C13.10:301

MOLECULAR DYNAMICS AND STRUCTURE OF SOLIDS

U.S. DEPARTMENT OF COMMERCE
NATIONAL BUREAU OF STANDARDS
SPECIAL PUBLICATION 301

C 13.10:301

PENNSYLVANIA STATE UNIVERSITY
JUN 26 1969
DOCUMENTS COLLECTION

UNITED STATES DEPARTMENT OF COMMERCE
Maurice H. Stans, *Secretary*
NATIONAL BUREAU OF STANDARDS • A. V. Astin, *Director*

Molecular Dynamics and Structure of Solids

Edited by
R. S. Carter and J. J. Rush

Institute for Materials Research
National Bureau of Standards
Washington, D.C. 20234

Based on Invited and Contributed Papers
2nd Materials Research Symposium
held at the NBS, Gaithersburg, Maryland
October 16–19, 1967

National Bureau of Standards Special Publication 301

Nat. Bur Stand. (U.S.), Spec. Publ. 301, 571 pages, (June 1969)
CODEN: XNBSA

Issued June 1969

For sale by the Superintendent of Documents, U.S. Government Printing Office
Washington, D.C. 20402 - Price $4.00

Foreword

The purpose of the annual symposia of the Institute for Materials Research of the National Bureau of Standards is to provide a forum for the presentation and exchange of information on the properties of materials and the development and improvement of measurement techniques.

"Molecular Dynamics and Structure of Solids," the second annual symposium of the Institute for Materials Research was held October 16–19, 1967 in the NBS laboratories at Gaithersburg, Maryland, and was attended by 250 university, government and industrial scientists from both the United States and abroad.

A major goal of the symposium was the encouragement of interdisciplinary cooperation in the study of the basic structural and dynamical properties of molecular solids. Such cooperation is essential if we hope to achieve a proper understanding and utilization of these materials. Topics and speakers were selected to demonstrate the correlation of various experimental techniques and the information they provide. This book, which documents the proceedings of the symposium, includes the complete text of invited lectures as well as summaries of the contributed papers and related discussions.

J. D. HOFFMAN, *Director*
Institute for Materials Research
National Bureau of Standards

C. O. MUEHLHAUSE,
General Chairman of the Symposium

Preface

This book represents the formal report of the second materials research symposium of the NBS Institute for Materials Research, which was held at the National Bureau of Standards from October 16–19, 1967. These symposia are intended to bring together authorities and workers in important areas of basic and applied materials research to provide an opportunity for communication of results and exchange of ideas and to assess current progress and future goals in such areas.

The subject of the symposium whose proceedings are presented here was "Molecular Dynamics and Structure of Solids." In the last decade there has been a virtual explosion of information on the basic dynamical and structural properties of molecular materials, which has been derived by a variety of spectroscopic and diffraction techniques, both new and old. The purpose of this symposium was to demonstrate and emphasize the correlation of the information obtained by the various experimental methods, while providing a review and discussion of important recent progress in the field of molecular solids. In this way it was hoped to stimulate among the participants, as well as readers of this book, a wider appreciation of techniques outside their own specialties and through this to encourage interdisciplinary cooperation.

The present volume contains the full text of the manuscripts on which invited lectures were based as well as summaries of all the contributed papers given at the symposium. The first part of the book provides, through a series of invited papers, an extensive introduction to the theory and practice of the major experimental techniques applied to the study of the molecular dynamics and structure of solids. These papers cover the fields of x-ray and neutron diffraction, infrared and Raman spectroscopy, neutron inelastic scattering and nuclear magnetic resonance spectroscopy. The rest of the volume is comprised of invited and contributed papers which discuss important recent work on lattice and molecular dynamics and molecular crystal structure. The results presented cover a wide range of molecular solids, including inorganic and organic crystals, hydrogen-bonded systems and polymers.

We believe that this volume clearly demonstrates the great advances which are being and can be made toward an understanding of the basic properties and intermolecular forces of solids through a complementary application of a variety of experimental methods.

PREFACE

The success of the symposium was made possible only because of the cooperation and enthusiasm of many people in the Institute for Materials Research and the National Bureau of Standards. Special thanks are due to Dr. V. W. Myers, Assistant General Chairman; Mr. F. J. Shorten, Arrangements Chairman; and Mr. H. T. Yolken, Social Chairman, for the symposium. The Program Committee members are to be commended for creating an excellent program and also for their advice and assistance in preparing manuscripts for publication in this book.

Although the entire staff of the NBS Office of Technical Information and Publications were particularly helpful in organizing and conducting the symposium, much expert assistance and advice were received from Messrs. W. R. Tilley, R. T. Cook, and G. T. Leighty. Mr. J. E. Carpenter advised on publishing the proceedings.

Finally, the editors wish to thank the many people who assisted in the various phases of the symposium and especially the preparation of these proceedings. In this regard, special recognition is extended to Mrs. Rosanne Dutrow who served as secretary, Miss Sandra Beall and Mrs. C. S. Damron who typed the manuscripts, and Mr. F. J. Shorten who coordinated the publication.

R. S. Carter
J. J. Rush

May 15, 1968

Abstract

This volume is based on material presented at the Second Materials Research Symposium of the National Bureau of Standards, held October 16–19, 1967. It provides a review of the application of spectroscopic and diffraction techniques to the study of the structure and dynamics of molecular solids. Invited papers on the theory and practice of the major experimental methods, including neutron and x-ray diffraction, neutron inelastic scattering, infrared and Raman spectroscopy and nuclear magnetic resonance, serve as a background for the more detailed presentation and discussion of results which follows. The topics covered in a series of invited and contributed papers include the lattice dynamics of molecular crystals, the spectroscopy and crystal structure of organic and inorganic solids and the dynamics of polymers.

Key Words: Molecular solid, crystal, polymer, molecular dynamics, lattice dynamics, crystal structure, rotation, vibration, spectroscopy, diffraction.

Library of Congress Catalog Card Number: 68-61721

Contents

Page

Foreword-- III

Preface--- v

INTRODUCTORY LECTURES

Theoretical Basis of Techniques for the Investigation of Molecular Dynamics and Structure of Solids*
ELLIOTT MONTROLL-- 3

The Contributions of Neutron and X-Ray Diffraction Techniques*
G. E. BACON-- 57

Infrared and Raman Studies on Molecular Structure and Motion in Condensed Phases*
G. R. WILKINSON-- 77

Neutron Inelastic Scattering Studies of Molecular Solids and Liquids*
P. A. EGELSTAFF-- 135

The Principles Involved in the Study of Molecular Motion in Solids by Nuclear Magnetic Resonance*
R. E. RICHARDS, F.R.S-- 157

STRUCTURE AND SPECTROSCOPY OF INORGANIC CRYSTALS

Spectroscopic and Diffraction Studies of Simple Hydrogen Bonds in Solids*
JAMES A. IBERS--- 177

Structure and Dynamics in Molecular Crystals: Some Comparisons*
WALTER C. HAMILTON--- 193

Dynamical Effects of Deuteron Intrabond Jumping in KD_2PO_4
V. HUGO SCHMIDT-- 219

The Detection of Atom Tunnelling in Solids
I. PELAH and Y. IMRY--- 223

Proton Delocalization in Inorganic Solids
J. J. FRIPIAT, P. G. ROUXHET, H. JACOBS, and A. JELLI-------------- 227

Structure Refinements, Thermal Motion and Madelung Constants of CdI_2- and $Cd(OH)_2$-Type Layer Structures
Y. M. de HAAN-- 233

The Aquated Hydrogen Ion: Single Crystal Diffraction Investigations of Compounds Containing the $(H_2O \cdot H \cdot OH_2)^+$ Ion
JACK M. WILLIAMS--- 237

Infrared Investigation of Ordering and Structural Changes in Ammonium Halides
C. W. GARLAND and N. E. SCHUMAKER---------------------------------- 241

---

*Invited papers.

CONTENTS

Page

Nuclear Magnetic Resonance and Neutron-Scattering Studies of Hindered Rotation in Phosphonium Iodide
T. C. Farrar and J. J. Rush ---------- 245

A Neutron Diffraction Study of Lithium Perchlorate Trihydrate
A. Sequeira and Ivan Bernal ---------- 249

The Structure of Several Uranyl Nitrate Compounds as Determined by Neutron Diffraction
M. H. Mueller and N. Kent Dalley ---------- 253

Infrared Spectral Studies as a Tool for Sensing the Environment About Water Molecules in Hydrates
J. Schiffer and D. F. Hornig ---------- 257

Nuclear Magnetic Resonance Studies of Molecular Motion in Clathrate Hydrates
C. A. McDowell and P. Raghunathan ---------- 261

Calculation and Analysis of Pulsed-NMR Line Shapes of Crystals
Marcel Kopp ---------- 265

The Vapor Pressure of CO/N_2 Solid Solutions
J. A. Morrison, D. M. T. Newsham, and R. D. Weir ---------- 269

Structural Study of Ti_5O_9
L. K. Keys ---------- 273

Significance of Weighting Schemes in an Anisotropic Least Squares Refinement of Ruby
J. W. McCauley and G. V. Gibbs ---------- 277

The Crystal Structure of $C_8Al_{2.1}B_{51}(AlB_{10})$
A. J. Perrotta, W. D. Townes, and J. A. Potenza ---------- 283

LATTICE DYNAMICS

Lattice Dynamics of Molecular Solids*
Gerald Dolling ---------- 289

Epithermal Neutron Inelastic Scattering from Metal Hydrides
S. S. Pan, M. L. Yeater, and W. E. Moore ---------- 315

Vibration Spectra of Hydrides Possessing the Cubic Perovskite Structure by the Inelastic Scattering of Cold Neutrons
Arnulf J. Maeland ---------- 319

Absorption of Light by the Sound Waves of Orientationally Disordered Crystals
E. Whalley ---------- 323

Lattice Vibrations in Some Simple Molecular Crystals
J. C. Laufer, J. E. Cahill, and G. E. Leroi ---------- 327

The Optical and Anharmonic Thermal Properties of a Diatomic Molecular Solid
George E. Jelinek ---------- 331

Neutron Scattering Studies of Molecular Vibrations in Ice
H. Prask and H. Boutin ---------- 335

---

*Invited paper.

CONTENTS

Page

Infrared Absorption Studies of Intermolecular Vibrations in the Low Frequency Region
Neil T. McDevitt, R. E. Witkowski, and W. G. Fateley 339

Optical Phonons in Mixed Sodium Potassium Tantalates
T. G. Davis, N. E. Tornberg, C. H. Perry and N. Knable 343

On the Second Order Elastic Constants of Molecular Solids
M. L. Klein 349

STRUCTURE OF ORGANIC CRYSTALS

Diffraction Studies of Molecular Dynamics in Organic Crystals*
K. N. Trueblood 355

Information on Molecular Motion Derived From Anisotropic Temperature Factor Coefficients
Carroll K. Johnson 381

Influence of Bonding Effects on Thermal Parameters as Determined by X-ray Diffraction
Philip Coppens 385

High Pressure Crystal Structure of Metal Free Phthalocyanine
R. S. Kirk 389

X-Ray Diffraction and Radiofrequency Spectroscopic Investigation of Dimethyltin Dichloride
Jack D. Graybeal and Domnic A. Berta 393

The Crystal and Molecular Structure of Tetraethylammonium Bis-(3)-1,2-Dicarbollylcuprate (II)
Richard M. Wing 397

Nuclear Magnetic Resonance Studies of Single Crystals of Trichloroacetic Acid
David C. Haddix and Paul C. Lauterbur 403

Thermal and Composition Expansion of Clathrates in the Ethylene Oxide-Water System
J. A. McIntyre and D. R. Petersen 407

SPECTROSCOPY OF ORGANIC CRYSTALS

Nuclear Magnetic Resonance and Molecular Motion in Organic Crystals*
E. R. Andrew 413

Far Infrared Spectra and Space Group of Crystalline Hydrazine and Hydrazine-d_4
F. G. Baglin, S. F. Bush, and J. R. Durig 437

Molecular Rotation in Condensed Phases of Simple Molecules
M. Blumenfeld 441

Correlation of Infrared and Inelastic Neutron Scattering Spectra of Solid Methane
Ashok K. Agrawal and Sidney Yip 449

---

* Invited paper.

Page

Theory of Phase Transitions in Solid Methanes
TSUNENOBU YAMAMOTO, YOSUKE KATAOKA, and HIDEO YASUDA 453

NMR Relaxation in Adamantane and Hexamethylenetetramine: Molecular Rotation and Diffusion
H. A. RESING 457

Thermodynamic Approach to Molecular Freedom, Especially in Plastically Crystalline Substances
EDGAR F. WESTRUM, Jr 459

Spectral Assignment in Inelastic Neutron Scattering Spectroscopy by Atomic Substitution Techniques
J. W. WHITE 463

Anisotropic Lattice Dynamic Studies of Organo-Tin Compounds by Mössbauer Spectroscopy
HANS A. STÖCKLER and HIROTOSHI SANO 469

DYNAMICS OF POLYMERS

Relaxation in Solid Polymers*
DAVID W. MCCALL 475

Low Frequency Vibrations in Polyethylene
W. R. MYERS and P. H. RANDOLPH 539

Neutron Scattering in Deuterated Polyethylene
L. A. FELDKAMP and J. S. KING 543

Epithermal Neutron Inelastic Scattering by Polyethylene
W. E. MOORE, G. J. KIROUAC, L. J. ESCH, K. W. SEEMANN, and M. L. YEATER 547

The Vibrational Properties of Polyoxymethylene
S. F. TREVINO and V. E. LAGARDE 553

Vibration Spectra of Polyglycine
V. D. GUPTA, S. TREVINO, and H. BOUTIN 559

Thermal Conductivity and Specific Heat of Amorphous Polymers Between 0.4 and 4 °K
C. L. CHOY, G. L. SALINGER, and Y. C. CHIANG 567

APPENDIX I—Symposium Committees 571

---

* Invited paper.

INTRODUCTORY LECTURES

THEORETICAL BASIS OF TECHNIQUES FOR THE INVESTIGATION OF MOLECULAR DYNAMICS AND STRUCTURE OF SOLIDS

ELLIOTT W. MONTROLL

University of Rochester, Rochester, New York 14627

The purpose of this introductory lecture is to review the basic ideas behind several experimental techniques employed in the investigation of the structure and molecular dynamics of solids. In the time allotted, I can hardly do more than drop a few names of topics and of the individuals who have developed them.

Unfortunately, the only man who could have given a masterful performance with such an assignment, Peter J. W. Debye, is no longer with us. For almost sixty years, from his early youth until his dying day, his imaginative, clearly presented investigations, as well as his dynamic personal enthusiasm, made his contributions to the subject of this conference greater than those of any other individual. Debye's Ph.D. thesis was concerned with light scattering, as were his last papers. This is not to imply that his career was spent rewriting his doctor's thesis. While his fundamental papers on scattering of light, x-rays, electrons and sound are all of great importance in the development of our subject, his research on lattice dynamics, polar molecules, electrolytes, magnetic cooling, transport processes, and properties of polymers are of at least equal importance. His work and style have always been an inspiration to me and I wish to dedicate this review to his memory.

1. Thermodynamic Properties [1] [1]

1.1. Information Available and not Available in Heat Capacity Measurements

While the variations of thermodynamic quantities with temperature, pressure, density, external magnetic field, etc., reflect only the large scale average behavior of a sample, they are important in indicating drastic changes in the long range order of a system which occur during phase transitions. When molecular interactions in a solid are described through a small number of parameters, thermodynamic data yield estimates of these parameters.

---

[1] Figures in brackets indicate the literature references at the end of this paper.

Theoretically, the thermodynamic properties of any substance are derivable from its Hamiltonian H, which, of course, contains the detailed laws of interaction between its various microscopic degrees of freedom. The first step in the derivation of formulas for these properties is to calculate the partition function

$$Z = \text{trace} \exp(-\beta H) \quad \text{with } \beta = 1/Tk_B \tag{1}$$

k_B being the Boltzmann constant. The internal energy and heat capacity (with a quantity x held constant) follow from well known statistical mechanical formulas (x might be volume, pressure, external magnetic field strength, etc.)

$$E = -\partial \log Z/\partial\beta, \quad C_x = (\partial E/\partial T)_x \tag{2}$$

Similar formulas exist for other thermodynamic quantities. Examples of four experimental heat capacity curves are given in figure 1.

The curve 1a is that of NaCl. Let us assume that the potential energy component of the Hamiltonian is the sum of the coulomb interactions between all charged particles in the crystal and a short range interaction which involves only nearest neighbor pairs. If this

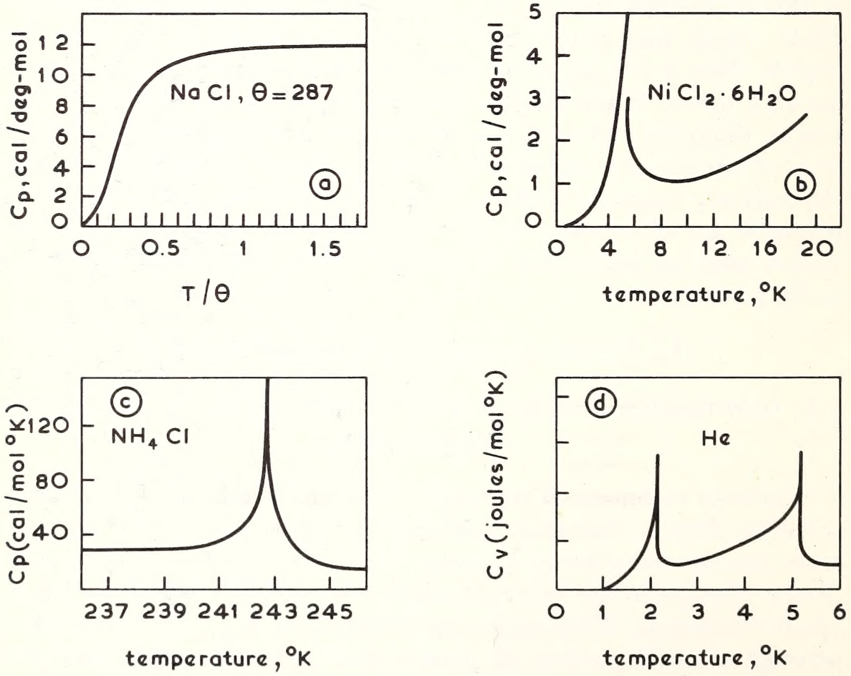

FIGURE 1. Four heat capacity curves.

short range interaction is expressed in terms of only two or three parameters, one could make a detailed analysis of the lattice vibrations of NaCl and find the set of parameters which would give the closest agreement with the experimental curves. On the other hand, if one had reason to believe that ten parameters would be necessary to properly characterize the Hamiltonian, the experimental data would not be sufficiently sensitive to assign reasonable values to all of them.

The curve 1b is the heat capacity of the antiferromagnetic material $NiCl_2 \cdot 6H_2O$ at very low temperatures [2]. The lattice vibrations make only a small contribution to the heat capacity in that range. The sharp rise followed by an even sharper fall is due to the development of spin disorder and the vanishing of the antiferromagnetic character of the crystal. The Hamiltonian in this case involves a spin-spin interaction which, to a first approximation, can be treated independently of the small vibrations of the lattice. The scheme of separating the Hamiltonian into several independent parts is employed in a number of the cases which we examine below.

Figure 1c is the heat capacity curve of NH_4Cl [3]. The peak is, as will be discussed in Section 2.2, associated with the transition from a low temperature ordered array with the ammonia group of each unit cell pointed in the same direction, with its symmetry axis along one of the cell diagonals, to a high temperature disordered array with these symmetry axes pointed randomly along the various cube diagonals. While thermodynamic data indicated the existence of an unusual event, it merely inspired the proposal of several possible models for the event; a clear picture developing only after the IR spectra was carefully analyzed. The model was substantiated through neutron scattering.

The heat capacity of liquid ^4He plotted in figure 1d exhibits two λ points [4]. The one at 2.1 °K suggested that the liquid was a bit strange. The investigation of transport properties revealed the peculiar superfluid state below T_c. The very low temperature heat capacity, being proportional to T^3, suggests phonons to be the elementary excitation in ^4He liquid. Rotons and vortex excitations are not immediately apparent from thermodynamic data. Such a variety of excitations and interactions of excitations exist at temperatures near the λ point that a satisfactory discussion of the logarithmic singularity of the heat capacity in that region has not yet been given. The high temperature λ point at 5.2 °K is associated with the gas-liquid phase transition.

1.2. Lattice Vibrations [5,6]

Lattice vibrations contribute to the thermodynamic properties of all solids. Most of the theory of these excitations (often called phonons) is based on the harmonic approximation in which atoms are assumed to suffer only small displacements from their equilibrium positions. The potential energy is chosen to be a quadratic form in the displacements of the various atoms from these equilibrium positions. The individual motions can be expressed as a linear combination of independent normal modes of vibration. A frequency ω is associated with each of these normal modes so that in a crystal composed of N unit cells with r atoms in each cell, there are $3rN$ frequencies. If $g(\omega)\,d\omega$ is the fraction of these in the range between ω and $\omega+d\omega$, then the contribution of the lattice vibrations to the heat capacity at constant volume is

$$C_v=3rNk_B\int_0^{\omega_L} g(\omega)\,(\hbar\omega\beta)^2\,\mathrm{csch}^2\,(\hbar\omega\beta)\,d\omega \tag{3}$$

The determination of the frequency spectrum $g(\omega)$ follows from the dynamical matrix of the crystal, a quantity which is derived from the crystal Hamiltonian which is written as

$$H=T+\Phi \tag{4}$$

T being the kinetic energy

$$T=\frac{1}{2}\Sigma\; m_k\,\dot{u}_\alpha^2\binom{l}{k} \tag{5}$$

and Φ the potential energy

$$\Phi=\Phi_0+\frac{1}{2}\Sigma\,\Phi_{\alpha\beta}\begin{pmatrix} l & l' \\ \kappa & \kappa' \end{pmatrix}u_\alpha\binom{l}{\kappa}u_\beta\binom{l'}{\kappa'}+\mathrm{O}(u^3). \tag{6}$$

The quantities

$$u_\alpha\binom{l}{\kappa}\text{ and }\Phi_{\alpha\beta}\begin{pmatrix} l & l' \\ \kappa & \kappa' \end{pmatrix}$$

represent respectively the displacement from equilibrium of the particle (of mass m_κ) located at the κth position in the lth unit cell (α running through the set of components x, y, and z) and the force constant which couples the displacement in the α direction of the κth atom in the lth cell with that in the α' direction of the κ' atom in the l' cell. The quantity Φ_0 is the vibrational potential energy in the equilibrium state with all atoms located at their equilibrium positions and

$$\Phi_{\alpha\beta}=\left[\frac{\partial^2\Phi}{\partial u_\alpha\binom{l}{\kappa}\partial u_\beta\binom{l'}{\kappa'}}\right]_0. \tag{7}$$

The evaluation of these second derivatives is also to be made at the equilibrium state.

The equations of motion of the vibrating lattice can be found from the Hamiltonian (4). In the small vibration harmonic approximation, the resulting equations are linear in the displacements u. Since boundary effects are generally uninteresting, one usually employs the Born-von Karman periodic boundary conditions in lattice vibration discussions. The periodic nature of the crystal implies that the αth component displacement of particle κ in cell l can be written as

$$u_\alpha\binom{l}{\kappa} = m_\kappa^{-1/2} u_\alpha(\mathbf{k}) \exp i[t\omega(\mathbf{k}) + 2\pi\mathbf{k}\cdot\mathbf{r}(l)]. \tag{8}$$

When this is substituted into the equations of motion

$$m_\alpha \ddot{u}_\alpha\binom{l}{\kappa} = \sum_{\beta, l',} \sum_{\kappa'} \Phi_{\alpha\beta}\binom{l\ l'}{\kappa\ \kappa'} u_\beta\binom{l'}{\kappa'} \tag{9}$$

one obtains a set of homogeneous equations whose solution exists only if the determinant of the coefficients of the displacements vanish. The matrix of the determinant is called the "dynamical matrix." The normal mode frequencies $\omega(\mathbf{k})$ associated with the wave vector $\mathbf{k}$ are solutions

$$\det\left\{D_{\alpha\beta}\binom{\mathbf{k}}{\kappa\ \kappa'} - \omega^2(\mathbf{k})\delta_{\alpha\beta}\delta_{\kappa\kappa'}\right\} = 0 \tag{10a}$$

where

$$D_{\alpha\beta}\binom{\mathbf{k}}{\kappa\ \kappa'} = (m_\kappa m_{\kappa'})^{-1/2} \sum_l \Phi_{\alpha\beta}\binom{l}{\kappa\ \kappa'} \exp[2\pi i\mathbf{k}\cdot\mathbf{r}(l)] \tag{10b}$$

The detailed dispersion relations

$$\omega = \omega(\mathbf{k}) \tag{11}$$

which are the roots of the characteristic determinants (10a) as a function of $\mathbf{k}$ are very sensitive to the detailed choice of force constants Φ. Hence, experiments such as the scattering of slow neutrons by crystals (see Section 2) which yield these dispersion curves can give good agreement with results deduced from theoretical models only if a good set of force constants have been used. Note that there are a number of branches of dispersion relations. For example, in the case of a monatomic cubic crystal, the dynamical matrix is 3x3 and there are three branches.

Thermodynamic averages (cf. eq 3 for the heat capacity) over the frequency spectrum or distribution function of the roots of (10a), (11), are much less sensitive to the detailed choice of the force constants and, therefore, do not produce as much information as experiments involving driven disturbances. Generally, to interpret the response of a crystal to coherent driving forces such as acoustic, electromagnetic, or matter (for example, neutrons) waves, one needs information about appropriate functions of the displacement vectors (8) as well as the dispersion relations (11). Hence, a richer picture of atomic and molecular motions must be available to interpret the experimentally observed responses.

We close our discussion of lattice vibrations of this section by summarizing some ideas about dispersion curves and frequency spectra. First consider the vibrations of a one-dimensional string of N atoms, each of mass m undergoing small vibrations when connected by springs with force constant γ. If u_j represents the displacement of the jth atom from its equilibrium position, the potential energy when the displacements are $u_1, u_2, \ldots,$ is

$$\Phi=\Phi_0+\frac{1}{2}\gamma\Sigma(u_j-u_{j+1})^2 \tag{12}$$

The dynamical matrix in this case is a scalar with

$$D(k)=-(\gamma/m)(e^{2\pi ika}-2+e^{-2\pi ika})=(4\gamma/n)\sin^2 \pi ka$$

so that the dispersion relation is

$$\omega(k)=\omega_L \sin \pi ka \quad \text{with} \quad \omega_L\equiv(4\gamma/m)^{1/2} \tag{13}$$

which is shown in figure 2.

The k associated with a preassigned value of ω is

$$\pi ak(\omega)=\sin^{-1}(\omega/\omega_L). \tag{14}$$

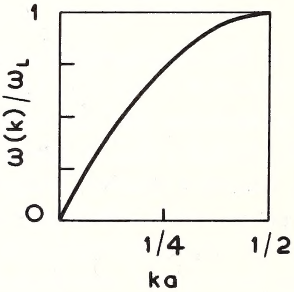

FIGURE 2. Dispersion curve $\omega=\omega(k)$ for linear chain.

The number of frequencies less than ω is proportional to $k(\omega)$. Hence the fraction of frequencies between ω and $\omega+d\omega$ is

$$a[k(\omega+d\omega)-k(\omega)]=a(dk/d\omega)d\omega=[a/\pi a\omega_L][1-(\omega/\omega_L)^2]^{-1/2}.$$

The normalization constant α is chosen to make the integral from 0 to ω_L be equal to 1. Hence,

$$\omega_L g(\omega)=\frac{2}{\pi}[1-(\omega/\omega_L)^2]^{-1/2} \text{ if } 0<\omega<\omega_L \tag{15}$$

Two and three dimensional dispersion relations and frequency spectra are often discussed in terms of curves or surfaces of constant frequency. For example, in the case of a two-dimensional square lattice, the determinant (10a) is 2×2 so that ω^2 is the solution of a quadratic equation for each $\mathbf{k}$ vector, $\mathbf{k}=(k_1,k_2)$. Since the elements of the dynamical matrix in this case are doubly periodic in $\mathbf{k}$ space, this is also true for $\omega(\mathbf{k})\equiv\omega(k_1,k_2)$. A triple periodicity exists in the $\omega(\mathbf{k})$ appropriate for three dimensional lattices. A typical set of curves of constant frequency are given in figure 3. The fraction of normal modes with frequency less than ω is the ratio of the area bounded by the curve $\omega(k_1,k_2)=\omega$ is

$$N(\omega)=(1/A)\iint\limits_{R(\omega)} dk_1dk_2$$

where A is the area of the full region of k space representing one period of $\omega(k_1,k_2)$.

We then find the frequency distribution function $g(\omega)$ to be

$$g(\omega)d\omega=N(\omega+d\omega)-N(\omega)=\frac{\partial N}{\partial\omega}d\omega=\frac{d\omega}{A}\frac{\partial}{\partial\omega}\iint\limits_{R(\omega)} dk_1dk_2$$

or in three dimensions

$$g(\omega)=\frac{1}{V}\frac{\partial}{\partial\omega}\iiint\limits_{R(\omega)} d^3k \tag{16}$$

where the volume integral extends over the interior $R(\omega)$ of the surface $\omega(k_1k_2k_3)=\omega$. This volume integral can be converted to the surface integral

$$g(\omega)=2\omega K\iint\limits_{S}[\{\nabla\omega(\mathbf{k})\}^2]^{1/2}dS \tag{17}$$

over the surface $\omega(k_1,k_2,k_3)=\omega$. The constant K depends on the lattice type.

The surface which is represented by the contour map in figure 3 for a 2D lattice has maxima, minima, and saddle points. The function

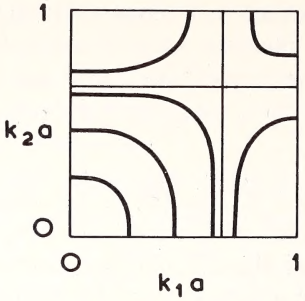

FIGURE 3. Curves of constant frequency for 2D square lattice.

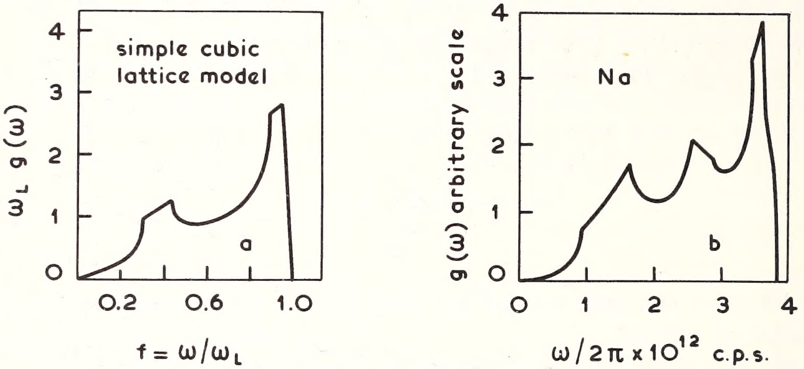

FIGURE 4. (a) Frequency spectrum of a simple cubic model lattice with nearest neighbor central and non-central forces. The central forces are 8 times as large as non-central ones. (b) Experimental frequency spectrum of sodium.

$g(\omega)$ (which is plotted in figure 4a) has a logarithimic singularity at the frequency associated with the saddle point [7]. The corresponding saddle points found in the 3D analogues of figure 3 lead to square root singularities [8, 6] as exhibited in figure 4 for model calculations and real materials. The best experimental method of investigating the dispersion relations and the frequency spectra is by neutron scattering experiments of the type discussed in section 2.2.

1.3. Contribution of Other Degrees of Freedom to Thermodynamic Properties

The first step in estimating the contribution of degrees of freedom other than small vibrations to thermodynamic properties is the construction of an appropriate Hamiltonian so that (1) and (2) can be applied.

In some cases this appears in a very natural way. For example, when permanent dipoles are associated with some interacting nuclei or with interacting groups in the molecule in each unit cell, the dipole-dipole Hamiltonian is just the sum of the potential energy of interaction of various dipole pairs (taken over all $i \neq j$)

$$H = \frac{1}{2} \sum_{i,j}{}' \left\{ \frac{\boldsymbol{\mu}_i \cdot \boldsymbol{\mu}_0}{r_{ij}^3} - \frac{3(\boldsymbol{\mu}_i \cdot \mathbf{r}_{ij})(\boldsymbol{\mu}_j \cdot \mathbf{r}_{ij})}{r_{ij}^5} \right\} \tag{18}$$

Here $\mathbf{r}_{ij}$ is the distance of separation between the i and jth dipole when the dipole moment vectors are $\boldsymbol{\mu}_i$ and $\boldsymbol{\mu}_j$.

In other cases a model Hamiltonian is constructed which summarizes the main features of the interaction but involves some simplification to make a theory possible. An important example is that used to characterize assemblies in which each lattice point can be in either of two states. One such assembly is a mixture of two components A and B such that any lattice site in the crystal is occupied by an A or B particle. One introduces a set of parameters $\{\sigma_j\}$ such that

$$\sigma_j = \begin{cases} +1 \text{ if lattice site } j \text{ is occupied by an A} \\ -1 \text{ if lattice site } j \text{ is occupied by a B} \end{cases} \tag{19}$$

Let ϵ_{AA}, ϵ_{AB}, and ϵ_{BB} represent, respectively, the energies of interaction of nearest neighbor AA, AB, and BB pairs. A given arrangement of A and B states on the lattice can be represented by a sequence (σ_1, σ_2, σ_3, . . .).

For example, in a line AABAB, the sequence would be (1, 1, −1, 1, −1). If only nearest neighbor interactions are relevant, then the total energy of interaction associated with the sequence σ_1, σ_2, . . . is

$$H(\sigma_1\sigma_2\ldots) = \sum_{i,j} \left\{ \frac{1}{2}\epsilon_{\mathrm{AB}}(1-\sigma_i\sigma_j) + \frac{1}{4}\epsilon_{\mathrm{BB}}(1-\sigma_i)(1-\sigma_j) + \frac{1}{4}\epsilon_{\mathrm{AA}}(1+\sigma_i)(1+\sigma_j) \right\} \tag{20}$$

where the summation runs over all nearest neighbor pairs. Clearly, if i and j are both A's, then $\sigma_i = \sigma_j = +1$ and the value of the (i, j) term in the bracket is ϵ_{AA}, etc. An alternative form is

$$H(\sigma_1, \sigma_2, \ldots) = \sum_{n\cdot n} \left\{ \frac{1}{4}\alpha - \frac{1}{2}H\mu(\sigma_i + \sigma_j) - J\sigma_i\sigma_j \right\} \tag{21a}$$

where

$$\alpha = 2\epsilon_{\mathrm{AB}} + \epsilon_{\mathrm{AA}} + \epsilon_{\mathrm{BB}}\ ;\ 2\mu H = \epsilon_{\mathrm{BB}} - \epsilon_{\mathrm{AA}} \tag{21b}$$

$$J = \frac{1}{4}(2\epsilon_{\mathrm{AB}} - \epsilon_{\mathrm{AA}} - \epsilon_{\mathrm{BB}}). \tag{21c}$$

If c is the coordination number (number of nearest neighbors to a given lattice point) and our crystal is composed of N lattice points, all energies can be measured relative to $Nc\alpha/8$ in which case we rewrite the Hamiltonian as

$$H(\sigma_1, \sigma_2, \ldots) = -\mu H \sum_j \sigma_j - J \sum_{n \cdot n} \sigma_i \sigma_j. \tag{22}$$

This is exactly the form of the Hamiltonian of the Ising model of a ferromagnet if one identifies μH with the product of a spin moment μ with an external magnetic field H and J with the spin-spin interaction between a pair of nearest neighbors.

In this model of ferromagnetism one lets

$$\sigma = \begin{cases} +1 \text{ if spin is ``up''} \\ -1 \text{ if spin is ``down''} \end{cases} \tag{23}$$

and postulates the interaction energy between neighboring spins to be

$$E = -J\sigma\sigma' = \begin{cases} -J \text{ if nearest neighbor pair of spins is parallel} \\ J \text{ if nearest neighbor pair of spins is antiparallel.} \end{cases} \tag{24}$$

In a ferromagnetic crystal $J > 0$ and in an antiferromagnetic one, $J < 0$. If our binary alloy has a ground state in which A and B atoms alternate on the lattice, then from (21c) $J > 0$ and the alloy is analogous to an antiferromagnetic crystal. It is analogous to a ferromagnetic one when $J > 0$ in eq (21c) so that the alloy separates into two immiscible phases at low temperatures, one being pure A and the other pure B.

A great deal is known about the thermodynamic and magnetic properties of the Ising model [9–15]. This can be translated into properties of our two component AB system and, indeed, into those of any system which describes a cooperative phase which is the result of each lattice point being able to appear in either of two possible states in such a manner that the state at a given lattice point is correlated with that of the neighboring lattice points.

1.4. Residual Entropy of Molecular Crystals

We close our discussion of thermodynamic properties with some remarks about the residual entropy problem. There are a number of materials whose entropy, with the lowering of temperature, reaches a a constant value which is much larger than the vibrational entropy should be. Most of these substances are hydrogen bonded, although there are some exceptions such as carbon dioxide and nitrous oxide.

Ice is probably the most studied example. Using measurements of the heat capacity of ice from very low temperatures to the melting point, Giauque and Stout [16] calculated an entropy $44.28 \pm .05$ cal/

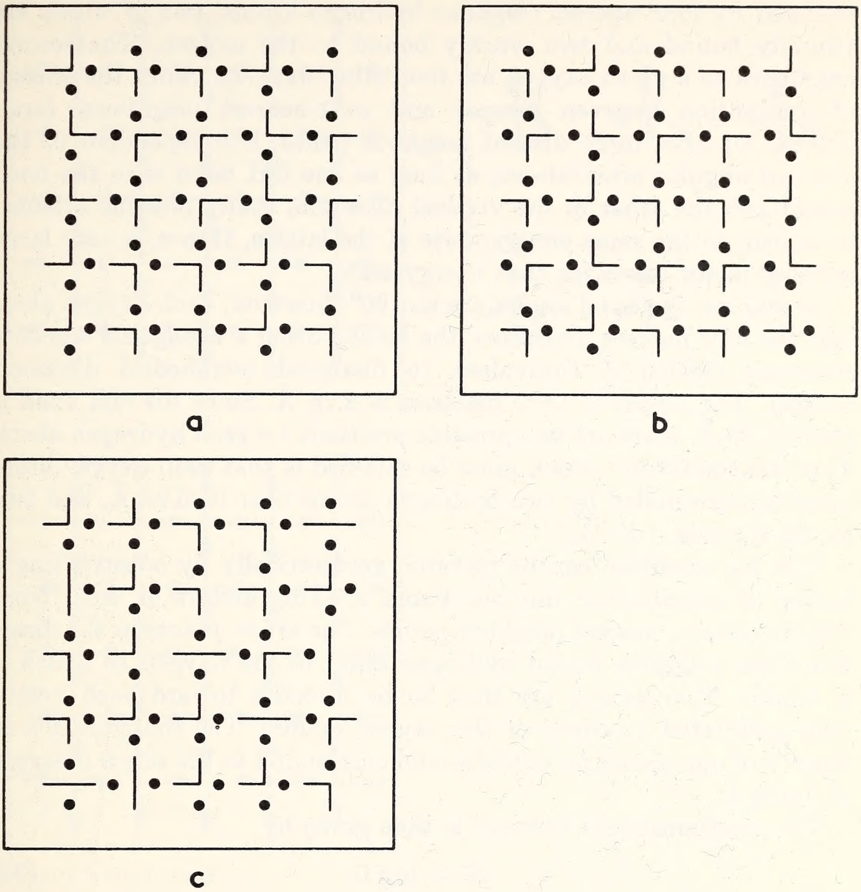

Figure 5. Configurations a and b correspond to 90° bond angle 2D ice. In real 3D ice all bond angles between a lattice point and any of its two nearest neighbors are the same. Hence a more reasonable 2D analogue would give equal weight to a linear and right angle molecule as in c.

deg/mol for gaseous water at 298.1 °K and 1 atmosphere pressure. This was 0.82±.05 cal/deg/mol smaller than that estimated by Giauque and Ashley [17] from an analysis of the band spectrum.

To give a qualitative idea of the source of the residual entropy in ice, let us first consider a two-dimensional crystal composed of a hypothetical water molecule whose bond angle between OH bonds is 90°. Several possible arrangements of our hypothetical water molecules on a square lattice are shown in figure 5. The heavy lines represent the strong OH bonds, while the light dot between hydrogen and oxygen represents the weak hydrogen bond between an oxygen of one molecule and a hydrogen of another. Clearly, every oxygen atom is surrounded by four nearest neighbor hydrogen atoms, two of which are strongly bound and two weakly bound to the oxygen. The second neighbors to a given oxygen are four other oxygens. Since the energy of interaction between nearest and next-nearest neighbors, (and, indeed, for even more distant neighbor pairs), is independent of the detailed angular orientations, as long as one OH bond is in the horizontal and the other in the vertical direction, many possible orientations lead to the same energy state of the lattice. Hence, a very large entropy factor exists for that energy state.

In real ice, the bond angles are not 90°; however, each oxygen atom still has four nearest neighbors, the lattice being a hexagonal wurtzite structure (which is equivalent to distorted tetrahedral diamond lattice). The observed O–O distance is 2.76 Å. Since the OH bond is about 0.95 Å, there are two possible positions for each hydrogen atom. The "ice condition" which must be satisfied is that each oxygen atom must be surrounded by two hydrogen atoms near it, 0.95 Å, and two on the far side, 1.81 Å.

This ice condition can be pictured geometrically by constructing a lattice of coordination number 4 and drawing arrows on each bond which connects nearest neighbor points. The arrow points in the direction from a tightly bound hydrogen atom to the oxygen to which it is bound. Two arrows are then to be directed toward each vertex (the postulated locations of the oxygen atoms). The configuration in figure 5 of our square ice model would correspond to the arrow diagram of figure 6.

The configurational entropy is then given by

$$S=k \log \Omega, \tag{25}$$

Ω being the number of ways arrows can be assigned to a lattice so that the ice condition "two in, two out of each vertex" is satisfied. As a first estimate, let us neglect the ice condition. Then, since each of the $2N$ bonds (in a lattice containing N water molecules) can have an arrow in either direction, $\Omega_o=2^{2N}$ and

$$S_o=Nk \log 4. \tag{26}$$

Pauling [18] improved this estimate by assuming that all vertices are independent but included the ice condition with that approximation. A typical vertex is the point 0 in figure 6. Of the sixteen possible arrow configurations for the four bonds in the figure, only six are consistent with the ice condition. Hence, only $(6/16)^N$ of the Ω_0 configurations are realized and we have the Pauling estimate

$$\Omega_p=2^{2N}(6/16)^N$$

so that

$$S_p=Nk \log (3/2)$$

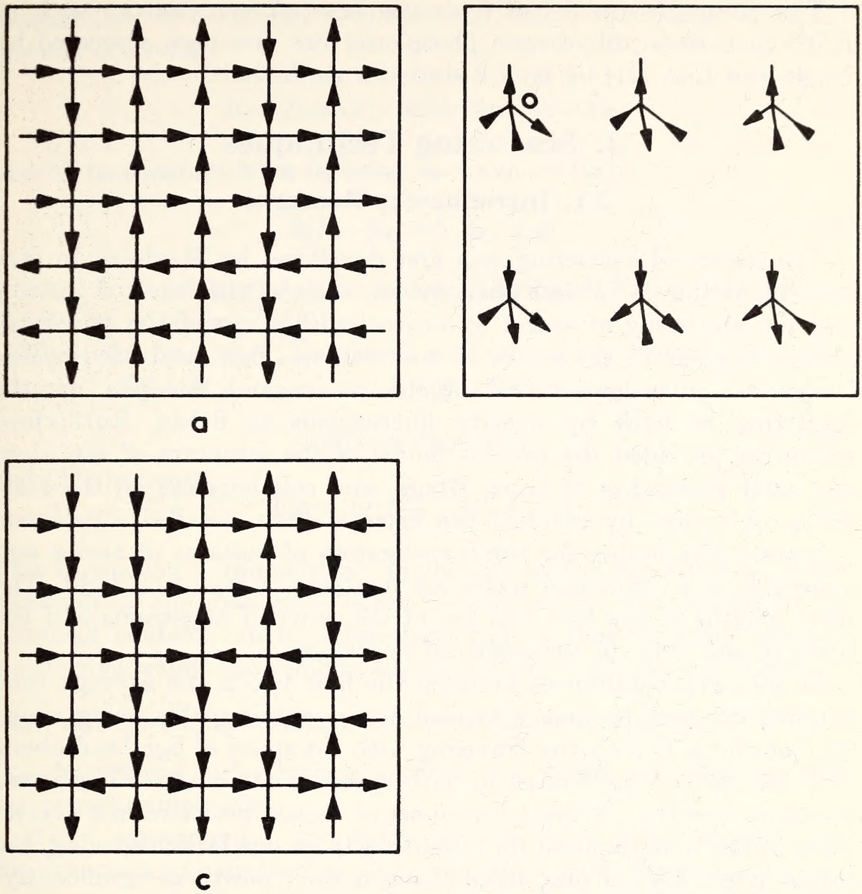

Figure 6. Diagrams (a) and (c) are arrow configurations which correspond to bond configurations in (5a) and (5b). Diagram (6c) shows which of the 16 possible arrow configurations in a model of ice satisfy the ice condition of two strong and two weak bonds.

which corresponds to the residual entropy of 0.805 cal/deg/mol in very good agreement with the observed value mentioned above.

The calculation becomes very complicated when the proper dependence of various vertices is employed. This was done by Nagle [19] who found the entropy to be $S=0.8145\pm0.0002$ cal/deg/mol. By the same method used for real ice, Nagle also gave the estimate for the "square ice" model

$$\Omega^{1/N}=1.540\pm.001$$

which agrees well with the exact value recently determined by E. Lieb

$$\Omega^{1/N}=(4/3)^{3/2}=1.5396007.$$

The Slater [20] model of hydrogen bonded ferroelectrics such as KDP (potassium dihydrogen phosphate) has also been discussed by Nagle and Lieb [21] by lattice statistics methods.

2. Scattering Techniques

2.1. Introductory Remarks

The theory of scattering was first developed by Rayleigh to give an explanation of natural phenomenon such as the color of the sky and the scattering of sound by obstacles. The use of the scattering technique to probe the nature of materials was first motivated by the theoretical investigations of Smoluchowski and Einstein on the scattering of light by density fluctuations in fluids. Rutherford scattering provided the present model of the structure of the atom and early researches of Laue, Bragg, and collaborators on the scattering of x rays by crystals has exposed their detailed structures.

Appropriate probes for the investigation of motions of atoms and molecules in a condensed phase are neutrons, x rays, and light. The wave lengths of the first two are of the order of angstroms and the latter of the order of thousands of angstroms.

An important difference between the first two is the average time required by each to span a typical lattice spacing, this being about 10^{-18} sec for a 10 kv x ray traveling with the speed of light and about 10^{-13} sec for a 5 meV neutron with speed of 10^5 cm/sec. The x ray travels so fast that it sees a frozen set of atomic positions in a crystal while in the time required for a neutron to go one lattice spacing, the atoms in the crystal may have changed their positions significantly. Furthermore, the energy of a slow neutron might be less than or equal to that of an atom with which it collides so that a considerable energy exchange might occur. The energy of an x ray hardly changes as it is scattered by a crystal.

The determination of crystal structures by x rays is based on the interference between x rays reflected from successive layers of atoms while a more productive analysis of neutron scattering data involves inelastic effects.

2.2. Inelastic Neutron Scattering [22]

Let an incident beam of monoenergetic slow neutrons of wave length λ greater than twice the largest lattice spacing in the crystal be scattered through an angle θ. Through its interaction with the crystal during the scattering processes, its initial energy E_I and wave number k_I is changed to the final values E_f and k_f. This change in energy and momentum is accomplished through the creation or annihilation of a phonon in the crystal. Since the energy of such a phonon is $E=\hbar\omega$,

$$E_F-E_I=(k_F^2-k_I^2)\hbar^2/2m=E=\hbar\omega \tag{27}$$

and its momentum is $\hbar\mathbf{q}$ ($\mathbf{q}$ being its wave vector),

$$\hbar(\mathbf{k}_I-\mathbf{k}_F)=\hbar(2\pi\boldsymbol{\tau}+\mathbf{q}) \tag{28}$$

where $\boldsymbol{\tau}$ is an arbitrary lattice vector. When $\mathbf{q}=0$ this equation is just the Bragg scattering formula.

Since the frequency associated with the wave vector $\mathbf{q}$ has the property $\omega(\mathbf{q})\equiv\omega(\mathbf{q}+2\pi\boldsymbol{\tau})$, (28) is equivalent to

$$\omega(\mathbf{q})=\omega(\hbar[\mathbf{k}_I-\mathbf{k}_F]), \tag{29}$$

and (27) becomes

$$\hbar(k_F^2-k_I^2)/2m=E=\hbar\omega(\mathbf{q}) \tag{30}$$

This expression is immediately applicable to the experimental determination of the dispersion curve $\omega=\omega(\mathbf{q})=E/\hbar$. The energy of the scattered neutron can be determined from a time of flight measurement which yields the velocity which, in turn, yields $|\mathbf{k}_F|=\hbar^{-1}(2mE_I)^{1/2}$ since $E_I=\frac{1}{2}m\mathrm{v}^2$. By scanning a large number of angles, a number of $(\mathbf{k}_I-\mathbf{k}_F)$ values and, hence, a number of $\mathbf{q}$ values are obtained with the corresponding $\omega(\mathbf{q})$.

Many experimental dispersion curves have been obtained by Brockhouse and collaborators [23] with the Chalk River reactor, and by Hughes and others with the Brookhaven reactor in the late 1950's and early 1960's. This work has been developed further by others and provides a great deal of our present knowledge of phonons in solids. Several typical dispersion curves are shown in figure 7. Much of the basic theory was done by van Hove [24, 25] and Placzek and, indeed, while Placzek's papers are not numerous, he masterminded and inspired many early developments in the use of neutrons as a probe for the investigation of lattice vibrations.

Neutrons are also useful in a search for rotational motions in crystals. The basis of the anomolous heat capacity of the halides of ammonia mentioned in Section 1 has been investigated by this method.

Two competing theories were proposed when the anomaly was first observed. Pauling suggested that, below the transition temperature, the NH_4 group undergoes torsional oscillations and that above the transition temperature rotates freely. Frenkel proposed that, below the transition temperature, each NH_4 group is pointed in the same direction with its symmetry axis along one of the same cell diagonal,

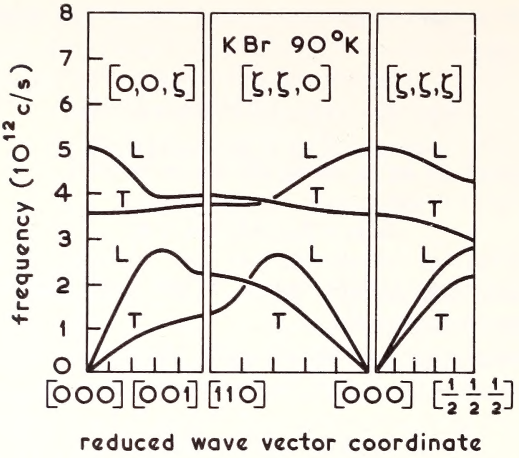

FIGURE 7. Dispersion curves in various directions for KBr.

and that, above the transition temperature, the NH_4 symmetry axes are pointed randomly along the various cubic unit cell diagonals. Hence, torsional vibrations would occur both below and above the transition temperatures, but about the same diagonal axis in each unit cell below T_c and about random diagonals above the unit cell. No free rotation would exist above the transition temperature.

Hornig [26], through a complicated analyses of the infrared spectrum of the halides and the deuterated halides of ammonia, proved the Frenkel model to be correct. It was verified to be correct by Palevsky [22] by inelastic neutron scattering in the following simple, yet elegant, manner. The intensity of neutrons scattered from the crystal of interest is plotted as a function of energy (see fig. 8) at temperatures below and above the transition temperature. In the case of NH_4Br, two sharp peaks are evident. The one at 48×10^{-3} is associated with the torsional oscillations of interest and the lower frequency 24×10^{-3} ev with the internal optical vibrations in the NH_4 ion. The main qualitative difference between the high and low temperature scattering intensity curves of figure 8 is the line broadening. Notice that the torsional line is still very strong above the transition temperature. In the case of certain organic crystals containing CH_3 groups, the peak associated with torsional vibrations disappears at the transitional temperature, indicating that these groups rotate freely without a restoring force.

Neutrons are also very useful for the investigation of the elementary excitations in liquid ^4He. The heat capacity of ^4He at very low temperatures is proportional to T^3 as is that of crystals. This and other observations have been attributed by Landau to be due to phonons

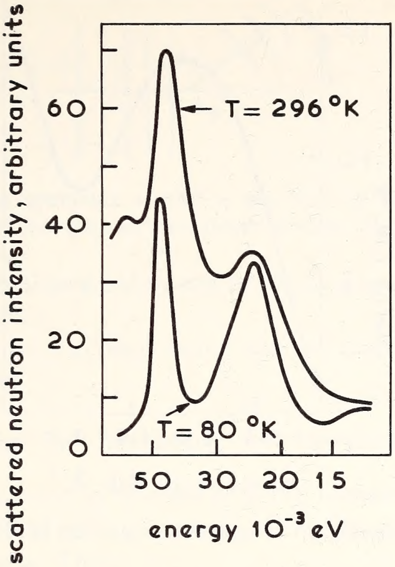

FIGURE 8. Variation of neutron scattered intensity with angle in NH_4Br.

as an elementary excitation in liquid helium. Since a liquid is unstable to shear, these phonons are longitudinal only. The energy of such phonons is proportional to their momentum (or wave number). At higher temperatures where deviations from the T^3 law occur, he postulated the existence of more complicated excitations which he called rotons and which have the energy, momentum relation

$$E=\Delta+(p-p_0)/2\mu \tag{31}$$

where Δ is a minimum energy and p_0 a minimum momentum required to form a roton and μ is its effective mass.

A direct way to verify the existence of rotons would be to observe the energy spectrum of slow neutrons which have been scattered by rotons in essentially the same manner that the dispersion curve for phonons was obtained for crystals. This was first done by Palevsky, Otnes, and Larsson [27]. The data of a number of groups [28–30] is combined in figure 9 to give the complete E–p dispersion curve at 1.1 °K. With increasing temperatures, interacting vertices and other more complicated excitations develop which are not so clearly understood. The theoretical basis for the logarithmic singularity of the heat capacity at the λ point is not understood. Above the λ point the neutron scattering by ^{4}He liquid is essentially that of classical liquids.

We now proceed with the theory of purely elastic scattering of plane waves of various sorts by scattering centers whose locations are correlated.

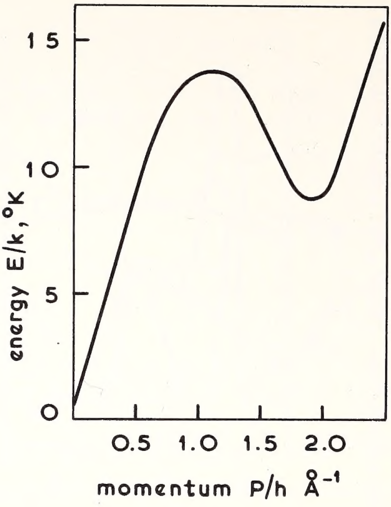

FIGURE 9. Dispersion curve for He II.

2.3. Elastic Scattering by Correlated Scattering Centers [31, 32]

The formulation of elastic scattering of various probes by correlated scattering centers is essentially the same. We follow the geometry shown in figure 10. The scattering wave function of the lth scattering center has the form

$$\psi_l=\frac{1}{R}f_l(\theta)\, e^{ikR}e^{ik(\mathbf{s}_0-\mathbf{s}_1)\cdot\mathbf{r}_l} \tag{32}$$

$\mathbf{s}_0$ and $\mathbf{s}_1$ being the direction of the incident and scattering wave, and r_l its position. If we let

$$\mathbf{q}=k(\mathbf{s}_0-\mathbf{s}_1) \text{ then } |\mathbf{q}|=2k \sin\frac{1}{2}\theta, \tag{33}$$

θ being the scattering angle. The total scattered wave function from all scatterers is

$$\psi=\Sigma\psi_l \tag{34}$$

and the scattered intensity at an angle θ, a distance R from the scatterer, is

$$I(\theta)=R^2|\psi|^2{}_{Av} \tag{35}$$

where the average is to be taken over the distribution function of the location of the scattering centers. Then

$$I(\Theta)=\Big<\sum_{l,\,m}f_l(\theta)f_m^*(\theta)e^{i\mathbf{q}\cdot(\mathbf{r}_l-\mathbf{r}_m)}\Big>_{Av} \tag{36}$$

In the derivation of this formula, it is assumed that no multiple scattering occurs; i.e., that each scatter is acted on by the incident

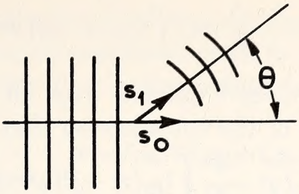

FIGURE 10. Scattering geometry s_0 and s_1 are respectively unit vectors in the direction of the incident and scattered beams. θ=scattered angle.

beam as though no other scatters are present. Hence, only interference effects are important.

There are a number of important special cases of (36) which we discuss individually.

2.4. Scattering by an Assembly of Identical Scatterers [33]

This case is important in the use of x-ray scattering for the investigation of the pair distribution function of liquids and crystal structure of monatomic lattices. Then

$$f_l(\theta)f_m^*(\theta)=|f(\theta)|^2 \text{ independently of } l \text{ and } m \tag{37}$$

and

$$I(\theta)=|f(\theta)|^2\Big\langle N+\sum_{l\neq m} \exp i\mathbf{q}\cdot(\mathbf{r}_l-\mathbf{r}_m)\Big\rangle \tag{38}$$

If we let $\rho_2(r_l,r_m)\, dr_l dr_m$ be the probability of finding one scatterer in dr_l and another in dr_m, the average of the double sum in (38) is equal to

$$\int_V d^3r_1 \int_V d^3r_2\, \rho_2(\mathbf{r}_1, \mathbf{r}_2) \exp [i\mathbf{q}\cdot(\mathbf{r}_1-\mathbf{r}_2)]. \tag{39}$$

Since the pair distribution function can be written (ρ_1 is number density, N/V)

$$N/V^2+[\rho_2(r_1,r_2)-\rho_1^2], \tag{40}$$

so that

$$I(\theta)=N|f(\theta)|^2[1+I_1+I_2] \tag{41}$$

where

$$I_1=\frac{N}{V^2}\int_V\int d^3r_1\, d^3r_2 \exp [ik(\mathbf{s}_0-\mathbf{s}_1)\cdot(\mathbf{r}_1-\mathbf{r}_2)] \tag{42}$$

depends on the geometry of the container of scatterers and

$$I_2=\frac{1}{N}\iint d^3r_1 d^3r_2[\rho_2(\mathbf{r}_1, \mathbf{r}_2)-\rho_1^2] \exp i\mathbf{q}\cdot(\mathbf{r}_1-\mathbf{r}_2) \tag{43}$$

In the case of spherically symmetrical scatterers, ρ_2 is a function only of $r=|(r_1-r_2)|$ and, as $r\rightarrow\infty$, $\rho_2\rightarrow\rho_1^2$. Hence we can let $|(r_1-r_2)|\equiv r$ be the first variable of integration and write (43)

$$I_2=\frac{1}{N}\int_v d^3r_2\int[\rho_2(r)-\rho_1^2]\,e^{i\mathbf{q}\cdot\mathbf{r}}d^3r \tag{44}$$

where the integration over r extends over all space. The r_2 integration yields the volume of the container so that

$$I_2(q)=\frac{V}{N}\int[\rho_2(r)-\rho_1^2]\,e^{i\mathbf{q}\cdot\mathbf{r}}d^3r$$

$$=\rho_1\int G(r)e^{i\mathbf{q}\cdot\mathbf{r}}d^3r \tag{45}$$

where $G(r)$ is the radial distribution function defined by

$$G(r)\equiv-1+\rho_1^{-2}\rho_2(r). \tag{46}$$

The angle integration in (19) can be performed immediately since $G(r)$ depends only on r. Let γ be the angle between $(\mathbf{s}_0-\mathbf{s}_1)$ and $\mathbf{r}$, then

$$(\mathbf{s}_0-\mathbf{s}_1)\cdot\mathbf{r}=2r\sin\frac{1}{2}\theta\cos\gamma \tag{47}$$

(since $(\mathbf{s}_0-\mathbf{s}_1)=2\sin\frac{1}{2}\theta$). Since $d^3r=4\pi r^2\sin\gamma\, d\gamma\, dr$, the γ integration yields

$$I_2(q)=4\pi\rho_1\int_0^\infty G\,(r)\,\frac{\sin 2rq}{2rq}\,r^2dr. \tag{48}$$

If the scattering function $I_2(q)$ can be measured experimentally, eq (47) can be inverted to yield the radial distribution function $G(r)$. This has been done for a number of monatomic liquids by the analysis of x-ray scattering data. A review of this subject has been published by Gingrich [31]. The radial distribution functions of liquid argon thus determined are plotted in figure 11.

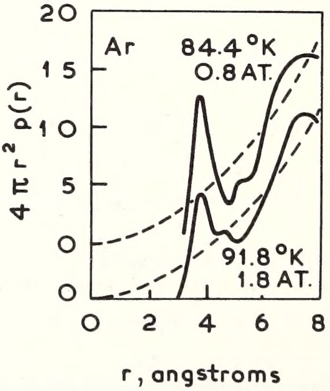

FIGURE 11. Radial distribution function of argon as obtained from x-ray scattering data.

While the pair distribution function can also be used in a discussion of periodically distributed scatterers such as crystals, it is simpler to return to (36) and (38). The lattice points $\mathbf{r}_l$ at which scatterers are located is

$$\mathbf{r}_l = l_1\mathbf{a}_1 + l_2\mathbf{a}_2 + l_3\mathbf{a}_3 \tag{49}$$

where $\mathbf{a}_1$, $\mathbf{a}_2$, and $\mathbf{a}_3$ are the primative vectors of a unit cell and l_1, l_2, and l_3 run through the integers 1, 2, . . ., N. Then the sum $\Sigma\psi_l$ in (34) has the form

$$\begin{aligned}\sum\psi_l &= R^{-1}f(\Theta)e^{ikR}\prod_{j=1}^{3}\sum_{l_j=1}^{N} e^{ik\cdot(\mathbf{s}_0-\mathbf{s}_1)\cdot\mathbf{a}_j l_j}\\ &= R^{-1}f(\Theta)e^{ikR}\prod_{j=1}^{3}\frac{e^{ik(\mathbf{s}_0-\mathbf{s}_1)\cdot\mathbf{a}_j}\{1-\exp iNk(\mathbf{s}_0-\mathbf{s}_1)\cdot\mathbf{a}_j\}}{\{1-\exp ik(\mathbf{s}_0-\mathbf{s}_1)\cdot\mathbf{a}_j\}}\end{aligned} \tag{50}$$

so that

$$I(\Theta) = \left|\sum\psi_l\right|^2 = N^6\frac{f(\Theta)^2}{R^2}\prod_{j=1}^{3}\frac{\sin^2\{1/2k(\mathbf{s}_0-\mathbf{s}_1)\cdot\mathbf{a}_j N\}}{N^2\sin^2\{1/2k(\mathbf{s}_0-\mathbf{s}_1)\cdot\mathbf{a}_j\}} \tag{51}$$

The averaging operation over positions in (35) is not included here because it is assumed that the scattering points are fixed. In real crystals there are small vibrations about the lattice points defined by (49), each scatterer having a Gaussian distribution about the lattice points, the dispersion being small at low temperatures and large at high temperatures. However, we neglect this effect now.

As $N\to\infty$ we find that

$$L(A) \equiv \frac{\sin^2 1/2NA}{N^2\sin^2 1/2A} = \begin{cases}1 \text{ if } A = 2\pi m & m = 0, \pm 1, \pm 2, \ldots\\ 0 \text{ otherwise}\end{cases} \tag{52}$$

Hence, in this limit the product of sine functions in (25) has the value

$$\begin{cases}1 \text{ if } k(\mathbf{s}-\mathbf{s}_1)\cdot(\mathbf{a}_1, \mathbf{a}_2, \mathbf{a}_3) = 2\pi(m_1, m_2, m_3)\\ 0 \text{ otherwise}\end{cases} \tag{53}$$

Hence, $I(\theta)$ is proportional to N^6 if the three eq (27) are satisfied and of lower order in N otherwise. Then if $N\sim 10^7$, the intensity is much greater at points at which (53) is satisfied. The lattice characterized by (49) has a reciprocal lattice defined by the points

$$\mathbf{r}^*(m_1, m_2, m_3) = m_1\mathbf{a}_1^* + m_2\mathbf{a}_2^* + m_3\mathbf{a}_3^* \qquad m_j = 0, \pm 1, \pm 2, \ldots \tag{54}$$

where the $\mathbf{a}_j^*$ satisfy

$$\mathbf{a}_j^*\cdot\mathbf{a}_k = \delta_{jk} \qquad j, k = 1, 2, 3. \tag{55}$$

It is clear that if a beam scattered from a periodic lattice impinges on a photographic plate, the points which correspond to scattering angles defined by

$$k(\mathbf{s}_0-\mathbf{s}_1)/2\pi=m_1\mathbf{a}_1^*+m_2\mathbf{a}_2^*+m_3\mathbf{a}_3^* \tag{56}$$

are identified by black spots on the positive made from the plate. This array of spots is, of course, the well-known Laue pattern for scattering by the periodic array. Note that $k=2\pi/\lambda$, λ being the wave length, and $|\mathbf{a}^*_j|=1/|\mathbf{a}_j|$ where $|\mathbf{a}_j|$ is a typical spacing between neighboring lattice points. Hence λ must be of the order of $|a_j|$ if integral values of the m_j can be found so that (56) is satisfied; in order to obtain Laue spots, the wave length of the scattered radiation must be of the same order of magnitude as the interatomic spacing as is the case in the scattering of x rays by crystals.

Real crystals are not composed of static particles but are, as was emphasized in section 1, constantly in thermal motion with each particle vibrating around its equilibrium position. Hence, the position of the lth lattice point should not be expressed as (49) but rather, as

$$\mathbf{r}(l)=l_1\mathbf{a}_1+l_2\mathbf{a}_2+l_3\mathbf{a}_3+\mathbf{u}(l) \tag{57}$$

where $u(l)$ is a normally distributed random component with mean value zero and average square

$$<u^2(l)>=(\hbar/6Nm)\sum_{k,j}[\omega_j(\mathbf{k})]^{-1}\coth\,[1/2\beta\hbar\omega_j(k)] \tag{58}$$

in the case of a monatomic lattice can be determined from the theory of lattice vibrations. As usual $\beta=1/Tk_B$, and $\omega_j(\mathbf{k})$ is the normal mode frequency in branch j which corresponds to the wave vector $\mathbf{k}$. This causes the broadening of a Laue spot and reduces its intensity by the Debye-Waller factor $\exp{-2W}$ where

$$W=8\pi^2<u^2(l)>\lambda^{-2}\sin^2\theta, \tag{59}$$

λ being the wave length of the incident x ray. A measurement of the factor W as a function of the temperature gives information on the temperature variation of the mean square displacement of a lattice point from its equilibrium position.

2.5. X-Ray Scattering by Molecular Crystal [33, 34]

The purpose of crystallographic studies today is to determine the structure of complex molecules from the x-ray diffraction patterns produced by them while they are in a crystalline state. With this in mind, we shall generalize our formulae of section 3 to the case of more than one particle per unit cell.

Let each unit cell contain l-atoms and let $\mathbf{r}(n)$ be the vector which connects the origin of our coordinate system to a local reference point in the nth unit cell. We shall locate the local reference points at equivalent points in the various unit cells and represent the positions of the l-atoms in the nth unit cell by

$$\mathbf{r}(n)+\boldsymbol{\rho}_j \qquad (j=1,2,\ldots l)$$

If f_j is the scattering factor of the jth atom in each cell, the total scattered wave function of our crystals is

$$\psi=\frac{1}{R}\sum_{j=1}^{l}\sum_{n} f_j \exp\left[k\mathbf{s}\cdot(\mathbf{r}(n)+\boldsymbol{\rho}_j)\right] \tag{60a}$$

$$=N^3R^{-1}F(\mathbf{s})L(\mathbf{s}) \tag{60b}$$

where

$$F(\mathbf{s})=\sum_{j=1}^{l} f_j e^{ik\mathbf{s}\cdot\boldsymbol{\rho}_j} \quad\text{and}\quad L(\mathbf{s})=N^{-3}\sum_{n} e^{ik\mathbf{s}\cdot\mathbf{r}(n)} \tag{61}$$

Since as $N\rightarrow\infty$ eq (55) implies

$$|L(\mathbf{s})|^2=\begin{cases}0 \text{ if } \mathbf{s}/\lambda\neq\mathbf{r}^*\\ 1 \text{ if } \mathbf{s}/\lambda=\mathbf{r}^*,\end{cases} \tag{62}$$

$\mathbf{r}^*$ being any lattice point on the reciprocal lattice, and that $|\psi|^2$ vanish unless $\mathbf{s}=\lambda\mathbf{r}^*$. If $\mathbf{h}$ is a given lattice point on the reciprocal lattice, the scattered intensity associated with that point is proportional to

$$R^2|\psi(\lambda\mathbf{r}^*)|^2=N^6|F(\mathbf{h})|^2 \tag{63}$$

where

$$F(\mathbf{h})=\sum_{j=1}^{l} f_j\exp 2\pi i(h_1x_1^j/|\mathbf{a}_1|+h_2x_2^j/|\mathbf{a}_2|+h_3x_3^j/|\mathbf{a}_3|) \tag{64}$$

(x_1^j, x_2^j, x_3^j) being the coordinate of the jth particle in a given unit cell.

It is clear from (60–63) that the geometrical pattern of x-ray spots or lines from a given crystal depends only on the manner in which unit cells are stacked together, while the intensity of the various spots or lines is determined by the detailed molecular structure in a typical unit cell.

The x-ray scattering is due to the electrons in the crystal and the scattering factor of a given atom depends on the electron density in the atom. Hence, the function $F(\mathbf{h})$ should be expressed in terms of an electron density function $\rho(\mathrm{r})$ rather than the point scattering factors f_j. The appropriate generalization of (64) is then

$$F(\mathbf{h})=v\int_0^1 \rho(a\zeta)\exp(2\pi i\mathbf{h}\cdot\boldsymbol{\zeta})d^3\zeta \tag{65}$$

where v is the volume of a unit cell and

$$\zeta_\mu = x_\mu / |a_\mu| \qquad \mu = 1, 2, 3 \tag{66}$$

and $\rho(a\zeta)$ is defined by

$$\rho(\mathbf{r}) \equiv \rho(a_1\zeta_1,\ a_2\zeta_2,\ a_3\zeta_3) \equiv \rho(a\zeta) \tag{67}$$

Then, if (65) is inverted

$$\rho(\mathbf{r}) = v^{-1} \sum_h F(\mathbf{h}) e^{-2\pi i \mathbf{h}\cdot\zeta} \tag{68}$$

Generally the function $F(\mathbf{h})$ is complex so that it can be expressed as

$$F(\mathbf{h}) = |F(\mathbf{h})| \exp i\alpha(\mathbf{h}) \tag{69}$$

It is to be noted from (68) that since the density is real

$$F^*(\mathbf{h}) = F(-\mathbf{h}) \tag{70}$$

and

$$e^{-i\alpha(\mathbf{h})} = e^{i\alpha(-\mathbf{h})} \text{ so that } \alpha(\mathbf{h}) = -\alpha(-\mathbf{h}). \tag{71}$$

Hence

$$\begin{aligned} \rho(\mathbf{r}) &= \frac{1}{2} v^{-1} \sum_h [F(\mathbf{h}) e^{-2\pi i \mathbf{h}\cdot\zeta} + F(-\mathbf{h}) e^{2\pi i \mathbf{h}\cdot\zeta}] \\ &= v^{-1} \sum_h |F(\mathbf{h})| \cos [2\pi \mathbf{h}\cdot\zeta - \alpha(\mathbf{h})]. \end{aligned} \tag{72}$$

Unfortunately scattering intensity measurements as indicated by eq 63 yield only $|F(\mathbf{h})|$ but not the phases $\alpha(\mathbf{h})$ which are necessary in (72) to yield the electron density function $\rho(\mathbf{r})$ and, thus, the structure.

The problem is somewhat simplified in the case of centrosymmetric molecules with

$$\rho(\mathbf{r}) = \rho(-\mathbf{r})$$

for then employing (68)

$$\rho(\mathbf{r}) = \tfrac{1}{2}[\rho(\mathbf{r}) + \rho(-\mathbf{r})]$$

$$= v^{-1} \sum_h F(\mathbf{h}) \cos (2\pi \mathbf{h}\cdot\zeta)$$

$$= v^{-1} \sum_h |F(\mathbf{h})| [\cos \alpha(\mathbf{h}) + i \sin \alpha(\mathbf{h})] \cos (2\pi \mathbf{h}\cdot\zeta) \tag{73}$$

If the cosine in (72) is expanded and the resulting $\rho(r)$ is compared with the above expression, one finds $\sin\alpha(\mathbf{h}) = 0$ so that $\alpha(\mathbf{h}) = 0$ or π and $\cos\alpha(\mathbf{h}) = \pm 1$. Hence, the density function for centrosymmetric structures is of the form

$$\rho(\mathbf{r}) = v^{-1} \sum_h \pm |F(\mathbf{h})| \cos (2\pi \mathbf{h}\cdot\zeta). \tag{74}$$

We can discuss the trials and tribulations of the x-ray crystallographer through an examination of this formula.

Various combinations of the + and − signs must be picked, the sums evaluated and densities plotted at a large number of points in the unit cell. If an incorrect choice of signs is made, $\rho(\mathbf{r})$ usually becomes negative or a ridiculous structure appears. In the era before the invention of the high speed computer, it was very tedious to calculate each three-dimensional Fourier series and it sometimes required months to determine a structure. As with practicers of many professions in which heartbreaking or backbreaking consequences result from poor judgment or luck, a special spirit of companionship and rivalry existed between crystallographers which was not always evident among workers in other branches of physics.

Various technical tricks have been developed to speed up computations. These are discussed in crystallography books. Some are, however, of general interest.

The density auto-correlation function, (generally known in crystallography as the Patterson function)[35]

$$P(\boldsymbol{\delta})=\int_v \rho(\mathbf{r})\rho(\mathbf{r}+\boldsymbol{\delta})d^3r \tag{75}$$

has the property that is becomes a maximum when the vector with components $(\delta_1/a_1,\delta_2/a_2,\delta_3/a_3)$ corresponds to some vector between atoms in the unit cell. Since as we shall see below it depends only on $|F(\mathbf{h})|^2$ or measured intensities, it can be computed directly without any knowledge of phases.

Eq 68 yields

$$P(\boldsymbol{\delta})=v^{-2}\sum_{h,}\sum_{h'}F(\mathbf{h})F(\mathbf{h}')e^{-2\pi i\mathbf{h}\cdot\delta}\int_v e^{-2\pi i(\mathbf{h}+\mathbf{h}')\cdot \mathbf{r}}\,d^3r.$$

The r integral vanishes unless $\mathbf{h}+\mathbf{h}'=0$ in which case it has the value v, the volume of a unit cell. Hence, in view of (44)

$$\begin{aligned}P(\boldsymbol{\delta})&=v^{-1}\Sigma|F(\mathbf{h})|^2\exp(-2\pi i\mathbf{h}\cdot\boldsymbol{\delta})\\&=v^{-1}\Sigma|F(\mathbf{h})|^2\cos(2\pi\mathbf{h}\cdot\boldsymbol{\delta})\end{aligned} \tag{76}$$

since the Patterson function $P(\boldsymbol{\delta})$ is real.

Unfortunately the distribution of distances between atoms which is found from $P(\boldsymbol{\delta})$ does not always determine atomic positions. However, when a heavy atom exists in each unit cell, the Patterson function has very strong peaks at those values of $\boldsymbol{\delta}$ which represent the vector separation between other atoms and the heavy atom. If in (64) $j=1$ represents the $f_1\gg f_j$ for $j>1$ so that terms in $P(\boldsymbol{\delta})$ which are independent of f_1 can be neglected and

$$P(\boldsymbol{\delta})\sim v^{-1}\sum_h\{f_1^2+f_1\sum_j f_j\cos 2\pi\mathbf{h}\cdot(\zeta_1-\zeta_j)\cos 2\pi\mathbf{h}\cdot\boldsymbol{\delta}\} \tag{77}$$

if $\boldsymbol{\delta} \neq \pm(\zeta_1 - \zeta_j)$, there is a strong cancellation that results in the summation over **h** because the products of cosines can be expected to be negative as often as they are positive. On the other hand, when $\boldsymbol{\delta} = \pm(\zeta_1 - \mathbf{h}_j)$, the product of cosines is always positive so $P(\boldsymbol{\delta})$ has peaks for these values of $\boldsymbol{\delta}$ from which the positions of all atoms in the unit cell relative to the heavy atom can be determined.

2.6. Scattering of Electromagnetic Waves by Spacial and Temporal Fluctuations in a Medium

Let us suppose that the wavelength of the radiation to be scattered by a medium is much longer than the average distance between particles making up the medium. Then the medium might be characterized as a continuous one with local fluctuations in density, temperature, etc. It can then be divided into a large number of identical cells of the volume δV which are still small compared with the wavelength, but contain a large number of particles. The quantity $f_l(\theta)$ in eq (36) has the form

$$f_l(\theta) = \alpha_l u(\theta) \tag{78}$$

where the polarizability α_l of the lth cell depends on the deviation of the local dielectric constant $\epsilon(r_l)$ from the mean value ϵ_0

$$\alpha_l = \Delta\epsilon(r_l)\delta V/4\pi, \qquad \Delta\epsilon(r) \equiv [\epsilon(r) - \epsilon_0]/\epsilon_0 \tag{79}$$

and $u(\theta)$ is the angular dependence of Rayleigh scattering with [36]

$$|u(\theta)|^2 = \frac{1}{2} I_0 k^4 (1 + \cos^2\vartheta) \tag{80}$$

for unpolarized light, I_0 being the incident intensity and somewhat different factors appearing for other polarizations of the incident beam.

Then, when the average (36) is converted to an integral by letting $\delta V \rightarrow 0$

$$I(\theta) = \frac{|u(\theta)|^2}{16\pi^2} \iint \langle \Delta\epsilon(r_2)\Delta\epsilon^*(\mathbf{r}_1) \rangle \exp i\mathbf{q} \cdot (\mathbf{r}_2 - \mathbf{r}_1) d^3r_1 d^3r_2. \tag{81}$$

A variation in the dielectric constant can be expressed in terms of variations in the density and temperature through

$$\Delta\epsilon = \left(\frac{\partial\epsilon}{\partial\rho}\right)\Delta\rho + \left(\frac{\partial\epsilon}{\partial T}\right)\Delta T. \tag{82}$$

Since $\Delta\rho$ and ΔT are statistically independent. [37]

$$I(\theta)=\frac{|u(\theta)|^2}{16\pi^2}\left\{\left(\frac{\partial\epsilon}{\partial\rho}\right)^2\iint<\Delta\rho(\mathbf{r}_1)\Delta\rho(\mathbf{r}_2)> \exp i\mathbf{q}\cdot(\mathbf{r}_2-\mathbf{r}_1)d^3r_1d^3r_2\right.$$
$$\left.+\left(\frac{\partial\epsilon}{\partial T}\right)^2\iint<\Delta T(\mathbf{r}_1)\Delta T(\mathbf{r}_2)> \exp i\mathbf{q}\cdot(\mathbf{r}_2-\mathbf{r}_1)d^3r_1d^3r_2\right\}. \tag{83}$$

In the liquid state $|\partial\epsilon/\partial T|<<|\partial\epsilon/\partial\rho|$ so that only the density fluctuation contribution to $I(\theta)$ is important. While our main interest here is in molecular motions in solids some remarks will be made concerning scattering from liquids especially at temperatures near phase transitions where critical opalescence occurs. Similar formulae apply to neutron scattering by magnetic materials near their curie temperature [38].

If we let $\mathbf{r}_2-\mathbf{r}_1=\mathbf{r}$, the first integral in $I(\theta)$ can be written as

$$V\int<\Delta\rho(0)\Delta\rho(\mathbf{r})> \exp i\mathbf{q}\cdot\mathbf{r}\; d^3r \tag{84}$$

since the correlation between two points depends only on the distance between them. The integration with respect to r_1 contributes the volume of the container, V, when the correlation is short ranged. The theory of density fluctuations in fluids which is usually used in scattering calculations is that of Ornstein and Zernike. In their theory one finds [39, 40]

$$<\Delta\rho(0)\Delta\rho(r)>\sim(kT/4\pi r g_1)\exp[-r(g_0/g_1)^{1/2}] \tag{85}$$

as $r\rightarrow\infty$ and

$$<[\Delta\rho(0)]^2>=\begin{cases} kT\rho/g_0 & \text{if } \partial p/\partial\rho\neq 0\\ ckTv^{5/3}g_1 & \text{if } \partial p/\partial\rho=0\end{cases} \tag{86}$$

where

$$g_0=\rho^{-1}\partial p/\partial\rho$$

and g_1 is related to a certain second derivative of the free energy of the fluid, but for our application here it might be considered only as a slowly varying function of the temperature which is to be determined experimentally. The quantity c is a dimensionless constant.

It can be shown that generally the required Fourier transform (84) can be written as

$$V\int\langle\Delta\rho(0)\Delta\rho(\mathbf{r})\rangle \exp i\mathbf{q}\cdot\mathbf{r}\; d^3r=\frac{VkT}{g_0+g_1q^2+O(q^4)} \tag{87}$$

In the Ornstein-Zernike theory all terms of order higher than q^2 are neglected in the denominator. Hence to this approximation, in fluids

$$I(\theta)=\frac{|u(\theta)|^2}{16\pi^2}\left(\frac{\partial\epsilon}{\partial\rho}\right)^2\frac{VkT}{g_0+g_1q^2} \tag{88}$$

The pressure derivative of the index of refraction is generally easier to determine than the density derivative. Hence we write

$$\frac{\partial\epsilon}{\partial\rho}=\left(\frac{\partial\epsilon}{\partial p}\right)\left(\frac{dp}{d\rho}\right)=\rho g_0\frac{\partial\epsilon}{\partial p} \tag{89}$$

and remember that

$$|q|=2k\sin \tfrac{1}{2}\theta.$$

It should also be noted that g_0 is related to the compressibility through

$$g_0=\rho^{-1}\partial p/\partial\rho=1/\kappa\rho^2 \text{ with } \kappa=-v^{-1}\partial v/\partial p \tag{90}$$

where v is the specific volume, $v=1/\rho$.

The manner in which experimental scattering data is usually presented is shown in figure 12 with $1/I(\theta)$ plotted as a function of q^2. The curves should be straight lines according to the OZ theory with

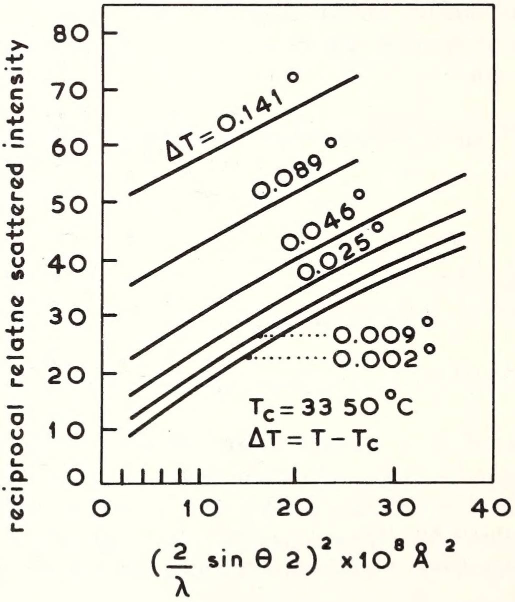

FIGURE 12. Plot of reciprocal relative scattering intensity as a function of $[(2/\lambda)\sin\theta/2]^2$ for mixture 40.6 wt. percent n-Dodecane in β, z′-dichloroethyl ether. See paper by B. Chu in reference 41.

the intercept at the origin at the critical temperature. While there is considerable interest in finding experimental deviations from straight lines, one has to work very hard to do so in a controlled way. A general discussion of these slight deviations by several authors is given in reference [41].

With the availability of intense monochromatic laser sources, light scattering experiments in both liquids and solids can be expected to be of increasing importance. The spectrum as well as the intensity of the scattered light can be observed. It is related to time dependent correlations in condensed material. We now review the ideas behind the relationship between time dependent correlations and the spectrum of scattered light.

2.7. Time Dependent Correlations and the Spectrum of Scattered Light [44–46]

While statistically there is an equilibrium number of fluctuations of a given magnitude in a fluid, as has been discussed earlier, individual fluctuations develope spontaneously and then die away or are propagated away. For example, sound waves of various frequencies and directions are generated at a given temperature T through thermal excitations in fluids and crystals. A given one of these sound waves yields spacially periodic density fluctuations. Light waves at the proper Bragg angle related to the wave length and spacing between planes of density fluctuations are reflected in the same manner that x rays are reflected from crystal planes [42]. Also, a local entropy or temperature fluctuation, when formed, disappears according to Fourier's law or heat flow.

Time dependent fluctuations induce changes in the spectrum of the scattered light. The reflecting planes which give rise to Bragg reflections move either toward or away from the observer. Hence the scattered light suffers a Doppler shift in frequency and has two peaks symmetrically placed on each side of the unscattered frequency. This type of scattering is called Brillouin scattering after the predictor of the effect. Landau and Placzek [43] pointed out that temperature fluctuations are dispersed according to Fourier's law of heat flow and give rise to the frequency broadening of the incident light.

The time dependent fluctuations in an electric field can be discussed in terms of their autocorrelation function. The Rayleigh formula for the scattered electric field at time t, at a point a distance R away from the scattering medium and at an angle θ relative to the direction of the incident wave is

$$E(R, t)=\left(\frac{2\pi}{\lambda}\right)^2 \frac{E_0}{R} \sin\theta \, e^{i(kR-t\omega_0)} \int_v \alpha(r, t) e^{i\mathbf{k}\cdot\mathbf{r}} \, d^3r \qquad (91)$$

Since only the variations from the mean polarizability give rise to scattering in direction $\theta \neq 0$,

$$E(R,\, t)=\left(\frac{2\pi}{\lambda}\right)^2 \frac{E_0}{R} \sin\theta\; e^{i(kR-t\omega_0)}\left(\frac{\delta V}{4\pi}\right)(2\pi)^{3/2}\delta\epsilon(k,\, t) \tag{92}$$

since

$$\delta\alpha(t)=\delta V\delta\epsilon(t)/4\pi \text{ with } \delta\epsilon=(\epsilon-\epsilon_0)/\epsilon_0$$

we let $\delta\epsilon(k,t)$ be the Fourier transform of the variation in the dielectric constant

$$\delta\epsilon(k,\, t)=\frac{1}{(2\pi)^{3/2}}\int \delta\alpha(r,\, t)e^{i\mathbf{k}\cdot\mathbf{r}}\, d^3r.$$

The auto correlation function in the field, neglecting the correlation between different spacial fluctuations is obtained by averaging the product

$$B^*(R,\, t)E(R,\, t+\tau)=\left(\frac{2\pi}{\lambda}\right)^4 \frac{|E_0|^2}{R^2} \sin^2\theta\; e^{-it\omega_0}(\delta V)^2\frac{\pi}{2}\delta\epsilon^*(k,\, t)\delta\epsilon(k,\, t+\tau) \tag{93}$$

In the remainder of this section we will not explicitly include the dependence of $\epsilon(k,t)$ on k but remember that we are always dealing with the kth Fourier component of the dielectric constant.

The spectral analysis of the light scattered can be discussed in terms of that of $E(t)$. However, the Fourier transform of $E(t)$ taken over an infinite time interval does not exist. The harmonic analysis of $E(t)$ is possible if averages are taken over long intervals of duration T where one redefines $E(t)$ so that

$$\mathbf{E}(t)=\begin{cases} 0 \text{ if } |t|>\frac{1}{2}T \\ \text{scattered electric field if } |t|<\frac{1}{2}T. \end{cases} \tag{94}$$

If the Fourier representation of E(t) is

$$E(t)=\int_{-\infty}^{\infty} e^{-i\omega t}S_T(\omega)d\omega \tag{95}$$

then its auto correlation function is (after employing (71) and integrating over t)

$$\begin{aligned} \mathcal{E}_T(\tau)&=\frac{1}{T}\int_{-T/2}^{T/2} \mathbf{E}^*(t)\mathbf{E}(t+\tau)dt \\ &=\int_{-\infty}^{\infty}\int e^{-i\tau\omega'}S_T(\omega)S^*{}_T(\omega')\frac{\sin T(\omega'-\omega)/2}{T(\omega'-\omega)/2}\, d\omega d\omega' \end{aligned} \tag{96}$$

Now let $z=T(\omega'-\omega)$ and employ ω and z as the variables of integration. Then

$$\mathcal{E}_T(\tau)=\frac{2}{T}\iint_{-\infty}^{\infty} e^{-i\tau\omega}e^{2iz\tau/T}S_T(\omega)S_T^*(\omega+2zT^{-1})\,\sin z\,dz\,d\omega/z$$

As $T \rightarrow \infty$ the z integration yields

$$\mathcal{E}_T(\tau)=\int_{-\infty}^{\infty} e^{-i\tau\omega}\lim_{T\to\infty} 2\pi\frac{|S_T(\omega)|^2}{T}\,d\omega \tag{97}$$

This result is consistent with the application of Parseval's Theorem to the determination of

$$<|E(t)|^2>\equiv\frac{1}{T}\int_{-T/2}^{T/2}|\mathbf{E}\,(t)|^2dt=2\pi\int_{-\infty}^{\infty}\frac{|S_T(\omega)|^2}{T}\,d\omega \tag{98}$$

The quantity

$$G(\omega)=2\pi\lim_{T\to\infty} T^{-1}|S_T(\omega)|^2 \tag{99}$$

is just the power spectrum of $\mathbf{E}(t)$. Furthermore, by inverting (97)

$$G(\omega)=\frac{1}{2\pi}\int_{-\infty}^{\infty}\mathcal{E}_T(\tau)\,e^{i\tau\omega}d\tau$$

$$=\frac{1}{2\pi}\int_{-\infty}^{\infty} d\tau<\mathbf{E}^*(t)\mathbf{E}(t+\tau)>_t e^{i\tau\omega} \tag{100}$$

The above formulae are, of course, the standard Wiener-Khinchine formulae.

The power spectrum of the scattered light can then be expressed in terms of the time dependent fluctuations in the dielectric constant through eq (92). Hence

$$G(\omega)=2|\mathbf{E}_0|^2\frac{(\delta V)^2}{r^2}\left(\frac{2\pi}{\lambda}\right)^4\frac{\sin^2\theta}{(2\pi)^3}\int_{-\infty}^{\infty} d\tau<\delta\epsilon^*(t)\delta\epsilon(t+\tau)>e^{i\tau\omega} \tag{101}$$

Actually, in various laser experiments, the spectral density function $G(\omega)$ is not obtained directly but it can be obtained from the experimental arrangement sketched in figure 13. A signal which is the photon current whose magnitude is $|\mathbf{E}(t)|^2$ is picked up on a phototube. The resulting electric current is amplified and sent through a spectrum analyzer which yields:

$$G(\omega)=\frac{1}{2\pi}\int<i(t)i(t+\tau)>_t e^{i\tau\omega}d\tau, \tag{102}$$

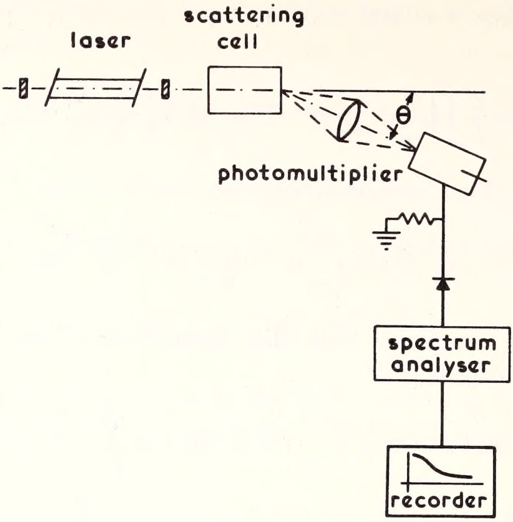

FIGURE 13. Block diagram of "self beating" spectrometer.

$i(t)$ being the electric current which is proportional to $|\mathbf{E}(t)|^2$. Hence the quantity which is Fourier analyzed is

$$<|\mathbf{E}(t+\tau)|^2|\mathbf{E}(t)|^2>$$

However, it can be shown that if the real and imaginary parts of $\mathbf{E}(t)$ are Gaussianly distributed, random variables, then

$$<|\mathbf{E}(t+\tau)|^2|\mathbf{E}(t)|^2>=<|\mathbf{E}(t)|^2>+|<\mathbf{E}(t+\tau)\mathbf{E}^*(t)>|^2 \tag{103}$$

and an experiment which yields the properties of the autocorrelation function of $|\mathbf{E}(t)|^2$ also yields those of $\mathbf{E}(t)$.

The spectral analysis of the scattered electric field depends on the statistical characteristics of the dielectric. Since

$$\delta\epsilon=\left(\frac{\partial\epsilon}{\partial p}\right)\delta p+\left(\frac{\partial\epsilon}{\partial s}\right)\delta s, \tag{104}$$

and since (c_p=specific heat per unit volume)

$$T(\delta s)_p=c_p(\delta T)_p, \tag{105}$$

$$\delta\epsilon=\left(\frac{\partial\epsilon}{\partial s}\right)_p\frac{c_p}{T}(\delta T)_p+\left(\frac{\partial\epsilon}{\partial p}\right)_s(\delta p)_s. \tag{106}$$

Temperature fluctuations decay according to the heat equation

$$\frac{\partial}{\partial t}\delta T(\mathbf{r},t)=\frac{\lambda}{c_p}\nabla^2\delta T(\mathbf{r},t) \tag{107}$$

where λ is the thermal conductivity and c_p is the heat capacity at constant pressure. In k-space

$$\frac{\partial}{\partial t}\delta T(\mathbf{k}, t) = -\frac{\lambda k^2}{c_p}\delta T(\mathbf{k}, t)$$

so that

$$\delta T(\mathbf{k},t) \equiv T_0 e^{-|t|\Gamma(\mathbf{k})} \tag{108}$$

where the life time of a temperature fluctuation is

$$[\Gamma(\mathbf{k})]^{-1} = c_p/\lambda \mathbf{k}^2. \tag{109}$$

Following Brillouin, pressure fluctuations are associated with thermally excited sound waves. These fluctuations modulate the dielectric constant and give rise to Bragg-type scattering. They are damped by viscosity in a fluid system and by thermal conduction in both fluids and crystals. Generally one can express the k component of the pressure fluctuation by

$$\delta p(\mathbf{k},t) = p_0 \exp\{\pm it\Omega(\mathbf{k}) - |t|\Gamma_p(\mathbf{k})\}. \tag{110}$$

The ± corresponds to the two directions that the wave of frequency $\Omega(k)$ can propagate.

Since, in a linear theory, temperature and pressure fluctuations are uncorrelated, the contributions of (108) and (110) to (101) are additive. Then from (110) the pressure fluctuation contribution to (101) is proportional to

$$\int_{-\infty}^{\infty} e^{-|\tau|\Gamma_p(\mathbf{k})} e^{i\tau(\omega \pm \Omega(\mathbf{k}))} d\tau = \frac{1}{\pi} \frac{\Gamma_p(\mathbf{k})}{[\omega \pm \Omega(\mathbf{k})]^2 + \Gamma_p^2(\mathbf{k})} \tag{111}$$

The Lorentzian character of this quantity has been verified experimentally to high precision by G. Benedik and his collaborators [44].

3. Relaxation and Resonance Techniques

3.1. Dielectric Relaxation [47, 48]

In 1913, after completing his work on specific heats and before undertaking his long investigation of the effect of lattice vibrations on scattering of x-rays, Debye attempted to understand the anomalous dispersion of long wavelength radio waves by some liquids. Experimental data had been collected by Drude and others, but no physical basis had been given to the phenomenon.

Debye attributed the anomalous dispersion to permanent dipole moments of the molecules composing the material under investigation. He argued that, while at low frequencies, the molecular dipoles could change their orientation in phase with the periodic variation of the driving field, at high frequencies, the "viscous" character of the fluid prevents the molecules from keeping up with the field. Hence, if the electric field has the periodic form

$$\mathbf{E}=\mathbf{E}_0 \cos \omega t \tag{112}$$

then the polarization lags the driving field. Since the electric polarization, P, in the equation

$$\mathbf{D}=\mathbf{E}+4\pi\mathbf{P} \tag{113}$$

lags the external field, the electric displacement has a component which also lags it. One often assumes that

$$\mathbf{D}=\mathbf{D}_0 \cos (\omega t-\phi)=\mathbf{D}_1 \cos \omega t+\mathbf{D}_2 \sin \omega t \tag{114}$$

where

$$\mathbf{D}_1=\mathbf{D}_0 \cos \phi \text{ and } \mathbf{D}_2=\mathbf{D}_0 \sin \phi. \tag{115}$$

It is generally observed that D_0 is proportional to E_0. Then one can write

$$\mathbf{D}_1=\mathbf{E}_0\epsilon_1(\omega) \text{ and } \mathbf{D}_2=\mathbf{E}_0\epsilon_2(\omega) \tag{116}$$

where the first dielectric constant $\epsilon_1(\omega)$ is associated with the component of the electric displacement which is in phase with the external field and $\epsilon_2(\omega)$ with that 90° out of phase with E. The quantity

$$\tan \phi=\epsilon_2(\omega)/\epsilon_1(\omega) \tag{117}$$

is sometimes used to characterize a material.

The above formulae can be summarized in a compact notation by assuming that the electric field has the form

$$\mathbf{E}=\mathbf{E}_0 e^{-i\omega t} \tag{118}$$

and

$$\mathbf{D}=\mathbf{D}_0 e^{(-i\omega t-\phi)}=\epsilon\mathbf{E} \tag{119}$$

where ϵ is interpreted to be a complex dielectric constant. If one writes it as

$$\epsilon=\epsilon_1+i\epsilon_2 \tag{120}$$

then it is easy to verify that ϵ_1 and ϵ_2 are to be identified with the two dielectric constants. On this basis, ϵ_2 is often called the imaginary part of the dielectric constant.

The quantity $\epsilon_2(\omega)$ is also a measure of the energy absorbed by the sample from the external driving field. It can be shown from a thermodynamic discussion of dielectrics in an alternating electric field that the energy absorbed per cycle is

$$-\frac{1}{4\pi}\int \mathbf{E}\cdot d\mathbf{D} = -\frac{\omega}{8\pi^2}\int_0^{2\pi/\omega} \mathbf{E}\cdot(\partial\mathbf{D}/\partial t)dt$$

$$=\omega \mathbf{E}_0^2\epsilon_2(\omega)/8\pi. \tag{121}$$

Hence an experimental measurement of energy absorption is a measurement of the imaginary component of the dielectric constant. Since the polarization **P** in eq (109) is related to the electric susceptibility χ_e by $\mathbf{P}=\chi_e\mathbf{E}$,

$$\chi_e=(\epsilon-1)/4\pi. \tag{122}$$

The real and imaginary parts of the dielectric constant (and, indeed, of the susceptibility) are not independent, but are related through the Kronig-Kramers relation [49].

In order to employ the formal ideas above in the discussion of molecular motions, one must make a model of these motions. This was first attempted by Debye [47] through a theory of molecular rotation analogous to the Einstein Theory of Brownian Motion. In the case of a fluid, the torque on a given polar molecule (of dipole moment μ) to turn it in the direction of the field is

$$\mathrm{M}=-\mu E\sin\theta. \tag{123}$$

The influence of collisions with other molecules gives rise to a frictional torque which keeps the angular velocity to a constant value with

$$M=\zeta d\theta/dt \tag{124}$$

where ζ is the friction constant. According to Stokes law for the rotation of a sphere of radius a in a fluid

$$\zeta=8\pi\eta a^3, \tag{125}$$

η being the viscosity of the fluid. The mean square random angle due to rotational Brownian motion is in time δt

$$<\theta^2>/4\delta t=kT/\zeta. \tag{126}$$

Debye then made a detailed analysis of the mean moment of a dipole under the influence of a periodic electric field of field intensity $\mathbf{E}=\mathbf{E}_0\exp(-i\omega t)$ and found it to be, at time t

$$<\mathbf{m}>=\frac{\mu^2}{3kT}\frac{\mathbf{E}}{(1-i\omega\tau)}=\frac{\mu^2e^{-i\omega t}\mathbf{E}_0}{3kT(1-i\omega\tau)} \tag{127}$$

where the relaxation time τ is

$$\tau=\zeta/2kT \tag{128}$$

On this basis, the polarization **P** in equation (113) is proportional to $(1-i\omega\tau)^{-1}$. The same mechanism implies that if a constant field E_0 is suddenly switched off at time $t=0$, then the mean moment after time t would be

$$<\mathbf{m}>=\frac{\mu^2}{3kT}\mathbf{E}_0 \exp(-t/\tau). \qquad (129)$$

All of these ideas can be summarized through the introduction of the transfer function $\alpha(t)$ which relates the electric displacement at time t to the electric field at times earlier so that

$$\mathbf{D}(t)=\epsilon_\infty\mathbf{E}(t)+\int_0^t \mathbf{E}(t')\alpha(t-t')dt' \qquad (130)$$

where ϵ_∞ is the infinite frequency dielectric constant. Alternatively,

$$\mathbf{D}(t)=\epsilon_\infty\mathbf{E}(t)+\int_0^t \mathbf{E}(t-t'')\alpha(t'')dt'' \qquad (131)$$

If the external field is periodic

$$\mathbf{D}(t)=\mathbf{E}_0\epsilon_\infty e^{-i\omega t}+\mathbf{E}_0 e^{-i\omega t}\int_0^t \alpha(t'')\exp(i\omega t'')dt''. \qquad (132)$$

When the memory function $\alpha(t)$ dies out in a finite time as it would if it had the form

$$\alpha(t)=\alpha_0 \exp(-t/\tau) \qquad (133)$$

then the upper limit on (132) could be made infinite so that

$$\mathbf{D}(t)=\mathbf{E}_0 e^{i\omega t}\{\epsilon_\infty+\int_0^\infty \alpha(t)\exp(i\omega t)dt\}. \qquad (134)$$

When $\alpha(t)$ has the decaying experimental form (133)

$$\mathbf{D}(t)=\mathbf{E}_0 e^{-i\omega t}\{\epsilon_\infty+\tau\alpha_0(1-i\omega\tau)^{-1}\} \qquad (135)$$

which is the form one would obtain from (112) and (127). The static dielectric constant ϵ_s would follow from the special choice $\omega=0$. Hence,

$$\alpha_0=(\epsilon_s-\epsilon_\infty)/\tau \qquad (136)$$

and from (119), (120), and (135),

$$\epsilon_1(\omega)-\epsilon_\infty=(\epsilon_s-\epsilon_\infty)/(1+\tau^2\omega^2) \qquad (137a)$$

$$\epsilon_2(\omega)=\tau\omega(\epsilon_s-\epsilon_\infty)/(1+\omega^2\tau^2) \qquad (137b)$$

and

$$\tan\phi=\epsilon_2/\epsilon_1=(\epsilon_s-\epsilon_\infty)\omega\tau/(\epsilon_s+\epsilon_\infty\omega^2\tau^2). \qquad (138)$$

The energy absorption is a maximum at the peak of the function $\epsilon_2(\omega)$, i.e., at the frequency for which $\omega\tau = 1$. This then gives a measurement of ϵ_2 which can then be expressed in terms of the molecular parameters which characterize the relaxation process.

In many materials, all dipoles are not exposed to the same internal electric fields. Hence there may be a number, or indeed a spectrum of relaxation times. The experimental data would then not be consistent with (137a) and (137b). Generally one can introduce a distribution function for relaxation times such that

$$\alpha(t) = \int_0^\infty e^{-t/\tau} y(\tau) d\tau/\tau. \tag{139}$$

When substituted into (134), the t integration can be performed to yield

$$\epsilon_1(\omega) - \epsilon_\infty = \int_0^\infty \frac{y(\tau)d\tau}{1+\omega^2\tau^2} \tag{140a}$$

$$\epsilon_2(\omega) = \int_0^\infty \frac{\omega\tau y(\tau)d\tau}{1+\omega^2\tau^2} \tag{140b}$$

(140) is equivalent to (137) if

$$y(\tau) = (\epsilon_s - \epsilon_\infty)\delta(\tau - \tau') \tag{141}$$

and after integration, the prime is removed from the τ'.

A number of detailed molecular models have been made and many materials investigated through the above ideas [50]. Dielectric relaxation methods have been especially helpful in studying molecular mechanisms in polymers [51].

3.2. Nuclear Magnetic Resonance

While experiments of polar molecules were already fashionable in the late 1920s and early 1930s, magnetic resonance techniques were not developed until much later, mainly since paramagnetic susceptibilities are a factor 10^3–10^4 smaller than electric susceptibilities. The theory was started in a paper by Waller [52] in 1932 and followed up by Kronig, Casimer, Van Vleck, Du Pre, Broer, Debye and others [53].

G. J. Gorter tried unsuccessfully to detect lattice heating resulting from nuclear magnetic resonance absorption. His materials had too long a relaxation time for nuclear spins to achieve equilibrium with the lattice. However he contributed many ideas to the development of the subject. Zavoisky [54] measured a barely resolved electron magnetic resonance absorption in manganese and cupric ions in crystals in 1945. Cummerow and Halliday [55] soon afterward observed a well-resolved resonance in $MnSO_4 \cdot 4H_2O$. Proton resonances were found by Purcell, Pound, and Torrey [56] and Bloch, Hansen and Packard [57]. The field quickly blossomed into one of the most active branches of physics. A short survey of the entire field has recently been published by G. Pake [58] and excellent textbooks have been written by C. P. Slichter [59] and Abragam [60]. We will outline some of the main ideas behind the field and discuss their application to the investigation of certain phase transitions in solids.

Resonance techniques are applied to particles such as electrons and nuclei which, in a given state, have a total magnetic moment $\boldsymbol{\mu}$ and an angular momentum $\mathbf{J}$. These two vectors can be taken as parallel and related by

$$\boldsymbol{\mu}=\gamma\mathbf{J}, \tag{142}$$

γ being the gyromagnetic ratio. $\mathbf{J}$ can be expressed in terms of a dimensionless angular momentum $\mathbf{I}$ by

$$\mathbf{J}=h\mathbf{I} \tag{143}$$

It is well known that if a particle with a magnetic moment is placed in a magnetic field H, its energy levels are

$$E=-\gamma\hbar Hm \text{ with } m=I,I-1. \; . \; . \; .,-I \tag{144}$$

The separation between successive levels is the constant γhH. Electromagnetic radiation of frequency

$$\hbar\omega=\gamma\hbar^{H}=\Delta E \text{ or } \omega=\gamma H \tag{145}$$

would induce transitions in a sample composed of the particles described above. A schematic experimental arrangement is sketched in figure 13.

The sample is placed in a static magnetic field in the z direction, H_0. Then an r–f magnetic field H_1 of frequency ω is applied perpendicular to H_0. The r–f power absorbed by the sample can be deduced by measuring the Q of the coil. The power absorbed will be greatest at the resonance frequency.

Since the formula for the resonance frequency does not depend on $\hbar$, one would expect to be able to make a classical analysis of the situation. This, indeed, is very useful in the description of the relaxation processes which occur when the magnetic particle is not isolated as, for example, through the spin lattice interaction when the particle is imbedded in a crystal. The classical analysis of this situation was first made by F. Bloch [61].

The equation of motion for the magnetic moment under the influence of a torque provided by a magnetic field **H** is

$$d\mathbf{J}/dt=\boldsymbol{\mu}\times\mathbf{H} \tag{146}$$

or from (142)

$$\frac{d\boldsymbol{\mu}}{dt}=\boldsymbol{\mu}\times\gamma\mathbf{H} \tag{147}$$

If $H=H_0$, a static field in the z direction, $\boldsymbol{\mu}$ rotates at an angular velocity $\boldsymbol{\Omega}=-\gamma\mathbf{k}H_0$ (**k** is the unit vector in the z direction). The angular frequency

$$\omega_0=\gamma H \tag{148}$$

is the Larmor frequency and is identical with the resonance frequency (145). A detailed discussion of the solution of (147) has been given in reference [56] for the case when H_0 has two parts consisting of a static field H_0 in the z direction and an alternating field normal to it with

$$H_x=H_1\cos\omega t;\ H_y=H_1\sin\omega t \tag{149}$$

The bulk magnetization of a crystalline sample is $\mathbf{M}=\Sigma\boldsymbol{\mu}_i$. At thermal equilibrium in the absence of an external field, one would expect $\mathbf{M}=0$. However, in the presence of a static magnetic field $\mathbf{H}_0$ in the z direction and a small r–f field normal to it, a non-vanishing moment **M** develops. Its time variation is in many situations well described by Bloch's phenomenological equations (with $\mathbf{M}_0=\chi_0\mathbf{H}_0$, χ_0 being the static magnetic susceptibility)

$$dM_z/dt=\gamma(\mathbf{M}\times\mathbf{H})_z+(M_0-M_z)/T_1 \tag{150a}$$

$$dM_x/dt=\gamma(\mathbf{M}\times\mathbf{H})_x-M_x/T_2 \tag{150b}$$

$$dM_y/dt=\gamma(\mathbf{M}\times\mathbf{H})_y-M_y/T_2 \tag{150c}$$

which involve two relaxation times. The time constant T_1 is the rate at which an assembly of spins in a magnetic field come to equilibrium with a reservoir of phonons as the magnetic moments take on their Boltzmann distribution among their various Zeeman states (144). A possible mechanism for T_2 is somewhat analogous to the relaxation phenomenon involving electric dipoles as discussed in Section 3.1. Each spin is influenced by local fields due to neighboring spins at slightly different locations so that if, initially, all spins are precessing in the same manner, these fluctuations would soon take them out of plane and eventually the system would be randomized. Generally, T_2 is less than T_1.

One would expect the Bloch model to yield resonance functions for the magnetic susceptibility which are analogous to (137). When the Bloch equations are solved relative to the driven magnetic fields

$$H_x(t) = H_{x_0} \exp(-i\omega t) \quad , \quad H_z = H_0 = \text{constant} \tag{151}$$

in the regime H_x small, the magnetic susceptibility has the form

$$\chi = \chi' + i\chi'' \tag{152}$$

with

$$\chi' = \frac{1}{2}\chi_0\omega_0 T_2(\omega_0 - \omega) T_2/[1 + (\omega - \omega_0)^2 T_2] \tag{153a}$$

$$\chi'' = \frac{1}{2}\chi_0\omega_0 T_2/[1 + (\omega - \omega_0)^2 T_2]. \tag{153b}$$

The Larmor frequency $\omega_0 = H_0$ did not appear in the Debye theory because in the polar molecule case there was no constant aligning field and no Larmor precession about it. With the aid of (153b) experimental data on χ'' could then yield information about molecular motions in solids provided that one had models that could be used for a calculation of χ''.

The average power absorbed per cycle in a sample of magnetic material in a periodic field H_{pert} is the direct analogue of (121) using the imaginary part of the magnetic susceptibility (122) instead of the dielectric constant. In a sample of volume V, it is averaged over one cycle,

$$<\text{P}> = \frac{1}{2}\omega\chi'' H_{x_0}^2 V. \tag{154}$$

This quantity can be calculated directly by standard quantum mechanical time dependent perturbation theory for a given model. The basic time independent Hamiltonian for an assembly of dipoles in a solid can be taken as

$$H = \sum_k \mu_{zk} H_0 + \sum_{j,k} H_{j,k} \tag{155}$$

where $H_{j,k}$ is a sum of dipole-dipole interactions. When an r-f magnetic field in the x direction is switched on, a time dependent perturbing Hamiltonian must be added

$$H_{\text{pert}} = -\sum_k \mu_{x,k} H_{x_0} \cos \omega t = -\mu_x H_{x_0} \cos \omega t, \tag{156}$$

μ_x being the x component of the total moment. The power absorbed in the sample depends on the number of transitions from a set of initial states a of the Hamiltonian to final states b such that $|E_b - E_a| = \hbar\omega$.

From second order perturbation theory, the transition probability is just the time average of the square of the matrix element of the perturbation; i.e., it is proportional to [59,60]

$$H_{x0}^2|(a|\mu_x|b)|^2.$$

The power is also proportional to $\hbar\omega$, the energy absorbed per transition. After one goes through the detailed energy balance calculation and substitutes the results into (154) he finds

$$\chi''(\omega)=\frac{\hbar\omega\pi}{2kTZ}\sum_{E_aE_b}e^{-\beta E_a}|(a|\mu_x|b)|^2[\delta(E_a-E_b-\hbar\omega)+\delta(E_a-E_b+\hbar\omega)] \tag{157}$$

where Z is just the partition function

$$Z=\sum_a \exp(-\beta E_a).$$

The Boltzmann factor $Z^{-1}\exp(-\beta Ea)$ appears in (157) because it is the probability that the state a is occupied initially. The delta function insures that only those transitions are counted for which $|E_a-E_b|=\hbar w$. Then

$$\chi''(\omega)=\frac{\hbar\omega\pi}{2kTZ}\sum{}' e^{-\beta E_a}|(a|\mu_x|b)|^2 \tag{158}$$

where the summation is to be taken over all states a and b such that

$$|E_a-E_b|=\hbar\omega.$$

In order to calculate the susceptibility $\chi''(\omega)$ from (158) we must know the energy levels of our system of interacting spins. This is, of course, a very difficult problem to solve. However, as a first approximation, one might choose the E_a to be the Zeeman energy levels. When they are examined in some detail, it is found that $E_a/kT<<1$ under the conditions of the usual resonance experiments. Hence the factor $\exp-\beta E_a$ can be omitted from (157). On that basis, the line shape is characterized by the function [59,60]

$$f(\omega)=\frac{1}{2}\sum_{a,b}|(a|\mu_x|b)|^2[\delta(E_a-E_b-\hbar\omega)+\delta(E_a-E_b+\hbar\omega)]. \tag{159}$$

This quantity is still difficult to calculate, but van Vleck [62] noticed that various moments of $f(\omega)$, $\int\omega^n f(\omega)\,d\omega$, can be obtained without too much trouble. First consider

$$\int_0^\infty f(\omega)d\omega=\frac{1}{2}\int_{-\infty}^\infty f(\omega)d\omega=\frac{1}{4}\sum_{a,b}|(a|\mu_x|b)|^2\int_{-\infty}^\infty [\delta(E_a-E_b-\hbar\omega) +\delta(E_a-E_b+\hbar\omega)]d\omega. \tag{160}$$

Since there is some frequency such that $E_a - E_b = \hbar\omega$, the summation extends over all a and b. The sum is, however, just the trace of the operator μ_x^2 and

$$\int_0^\infty f(\omega)d\omega = \frac{1}{2}\ \text{trace}\ \mu_x^2 \tag{161}$$

Since the trace is independent of the choice of base wave functions, one can use the Zeeman wave functions to perform the calculations to obtain

$$\int_0^\infty f(\omega)d\omega = \frac{1}{2\hbar}\,\delta^2\hbar^2\frac{I(I+1)}{3}\,N(2I+1)^N. \tag{162}$$

The second moment is proportional to

$$\begin{aligned}\int_0^\infty \omega^2 f(\omega)d\omega &= 1/2\int_{-\infty}^\infty \omega^2 f(\omega)d\omega \\ &= 1/2\sum_{a,b}(E_a - E_b)^2|(a|\mu_x|b)|^2 \\ &= -\frac{1}{2\hbar^3}\,tr[H,\mu_x]^2.\end{aligned} \tag{163}$$

Again the Zeeman wave functions can be used to calculate the trace. It is somewhat more difficult to express the odd moments as traces, but it can still be done. One finds, for example,

$$\int_0^\omega \omega f(\omega)d\omega = \omega_0. \tag{164}$$

A calculation of the trace $[H,\mu_x]^2$ implies that when all particles with magnetic moments are the same,

$$\begin{aligned}<(\omega-\omega_0)^2> &= \left\{\int_0^\infty (\omega-\omega_0)^2 f(\omega)\,d\omega \Big/ \int_0^\infty f(\omega)\,d\omega\right\} \\ &= \frac{3}{4}\gamma^4\hbar^2 I(I+1)\frac{1}{N}\sum_{j,k}(1-3\cos^2\theta_{j,k})^2/r_{j,k}^6.\end{aligned} \tag{165}$$

A similar formula exists when there are several different particles with different magnetic moments in each unit cell. In that case a contribution to the second moment comes from each type of pair interaction. The γ^4 is replaced by $\gamma_A^2\gamma_B^2$, A and B being two species. These formulae can be used to determine the distances between hydrogens in certain organic crystals, a measurement which cannot be made by x-ray analysis.

A very nice investigation of crystals of benzene and deuterated benzene has been made by Andrew and Eades [63]. The magnetic moments of the deuteron and proton differ by a factor of 2 and the γ value of the proton is about 7 times that of the deuteron. On this basis, the resonance widths which are given by the second moments differ appreciably between the undeuterated and partially deuterated crystals. From these differences, the various H–H and C–H distances in the benzene molecule were obtained.

Certain phase transitions in molecular crystals have been studied by NMR techniques [64]. The magnetic field H in the Larmor frequency formula should have two components, the external field H_0 and the local field, due to the existence of other dipoles, H_{loc}.

If the absorption is plotted as a function of the external field at constant frequency the width of the resonance curve depends on several variables, including the local field H_{loc}. At low temperatures in weak fields the magnetic moments of the various magnetic nuclei are oriented at random. Hence a wide variety of local fields might exist for each nucleus, each possible field yielding a different Larmor frequency. This variety is one of the contributors to the width of the resonance curve. Qualitatively the line width is reduced by any process which averages out the local field. The free rotation of the molecules would make the local fields at the various lattice points roughly the same. The rotational frequencies are usually much higher than the resonance frequency. On this basis, one would expect a considerable narrowing of the line width as a crystal passes through transition into a free rotation state. In the case of an order-disorder transition, there may or may not be a narrowing of the line width in passing through a transition. The effect would depend on the flipping frequency in going from one state to another and, possibly, on the molecular orientation in the various state.

In general, it is true that if only a slight or no change occurs in the line width at the transition, an order-disorder transition has taken place. A rapid narrowing of the line width indicates the possibility of a rotational transition, but does not completely rule out the possibility of an order-disorder transition without further investigation.

Experimental evidence indicates that HCl, HBr, HI, H_2S, H_2Se and NH_4Cl undergo order-disorder transitions at the λ-point temperature of the specific heat.

The work of Andrew and Eades [63] mentioned above shows conclusively that benzene molecules enjoy a free rotation at temperatures above the λ-point. The variation in the second moment of $f(\omega)$ as observed, is plotted in figure 14. Andrew and Eades used the appropriate extension of (165) to calculate the second moment in the free rotation made and found the variation from that in the rigid lattice to be exactly the 8.1 G^2 which was observed experimentally.

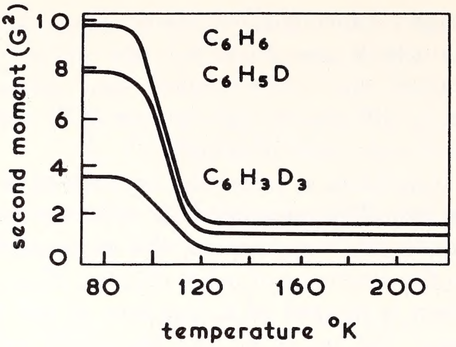

FIGURE 14. Temperature variation of second moment of absorption line for three isotopic species of benzene (Reference 63).

4. Infrared Spectra

One of the most productive schemes for investigating motions in polyatomic molecules in the gas phase has been through their infrared spectrum. While this is sometimes more difficult to interpret in a condensed phase, infrared spectroscopy is still an important technique even in condensed systems. The basic principles of molecular spectroscopy as well as results of researches on an enormous number of molecules are reviewed in Herzberg's various books [65, 66].

Our brief survey will be presented in three stages. We first outline the manner in which the infrared spectrum of diatomic molecules develops. Then the ideas which are needed when more degrees of freedom exist will be added, and finally some aspects of the infrared spectra of solids will be discussed.

4.1. Diatomic Molecules

The energy levels and wave functions of various models of diatomic molecules are easily calculated by methods of elementary quantum mechanics. At the lowest degree of sophistication such a molecule might be considered as a rigid dumbbell with a moment of inertia I. Then in addition to the various translational energy levels which are the same as those of a point particle of the same mass, it has rotational energy levels.

$$E_R = J(J+1)\,\hbar^2/2I;\ J=0,\ 1,\ 2,\ .\ .\ . \tag{166}$$

and wave functions which are surface harmonics. The rigidity of the dumbbell might be relaxed so that its two atoms might then undergo small vibrations about an equilibrium separation distance. Their vibrational energy levels would then be:

$$E_v = (n+\frac{1}{2})\,\hbar\omega;\ n=0,\ 1,\ 2,\ .\ .\ . \tag{167}$$

where the fundamental frequency is related to the reduced mass, μ, and the second derivative, k, of the interatomic potential energy of interaction evaluated at equilibrium separation distance:

$$\omega=(k/\mu)^{1/2} \tag{168}$$

At higher levels of sophistication vibrational-rotational interaction might be included since the moment of inertia of a non rigid molecule varies with its vibrational state and the force constant k would change slightly in higher rotational states. Furthermore anharmonicities are important in higher vibrational states. A detailed analysis of these complications is given in Herzberg's excellent book on Spectra of Diatomic Molecules [65].

These molecules have been investigated through their spectra. The coupling to a driving electromagnetic field which is relevant to the optical region of the spectrum is made through the electric dipole moment of the molecule, permanent or induced. The observed molecular spectra is composed of frequencies which are proportional to the energy differences between pairs of levels through which transitions are induced by the driving field. The quantities which tell whether a transition is allowed and which give a measure of the intensity of spectral lines resulting from an allowed transition are the matrix elements of the components of the electric moment, M, of the molecule

$$R_\alpha^{mn}=(n|M_\alpha|m) \tag{169}$$

$\alpha=1,2,3$ represent respectively the x, y and z components of M. Also n and m represent energy levels which normally are available to the molecule in the absence of the driving field. It can be shown by quantum mechanical perturbation theory that the intensity of an emission line which corresponds to the transition $n \rightarrow m$ is

$$I_{em}^{nm} \propto \omega_{nm}^{4}|R^{nm}|^2 \tag{170a}$$

while that of an absorption line is

$$I_{ab}^{nm} \propto \omega_{nm}|R^{nm}|^2 \tag{170b}$$

Let us suppose that the dipole moment can be expressed as

$$M_\alpha=M^{(0)}+u_\alpha M_\alpha{}^{(1)} \tag{171}$$

A permanent moment, $M^{(0)}$, exists when the two atoms comprising the diatomic molecules are different because of the difference in charge distribution in the two atoms. Symmetry forces $M^{(0)}$ to be zero when the two atoms are identical. Here u_α is the α component of the separation distance.

In the rigid dumbbell model $M^{(1)}=0$ and the x, y, and z components of $M^{(0)}$ are the magnitude of the permanent dipole moment multiplied by the appropriate angle dependent function which takes the projection of the dipole moment vector in the x, y, or z direction. When these products are substituted into (169) and the n and m of (169) represent rotational states J and J' the only nonvanishing matrix elements of (169) are those with $J-J'=\pm 1$. The difference between the energy in the higher and next lower rotational states (J and $J-1$) is

$$\Delta E=\hbar^2(J+1)/I \qquad (172)$$

so that the rotational spectrum consists of a sequence of regularly spaced lines with a separation of $\hbar^2/I$ between neighbors. These are generally in the far infrared region.

The selection rules for the vibrational spectrum are obtained by substituting (171) into (169) and interpreting n and m to be vibrational states. The appropriate wave functions are the products of a Gaussian factor and Hermite polynomials. From their orthogonality properties a constant dipole moment, $M^{(0)}$, contributes nothing to R_α^{mn} when $m\neq n$.

In a linear molecule there is only one displacement component in the induced dipole moment (the second term in 171). We let x be the deviation of the separation distance from its equilibrium value. The only nonvanishing matrix elements of x correspond to $n=m\pm 1$. Hence only vibrational transitions from a given level to its closest neighboring levels are possible. Since vibrational levels are equally spaced, ΔE is the same for all possible transitions which lead to emission and for all transitions resulting from absorption. Therefore there is a single line in the vibration spectrum for the simple harmonic model with a linear electric moment function (171). It is generally in the near infrared spectrum. There is an isotopic shift which can be estimated by noting the change in reduced mass as given by (168).

The vibrational model can be made more sophisticated in two ways. First by adding cubic, quartic, etc., terms to the harmonic interaction potential, and second by adding quadratic, cubic etc., terms to the induced dipole moment contribution to (171). Both of these changes make transitions $|n-m|=2, 3, \ldots$ possible as well as $n=m\pm 1$. However, the intensity of the associated lines decreases rapidly with increasing $|n-m|$.

The rotation spectrum yields information about the moment of inertia and internuclear distances. The vibration spectrum gives force constants and other properties of the interaction potential.

The Raman spectra is the change in the spectra of light scattered by molecules. As was discussed in section 2, Rayleigh scattering depends on the polarization of the scatterer, $\mathbf{P}=\alpha\mathbf{F}$, α being the polarizability and $\mathbf{F}$ the electromagnetic field vector of the incident wave. In the quantum theory of light scattering one must calculate the matrix element of P

$$(n|\mathbf{P}|m)=\int\psi_n^*\alpha\mathbf{F}\psi_m\mathrm{dr},$$

which, in the case of a periodic driving force $\mathbf{F}=\mathbf{F}_0\cos\omega_0t$ of frequency ω_0 can be written as

$$(n|\mathbf{P}|m)=\mathbf{F}_0\cos\omega_0t\int\psi_n^*\alpha\psi_m\ \mathrm{dr}.$$

The time dependent factors in ψ_n^* and ψ_m are respectively $\exp(iE_nt/\hbar)$ and $\exp(-iE_mt/\hbar)$ so that (the φ's being spacial dependent part of wave functions)

$$(n|\mathbf{P}|m)=\frac{1}{2}\mathbf{F}_0\{\exp it(\omega_0-[E_m-E_n]/\hbar)+\exp-it(\omega_0+[E_m-E_n]/\hbar)\}\int\varphi_n^*\alpha\varphi_m\mathrm{dr}.$$

If α is not a constant but depends on either angle or separation distance, then the scattered light is composed of light of the incident frequence ω_0 as well as the Raman frequencies.

$$\omega_0\pm(E_m-E_n)/\hbar \tag{173}$$

for the (n, m) pairs which correspond to non-vanishing matrix elements. For reasonable models of the polarizability function α it can be shown that the selection rules for rotational Raman lines are $\Delta J=\pm 2$, ± 4, etc., with the intensity diminishing rapidly with increasing $|\Delta J|$. The main vibrational Raman lines correspond to $\Delta n=\pm 1$. It should be emphasized that by the proper choice of ω_0, Raman lines can be put in various regions of the spectrum.

4.2. Polyatomic Molecules [66, 69]

The rotational energy levels of molecules composed of more than two atoms differ somewhat from those of diatomic molecules since such molecules generally have three non-vanishing moments of inertia rather than one. A simple formula exists for the energy levels in the case of symmetrical "top" molecules; i.e., those such that $I_z=I_A$, and $I_x = I_y = I_B$. It was shown many years ago by Reiche and Radamacher [67] that

$$E = \frac{1}{2}\hbar^2[J(J+1)/I_A + \Omega^2(1/I_B + 1/I_A)]$$

$$\Omega = 0, \ \pm 1, \ \pm 2, \ . \ . \ . \quad \text{and } J = |\Omega|, |\Omega| + 1, \ . \ . \ .$$

There is actually a very small I_B in diatomic molecules because the constituent atoms are not points but have an extended electron cloud which is sufficient to give them a small I_B. Then for a fixed Ω the ΔE's are the same as they would be in the absence of the Ω^2 term. However, in a complete careful analysis of diatomic spectra, bands which correspond to various values of Ω can be picked out.

Molecules without symmetrical tops (i.e., the case $I_x \pm I_y \pm I_z$) do not have a closed formula for the energy levels. Rather comprehensive tables of energy levels and selection rules do exist however [68].

An extra property of sufficiently complicated polyatomic molecules is that an internal free rotation might exist which could be infrared active. There is a considerable literature on the nature of the angular dependent internal potential barriers which must be overcome if some internal part of the molecule is to rotate freely. The molecule CH_3OH has an internal rotation as does C_2H_6. The details of these rotations have been deduced from band spectra.

As the pressure of a gas composed of polyatomic molecules is increased the individual spectral lines of the infrared and Raman spectra become broader and broader due to molecular collisions. In the liquid state the molecules do not generally show a rotational fine structure, H_2 being one of the rare exceptions. In dilute solutions one occasionally does find a rotational fine structure.

In solids rotational degrees of freedom are generally repressed and are replaced by librations or vibrations about preferred axes. Often the best way to investigate the vibrational states of a polyatomic molecule is through the spectra in its solid state at very low temperatures. Since there is no rotation, any effect of rotations on vibrations in the gaseous state has disappeared as well as effects of anharmonicity. Hence the vibrational lines become much sharper.

If an internal free rotation develops at a phase transition it can be observed by the appearance of rotational bands. The negative case of the ammonium halides was mentioned earlier. The absence of the rotational bands both below and above the phase transition is evidence that the transition is an order-disorder one.

The vibrational spectra of a polyatomic molecule is deduced by making a normal mode analysis of the small vibrations which the molecule might undergo. A model for a given molecule is given in terms of a set of masses and force constants which then appear as elements in the characteristic determinant whose roots yield the normal mode frequencies. There are two difficulties in this approach. First, when the molecule becomes large the characteristic determinant becomes large and unwieldy. When symmetries exist in the molecule, group theoretical methods are very useful in factoring the determinant into several smaller ones. Second, one does not know the various force constants a priori.

In simple symmetric molecules such as C_2H_2, SO_2, or CH_4 there are not many force constants and the small vibration analysis can be done easily with them as parameters. A pattern becomes clear so that with only very rough estimates of the force constants a correspondence of observed spectral lines with normal modes can be made. Then the experimental data can be used to obtain precise values for the force constants. Checks can be made or more information gained when required by observing shifts in the spectra when various isotopic substitutions are made. After a number of small molecules are well analyzed one can proceed to slightly more complicated ones, using some of the established force constants where similar interactions exist in the complicated case. With these and other tricks quite a collection of information on motions of rather complicated molecules has been established.

The vibrations of diatomic and polyatomic molecules generally change very little in going from the vapor to the liquid to the solid state. When slight shifts occur they can sometimes be used to discuss the interaction between molecules in the condensed phase. Most changes in fundamental frequencies are less than 5 percent and the magnitude of the changes diminish with increasing temperature. Certain qualitative differences may also appear. For example degenerate modes which correspond to the same frequency may be split due to crystal fields and transitions which were forbidden might be allowed through the intermolecular interaction.

Since most solids are not very transparent, experiments can only be performed when very thin specimens can be made. There are a number of complicated molecules of biological interest which can be prepared only in minute quantities as a powder. Their absorption spectrum can now be investigated by suspending them in a rather transparent material such as Nujol paste. Whatever the method used for sample preparation of biological materials, great care must be taken. A discussion of techniques and precautions are given in reference [70].

Lists of frequencies of various bonds resulting from motions of important fragments and groups in organic molecules have been assembled [71]. Bonds in complicated molecules can then be identified from such compilations even when detailed molecular structures are not known or when the molecule is so complex that the mathematical analysis of its vibrations become unwieldy.

Protein molecules sometimes exist in several states, one being biologically active and the other not. Spectroscopic methods might be used as a tool to investigate the changes in structure or molecular motions which are responsible for the difference in the activity. The DNA molecule in solution changes from a double helix structure to a random coil structure in which the hydrogen bonds which hold the two strands of the helix together are broken. A critical temperature range of a few degrees exists in which this transition occurs with the double helix structure being the low temperature form and the random coil the high temperature form. The transition is generally followed by observing the change in magnitude of an absorption peak at 2600 Å. The stacking of various base groups in the ordered double helix structure produces a depression in the absorption. With the breaking of hydrogen bonds, the absorption at 2600 Å increases to higher values in the disordered denatured state [72].

4.3. More About Crystal Lattices [73–76]

The remarks made above for molecular crystals are not valid for ionic crystals such as NaCl. In the cases discussed above the high frequency internal vibrations are almost uncoupled from the low frequency lattice vibrations. In the ionic crystals one effectively has a giant molecule with all close neighbor interactions being of the same order of magnitude.

In optical experiments on these materials, one generally uses a very thin slab of material and measures the intensities of the incident, reflected and transmitted beams. Through energy conservation

$$I_0 = I_R + I_T + I_A$$

I_A being the absorbed intensity. In terms of the reflectivity $R = I_R/I_0$, transmitivity T, and absortivity, A,

$$1 = R + T + A$$

so that measurements in R and T yield information about A.

The optical properties of the sample are directly related to the frequency dependent complex dielectric constant discussed in section 3.1. This quantity is in turn connected to atomic and molecular motions in the material of interest. The various formal expressions of section 3.1 are applicable to this problem.

The optical spectroscopy of crystals is concerned with driving wavelengths much longer than the lattice spacings so that an external driving field of the form

$$E = E_0 \exp i(2\pi \mathbf{k} \cdot \mathbf{r} - \omega t) \tag{174}$$

is considered in the long wave length limit k=0 and no spacial dispersion is included in the theory. Hence the only part of the lattice dispersion curves (see figure 7) which is relevant to this technique is the k=0 asymptote of the optical branch of lattice vibrations.

In the simplest theory of the dielectric constant of an ionic crystal one assumes that the lattice is composed of springs and point nonpolarizable masses. Then in an electric field the positive and negative ions separate, the restoring force of each type of ion being proportional to an effective mass of that type. The longitudinal and transversal vibrations are assumed to be independent of each other for waves traveling in symmetry directions in cubic crystals. One then writes Newton's equation of motion for a typical positive ion (in a two component lattice such as NaCl) in an effective electric field which is the sum of the external driving field and the local field due to all other ions. A similar equation is written for the negative ions and the difference between the two accelerations are taken to obtain the equations for the transverse optical vibrations

$$m\ddot{u}_T+m\gamma_t\dot{u}_T+m\omega_0^2u_T=e^*E_{T\mathrm{eff}} \tag{175}$$

where $u_T=x_{+T}-x_{-T}$ is the relative displacement of a nearest pair of changes, m is the reduced mass $m=m_+m_-/(m_++m_-)$, $m\omega_0^2$ the restoring force constant, $\gamma_T=1/\tau_T$, the damping constant, and $E_{T\mathrm{eff}}$ the effective transverse electric field. The effective charges of the ions are defined as $\pm e^*$. The transverse polarization of the medium is

$$P_T=ne^*(x_{+T}-x_{-T})=ne^*u_T. \tag{176}$$

The procedure for choosing an appropriate form for the effective field $E_{T\mathrm{eff}}$ was discussed many years ago by Lorentz [77]. When the lateral dimensions of the medium are large compared with the wavelength and when the medium is cubic,

$$E_{Teff}=E_{Text}+(4\pi/3)P_T \tag{177}$$

the last term being the so-called Lorentz field and $E_{T\mathrm{ext}}$ the external electric field which drives the transverse vibration. Now, if we set $k=0$ in (174) and call $E_{T\mathrm{ext}}=E_0\exp-i\omega t$ and furthermore write

$$u_T(\omega)=\frac{(e^*/m)E_0}{\omega_T^2-\omega^2-i\omega\gamma_T}, \tag{178}$$

then

$$P_T(\omega)=\frac{(ne^{*2}/m)E_0}{\omega_T^2-\omega^2-i\gamma_T\omega}=\chi_T(\omega)E_0 \tag{179}$$

where

$$\omega_T^2=\omega_0^2-(4\pi/3)ne^{*2}/m \tag{180}$$

and the transverse electric susceptibility $\chi_T(\omega)$ is related to the transverse dielectric constant through (122). The "plasma frequency" is defined through the second term in (180)

$$\omega_p^2=(4\pi/3)ne^{*2}/m. \tag{181}$$

The real and imaginary parts of the dielectric constant then have forms essentially the same as those discussed in section 3.

$$\epsilon_{TR}(\omega)=1+\frac{\omega_p^2(\omega_T^2-\omega^2)}{(\omega_T^2-\omega^2)^2+\gamma_T^2\omega^2} \tag{182a}$$

$$\epsilon_{TI}(\omega)=\frac{\omega_P^2\gamma_T\omega}{(\omega_T^2-\omega^2)^2+\gamma_T^2\omega^2} \tag{182b}$$

The damping constant γ_T vanishes in a purely harmonic theory. However, if the original lattice vibration hamiltonian has anharmonic forces or if the dipole moment term (171) has additional non-linear terms in the displacements u, γ_T can be calculated form perturbation theory in a manner analogous to the derivation of (158). It involves so-called multiphonon processes. A similar discussion of the longitudinal dielectric constant can be made.

When one relaxes the initial hypothesis that the atoms in the lattice are point non-polarizable objects, then the atomic polarizabilities must be included in the above discussion. This was first done by Szigeti [78].

All of the above mentioned elaborations as well as discussions of experimental data and generalizations to systems with more complicated unit cells than one finds in NaCl lattices can be found in recent reviews by E. Burstein [74, 75] and collaborators and by D. H. Martin [76].

5. Discussion

E. R. Lippincott: (University of Maryland): My question is associated with the singularities that show up in the heat capacity curves. Is it always true that these singularities show up when you have cooperative motion? Is it necessary to have a cooperative phenomenon to have a singularity?

E. Montroll: I think all the sharp singularities come from some kind of cooperative phenomena. I don't know of any exception.

6. References

[1] W. Nernst and F. Lindemann, Zeit für Elektrochemie und Angewandte Physikalische Chemie **17,** 817 (1911).

[2] W. K. Robinson and S. A. Friedberg, Phys. Rev. **117,** 402 (1960).

[3] A. Lawson, Phys. Rev. **57,** 417 (1940).

[4] M. R. Moldover and W. A. Little, Critical Phenomenon NBS Publication 273 (editors M. S. Green and J. V. Sengers) p. 79 (1966). See also M. J. Buckingham and W. M. Fairbank, Prog. in Low Temp. Phys. **3,** 80 (1961).

[5] Dynamical Theory of Crystal Lattices, M. Born and K. Huang, Clarendon Press, Oxford, (1954).

[6] Theory of Lattice Dynamics in the Harmonic Approximation, A. Maradudin, E. Montroll and G. Weiss, Academic Press, New York, (1963).

[7] E. W. Montroll, J. Chem. Phys. **15,** 575 (1947).

[8] L. van Hove, Phys. Rev. **89,** 1189 (1953).

[9] L. Onsager, Phys. Rev. **65,** 117 (1944); B. Kaufman and L. Onsager Phys. Rev. **76,** 1244 (1949).

[10] E. Montroll, R. Potts, and J. Ward, J. Math. Phys. **4,** 308 (1963).

[11] G. F. Newell and E. W. Montroll, Rev. Mod. Phys. **25,** 353 (1953).

[12] C. Domb, Advances in Physics **9,** 149 (1960).

[13] M. E. Fisher, Reports on Progress in Physics **30** (part 2), (1967).

[14] T. Schultz, D. Mattis, and E. Lieb, Rev. Mod. Phys. **36,** 856 (1964).

[15] G. A. Baker Jr. Advances in Theoretical Physics **1,** 1 (1965).

[16] W. F. Giauque and J. W. Stout, J. Am. Chem. Soc. **58,** 1144 (1936).

[17] W. F. Giauque and M. Ashley, Phys. Rev. **43,** 81 (1933).

[18] L. Pauling, J. Am. Chem. Soc. **57,** 2680 (1935).

[19] J. F. Nagle, J. Math. Phys. **7,** 1484 (1966); **7,** 1492 (1966).

[20] J. Slater, J. Chem. Phys. **9,** 16 (1941).

[21] E. Lieb, Phys. Rev. Letters **18,** 692 (1967).

[22] H. Palevsky, Brookhaven Lecture Series number 66, (1967).

[23] cf. B. N. Brockhouse, Aarhus Summer School Lectures 1963, p. 211, (W. A. Benjamin, Inc., N.Y.).

[24] G. Placzek and L. van Hove, Phys. Rev. **93,** 1307 (1954).

[25] L. van Hove, Phys. Rev. **95,** 249 (1954).

[26] E. L. Wagner and D. F. Hornig, J. Chem. Phys. **18,** 296 (1950).

[27] Palevsky, Otnes, and Larson, Phys. Rev. **112,** 11 (1958).

[28] Yarnell, Arnold, Bent, and Kerr, Phys. Rev. **113,** 1358 (1959).

[29] D. G. Henshaw, Phys. Rev. Letters **1,** 127 (1958).

[30] Henshaw, Woods, and Brockhouse, Bull. Am. Phys. Soc. **5,** 12 (1960).

[31] N. S. Gingrich, Rev. Mod: Phys. **15,** 90 (1943). For more recent review see K. Furukawa, Reports on Prog. of Phys. **25,** 396 (1962).

[32] W. L. Bragg, The Crystalline State I, G. Bell and Sons, London, (1933), and R. W. James, The Crystalline State II, G. Bell and Sons, London (1954).

[33] J. Bouman, Handbuch der Physik, **32,** p. 96–237 (see especially p. 218–236), 1957.

[34] H. Lipson and W. Cochran, The Crystalline State III, G. Bell and Sons, London, (1953).

[35] A. L. Patterson, Phys. Rev. **46,** 373 (1934).

[36] Light Scattering by Small Particles, H. C. van de Hulst, Wiley, New York, (1957).

[37] P. Debye, J. Appl. Phys. **15,** 338 (1944).

[38] W. Marshall, Critical Phenomenon, NBS Publication 273, p. 135 (1966).

[39] L. S. Ornstein and F. Zernicke, Proc. Acad. Sci. Amsterdam **17,** 793 (1914).

[40] Theoretical Physics in the Twentieth Century, p. 161, M. Fierz, Interscience, New York, (1960).

[41] Phase transitions, NBS Publication 273 (Ed. M. S. Green and J. V. Sengers).

[42] L. Brillouin, Ann. Phys. **17,** 88 (1922).

[43] L. Landau and G. Placzek, Physik. Z. Soviet Union **5,** 172 (1934).

[44] N. C. Ford, Jr., and G. B. Benedek, Phys. Rev. Letters **15,** 649 (1965). Critical Phenomenon NBS Publ. 273, p. 150 (1966).

[45] G. B. Benedek and K. Fritsch, Phys. Rev. **149,** 647 (1966).

[46] S. S. Alpert, Critical Phenomenon, NBS Publication 273, p. 157 (1966).

[47] Polar Molecules, P. Debye, Chemical Catalog Co., New York, (1929).

[48] Theory of Dielectrics, H. Fröhlich, Clarendon Press, Oxford, (1958).

[49] R. Kronig, J. Am. Op. Soc. **12,** 547 (1926): H.A. Kramers, Atti del Congress Internationale de Fisica Como (1927).

[50] W. Kauzmann, Rev. Mod. Phys., **14,** 12 (1942).

[51] Viscoelastic Properties of Polymers, J. Ferry, Wiley, New York, (1961).

[52] I. Waller, Zeit, f. Physik **79,** 370 (1932).

[53] Paramagnetic Resonance, C. J. Gorter, Elsevier, Amsterdam, (1947).

[54] E. J. Zavoisky, J. Phys. USSR **10,** 197 (1946).

[55] R. L. Cummerow and D. Halliday, Phys. Rev. **70,** 433 (1946).

[56] E. M. Purcell, H. C. Torrey, and R. V. Pound, Phys. Rev. **69,** 37 (1946).

[57] F. Bloch, W. W. Hansen, and M. Packard, Phys. Rev. **70,** 474 (1946).

[58] G. Pake, Proceedings of Conference on Magnetic Resonance, Cairo (1967).

[59] Principles of Magnetic Resonance, C. P. Slichter, Harper and Row, (1963).

[60] Principles of Nuclear Magnetism, A. Abragam, Clarendon Press, Oxford, (1961).

[61] F. Bloch, Phys. Rev. **70,** 460 (1946).

[62] J. H. van Vleck, Phys. Rev. **74,** 1168 (1948).

[63] E. R. Andrew and R. G. Eades, Proc. Roy. Soc. **A218,** 537 (1953).

[64] N. L. Alpert, Phys. Rev. **75,** 398 (1949).

[65] Molecular Spectra and Molecular Structure, I. Spectra of Diatomic Molecules, G. Herzberg, van Nostrand, New York, (1950).

[66] Molecular Spectra and Molecular Structure, II. Infrared and Raman Spectroscopy, G. Herzberg, van Nostrand, New York, (1946).

[67] F. Reiche and H. Radamaker, Z. Phys. **39,** 444 (1926).

[68] Cf. C. W. King, R. M. Haimer and P. C. Cross, J. Chem. Phys. 11, 27 (1943) **17,** 826 (1949).

[69] D. F. Hornig, J. Chem. Phys. **16,** 1063 (1948).

[70] J. Lecomte, Advances in Chem. Phys. **7,** 408 (1964).

[71] R. N. Jones and C. Sandorfy, Chemical Applications of Spectroscopy (Vol IX of Technique of Organic Chemistry, Ed. A. Weissberger, Interscience, New York, (1956).

[72] P. Doty, J. Polymer Sci. **55,** 1 (1961).

[73] Dynamical Theory of Crystal Lattices, M. Born and K. Huang, Clarendon Press, Oxford, (1954).

[74] E. Burstein, Aarhus Summer School Lectures 1963, p. 276 (W. A. Benjamin Inc. N.Y.).

[75] E. Burstein, S. Iwasa, and Y. Sawada, Redic. della Scuola Int. de Fisica Enrico Fermi XXXIV Corso 421 (1966).

[76] D. H. Martin, Advances in Physics, **14,** 39 (1965).

[77] Theory of Electrons, H. A. Lorentz, (Teubner 1909, Dover reprint 1953).

[78] B. Szigeti, Trans. Faraday Soc. **45,** 155 (1949).

THE CONTRIBUTIONS OF NEUTRON AND X-RAY DIFFRACTION TECHNIQUES

G. E. BACON

The University, Sheffield 10, England

1. Introduction

The applications of neutrons and x rays in studying molecular dynamics and the structure of solids depend particularly on four factors.

1. The quantitative way in which individual atoms scatter a beam of neutrons or x rays.
2. The relation between neutron and x ray wavelengths and interatomic and intramolecular distances.
3. The absorption coefficients, or, more important, the penetrabilities of these radiations for solids and liquids.
4. The energies of neutrons and x-ray photons in relation to the energies of acoustic, vibrational and rotational quanta.

We can say at the outset, as indicated in figure 1, that neutrons of thermal energy have not only the right wavelengths to determine atomic positions by a study of the diffraction effects between neighbouring atoms, but also the right energies to assess the dynamical behaviour of solids—this being a consequence of the near equivalence of the neutron energy and that of a quantum of energy for a lattice vibration, a molecular vibration or a molecular rotation. On the other hand x rays are favourable only from the first point of view and infrared radiation is favourable only from the second.

Although neutrons and x rays, and indeed electrons, are employed with the common aim of producing a view of both the static arrangement and the dynamic motion of the atoms in a solid, yet the details of the pictures which they yield are really totally different. This happens because the different radiations see different things: x rays measure electron density, electrons measure electric potential and neutrons measure nuclear density, often considerably modified because of resonance effects in neutron-nuclear scattering. We can consider the magnitude of the scattering by an atom in terms of the amplitude of the scattered wave for an incident wave of unit amplitude. At distance r this is represented by $-\frac{b}{r}$ where b is called the

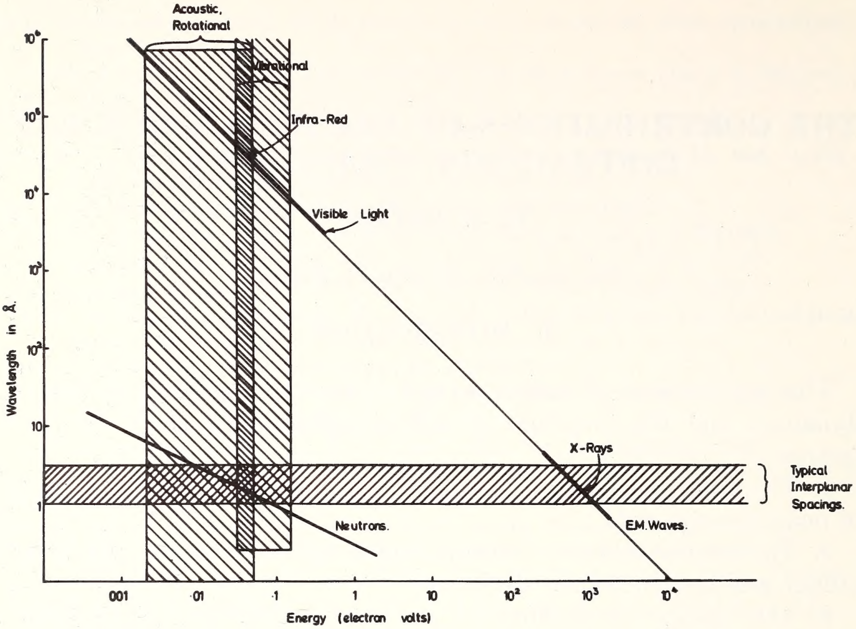

FIGURE 1. The relation between wavelength and energy for neutrons and electromagnetic radiation. Also indicated is the normal range of interplanar spacings and the range of energy quanta for acoustic and molecular motions.

"scattering length". For x rays the value of b is proportional to the number of extranuclear electrons, i.e., the atomic number Z, being in fact equal to $\left(\frac{e^2}{mc^2}\right) Z$, which takes values in the range 10^{-11}–10^{-12} cm. Since the electron cloud has dimensions of the same order as the x-ray wavelength (for diffraction wavelengths) the amplitude of scattering falls off fairly rapidly as the angle of scattering, 2θ, increases. When $(\sin \theta)/\lambda$ is 0.5 Å^{-1}, i.e., at $\theta=50°$ for Cu $K\alpha$ radiation, the scattering amplitude has fallen to about a half of its initial value. Neutron scattering amplitudes are rather lower, averaging 0.62×10^{-12} cm, and do not vary very substantially from atom to atom. Practically all atoms lie within the range of a half to twice this mean value and, because of the resonance effects which we have already mentioned, the variation from atom to atom is rather haphazard. Since the dimension of the nucleus is 10^{-12} cm, i.e., much smaller than the neutron wavelength, the scattering is isotropic.

Figure 2 contrasts the scattering amplitudes for x rays and neutrons and a detailed consideration of this figure will indicate many of the applications of neutron beams to solving problems which are intractable to x rays. Before looking at this feature more closely it is worth completing the overall picture by noting the absolute values of scattering amplitude for *electron* beams. These values are of the order of 10^{-8} cm i.e. several orders of magnitude larger than those for neutrons and x rays, with the result that electron diffraction studies are applicable to gases, thin films and surfaces, whereas x rays and neutrons deal with specimens which are of the order of millimetres in thickness. Indeed specimens with centimetre dimensions can often be employed in neutron investigations.

Conventional diffraction studies with x rays and neutrons have two major aims:

1. To determine the size and shape of the unit cell, which by continued repetition in 3-dimensions builds up the solid.

2. To determine the details of the arrangement of atoms in the unit cell i.e. to locate the individual atoms within the cell—and this means not only defining their equilibrium positions but also providing a dynamic picture of their thermal motion. The determination of the size of the unit cell is simple and straightforward. It can easily be done to an accuracy of 1 part in 10,000 and with more difficulty to 1 in 100,000. However there is in principle no direct way of determining the location of the atoms in the unit cell, but in practice solutions have

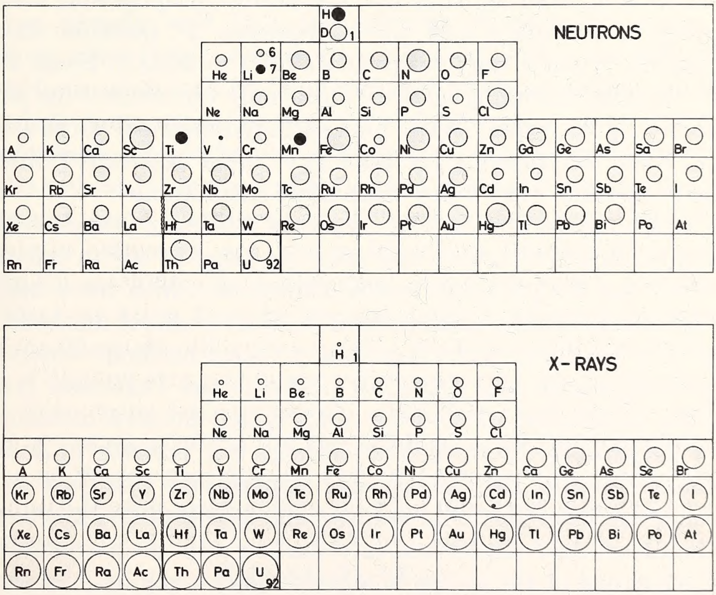

FIGURE 2. A diagrammatic representation of the variation of the scattering amplitudes of the elements for (i) neutrons and (ii) x rays. The areas of the circles are proportional to the *amplitude* of the scattered wave: for neutrons the scale of the drawing is ten times larger than for x rays.

been provided for many substances by incorporating suitable amounts of labour, time and ingenuity, which increase in quantity as we progress from simple structures up to the few proteins which have been analyzed in detail.

2. Crystal Structure Analysis

In all respects the crystal is the 3-dimensional analogue of the optical diffraction grating so that the spectral *positions*, when the crystal is illuminated with monochromatic radiation, are determined by the grating spacing; i.e., the unit cell size, whereas the spectral intensities are determined by the line shape and its transmission factor; i.e., the content of the unit cell. Conversely, having made measurements with x rays we can determine the electron density at any point in the unit cell by making a three-dimensional summation of terms which are proportional to the amplitudes of the 3-dimensional set of spectra. In the same way, measurements of neutron spectra will give a calculation of the nuclear density in the material. In each case the drawback to this procedure is that we require to know the spectral amplitudes in both magnitude and phase, . . . and there is no direct way of measuring phase. For centrosymmetrical structures the phase can be either 0° or 180° so that there are simply two alternatives for each term in the summation but, even so, it is not a practical proposition, even with computers, to calculate and choose between 2^n possible structural arrangements when n may range from 1000 to 20,000. Even $2^{30}=10^9$ and 10^9 seconds, assuming that we allow only one second for perusing each result, is 35 years. With noncentrosymmetrical structures the phase of each amplitude may take any value between 0° and 360° and the problem is even more completely intractable.

The task of determining the structure therefore becomes that of determining phases by a trial and error sequence in which calculations are carried out for plausible model structures which have been suggested by chemical information, reinforced by indirect methods which may be very helpful in particular cases. Of such methods which have a fairly general application the most useful is the Patterson synthesis which is a summation of Fourier terms which involve intensities instead of amplitudes. From such a synthesis it is possible to determine interatomic vectors i.e., interatomic separations specified in both magnitude and direction. The resulting pattern obtained in this way is often confused, but significant information can be extracted fairly readily when one of the atoms in a molecule is much heavier than the others. Another method of fairly general application is that of isomorphous replacement, which can be applied, for example with the alums, in the case of a series of isomorphous compounds which differ in composition only in respect of one particular atom. By noting whether replacement by a heavier atom causes an increase or decrease of intensity of individual reflections it is possible to draw conclusions regarding their phases. It is of course necessary to assume that the remainder of the structure is completely unchanged by these substitutions.

We can mention two other methods which may be applied to phase determination.

2.1. Anomalous Scattering

If the wavelength of an incident beam of x rays lies in the neighbourhood of an absorption edge for one of the scattering atoms then the scattering amplitude of the latter becomes complex rather than real. For CuKα radiation this occurs particularly for atoms of iron and cobalt. It can be shown that in such cases the usual equality of intensity between reflections $(h\ k\ l)$ and $(\overline{h\ k\ l})$, known as Friedel's Law, will break down in structures which do not possess a centre of symmetry. From the differences in intensity it is possible to calculate phase angles. We shall discuss this behaviour later in relation to neutron diffraction for which, for certain atoms, the effects are much more marked.

2.2. Statistical Relations and Direct Methods

We have already said that the solution of most structures has depended on using "trial and error" methods in which the diffraction data have been reinforced by incorporating much subsidiary physical and chemical information. It would be of enormous value if this intuitive information could be put in at the outset of an analysis, rather than at the end, and it is worthwhile asking whether it can be described in any general terms. There are in fact two important principles which, consciously or otherwise, are used as criteria in deciding whether any artificially or mechanically determined structure could possibly be correct. First, we know that the electron density can never be negative anywhere in the unit-cell and, secondly, we know that structures are built out of discrete atoms of fairly well-known size, shape and electron content. These facts lead to certain statistical relationships and restrictions of the signs of the Fourier coefficients of related reflections. For example Harker and Kasper [1][1] in 1958 gave the following inequalities which exist among the structure factors of a centrosymmetric structure.

$$\mathrm{F_H}^2 \leq \tfrac{1}{2}F_0(\mathrm{F_0}+\mathrm{F_{2H}}) \qquad (1)$$

$$(\mathrm{F_H}+\mathrm{F_{H'}})^2 \leq (\mathrm{F_0}+\mathrm{F_{H+H'}})(\mathrm{F_0}+\mathrm{F_{H-H'}}) \qquad (2)$$

$$(\mathrm{F_H}-\mathrm{F_{H'}})^2 \leq (\mathrm{F_0}-\mathrm{F_{H+H'}})(\mathrm{F_0}-\mathrm{F_{H-H'}}) \qquad (3)$$

---

[1] Figures in brackets indicate the literature references at the end of this paper.

where F_H stands for F_{hkl}, $F_{H+H'}$ stands for $F_{h+h', k+k', l+l'}$ and F_0 is F_{000} in the forward direction and therefore equals N, the total number of electrons in the unit-cell.

The first of these inequalities establishes a relation between F_{hkl} and $F_{2h, 2k, 2l}$ which may serve to determine the sign of the latter. To take a simple example quoted by Ewald [2]: if $|F_H| = 0.8N$ and $|F_{2H}| = 0.45N$ then inequality (1) gives

$$0.64\ N^2 \leq \tfrac{1}{2}N(N \pm 0.45N).$$

This can only hold if we take the + sign, i.e., if the sign of F_{2H} is positive. For a full account of the development of this technique of analysis and of its use in structure determination reference is made to articles by Karle [3] and Woolfson [4].

2.3. Structural Refinement and Thermal Motion

By a combination of methods of the type we have discussed, and with a degree of difficulty which may vary enormously for different compounds, we can arrive at a structure which is largely correct and in which the atomic coordinates are probably within 0.1 Å of the truth. There are various ways, such as by calculating the Reliability Index or Discrepancy Factor, in which we can express the likely accuracy of the structure at this stage. A process of structural refinement then follows and this provides a convenient point in our survey to introduce the topic of thermal motion. Because of an atom's thermal energy it undergoes motion about its equilibrium position and in order to specify this motion completely requires six parameters, in addition to the three coordinates which define its equilibrium position. The motion may be substantially different in different directions in a manner which depends on the crystal symmetry and the type of structure: for example, in a layer structure the displacements perpendicular to the layers will be much greater than those in their plane. There now exists an accumulated volume of knowledge which permits, at any temperature, a good estimate of the thermal motion of an atom and a rough guess at its anisotropy. These preliminary values of the thermal parameters and the initial values of the coordinates have to be refined. In earlier days this was usually done by Fourier refinement, involving cycles of recalculation of phases and production of electron-density maps, but is is now more often done by least-squares analysis, which is generally more adaptable to automatic computers. The final outcome is a list of atomic coordinates, correct to 0.01 Å or often better, and a description of the ellipsoid of thermal motion for each atom, specifying the magnitudes and orientations of its axes. The overall accuracy will depend very much on the particular compound and especially on the way in which this will decide the ratio between the number of independent reflections which are measured and the number of parameters which have to be determined. Thus, in a neutron diffraction study of sucrose Brown and Levy [5] had 2800 independent measurements of spectral intensities from which to determine about 400 parameters: in the analysis of myoglobin 17,000 reflections were measured but there were 21,500 parameters needed to define the structure completely and 11,340 if the hydrogen atoms were left out altogether, (Phillips, [6]).

The foregoing account of the principles of structural analysis is applicable to either x-ray or neutron diffraction. It is an unfortunate fact however that a suitable neutron source costs between 10^3 and 10^4 times as much as an x-ray set and that, even then, the number of quanta in unit area of its incident beam is less by a similar order of magnitude. It is of course these facts, leading to a scarcity of suitable nuclear reactors, which limits the pace of advancement of neutron beam work in investigating solids and liquids. It is therefore necessary to ensure that, with any material or structure, all the progress which can be achieved with x-rays is made first and that the neutron crystallographer starts where his x-ray colleague leaves off. Our aim now, therefore, is to see what the former can do which the latter cannot. We return to an examination of figure 2.

3. The Contribution of Neutron Diffraction

The most important feature of figure 2 from the point of view of molecular structure determination is that hydrogen is revealed as a respectable scatterer of radiation. Its scattering length of -0.38×10^{-12} cm is rather below the average value of 0.62×10^{-12} cm, but not unduly so. Moreover, deuterium has a scattering amplitude which just about equals the average, so that extremely good location of hydrogen atoms can be achieved in those cases where deuterium substitution can be effected. Moreover the fact that H, D have scattering lengths of opposite sign, so that hydrogen appears in atomic projections as *negative* scattering density, means that the two isotopes can be very readily distinguished in mixed systems. In practice deuterium substitution is very valuable if studies have to be confined to powdered materials but practically all single-crystal studies have been achieved with ordinary hydrogen-containing material.

3.1. Hydrogen Atoms and Thermal Motion

The importance of the accurate location of the hydrogen atoms is not simply that it completes the picture of the molecule. Very often there are hydrogen atoms on the outsides of molecules and they are accordingly at large distances from the centre of mass, so that any molecular rotations will therefore be revealed very clearly in the motions of the hydrogen atoms. This point is well illustrated in figure 3 which shows a relatively old and primitive projection by neutron diffraction of the hydrogen atoms in solid benzene (Bacon, Curry and Wilson [7]). In this figure the contours for hydrogen are drawn on a slightly closer scale than for the carbon atoms in order to emphasize the accuracy which is obtainable. From this analysis it was possible to determine, for example, the r.m.s. angular oscillation of the molecule as 8°, 4.5° and 3° of arc at –3°, –55° and –135 °C respectively. The inferior visibility of the hydrogen atoms for x rays is indicated in figure 4 which compares the neutron picture for a benzene molecule with that of the x-ray result for anthracene. A further simple example of the elucidation of thermal motion by studying the peripheral hydrogen atoms is provided by figure 5, which shows projections for the molecule of potassium hydrogen bis-phenylacetate (Bacon and Curry, [8]). The increasing movement as we go outward to the end of the molecule, associated with an oscillation about the atom C_3, is indicated by the varying diffuseness of the contours of the hydrogen atoms deduced respectively from observations at room temperature and at 120 °K.

Over the past 3 or 4 years the introduction of higher-flux reactors and automatic diffractometers has both vastly reduced the labour of data collection and much improved the accuracy of parameter

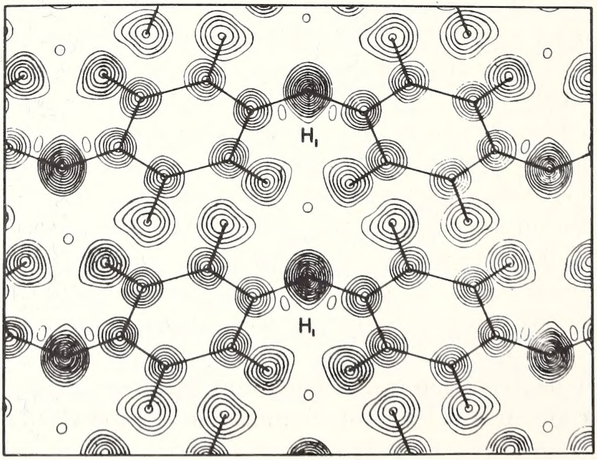

Figure 3. A projection of the molecular structure of solid benzene as computed from neutron diffraction observations. The contours for the hydrogen atoms are more closely spaced than those of the carbon atoms, in order to indicate the precision attained. In projection, hydrogen atoms from neighbouring molecules overlap at positions such as H_1.

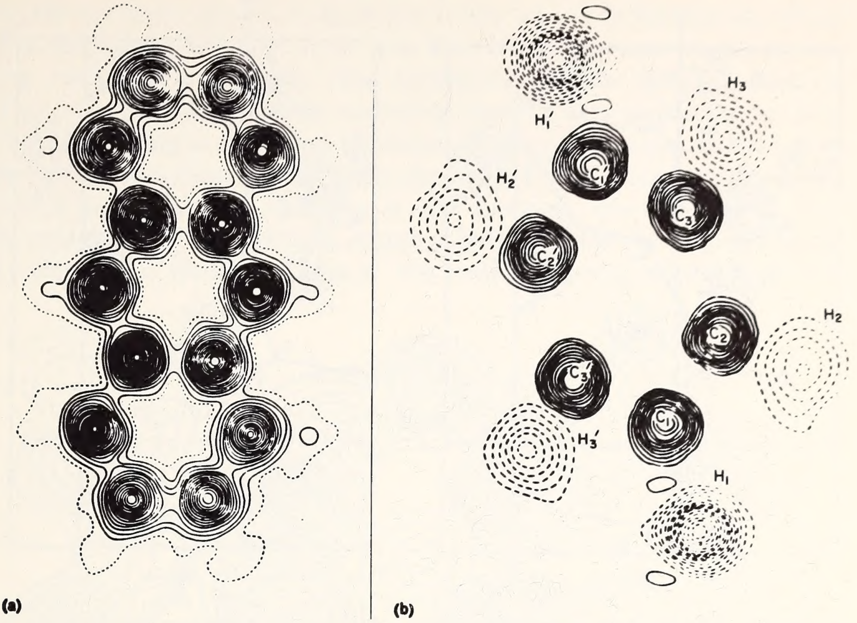

FIGURE 4. A comparison of the relatively insignificant detail of the hydrogen atoms revealed by x rays in an anthracene molecule (a) compared with the full detail provided by neutrons for the benzene ring in solid benzene itself (b). Pairs of hydrogen atoms overlap at H_1, H_1' in the projection (b). View (a) is based on Sinclair et al. Acta Cryst. *3*, 251, 1950.

determination by making possible full 3-dimensional analyses. Very good examples of the accuracy which is now obtainable is provided by the work of Brown and Levy on sucrose [5] and glucose [9]. In the former analysis, to which we have already referred, the coordinates of the carbon and oxygen atoms were determined to an accuracy of 0.003 Å and the hydrogen atoms to 0.007 Å. Figure 6 indicates the shape of the molecule of sucrose viewed along the a axis, together with the structural formula of the molecule placed in the same orientation. The two intramolecular hydrogen bonds are of particular interest. The final coordinates varied by from 0.06 to 0.91 Å from the starting values and this analysis demonstrates that, quite apart from the precision in the information about the hydrogen atoms, the general accuracy of neutron determinations is at least as satisfactory as for an x-ray study of a crystal of comparable complexity. Perhaps the most ambitious study attempted, and achieved, so far is that of the acid derivative of vitamin B_{12} reported by Moore, Willis and Hodgkin [10]. The complexity here is an order of magnitude greater than for sucrose and there are 228 atoms in the asymmetric unit of the structure. From about 1500 reflections 820 parameters were determined,

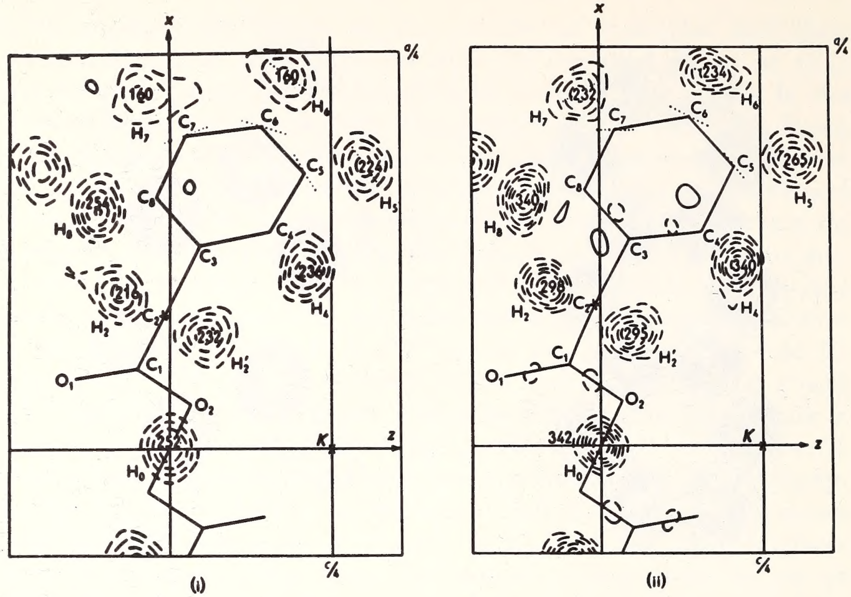
x
½
O
160
H₇
C₇
C₆
H₆
C₅
224
H₅
C₈
254
H₈
C₃
C₄
234
H₄
216
H₂
C₂
232
H₂'
C₁
O₁
O₂
252
H₀
K
z
(i)
233
234
265
340
298
295
342
(ii)

FIGURE 5. The neutron scattering density due to the hydrogen atoms alone in potassium hydrogen bis-phenylacetate KH (C_6 H_5 CH_2 $COO)_2$ at (i) 290 °K (ii) 120 °K indicating, by the diffuseness of the contours, both the enhanced thermal motion at room temperature and the oscillation of the ends of the molecules about C_3.

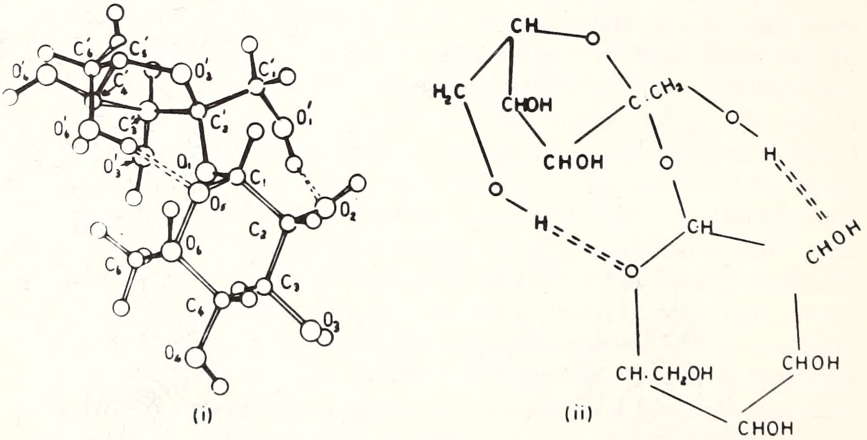
O₆'
C₆'
C₅'
C₄'
O₂'
C₁'
O₁'
O₄'
C₃'
C₂'
O₃'
O₁
C₁
O₅
O₂
C₂
O₆
C₆
C₃
C₄
O₃
O₄
(i)
CH
O
H₂C
CHOH
C.CH₂
CHOH
O
O
H
CH
H
O
CHOH
CH.CH₂OH
CHOH
CHOH
(ii)

FIGURE 6. A projected view of the structure of sucrose along the a axis, from the results of Brown and Levy, together with a structural formula for the molecule placed in the same orientation.

so the accuracy of the study is inevitably less than for sucrose, where the reflection/parameter ratio was 7:1. However some very convincing chemical information was forthcoming from the B_{12} analysis. Figure 7 shows the neutron scattering density over the corrin nucleus. It is interesting to note that for neutrons the cobalt atom at the center is the lightest atom in the molecule (with a scattering length of only 0.25×10^{-12} cm) and nitrogen is the heaviest ($b=0.94\times10^{-12}$ cm), in contrast to the x-ray case, where cobalt is by far the heaviest atom. In figure 8 is illustrated one of the methyl groups, establishing that

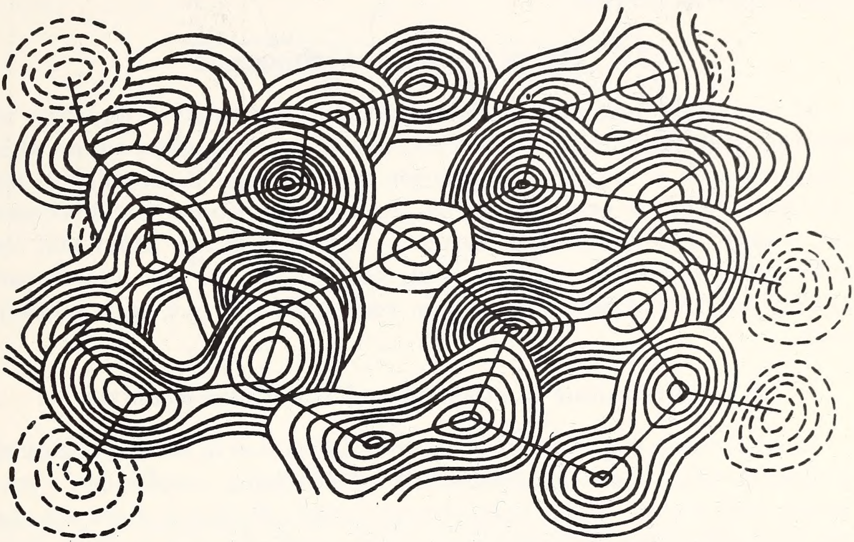

FIGURE 7. The neutron scattering density over the corrin nucleus of the molecule of a monocarboxylic acid derivative of Vitamin B_{12} (from Moore, Willis and Hodgkin, Nature *214*, 130, 1967).

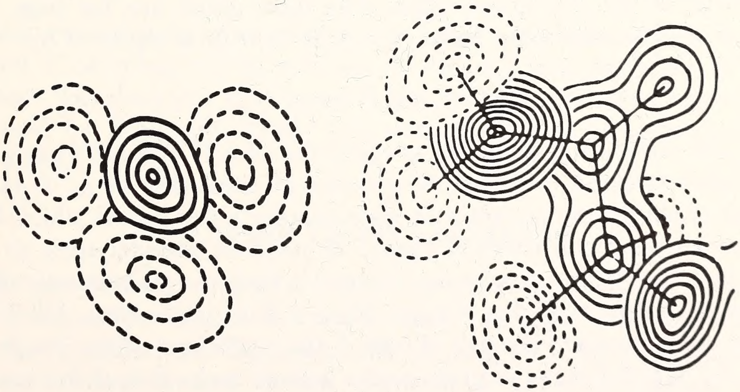

FIGURE 8. Details of (i) a methyl group, indicating non-rotation, and (ii) a group conclusively identified as acetamide in the B_{12} derivative (by courtesy of Nature, as for figure 7).

this is *not* in free rotation about the single bond which links it to the ring carbon atom, and also one of the acetamide groups. The detail of the latter is in fact important in establishing the nature of this group, showing conclusively that the atoms are $CO\cdot NH_2$ and cannot be $COOH$. Both the sucrose and B_{12} studies were carried out using reactors which gave a neutron flux of about 5×10^{13} neutrons cm^{-2} sec^{-1} and employed crystals measuring about 2 mm. With the higher-flux reactors which are now coming into use in the U.S.A. it should be possible to carry out comparable investigations with crystals less than 1 mm^3 in volume.

3.2. 'Heavy Element' Compounds

At the other end of the Periodic Table the relative equality of scattering amplitudes means that studies of uranium compounds with elements such as oxygen and nitrogen are no longer made difficult by the overwhelming contribution of the uranium atoms which occurs for x rays. For neutrons, nitrogen is almost a heavy atom and its substantial difference from oxygen means that the two atoms can readily be distinguished in organic compounds, as we have already seen.

3.3. Anomalous Scattering and the Phase Problem

Most of the opportunities for neutron diffraction in solving chemical problems arise from the differences in scattering amplitudes, compared with x rays, which figure 2 summarises. However there are one or two factors of a different kind which merit discussion. First, it is found that anomalous scattering effects are, in a few cases, much larger than what is found for x rays. In figure 9(i) is plotted a typical variation of scattering amplitude with x-ray wavelength in the neighbourhood of an absorption edge. The data given are for iron. The normal atomic scattering factor f_0, which is real, is replaced by

$$f=f_0+\Delta f'+i\Delta f''.$$

Near the absorption edge the magnitudes of $\Delta f'$ and $\Delta f''$ are about equal and amount to about 20 percent of the value of f_0. A rather similar phenomenon occurs with neutrons for a few nuclei which have resonances near the thermal region of neutron energy, such as B^{10}, Cd^{113} and Sm^{149}. The interesting feature is that the anomalous effects are much larger than for x rays. Figure 9(ii) gives data for Cd^{113}. At the resonance wavelength of 0.68 Å the coefficient of the imaginary term, $\Delta f''$, is 7.6 times as great as the normal real value of the scattering amplitude far from resonance. There are therefore very good prospects of accurate phase-determination for structures in which one

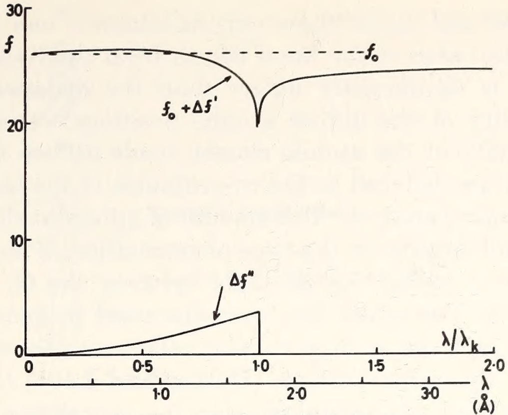

(i) X-ray Scattering Amplitude for Fe

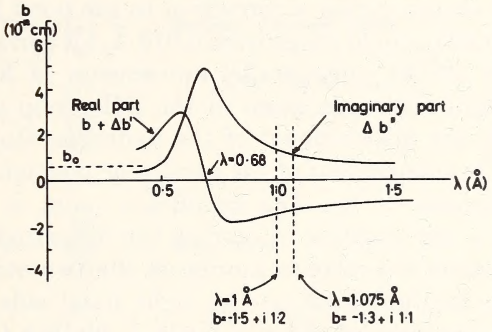

(ii) Neutron Scattering Amplitude for Cd^{113}

FIGURE 9. A comparison of the anomalous scattering for x ray and neutrons. At (i) are shown the real and imaginary contributions to the scattering amplitude f of Fe as a function of the x-ray wavelength. (ii) Shows the corresponding parameters for the isotope Cd^{113} for neutrons.

of these anomalously scattering atoms can be incorporated. A formal method of carrying out an analysis by making measurements at two different wavelengths, one on each side of the resonance, has been discussed by Dale and Willis [11] with a view to determining the structure of insulin.

3.4. Bond-Length Corrections

We have already mentioned that hydrogen atoms often occur on the outside of molecules and accordingly are sensitive indicators of molecular oscillations. Superimposed on any oscillatory motion will be translational motion of the molecule as a whole together with random motion of the hydrogen atom relative to the immediate neighbour to which it is bonded. Very often the resultant motion is large and anisotropic and under these circumstances it can be shown that the equilibrium value of the bond length from the hydrogen atom to its neighbour is significantly longer than the distance between the centre of gravity of the diffuse atomic positions. It is of course the centres of gravity of the atomic clouds, made diffuse by the thermal motion, which are deduced as the co-ordinates of the atoms by a Fourier or least-squares analysis. The amount of apparent shortening of the bond length will depend on the type of correlation, if any, which exists between the two atoms, for example between the O, H atoms in a hydroxyl group. The effect has been discussed in general by Busing and Levy [12] and also with particular relation to the case of calcium hydroxide by the same authors (Busing and Levy, [13]). Figure 10 indicates a variety of possibilities for the correlation of movement between the two atoms, giving a correction to the bond length which, in the case of $Ca(OH)_2$, could range from 0.016 Å, for correlated parallel movements, to 0.125 for anti-parallel movements. A likely type of motion for the light hydrogen atom in the OH group is the "riding motion" in which the displacement of the hydrogen atom relative to the oxygen atom is independent of the particular position in which the oxygen atom happens to be. The significant point is that in any practical case it is not possible to correct the measured bond-length unambiguously unless the relative motion of the two atoms is known or assumed. The results shown at the right hand side of figure 10 indicate how the uncorrected value of 0.936 Å for the O–H distance in $Ca(OH)_2$ could be increased to as much as 1.061 Å, but the plausible assumption that the hydrogen atom "rides" on the oxygen atom would give a corrected length of 0.981 Å. It is interesting to note also that there is a large correction to the position of the terminal hydrogen atom which appears at the bottom of the sucrose molecule in figure 6. The motion of this atom is large because it is not restrained in position by any hydrogen bonding. If we assume that the hydrogen atom rides on the oxygen atom O_4 then the measured O–H bond length of 0.89 Å is corrected to 0.94 Å.

A more simple, but somewhat related, limitation in interpretation of electron or nuclear density patterns is the familiar one of trying to distinguish between statistical and dynamic disorder. A well-known example is the hydrogen bond in KH_2PO_4 where it is not possible, by diffraction methods alone, to distingush between the alternatives of anisotropic thermal motion and a random distribution of hydrogen atoms among two sets of atomic sites provided by a potential well with a double minimum. In the related problem of $NaHF_2$ and $NaDF_2$ McGaw and Ibers [14], by considering both infrared and diffraction data, came to a definite conclusion in favour of a centred bond with anisotropic motion.

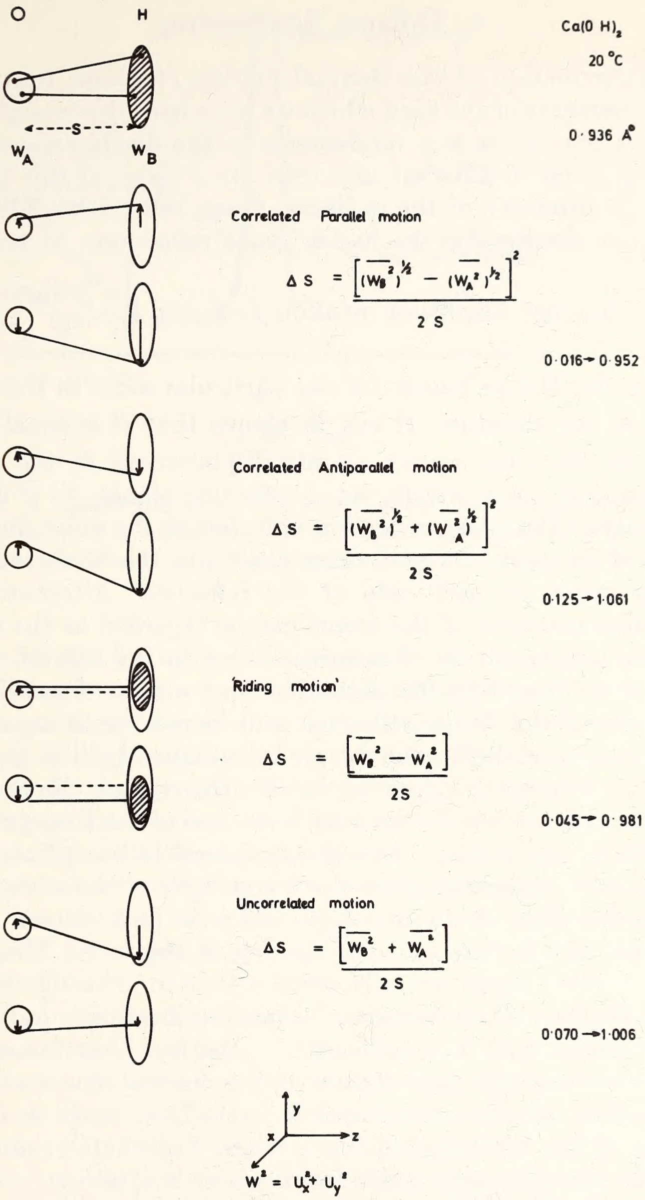
O
H
Ca(O H)$_2$
20 °C
S
W_A
W_B
0·936 Å
Correlated Parallel motion
$\Delta S = \frac{\left[(\overline{W_B^2})^{1/2} - (\overline{W_A^2})^{1/2}\right]^2}{2S}$
0·016→0·952
Correlated Antiparallel motion
$\Delta S = \frac{\left[(\overline{W_B^2})^{1/2} + (\overline{W_A^2})^{1/2}\right]^2}{2S}$
0·125→1·061
'Riding motion'
$\Delta S = \frac{\left[\overline{W_B^2} - \overline{W_A^2}\right]}{2S}$
0·045→0·981
Uncorrelated motion
$\Delta S = \frac{\left[\overline{W_B^2} + \overline{W_A^2}\right]}{2S}$
0·070→1·006
y
x
z
$W^2 = U_x^2 + U_y^2$

FIGURE 10. A summary of possible correlations of motion for two atoms, such as the O, H atoms in the hydroxyl groups of Ca(OH)$_2$, together with values for bond-length correction appropriate to each case.

4. Diffuse Scattering

The determination of the thermal motion of atoms from diffraction measurements of the kind which we have been discussing depends on the fact that there is a randomness in the displacements of corresponding atoms in different unit cells. As a result of this there is a reduction in intensity of the ordinary Bragg reflections. This reduction becomes greater for the higher angle reflections, in accordance with the structure amplitude relation $f=f_0 \exp\left(\frac{-B \sin^2\theta}{\lambda^2}\right)$ where B is the Debye Factor for the particular atom in the relevant direction in the structure. It can be shown that B is equal to $8\pi^2\overline{u^2}$ where $\overline{u^2}$ is the mean-square atomic displacement in the direction of the normal to the particular set of reflecting planes. As $\overline{u^2}$ increases, the intensity of the Bragg reflection falls, but at the same time diffuse reflection of x rays or neutrons takes place into the background, thus producing wings on each side of the reflection. Alternatively the thermal displacements of the atoms can be regarded as the resultant of a continuous spectrum of acoustic waves in the crystal. Each individual wave would scatter radiation into a pair of satellites, one on each side of the Bragg reflection and increasing in separation as the acoustic wavelength gets shorter. Consequently it is possible in principle to deduce the dispersion law for the crystal vibrations from the variation of intensity in the neighbourhood of the Bragg reflection.

In figure 11 the distance from the reciprocal lattice point at which the intensity is measured gives the wavelength of the acoustic wave and from the value of the intensity, which is proportional to $1/\omega_k^2$, it is possible to calculate ω_k the frequency of the wave. This method has been applied experimentally using x rays in investigations such as that of Walker [15] who studied the lattice vibrations of aluminium. However the method is complicated by the fact that the scattering consists not of a single mode but several acoustical modes and several optical modes, as well as quite different effects such as Compton scattering of the incident beam of x rays. Fortunately, much more favourable circumstances exist for neutron scattering, simply because of the quite different energy values for x rays and neutrons of the same wavelength. If we express the data of figure 1 in a different way, we can show that for a wavelength of 1 Å the energy of an x ray is about $3\times10^{18}h$, where h is Planck's constant, whereas for a neutron of the same wavelength the energy is only $1.5\times10^{13}h$. When the incident radiation is scattered by an acoustic wave it loses or gains energy, representing a quantum of lattice energy which is of

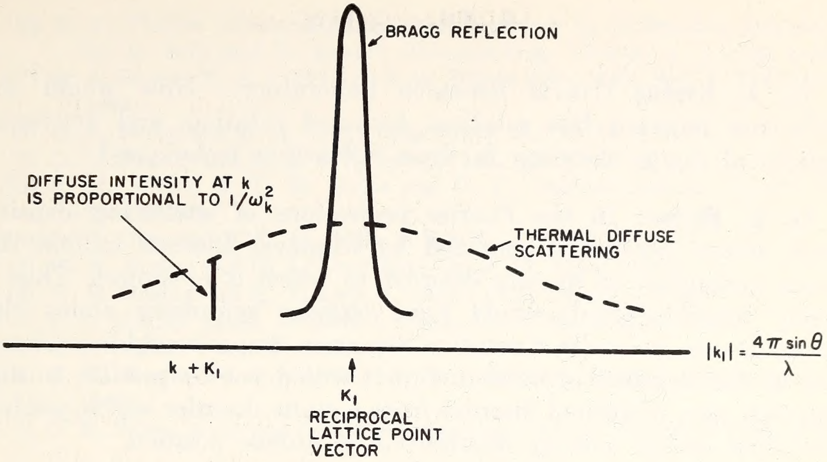
BRAGG REFLECTION
DIFFUSE INTENSITY AT k IS PROPORTIONAL TO $1/\omega_k^2$
THERMAL DIFFUSE SCATTERING
$k + K_1$
K_1
RECIPROCAL LATTICE POINT VECTOR
$|k_1| = \frac{4\pi \sin\theta}{\lambda}$

FIGURE 11. A representation of the diffuse scattering, comprised of a pair of satellites for each acoustic wave in the spectral distribution, which is superimposed on the Bragg scattering at each point of the reciprocal lattice.

the order of 10^{13} *h*. It therefore happens that the change of energy, and wavelength, of the x ray is negligibly small and impossible to measure experimentally, whereas for neutrons the fractional change of wavelength is very substantial. It therefore becomes practicable to explore the diffuse scattering of neutrons in full detail by measuring the velocity of the neutrons after they have been scattered. It is then possible to deduce both their momentum and energy and, in turn, the relation between frequency and wave-number (i.e., the dispersion law) for the crystal vibrations. The practical applications of this principle will be discussed in a subsequent paper on inelastic neutron scattering.

In this survey we have restricted ourselves to the consideration of the scattering of neutrons by the nuclei of atoms, this being the aspect which is important in the determination of molecular structure in chemical terms, and of molecular motion. For completeness we mention that in materials which contain atoms with unpaired electron spins it is possible to determine magnetic structures in an analogous way to chemical structures, by observing the additional scattering of the neutron beam by the unpaired electrons. Moreover from a study of the diffuse magnetic scattering it is possible to discover the transmission properties for waves of magnetic spin. For an account of these applications the reader is referred to the literature (Bacon [16], [17]).

5. Discussion

H. A. Resing (Naval Research Laboratory): How would the difference between free rotation, hindered rotation, and activated rotational jumps show up in these diffraction techniques?

G. E. Bacon: In the Fourier projections of scattering density each atomic portrait is modified by whatever thermal motion the atom undergoes, or by any disorder to which it is subject. Thus a freely rotating group would have circular symmetry about the rotation axis. In hindered rotation, the atom shapes would be smeared out in the direction of motion. But it would not be possible to distinguish, say, rotational disorder from a static disorder which yielded the same overall average distribution of atomic position.

J. J. Rush (National Bureau of Standards): Could you comment on the relative accuracies of electron and neutron diffraction in determining hydrogen positions?

G. E. Bacon: It would be reasonable to take a factor of three or four in favor of neutrons. Not only is the visibility of hydrogen relative to other atoms higher for neutrons—say by a factor of two or three in relation to a carbon atom—but also it is very much easier to interpret accurately the measured spectral intensities in terms of the structure amplitude factors of the unit cell.

D. T. Goldman (National Bureau of Standards): Could you comment on how light scattering might fit into this general picture of determination of structure by scattering techniques?

G. E. Bacon: I would not expect any detail of the unit cell to be revealed by optical wavelengths, but information on particle size and texture could be forthcoming from samples of suitable transmission or reflectivity.

6. References

[1] D. Harker and J. S. Kasper Acta Cryst. **1**, 70–75 (1948).

[2] P. P. Ewald Fifty Years of X-ray Diffraction; Utrecht, Oosthoek p. 116 (1962).

[3] J. Karle Advances in Structure Research by Diffraction Methods **1** Ed. R. Brill; Braunschweig, Vieweg: p. 55–89 (1964).

[4] M. M. Woolfson Chap. IX of The Determination of Crystal Structures Third Edition, by H. Lipson and W. Cochran; Bell, London (1966).

[5] G. M. Brown and H. A. Levy Science **141**, 921–3, (1964).

[6] D. C. Phillips Advances in Structure Research by Diffraction Methods **2.** Ed. R. Brill and R. Mason, Braunschweig, Vieweg: p. 75–140 (1966).
[7] G. E. Bacon, N. A. Curry and S. A. Wilson Proc. Roy. Soc. A. **279,** 98–110 (1964).
[8] G. E. Bacon and N. A. Curry Acta Cryst. **13,** 717–21 (1960).
[9] G. M. Brown and H. A. Levy Science **147,** 1038–9 (1965).
[10] F. M. Moore, B. T. M. Willis and D. C. Hodgkin Nature, London **214,** 130–3 (1967).
[11] D. H. Dale and B. T. M. Willis A.E.R.E. -R **5195** (1966).
[12] W. R. Busing and H. A. Levy Acta Cryst. **17,** 142–6 (1964).
[13] W. R. Busing and H. A. Levy J. Chem. Phys. **26,** 563–8 (1957).
[14] B. L. McGaw and J. A. Ibers J. Chem. Phys. **39,** 2677–84 (1963).
[15] C. B. Walker Phys. Rev. **103,** 547–57 (1956).
[16] G. E. Bacon Neutron Diffraction 2nd Edition—Oxford, Clarendon Press (1962).
[17] G. E. Bacon X-ray and Neutron Diffraction, Oxford, Pergamon Press (1966).

INFRARED AND RAMAN STUDIES ON MOLECULAR STRUCTURE AND MOTION IN CONDENSED PHASES

G. R. WILKINSON

Department of Physics
King's College, Strand, London, England

1. Introduction

Although infrared and Raman spectroscopy [1, 2, 3, 4, 5][1] are very mature fields of study, it is only recently with instrumental advances in the far infrared region and with the use of lasers for Raman excitation that complete vibrational spectra including polarization data can be readily obtained.

The amount of data already collected on the vibrational spectra of "molecules in liquids" or "molecules in powdered solids" is immense, as there is hardly a chemistry research department without at least one infrared spectrometer. The stage of virtually automatic recording was reached and widely applied over a decade ago and there are now several thousand such instruments in daily use. The structure of many molecules has been deduced by infrared and Raman spectroscopy. However much of the day to day interpretation is of a semiempirical nature and is usually directed towards the presence or absence of vibrational frequencies which are characteristic of specific chemical groups, e.g. CH_3 groups [4]. Often the spectra are only used to characterize substances, i.e. as spectral fingerprints or to determine the presence and purity of chemical materials. In comparison the number of complete studies on crystalline solids treated from the point of view of *lattice* dynamics [6, 7] is rather small.

Two questions will first be answered to try and clear up two frequent misunderstandings about infrared and Raman spectroscopy.

First, "can infrared and Raman spectroscopy be used to determine *without ambiguity* the structure of a solid?" The straight answer is "no." In the gas phase the rotational energy of molecules is quantised, and consequently if the rotational structure can be resolved and the moments of inertia found, bond lengths and bond angles can be deduced, provided sufficient isotopic species are available [5].

---

[1] Figures in brackets indicate the literature references at end of this paper.

In the solid or liquid phase completely free rotation is in general not permitted, so only vibrational energy levels may be determined and the best that can be done is to deduce the symmetry of the molecule and, in favourable cases, to assign to which point group the unit cell belongs. Little information can be deduced on interatomic distances.

The second question is "can infrared and Raman spectroscopy be used to obtain the complete vibrational spectrum of a solid?" Once again the answer is "no." Infrared and Raman spectroscopy only gives readily interpretable information about the long wavelength spectrum (i.e., for $\mathbf{k}=2\pi/\lambda=0$, where λ is the phonon wavelength). However, it must be made clear that in many ways this is the great advantage of these techniques, since it leads to spectra that are comparatively simple. These are, consequently, fairly easy to interpret, especially as selection rules for infrared and Raman activity can be readily calculated for different modes of vibration. It is necessary to point out that in spectroscopic literature the term "the vibrational spectrum of" is usually understood to mean for $\mathbf{k}=0$.

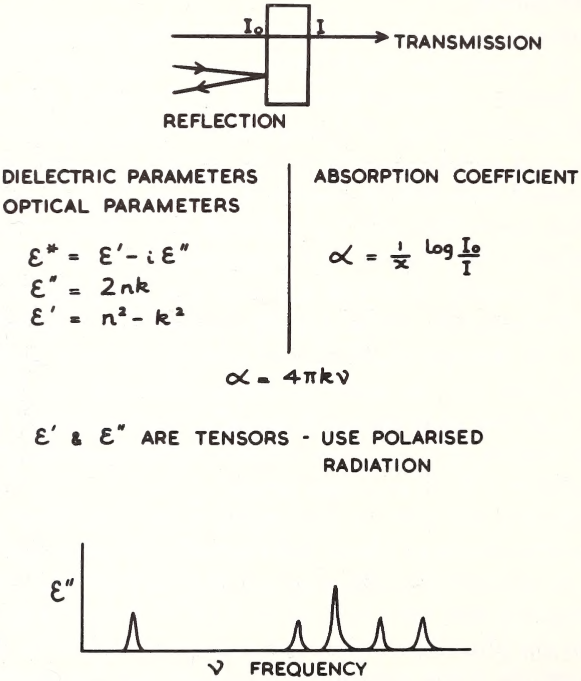
I_o
I
TRANSMISSION
REFLECTION
DIELECTRIC PARAMETERS
OPTICAL PARAMETERS
ABSORPTION COEFFICIENT
$\varepsilon^* = \varepsilon' - i\varepsilon''$
$\varepsilon'' = 2nk$
$\varepsilon' = n^2 - k^2$
$\alpha = \frac{1}{x} \log \frac{I_o}{I}$
$\alpha = 4\pi k \nu$
ε' & ε'' ARE TENSORS - USE POLARISED RADIATION
ε''
ν FREQUENCY

FIGURE 1. As illustrated in the figure infrared spectroscopy involves the measurement of the transmission or the reflection spectrum as a function of the frequency of the radiation. The transmission spectrum can be used to obtain the absorption coefficient α. In the case of very strong absorption bands the reflection spectrum can be measured to give the dielectric parameters ϵ' and ϵ''.

Infrared spectroscopy either involves the determination of the absorption coefficient as a function of frequency from transmission experiments or the computation of complex dielectric parameters ϵ^*, and optical parameters n^* from reflection measurements (see fig. 1). Resonances in these spectra then reveal the $\mathbf{k}=0$ phonon frequencies which are infrared active. Raman spectroscopy involves measurements on the interchange of energy between light quanta and the molecules or crystal scattering the light, as illustrated in figure 2. The shifts in frequency between the Raman lines and the exciting line give vibrational frequencies of the molecule or solid. The energy lost or gained by the photons being absorbed or emitted as vibrational quanta by the molecule or lattice is

$$h\nu_s = h\nu_i \pm h\nu_{\mathrm{vib}}$$

where ν_s, ν_i, and ν_{vib} are the frequencies of the scattered and incident radiation and the frequency of the vibration excited. The quantities eventually found are the components of the polarizability tensor α_{ij}, from which the symmetry of the vibration can be deduced. Brillouin scattering [6] is a form of Raman scattering which involves the acoustic vibrations of a solid or liquid.

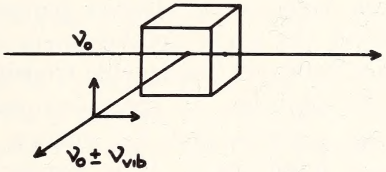

THE POLARIZABILITY TENSOR α IS MEASURED.

$$\begin{bmatrix} \alpha_{xx} & \alpha_{xy} & \alpha_{xz} \\ \alpha_{yx} & \alpha_{yy} & \alpha_{yz} \\ \alpha_{zx} & \alpha_{zy} & \alpha_{zz} \end{bmatrix}$$

$$\alpha = \alpha^\circ + \left(\frac{\partial \alpha}{\partial q}\right)_0 q$$

FIGURE 2. Raman spectroscopy involves the measurement of the change in frequency of radiation scattered by matter. The intensity depends upon the polarization of the incident and scattered radiation and upon the polarizability tensor α_{ij} of the material. The tensor is symmetric, i.e., $\alpha_{zx}=\alpha_{xz}$, and the components of interest in Raman spectroscopy are $\left(\frac{\partial \alpha_{ij}}{\partial q}\right)_0$.

In anisotropic crystals it is essential to use polarized radiation to obtain the spacial dependence of the absorption coefficient α or the dielectric parameters ϵ^* and to determine the components of the polarizability tensor α_{ij}. (note the distinction between α and α_{ij}!)

Perhaps the greatest advantage in infrared and Raman spectroscopy is the very wide range of materials whose vibrational spectra may be explored. Crystals, amorphous solids including glasses, polymers and liquids may be studied; metals however are completely excluded. Only small quantities of substances are required. Good spectra can frequently be obtained from milligrams of material if microtechniques are employed. A further advantage is the precision with which $k = 0$ frequencies may be measured. An accuracy of ± 0.2 cm^{-1} or ± 0.2 millielectron volts is not difficult to achieve over the whole range of vibrational frequencies. Spectral resolutions of 0.25 cm^{-1} for infrared and 1 cm^{-1} for Raman are routinely obtained from commercially available spectrometers. As a consequence of this precision, frequency shifts resulting from isotopic substitution can be measured very accurately. This provides a very powerful method of assigning resonances to particular modes of vibration.

The wide range of units used to measure phonon energies is a constant source of frustration to lattice dynamicists. Frequencies or phonon energies are often quoted in cycles/sec, radians/sec, wavenumbers, millielectron volts or as Debye temperatures. Spectroscopists have long used the wave number measured in cm $^{-1}$ both to denote photon and vibrational frequencies. Considerable advantages would result from the adoption by spectroscopists of the electron volt both for photon energies and for energy levels in matter. (1 millielectron volt = 8.067 cm^{-1}). It is worthwhile recalling here that kT at normal temperature $\sim 300°$ K is about 25 millielectron volts or 200 cm $^{-1}$. The ratio $h\nu/kT$ is of the greatest importance in any consideration of the thermal population of vibrational energy levels.

Fundamental vibrational frequencies of molecules or for one phonon processes in crystals extend over the range 0 to 4500 cm^{-1}, i.e., 0–600 millielectron volts, the upper limit being the frequency of vibration of the hydrogen molecule. Frequencies associated with stretching vibrations [4] are $\sim$3600 cm^{-1} for free O–H, $\sim$3000 cm^{-1} for C–H, $\sim$1100 cm^{-1} for C–F, and $\sim$500 cm^{-1} for C–I.

The whole of spectroscopy is dominated by the concept of symmetry, and the optical spectra of crystals is no exception. Without the aid of group theory all but the spectra of the simplest systems would be almost impossible to comprehend. In this article the symmetry of modes of vibration are designated by the Schoenflies notation which has been adopted by Mulliken and used by nearly all the workers in the field of molecular vibrations.

2. Molecular and Crystal Vibrations

2.1. The Vibration of Isolated Molecules

A molecule containing n atoms has $3n$ degrees of freedom. Of these, three describe translation of the molecule as a whole and three describe rotation of the molecule as a whole. Thus the number of fundamental modes of vibration is just $3n-6$, as illustrated in figure 3 for the water molecule. If all the atoms lie in a straight line, however, there are only two rotational axes of significance; consequently in this case the total number of vibrations is $3n-5$.

The relationship between vibration frequencies, force constants, atomic masses, and geometry is fully treated in a number of texts [1, 2, 8]. Hence it will only be necessary here to outline some of the essential features of the vibrations of isolated polyatomic molecules.

If an atom is displaced from its equilibrium position in a polyatomic molecule a force f_{ij} acts tending to return the atom to its equilibrium position. In the harmonic approximation the force is

$$f_{ij}=\frac{\partial^2 V}{\partial q_i \partial q_j}.$$

Displacement coordinates q are most conveniently taken in terms of increments of valence bond lengths and bond angles. The $(3n-6) \times (3n-6)$ square array of f_{ij} values is termed an F matrix. The inverse kinetic-energy matrix in valence coordinates is called a G matrix. If E is a unit matrix and $\lambda=4\pi^2c^2\nu^2$, then the secular equation in valence coordinates v_i is

$$(GF-\lambda E)v=0.$$

If the force constants are not known, then in general they cannot be determined from the frequencies without simplifying assumptions, for there are $\frac{1}{2}(3n-6)(3n-6+1)$ different force constants for the completely general quadratic force field, but only $3n-6$ equations.

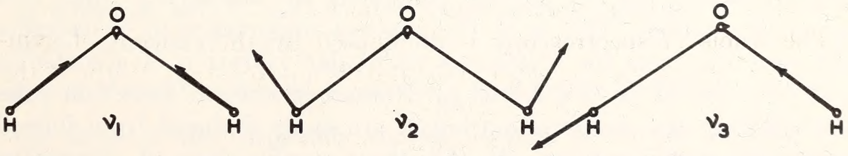

FIGURE 3. The normal modes of vibration of the water molecule. In free space the frequencies are ν_1 3652 cm^{-1}, ν_2 1595 cm^{-1} and ν_3 3756 cm^{-1}.

It is convenient to define an L matrix which is a collection of normalized eigenvectors or solutions of the secular equation. The elements of this L matrix are the normal coordinates

$$v_i = \sum_{j}^{3n-6} l_{ij}\, Q_j.$$

Hence l_{ij} is the charge of the valence coordinate v_i per unit charge of normal coordinate Q_j.

Usually the force constants cannot be determined from experimentally determined frequencies without further information or without making approximations. This problem may be overcome by obtaining data from isotopically substituted molecules, using symmetry operations to factor the secular equation, or by making approximations about the nature of the force field. The use of isotopically substituted molecules coupled with symmetry factoring represents the only way of obtaining nonapproximate force constants for larger molecules.

The general quadratic force field can be approximated by setting certain values of F which are expected to be small to be zero. In the "central force" approximation all internal coordinates are defined as distances between atoms, and consequently in simple molecules the central force constants can be uniquely determined from the observed frequencies. In practice this force field has not proved to be very satisfactory. From a chemical point of view the "valence force field" has attractions. In it the force constants are expressed in terms of the valence internal coordinates which involve changes in valence bond lengths and angles. This leads to an F matrix which is now diagonal. Consequently the expansion and solution of the secular equation is much simplified.

The Urey-Bradley force field neglects all off-diagonal elements in the F matrix but includes central forces between closely adjacent nonbonded atoms. It is essentially a combination of the "central force" and "valence force" approximations. It has the advantage of giving force constants that should be transferable among similar molecules without introducing large error.

If a molecule possesses elements of symmetry, the description of the vibrations can be greatly simplified by classifying them into symmetry species. This is of the greatest importance in considering the selection rules for whether a particular vibration of a molecule will be detected in its infrared or Raman spectrum. Selection rules for overtone and combination bands are easily deduced from formal symmetry considerations [1]. All these applications of symmetry considerations can conveniently be performed using group theoretical methods.

The intensities of lines in the infrared absorption spectrum and and Raman spectrum are determined respectively by the matrix elements

$$\int \psi_{\mathrm{v1b2}} \mu_j \psi_{\mathrm{v1b1}} d\tau \text{ and } \int \psi_{\mathrm{v1b2}} \alpha_{ij} \psi_{\mathrm{v1b1}} d\tau$$

of the dipole moment μ_j and polarizability tensor α_{ij} of the molecule. There is an infrared absorption line at a fundamental frequency ν_0 if the corresponding normal coordinate q_β transforms in the same way as one of the dipole moment components μ_x, μ_y, μ_z. The Raman spectrum contains the fundamental line of frequency shift ν_0 if q_β transforms in the same way as one of the polarizability components α_{ij}. The polarizability may be expanded in terms of the normal coordinates

$$\alpha_{ij}=\alpha_{ij}^0+\sum_{i=1}^{3n-6}\left(\frac{\partial \alpha_{ij}}{\partial q_i}\right)_0 q_i+\sum_{\substack{i=1\\ j=1}}^{3n-6}\left(\frac{\partial^2 \alpha_{ij}}{\partial q_i \partial q_j}\right)_0 q_i q_j+\dots .$$

All modes of oscillation coming under the totally symmetric classes are always Raman active.

If a centre of inversion is one of the elements in the group, all modes which are antisymmetric with respect to it are Raman inactive. All normal modes which are symmetric with respect to a centre of inversion are infrared inactive.

2.2. The Vibrations of a Diatomic Lattice

The essential features of the vibrational spectrum of a solid are best illustrated by a consideration [6, 9] of a diatomic lattice such as diamond, NaCl or ZnS. For such a lattice the ν versus $\mathbf{k}$ dispersion curves consist of three optical branches and three acoustic branches (see fig. 4). For crystals such as diamond, silicon or germanium, the transverse optical branches are degenerate with the longitudinal optical branches at $\mathbf{k}=0$. In NaCl or ZnS-type crystals the transverse optic and longitudinal optic branches are not degenerate at $\mathbf{k}=0$. In the optic modes the atoms vibrate against one another. If the ions are oppositely charged, this type of motion may be excited by an electromagnetic wave of the appropriate frequency. The mode of vibration which leads to the atoms moving together is referred to as an acoustical mode. The group velocity of such a wave propagating through the solid is $v_g=2\pi\frac{\partial \nu}{\partial k}$ and hence is directly related to the slope of the dispersion curves. It may be noted that for $\mathbf{k}=0$ and $\mathbf{k}=\frac{\pi}{a}$ the velocity of propagation of optical modes is zero, corresponding to standing waves in the solid. The velocities of transverse

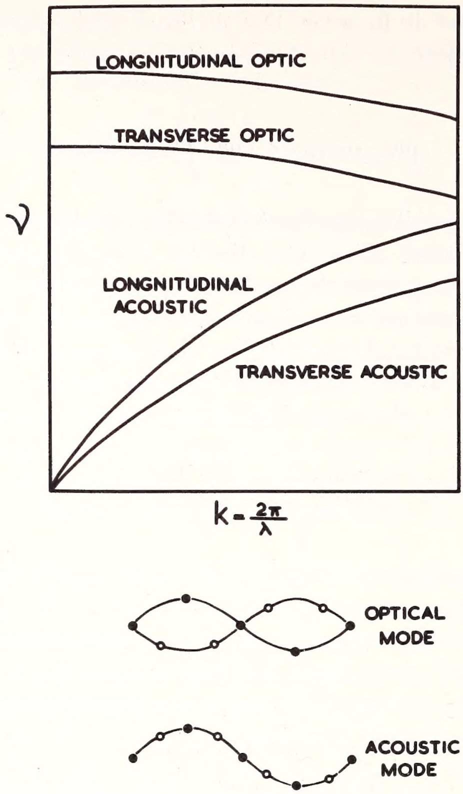

FIGURE 4. The dispersion curves of frequency ν versus wave vector $\mathbf{k}$ for a diatomic lattice such as sodium chloride. In an optic mode the displacement of the atoms leads to a net displacement of electric charge, but not in an acoustic mode. The transverse modes are doubly degenerate. Infrared spectroscopy can be used to determine the frequencies of ν_{LO} and ν_{TO} at $\mathbf{k}=0$.

acoustic and longitudinal acoustic waves for $\mathbf{k}=0$ may be measured by several different methods. In a polar crystal the form of the ν versus $\mathbf{k}$ curves near $\mathbf{k}=0$ are modified in the presence of electromagnetic radiation. Hence considerable caution must be exercised in describing an electromagnetic wave in a crystal, if the frequency of the radiation corresponds closely to some excitation frequency of the solid. The "mixture" of photon and phonon or photon and exciton must be considered together.

2.3. The Vibrations of Molecular Crystals

At first encounter the problem of classifying the vibrations of a molecular crystal containing perhaps a hundred atoms would appear to be a hopeless task. However in practice the problem is a tractable

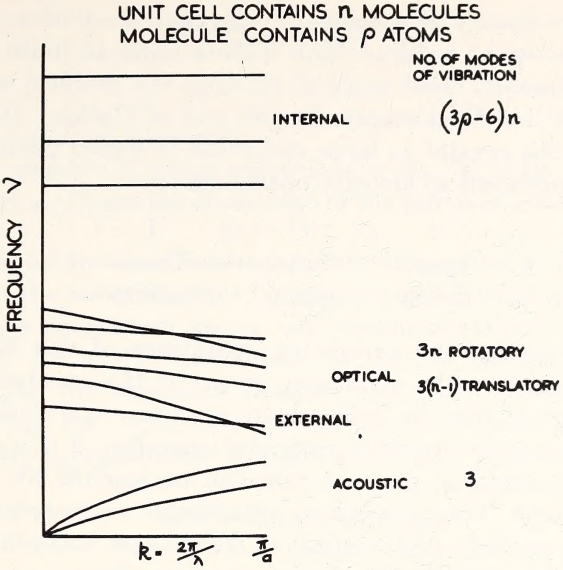

Figure 5. Schematic diagram of the dispersion curves for a molecular crystal containing n molecules each containing ρ atoms. The modes of vibration are divided into internal and external modes. In general the internal modes show little change of frequency ν with wave vector **k**.

one, as the forces between the atoms in a molecule are very much greater than the forces between the molecules, and hence a considerable simplification can be made in considering the vibrations of molecular crystals. We can distinguish between internal modes of vibration, i.e., intramolecular modes, and external modes of vibration, i.e., intermolecular modes, The latter involve the vibration of molecules with respect to one another. If the unit cell contains n molecules, each with ρ atoms, then the total number of modes of vibration is $3n\rho$. Of these $(3\rho-6)n$ are internal modes of vibration and $6n$ external modes of vibration. Of the latter $3n$ are rotatory in nature, $3(n-1)$ are translatory and 3 correspond to the motion of the unit cell as a whole—i.e., in the crystal they are acoustic modes. Dispersion curves for such a crystal are shown in figure 5. Thus for a unit cell containing 2 nonlinear molecules with 3 atoms each there would be 6 internal modes. Of the 12 external modes, 6 are rotatory, 3 translational optic and 3 translational acoustic. Each of the three internal modes will be observed as doublets if the interaction between the molecules is strong enough to lead to a measurable splitting. For unit cells containing linear molecules, rotation about the molecular axis need not be considered, and hence there are $(3\rho-5)n$ internal modes, $2n$ rotatory modes and $3(n-1)$ translatory modes and 3 acoustic modes.

In order to classify the modes of vibration $k=0$ of a crystal, the space group must be reduced from infinite order to finite order. The two most frequently used ways of tackling the problem are those of Bhagavantam and Venkatarayuda [10] and of Halford, [11, 12]. The former treat the crystal as large molecules in which primitive translations are equivalent to identity operations:

$$\begin{array}{ccccc} \mathrm{S} & = & \mathrm{U} & \times & \mathrm{I} \\ \text{space} & & \text{factor} & & \text{Trans-} \\ \text{group} & & \text{group} & & \text{lations} \end{array}$$

They then consider the symmetry operations of the factor group (which is defined as the symmetry group of the smallest unit from which the crystal may be built up by primitive translations) taking an atom as invariant under a particular operation if it is carried into an equivalent position, i.e., one that can be reached by a primitive translation alone. Thus the set of unreducible representations which are totally symmetric with respect to translation, according to one of which each normal mode transforms, are given by

$$\Gamma^{(v)}=\Gamma^{(s)}$$

The alternative method, due to Halford, is to consider the site symmetry of particular molecular groups and use correlation tables for the species of a group and its subgroups to determine the effect of the lattice on the vibrations of the isolated molecules. Since all the operations of the factor group can be obtained by taking all possible products of the operations contained in the site groups, the two methods give identical results and both have been used in the discussion of the spectra of various crystals.

The factor group defined above is situated at each lattice point of the Bravais cell of the crystal under consideration, and hence it is at the centre of the symmetric unit cell which is invariant under the point group isomorphic with the space group of the crystal. The corresponding reciprocal lattice in **k** space is also invariant under the same point group operating about one of its lattice sites. This site is at the centre of the Brillouin zone, where the group of the wave vector is that of the entire group. Thus a classification of the modes of the crystal are obtained by applying the above methods to the factor group. Other special points in the zone have lower symmetries, while general points have representations of the group of pure translations corresponding to the $\mathbf{k}=0$ vector in question.

A brief review of Bhagavantam and Venkatarayuda's method will now be given.

In the B and V method N_k, the number of times an irreducible representation Γ is contained in another representation, is given by

$$N_k=\frac{1}{N}\sum_j h_j\chi_k(R)\chi_j'(R)$$

where

N is the order of the group.
h_j is the number of group operations in the jth class.
$\chi_j(R)$ and $\chi_k(R)$ are the characters of the group operations Γ_i and Γ_k.

The normal modes are classified by a suitable choice of the representation Γ, and the selection rules for infrared and Raman are determined by using the translation vector and symmetric tensor representation respectively for Γ. If Γ ls defined by all $3N$ cartesian coordinates comprising all the degrees of freedom, the distribution of the normal modes among the symmetry species can be found by substituting the following expression for χ_j into the formula above for N_k:

$$\chi_j'(n_i)=\omega_R(\pm 1+\cos\phi_R).$$

Here ω_R is the number of atoms invariant under the operation R, and ϕ_R is the angle of rotation taking the signs $+ve$ for proper and $-ve$ for improper rotations.

The modes of vibration can be further classified as follows:
Acoustic modes: In the acoustic modes the unit cell moves as one unity, so in this case $\omega_R=1$ and

$$\chi_j'=\pm 1+\cos 2\phi_R.$$

This also gives the selection rules for infrared absorption, since the dipole moment transforms in the same way as for pure translations.
Translatory external modes: In this case we have

$$\chi(T')=[\omega_R(s)-1][\pm 1+\cos 2\phi_R]$$

where $\omega_R(s)$ is the number of structural groups which remain invariant.
Rotatory external modes: These transform as the angular momentum P, i.e.,

$$\chi(R')=\omega_R(s-p)\chi(p)$$
$$\chi(p)=1\pm 2\cos\phi_R$$

where $\omega_R(s-p)$ is the number of polyatomic groups which remain invariant. The monoatomic groups do not contribute since they have no rotational degrees of freedom. In the case of linear molecules or ions, there are only two degrees of freedom, and the character $\chi(p)$ for a rotation about the molecular axis is $\pm 2\cos\phi_R$ and that for rotations perpendicular to it is zero.

Internal modes: Finally the number of internal modes may be found by subtracting the sum of the acoustic, translatory and rotatory external modes from the total number. Where there are more than two structural groups, the number of internal modes due to each can be found by ignoring first one then the other. As shown previously, if there are n identical molecules in the unit cell then the total number of internal modes is $(3\rho-6)n$ if the molecules are non linear, but $(3\rho-5)n$ if they are linear.

The mean displacement of atoms in a particular vibrational state is of interest in the interpretation of observations of lattice dynamics by several different techniques [7], e.g. x-ray scattering. If the normal modes of vibration for different frequencies have been completely calculated using experimental data for the frequencies, then the mean-square displacements of the different atoms involved in any normal mode can be found. Thus the mean displacement of an atom in a diamond-type lattice due to the excitation of the single optical phonon of frequency ν_0 is given by

$$\langle r^2\rangle=\frac{h}{8\pi M\nu_0}$$

where M is the mass of the atom (e.g., C, Si, Ge, or Sn). Typical root-mean-square displacements are of the order of 0.01 Å to 0.1 Å.

3. Spectroscopic Methods

3.1. Fundamentals of Infrared Spectroscopy—Dielectric Parameters

A normal mode of vibration in a crystal gives rise to infrared absorption if the displacement of the atoms leads to the generation of a dipole moment. Usually it is the infrared absorption spectrum that is measured by a spectrometer; however, as absorption coefficients in the infrared are frequently very large, experimental difficulties arise in obtaining thin enough samples. In such cases it is frequently necessary to measure the reflection spectrum and then to calculate the dielectric parameters for the solid as described below Dielectric parameters are to be preferred to absorption coefficients or indices and to refractive indices because ϵ' and ϵ'' are much more readily compared with theory. Absorption coefficients due to one-phonon processes vary over as much a range as three orders of magnitude. Whereas a film only a fraction of a micrometre thick is necessary for the study of the single resonance in alkali halides, a crystal almost a millimetre thick is necessary to study absorption due to intermolecular vibrations in crystals containing nonpolar molecules.

A discussion will first be given of the various parameters that may be used to characterize the optical properties of solids and the relationship between them (see fig. 1). The optical properties of a crystal may be characterized by the complex refractive index

$$n^*=n-ik$$

where n is the refractive index and k the absorption index. Alternatively the complex dielectric parameter

$$\epsilon^*=\epsilon'-i\epsilon''$$

may be used. From Maxwell's electromagnetic theory

$$n^{*2}=\epsilon^*.$$

Hence

$$\epsilon'=n^2-k^2$$

$$\epsilon''=2nk$$

The absorption coefficient α is defined by the equation

$$I=I_0e^{-\alpha x}$$

where I_0 is the electromagnetic energy incident on the sample of thickness x, and I is the transmitted energy. α is related to the absorption index by

$$\alpha=4\pi k\nu$$

where ν is the wave number of the radiation.

The conductivity of a dielectric can be shown to be

$$\sigma=nk\nu=\frac{\epsilon''\nu}{2}.$$

The dielectric parameters are obtained from a study of the reflection spectrum of a crystal.

The reflected amplitude at normal incidence r is given by

$$r=\frac{n-ik-1}{n-ik+1}.$$

If the phase change on reflection is θ then

$$r=|r|\exp(i\theta).$$

Since $|r|=\sqrt{R}$, where R is the fraction of the energy reflected, this equation can be used to give values of n and k.

$$n = \frac{1-R}{1+R-2\sqrt{R}\cos\theta}$$

$$k = \frac{-2R\sin\theta}{1+R-2\sqrt{R}\cos\theta}.$$

A determination of the real part of the response of a system as a function of frequency can give, via the Kramer-Kronig relations, the imaginary part of the response of the system, and vice versa. The reflectivity function $R(\nu)$ and its associated phase $\theta(\nu)$ satisfy these conditions [13]. Thus if R is known as a function of frequency between $\nu=0$ and $\nu=\infty$, the value of $\theta(\nu)$ may be determined by an integral transform. The transform linking θ with R is

$$\theta_m = \frac{2\nu_m}{\pi}\int \frac{\mathrm{Log}\sqrt{R}d\nu}{\nu^2-\nu_m^2}$$

where ν_m is a given frequency at which the value of θ is required. In principle the reflection coefficient must be measured over an infinite frequency range. However, various approximations can be made so that usually only infrared measurements are required.

Classical dispersion theory provides the simplest approximation to an understanding of the optical and dielectric parameters in terms of the motion of the atoms in a crystal. Consider a set of particles of mass m and charge e each bound to a fixed centre by a force, where x is the particle displacement and ω_0 the natural vibration frequency. Suppose the effective electric field is F and γ is a damping constant; then the equation of motion is

$$m\ddot{x}+m\gamma\dot{x}+m\omega_0^2x=eF.$$

The solution is of the form

$$x = \frac{eF}{m}\,\frac{1}{\omega_0^2-\omega^2-i\gamma\omega}$$

If N is the number of particles per unit volume, then the polarization is Nex, and hence the dielectric parameter

$$\epsilon = 1+\frac{4\pi P}{3} = 1+\frac{4\pi Nex}{E}$$

as

$$F = E+\frac{4\pi}{3}P$$

also

$$\epsilon = \epsilon_\infty + \frac{4\pi NQ'^2}{\mu}\left(\frac{1}{\omega_0^2-\omega^2-i\omega\gamma}\right)$$

where Q' is the effective charge associated with the vibration

Hence
$$\frac{4\pi NQ'^2}{\mu\omega_0^2}=\epsilon_0-\epsilon_\infty=\frac{4\pi(\epsilon_0+2)^2z^2e^2}{9\mu\omega_0^2V_0}.$$

Let
$$\epsilon_0-\epsilon_\infty=4\pi\rho$$

so
$$\rho=\frac{NQ'^2}{\mu\omega_0^2}$$

$$\epsilon_\nu^*=n^{*2}=\epsilon_\infty+\frac{4\pi\rho\omega_0^2}{\omega_0^2-\omega^2-i\gamma\omega}$$

$$\epsilon_\nu'=n^2-k^2=\epsilon_\infty+\frac{4\pi\rho(\omega_0^2-\omega^2)\omega_0^2}{(\omega_0^2-\omega^2)^2+\gamma^2\omega^2}$$

$$\epsilon_\nu''=2nk=\frac{4\pi\rho\omega_0^2\gamma\omega}{(\omega_0^2-\omega^2)^2+\gamma^2\omega^2}.$$

The damping constant here has the dimensions of frequency, so that a reduced damping constant is defined such that $\gamma_0=\frac{\gamma}{\omega}$.

A quantum mechanical treatment of the vibrational frequencies of simple lattices such as the alkali halides leads to basically similar equations to those derived classically. Cowley [14] has shown that

$$\epsilon_\nu^*=\epsilon_\infty'+\frac{\nu_0^2(\epsilon_0'-\epsilon_\infty')}{(\nu_0^2-\nu^2)^2+2\nu_0[\Delta_\nu-i\Gamma_\nu]}$$

Hence

$$\epsilon_\nu'=\epsilon_\infty'+\frac{\nu_0^2(\epsilon_0'-\epsilon_\infty')[(\nu_0^2-\nu^2)+2\nu_0\Delta_\nu]}{[(\nu_0^2-\nu^2)^2+2\nu_0\Delta_\nu]^2+4\nu_0^2\Gamma_\nu^2}$$

$$\epsilon_\nu''=\frac{\nu_0^2(\epsilon_0'-\epsilon_\infty)2\nu_0\Gamma_\nu}{[(\nu_0^2-\nu^2)^2+2\nu_0\Gamma_\nu]^2+4\nu_0^2\Gamma_\nu^2}$$

As mentioned above, $\Gamma_\nu=\frac{\gamma_0\nu}{2}$ and consequently, according to classical theory, the damping "constant" is actually proportional to the frequency ν. Δ_ν represents a shift in frequency from the classical frequency ν_0 due to anharmonicity.

The variation of Γ_ν with frequency can be calculated from the experimentally determined quantities in the equation:

$$\Gamma_\nu=\frac{(\epsilon_0'-\epsilon_\infty')\nu_0\epsilon_\nu''}{2[(\epsilon_\nu'-\epsilon_\infty')^2+\epsilon_\nu''^2]}.$$

Expressions for Γ_ν and Δ_ν have been given by Cowley [14].

The real and imaginary parts of the dielectric parameter ϵ' and ϵ'' are related to one another. Thus if ϵ_ν'' is known for all frequencies then

ϵ'_ν can be calculated for any particular frequency using Kramer-Kronig equations

$$\epsilon'_{\nu_0}=\epsilon'_\infty+\frac{2}{\pi}\int_0^\infty\frac{\nu\epsilon''_\nu d\nu}{\nu^2-\nu_0^2}$$

$$\epsilon''_{\nu_0}=-\frac{2\pi\nu_0}{\pi}\int_0^\infty\frac{(\epsilon'_{\nu_0}-\epsilon_\infty)d\nu}{\nu^2-\nu_0^2}.$$

The first equation is especially valuable for calculating the zero frequency dielectric parameter ϵ'_0, which is usually referred to as the dielectric constant.

If ϵ'_∞ is taken as the dielectric parameter in the γ-ray region, where it is experimentally found to be very close to unity, then the equation can be written

$$\epsilon'_0-1=\frac{2}{\pi}\int\epsilon''_\nu d(\log\nu).$$

Hence if ϵ''_ν is measured throughout the electromagnetic spectrum and then plotted against the logarithm of frequency, the area under the curve is $\pi/2(\epsilon'_0-1)$. From this curve the effects on the dielectric constant ϵ'_0 of various vibrational or electronic processes may be readily appreciated.

The dielectric parameters are tensors and consequently it is essential to use polarized radiation when recording the infrared absorption and reflection spectra of all but cubic crystals. Thus, with an orthorhombic crystal the reflection has to be measured with the electric vector parallel to the *a*, *b*, and *c* axes. When obtaining the reflection spectra from the *bc* plane of a monoclinic crystal, it is necessary to rotate the plane of polarization of the electric vector.

The longitudinal optic frequency ν_{L0} can be found for $\mathbf{k}=0$ by noting that it is the frequency for which $\epsilon'=0$. It can be measured directly in cubic crystals by a method due to Berriman [15]. A thin film is deposited on a metal surface, and then the reflection spectrum is measured with an angle of incidence of about 30°, using infrared radiation plane-polarized with a component perpendicular to the film surface. A marked fall in the reflectivity occurs when $\epsilon'=0$ and gives the frequency of the longitudinal optic mode at $\mathbf{k}=0$.

If the low and high frequency limits, ϵ'_0 and ϵ'_∞, are known, then ν_{L0} may be calculated from a relationship first given by Lyddane, Sachs, and Teller [16]

$$\nu_{L0}=\left(\frac{\epsilon'_0}{\epsilon'_\infty}\right)^{1/2}\nu_{T0}.$$

This equation may be generalized for cubic crystals having infrared active vibrations as follows:

$$\prod_j^n\left(\frac{\nu_{L0}(i)}{\nu_{T0}(i)}\right)^2=\frac{\epsilon'_0}{\epsilon_\infty}.$$

A similar type of expression holds for the two principal dielectric parameters of uniaxial crystals.

3.2. Fundamentals of Raman Spectroscopy of Crystals—the Polarizability Tensor

Raman spectroscopy of crystals involves the inelastic scattering of photons. The energy lost or gained by the photons is used to create an annihilate phonons in the crystal. Annihilation of phonons can only occur if the phonon energy $h\nu_{vib}$ is not large compared with kT, as the phonon population has a temperature dependence of the form

$$\frac{1}{\exp\left(\frac{h\nu}{kT}\right)-1}.$$

Anti-Stokes components of the Raman spectrum are rarely detectable at normal temperatures for frequencies greater than about 800 cm^{-1}, i.e., phonon energies larger than about 100 millielectron volts.

The essential features of Raman spectroscopy can be understood using the following simplified argument [7]. Let α_{ij} be the electronic polarizability and q the displacement:

$$q=q_0e^{2\pi i\nu_{\mathrm{vib}}t}.$$

If monochromatic electromagnetic radiation of frequency ν_0 is applied:

$$E=E_0e^{2\pi i\nu_0t}$$

where E is the electric field. Then, since α_{ij} may be expanded as a power series as the polarizability changes with the vibrational motion of the atoms

$$\alpha_{ij}=\alpha_0+\alpha_1q+\alpha_2q^2+\ .\ .\ .$$

where

$$\alpha_1=\left(\frac{\partial\alpha_{ij}}{\partial q}\right)_0 \textit{and } \alpha_2=\left(\frac{\partial^2\alpha_{ij}}{\partial q^2}\right)_0.$$

We then get an induced dipole moment M with a component:

$$M=\alpha_1q_0E_0e^{2\pi i(\nu_0\pm\nu_{\mathrm{vib}})t},$$

which leads to Raman radiation at frequencies $\nu_0\pm\nu_{vib}$.

The terms α_1 then give rise to one phonon processes; in order to account for second-order Raman scattering, which involves the creation or destruction of two phonons, α_2 must be considered.

In general α_{ij} is a tensor with components that may be measured using polarized radiation

$$\begin{bmatrix} \alpha_{xx} & \alpha_{xy} & \alpha_{xz} \\ \alpha_{yx} & \alpha_{yy} & \alpha_{yz} \\ \alpha_{zx} & \alpha_{zy} & \alpha_{zz} \end{bmatrix}$$

Relative values of α_{ij} have been listed by Loudon [17] for the Raman-active modes of vibration of crystals of different point groups. For example, for an orthorhombic crystal with point group D_{2h}, the polarizability tensors take the following form for the Raman-active modes of symmetry A_g, B_{1g}, B_{2g}, B_{3g}.

$$\begin{array}{cccc} Ag & B_{1g} & B_{2g} & B_{3g} \\ \begin{bmatrix} a & & \\ & b & \\ & & c \end{bmatrix} & \begin{bmatrix} & d & \\ d & & \\ & & \end{bmatrix} & \begin{bmatrix} & & e \\ & & \\ e & & \end{bmatrix} & \begin{bmatrix} & & \\ & & f \\ & f & \end{bmatrix} \end{array}.$$

Consequently by measuring α_{ij} using polarized radiation the symmetries of the vibrational modes corresponding to different Raman lines can be identified. Thus only α_{xx}, α_{yy}, α_{zz} are finite for A_g modes and α_{yx}, α_{xy} for B_{1g} modes.

A rigorous analysis of Raman scattering from a crystal has been given by Cowley [18], who has obtained the following results. The intensity of Raman scattering per unit solid angle is given by the expression

$$I=\frac{8\pi\nu_0^4}{2c^3}\sum_{\alpha\beta\gamma\delta} n_\alpha n_\beta I_{\alpha\beta\gamma\delta} E_\gamma E_\delta,$$

in which the polarization of the electric vectors of the scattered radiation is defined by the unit vector **n** and the electric vector of the radiation by **E**. Further

$$I_{\alpha\beta\gamma\delta}=\sum_{V'} < V|P^*_{\alpha\gamma}|V' > < V'|P_{\beta\delta}|V > \delta\left(\nu-\frac{E_\nu-E_{\nu'}}{h}\right)$$

where the operators for the optical polarizability tensor are designated by P, and the change in frequency of the radiation by ν. The expression is taken over a thermal average of all the initial states V'.

The line profile, of the scattered Raman radiation has been shown by Cowley[18] to be

$$I_{\alpha\beta\gamma\delta}=\frac{1}{2\pi}\,\frac{1}{[\exp\,(h\nu/RT)-1]}\,\frac{\sum P^*_{\alpha\gamma}P_{\beta\delta}\,\nu_0^2\Gamma_\nu}{\{\nu_0^2-\nu^2+2\nu\Delta_\nu\}^2+4\nu_0^2\Gamma_\nu^2}$$

Hence the line profile for Raman scattering is of the same general form as found for the imaginary part of the dielectric parameter ϵ'' found by infrared spectroscopy.

The term Brillouin scattering[6] is used to denote scattering involving acoustic modes in solids or liquids. For the Stokes component of the scattering the fractional shift in the frequency of the radiation is

$$\frac{\Delta\nu}{\nu}=\frac{2nV}{c}\sin\frac{\theta}{2},$$

where θ is the angle between the direction of observation and the original direction of propagation of light, n is the refractive index, V is the velocity of propagation of the acoustic phonon, i.e., the sound velocity, and c is the velocity of electromagnetic radiation. As V/c is small ($\sim 10^{-5}$), Brillouin shifts are only of order of 1 cm^{-1}, and hence a good Fabry-Perot spectrometer is needed for the observation of the frequency shift. In general for a solid there are three acoustic branches for a single direction of propagation and consequently three Stokes and three anti-Stokes components. However, in a liquid there is only one velocity, as transverse waves cannot be propagated through liquids, except perhaps for very short wavelengths. From a measurement of the velocity of acoustic waves the elastic constants can be deduced.

3.3. Selection Rules

The selection rules for infrared absorption and Raman scattering in crystals can be derived by taking into consideration

(a) conservation of energy,
(b) conservation of momentum or wave vector, and
(c) the magnitude of the transition moments.

In infrared absorption (a) leads to the requirement that in a one-phonon process the photon energy must equal the energy of the phonon that is created. Since the wavelength of infrared radiation or visible radiation used for Raman spectroscopy is very large compared with the dimensions of a unit cell, we can effectively set the wavevector of the electromagnetic radiation to zero. Consequently, in a one phonon process in both infrared and Raman spectroscopy only long-wavelength vibrations are excited, i.e., those for which $\mathbf{k}=0$. In two phonon processes in both infrared and Raman spectroscopy we must have

$$\mathbf{k}_1+\mathbf{k}_2=0$$

where $\mathbf{k}_1$ and $\mathbf{k}_2$ are the phonon wave vectors. Consequently the transitions are not confined to $\mathbf{k}=0$ but to any value of $\mathbf{k}$, provided that the equation above holds. Two-phonon processes then call for a consideration of the combined density of vibrational states in which the number of modes of vibration are computed taking the branches of the dispersion curves in pairs for a common **k** value.

In a two phonon process which involves an internal mode of vibration for which the frequency ν varies very little with wavevector, the combined density of states approximates—at least in a cubic crystal—to the density of vibrational states spectrum. This is important for a discussion of the absorption that occurs on the high and low frequency sides of many absorption lines due to internal modes.

From the above discussion it is clear that when $d\nu/dk$, or more rigorously, when $\nabla_k\nu$ is either zero or has a slope discontinuity, there are likely to be slope discontinuities in the combined density of states, which may be reflected in infrared and Raman spectra involving two phonon processes. Points in the Brillouin zone where each of the components of $\nabla_k\nu=0$ are known as critical points.

The intensity of infrared absorption or Raman scattering depends upon the matrix elements $|M^{VV'}|$ and $|\alpha_{ij}^{VV'}|$. For infrared absorption the transition moment is:

$$|M^{VV'}|^2=\int \psi_V M(\mathrm{q})\psi_{V'}d\tau$$

where

$$M(\mathrm{q})=m_0q_0+\sum_{ij} m_{ij}q_iq_j+\sum_{ijk} m_{ijk}q_iq_jq_k.$$

For Raman scattering we must consider the matrix elements

$$[\alpha_{ij}^{VV'}]=\int \psi_V\alpha_{ij}\psi_{V'}d\tau=\alpha^0_{ij'}\int \psi_V\psi_{V'}d\tau$$
$$+\sum\frac{\partial\alpha_{ij}}{\partial q}\int\psi_V q\psi_{V'}d\tau+\sum\frac{\partial\alpha_{ij}}{\partial q_i\partial q_j}\int\psi_V q_iq_j\psi_{V'}d\tau$$

As $\int\psi_V\psi_{V'}d\tau$ is zero, the intensity of first-order Raman scattering depends upon

$$\left|\frac{\partial\alpha_{ij}}{\partial q}\right|^2\left|\int\psi_V q_i\psi_{V'}d\tau\right|^2.$$

As in the case of isolated molecules the activity—infrared or Raman—requires the evaluation of $\int\psi_V \mathrm{q}\psi_{V'}d\tau$. In general, numerical solutions are not possible; however, by using symmetry considerations and group theoretical methods, the various modes can be assigned as infrared or Raman active, although the intensities cannot be calculated.

3.4. Effect of Temperature and Pressure on Spectra

The infrared and Raman spectra of crystals are frequently strongly temperature dependent. A reduction in temperature results in the freezing out of thermal phonons and hence to the disappearance of the two-phonon transitions which involve the annihilation of thermal phonons. As a consequence of reduction by cooling of the number of processes available for phonon-decay, damping factors Γ_ν are decreased, and absorption lines are usually considerably sharper at low temperatures. Lattice spacings usually decrease on cooling, and hence force constants are increased and with them vibrational frequencies. Similarly an increase in pressure invariably leads to the raising of frequencies. Such temperature and pressure information is particularly valuable in studies aimed at the understanding of intermolecular forces, as the variation of frequencies with intermolecular distances may be deduced.

Perhaps the most interesting type of changes in infrared and Raman spectra are those which accompany changes of phase. Changes in both infrared and Raman spectra can be followed with comparative ease. As the structure changes so do selection rules; these can be correlated with the two crystal structures involved. Small changes in molecular or site symmetry or the onset of hindered rotation can be detected.

Many materials have a low-frequency mode of vibration which is strongly temperature-dependent, and the study of these is adding much to our understanding of ferroelectric transitions [19, 20, 21]. A ferroelectric crystal is one which has a spontaneous electric dipole moment. Usually the dielectric constant as measured at low frequencies has a high value and a temperature dependence of the following type:

$$\epsilon_0' = \frac{c}{T-T_c}.$$

In certain crystals the ferroelectricity results from a low-frequency vibration becoming unstable as the temperature approaches the ferroelectric transition temperature T_c. As shown above

$$\epsilon_0' = 1 + \frac{2}{\pi}\int \frac{\epsilon'' d\nu}{\nu}$$

Hence if one of the vibrational frequencies changes with temperature, the value of ϵ'_0 will alter if ν for the mode approaches zero. It is usually found that $\nu^2 \sim (T-T_c)$.

3.5. Instrumentation

Infrared and Raman spectrometers have been available commercially for many years and have been developed to the stage where the recording of spectra is virtually automatic. Most of the labour now involved in obtaining spectra lies in sample preparation, e.g., in growing suitable crystals and determining the principal axes so as to enable spectroscopic studies to be correlated with the structure.

Most infrared spectrometers [22] employ a blackbody source and use a grating monochromator with filters to cut out overlapping orders. Good detectors are available for whole infrared regions. Nonselective types such as thermopiles and Golay detectors are usually incorporated into commercial instruments. Performance can be improved by using cooled photoconductive detectors, but these are frequency selective and only function over comparatively narrow spectral ranges.

Nearly all commercial infrared spectrometers are of the double beam type and produce a record on preprinted paper of the percentage transmission as a function of frequency. A good general purpose spectrometer will enable infrared spectra to be obtained between the limits 200 cm^{-1} to 4000 cm^{-1}, with a resolution better than 0.5 cm^{-1} and a signal to noise ratio exceeding 50/1. In such an instrument grating and filter changes are automatic. Polarizers of the wire grid type are now available to permit the recording of polarized spectra throughout the infrared region. For the study of the absorption spectra of small crystals or polymers, microilluminators have been developed which enable infrared spectra to be obtained from areas as small as 1 mm by 0.1 mm. The beam condensors that are used are usually of the reflecting microscope type.

One of the most important developments in infrared spectroscopy in recent years has been the opening up of the far infrared region (i.e., approximately from 5 cm^{-1} to 200 cm^{-1}) for routine studies. This frequency range is very important, as most intermolecular vibrational frequencies occur within it. Spectroscopy in this region suffers from the difficulty that there are as yet no readily tunable monochromatic sources, and blackbody radiation in this range is weak. Hence, it is essential that the form of spectrometer should have a high efficiency interferometers of the Michelson type [23, 24] are now commercially available for work in the far infrared region. In these interferometers, radiation of all frequencies passed by a filter falls simultaneously on the detector, instead of successively as in conventional monochromators. On scanning the movable reflector, an interferogram $I(x)$ is produced from which it is possible to obtain the spectral intensity $G(\nu)$ by means of a Fourier transformation

$$G(\nu)=\int I(x)\cos(2\pi\nu x)dx.$$

The actual computation is usually carried out using a digital computer. If the distance moved by the scanning mirror is l, then the resolution is given by $\Delta\nu \sim 1/2l$ thus if $l = 5$ cm then $\Delta\nu \sim 0.1$ cm^{-1}. Even at liquid-helium temperature very few intrinsic absorption bands in solids are narrower than 1 cm^{-1}; hence reliable measurements can now be made on band contours throughout the infrared region.

The power of Raman spectroscopy has been radically improved by the introduction of lasers as sources. These, combined with double monochromators with very low scattered-light factors and extremely sensitive photomultipliers, now make it routinely possible to obtain good resolution Raman spectra with high signal-to-noise ratios from comparatively small specimens, e.g., crystals weighing a few milligrams. This is largely due to the high radiation density which can be produced in the specimen. In view of the fact that the beam is narrow and parallel, accurate polarization measurements are now possible. Further, the beam geometry is such that the recording of Raman spectra at variable temperatures and pressure are much facilitated. Although ionised argon lasers (Green line 5145 Å, 19,440 cm^{-1}) are being used for Raman spectroscopy, most work so far done has been with continuous He/Ne lasers with power outputs between 25 and 100 milliwatts. This type of laser provides a highly monochromatic source at 15,800 cm^{-1} (6238 Å). It is usual with many samples to obtain Raman spectra as close as 30 cm^{-1} to the exciting line. The red source enables many coloured samples to be examined, as absorption by most coloured compounds is less for red light than for blue or green. The output from these lasers is plane polarized, and hence a quarter wave plate is necessary to rotate the plane of polarization through 90°. A piece of polaroid is adequate as an analyser; however, in view of grating polarization, it is essential that a circular polarizer should be placed in the path of the Raman radiation between the analyser and the monochromator.

4. Experimental Studies on Specific Systems

The general principles just developed will now be applied to some specific systems. No attempt will be made to give a complete review of all studies that are worthy of notice. Here we discuss some examples that illustrate the type of work that has been carried out on a very wide range of materials. In some cases the studies give information about the frequencies and types of vibration. In other cases the data is used to reveal changes in molecular configuration.

4.1. Classification of Crystalline Solids

It would be very convenient for a discussion of the properties of crystals if a satisfactory classification of different crystal types existed which would bring together those with similar physical properties. The following frequently used classification distinguishes between different types of crystals: molecular, covalent, ionic, and metallic.

Unfortunately such a division is of limited value for classification purposes, as in many crystals bonding of an intermediate character is found, and in others different types of bonding operates between different constituent atoms. Thus the semiconductors silicon and germanium are transitional cases between covalent solids and metals. Silicon carbide is borderline between covalent and ionic. Calcite, $CaCO_3$ has both molecular and ionic character.

However, the classification does have the advantage that the prototypes do show quite distinct physical properties. From the point of view of the infrared and Raman properties of these main divisions, metals represent the only group whose vibrational spectra cannot be studied. As the emphasis in this review is on molecular crystals, only brief mention will be made to pure covalent crystals such as silicon. Ionic crystals warrant much further discussion in view of the importance of molecular ions in many inorganic systems.

A further classification is according to the space group of the crystal, and as already seen, a knowledge of this together with the number of atoms in the unit cell leads immediately by group theoretical methods to a classification of the activity—infrared or Raman—of the different modes of vibration. In the following discussion the representations to which the modes of vibration belong are listed by Γ. (IR) and (R) indicate infrared and Raman activity respectively, and (F) means forbidden. The notation $\perp$ or $\|$ means that the infrared transition is perpendicular or parallel to the optic axis of the crystal. The acoustic modes are not included.

4.2. Elemental Covalent Crystals

The group IVb elements, carbon (diamond), silicon, and germanium form covalent cystals with the diamond structure and as such may be considered as giant molecules. The symmetry of the unit cell is such that no one phonon absorption should be observed in the infrared, and consequently thin slabs of the pure crystals are essentially transparent over most of the infrared region. As the oscillator strength $|M^{VV'}|^2$ is effectively zero, the transverse optic and longitudinal optic modes are degenerate at the zone centre. They are Raman active and the Raman spectra of diamond, silicon, and germanium are known. As pointed out previously, a knowledge of this frequency together with the mass of the atom enables the root-mean-square amplitude of the atoms in this mode of vibration to be calculated.

4.3. Ionic Crystals

Ionic crystals have played a very important role in the development of studies relating infrared and Raman spectra to lattice dynamics. This has resulted experimentally from the availability of many crystals of good optical quality. From the point of view of theory, the comparative simplicity of the structure of crystals such as the alkali halides and alkaline earth fluorides permits the calculation of reliable phonon dispersion curves.

Oscillator strengths in ionic crystals are usually high; hence it is essential that the infrared reflection spectra should be measured and the dielectric parameters determined, rather than attempting to obtain the absorption spectra of powdered material.

a. NaCl Type

All the alkali halides have this structure with the exception of CsCl, CsBr, and CsI, which have the CsCl structure. The space group is O_h, there is one formula unit/unit cell and the selection rule is $\Gamma = F_{1u}(\mathrm{IR})$.

There are six branches to the phonon dispersion curves. Three are acoustic branches and three optic. The longitudinal optic and doubly degenerate transverse optic mode frequencies at $\mathbf{k}=0$ are split by an amount which depends on the oscillator strength associated with the F_{1u} vibration. Only the ν_{TO} at $\mathbf{k}=0$ is infrared active, and extensive studies have been made by many workers [9, 20] on the absorption and

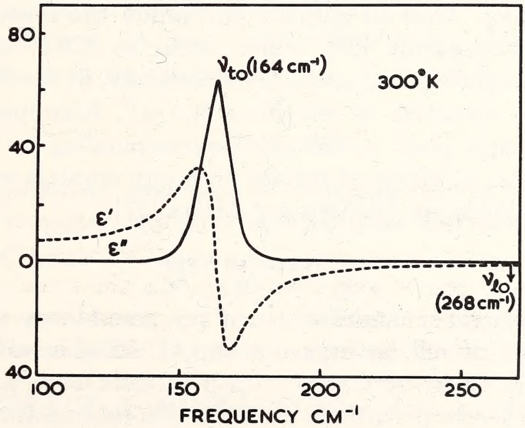

FIGURE 6. The dielectric parameters ϵ' and ϵ'' for sodium chloride in the region of the resonance due to the excitation of the transverse optical mode at $\mathbf{k}=0$, which has a frequency of 164 cm⁻¹. The frequency for which $\epsilon'=0$ (268 cm⁻¹) gives the frequency of the longitudinal optic mode at $\mathbf{k}=0$.

reflection spectra in order to obtain the dielectric parameters ϵ' and ϵ'' and to connect these with the properties of the lattice. The dielectric parameters for NaCl are illustrated in figure 6. Much current interest now centres on the calculation of Γ_ν, the frequency and temperature-dependent damping factor which is an inverse measure of the lifetime of the phonon and which depends essentially upon the rate at which the TO phonons are converted into two phonons.

The second-order Raman scattering involves two phonon processes [7]. These, like the two phonon absorption in the infrared, extend over a wide frequency range, as transitions may occur for any value of the wavevector **k** provided that:

$$\mathbf{k}_1 \pm \mathbf{k}_2 = 0.$$

Many other crystals with the NaCl structure besides the alkali halides have been studied by infrared spectroscopy [9], e.g., AgCl, AgBr, TlCl, TlBr, MgO, CaO, PbS, PbTe, NiO.

b. Zinc Blende Type

Many crystals have this structure. There is one formula unit/unit cell having space group T_d^2 with $\Gamma = F_{2u}(\mathrm{IR})$. They differ from the alkali halides in that each ion is surrounded by four not six near neighbours. There is no centre of inversion, so that although the phonon dispersion curves have generally the same form as those for NaCl type lattices, the selection rules are now different. The $\mathbf{k}=0$ transverse optic mode is strongly infrared active and is also Raman active. As the crystal is piezoelectric the $\mathbf{k}=0$ longitudinal optic mode is Raman active. Thus in gallium phosphide the most intense lines in the Raman spectrum [25], which occur at 366.5 cm^{-1} and 403.8 cm^{-1}, give the values of ν_{TO} and ν_{LO} respectively, at $\mathbf{k}=0$. In the infrared absorption spectrum of thin films of GaP, Kleinman and Spitzer [26] found a single peak at 366 cm^{-1}, corresponding to the excitation of the ν_{TO} mode. A review of results on many crystals with this structure has been given by Gielisse and Mitra [27].

c. Wurtzite Type

This is a hexagonal modification of the zinc-blende type with two formula units/unit cell and space group C_6^4. The selection rules are:

$$\Gamma = A_1(\mathrm{IR}, \|, \mathrm{R}) + 2B_1(F) + E_1(\mathrm{IR}, \perp, \mathrm{R}) + 2E_2(\mathrm{R}).$$

The most important crystals with this structure are II–VI compounds such as ZnO, CdS, and CdSe [28]. The wurtzite structure is a slightly distorted zinc blende structure in which the change in nearest and next-nearest neighbour distances is small, and consequently the anisotropy is small. There are 12 phonon branches, of which three are acoustic. Of the nine optical branches there is one A, and a doubly degenerate E mode, which is both Raman and infrared active, two doubly degenerate E_2, which are Raman active only, and two inactive B_1 modes.

Dispersion curves for CdS have been calculated by Birman [29] using a mixed valence-coulomb force field. At 77 °K CdS shows a strong enhancement of the Raman spectrum [30] recorded with an ionised argon laser, as the exciting line is close to the absorption edge and consequently a Resonance Raman effect occurs.

d. Cinnibar (HgS)

This form of mercuric sulphide has three formula units in a hexagonal unit cell of symmetry D_3^4. Hence there should be eighteen branches to the phonon dispersion curves, and:

$$\Gamma = 2A_1'(\mathrm{R}) + 3A_2''(\mathrm{IR}, \|) + 5E'(\mathrm{IR}, \perp, \mathrm{R})$$

The Raman active A_1' modes occur at 43 cm^{-1} and 256 cm^{-1}, whilst the A_2'' modes that are infrared active are at 36, 102, and 336 cm^{-1}. The E' type vibrations are found at 83, 82, 100, 280 and 343 cm^{-1} in the infrared and at 72, 88, 108, 282, and 343 cm^{-1} in the Raman spectrum. There are also Raman peaks at 202, 290, and 351 cm^{-1}.

As there is no centre of inversion in the unit cell, the longitudinal optic modes would be expected to be Raman active. Presumably the 290 cm^{-1} and 351 cm^{-1} peaks are LO modes. The measurement of the polarizability tensor for the crystal is complicated by the fact that cinnibar has a very high optical rotatory power. The Raman spectrum is enhanced by resonance when using red He/Ne laser excitation, as the exciting line frequency is very close to the absorption edge of HgS.

e. Fluorite Type

The most commonly encountered members of this group are the alkaline-earth fluorides. All have one formula unit in a unit cell of space group O_h^5 with

$$\Gamma = F_{1u}(\mathrm{IR}) + F_{2g}(\mathrm{R}).$$

There are nine branches to the phonon dispersion curves. LO_1 and TO_1 are split at $\mathbf{k}=0$ by an amount which depends on the oscillator strength of the ν_{TO} vibration. LO_2 and TO_2 are degenerate at $\mathbf{k}=0$. The infrared active mode involves the vibration of the metal ions against the cage of surrounding anions. ν_{TO} is strongly infrared active and strong reflection occurs in the far infrared between the TO and LO frequencies. TO_2 and LO_2 are Raman active for $\mathbf{k}=0$. Crystals of this type which have been studied include CaF_2, SrF_2, BaF_2, CdF_2, PbF_2, $SrCl_2$, and UO_2 [31].

f. Quartz

SiO_2 has 3 formula units/unit cell of space group D_3. Hence there are 27 branches to the phonon dispersions, which have recently been calculated by Elcombe [33]

$$\Gamma = 4A(\mathrm{R}) + 4B(\mathrm{IR}, \parallel) + 8E(\mathrm{IR}, \perp)$$

The infrared [32] and Raman spectra of quartz have been recorded by several workers as a function of temperature. Recently a detailed Raman study has been carried out as a function of temperature from 77 °K to 888 °K, and was directed towards elucidating the nature of $\alpha \rightarrow \beta$ quartz transition which occurs at 846 °K. The α phase has symmetry D_3 whilst the high temperature form (β-quartz) has symmetry D_6.

$$\Gamma = A_1 + 3B_2 + 2A_2 + 2B_1 + 4E_1 + 4E_2$$

$$4A_1 \rightarrow A_1 + 3B_2,\ 4A_2 \rightarrow 2A_2 + 2B_1,\ 8E = 4E_1 + 4E_2$$

Shapiro [34] et al., have shown that the line at 147 cm^{-1} increases in intensity and decreases in frequency as the transition temperature is approached. A logarithmic plot for this line shows that $\nu^2 \sim (T - T_c)^{1/2}$, which is quite different from the form $\nu^2 \sim (T - T_c)$ for ferroelectric modes. A definitive identification of the 147 cm^{-1} band has not as yet been made.

From a Raman spectroscopy [35] point of view, quartz is interesting in that several longitudinal modes are strongly active and their frequencies agree well with the positions for $\epsilon' = 0$ determined from an infrared analysis of the reflection spectra.

g. Rutile (TiO_2)

This structure has two formula units/unit cell of space group D_{4h}. In MgF_2, for example, the magnesium ions are located at sites with D_{2h} symmetry and fluorine ions occupy sites having C_{2v} symmetry.

$$\Gamma = A_{1g}(\mathrm{R}) + A_{2g}(\mathrm{F}) + A(_{2u}(\mathrm{IR}, \parallel)$$

$$+ B_{1g}(\mathrm{R}) + B_{2g}(\mathrm{R}) + 2B_{1u}(\mathrm{F}) + E_g(\mathrm{R}) + 3E_u(\mathrm{IR}, \perp).$$

Thus in the infrared three resonances occur with the electric vector of the radiation perpendicular to the c axis and one with the electric vector parallel to the c axis [36]. The Raman active modes have been identified [37] and assigned to A_{1g}, E_g, B_{1g}, and B_{2g} by determining the form of the polarizability tensor. Dispersion curves ν versus $\mathbf{k}$ have been calculated for MgF_2 using a rigid ion model and adjusting force-constant parameters and the effective charge on the ions to give the best fit with experimentally observed values.

Other crystals with this structure that have been studied include ZnF_2, FeF_2, and MnF_2 [37].

h. Brucite and Portlandite

$Mg(OH)_2$ and $Ca(OH)_2$ have one formula unit/unit cell which has space group D^3_{3d}. In this structure layers of hydroxide ions are separated by layers of Ca^{++} or Mg^{++} ions.

$$\Gamma = A_{1g}(\mathrm{R}) + A_{1u}(\mathrm{F}) + A_g(\mathrm{F}) + 2A_{2u}(\mathrm{IR}, \|) + 2E_g(\mathrm{R}) + 2E_u(\mathrm{IR}, \perp).$$

Of these A_{1g} and one A_{2u} correspond to internal modes, and the rest involve external modes [38], i.e.,

$$A_{2u}(\mathrm{IR}, \|) + 2E_g(\mathrm{R}) + 2E_u(\mathrm{IR}, \perp)$$

The values of the infrared measured frequencies are $Mg(OH)_2$—361 ($\perp$), 416 cm^{-1} ($\perp$) and 461 cm^{-1} ($\|$), and for $Ca(OH)_2$—288 cm^{-1} ($\perp$), 373 cm^{-1} ($\perp$) and 334 cm^{-1} ($\|$). The 416 cm^{-1} and 373 cm^{-1} bands are assigned to rotatory modes of the hydroxyl ion and the others to translatory motion (see fig. 7).

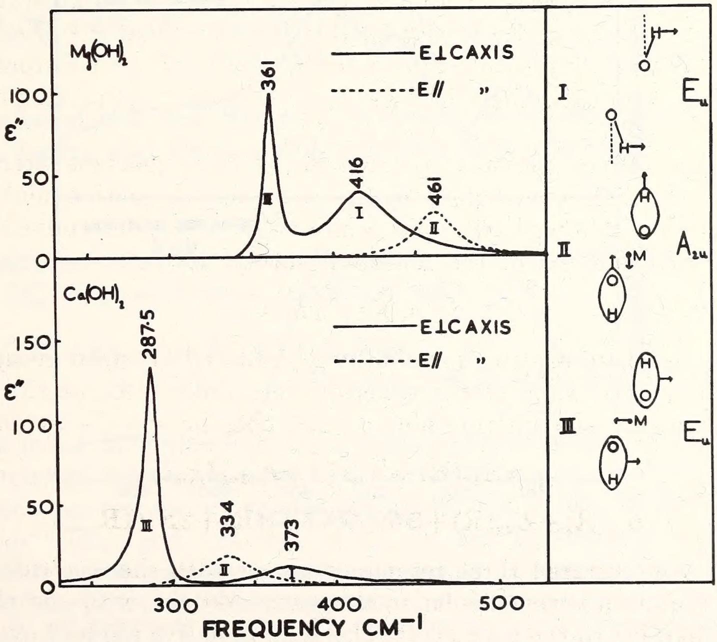

FIGURE 7. The dielectric parameters ϵ'' for $M_g(OH)_2$ and $Ca(OH)_2$ measured parallel and perpendicular to the c axis of the crystals. The assignments of the corresponding modes are designated I, II and III.

On either side of the infrared absorption due to the O—H stretching vibration, observed with direction of propagation of the radiation along the crystal *c* axis, are two broad absorption bands. The low frequency absorption disappears on cooling to liquid helium temperature. This is a example of an internal mode of vibration combined with an external mode of vibration. As discussed previously, since the wave vector $\mathbf{k}$ may have any value in the Brillouin zone such that $\mathbf{k}_{\mathrm{int}} \pm \mathbf{k}_{\mathrm{ext}} = 0$, and as there is little dispersion for the internal O—H vibration, the absorption might be expected to approximate to partial density-of-states spectum.

Figure 8 shows a comparison of the infrared absorption on the low frequency side of the internal O—H stretching frequency compared with the neutron scattering data of Pelah et al. [39]. In the neutron-spectrum the scattering is mainly from the hydrogen atoms. However, the spectra might be expected to be comparable, as the hydrogen atom in the hydroxyl ion is almost exclusively involved in the rotatory motion due to its small mass compared with oxygen, and of course, in

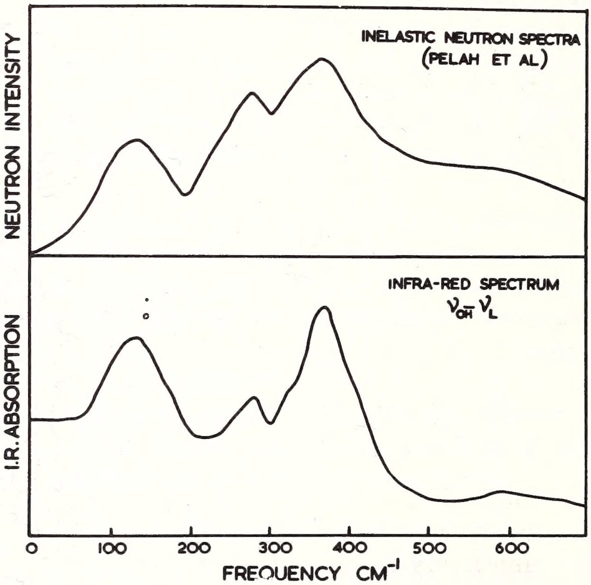

FIGURE 8. A comparison of the inelastic neutron scattering spectrum of $Mg(OH)_2$ with the infrared absorption spectrum measured with the electric vector of the radiation propagating along the *c* axis. The infrared absorption for the lattice vibrations are observed in combination with the O—H stretching vibration and $\nu_{OH} - \nu_L$ is plotted. The marked similarity results from the fact that all the lattice modes lead to a movement of the hydrogen atoms which are principally responsible for the neutron scattering.

translatory motions it has the same motion as that of the hydroxyl ion as a whole.

Recently Oehler [40] has calculated the dispersion curves for $Ca(OH)_2$ and $Mg(OH)_2$, using the frequencies of the external modes given above and has compared his results with the combination bands which occur in the 3600 cm^{-1} region. The agreement is satisfactory, and clearly shows that the assignment of the "wing" absorption is essentially correct.

i. LaF_3

There are six formula units in the unit cell of symmetry D_{3d}^{4}.

$$\Gamma = 5A_{1g}(\mathrm{R}) + 12E_g(\mathrm{R}) + 6A_{2u}(\mathrm{IR}, \| c) + 11E_{1u}(\mathrm{IR}, \perp c).$$

Raman spectra [41] have been reported for LaF_3, CeF_3, PrF_3, and NdF_3 all of which have this structure.

j. $LaCl_3$

Lanthanum chloride crystallizes in a hexagonal dipyramidal type of unit cell of space group C_{6h}^{2}, with two formula units/unit cell. The La^{3+} ions have site symmetry C_{3h} and Cl^- site symmetry C_s.

$$\Gamma = 2A_g(\mathrm{R}) + 2B_{2u}(\mathrm{F}) + 6E_g(\mathrm{R}) + 6E_{1u}(\mathrm{IR}, \perp) \\ + 2A_u(\mathrm{IR}, \perp) + 2B_u(\mathrm{F}) + 2E_{1g}(\mathrm{R}) + E_{2u}(\mathrm{IR}, \perp).$$

The infrared [42] and Raman [43] spectra have been measured for $LaCl_3$, $LaBr_3$, and $PrCl_3$, which have the same structure.

k. KHF_2

Potassium bifluoride has a tetragonal unit cell belonging to space group D_{4h}^{14} with two formula units/unit cell.

$$\Gamma = A_{1g}(\mathrm{R}) + 2A_g(\mathrm{F}) + B_{1g}(\mathrm{R}) + B_{2g}(\mathrm{R}) \\ + 2E_g(\mathrm{R}) + A_{1u}(\mathrm{F}) + 2A_{2u}(\mathrm{IR}, \|) + B_{1u}(\mathrm{F}) + 4E_u(\mathrm{IR}, \perp).$$

The linear bifluoride ions lie in planes perpendicular to the c axis. The external modes expected in the infrared are A_{2u} and $2E_u$, both of which are translatory modes and occur (fig. 9) at 146 cm^{-1} (A_{2u}) 130 cm^{-1} (E_u) and 174 cm^{-1} (E_u). In the low-frequency Raman spectrum one B_{1g} mode of a rotatory nature is expected and two E_g modes, one of which is rotatory and the other translatory. Mathieu [44] has reported a Raman line at 100 cm^{-1}, and as this has also been observed by neutron scattering [45], it would appear to be a translatory mode, as a rotatory mode would not involve an appreciable motion of the hydrogen atoms, which are the predominant scatterers in

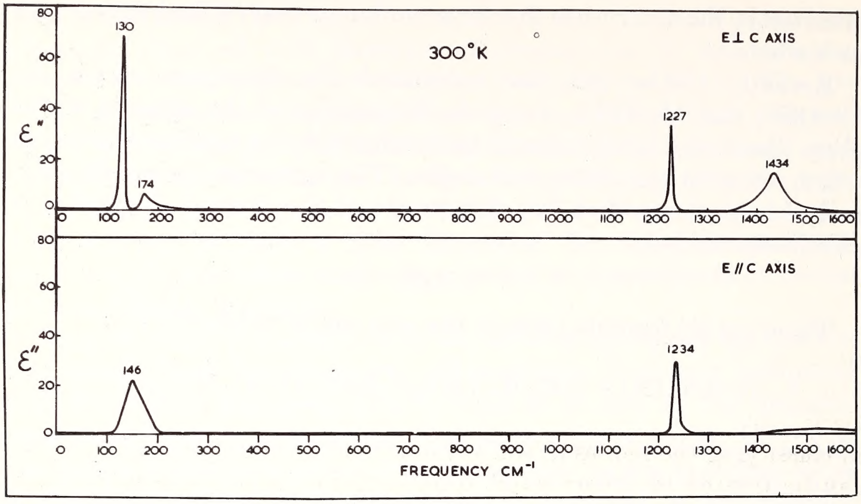

FIGURE 9. The dielectric parameter ε'' for potassium bifluoride KHF_2 measured with the electric vector parallel and perpendicular to the *c* axis of the crystal. The high frequency resonances are due to the internal modes of the bifluoride ion. The 1434 cm^{-1} band is the antisymmetric stretching mode whilst the degenerate bending mode which involves the off-axis motion of the hydrogen atom is split by the crystal field—the frequencies being 1227 (⊥) and 1234 cm^{-1} (||). The low-frequency modes involve the motion of the bifluoride ion with respect to the potassium ion.

the neutron spectrum. A line at 140 cm^{-1} is also found in the Raman spectrum.

The internal modes of the bifluoride ion are of interest, as this is one of the simplest examples of a very strong hydrogen bond. The symmetric stretching mode of vibration should only be active in the Raman spectrum [44]. It has been found to occur at approximately 600 cm^{-1}. The antisymmetric stretching vibration gives rise to a resonance in the ε'' spectrum at 1440 cm^{-1}, with a half width of 40 cm^{-1}. The values quoted for $\Delta\nu_{1/2}$ in the literature are wrong, as they were obtained by infrared absorption measurements and not by reflection measurements. The degeneracy of the mode in which the hydrogen atom vibrates perpendicular to the bifluoride axis is removed by the crystal field, and the frequencies are 1234 cm^{-1} for the mode in which the H atom moves parallel to the *c* axis and 1227 cm^{-1} for perpendicular to the axis.

1. Corundum (α-Al_2O_3)

The rhombohedral cell contains two formula units/unit cell and belongs to space group D_{3d}^6. There are thirty branches to the phonon dispersion curves.

$$\Gamma = A_{1g}(\mathrm{R}) + 2A_{1u}(\mathrm{F}) + 3A_{2g}(\mathrm{F}) + 2A_{2u}(\mathrm{IR}, \|) + 5E_g(\mathrm{R}) + 4E_u(\mathrm{IR}, \perp).$$

As the unit cell has a center of symmetry, all the Raman-active modes are infrared forbidden or vice versa. The Raman frequencies [46] are (A_{1g}, 418 cm^{-1} and 645 cm^{-1}) and (E_g, 378, 432, 451, 578, and 751 cm^{-1}), and for the infrared active modes (A_{2u}, 399 and 594 cm^{-1}) and (E_u, 385 450 576 and 640 cm^{-1}).

Other crystals with this structure are Fe_2O_3 and Cr_2O_3.

m. Barytes ($BaSO_4$)

Crystals of this class, which include $SrSO_4$ and $PbSO_4$, are orthorhombic with space group V_h^{16} and have four formula units/unit cell; hence there are 72 modes of vibration. Infrared reflection spectra for $BaSO_4$ are shown in figure 10. A considerable simplification occurs in classifying the modes in this crystal from the fact that the SO_4^{-2} ion can be treated to a very good approximation as a single entity with nine internal modes of vibration. In the isolated sulphate ion only four are different. The first mode is a symmetric stretching frequency which is nondegenerate. There is a doubly degenerate deformation mode, a triply degenerate stretching and triply degenerate bending mode.

$$\left.\begin{array}{l} \Gamma_{\mathrm{ext}} = 4B_{1u}(\mathrm{c}) + 3B_{2u}(\mathrm{b}) + 4B_{3u}(\mathrm{a}) \\[1em] \Gamma_{\mathrm{int}} = 4B_{1u}(\mathrm{c}) + 3B_{2u}(\mathrm{b}) + 6B_{3u}(\mathrm{a}) \end{array}\right\}\text{Infrared Active}$$

$$\left.\begin{array}{l} \Gamma_{\mathrm{ext}} = 5A_g + 4B_{1g} + 5B_{2g} + 4B_{3g} \\[1em] \Gamma_{\mathrm{int}} = 6A_g + 3B_{1g} + 6B_{2g} + 3B_{3g} \end{array}\right\}\text{Raman}$$

The sulphate ion has site symmetry C_s in the lattice. Bhagavantam's method [10] gives only the number of vibrations belonging to each symmetry species, whereas Halford's method [11] shows which free-ion vibrations give rise to which crystal vibrations, and hence gives an indication of the frequencies to be expected for the various modes of vibration. The correlation table for the sulphate ion in the barytes lattice is

$$\begin{tikzcd}
\text{Free Ion} & \text{Site} & \text{Lattice} \\
T_d & C_s & V_h \\
\nu_1 A_1 \arrow[dr, dash] & & A_{1g}(\mathrm{R}) + B_{1u}(\|c) \\
 & A' \arrow[ur, dash] \arrow[dr, dash] & \\
\nu_2 E \arrow[ur, dash] & & B_{2g}(\mathrm{R}) + B_{3u}(\|a) \\
 & & B_{1g}(\mathrm{R}) + A_{1u}(\mathrm{F}) \\
\nu_3, \nu_4 F_2 \arrow[uuur, dash] \arrow[r, dash] & A'' \arrow[ur, dash] \arrow[dr, dash] & \\
 & & B_{3g}(\mathrm{R}) + B_{2u}(\|b)
\end{tikzcd}$$

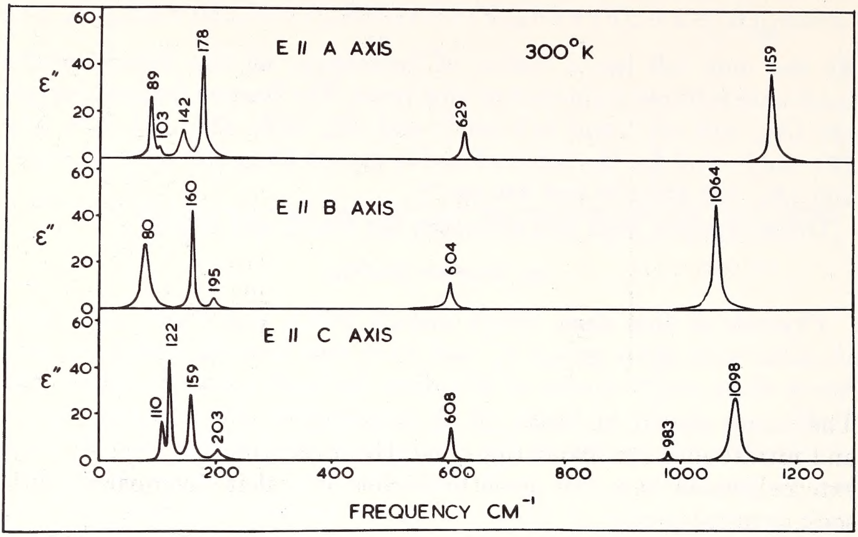

FIGURE 10. The dielectric parameters for barytes ($BaSO_4$) measured with the electric vector of the infrared radiation parallel to the *A*, *B* and *C* axes of the orthorhombic crystal. The resonances above 400 cm^{-1} are due to the excitation of internal modes of vibration of the SO_4^{2-} ions, those below to the external modes. Note the large anisotropy in the frequency of the ν_3 vibration 1159 cm^{-1} ∥ to *A*, 1064 cm^{-1} ∥ to *B* and 1098 cm^{-1} ∥ to *C*.

For instance for the ν_2 symmetric bending vibration of the sulphate SO_4^{-2} ions, the observed Raman frequencies are A_{1g}, B_{1g}, B_{2g}, B_{3g}, while for the very weak infrared transition $B_{1u}\|c=451$ cm^{-1}, $B_{2u}\|b=474$ cm^{-1} and $B_{2u}\|a=468$ cm^{-1}.

n. Calcite

$CaCO_3$ has long attracted the attentions of infrared and Raman spectroscopists in view of its comparatively simple structure and ready availability. The space group is D_{3d}^6 with two formula units/unit cell.

$$\Gamma=A_{1g}(\mathrm{R})+2A_{2g}(\mathrm{F})+3A_2(\mathrm{IR},\|)+5E_u(\mathrm{IR},\perp)$$

The internal modes of the carbonate ion CO_3^{-2} can be distinguished from the external modes. Two A_{2u} and three E_{2u} external modes are observed in the far infrared region, as expected. Two Raman external modes of symmetry E_g occur. The high-frequency Raman mode is a rotatory mode involving the planar carbonate ion, and the low-frequency mode is a translatory one. Sodium nitrate has the same structure and a very similar vibrational spectrum. The frequencies are:

		Calcite ($CaCO_3$)	$NaNO_3$
Internal	ν_1 A_{1g}	1086.3 cm^{-1}	1068.8 cm^{-1}
	ν_2 A_{2u}	870.5	834.6
	ν_3 E_u	1435.9	1385.9
	ν_4 E_u	712.5	726
External	A_{2u}	92 cm^{-1}	50 cm^{-1}
	A_{2u}	306	205
	E_u	102	87
	E_u	224	176
	E_u	296	208
	E_g	156.1	100
	E_g	281.8	185.8

The frequencies of the internal modes of vibration of the carbonate and nitrate ions are about the same. However, the frequencies of the external modes are consistently higher in calcite compared with sodium nitrate.

Aragonite is another form of $CaCO_3$ with four formula units in the orthorhombic unit cell with V_h^{16} symmetry. The vibrational spectrum is much more complicated than that for calcite and there are 60 branches to the phonon dispersion curves. Whilst the site symmetry in calcite is D_3, it is C_s in aragonite. As a consequence of this, the totally symmetric stretching vibrations of the carbonate ion are infrared active in aragonite, but not in calcite. Similarly the degenerate stretching and bending modes are split in aragonite.

o. Sodium Nitrite ($NaNO_2$)

The unit cell, which contains two formula units, is orthorhombic with space group C_{2v}^{20}.

$$\Gamma_{\text{int}} = 2A_1(\text{IR}\|b,\ \text{R}) + B_1(\|c,\ \text{R})$$

$$\Gamma_{\text{ext}} = A_1(\text{IR}\|b,\ \text{R}) + A_2(\text{R}) + 2B_1(\|c,\ \text{R}) + 2B_2(\|a,\ \text{R}).$$

Of the external modes, the translatory ones are $A_1+B_1+B_2$ whilst the rotatory types are $A_2+B_1+B_2$.

It may be noted that all the infrared active modes are also Raman active, and hence longitudinal optic modes would also be expected to be active in the Raman spectum. The frequencies of the internal modes are (825 cm^{-1} A_1, ν_2) (1327 cm^{-1} A_1, ν_1) and (1280 cm^{-1} B_1, ν_3). The Raman-active external modes occur at (119 cm^{-1} A_2), (153 cm^{-1} B_1), (177 cm^{-1}, B_1) and (220 cm^{-1}, B_2).

Sodium nitrite is ferroelectric; below its transition point at 163 °C all the NO_2^- groups have identical orientations. The Raman frequencies [47] of the external modes as a function of temperature are

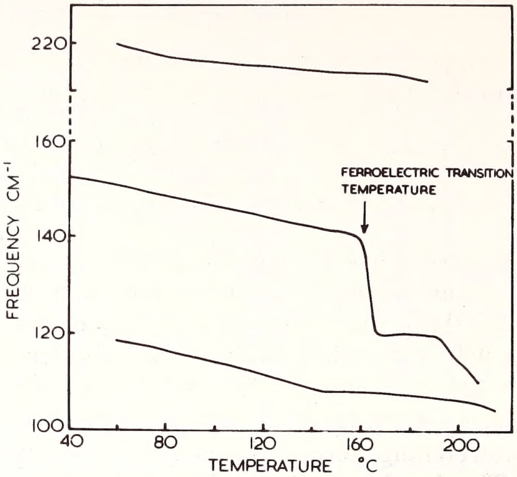

FIGURE 11. The variation with temperature of the Raman frequencies of external modes in sodium nitrite $NaNO_2$. Note the large change in frequency at the ferroelectric transition temperature for one of the modes of vibration. (Chisler and Shur [47]).

shown in figure 11. Only the 153 cm^{-1} band shows a marked change at the transition temperature; hence it is concluded that the phase transformation is due to a reorientation of the NO_2^- group around an axis perpendicular to the anion plane. Above 163 °C the space group of the crystal has been shown to be V_h^{25}. In the high temperature phase

$$\Gamma=A_g+2B_{1u}+2B_{2u}+2B_{3u}+B_{1g}+B_{2g}.$$

p. Scheelite

$CaWO_4$ has two formula units in the tetragonal unit cell of space group C_{4h}^6.

The **k**=0 vibrational spectrum can be divided into modes which involve the internal motion of the tungstate WO_4^{-2} ions, which in free space are tetrahedral, and external modes.

$$\Gamma=3A_{1g}(R)+5A_{2g}(R)+5E_g(R)+4A_u(IR, \|c)+3B_u(F)$$

Thus the infrared spectrum should show four modes [48] with the electric vector parallel to the c axis and four with the electric vector perpendicular to the axis. Examples that have been studied so far include $CaWO_4$, $SrWO_4$, $CaMO_4$, and $SrMO_4$. Thirteen Raman-active modes are predicted, and these have been recently observed and assigned using laser-Raman spectroscopy [49].

q. Zircon

$ZrSiO_4$ is tetragonal with two formula units/unit cell. The space group is D_{4h}^{19} and the site symmetry of the silicate ion is S_4.

$$\Gamma = 2A_{1g}(\mathrm{R}) + A_g(\mathrm{F}) + 4B_{1g}(\mathrm{R}) + B_{2g}(\mathrm{R}) + 5E_g(\mathrm{R}) \\ + A_{1u}(\mathrm{F}) + 3A_{2u}(\mathrm{IR}, \parallel) + B_{1u}(\mathrm{F}) + B_{2u}(\mathrm{F}) + 4E_u(\mathrm{IR}, \perp)$$

Thus in the infrared three resonances should be expected with the electric vector of the radiation parallel to the *c* axis, and four with it perpendicular to the *c* axis. The parallel frequencies are 338 cm^{-1}, 608 cm^{-1}, and 989 cm^{-1}, while the perpendicular frequencies are 288 cm^{-1}, 389 cm^{-1}, 431 cm^{-1}, and 885 cm^{-1}. Of the frequencies of vibration of the silicate ions SiO_4^{-4}, those at 885 cm^{-1} and 989 cm^{-1} are due to antisymmetric stretching vibrations which differ in frequency due to the crystal field. The band at 608 cm^{-1} is due to the antisymmetric vibration ν_4. All the expected Raman modes have been observed.

4.4. Molecular Crystals

Usually the forces between molecules in a crystal are weak compared with the atomic forces within the molecules themselves. Consequently it is usually easy to distinguish between external and internal modes of vibration. A good test to carry out when a suitable solvent is available is to measure the infrared and Raman spectra in solution. If an absorption line persists in solution, then the associated vibrational mode must involve an internal motion of the atoms within the molecule.

The infrared absorption due to intermolecular vibrations in crystals is usually weak and is especially weak if the molecules are nonpolar [50]. The infrared reflectivity is rarely sufficiently great to enable measurements to be made of the dielectric parameters. Hence only the absorption coefficient α is usually measured. In anisotropic crystals polarized radiation must be used. Much of the interest in studying the spectra involving internal modes of vibration is in determining accurately the splitting in bands due to intermolecular interaction. For such observations it is preferable to work at low termperatures with a high resoution spectrometer.

a. Hydrogen

The infrared and Raman spectra of crystalline hydrogen has been studied in great detail [51]. The spectra shown in figure 12 indicate clearly that free rotation can exist in the solid state. Although the internal mode is strongly Raman active [52], para hydrogen is not infra-active until ortho hydrogen is added [53]. The spacing of the rotational lines confirms that there is very little change in the internuclear distance in going from the gaseous to condensed phases.

b. Chlorine, Bromine, Iodine (Cl_2,Br_2I_2)

These gases condense to form orthorhombic crystals of space group V_h^{18}. The molecules are located at sites of symmetry C_{2h}.

$$\Gamma_{\text{Trans}} = A_u + B_{1u}(\text{IR}, \|c) + B_{2u}(\text{IR}, \|b)$$
$$\Gamma_{\text{Rot}} = A_g(\text{R}) + B_{1g}(\text{R}) + B_{2g}(\text{R}) + B_{3g}(\text{R})$$
$$\Gamma_{\text{Int}} = A_g(\text{R}) + B_{3g}(\text{R})$$

The B_{1u} and B_{2u} modes are found in the infrared absorption spectrum: Cl_2(62 cm^{-1}, 92 cm^{-1}), Br_2 (49 cm^{-1}, 74 cm^{-1}), I_2 (41 cm^{-1}, 65 cm^{-1}). The infrared forbidden transitions involving internal modes of vibration are found to be weakly active in the infrared, but slightly shifted from the gas values (given in brackets): Bromine 298 cm^{-1} (323 cm^{-1}), Iodine 211 cm^{-1} (215 cm^{-1}).

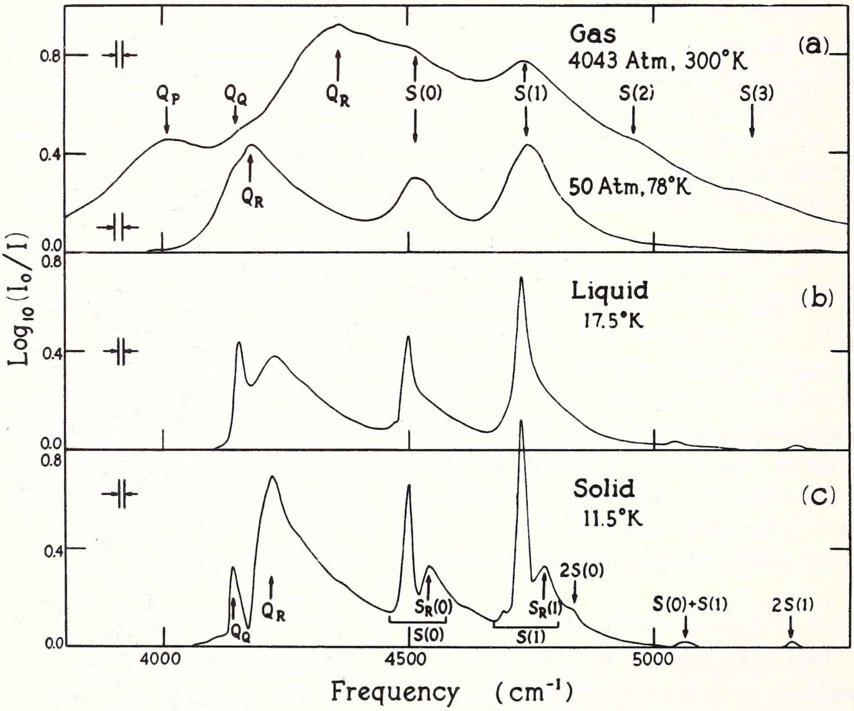

FIGURE 12. The infrared absorption spectrum of hydrogen in the gas, liquid and solid phases. The spectra show evidence for quantised rotation in the condensed phases as well as in the gas. (Welsh et al. [52]).

c. Carbon Dioxide (CO_2)

Of particular interest are molecular crystals which contain simple molecules which have been extensively studied in the gas phase, both at low pressure so that the vibrational energy levels are known, and at high pressures so that information on intermolecular forces in the gas phase can be obtained. One such system is solid carbon dioxide.

Carbon dioxide condenses to form cubic crystals of space group T_h^6 containing four linear molecules. The external modes are found from

$$\Gamma = A_u(\mathrm{F}) + E_u(\mathrm{F}) + E_g(\mathrm{R}) + 2F_u(\mathrm{IR}) + 2F_g(\mathrm{R}).$$

The E_g and $2F_g$ modes should be Raman active, whilst $2F_u$ infrared-active modes are to be expected. The observed values for the infrared-active [54, 55] vibrations are 67 and 113 cm^{-1}, and for Raman [57] the frequencies 90.5 and 131 cm^{-1} for the F_g modes and 73 cm^{-1} for the E_g mode. Pople and Walmsley [56, 58] have used a Leonard-Jones 6–12 potential of the form

$$4\epsilon\left\{\left(\frac{R_0}{R}\right)^{12} - \left(\frac{R_0}{R}\right)^{6}\right\}$$

together with an electric quadrupole interaction of the form θ/R^5, where θ is the electric quadrupole moment of CO_2. Reasonable agreement with the observed frequencies is obtained.

In the region of the ν_2 and ν_3 internal vibrational modes, summation bands of the type internal ± external occur [59], and as discussed previously, these are density-of-states type spectra. Features in the infrared spectrum involving combinations with the ν_3 internal antisymmetric stretching vibration and the ν_2 bending vibration differ by 110 and 114 cm^{-1} from the internal mode frequencies. Similarly there are features which differ in frequency by 78 cm^{-1} and 77 cm^{-1}.

d. Hydrogen Chloride (HCl and DCl)

Extensive infrared and Raman studies have been made on the hydrogen halides. Of these only HCl will be discussed here. Solid HCl and DCl undergo a phase transition at 98 °K and 105 °K respectively. Their structures [60, 61] have recently been shown to be isomorphous. The unit cell has four molecules and is orthorhombic with space group C_{2v}^{12} below the transition temperature, and cubic above. In the orthorhombic form the molecules are hydrogen bonded in planar zig-zag chains, all oriented the same way (i.e., to give a net dipole moment) and arranged in layers parallel to the (001) plane. In the cubic form the chlorine atoms form a face centred lattice; however, the structure is disordered as the hydrogen bonds are irregularly arranged. As there are four molecules in the unit cell in the low temperature phase, it is expected that there should be 9 translational modes, of which 6 should be both infrared and Raman active and 3 Raman active only. Eight rotatory modes should be expected, of which six should be infrared and Raman active and two only Raman active. Four internal modes are predicted, all of which should be Raman active and three infrared active.

Experimentally only two translational modes are clearly apparent at 86 cm^{-1} and 109 cm^{-1} in the far infrared spectrum, while the number of rotatory modes is at least four. There are three comparatively strong infrared bands [62] due to internal motion at 2707, 2718, and 2758 cm^{-1} and four corresponding ones in the Raman spectrum at 2705 cm^{-1}, 2720 cm^{-1}, 2748 cm^{-1}, and 2758 cm^{-1}, all measured at 77 °K.

On passing through the transition to the cubic disordered hydrogen-bonded phase, the infrared absorption bands due to the internal vibration merge to give a single broad peak at 2780 cm^{-1}. The increase in frequency is due to the 0.2 Å increase in the hydrogen bond length on going from the orthorhombic to cubic phase. Only a small increase in frequency to 2787 cm^{-1} and an increase of from 44 cm^{-1} to 59 cm^{-1} in half-width is found on melting. The gas-phase band centre occurs at 2886 cm^{-1}.

e. Mercurous Chloride (Hg_2Cl_2)

The tetragonal unit cell has one molecule in the unit cell which has space group D_{4h}^{17}

$$\Gamma = 2A_{1g}(\mathrm{R}) + A_{2u}(\mathrm{IR}, \|) + 2E_g(\mathrm{R}) + E_u(\mathrm{IR}, \perp)$$

There are five internal modes of vibration in a linear molecule containing 4 atoms. The Raman lines [64] at 167 cm^{-1} and 270 cm^{-1} are highly polarized and must correspond to A_{1g} modes, leaving the lines at 42 cm^{-1} and 140 cm^{-1} to be E_g modes. The low-frequency mode is clearly the rotatory mode, and the higher frequency mode involves a bending vibration of the molecule. In the infrared a 33 cm^{-1} peak is assigned to the E_u bending mode and a 110 cm^{-1} peak to the A_{2u} stretching mode [65].

f. Naphthalene

This crystal has a monoclinic unit cell containing two molecules. The space group is C_{2h}^5, to which many simple organic crystals belong.

$$\Gamma_{\mathrm{ext}} = 3A_g(\mathrm{R}) + 3B_g(\mathrm{R}) + 2A_u(\mathrm{IR}) + B_{1u}(\mathrm{IR}).$$

The A_g and B_g modes which are Raman active are three pairs of rotatory modes. The frequency difference between the A_g and B_g

types which correspond to the in-phase and out-of-phase motions is small. The three modes do not consist of rotatory modes about the principal axes of inertia of the naphthalene molecule. The Raman frequencies at 100 °K are 56 and 66 cm^{-1}, 82 and 86 cm^{-1}, and 120 and 140 cm^{-1}.

Two absorption bands are readily observed in the far infrared absorption of the *ab* face, one an A_u mode at 72 cm^{-1}, as shown by its polarization parallel to the *b* axis, and another at 103 cm^{-1} perpendicular to the *b* axis.

Recently Pawley [66] has calculated the dispersion curves for both naphthalene and anthracene using a potential function of the form

$$V(r) = -\frac{A}{r^6} + B \exp(-\alpha r) \cdot$$

The frequencies calculated for the Raman-active and infrared-active modes are in satisfactory agreement with experimental values for naphthalene. The agreement for anthracene is less good. However, it is clear that the dispersion curves would be improved by using the accurately determined infrared and Raman frequencies in the calculation.

g. Iodoform

CI_3H has a single molecule of D_{3h} symmetry in a trigonal unit cell. Iodoform provides one of the best examples for studying the combination of internal modes with external modes, as all the C—H bonds are parallel to the *c* axis. Hexter [67] was the first to show that if the infrared spectrum is obtained with the radiation propagating along the C—H direction, so that the absorption due to the excitation of the C—H stretching vibration is weak, then "wings" can be observed on either side of the C—H resonance frequency near 3000 cm^{-1}, as is shown in figure 13. This is a clear case of internal ± external modes giving a partial density of states type spectrum [68]. The high frequency cutoff appears at about 50 cm^{-1}. Similar structure has been observed in combination with the C—I symmetric bending frequency at 154 cm^{-1} in the far infrared region.

h. Hexamethylbenzene

$C_6(CH_3)_6$ contains a single molecule in a monoclinic unit cell, with the molecule parallel to the *ab* face. Many studies have been carried out using different physical techniques [69, 70] to study the phase changes which occur at low temperature. When the hydrogen atoms are considered, the symmetry of the molecule is determined by the orientation of the methyl groups. Figure 14 shows the polarized infrared absorption spectrum at different temperatures for a *bc* face.

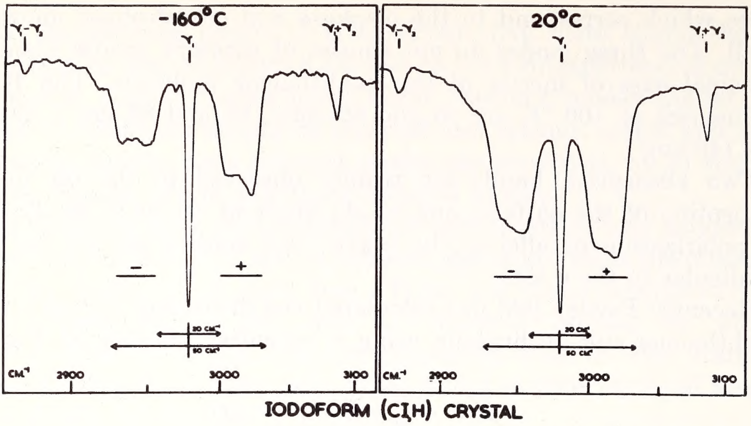

FIGURE 13. The infrared absorption spectrum of Iodoform (CI_3H) at 20 °C and −160 °C, observed with the direction of propagation of the radiation along the *c* axis of the crystal. This is the direction along which all the C—H bands occur. The "wings" on either side of the main absorption due to the C—H stretching vibration are "partial density of vibrational states" type spectra.

The 2950 cm^{-1} band is associated with CH_3 stretching, the 1450 cm^{-1} band with CH_3 deformation and 1050 cm^{-1} band with C—CH_3 stretching. A sharp change in the rate of increase of the absorption at 2950 cm^{-1} with temperature occurs at about 165 to 170 °K. An anomaly has also been found in the specific heat curve at this temperature whilst the NMR line width decreases between 135 °K and 210 °K. Corresponding Raman studies have also been made. It appears that the changes are associated with the rotation of methyl groups about their triad axes.

i. Zeise's salt ($K^+(PtCl_3C_2H_4)^-H_2O$)

This crystal is monoclinic with two formula units/unit cell. The anion has symmetry C_{2v}. The interest in this crystal in the present discussion lies in (a) the orientation of C_2H_4 molecule (b) the fact that water molecule is very weakly hydrogen bonded, one of the very few examples known where this is so in a crystal.

From polarized infrared and Raman experiments it has been shown that the long axis of the ethylene molecule lies perpendicular to the $PtCl_3$ plane. The infrared spectrum for C_2H_4 and the fully deuterated C_2D_4 are shown in figure 15. Zeise's salt contains two water molecules in the unit cell. The half widths of the absorption bands due to the O—H stretching vibrations are about 10 cm^{-1} and hence very little hydrogen bonding occurs. The translatory and rotatory motions are

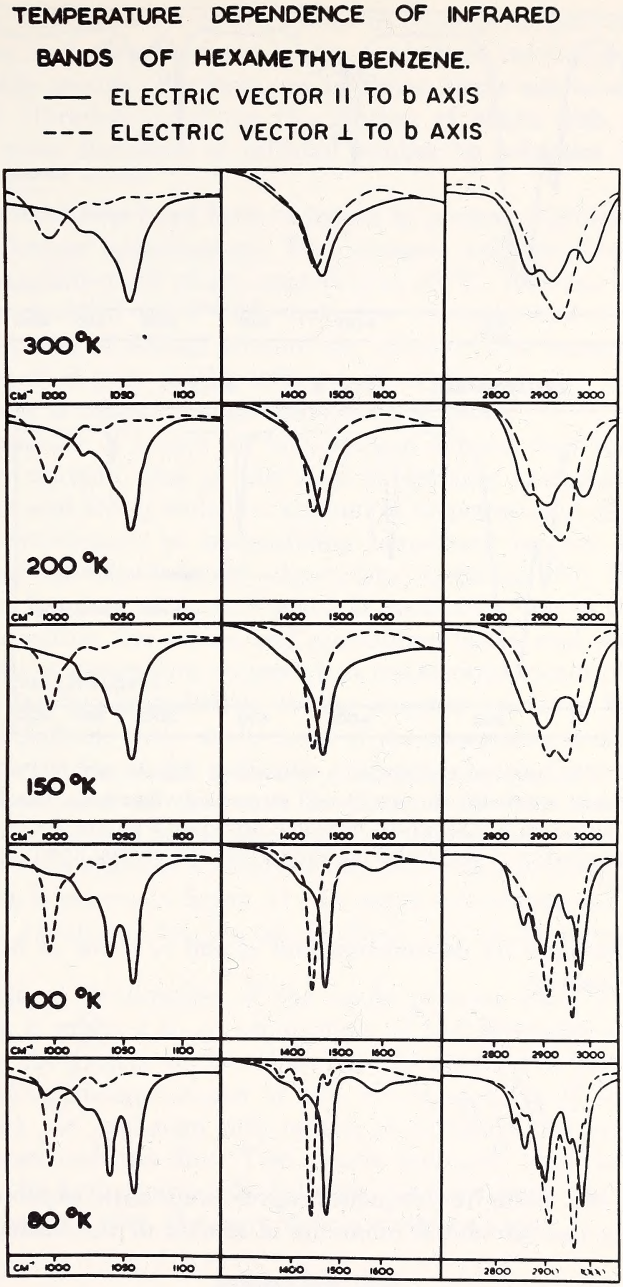

Figure 14. The temperature dependence of the infrared absorption spectrum of hexamethylbenzene measured with the electric vector of the radiation parallel and perpendicular to the *b* axis. The three regions shown correspond to C—CH stretching vibration (~1050 cm^{-1}), the CH$_3$ deformations (~1450 cm^{-1}) and the methyl stretching vibrations (~2900 cm^{-1}).

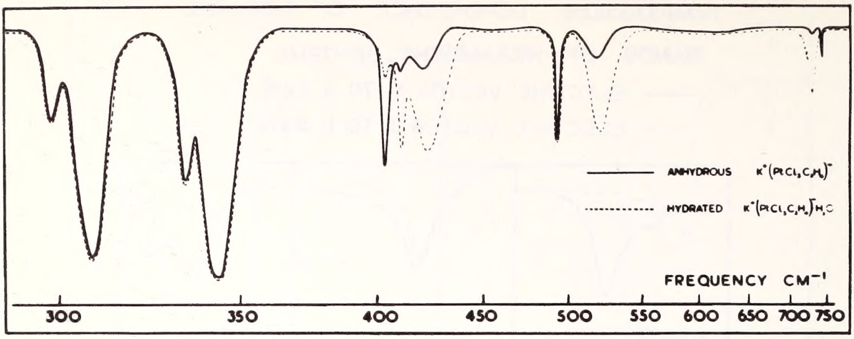

DEUTERATED ZEISE'S SALT

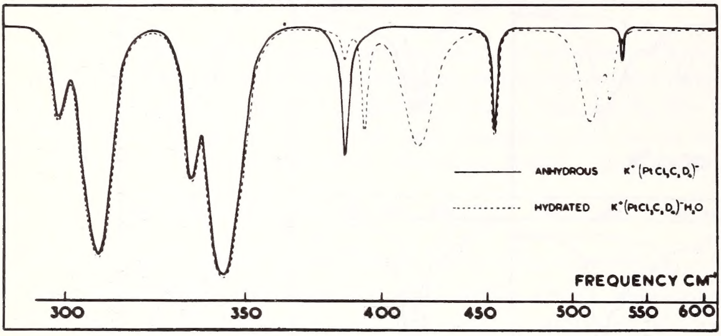

FIGURE 15. The infrared absorption spectrum of Zeise's salt $K(PtCl_3C_2H_4)H_2O$ The strongest bands are due to Pt—Cl stretching vibrations. Bands due to the external vibration of the water molecule are clearly shown by comparing the absorption spectra of the anhydrous salts with both normal and fully deuterated Zeise's salt.

readily identified by deuteration and ν_4 and ν_5 occur at 517 and 420 cm^{-1} (see below).

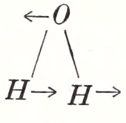

ν_4

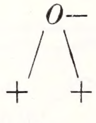

ν_5

For D_2O the shifts in frequency agree well with expected values, considering the calculated moments of inertia of the various species.

4.5. Polymers

With the production of new synthetic polymers in ever increasing numbers and with the isolation of many high polymers of natural origin, it is understandable that the volume of publications on the study of their vibrations is growing steadily [71]. It is convenient in discussing the vibration of a polymer to distinguish between skeletal vibrations, including torsional modes, and those involving the vibration of side groups. Furthermore in fibres there are intermolecular modes of vibration involving the motion of chain with respect to chain. A good discussion of infrared studies on polymers is given in reference 72.

Phase transitions have been observed in several polymers by infrared and Raman spectroscopy. For instance polytetrafluoroethylene undergoes a first-order phase transition at 20 °C. This has been shown to be the result of the PTFE molecular chains, which are compact helices, slipping or rolling around one another. The transition results in a marked change in the infrared absorption at 630 cm^{-1} as the temperature is raised through the transition point.

The structure of nearly all biopolymers depend very markedly on the water content. One of the most interesting examples of this is the nucleic acid DNA, which on account of its presence in chromosomes and its involvement in transmitting hereditary factors, is of some importance. In the infrared absorption spectrum [73] there is an absorption band at 1650 cm^{-1} which is essentially due to the in-plane vibrations within the purine and pyrimidine bases, and consequently the maximum absorption occurs when the electric vector of the infrared radiation is perpendicular to the polymer axis (see fig. 16). We define the dichroic ratio as the ratio of the absorption coefficient with the electric vector of the radiation perpendicular to the polymer axis to the absorption at the same frequency with the electric vector parallel to the axis. The variation in the observed dichroic ratio at 1650 cm^{-1} when the oriented crystalline film is exposed to different relative humidities is shown in figure 17. As water is removed the bases tilt; the angle calculated for the tilt is about 15° at 70 percent relative humidity.

The rate of deuteration of the labile protons when a crystalline DNA film is exposed to an atmosphere of D_2O is readily followed by observing the growth of N—D and O—D absorption bands and the corresponding disappearance of the N—H and O—H bands. It is found that the exchange rate occurs at virtually the same rate as D_2O diffuses into the film. This clearly indicates that the hydrogen atoms in the hydrogen bonds between the base pairs are constantly being exchanged with the surrounding water protons.

4.6. Liquids

Infrared and Raman spectroscopy are potentially powerful methods of determining the motion of molecules in liquids. In a liquid all

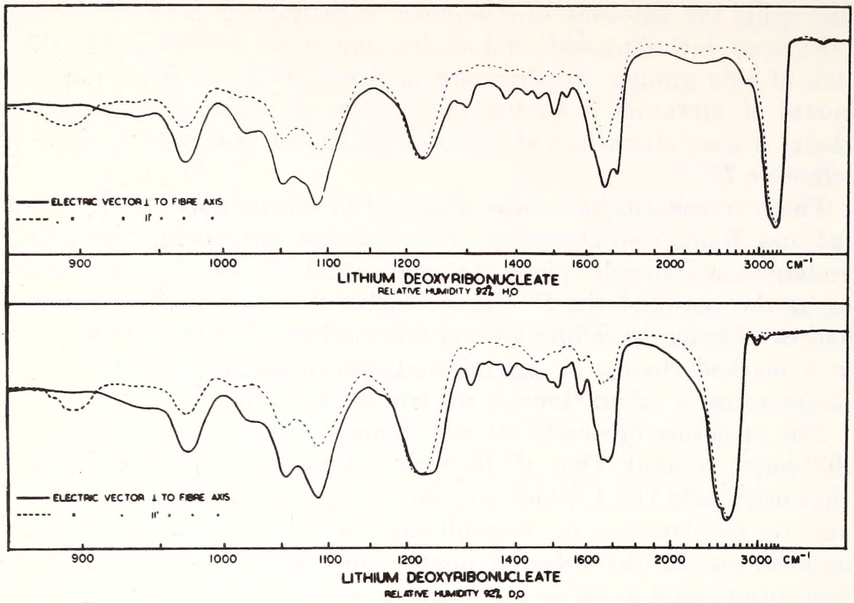

FIGURE 16. The infrared absorption spectrum of lithium deoxyribonucleate (DNA) obtained using polarized radiation and a reflecting microscope. The top spectrum was obtained when the salt was in equilibrium with a 92 percent relative humidity of H_2O and the lower with the same R.H. of D_2O. Note the exchange of labile hydrogen atoms. The bands in the 1650 cm^{-1} region which show maximum absorption when the electric vector is perpendicular to the fibre axis are due to in-plane vibrations of the base-pairs.

long range order is lost [74]; hence it is no longer possible to identify the unit cell which simplified the discussion of $\mathbf{k}=0$ infrared and Raman spectra. However, in general the change in intramolecular frequencies in going from liquid to crystal is small, as might be expected, since the first-neighbour intermolecular distances are not radically changed. Absorption due to intermolecular vibration is spread over a wider range in the liquid than in the corresponding crystal.

In liquids the vibration of molecule with respect to molecule would be expected to be aperiodic. A simple theory considers that the dielectric parameters may be calculated by setting ν_0, the resonance frequency, to zero, and by replacing the damping constant by a relaxation time τ. Then

$$\epsilon' = \epsilon'_\infty + \frac{\epsilon'_0 - \epsilon'_\infty}{1+4\pi^2\nu^2\tau^2}$$

$$\epsilon'' = \frac{\epsilon'_0 - \epsilon'_\infty}{1+4\pi^2\nu^2\tau^2}$$

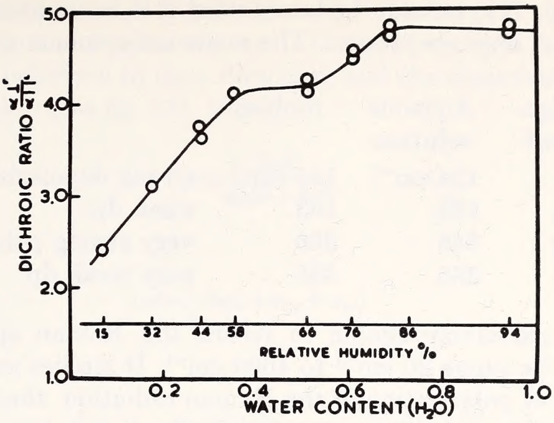

Figure 17. The variation of the dichroic ratio of the in-plane vibrations of the bases ($\sim 1650\ \text{cm}^{-1}$) with water content. The scale at the bottom shows both the relative humidity of the atmosphere to which the sample was exposed as well as the water content. The latter was measured by determining the intensity of the H_2O band in the $3300\ \text{cm}^{-1}$ region.

where τ may be thought of as the average time required by a molecule to rotate one radian, or as a correlation time.

Resonances in ϵ^* associated with the excitation of internal modes of vibration can be represented quite well by classical oscillator functions of the type used for solids. Recently attempts have been made by Gordon to use the band contours of both infrared and Raman lines of liquids [75] to obtain correlation times.

Chemists have long made use of the infrared and Raman spectra of pure liquids or solutions to determine the structure of molecules. By structure here we mean symmetry, as it is not possible to deduce bond lengths and angles in condensed phases by spectroscopy. The procedure involves the recording of infrared and Raman spectra. In the latter case it is very valuable to measure the depolarization values, as important conclusions about symmetry can be drawn from them. By noting the coincidence or noncoincidence of infrared absorption lines with Raman lines, further information can be obtained about the symmetry of the molecule.

We will now consider in more detail measurements of the Raman spectra of liquids.

As an example of the use of Raman spectroscopy to obtain the structure of a molecule, we take the case of Gallium dichloride, $GaCl_2$. In solution and in the melt the structure has been shown to be ionic and of the form $Ga^+GaCl_4^-$. The assignments show that the Raman spectrum [76, 77] can only be interpreted if it is assumed that tetrahedral $GaCl_4^-$ ions are present. The mode assignments are as follows:

Assignment	Aqueous solution	molten	
$\nu_2(E)$	114 cm^{-1}	115 cm^{-1}	strong depolarized
$\nu_4(F_2)$	148	153	weak dp.
$\nu_1(A_1)$	346	356	very strong polarized.
$\nu_3(F_3)$	386	380	very weak dp.

It is comparatively simple to record the Raman spectrum of a liquid over the range 30 cm^{-1} to 4000 cm^{-1}. If studies are carried out on the state of polarization of the Raman radiation, then information can be obtained about the symmetry of vibration associated with any Raman line. On account of motion in a liquid, space-fixed axes (x, y, z) no longer coincide with the axes of the polarizability ellipsoid x', y', z', which are fixed in the molecule. However, it is possible to measure experimentally the depolarization ratio, which is defined as:

$$\rho = \frac{\mathbf{p}_y^2}{\mathbf{p}_z^2} = \frac{I_\perp}{I_\parallel}$$

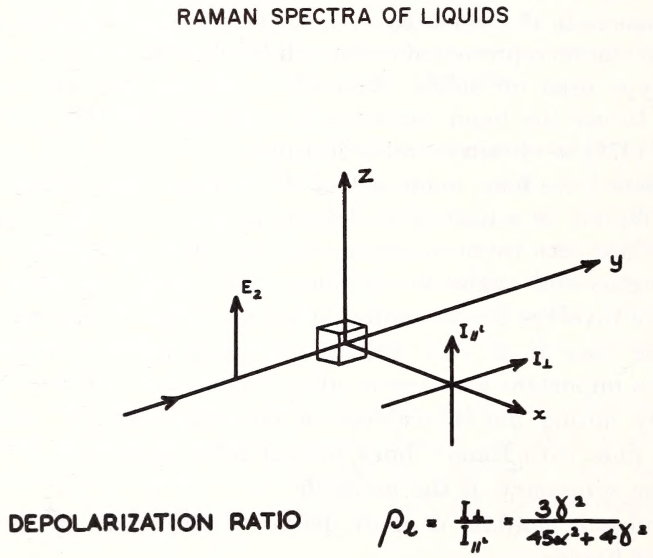
RAMAN SPECTRA OF LIQUIDS
Z
y
E_z
$I_\parallel{}'$
$I_\perp$
x
DEPOLARIZATION RATIO
$\rho_\ell = \frac{I_\perp}{I_\parallel{}'} = \frac{3\gamma^2}{45\alpha^2+4\gamma^2}$

FIGURE 18. As illustrated in the figure, the dipolarization ratios of liquids may be measured by using polarized exciting radiation (E in the z direction) and then observing the scattered Raman radiation with a polarizer set first parallel and then perpendicular to the z direction. The depolarization ratio is given by $\rho = I\perp/I\parallel$.

in which p_y^2 and p_z^2 are proportional to the intensities of the scattered radiation with y and z polarizations. If the incident light moves in the y direction, is polarized in the z direction, and the observation is made in the x direction (see fig. 18), then

$$\rho=\frac{3\gamma^2}{45\alpha^2+4\gamma^2}$$

where

$$\alpha=\frac{1}{3}(\alpha_{xx}+\alpha_{yy}+\alpha_{zz})$$

and

$$\gamma^2=\frac{1}{2}[(\alpha_{xx}-\alpha_{yy})^2+(\alpha_{yy}-\alpha_{zz})^2+(\alpha_{zz}-\alpha_{xx})^2+6(\alpha_{xy}{}^2+\alpha_{yz}{}^2+\alpha_{zx}{}^2)].$$

If $\alpha_{xx}=\alpha_{yy}=\alpha_{zz}$ and $\alpha_{xy}=\alpha_{yz}=\alpha_{zx}=0$, then $\rho=0$. For example, for a totally symmetric "breathing" vibration in a tetrahedral molecule XY_4 or octrahedral molecule XY_6, the line is completely polarized. If $\alpha_{xx}=\alpha_{yy}=\alpha_{zz}=0$, then $\rho=3/4$ and the line is said to be completely depolarized.

Hence all Raman lines due to fundamental modes of vibration belonging to totally symmetric species are polarized ($\rho<3/4$) and all Raman lines of other species are depolarized ($\rho=3/4$).

Liquid water presents very many difficulties to experimental spectroscopists. Its infrared absorption is very intense [78] whilst the Raman spectrum is weak. However, there is now available good data to attempt to understand the various spectral features. Figure 19 shows the dielectric parameters for water. Two quite distinct regions can be distinguished, the region below 1000 cm^{-1} which results from intermolecular motion, and the region above in which resonance due to intramolecular vibrations occur, corresponding to the ν_1, ν_2, and ν_3 vibrations.

The main step in ϵ' occurs at about 0.5 cm^{-1} in the microwave region and is associated with the reorientation of the water molecules. Two steps in ϵ' and ϵ'' can be distinguished in the low frequency infrared region at 600 cm^{-1} and 165 cm^{-1}, which shift to 460 cm^{-1} and 150 cm^{-1} in D_20. The first is clearly to be associated with a rotatory motion, as the ratio of 1.4 is roughly what can be expected from the known moments of inertia, and the second to a translatory motion. The peak occurs at 470 cm^{-1} in the Raman spectrum and is clearly due to a similar rotatory motion. In both the infrared and Raman spectra there is a peak in the 2100–2130 region which involves the combination of the internal bending vibration ν_2 with the rotatory external mode at 470 cm^{-1}.

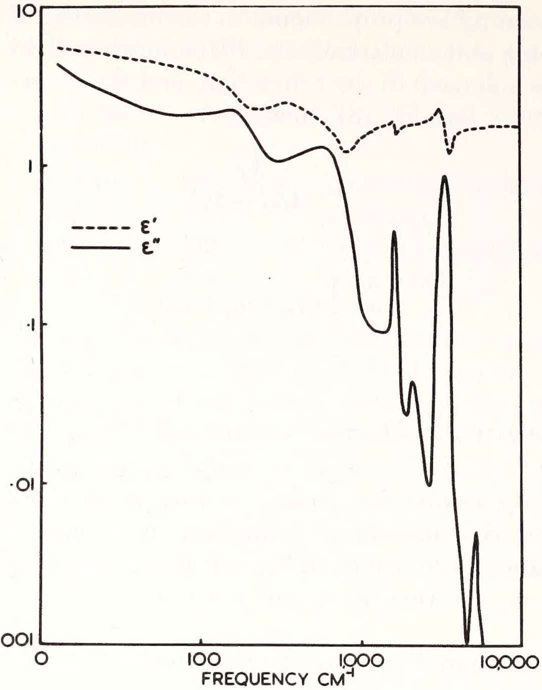

FIGURE 19. The dielectric parameters ϵ' and ϵ'' of water in the infrared region. The large fall in ϵ' in the region below 1 cm^{-1} is not shown. The resonances in ϵ'' are at 165 cm^{-1}, which involves a translatory motion of the water molecules, and at 600 cm^{-1}, which is due to a rotatory motion. The peak ~1600 cm^{-1} is due to the internal bending mode of vibration whilst that ~3300 is due to stretching modes. The band ~5000 cm^{-1} is due to a combination of the stretching and bending modes, whilst the ~2100 cm^{-1} peak is a combination of the bending mode with a rotatory-type external mode.

4.7. Hydrogen Bonding

Infrared spectroscopy provides the most sensitive method of determining whether hydrogen bonding occurs in a crystal or liquid [79]. If it does, then the absorption bands associated with O–H and N–H stretching vibrations (~3500 cm^{-1}) are shifted to lower frequencies and are broadened. Many different explanations have been put forward. However, none is yet sufficiently developed to permit detailed quantitative calculation of the shifts.

Spectroscopic studies in the solid phase, in which donor-acceptor distances are well known, have been very fruitful. There is found to be for the O–H stretching vibration a good correlation between the frequency shift and the oxygen-oxygen distance. Consequently the measurement of such O–H frequency shifts can now be used with a fair measure of confidence, to measure these separations.

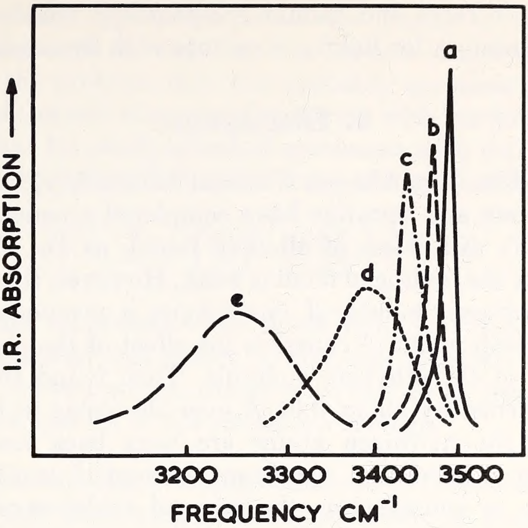

Figure 20. The infrared absorption spectrum due to the excitation of the N—H stretching vibration of indole in different solvents: (a) hexane, (b) carbon disulphide (c) benzene (d) methylthiocyanate (e) N;N dimethylacetamide. The spectra clearly show the specific interaction of the N—H group with the solvent. In general the greater the frequency shift, the greater the interaction.

Figure 20 shows the infrared absorption [80] associated with the N–H stretching vibration in indole measured in different solvents. It will be noted that the bond has a different shift and different half-width in different solvents, which clearly indicates the presence of specific interactions between the solute and solvent, i.e. the presence of hydrogen bonds.

5. Conclusions

In this article it has only been possible to outline briefly the role of infrared and Raman spectroscopy in elucidating the structure and motion of molecules. The wide success of these methods as structural diagnostic tools depends experimentally in no small measure on the relative ease with which the vibrational spectra of any solid or liquid can be obtained, and on the wave-vector selection rule that restricts one phonon transitions to $\mathbf{k}=0$. This makes infrared and Raman vibrational spectra much simpler than the corresponding density of vibrational states. Progress in interpretation of spectra will be furthered by corresponding studies on the same materials by a wide range of physical techniques. If in the introduction we stressed some of the difficulties in using optical spectroscopy for structure determination and for complete lattice dynamics studies, then we close with the claim that infrared and Raman spectroscopy are the most widely applicable techniques for linking structure with dynamics.

6. Discussion

W. C. Hamilton (Brookhaven National Laboratory): My colleagues Drs. Klanderman and Spratley have completed a neutron diffraction study of Zeise's salt. First of all they found, as Dr. Wilkinson has suggested, that the hydrogen bond is weak. However, there are definite O—H—Cl hydrogen bonds—if one adopts a geometrical criterion. A more interesting point of course is the effect of the coordination on the geometry of the ethylene molecule. They found that the C═C bond is lengthened by about 0.01 Å over the value in free ethylene. Furthermore, the hydrogen atoms are bent back away from the platinum atom a small but significant amount. I would like to ask Dr. Wilkinson to comment on the infrared evidence on these latter two points.

G. R. Wilkinson: The infrared absorption spectrum of the water molecule in Zeise's salt shows that the hydrogen bonding is very weak indeed. The criterion used being the shift in the ν_1 and ν_3 stretching-vibration frequencies and the halfwidth of the absorption bands. The frequency shift for ν_1, ν_2, and ν_3 from the gas phase values are -187 cm^{-1}, $+19$ cm^{-1}, and -227 cm^{-1} whilst the halfwidths $\Delta\nu_{1/2}$ for ν_1 and ν_3 are only 10 cm^{-1} and 15 cm^{-1} in the salt. These line widths are the narrowest that I have encountered for water molecules in the condensed phase.

As far as the double bond length is concerned, infrared spectroscopy is unable to give any information of the precise change of bond length. However it does reveal that the force constant of the C═C bond is reduced, and the frequency of the stretching vibration is reduced from the value 1623 cm^{-1} in ethylene gas to 1516 cm^{-1} on coordination with platinum.

R. Summitt (Department of Physics, Michigan State University): Would you please comment on the effect of specimen size on the infrared and Raman spectra of solid materials.

G. R. Wilkinson: Particle size has an appreciable effect on infrared spectra, especially in the case of very strong absorption bands such as occurs in ionic crystals. In fact it is frequently impossible to obtain a true absorption spectrum with many inorganic powders—the literature is full of spectra that are supposed to be infrared absorption spectra but which are in fact reflection spectra or rather $(1—R\nu)$

spectra. For weak absorption bands the quality of the spectra can be greatly improved by reducing the particle size d such that $d \ll \lambda$.

However, the problem that you probably are more interested in is the change of the real vibrational spectrum with particle size. Fröhlich has shown that for small spherical specimens with $d < \lambda_p$, where λ_p is the wavelength of the polarization wave of angular frequency ω_s:

$$\left(\frac{\omega_s}{\omega_t}\right)^2 = \frac{\epsilon_0 + 2}{\epsilon_\infty + 2}.$$

Here ω_t is the transverse optic mode frequency for large crystals. Hass[1] has extended this theory to elliptical cylinders of semiinfinite length. You[2] have used this theory with success to interpret the infrared absorption spectra of fibrous silicon carbide.

G. Dolling (Oak Ridge National Laboratory): I have a rather general question to ask concerning the interpretation of Raman scattering spectra, with perhaps a specific reference to naphthalene. Symmetry arguments tell us that several modes may be Raman active. One then observes several peaks in the spectrum. How do you go about assigning in detail the correct normal-mode labels to each of the observed peaks? And do your assignments in the case of naphthalene really agree, in detail, with the calculations of Pawley? Are there any qualitative discrepancies?

G. R. Wilkinson: In general the methods used to classify Raman modes of vibration are as follows. The first approach is to consider the spectra of similar molecules; e.g., methyl vibrations were identified by early workers in this field by considering the spectra of a range of substances known to contain methyl groups. The next approach involves the observation of shifts in spectral lines on isotopic substitution, and their comparison with theoretically predicted values. Internal modes of vibration can be distinguished from external modes of vibration, as in general they will still occur in solution or in melts. Finally, using polarized radiation to measure the relative magnitudes of the components of the polarizability tensor, the symmetry class to which the vibration belongs may be assigned. The assignments for naphthalene agree in a qualitative rather than quantitative way with Pawley's calculations for the $\mathbf{k}=0$ spectra.

Jerome Schiffer (Temple University): In a crystal such as naphthalene, how sensitive are the calculated forms of the dispersion curves to the form taken for the intermolecular potential energy?

---

[1] M. Hass, Phys. Rev. Letters **13**, 429 (1964).

[2] R. Summitt, Spectrochemica Acta **23A**, 2857 (1967).

G. R. Wilkinson: As yet there is no experimental data on the complete dispersion curves for naphthalene, so it is not possible to answer the question whether a potential of the form

$$V(r)=-\frac{A}{r^6}+B\exp(-\alpha r)$$

can be adjusted to fit the curves. However, preliminary calculations suggest that it is not even possible to fit the $\mathbf{k}=0$ frequencies exactly.

W. Fateley (Carnegie Mellon University): Should we call the far infrared absorptions in liquids "pseudo lattice" vibrations?

G. R. Wilkinson: I used the term "pseudo lattice" modes in liquids to draw attention to the similarity between the infrared absorption in liquids and the corresponding absorption in crystals of the same substance due to lattice modes. However, if you object then maybe we should refer to them as collective molecular motions with correlation or relaxation times τ.

J. J. Rush (National Bureau of Standards): I was very interested in the results you presented on hexamethylbenzene, which showed changes in internal modes with temperature. A few years ago we measured neutron spectra for hexamethylbenzene, above and below its λ transition at 115 °K. We were able to directly observe the torsional vibrations of the methyl groups. These showed a dramatic change around the λ point, indicating changes in the barrier to rotation. These results, as well as some recent u.v. absorption spectra suggest that the λ transition is related to a distortion of the molecule. Are the changes you have observed in the I.R. spectra consistent with such a transition mechanism?

G. R. Wilkinson: The infrared absorption spectra show no evidence that can be unambiguously interpreted as due to a marked distortion of the hexamethylbenzene molecules. However, the possibility cannot be completely ruled out. There is a very marked change in infrared absorption associated with methyl vibrations which is interpreted as being due to a reorientation of the methyl groups. The Raman spectrum shows that if the hydrogen atoms are considered, then there is more than one molecule in the unit cell—at least in the high temperature phase.

E. R. Andrew (Nottingham University): May I add to the discussion on solid hexamethylbenzene? Allen and Cowking in our laboratory have measured the nuclear magnetic resonance spin-lattice relaxation time T_1 which gives a measure of the rate of reorientation of the methyl groups. At the 116 °K transition there is a discontinuous change of a factor of about three in T_1. Below 116 °K the correlation time of the reorientation is characterized by an activation energy of 1.9 kcal/mole, while above 116 °K it is 1.6 kcal/mole.

G. R. Wilkinson: I would be very interested to know what is the rate of reorientation of the methyl groups. It is important to know how this compares with the lifetime of the methyl vibrational states.

7. References

[1] A standard text on infrared and Raman spectroscopy is, Infrared and Raman Spectra of Polyatomic Molecules, G. Hertzberg (Van Nostrand, New York, 1945).
[2] A good text on the vibration of molecules, which makes extensive use of symmetry considerations and gives a full discussion of the determination of force constants is, Molecular Vibrations, E. B. Wilson, J. C. Decius and P. C. Cross (McGraw Hill Book Co., New York, N.Y., 1955).
[3] An extensive coverage of infrared and Raman spectroscopy can be found in the volume, Infrared Spectroscopy and Molecular Structure, edited by M. Davies (Elsevier, Amsterdam, 1963).
[4] A systematic approach to the classification of characteristic frequencies can be found in, The Infrared Spectra of Complex Molecules, L. J. Bellamy (Methuen, London, 1958).
[5] A very thorough discussion of vibration-rotation spectra in the gas phase can be found in, Molecular Vibrators, H. C. Allen and P. C. Cross (John Wiley & Sons, New York, N.Y., 1963).
[6] There are several sections devoted to the optical properties of lattice vibrations in, Dynamical Theory of Lattice Vibrations, M. Born and K. Huang (Oxford University Press, London, 1954).
[7] A more recent edited volume on phonons is, Phonons in Perfect Lattices and in Lattices with Point Imperfections, R. W. H. Stevenson (Plenum Press, New York, 1966).
[8] A concise outline of the theory of vibrations of isolated molecules can be found in, Chemical Infrared Spectroscopy, Vol. **1**, ch. 8, W. J. Potts (John Wiley & Sons, New York, N.Y., 1963).
[9] A full discussion of the infrared and Raman spectra of diatomic lattices has been given by Burstein in, Lattice Dynamics, edited by R. F. Wallis (Pergamon Press, London, 1964).
[10] S. Bhagavantam and T. Venkataryuda, Proc. Indian Acad. Sci. **9**, 224 (1939).
[11] R. S. Halford, J. Chem. Phys. **14**, 8 (1946).
[12] H. Winston and R. S. Halford, J. Chem. Phys. **17**, 607 (1949).
[13] W. C. Price and T. S. Robinson, Proc. Phys. Soc. **B66**, 969 (1953).
[14] R. A. Cowley, Advances in Physics **12**, 421 (1963).
[15] D. W. Berriman, Phys. Rev. **130**, 2193 (1963).
[16] R. Lyddane, R. Sachs and E. Teller, Phys. Rev. **59**, 673 (1941).
[17] R. Loudon, Advances in Physics **13**, 423 (1964).
[18] R. A. Cowley, Proc. Phys. Soc. **84**, 281 (1964).
[19] W. Cochran, Advances in Physics **9**, 387 (1960).
[20] A. S. Barker and M. Tinkham, Phys. Rev. **125**, 1527 (1962).
[21] C. H. Perry and T. F. McNelly, Phys. Rev. **154**, 456 (1967).

[22] For an account of the fundamentals of techniques see, Infrared Physics, J. T. Houghton and S. D. Smith (Oxford University Press, Oxford, England, 1966).
[23] H. A. Gebbie and G. A. Vanasse, Nature **178,** 432 (1956).
[24] Spectroscopic Techniques for Far Infrared and Millimetre Waves, edited by D. H. Martin (North Holland, Amsterdam, 1967).
[25] M. V. Hobden and J. P. Russell, Physics Letters **13**, 39 (1964).
[26] D. A. Kleinman and W. G. Spitzer, Phys. Rev. **119,** 110 (1960).
[27] S. S. Mitra and P. J. Gielisse, Progress in Infrared Spectroscopy, Vol. **2,** edited by H. A. Szymanski (Plenum Press, New York, 1964).
[28] C. H. Perry, H. Geick, and S. S. Mitra, J. Appl. Phys. **37,** 1994 (1966).
[29] M. A. Nusimovici and J. L. Birman, Phys. Rev. **156,** 925 (1967).
[30] B. Tell, D. C. Damen and S. P. S. Porto, Phys. Rev. **144,** 771 (1966).
[31] J. D. Axe and G. D. Pettit, Phys. Rev. **151,** 676 (1966).
[32] W. G. Spitzer and W. Kleinman, Phys. Rev. **121,** 1324 (1962).
[33] M. M. Elcombe, Proc. Phys. Soc. **91,** 947 (1967).
[34] S. M. Shapiro, D. S. O'Shea and H. Z. Cummins, Phys. Rev. Letters **19,** 361 (1967).
[35] J. F. Scott and S. P. S. Porto, Phys. Rev. **161,** 903 (1967).
[36] A. S. Barker and M. Tinkham, Phys. Rev. **125,** 1527 (1962).
[37] S. P. S. Porto, P. A. Fluery and T. C. Damen, Phys. Rev. **154,** 522 (1967).
[38] S. S. Mitra, Solid State Physics **13** (Academic Press, New York, 1962).
[39] I. Pelah, K. Krebs and Y. Imry, J. Chem. Phys. **43,** 1846 (1965).
[40] O. Oehler, Thesis for Doctor of Science Technische Hochschule Zurich (1967).
[41] R. P. Baumann and S. P. S. Porto, Phys. Rev. **161,** 842 (1967).
[42] H. H. Caspers, J. Murphy and R. A. Buchanan, J. Chem. Phys. **40,** 743 (1964).
[43] J. T. Hougen and S. Singh, Proc. Roy Soc. **A277,** 193 (1964).
[44] J. P. Mathieu and L. Coutoure, Compt. Rend. **228,** 1054 (1950).
[45] H. Boutin, G. J. Safford and V. Brajovic, J. Chem. Phys. **39,** 3135 (1963).
[46] S. P. S. Porto and R. S. Krishnan, J. Chem. Phys. **47,** 1009 (1967).
[47] E. V. Chisler and M. S. Shur, Phys. Stat. Solidi. **19,** 163 (1966).
[48] A. S. Barker, Phys. Rev. **135,** 742 (1964).
[49] S. P. S. Porto and J. F. Scott, Phys. Rev. **157,** 716 (1967).
[50] O. Schnepp, J. Chem. Phys. **46,** 3983 (1967).
[51] W. Vedder and D. F. Hornig, Infrared Spectra of Crystals, in Advances in Spectroscopy, edited by H. W. Thompson (Interscience, New York, 1961).
[52] V. Soots, E. J. Allin and H. L. Welsh, Can. J. Phys., 1985 (1965).
[53] E. J. Allin, W. F. J. Hare and J. C. F. MacDonald, Phys. Rev. **98,** 554 (1955).
[54] A. Ron, and O. Schnepp, J. Chem. Phys. **46,** 3991 (1967).
[55] A. Anderson and S. H. Walmsley, Molecular Physics **7,** 583 (1964).
[56] S. H. Walmsley and A. Anderson, Molecular Physics **7,** 411 (1964).
[57] J. E. Cahill, J. C. Laufer and G. E. Leroi, J. Chem. Phys. 47, 3678 (1967).
[58] S. H. Walmsley and J. Pople, Molecular Physics **8,** 345 (1964).
[59] D. A. Dows, Spectrochim. Acta **13,** 308 (1959).
[60] E. Sandor and R. F. C. Farrow, Nature **213,** 171 (1967).
[61] E. Sandor and R. F. C. Farrow, Nature **215,** 1265 (1967).
[62] L. C. Brunel and H. Peyron, C. R. Acad. Sci. **264C,** 821 (1961).
[63] A. Anderson, H. A. Gebbie and S. H. Walmsley, Molecular Physics **7,** 401 (1964).
[64] I. R. Beattie, Chemistry in Britain **3,** 347 (1967).
[65] A. Hadni and J. P. Mathieu, C. R. Acad. Sci. **252,** 1585 (1961).
[66] G. S. Pawley, Phys. Stat. Solidi **20,** 347 (1967).
[67] R. M. Hexter, J. Chem. Phys. **24,** 1186 (1955).

[68] W. C. Price and G. R. Wilkinson, J. Phys. Chem. Solids **18,** 74 (1961).

[69] E. R. Andrew, J. Chem. Phys. **18,** 607 (1950).

[70] J. J. Rush and T. I. Taylor, J. Chem. Phys. **44,** 2749 (1966).

[71] H. Tasumi and S. Krimm, J. Chem. Phys. **46,** 755 (1967).

[72] For a discussion of the theory and practice of infrared studies on polymers see, Infrared Spectroscopy of High Polymers, R. Zbinden (Interscience, New York, 1964).

[73] G. R. Wilkinson, W. C. Price and E. M. Bradbury, Spectrochim. Acta **14,** 284 (1959).

[74] Introduction to the Liquid State, Edited by P. Egelstaff (Academic Press, New York, 1967).

[75] R. G. Gordon, J. Chem. Phys. **43,** 1307 (1965).

[76] L. Woodward, N. N. Greenwood, J. R. Hall and I. Worrall, J. Chem. Soc. 1505, 1958).

[77] J. Nixon and R. A. Plane, J. Am. Chem. Soc. **84,** 4445 (1962).

[78] G. W. Chantry, H. A. Gebbie, B. Lassier and G. Wyllie, Nature **214,** 163 (1967).

[79] The Hydrogen Bond, G. C. Pimentel and A. L. McClellan (Reinhold, New York, 1960).

[80] W. C. Price, W. F. Sherman and G. R. Wilkinson, Proc. Roy. Soc. **255,** 5 (1960).

NEUTRON INELASTIC SCATTERING STUDIES OF MOLECULAR SOLIDS AND LIQUIDS

P. A. EGELSTAFF

Atomic Energy Research Establishment, Harwell, England

1. Introduction

The study of condensed matter involves a detailed description of atomic positions and motions, and relevant data may be obtained from the analysis of radiation scattering experiments. Many types of radiation are available each of which has different virtues, although a common function is measured in all such experiments. A monochromatic beam of radiation falls upon a specimen and the radiation scattered through an angle θ is studied. This scattering process involves the transfer of momentum (usually denoted by $\hbar \mathbf{Q}$) between the radiation and the specimen, and the scattered intensity is proportional to the probability $S(\mathbf{Q},\omega)$ that the specimen takes an energy $\hbar\omega$ from the radiation. In order to compare several types of radiation it is useful to compare their wavelengths and energies as shown in table 1. The wavelength region of greatest interest is around 3 Å because that corresponds to a typical spacing between the atoms of condensed matter. The energy difference between the incident and scattered beams should correspond to the allowed energy levels in the specimen, that is 0.01 to 0.1 eV in typical cases. Thus δE (expt) in table 1 should be of this order. It is seen that neutrons meet both of these requirements while electromagnetic radiation meets either one or the other (x rays providing a suitable wavelength range and light providing a suitable energy range).

TABLE 1. Wavelength and energy of various types of radiation

Radiation	Wavelength Å	Approx. momentum $=2\pi/\lambda A^{-1}$	Energy	Approximate δE (expt) eV
1 Neutrons	1–10	2	100–1 meV	10^{-1}–10^{-3}
2 X rays	0. 5–2	1	~10 keV	Wide
3 Light	4000–6000	$\sim 10^{-3}$	~10 eV	10^{-1}–10^{-3}
4 Electrons	~0. 1	0. 1	~50 keV	Wide

These points may be made more clearly in a diagram showing the regions of momentum and energy transfer space covered by each technique. This diagram is given as figure 1. Logarithmic scales have been used in order to locate the axes at the energy and momentum values quoted above. It can be seen that neutrons cover the central region of the diagram and hence may be expected to have the widest application. The periphery of this figure is covered by electromagnetic radiation because of the restrictions indicated in table 1. A striking feature of the diagram is the extent of the blank spaces which present day techniques do not cover. It can be seen that different techniques can be used to study different parts of the function $S(\mathbf{Q},\omega)$, and consequently the data obtained cannot be synthesised into a single result without further theoretical analysis.

In addition to such basic points, there are many questions of theoretical or experimental detail which can affect the quality or type of data obtained. Some of these points are summarized in table 2. Columns 1–5 correspond to the remarks made above. Column 6 lists points which affect the interpretation of the data, in terms of the function $S(\mathbf{Q},\omega)$, arising from the nature of the scattering process.

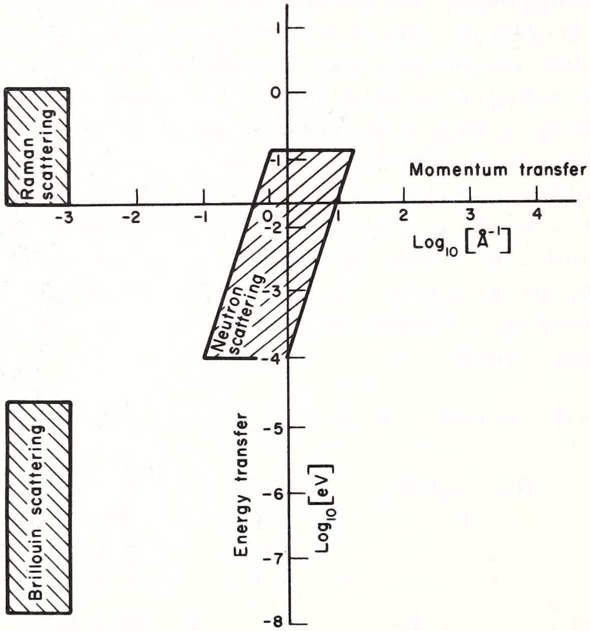

FIGURE 1. Momentum-Energy Space diagram, illustrating the regions covered by various radiation scattering techniques (from Egelstaff, P. A., 1966 IAEA meeting on "Research Applications of Repetitively Pulsed Boosters and Reactors").

TABLE 2. Summary of radiation techniques

(1)	(2)	(3)	(4)	(5)	(6)	(7)		
						Experimental Possibilities		
Radiation	Target	Data type	Momentum range (Q)	Energy range (ω)	Interpretation	Isotopic variation	Observation of hydrogen	Use of high/low cross section
1 Neutrons	Nucleus	Nuclear position correlation.	Wide	Wide	Straightforward.	Yes	Yes	Yes, for specimens containing H^1 or A^{36}.
2 X rays	Electron cloud.	Atomic position correlation.	Wide	Integrated.	Form factor.	No	Difficult	Yes, for specimens containing heavy and light elements.
3 Light	Electron cloud.	Atomic position correlation.	Small	Wide	Selection rules.	No	Yes, if large dipole moment.	Yes, for specimens containing high/low dipole moments.
4 Electrons	Charge cloud.	Atomic position correlation.	Wide	Integrated.	Form factor.	No	Difficult	As for X rays.

Column 7 lists three experimental points. Variation of isotopic ratios (e.g., *H*/*D* ratio) can be a powerful technique for isolating particular modes of motion since the scattering law [$S(\mathbf{Q},\omega)$] can be altered without altering the chemical nature of the sample. This possibility is open to neutron scattering only because neutrons interact with the nuclei, in contrast to the other cases listed where the interaction is through the electrons or electric charge. For studies of many molecular systems, the observation of hydrogen positions and motions is important, and the difficulty of doing this is indicated briefly in the table. Because the thermal neutron cross section of a proton is approximately 10 times that of a typical nucleus, the observation of protonic movements is relatively easy. As will be shown later, it is necessary to deuterate a sample in order to measure "hydrogen" positions in a crystal structure; the deuterium cross section is similar in magnitude to that for other nuclei. Motions involving hydrogen atoms are also observed in light scattering if the electric dipole moment is large enough to enhance the scattering due to a particular protonic mode. For x-ray or electron scattering experiments hydrogen is almost invisible. Finally a useful technique is the relative enhancement of the scattering from a particular group in a molecular system. For neutrons scattering this can be done by deuterating those parts of an organic molecule which it is desired not to observe. In this case scattering from the remaining hydrogenous groups (e.g., CH_3 —) can be examined. As will be explained later this method is useful for the study of molecular dynamics but not for structure work. An analogous technique can be used in x-ray structural studies for those cases where a heavy element can be placed at given points in a molecule. Due to the relatively large scattered x-ray intensity from heavy elements compared to light elements the location of such points is obtained. Thus the uses of this technique with neutron or x radiation are complementary, one providing dynamical and the other structural information.

In the following section the theory of neutron scattering will be outlined briefly, while later sections will be devoted to particular cases of neutron inelastic scattering by molecular systems.

2. Nuclear Scattering of Neutrons [1] [1]

The cross section for the scattering of radiation by matter has been described many times in the literature (e.g., Van Hove [2], Sjölander [3]). The method followed is (essentially) the same for each kind of radiation, differing only in detail, and in the following the principal steps in the theory of the scattering of thermal neutrons will be given. These steps are as follows:

---

[1] Figures in brackets indicate literature references at the end of this paper.

(a) For low energy (thermal) neutrons only s-wave nuclear scattering is important (because the neutron wavelength $\gg$ nuclear diameter).

(b) *s*-wave scattering cross sections (for an isolated stationary nucleus) are spherically symmetric and independent of neutron energy.

(c) The nuclear size is much smaller ($\sim 10^{-5}$) than the neutron wavelength and the interatomic distances hence we may write for the *i*th nuclear potential $V(r)$:

$$V_i(r) = \text{constant } \delta\ (\mathbf{r} - \mathbf{r}_i)$$

where $\mathbf{r}_i$ is the position of the *i*th nucleus.

(d) The overall perturbation is small (e.g., although the nuclear potential is very strong within its range, the intensity scattered by a single nucleus is very small) so that the Born approximation is valid.

(e) The constant in (c) is determined by fitting the Born cross section for epi-thermal neutrons to the measured "free atom" cross section. This constant is (conventionally) written:—

$$\frac{2\pi\hbar^2 b}{m}$$

where m is the neutron mass and b is a length (positive for hard-sphere scattering) called the bound atom scattering length. [The free atom cross section is equal to $4\pi\left(\frac{A}{A+1}\right)^2 b^2$ where A is the ratio of nuclear to neutron masses.]

(f) Therefore, the scattering amplitude for a system of N atoms is—

$$a(\Theta) \simeq \sum_{i=1}^{N} b_i \int d\mathbf{r}' e^{i\mathbf{Q}\cdot\mathbf{r}'} \delta(\mathbf{r}' - \mathbf{r}_i)$$

The essential point which has been given in step (f) is that the scattering amplitude in the Born approximation is expressed as the Fourier transform of the scattering potential. Since the scattering potential consists of a δ-function point for each atom we get a Fourier transform of the atomic positions. However, so far the atoms have been assumed to be fixed in space, and in order to allow for atomic motions the following point is considered.

(g) If the atoms are moving about on a timescale comparable with the value of $\frac{\hbar}{\delta E}$ then the time dependence of the atomic positions given in the formula in (f) above must be considered. Essentially the neutron wave suffers a Doppler shift, which is observed through the energy spectrum of the scattered neutrons. The condition for the conservation of energy in the scattering process may be represented as a Fourier transformation, so that the required scattering amplitude involves a Fourier transformation between time and energy. Thus the scattering amplitude involves both space and time Fourier transformations.

There is one final point to be considered, namely that an observable cross section is given by the square modulus of the scattering amplitude and for this reason it involves a product of two terms of the kind given under (f) above. These two functions give a "pair correlation function," and the cross section formula becomes finally the Fourier transformation of the pair correlation given at eq. (1):

$$G(\mathbf{r},\ \tau)=\frac{1}{N}\sum_{n,\,m}<\delta[\mathbf{r}+\mathbf{r}_n(0)-\mathbf{r}_m(\tau)]> \tag{1}$$

where $\mathbf{r}_m$ (τ) is the position of the mth atom at time τ. A subscript "s" will be used to denote the self term, that is the term for which $n=m$ in eq. (1).

The form of the correlation function shown here applies to a classical system, eqs (1) and (2) are taken from Van Hove [2] to whom this formalism is due.

The cross section is:

$$\frac{d^2\sigma}{d\Omega d\omega}=b^2\frac{k}{k_0}\int \exp i(\mathbf{Q}\cdot\mathbf{r}-\omega\tau)[G(\mathbf{r},\ \tau)-\rho]d\mathbf{r}d\tau \tag{2}$$

where b is the scattering length for a single bound atom and ρ is the average density of the system.

It is possible to consider two types of correlation functions. Referring to eq (1) the first of these is the case for which the two atoms n and m are the same; this correlation describes the average motion of a single atom and is therefore known as the self correlation function. The second type of correlation function is that for which n and m may take on any values, so that all atoms in the system are considered. This function is known as the coherent correlation function. The techniques which are used in neutron scattering work to separate the G function into these two parts depend upon the fact that different isotopes of the same element may have different scattering lengths and also that different spin states of the same isotope may have different scattering lengths. Thus the separation depends upon making measurements with the system in the same chemical state but in different nuclear states.

An important case of this kind is that of hydrogen. Here the scattering amplitude for the case of neutron and nuclear spins parallel is almost equal in magnitude but of opposite phase to the case of neutron and nuclear spins anti-parallel. Thus constructive interference of the scattered wavelets cannot occur and the scattered wave from each nucleus escapes from the specimen without being modified by interference effects. For this reason the neutron scattering by hydrogenous systems is proportional to the transform of the self-correlation function. That is it corresponds to the motions of single protons. In addition since the scattering cross section for protons is (fortuitously) about 20 times greater than that for carbon nuclei the neutron scattering by an organic molecule can be related to the motion of its hydrogen atoms only.

Another case is that for deuterium where the scattering lengths for parallel and anti-parallel spins are different. Here some constructive interference occurs and the coherent G function is observed. The coherent cross section for deuterium is similar in magnitude to that for carbon and many other elements so that interference between the wavelets scattered by all the atoms of a molecular system has to be considered. In this way the structure of a molecular system can be studied. In addition deuterium has a small incoherent cross section which gives a background to some experiments.

In summary, the cross section for hydrogen is large and incoherent while that for deuterium is of normal size and coherent.

3. Neutron Spectrometers [4, 5]

During the past decade many different types of neutron spectrometers have been developed. In each case, however, their success rests upon the determination of either the neutron wavelength or velocity. Either neutrons of a given wavelength are reflected from a single crystal in the same manner as used for x rays, or neutrons of a given velocity are selected by a system of shutters opening at pre-selected times. The neutron energy is then determined from the relationships:

$$E=\frac{1}{2}\,mv^2=\frac{h^2}{2m\lambda^2} \tag{3}$$

where m is the neutron mass, v is its velocity and λ is its wavelength For inelastic scattering measurements the system is complicated by the fact that two spectrometers are required. One is used to determine the energy and direction of the neutron beam falling upon the sample while the second is used to determine the energy and direction of scattered neutrons. Two of the most widely used spectrometers will be described briefly in the following.

A schematic diagram of a "3-axis" neutron spectrometer is given at figure 2. The beam of neutrons from the reactor has an approximately Maxwellian distribution of velocities giving the wavelength distribution shown in the inset. It is usual to collimate it to the desired angular definition before it falls upon the monochromatic crystal, so that the number of unwanted neutrons escaping from the reactor is kept to a minimum. Bragg reflection from the monochromatic crystal provides a beam at roughly the wavelength shown in the inset. This position on the Maxwellian peak is chosen so as to minimize the intensity of the second order reflections from the crystal. The angle between the sample table and the incident beam can be varied to allow the Bragg angle (and hence the reflected wavelength) of the crystal monochromator to be altered. The resolution of the incident wavelength is determined by the angular spread in the beam and the crystal mosaic according to the relation:

$$\frac{\Delta\lambda}{\lambda} \simeq \frac{\Delta\Theta_B}{\tan\Theta_B} \tag{4}$$

where Θ_B is the Bragg angle.

An analyzing crystal spectrometer is set up at a given (adjustable) scattering angle, and is set to Bragg reflect neutrons of a given wavelength into the neutron detector. A data point is then obtained as a ratio of the detected intensity to the beam monitor intensity. An instrument of this type provides a measurement of intensity at a given point in (ω-Q) space. By resetting three out of the four possible variables (two Bragg angles, angle of scatter and sample orientation) another given point in (ω-Q) space may be reached. In this way a chosen locus may be followed point by point. For this reason the three axis spectrometer is especially valuable for the study of lattice vibrations since, as discussed in section 4, a given lattice mode will give an intensity peak at one point of (ω-Q) space only.

A schematic diagram of a cold neutron scattering spectrometer is shown at figure 3. In this instrument a beam of low energy neutrons ($E << kT$) is allowed to fall on the sample and their energy change on scattering is measured. To enhance the number of low energy neutrons in the beam a small volume of liquid hydrogen is maintained near the center of the reactor. The effect of the liquid hydrogen moderator is to modify the usual Maxwellian spectrum as shown in the inset to figure 3. A beam of neutrons from the moderator is allowed to pass through a "Be filter," which is a block of polycrystalline beryllium metal held at liquid nitrogen temperatures. Neutrons of wavelengths greater than 4 Å will pass through the filter almost without collision, since their wavelength is too great for Bragg reflection and the cross section for scattering by lattice modes has

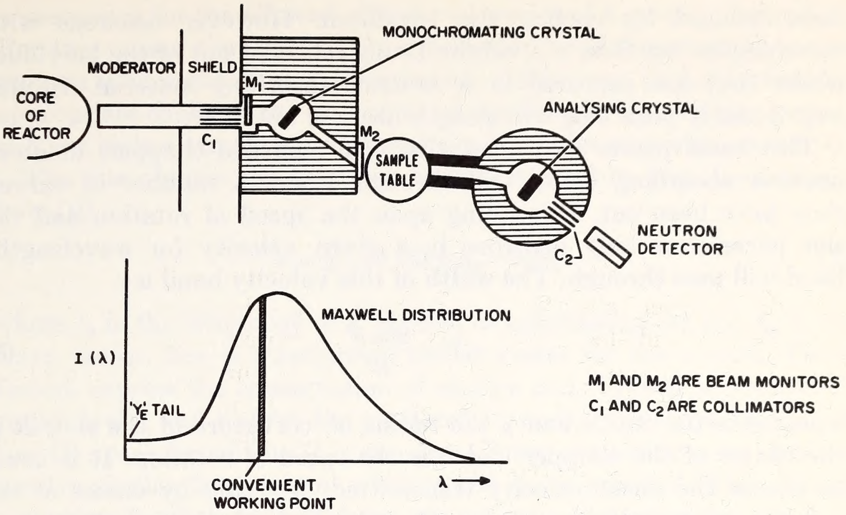
MONOCHROMATING CRYSTAL
MODERATOR
SHIELD
M1
CORE OF REACTOR
C1
M2
ANALYSING CRYSTAL
SAMPLE TABLE
NEUTRON DETECTOR
C2
MAXWELL DISTRIBUTION
I (λ)
'Y'E TAIL
CONVENIENT WORKING POINT
λ ⟶
M1 AND M2 ARE BEAM MONITORS
C1 AND C2 ARE COLLIMATORS

FIGURE 2. Diagram of a typical 3-axis neutron spectrometer: A horizontal section through the apparatus is shown. The inset shows the wavelength distribution from a reactor, and the usual working point for the monochromating crystal.

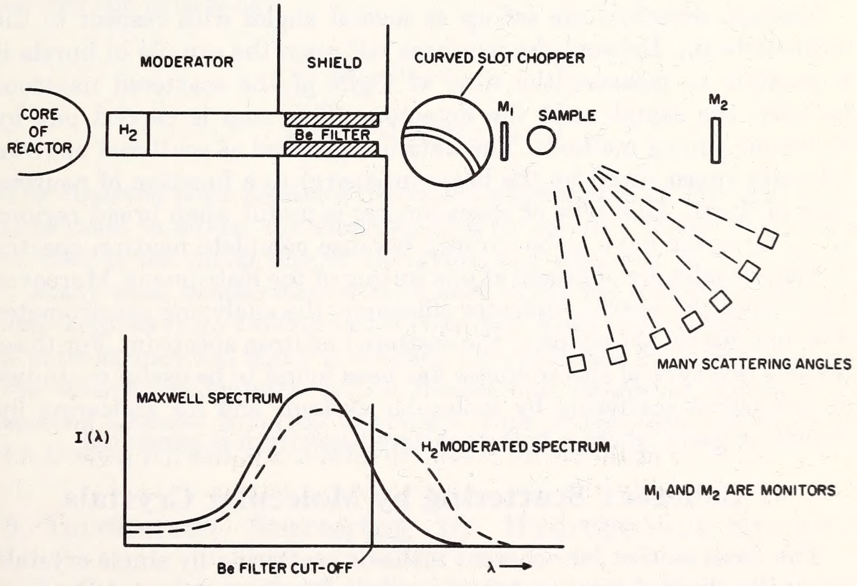
MODERATOR
SHIELD
CURVED SLOT CHOPPER
CORE OF REACTOR
H2
Be FILTER
M1
SAMPLE
M2
MANY SCATTERING ANGLES
MAXWELL SPECTRUM
I (λ)
H2 MODERATED SPECTRUM
M1 AND M2 ARE MONITORS
Be FILTER CUT-OFF
λ ⟶

FIGURE 3. Diagram of a cold neutron apparatus: A vertical section through the apparatus is shown. The inset shows the spectrum modification caused by the liquid hydrogen moderator.

been reduced by cooling the beryllium. However neutrons with wavelengths less than 4 Å can be Bragg reflected out of the beryllium where they are captured in a neutron absorbing material. In this way a nearly pure long wavelength beam is obtained.

This beam passes into a rotating disc (called a chopper) made of neutron absorbing metal and through which a number of curved slots have been cut. Depending upon the speed of rotation and the slot parameters only neutrons in a given velocity (or wavelength) band will pass through. The width of this velocity band is:

$$\Delta V = \frac{8d\omega\rho^2}{R^2} \tag{5}$$

where d is the width and ρ the radius of curvature of the slot, R is the radius of the chopper and ω is the speed of rotation. It is usual to choose the mean velocity transmitted ($V=2\omega\rho$) by choice of the rotational speed, and in this case the relative resolution is independent of velocity according to the relation:

$$\frac{\Delta V}{V} = \frac{4d\rho}{R^2} \tag{6}$$

Typical values for $\Delta V/V$ are 6 percent to 10 percent at 5 Å.

Neutron detectors are set up at several angles with respect to the incident beam. Because the neutrons fall upon the sample in bursts it is possible to measure the time of flight of the scattered neutrons between the sample and the detectors. This step is carried out by electronic timing methods. The data is registered as scattered neutron intensity (normalized by the beam intensity) as a function of neutron time of flight. This type of spectrometer is useful when broad regions of (ω–$\mathbf{Q}$) space have to be covered because complete neutron spectra at many angles are obtained at one setting of the instrument. Moreover apart from the neutron detector efficiency, the analyzing spectrometer does not distort the shape of the scattered neutron spectrum. For these reasons this type of spectrometer has been found to be useful in studies of incoherent scattering by molecular systems and for scattering by liquids or gases where a broad scattered spectrum is generated.

4. Coherent Scattering by Molecular Crystals

The cross section for coherent inelastic scattering by single crystals is usually divided into contributions from the interaction of the neutron and the crystal involving one, two, etc., vibrational quanta (phonons). The most useful information is obtained from the one phonon cross section; namely the relationship between frequency and wave vector for the allowed vibrational modes of a given polarization. For this reason that part of the interaction involving more than one phonon is thought of as a background which must be kept small by appropriate choice of the experimental conditions. Usually this means, not too high a temperature or magnitude of the scattering vector $\mathbf{Q}$.

The one phonon cross section is proportional to (e.g. Lomer and Low [1])

$$\delta(\omega \pm f_\epsilon)\, \delta\, (\mathbf{Q} \pm \mathbf{q}_\epsilon - 2\pi\tau) \tag{7}$$

where f_ϵ is the frequency of a phonon of polarization (ϵ) and $\mathbf{q}_\epsilon$ is its wave vector. $2\pi\tau$ is a reciprocal lattice vector for the crystal. These factors express the conservation of energy and "crystal momentum" respectively, and restrict the scattered intensity to narrow regions of ($\omega - \mathbf{Q}$) space for which (7) is non-zero. Bragg scattering cross sections involve similar factors from which f and $\mathbf{q}$ are omitted. Thus Bragg scattering is distinguished from one phonon scattering by the fact that it is an elastic rather than an inelastic process. On the other hand multiphonon processes give rise to a factor $\delta\ (\mathbf{Q} \pm \Sigma \mathbf{q} - 2\pi\tau)$ and since a range of energy transfers can meet this condition a broad energy spectrum is observed. Thus if a neutron spectrometer has sufficient energy and momentum resolution the one phonon scattering will be seen as peaks of scattered intensity whose position is determined by solving the equations:

$$\left.\begin{aligned} &\frac{\hbar}{2m}\,(k_0^2 - k^2) = \hbar\omega \\ &\mathbf{k}_0 - \mathbf{k} = \mathbf{Q} = 2\pi\tau \pm \mathbf{q}(\omega) \end{aligned}\right\} \tag{8}$$

The observed peak positions determine experimentally the locus $\mathbf{q}(\omega)$. It is usual to adjust the direction of $\mathbf{q}$ by suitable choice of $\mathbf{Q}$ and τ so that it lies along one of the symmetry direction of the crystal.

Many such measurements have been made for metal crystals and ionic crystals (e.g., Dolling and Woods [6]). Work on molecular crystals is in its infancy but many interesting new problems arise. For example the interaction between lattice modes and molecular modes is of especial interest. A review of current work in this field will be given by Dolling [7], and will not be discussed further here.

5. Incoherent Scattering by Hydrogenous Systems

As discussed in section 2 the incoherent scattering is related to the Van Hove correlation function for single atoms (denoted by the subscript s). It has been found convenient to make incoherent measurements at low values of $\mathbf{Q}$ because structure in the spectrum of inelastically scattered neutrons can be observed more easily than at high **Q** values. The reason for this may be seen via the example of the crystalline solid. In this case $S_s(\mathbf{Q},\omega)$ has the form (e.g., Lomer and Low[1]) in the classical limit:

$$S_s(\mathbf{Q},\omega)=e^{-\lambda Q^2}\left\{\delta(\omega)+\frac{kT}{M}Q^2\frac{\rho(\omega)}{\omega}+\left[\frac{kT}{M}Q^2\right]^2\int\frac{\rho(\omega-\omega')\rho(\omega')d\omega'}{2(\omega-\omega')^2\omega'^2}+\mathrm{O}(Q^6)\right\} \tag{9}$$

where $\rho(\omega)$ is the spectrum of normal modes and $\exp(-\lambda Q^2)$ is the Debye-Waller factor. The first term in this expansion corresponds to elastic scattering while the second term corresponds to one-phonon interactions, and the detailed structure of the phonon spectrum can be seen in this term. However the third term corresponds to two-phonon interactions and gives a broad spectrum due to the convolution integral. Finally the higher order terms, corresponding to multiphonon interactions give even broader spectral distributions. Thus the detail of the one phonon spectrum is best observed by allowing $Q\rightarrow 0$ for non zero values of ω.

To interpret the experimental data it is usual to make an approximation for the shape of $G_s(r,\tau)$—eq (1)—which will enable the higher order terms $\{\mathrm{O}(Q^4)\}$ in $S_s(\mathbf{Q},\omega)$ to be calculated from the first order term. This approximation is:

$$G_s(r,\tau)\simeq\frac{1}{\{\pi w^2(\tau)\}^{3/2}}\exp-\frac{r^2}{w^2(\tau)} \tag{10}$$

where $w^2(\tau)$ is the time dependent width of this Gaussian function. The velocity correlation function is obtained from $w^2(\tau)$ by double time differentiation. Since this approximation to the shape of $G_s(r,\tau)$ is needed only to correct the data for higher order contributions it does not introduce a large error into the determination of $z(\omega)$. This is particularly true if energies of levels are required only. A larger error enters the determination of the amplitude of molecular modes.

In general molecular systems undergo non-harmonic motions to which eq (9) does not apply. However the above result may be generalized by considering the velocity correlation function for a single atom. This function is the thermally averaged correlation between the velocity, $v(t)$, of an atom of time t and its velocity at a later time $(t+\tau)$. It is usual to discuss the spectral density of this function, since then particular modes of motion will appear as peaks whose area is proportional to the amplitude of the mode. In the case of a harmonic crystal lattice the spectral density is equivalent to the combined frequency spectrum of lattice modes and molecular modes. In other cases it has a shape dependent on the type of motion occurring.

It may be shown (e.g., Sjolander [8]) that the velocity correlation for a classical system is simply related to the scattering law, $S(Q,\omega)$, by the rule.

$$z(\omega)=\frac{1}{\pi}\int_0^\infty \cos\omega\tau \, <V(0)\cdot V(\tau)> d\tau=\omega^2\left[\frac{S_s(\mathbf{Q},\omega)}{\omega^2}\right]_{Q\rightarrow 0} \tag{11}$$

where $z(\omega)$ is the spectral density of the velocity correlation function. Thus most experiments on hydrogenous molecular systems are directed towards the determination of part of $z(\omega)$; usually that part between frequencies of $10^{12} - 10^{14}$ Hz.

It should be noted that every atomic motion makes a contribution to $z(\omega)$, and to isolate one type of motion within the whole spectrum requires some additional information. A knowledge of the approximate frequency and shape of a given rotational or vibrational contribution to $z(\omega)$ may be sufficient to identify it. In other cases however the temperature dependence or dependence on chemical form may be required. A particularly powerful technique is that of isotopic substitution (e.g., substitution of D for H) which will be discussed separately in section 7.

Another point of importance is that the cross sections can be measured on an absolute scale and their angular dependence determined. This provides information on the amplitude of molecular modes. If the mode of motion is anisotropic then the width function in eq (10) must be treated as a tensor rather than a scaler quantity. In the simplest case of a mode with cylindrical symmetry the difference between the Debye-Waller factors for elastic and inelastic scattering is sufficient to determine the amplitudes along the z- and x-axes.

6. Studies of Molecular Rotation

The technique described above is applicable to gaseous, liquid or solid systems but it has been used mainly to examine rotational or torsional modes of molecular systems. Data of this type are usually obtained by the cold neutron scattering technique shown in figure 3. An example is provided by liquid methylchloroform; the cold neutron spectrum (5.3 Å neutrons at a scattering angle of 60°) is shown in figure 4 [9]. The three peaks marked A, B, and C correspond to translational diffusion, quasi-lattice modes and torsional oscillation of the CH_3 group respectively. A spectrum such as this provides qualitative information on the separate identity of the different modes and quantitative information on their positions. The reduction of the raw data to $z(\omega)$ will change significantly the relative magnitudes of the peaks, by reducing the low frequency peaks relative to the high frequency one.

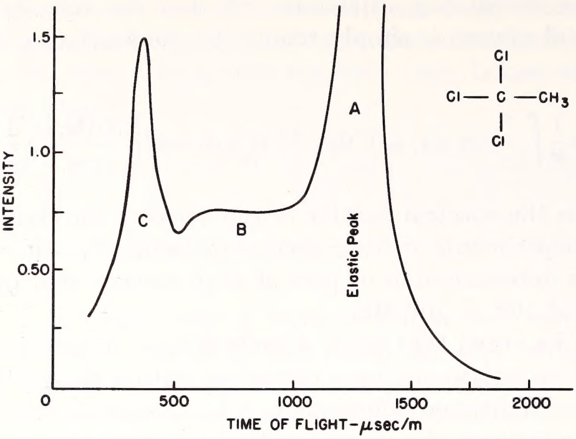

FIGURE 4. Cold neutron spectrum from liquid methyl-chloroform. The peaks marked A, B, and C correspond to translational motion, quasi-lattice vibrations and internal molecular rotations respectively. (Brier et al., [9])

The question of free or hindered rotation has been the object of many experiments. For example Janik et al. [10], studied both ammonium perchlorate and perchloric acid. These two systems have the same crystal structure but the NH_4^+ group is believed to be rotating almost freely while the H_3O^+ group is strongly hindered. The cold neutron spectra exhibited by these two materials are shown in figure 5a (4 Å neutrons scattered at 90°). For free rotation the data should take the form of a Maxwellian envelope (because the spacing of the rotational states is nearly continuous) and this is consistent with the data on NH_4ClO_4. However for hindered rotation—or torsional oscillation—the levels are more widely spaced and individual levels can be seen in the spectra, as is evident in the data on H_3OClO_4.

An analogous effect has been observed across the phase transition of hexamethylbenzene at 110°K. The data of Rush and Taylor [11] are shown in figure 5b (4 Å neutrons scattered at 60°). At low temperatures the CH_3-groups are undergoing torsional oscillation and the $1 \rightarrow 0$ transition (17 meV) can be seen in the spectrum. At temperatures above the transition the oscillation is modified, the rotational barrier is lowered and the peak moves to 15 meV. Additional broadening of this peak occurs due to the interaction of torsional and lattice modes. The barriers due to rotation were deduced by Rush and Taylor to be 1.35 ± 0.10 kcal/mole below and 1.07 ± 0.09 kcal/mole above the transition. A detailed description of this transition is not available but a change of molecular shape may explain the data. Further and more detailed neutron experiments would be worthwhile.

The rotation of the NH_4^+ group in NH_4Cl has been the subject of many experiments. Most of these experiments were carried out with

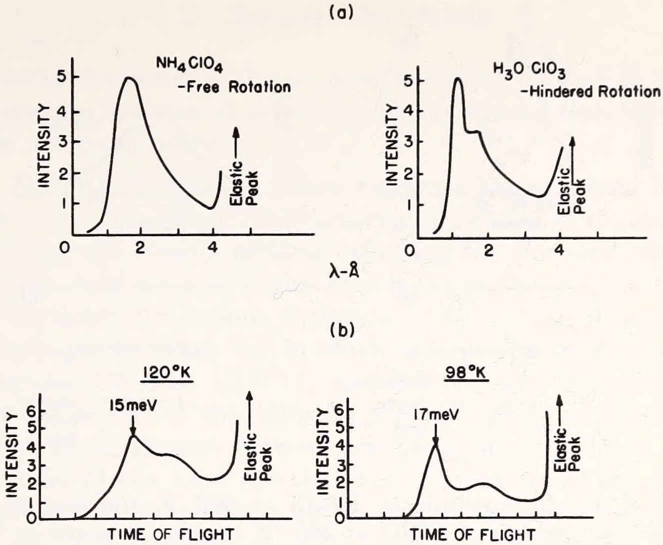

FIGURE 5. a. Cold neutron (4Å) spectra of ammonium perchlorate and perchloric acid (Janik et al., [10]) at an angle of 90°.

b. Cold neutron spectra (4Å) at an angle of 60° for Hexamethylbenzene at temperatures above and below the transition (Rush and Taylor [11]).

high energy (rather than low energy) neutrons. In such experiments a beam of high energy neutrons gives energy to the specimen and, usually, those scattered neutrons low enough in energy to pass through a beryllium filter are detected. Data of this kind obtained by Bajorek el al. [12] at 265 °K are shown in figure 6a. Of the several features shown by this spectrum the one marked by the arrow is due to the rotation of the NH_4^+ group (48 meV). The question of structure in this peak has been examined in detail by Venkataraman et al. [13]. Their data, giving an enlarged view of the peak at 300 °K are shown in figure 6b. It can be seen that the peak is a doublet; the explanation of which is illustrated at figure 6c. At 300 °K both the zero and first excited states are populated so that a neutron can lose energy by the two transitions shown in the figure. If the level spacings are not equal, a doublet will be seen in the neutron spectrum. It is possible to identify the components of the doublet by changing the temperature of the specimen so varying the intensity of the 1→2 transition relative to the 0→1 transition. Using this method Venkataraman et al. [13] showed that the 1→2 transition was of lower energy than the 0→1 transition.

A phase transition in NH_4Cl occurs at 243 °K and neutron scattering experiments made above and below the transition show that a shift in frequency of the rotational mode occurs; it moves to a higher

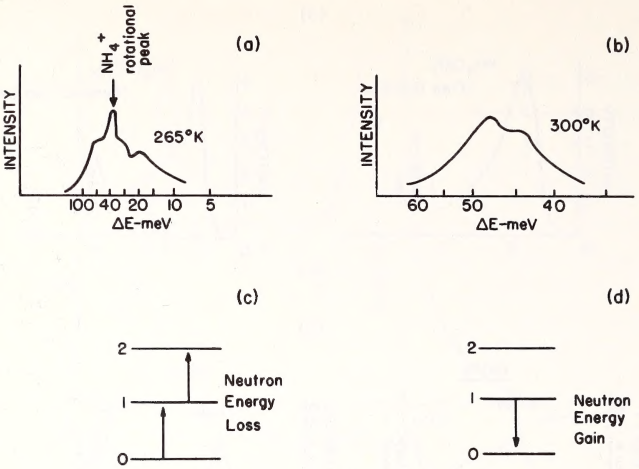

FIGURE 6. a. Energy spectrum of NH_4Cl at 265° K (Bajorek et al., [12]). b. Energy loss spectrum of NH_4Cl at 300 °K showing structure in rotational peak (Venkataraman et al., [13]). c. Levels excited in energy loss experiment.

frequency at the lower temperature. Although many neutron experiments have been carried out on NH_4Cl the resolution and temperature control were insufficient for a detailed study of this transition and further work remains to be done.

Other examples are discussed in the literature (e.g. Janik and Kolwalska [14]) which together with those given above show the value of neutron techniques in the study of molecular rotation. One possible direction for future studies may lie in the comparison of neutron and optical data to find the correlation function for the rotation of neighboring molecules. The neutron data concern the rotation of single molecules (because the incoherent scattering by protons is observed) but the optical data concern the rotational correlation function for all pairs of molecules in the system. Gordon [15] describes how the rotational correlation function may be derived from the optical data. It is usual to analyze these experiments through the assumption that the rotation of neighboring molecules is uncorrelated, and in this case only the self term will be observed so that the optical and neutron data will be in agreement. If, however, a careful comparison of the two types of data [one method of making this comparison is described by Agrawal and Yip [16]] shows up significant discrepancies then the rotational correlation of neighboring molecules can be expected to be important. Even the limited data available at present would seem to justify some comparisons of this type, (e.g. Agrawal and Yip [16]).

7. Special Methods

Because of the power of the neutron scattering method in the study of hydrogenous systems, it can be applied in special situations. Three examples are given below.

(a) *Isotopic Substitution.* Since neutrons are scattered by nuclei it is possible to change the scattering properties of the system (by changing the nuclei) without changing the chemical properties. The principal example of this kind is the replacement of hydrogen by deuterium in organic molecules. This technique is described in the paper by White [17] in which neutron spectra from the three molecules CH_3OH, CD_3OH, and CH_3OD are reported. In this way the motion of the different parts of the molecule may be observed as differences between the three spectra. More complex examples of this kind are the study of rotation of side groups of polymer chains, and the rotation of paraffin molecules by studying specimens deuterated at the ends or centers of the molecule.

A similar method is to replace hydrogen by fluorine since fluorine is relatively "invisible" to neutrons. However this often results in a change in physical or chemical properties and so does not have as wide an application as the former method.

(b) *The Study of Molecular Series.* The conventional technique of observing the frequency of a rotational or torsional mode as a function of molecular species may be used to advantage in neutron work. This is especially so in cases where one or two members of a series are symmetrical molecules which cannot be examined by optical methods. An example is provided by the chloroethanes. Allen et al. [18] studied the internal rotation of molecules from C_2H_6 to C_2Cl_6 by optical and thermodynamic methods, but for two members of the series the data were unsatisfactory. Recently these workers have used neutron spectroscopy to remeasure the frequencies of these two molecules with the results shown in table 3 and figure 4.

The interpretation of these data rests upon the assumption that the frequency of the torsional mode is independent of wave number. In this case neutron results are more reliable than the other data for the molecules chosen, and when taken with the other data for the lower and higher members of the series form a reasonably consistent set.

(c) *Motion of guest molecules (e.g., in xeolites).* The high neutron cross section of hydrogen makes it possible to observe the motion of a guest molecule in a lattice of low cross section materials. Examples are provided by natural or artificial xeolite—which normally consist of low cross section nuclei—and by clathrates

TABLE 3—Rotational barriers in chloroethanes

Molecule	C_2H_6	C_2H_5Cl	CH_3CHCl_2	CH_3CCl_3	CH_2ClCCl_3	$CHCl_2CCl_3$	C_2Cl_6
Thermodynamic data	3. 0			2. 8			
Optical data		3. 7	3. 3–3. 7		10. 0	14. 2	17. 5
Neutron data			5. 0	6. 0			

All values in kcal/mole.

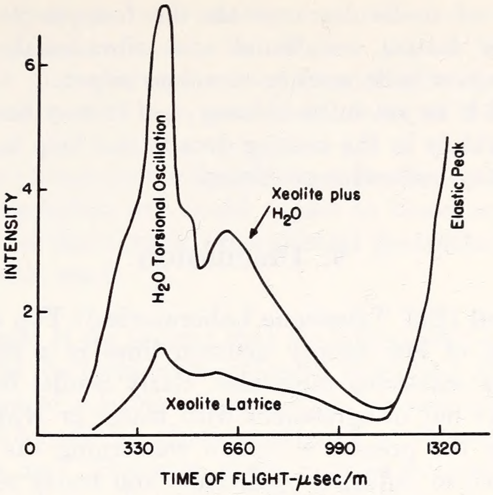

FIGURE 7. Spectra from the scattering of cold (5.3Å) neutrons by xeolite 3A containing H_2O at an angle of 20°. The lower curve is the scattering by the empty lattice. (Egelstaff et al., [19]).

if prepared in deuterated form. As an example, figure 7 shows the data of Egelstaff et al. [19] on H_2O in molecular sieve 3A. The additional scattered intensity due to the water is clearly visible over the scattering due to the xeolite lattice. These data can be analyzed to show the frequency spectra of the guest molecule, the amplitude of its vibrations and the time it spends at one site in the cage.

8. Conclusions

Over the past decade neutron spectrometers have been developed to the point where they can be employed as routine instruments. This in turn has led to the widespread use of neutron spectroscopy in the study of atomic and molecular dynamics. The analysis of the scattered neutron spectrum from a molecule can provide data on both the frequencies and amplitudes of translational, rotational and vibrational modes.

The technique is made more useful by the fortunate circumstance that the cross section for protons is abnormally large while that for deuterium is similar to other nuclei. Thus a wide range of organic molecules can be studied and the motion of each part of the molecule examined separately. Of especial interest is the comparison of neutron and optical data on rotational spectra in order to isolate the rotational correlations between neighbouring molecules.

In the case of molecular crystals the frequency—wave number relationship for lattice, rotational and vibrational modes can be measured. However little work is complete as yet.

This method is as yet in its infancy, but it may be expected to be applied more widely in the coming decade and help to provide a new insight into many molecular problems.

9. Discussion

D. W. McCall (Bell Telephone Laboratories): You mentioned that the broadening of low energy neutron lines is a reflection of self diffusion of the scattering molecules. Early results for self diffusion coefficients were not in agreement with tracer or NMR results. Can you summarize the present situation concerning the comparison of the neutron-derived diffusion coefficients and tracer results?

P. A. Egelstaff: There are several reasons for this discrepancy. One is that neutron measurements are made at high values of the momentum transfer where you observe the time for a diffusive step rather than the diffusion constant. This effect gives an observed width for the quasi-elastic peak which is less than that forecast by Ficks law. Another reason is that the spectral density of the velocity correlation function for protons in large organic molecules often has intense components at low frequencies. In contrast with the above effect this causes the width to be larger than predicted by Ficks law.

In general, the values of the momentum transfer used in neutron work are not small enough to be sure that the diffusion constant is measured properly, but as indicated above, other interesting information may be obtained from the data. For those cases (e.g., liquid sodium or liquid hydrogen) where one has reason to believe that Q is small enough, reasonable agreement with tracer or NMR work is found. However, even in these cases, the diffusion constant can be measured to a higher accuracy by the other methods, so that one should not look to the neutron method for good diffusion constant data. Rather one should exploit the new information made available by a tool which can probe at high Q values.

V. H. Schmidt (Montana State University): How fast a hindered rotation can be distinguished from a free rotation?

P. A. Egelstaff: The practical answer depends upon whether other modes of motion overlap or couple to the rotation being sought. However, if a molecule resides in a given orientation for 10^{-12} sec or longer the hindering is easily visible but if it resides for less than

10^{-13} sec it will appear as virtually free. This answer applies to a typical existing spectrometer, but if (see answer to Dr. Moore's question) a new phased chopper spectrometer is used, one might hope to push one limit to 10^{-11} sec and the other to 10^{-14} sec.

M. J. Moore (Rensselaer Polytechnique Institute): Could you comment on the resolution one could expect in these scattering experiments, in view of the various experimental parameters, e.g., chopper width, flight path, etc.?

P. A. Egelstaff: If we assume that the collimation angles are in the region of 2° and the incident wavelength is about 5 Å, then the average performance of existing spectrometers corresponds to resolutions ranging from 0.5 meV for elastic scattering to 10 meV for an energy transfer of 100 meV. However, there may be as much as a factor 10 difference in resolution between a filter-chopper apparatus mounted on a low flux reactor and a phased chopper apparatus mounted on a high flux reactor (e.g., the new cold neutron apparatus at the NBS reactor). A spectrometer of the latter type can have a resolution of 0.05 meV for elastic scattering and 0.5 meV for inelastic transition of 30 meV.

P. Coppens (Brookhaven National Laboratory): What are the prospects for observing overtones of molecular librations? Has information on anharmonicity of the librations been obtained?

P. A. Egelstaff: The cases of (lattice) modes in NH_4Cl and PH_4I have been studies already, but only a limited number of cases in which the level energy is ≤ 0.05 eV can be examined using present techniques. Future development, towards studying unharmonicity of internal modes of molecules, will become possible when strong neutron sources of about 0.25 eV are available (e.g., the linac pulsed neutron source). Some experiments of this kind have been conducted on metal hydrides by Yeater and co-workers at R.P.I. and by Whittemore and co-workers at G.A.

10. References

[1] Lomer, W. M. and Low, G. C., Ch. 1, Thermal Neutron Scattering, Ed. P. A. Egelstaff, Academic Press (London), (1965).

[2] Van Hove, L., Phys. Review **95**, 249, (1954).

[3] Sjolander, A., 72, Phonons and Phonon Interactions, Ed. T. A. Bak (New York: Benjamin), (1964).

[4] Brugger, R. M., Ch. 12, Thermal Neutron Scattering, Ed. P. A. Egelstaff, Academic Press (London), (1965).

[5] Iyengar, P. K., Ch. 3, Thermal Neutron Scattering, Ed. P. A. Egelstaff, Academic Press (London), (1965).
[6] Dolling, G. and Woods, D. B., Ch. 5, Thermal Neutron Scattering, Ed. P. A. Egelstaff, Academic Press (London), (1965).
[7] Dolling, G., These proceedings.
[8] Sjolander, A., Ch. 7, Thermal Neutron Scattering, Ed. P. A. Egelstaff, Academic Press (London), (1965).
[9] Brier, P. N. et al., To be published.
[10] Janik, J. A., Janik, J. M., Mellor, J. and Palevsky, H., J. Phys. Chem. Solids **25,** 1091, (1964).
[11] Rush, J. J. and Taylor, T. I. (1966), J. Chem. Phys. **44,** 2749, (1966).
[12] Bajorek et al., In Inelastic Scattering of Neutrons, Vol. II, 355, published by IAEA, Vienna, (1965).
[13] Venkataraman, G. et al., Report No. AEET 258, (1965).
[14] Janik, J. A. and Kowalska, A., Ch. 10, Thermal Neutron Scattering, Ed. P. A. Egelstaff, Academic Press (London), (1965).
[15] Gordon, R. B., J. Chem. Physics **43,** 1307, (1965).
[16] Agrawal, A. K. and Yip, S., These proceedings.
[17] White, J. W., These proeedings.
[18] Allen, G., Brier, P. N. and Lane, G. Trans Faraday Society **63,** 824, (1967).
[19] Egelstaff, P. A., Downes, J. and White, J., Proc. Soc. Chem. Ind., 306, (1968).

THE PRINCIPLES INVOLVED IN THE STUDY OF MOLECULAR MOTION IN SOLIDS BY NUCLEAR MAGNETIC RESONANCE

R. E. RICHARDS, F.R.S.

Physical Chemistry Laboratory, University of Oxford, Oxford, England

1. Introduction

Nuclear resonance lines in solids are often broadened either by magnetic dipole-dipole interactions with other spins in the crystal or by quadrupole coupling between the *electric* quadrupole moment of the nucleus and electric field gradients in the crystal; in special cases other mechanisms may also contribute to the line width. If molecular motion occurs in the solid with sufficient frequency, these interactions may be partially or completely averaged to zero; from the change of line shape and width it is often possible to characterize the axis or axes and the amplitudes of the molecular motion responsible for the changes of line width. The mechanisms of the various interactions which may cause line broadening in n.m.r. spectra are outlined briefly below and the conditions for line narrowing by molecular motion considered.

The magnetic dipole-dipole and electric quadrupole interactions also provide the most important process by which Zeeman energy can be transferred among the nuclei themselves, by so-called spin-spin relaxation, and by which energy may be exchanged between the nuclear spin system and the thermal motion of the molecules in the lattice, by spin lattice relaxation. These two processes are usually characterized by the spin-spin relaxation time, T_2, and the spin lattice relaxation time, T_1.

The nuclear spin lattice transitions are not stimulated by time independent effects, but only by interactions which are modulated at appropriate frequencies. In solids the transitions are induced by the magnetic dipole-dipole couplings or by the electric quadrupole couplings, which are modulated by molecular motion. By studying the variation of T_1 and T_2 with temperature, the frequency of the molecular motion and its temperature dependence can be found. The principles of these studies, and some of the complications which can occur, are discussed in the second part of the article.

The physical principles are most easily discussed using the so-called rotating frame of reference; for readers not familiar with the terminology involved, the basic ideas are outlined in the next section.

2. Magnetic Resonance

2.1. The Use of Rotating Coordinates

A nuclear magnet of moment, $\boldsymbol{\mu}=\gamma\boldsymbol{\rho}$, where γ is the gyromagnetic ratio and $\boldsymbol{\rho}$ is the nuclear angular momentum, experiences a torque when placed in an applied magnetic field, $\mathbf{H}_0$, so that its energy depends on its orientation in the applied field. The angular momemtum, $\boldsymbol{\rho}$, may be written as $\mathbf{I}h/2\pi$, where $\mathbf{I}$ is the spin angular momentum in units of $h/2\pi$, and the theory of quantum mechanics[1][1] requires that $\mathbf{I}$ has the magnitude $\sqrt{I(I+1)}$ and that the only measurable values of this vector are given by the magnetic quantum number, m, which may take on the values

$$-I,\ -I+1,\ -I+2,\ .\ .\ .\ .\ .\ -1,\ 0,\ +1,\ +2,\ .\ .\ .\ .\ +I,$$

each of these values corresponding to a particular orientation of the nuclear magnet in the applied field, $\mathbf{H}_0$. A nucleus may therefore occupy one of $(2I+1)$ orientations in $\mathbf{H}_0$, each of which corresponds to a particular energy level, and we may write the energy, E_m, as

$$E_m=-\boldsymbol{\mu}.\,\mathbf{H}_0=-H_0m.\frac{\gamma h}{2\pi} \tag{1}$$

For a nucleus with $I=\frac{1}{2}$, there are two energy levels with $E_m=-\frac{1}{2}H_0\gamma h/2\pi$ and $+\frac{1}{2}H_0\gamma h/2\pi$; the energy difference is $H_0\gamma h/2\pi$ and transitions between the levels may be stimulated by radiation of energy $h\nu_0=H_0\gamma h/2\pi$ or angular frequency $\omega_0=\gamma H_0$.

The combination of the torque exerted by the magnetic field on the moment $\boldsymbol{\mu}$ and the spin angular momentum $\mathbf{p}$ causes the nucleus to precess [2] about $\mathbf{H}_0$, according to the Larmor theorem, at an angular frequency,

$$\boldsymbol{\omega}_0=-\gamma\mathbf{H}_0, \tag{2}$$

and eq. (2) describes the motion of a nucleus in its particular energy level E_m (see fig. 1a). Note that the angular precession frequency is just equal to the angular frequency of the radiation required by the quantum theory to stimulate transitions of the nuclei from one energy level to another.

An observer in the fixed coordinate system x, y, z, (fig. 1a) would observe the nucleus precessing at angular frequency ω_0, and from eq

---

[1] Figures in brackets indicate the literature references at the end of this paper.

(2) he could measure the field H_0. If the observer now placed himself in a frame of reference $x'y'z'$, having the same z axis but with the x' and y' coordinates rotating about z in the same sense as the nuclear precession and at ω_0, the nucleus would appear to him to be stationary (fig. 1b). *In the rotating frame*, the effective magnetic field would then be zero, as measured by an observer using eq. (2).

A sample of finite size will contain many nuclei, all of which may not be in identical values of H_0, either because of magnetic field inhomogeneity, or because of magnetic interactions in the sample. If the $x'y'$ coordinates rotate at ω_0 corresponding to the mean value of H_0 applied to the sample, the observer in the rotating frame will see many nuclei stationary, but with some precessing slowly in either direction, corresponding to the distribution of magnetic fields about H_0, the apparent precession frequency being $\Delta\omega=\gamma\Delta H$ where ΔH is the deviation from the mean value of H_0.

We can now consider the resultant nuclear magnetization of a large number of nuclei. For $I=\frac{1}{2}$, the nuclei will be distributed between two energy levels or orientations in H_0, with more in the lower level than in the upper according to the Boltzmann distribution. There is therefore a small resultant magnetization along the z axis. However, because of the distribution of fields about H_0, there will be nuclei precessing about z at slightly different frequencies, so that they quickly spread out evenly, giving no resultant magnetization in the $x'y'$ plane, the precessing nuclei having a random distribution of phases with respect to one another. The resultant magnetization at thermal equilibrium may therefore be represented as in figure 1*c*.

To induce transitions of the nuclei among their energy levels, we have seen that a weak magnetic field must be applied which rotates at the Larmor frequency $\boldsymbol{\omega}_0=-\gamma\mathbf{H}_0$, i.e., a field rotating in the xy plane at ω_0 and in the sense of the nuclear precession. This field is usually represented by $\mathbf{H}_1$, and in the rotating frame it will appear to be stationary as shown in figure 2a. The effect of H_1 on the resultant

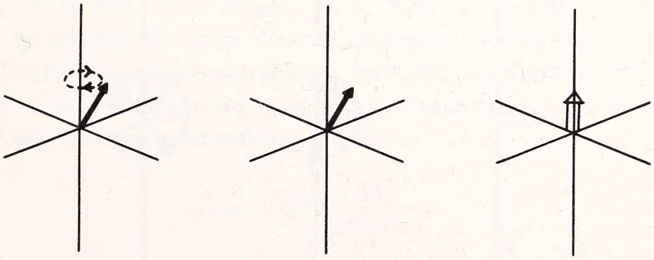

FIGURE 1. (a) Nuclear precession. (b) Nucleus in frame rotating at Larmor frequency. (c) Nuclear magnetisation.

nuclear magnetization can be seen from figure 2a to be to cause it to precess about H_1 at an angular frequency $\boldsymbol{\omega}_1 = -\gamma \mathbf{H}_1$ in the rotating frame.

After a time $t_\pi = \pi/\gamma H_1$ sec., the nuclear magnetization will have precessed through an angle π, so that the populations of the energy levels have been inverted (fig. 2b). If H_1 is turned off after this time, the spin system will return exponentially to thermal equilibrium (figs. 2c and 2d) with a characteristic time, T_1, called the spin-lattice or longitudinal relaxation time. This is the time constant for exchange of energy between the nuclear spins and the thermal motion of the lattice. The pulse of rotating H_1 which has been applied is known as a 180° pulse.

If we apply a 90° pulse instead of a 180° pulse, which will have a a length $t_\pi/_2 = (\pi/2)\gamma H_1$ sec., the nuclear magnetization will be turned into the xy plane (figs. 3 a and b) and immediately after the pulse it will point along the x' axis in the rotating frame. This rotating magnetisation in the xy plane gives the signal which is amplified and detected by the n.m.r. spectrometer.

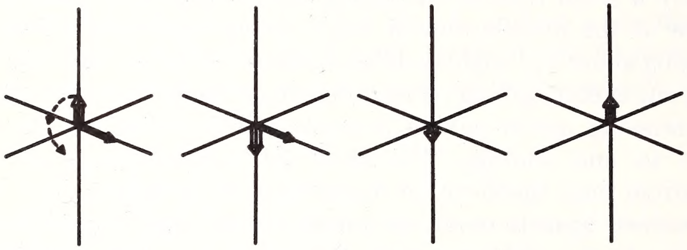

FIGURE 2. (a), (b) 180° pulse of H_1. (c), (d) decay of nuclear magnetisation.

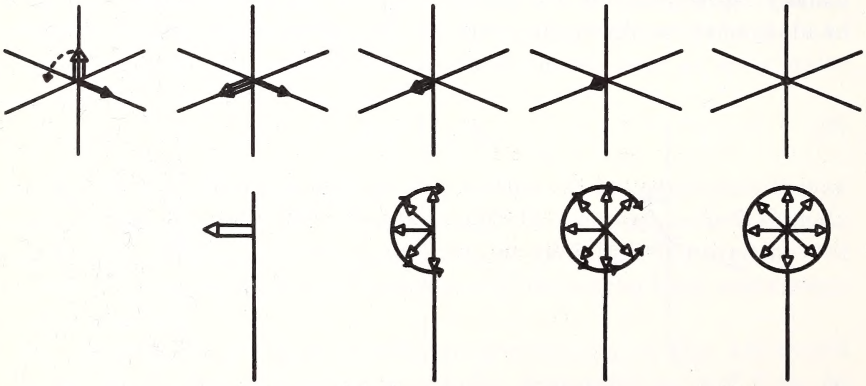

FIGURE 3. Decay of transverse magnetisation.

Because of the small variations of H_0 over the sample which come from magnetic field inhomogeneities and from the interactions between the nuclei, not all the spins precess at quite the same frequency, so the transverse magnetization in the *xy* plane decays as the nuclei lose phase with one another (fig. 3 c to e). The magnetization decays exponentially with a characteristic time, T_2, called the transverse or spin-spin relaxation time; T_2 is the time constant for the adiabatic exchange of energy *among the spins*. It is clear that the greater the range of H_0 over the sample resulting from magnetic interaction between the spins, the shorter will be T_2.

It is the study of the values ot T_1 and T_2 and their variation with temperature and applied magnetic field which can give information about molecular motion in solids.

2.2. The Correlation Time

We shall be concerned with the effects of molecular motion on T_2 and on T_1 and it will be convenient to characterise this motion by a correlation time τ_c.

If $f(t)$ is some function of the nuclear coordinates in the solid which has a zero average value, the product $f(t)\cdot f(t+\tau)$ will have a value not very different from $f(t)^2$ when τ is very small. On the other hand, when τ is long there will be little correlation between the values $f(t)$ and $f(t+\tau)$ and $f(t)\cdot f(t+\tau)$ will be small. This result is usually defined in terms of an autocorrelation function

$$G(\tau)=\overline{f(t)\cdot F(t+\tau)} \tag{3}$$

which is very small for $\tau \gg \tau_c$. The explicit form of the decay of the correlation function depends on the type of motion concerned, but for many processes $G(\tau)$ is assumed to fall off exponentially with τ. Thus

$$G(\tau)=\overline{f(t)^2}e^{-\tau/\tau_c} \tag{4}$$

in which τ_c is the "correlation time" for the motion. The function $f(t)$ may be represented as a Fourier spectrum of frequencies of motion, and the transform of the correlation function is known as the "spectral density," $J(\omega)$, which represents the power available at frequency ω. For an exponential correlation function

$$J(\omega)=\overline{f(t)^2}\cdot\frac{2\tau_c}{1+\omega^2\tau_c^2}. \tag{5}$$

From eq. (5) one can see that at low frequencies $J(\omega)$ is independent of ω, but when $\omega^2\tau_c^2\approx 1$, the value of $J(\omega)$ falls rapidly to zero. For a longer value of τ_c, $J(0)$ is larger, but the spectrum extends only to a lower limiting frequency (fig. 4).

3. Broadening of Nuclear Resonance Lines in Solids

3.1. Dipolar Broadening

In solids the line widths of resonances of nuclei with $I=\frac{1}{2}$ are usually determined by magnetic dipole interactions between the nuclei. A nucleus of magnetic moment μ produces a local field H_{loc} in its environment, of the order of

$$H_{\mathrm{loc}} \approx \frac{\mu}{r^3}$$

where r is the distance from the nucleus; at distances of a few Angstroms, H_{loc} turns out to be of the order of 1 G. H_{loc} has two components; there is a static component directed along the axis of H_0, and a rotating component in the xy plane at right angles to H_0 (fig. 5). The rotating component has, of course, the Larmor frequency ω_0 of the nucleus causing the field. The static component of this local field may reinforce or oppose the applied field, H_0, in the region of a

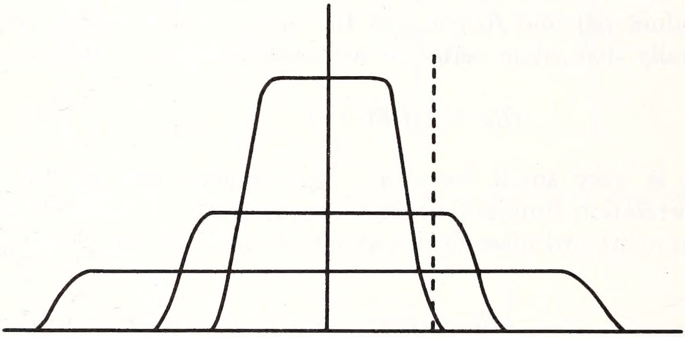

FIGURE 4. Variation of spectral density of thermal motion with frequency.

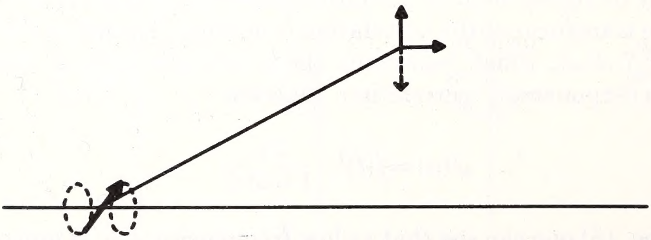

FIGURE 5. Local fields due to a magnetic dipole.

second nucleus, so that the resonance condition is spread over a range of fields of the order of H_{loc} and a broad line results.

The rotating component of the local field has just the right polarisation and frequency to induce transitions of another identical nucleus nearby, and the result is that the two nuclei exchange energy through their rotating local fields. This spin exchange causes a broadening of the resonance line by an amount comparable with the rotating field, and since this is of the same order as the static component of H_{loc}, it produces an additional broadening of comparable importance. Of course if the two nuclei are *unlike*, the rotating component of H_{loc} will have the wrong frequency for inducing transitions in the neighbouring nuclei, and the spin-spin interaction is then negligible, so that only the static component of H_{loc} contributes to the line width.

We have seen from section 2 that the line broadening can be expressed in terms of the spin-spin relaxation time T_2. The broader the spread of the static local fields, the more quickly the spins lose phase and the shorter is T_2; the spin exchange stimulated by the rotating components of the local fields between like spins also causes dephasing of the spins and further shortens T_2. Thus we may write

$$\frac{1}{T_2} \propto \gamma \Delta H \tag{6}$$

where ΔH is the line width and the proportionality factor is a number of order unity which depends on the detailed line shape.

3.2. Line Shapes

The detailed line shape can be calculated for nuclear resonances in crystals in which the nuclei are grouped in pairs or in groups of three, but for more complicated groups the calculation becomes tedious and the line shape uninteresting. For crystals containing pairs of nuclei the line is a broad doublet[3]; for groups of three nuclei it is a broad triplet[4], and for more complex grouping it is usually a shapeless hump.

However, in a most important paper [5], Van Vleck has shown that the mean square width, or second moment, of the absorption line from any configuration of nuclei in a single crystal is given by

$$\begin{aligned} <(\Delta H)^2>_{Av} &= \frac{3}{2} I(I+1) N_s^{-1} \gamma^2 \hbar^2 \sum_{j>k} \sum_{k} (3\cos^2\theta_{jk} - 1)^2 r_{jk}^{-6} \\ &+ \frac{N_s^{-1}}{3} \hbar^2 \sum_{j} \sum_{f} I_f(I_f+1) \gamma_f^2 (3\cos^2\theta_{jf} - 1)^2 r_{jf}^{-6} \end{aligned} \tag{7}$$

where γ and I refer to the nuclei at resonance, γ_f and I_f to other nuclei in the sample, θ_{jk} is the angle between the vector joining the

jth and kth nuclei and H_0, and r is the internuclear distance. For a powdered sample, the average is taken over all directions and we find

$$<(\Delta H)^2>_{Av} = \frac{6}{5} I(I+1) N_s^{-1} \gamma^2 \hbar^2 \sum_{j>k} \sum_{k} r_{jk}^{-6} + \frac{4}{15} \hbar^2 N_s^{-1} \sum_{j} \sum_{f} I_f(I_f+1) \gamma_f^2 r_{jf}^{-6} \tag{8}$$

4. Effect of Molecular Motion on Line Widths

If the molecules in a crystal are in motion, eq (7) for the second moment of the nuclear resonance must be modified to take account of the time dependence of θ_{jk}. If the motion is fast enough, the term $(3 \cos^2\theta_{jk} - 1)$ is replaced by its time average, which will depend on the type of motion. If the motion occurs about random axes, as for example is the case of the ammonium ion in ammonium chloride at room temperature, the time average value of $(3 \cos^2\theta_{jk} - 1)$ is zero and the intramolecular broadening vanishes. A narrow line is left, broadened only by intermolecular interactions which are not necessarily completely averaged by the motion. On the other hand, when the molecular motion is not random, but for example involves reorientation about only one axis, it is easy to calculate from eq (7) by how much the second moment is reduced in a particular case. In this way the measurement of the change of second moment from a low temperature where motion is slow, to a higher temperature where it is fast, can often be used to identify the type of molecular motion involved. For example the proton second moment of 1,2-dichloroethane is 18.2 G^2 at low temperatures and 7 G^2 at high temperatures. This is just the change expected for reorientational motion about the *C–C* axis [6].

In the particularly simple cases of nuclei grouped in pairs or in threes, it is also possible to calculate the change of line *shape* caused by molecular motion about various axes[3, 4]. Crystalline hydrazine sulphate gives a broad triplet proton resonance at 90 °K which shows the presence of $N_2H_6^{++}$ ions with the hydrogen atoms grouped at the corners of equilateral triangles of side 1.71 Å. At room temperature, however, the proton resonance is narrower, with a single peak, which can be fitted exactly to the calculated line shape for molecular motion about the C_3 axis of the triangles of protons, showing that in this substance the hydrazinium ion reorients itself about the *N–N* axis[7].

The molecular motion which is responsible for line narrowing may be free rotation, hindered rotation, libration, self diffusion or quantum mechanical tunnelling, and it is often possible to distinguish these types of motion from the amount by which the second moment is reduced and from its temperature dependence[8].

The critical frequency of molecular motion below which a broad line is observed and above which the line narrowing occurs can be deduced on the basis of a simple physical argument. An observer in a reference frame x', y', z' rotating at the Larmor frequency ω_0 will observe the nuclei of a rigid solid to be precessing, some forwards and some backwards, with a range of frequencies $\Delta\omega$, where $\Delta\omega$ is the nuclear resonance line width; the observer can thus measure the local magnetic fields experienced by the nuclei as a result of the dipole-dipole interactions.

If, however, the molecules are in motion, so that the local fields fluctuate many times during the period of a precession *in the local field,* (i.e., in the rotating frame), then the nuclei are no longer able to distinguish the local fields, and they all precess more nearly at the Larmor frequency ω_0 and the line width is reduced. The critical frequency for line narrowing is thus a frequency equivalent to the rigid-lattice line width. The full theory of the variation of line width with frequency of molecular motion may be found in reference[9]; the calculation of the line width for a particular model is easy for a rigid-lattice and for a lattice with rapid motion, but the line width and shape at frequencies of motion near the rigid-lattice line width are very difficult to calculate. The result depends in detail on the exact nature of the molecular motion, and hence on the correlation function assumed. However in their classic paper, Bloembergen, Purcell and Pound[10] proposed an approximate relationship between τ_c and the nuclear resonance line widths at temperatures above and below the transitions, assuming that τ varied exponentially with temperature according to an activation process. This equation has been discussed by Kubo and Tomita[11] and an improvement suggested, but even so it can only give an approximate value for the variation of τ_c with temperature near the line-width transition. It is, however, relatively easy to measure the variation of second moment of the nuclear resonance with temperature, and this is often used to find a preliminary estimate of the correlation time at a particular temperature[12].

Nuclei with $I > \frac{1}{2}$ usually possess, in addition to the magnetic dipole moment, an electric quadrupole moment, which may interact with an electric field gradient in the crystal. This electric quadrupole coupling [9] often far outweighs the dipole-dipole interaction and dominates the nuclear resonance spectrum.

Molecular motion which interrupts the quadrupole interaction produces an averaging effect as in the case of dipole coupling, and the critical frequency of motion required is similarly the frequency of the rigid lattice line width or splitting.

Relatively little work on molecular motion in crystals has been done on quadrupolar nuclei. Ketudat and Pound [12a] have observed the deuterium resonance in $LiSO_4 \cdot D_2O$ and conclude that the D_2O molecules reorient themselves about their twofold axes.

Chiba [12b] by the same method has been able to make a detailed study of the motion of the water molecules in $BaCl_2 \cdot D_2O$ and in a number of strongly hydrogen bonded crystals.

5. Effect of Molecular Motion on Relaxation Times

We have already seen (3.1) that the spin-spin or transverse relaxation time, T_2, is related to the resonance line width. The static components of local magnetic fields cause a range of nuclear precession frequencies, so that the nuclei lose phase; the rotating components of the local fields induce spin exchange and shorten T_2 still further. The value of T_2 therefore depends on local fields along the z direction which have frequency components near zero (static) and also on local fields in the xy plane which fluctuate at frequencies close to the Larmor frequency.

The spin-lattice, or longitudinal relaxation time, T_1, is concerned with changes of magnetisation along the z direction, and these changes can only be stimulated by local fields which fluctuate in the xy plane (2.1).

In order to analyze the effects of molecular motion on T_1 and T_2 we must therefore consider the spectral distribution of the fluctuations of the local nuclear magnetic fields caused by the motion.

5.1. Modulation of Dipole-Dipole Interactions by Molecular Motion

The modulation of dipole interactions by molecular motion, and its effect on the nuclear relaxation times was first set out by Bloembergen, Purcell and Pound [10]; the theory has since been extended and generalised and recent reviews may be found in references 9 and 13.

The classical dipolar energy of interaction, E, between two magnetic moments $\boldsymbol{\mu}_1$ and $\boldsymbol{\mu}_2$ is

$$E=\frac{\boldsymbol{\mu}_1 \cdot \boldsymbol{\mu}_2}{r^3}-\frac{3(\boldsymbol{\mu}_1 \cdot \mathbf{r})(\boldsymbol{\mu}_2 \cdot \mathbf{r})}{r^5} \tag{9}$$

where r is the radius vector from $\boldsymbol{\mu}_1$ to $\boldsymbol{\mu}_2$. Treating μ_1 and μ_2 as operators

$$\boldsymbol{\mu}_1=\gamma_1 \hbar \mathbf{I}_1$$
$$\boldsymbol{\mu}_2=\gamma_2 \hbar \mathbf{I}_2$$

The general dipolar Hamiltonian for N spins then becomes

$$\mathcal{H}_d=\frac{1}{2}\sum_j^N \sum_k^N \left[\frac{\boldsymbol{\mu}_j \cdot \boldsymbol{\mu}_k}{r_{jk}^3}-\frac{3(\boldsymbol{\mu}_j \cdot \mathbf{r}_{jk})(\boldsymbol{\mu}_k \cdot \mathbf{r}_{jk})}{r_{jk}^5}\right]. \tag{10}$$

Using spherical polar coordinates and the raising and lowering operators I^+ and I^-, the Hamiltonian may be written in the form

$$\mathcal{H}_d=\frac{\gamma_1\gamma_2\hbar^2}{r^3}\,[A+B+C+D+E+F] \tag{11}$$

where

$$A=I_{1z}I_{2z}(1-3\cos^2\theta)$$

$$B=-\frac{1}{4}\,[I_1^+I_2^-+I_1^-I_2^+](1-3\cos^2\theta)$$

$$C=-\frac{3}{2}\,[I_1^+I_{2z}+I_{1z}I_2^+]\sin\theta\cos\theta e^{-i\phi}$$

$$D=-\frac{3}{2}\,[I_1^-I_{2z}+I_{1z}I_2^-]\sin\theta\cos\theta e^{i\phi}$$

$$E=-\frac{3}{4}\,I_1^+I_2^+\sin^2\theta e^{-2i\phi}$$

$$F=-\frac{3}{4}\,I_1^-I_2^-\sin^2\theta e^{2i\phi}$$

When the molecules in the solid are in motion, the coordinates r, θ and ϕ vary randomly with time, and it is convenient to choose as space functions the terms

$$\begin{aligned} F_0&=(1-3\cos^2\theta)r^{-3}\\ F_1&=r^{-3}\sin\theta\cos\theta e^{\pm i\phi}\\ F_2&=r^{-3}\sin^2\theta e^{\pm 2i\phi} \end{aligned} \tag{12}$$

When these functions vary randomly with time, the corresponding spectral densities are

$$\begin{aligned} J_0(\omega)&=\overline{F_0(t)^2}\cdot j(\omega)\\ J_1(\omega)&=\overline{F_1(t)^2}\cdot j(\omega)\\ J_2(\omega)&=\overline{F_2(t)^2}\cdot j(\omega). \end{aligned} \tag{13}$$

If we assume an exponential correlation function (section 2.2) the normalised spectral density $j(\omega)$ becomes

$$j(\omega)=\frac{2\tau_c}{1+\omega^2\tau_c^2} \tag{14}$$

The functions in eq (13) thus describe the intensity of the frequency components at ω of the fluctuating dipolar fields in the solid arising from the molecular motion characterised by the correlation tine τ_c.

5.2. Effect of Motion on T_1

Spin-lattice relaxation involves transitions of nuclei which are stimulated by fluctuating fields in the xy plane, and which involve exchange of energy between the spins and the thermal molecular motion. The terms C, D, E and F of the Hamiltonian (eq 11) can induce spin-lattice relaxation, as can be seen from the spin operators involved. We are therefore concerned with $F_1(t)$ and $F_2(t)$ of eq (12). Terms C and D involve a single spin flip, requiring a frequency ω_0, but terms E and F represent double spin flips, requiring a frequency $2\omega_0$, where ω_0 is the nuclear Larmor frequency.

Terms C and D involve the function $F_1(t)$ and terms E and F the function $F_2(t)$ (eq 12). Spin lattice relaxation is therefore stimulated by spectral components $J_1(\omega_0)$ and $J_2\,(2\omega_0)$, i.e.,

$$\frac{\overline{F_1(t)^2}\cdot 2\tau_c}{1+\omega_0^2\tau_c^2} \text{ and } \frac{\overline{F_2(t)^2}\cdot 2\tau_c}{1+4\omega_0^2\tau_c^2}.$$

The functions F_1 and F_2 are measure of the local fields in the xy plane, and contain the internuclear distances. For example, for spin-lattice relaxation of a spin I interacting with several identical nuclei, provided their motions are not correlated, it turns out that [9],

$$\frac{1}{T_1}=\frac{3}{2}\gamma^4\hbar^2 I(I+1)\sum_k [J_{1,j,k}(\omega_0)+J_{2,j,k}(2\omega_0)]. \qquad (15)$$

For rotational motion

$$J_1(\omega_0)=\frac{4}{15}\cdot\frac{1}{r_{jk}^6}\cdot\frac{\tau_c}{1+\omega_0^2\tau_c^2};\ J_2(2\omega_0)=\frac{16}{15}\cdot\frac{1}{r_{jk}^6}\cdot\frac{\tau_c}{1+4\omega_0^2\tau_c^2}.$$

so

$$\frac{1}{T_1}=\frac{2}{5}\gamma^4\hbar^2 I(I+1)\left[\frac{\tau_c}{1+\omega_0^2\tau_c^2}+\frac{4\tau_c}{1+4\omega_0^2\tau_c^2}\right]\sum_k r_{jk}^{-6}.$$

For a group of identical nuclei this value is

$$\frac{1}{T_1}=\frac{2}{3}<(\Delta\omega)^2>_{Av}\left[\frac{\tau_c}{1+\omega_0^2\tau_c^2}+\frac{4\tau_c}{1+4\omega_0^2\tau_c^2}\right] \qquad (16)$$

where $<(\Delta\omega)^2>_{Av}$ is the second moment of the absorption line in angular frequency units.

When $\omega_0{}^2\tau_c^2<<1$ (eq 16) reduces to

$$\frac{1}{T_1}=\frac{2}{3}<(\Delta\omega^2)>_{Av}\cdot 5\tau_c$$

and T_1 is inversely proportional to τ_c. On the other hand, when motion is slow and $\omega_0^2\,\tau_c{}^2$ is large,

$$\frac{1}{T_1}=\frac{2}{3}<(\Delta\omega^2)>_{Av}\cdot\frac{2}{\omega_o^2\tau_c}$$

and T_1 is directly proportional to τ_c. Furthermore, the plot of T_1 against τ_c passes through a minimum value of T_1 when $\omega_0\tau_c \approx 0.6$, so that,

$$\left(\frac{1}{T_1}\right)_{\min}=\frac{2}{3}<(\Delta\omega^2)>_{Av}\cdot\frac{1.42}{\omega_o} \qquad (17)$$

Thus by following the variations of T_1 in a solid one can follow the variation of τ_c. For example, if τ_c is the correlation time for hindered reorientation in a solid, it is likely to vary exponentially with the temperature according to an equation of the form

$$\tau_c=\tau_o e^{V/RT}$$

In this case a plot of ln T_1 against $1/T$ will have two linear portion^S with a minimum given by eq (17). From the slopes of the linear parts, the value of the potential barrier, V, can be derived, and from the temperature of the minimum where $\omega_0\tau_c \approx 0.6$, the value of τ_0 can be obtained.

The formation of a minimum in the plot of T_1 against τ_c can be seen qualitatively from figure 4, if we remember that spin lattice relaxation is stimulated by thermal fluctuations near ω_0 and $2\omega_0$. When τ_c is small, at high temperatures, the correlation spectrum, $J(\omega)$, is very extended and the intensity near ω_0 is small, and T_1 is long. As τ_c increases, the intensities of the components near ω_0 increase and T_1 becomes shorter.

When $\omega_0^2\tau_c^2 \approx 1$, the intensities of the thermal fluctuations are at a maximum near ω_0 (fig. 4b) and T_1 reaches a minimum. As τ_c gets longer still, the correlation spectrum shrinks further back to frequencies below ω_0, and T_1 increases as the thermal fluctuations at the Larmor frequency die away again.

Many studies of molecular motions have been made, using T_1 measurements. For example, Andrew and Eades [14] have studied the change of second moment and of relaxation time with temperature for solid benzene. The change of second moment is consistent with reorientation of the benzene ring about its hexad axis. The value of T_1 passes through a minimum at about 170 °K and from the slopes of the plots of ln T_1 against $1/T$ at high and low temperatures, an activation energy for the motion of 3.95 kcal/mole was found.

Further measurements have been made by Anderson [15] on solid solutions of C_6H_6 in C_6D_6 from which it was possible to extrapolate the value of $(T_1)_{\min}$ from pure benzene to a crystal having C_6H_6 in C_6D_6 at infinite dilution. The value of $(T_1)_{\min}$ obtained corresponds to a relatively isolated benzene molecule, and was found to be 196 ± 8 msec at 50 Mc/s. The value of $(T_1)_{\min}$ can also be calculated from eq (17), using the known interproton distance in benzene, and is found to be 199 msec., in excellent agreement with the experimental result.

Such measurements of correlation times for molecular motion can be made not only as a function of temperature but also as a function of pressure; Anderson and Slichter [16] have measured the effect of pressure on molecular motion in camphor, benzene, hexamethylbenzene, ammonium chloride, and some *n*-alkanes, and have tabulated volumes of activation.

A considerable amount of work has been done on molecular motion in polymers. Connor, Blears and Allen [17] have studied proton spin-lattice relaxation in polypropylene oxides over a range of temperatures. Two T_1 minima were observed, one corresponding with motion of the chain backbone and the other with methyl group rotation. The measurements correlate well with dielectric and mechanical measurements of the chain backbone motion for which an activation energy of 10.5 kcal/mole was found.

Relaxation times in polymers are often complicated by "spin diffusion" at low temperatures. If the methyl groups at the end of a hydrocarbon chain are free to rotate, they may act as an energy "sink" for the whole spin system. Spin-spin relaxation, which in solids is much faster than spin-lattice relaxation, may conduct energy very efficiently from the methylene protons to the methyl groups, which by virtue of their rotation may be more strongly coupled to the thermal modes of the lattice.

This mechanism has been carefully studied [18, 19], and if it dominates spin-lattice relaxation in a hydrocarbon, one expects that (a) the T_1 minimum will occur at the same temperature for all members of a homologous series, (b) the value of $(T_1)_{\min}$ will be inversely proportional to the fraction of methyl protons, and (c) the activation energies for members of a homologous series would all be about the same and equal to that for the reorientation of the methyl groups.

The equations given above refer only to solids in which nuclear relaxation occurs by rotational motion among like nuclei. For other forms of motion, such as diffusion, similar arguments may be used, but different correlation functions may be involved.

Holcomb and Norberg [20] have studied the temperature dependence of relaxation times of lithium, sodium, and rubidium in the alkali metals and have determined the magnitude and temperature dependence of the self diffusion coefficients. Hultsch and Barnes [21] then determined the effects of pressure on these diffusion coefficients in lithium and sodium.

In solids where heteronuclear relaxation is important the situation is complicated by the possibility of non-exponential spin-lattice relaxation, so that one can no longer characterise the relaxation by a single time T_1. Nevertheless the results can be interpreted in terms of the usual models for molecular motion. For example Anderson and Slichter [22] have studied the motion of CF_3 groups in solid $C_6H_5CF_3$ and in solid *m*- and *p*- $C_6H_4(CF_3)_2$.

6. The Study of Very Slow Molecular Motion

The theory of spin-lattice relaxation which has been used in the above sections [9, 13] is valid only when $\tau_c < T_2$. We can observe line narrowing when τ_c is less than the rigid lattice value of T_2, and spin-lattice relaxation is most efficient when τ_c is of the order of the Larmor period.

By measuring low-field relaxation *in the rotating frame*, however, these restrictions can be extended to values of $\tau < T_1$. Since T_1 is nearly always much longer than T_2 in the rigid lattice, this means that much longer values of τ_c can be explored.

6.1. Measurement of Relaxation in the Rotating Frame

The low field relaxation time in the rotating frame may be measured by a number of methods, all of which involve aligning the nuclear magnetisation, which was initially along H_0, along the rotating field H_1. If H_1 is large enough to saturate the spin system, a magnetisation initially parallel to H_1 maintains its orientation [23] and decays with a time constant, usually termed $T_{1\rho}$.

Methods of aligning the magnetisation along H_1 have been described by Slichter and Holton [24], Hartman and Hahn [25], Meiboom [26] and by Jones, Douglass and McCall [27].

The method of Hartman and Hahn [25] is easily understood from figure 6, which shows the behaviour of the nuclear magnetisation

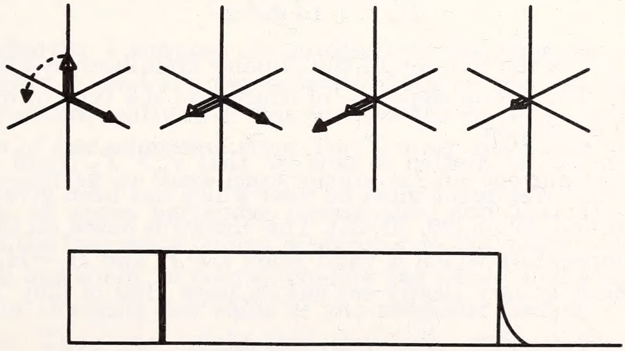

FIGURE 6. Measurement of T_1 in the rotating frame.

in the rotating frame. The field H_1 is applied at (a) for a time equivalent to a 90° pulse (section 2.1) until (b). When the nuclear magnetisation lies along the x' axis, H_1 having been applied along y', H_1 is not turned off but shifted in phase by 90°. (b) and (c) thus follow almost instantaneously.

The nuclear magnetisation is now aligned along H_1; it is allowed to relax in H_1 for a time, t, and then H_1 is turned off at (d). When H_1 is turned off, a free induction decay may be observed from the rotating magnetisation in the xy plane; its height measures the remaining magnetisation after time, t. By varying t, the time constant, $T_{1\rho}$, for the decay of magnetisation in the rotating frame may be measured.

6.2. Effects of Molecular Motion on $T_{1\rho}$

The theoretical interpretation of these measurements is complicated by the fact that H_1 is comparable with the dipole-dipole interaction energy, which cannot therefore be treated as a perturbation on the Zeeman energy.

However, if the correlation time for molecular motion is small compared with T_2 for the rigid lattice, the effect of dipolar coupling is greatly diminished and the Redfield theory [13] described in section 5 can still be applied. Calculation of $T_{1\rho}$ is then similar to that for the laboratory frame T_1, except that the Hamiltonian for the rotating frame only contains terms of the type E and F of eq (11). The frequency components of the correlation spectrum which cause relaxation are therefore only those at $2\omega_1$.

If we define the "local dipolar field", H_{loc} as

$$H_{\text{loc}}^2 = \frac{1}{3} < (\Delta H)^2 >_{\text{Av}}$$

then it turns out [28] that

$$\frac{1}{T_{1\rho}} = \frac{3\gamma^2 \tau_c (1-q) H_{\text{loc}}^2}{1+4\omega_1^2 \tau_c^2}$$

where $(1-q)$ is the fraction of the Dipolar Hamiltonian which is time dependent. This factor depends, of course, on the type of motion and the model concerned.

If the molecular motion is slow, so that $\tau_c > T_2$ (rigid lattice), a quite different treatment must be used which has been given in detail by Slichter and Ailion [29, 30, 31]. This theory is based on the concept of spin temperature which is valid when $\tau_c \gg T_2$ and $H_1 \approx H_{\text{loc}}$, and its physical basis is very clearly set out on page 1100 of [30]. The result is that

$$\frac{1}{T_{1\rho}} = \frac{2(1-p) H_{\text{loc}}^2}{\tau_c (H_1^2 + H_{\text{loc}}^2)}$$

where $(1-p)$ is a factor similar to, but not necessarily identical with $(1-q)$ of the fast motion condition.

The intermediate case, when $H_1 \approx H_{\mathrm{loc}}$ and $\tau \approx T_2$ is not properly described by either theory, so there is some ambiguity in the interpretation of a $T_{1\rho}$ minimum.

Ailion and Slichter [31] have studied $T_{1\rho}$ over a wide range of temperatures, and determined τ_c for self diffusion in lithium metal. They applied the BPP [10] and Redfield [13] theories to the high-temperature region where τ_c is short and the spin temperature theory to the low temperature region. In this way they were able to follow the variation of τ_c with temperature almost continuously from $\tau_c = 10^{-9}$ sec. to $\tau_c = 1$ sec.

The technique has been applied to a variety of systems, from an exhaustive study of molecular motion in crystalline H_2S by Look, Lowe and Northby [32] to a study of methyl-group rotation and spin diffusion in normal alkanes [28].

The correlation time for self diffusion in *d-l* and *d* camphor has been measured [27] in the temperature range 10 to 95 °C and found to vary from 70 μsec to 30 msec, corresponding to an activation energy of 15.4 Kcal/mole. The motion of the water molecules in gypsum has been further studied using these methods by Look and Lowe [33].

7. Discussion

W. C. Hamilton (Brookhaven National Laboratory): In the interpretation of relaxation-time measurements, a classical activated process is usually assumed in order to derive a potential barrier. Would you care to comment on the validity of this approximation, particularly in the case of low-barrier motions? I wonder whether one would obtain different barriers if one considered in detail the small and limited number of energy levels for a realistic potential function?

R. E. Richards: I suppose the justification for using the activated type of barrier is that it's the simplest thing to do, and that when you do it you frequently find that you get the expected temperature dependence of the relaxation time. But I must emphasize that what you are measuring in these experiments is just the intensity of the fluctuations at some particular frequencies, and that the barriers you get and the frequency factors do depend on the model you assume. In principal one could, of course, explore the whole of the correlation spectrum by changing the value of the magnetic field in a series of experiments. Then you might find that you couldn't describe the spectrum in terms of a single correlation time, and you might find that it varied in a complicated way with temperature, but you would have a very detailed picture of the motion. So far as I know, however, this is not being done very extensively at the present time.

8. References

[1] E. Feenberg and G. E. Pake, Notes on the Theory of Angular Momentum (Addison Wesley, Cambridge, Mass., 1963).

[2] Advances in Spectroscopy, Vol. II, H. W. Thompson, ed., p. 105 (Interscience Publishers, New York, 1961).

[3] G. E. Pake, J. Chem. Phys. **16,** 327 (1948).

[4] E. R. Andrew and R. J. Bersohn, J. Chem. Phys. **18**, 159 (1950).

[5] J. H. Van Vleck, Phys. Rev. **74,** 1184 (1948).

[6] H. S. Gutowsky, G. B. Kistiakowsky, G. E. Pake and E. M. Purcell, J. Chem. Phys. **17,** 972 (1949).

[7] L. Pratt and R. E. Richards, Trans. Faraday Soc. **49,** 744 (1955).

[8] J. G. Powles and H. S. Gutowsky, J. Chem. Phys. **23,** 1692 (1955),
E. O. Stejskal and H. S. Gutowsky, J. Chem. Phys. **28,** 385 (1958).

[9] A. Abragam, The Principles of Nuclear Magnetism (Oxford University Press, 1961).

[10] M. Bloembergen, E. M. Purcell and R. V. Pound, Phys. Rev. **73,** 679 (1948).

[11] R. Kubo and K. Tomita, J. Phys. Soc. Japan **9,** 88 (1954).

[12] G. W. Smith, J. Chem. Phys. **36,** 3081 (1962), J. Chem. Phys. **42,** 4229 (1965); W. P. Slichter, Fortschr. Hochpolymer Forsch. **1,** 35 (1958).

[12a] S. Ketudat and R. V. Pound, J. Chem. Phys. **26,** 708 (1957).

[12b] T. Chiba, J. Chem. Phys. **39,** 947 (1963), J. Chem. Phys. **41,** 1352 (1964).

[13] A. Redfield, Advances in Magnetic Resonance, Vol. 1, J. Waugh, ed., p. 1 (Academic Press, New York, 1966).

[14] E. R. Andrew and R. G. Eades, Proc. Roy. Soc. (London), **A218,** 537 (1953).

[15] J. E. Anderson, J. Chem. Phys. **43,** 3575 (1965).

[16] J. E. Anderson and W. P. Slichter, J. Chem. Phys. **44,** 1797 (1966).

[17] T. M. Connor, D. J. Clears and G. Allen, Trans. Faraday Soc. **61,** 1097 (1965).

[18] J. E. Anderson and W. P. Slichter, J. Phys. Chem. **69,** 3099 (1965).

[19] D. C. Douglass and G. P. Jones, J. Chem. Phys. **45,** 956 (1966).

[20] D. Holcomb and R. E. Norberg, Phys. Rev. **98,** 1074 (1954).

[21] R. A. Hultsch and R. G. Barnes, Phys. Rev. **125,** 1832 (1962).

[22] J. E. Anderson and W. P. Slichter, J. Chem. Phys. **43,** 433 (1965).

[23] A. G. Redfield, Phys. Rev. **98,** 1787 (1955).

[24] C. P. Slichter and W. C. Holton, Phys. Rev. **122,** 1701 (1962).

[25] S. R. Hartman and E. L. Hahn, Phys. Rev. **128,** 2042 (1962).

[26] S. Meiboom, J. Chem. Phys. **34,** 375 (1961).

[27] G. P. Jones, D. C. Douglass and D. W. McCall, Rev. Sci. Instr. **36,** 1460 (1965).

[28] D. C. Douglass and G. P. Jones, J. Chem. Phys. **45,** 956 (1966).

[29] D. Ailion and C. P. Slichter, Phys. Rev. Letters **12,** 168 (1964).

[30] C. P. Slichter and D. Ailion, Phys. Rev. **135A,** 1099 (1964).

[31] D. Ailion and C. P. Slichter, Phys. Rev. **137A,** 235 (1965).

[32] D. C. Look, I. J. Lowe and J. A. Northby, J. Chem. Phys. **44,** 3441 (1966).

[33] D. C. Look and I. J. Lowe, J. Chem. Phys. **44,** 2995 (1966).

STRUCTURE AND SPECTROSCOPY OF INORGANIC CRYSTALS

SPECTROSCOPIC AND DIFFRACTION STUDIES OF SIMPLE HYDROGEN BONDS IN SOLIDS

JAMES A. IBERS

Department of Chemistry and Materials Research Center, Northwestern University, Evanston, Illinois 60201

1. Introduction

In this lecture I shall attempt to summarize some studies of simple hydrogen-bonded systems in the solid state. The coverage is not extensive; it reflects my personal interests.

Simple hydrogen-bonded systems offer the advantage that not only diffraction studies of them are amenable to interpretation, but also spectroscopic studies. As I shall illustrate, it is essential that information from both spectroscopic and diffraction studies be available if one wishes to understand even the rudiments of potential functions applicable to simple hydrogen bonds in solids. Although spectroscopic studies have provided a wealth of information on more complex systems, this information is generally of a qualitative nature for several reasons: (1) the number of observed bands is never sufficient to enable a general force field calculation to be carried out; (2) in complex systems the assignment of bands to O–H vibrations is often complicated by the presence of many hydrogen atoms, some hydrogen bonded, some not, in the unit cell; (3) various complications arise from factor splittings if there are a number of formula units in the primitive cell; (4) application of selection rules may be hampered by insufficient knowledge of the site symmetry. It is really only for simple hydrogen-bonded systems in solids that the spectroscopic data are easily interpretable.

2. Criteria for Hydrogen Bonding

The presence of hydrogen bonds can be inferred from both energy and geometrical considerations. Energy considerations necessarily arise from thermodynamics and from spectroscopy, for spectroscopy is really the measurement of energy differences. These arguments are familiar: the high boiling point of water is ascribed to the formation of hydrogen bonds in the liquid. Geometrical considerations parallel the information obtainable from diffraction studies. A number of structures have been determined through x-ray diffraction studies. Most of these, until recently, did not yield precise, or perhaps even approximate, positions for hydrogen atoms. Nevertheless the presence of hydrogen bonding was inferred indirectly. If one found an O—O bond length of 2.50 Å, and if the geometry and chemistry were such that hydrogen bonding might occur, one would postulate an OHO bond, since under normal circumstance oxygen atoms do not approach one another closer than about 2.8 Å.

The development of neutron diffraction techniques over the past twenty years has enabled much more specific information to be obtained on the geometry of hydrogen bonds. This is because it is generally possible with the use of neutron diffraction to locate the positions of hydrogen atoms in crystals with certainty. The picture that has emerged here is somewhat different. Whereas for the A-H—B bond we spoke of a shortening of the A—B interaction over that predicted from the sums of the van der Waals radii of A and B as a criterion for hydrogen bonding, we now know that a much more general criterion is the shortening of the H—B bond distance relative to the van der Waals radii of H and B. This point is illustrated in table 1. We see from the data of table 1 that even for very weak hydrogen bonds, e.g., N-H—S, there is very good evidence for their existence based on this last criterion. Naturally this criterion has its parallel in spectro-

TABLE 1. Van der Waals Contact Distances and Observed Hydrogen Bond Distances (in Å) for Some Common Types of Hydrogen Bonds [a]

Bond type	A···B (calc)	A···B (obs)	H···B (calc)	H···B (obs)
F–H–F	2. 7	2. 4	2. 6	1. 2
O–H . . . O	2. 8	2. 7	2. 6	1. 7
O–H . . . F	2. 8	2. 7	2. 6	1. 7
O–H . . . N	2. 9	2. 8	2. 7	1. 9
O–H . . . Cl	3. 2	3. 1	3. 0	2. 2
N–H . . . O	2. 9	2. 9	2. 6	2. 0
N–H . . . F	2. 9	2. 8	2. 6	1. 9
N–H . . . Cl	3. 3	3. 3	3. 0	2. 4
N–H . . . N	3. 0	3. 1	2. 7	2. 2
C–H . . . O	3. 0	3. 2	2. 6	2. 3
N–H . . . S	3. 4	3. 4	3. 1	2. 4

[a] From Hamilton and Ibers, The Hydrogen Bond in Solids (Benjamin, New York, 1968).

scopic effects, for example in changes in the spectra of various hydrogen bonding species in CCl_4, which may be attributed to A-H—Cl interactions.

3. Neutron Diffraction and Symmetric (or Almost Symmetric) AHA Bonds

It is apparently not generally appreciated that for symmetric or nearly symmetric AHA bonds, there are no methods available which allow an unequivocal determination of the shape of the potential function. To take neutron diffraction as an example, one may pose the question: "How do I know that a given AHA bond is truly symmetric, with the ground-state level above a barrier, if any, in a symmetric potential well rather than that the bond is actually asymmetric, with the barrier of a symmetric double-minimum potential function above the ground-state level?" Moreover, one might further ask "If it is a symmetric double-minimum potential function, what information can I obtain about the tunneling frequency through the barrier," a question that is equivalent to asking the height of the barrier. In the solid state the symmetric double-minimum potential function can be thought of as arising from the configurations A–H—A and A—H–A in equal probability, that is from the arrangement A–½ H—½ H–A. We shall show that in a neutron diffraction experiment this arrangement cannot be distinguished from the A–H–A arrangement.

Consider the scattering density for neutrons for the FDF ion in $NaDF_2$ [1][1] as illustrated in figure 1. The solid curve is the observed scattering function, and this is easily reproduced by assuming a symmetric single minimum well (F-D-F) and a root-mean-square amplitude of the D nucleus along the bond of 0.140 Å. However, let us assume that we have a symmetric double-minimum potential function F–½ D—½ D–F. Then, as figure 1 illustrates, it is possible for the two "half-deuterium" scattering functions to add to give a total scattering density that is indistinguishable from that obtained from the single-minimum model. If the scattering densities from two models are equivalent, then these two models cannot be distinguished. Now how was the scattering density from each of the "half-deuterium" atoms obtained? The deuterium nuclei were arbitrarily displaced 0.09 Å along the bond from its center, and the appropriate root-mean-square amplitude of vibration along the bond was determined to give the results shown. You might say that I cannot arbitrarily adjust the root-mean-square amplitudes of vibration. I agree with you, but the only

---

[1] Figures in brackets indicate the literature references listed at the end of this paper.

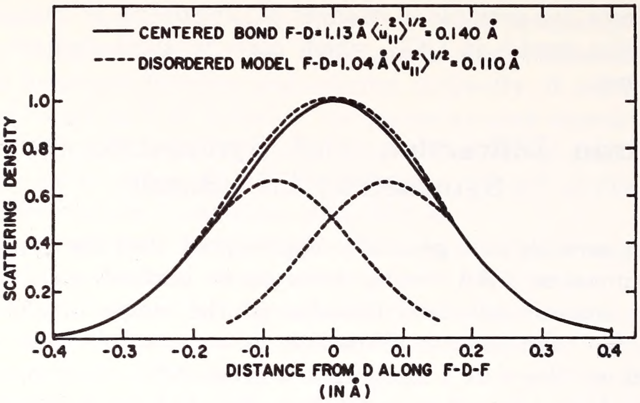

FIGURE 1. Scattering from two models of the FDF bond in $NaDF_2$ [1]. The solid line is the experimental curve and that calculated from the single-minimum centered model. The dotted line that nearly superimposes onto the solid line is the sum of the two half-deuterium peaks of the symmetric, double-minimum model.

model available from the neutron study alone is one in which the root-mean-square amplitudes of vibration and the positions of the deuterium atoms are among the variables to be determined. These interact so strongly that for an assumed position of the "half-deuterium" atoms there is evaluated from the data a root-mean-square amplitude of vibration along the bond which results in excellent agreement between observed and calculated scattering intensities. If a spectroscopist told me that he was certain that the deuterium atom has a certain root-mean-square amplitude of vibration along the FDF bond at a given temperature, then I would be pleased to include this information in my model and determine the position of the deuterium atom.

In the absence of a quantitative description of the vibrations of solid $NaDF_2$, it seems unlikely that any spectroscopist will volunteer such precise information. Nevertheless, spectroscopy does provide very useful information on this problem. Let us consider the FDF ion in $NaDF_2$ as an isolated, linear, symmetric triatomic group. Then the only modes in the crystal in which the F and D atoms move differently along the FDF bond are the symmetric and antisymmetric stretching modes. Let r_1 and r_2 be the instantaneous displacements from equilibrium of the bonds F_1-D and $D-F_2$. Then the normal coordinates for the stretching modes of the system are

$$\begin{aligned} Q_1 &= (\mu_1/2)^{\frac{1}{2}}(r_1+r_2) \qquad \mu_1 = m_F \\ Q_3 &= (\mu_3/2)^{\frac{1}{2}}(r_1+r_2) \qquad \mu_3 = m_D m_F/(2m_F+m_D). \end{aligned} \tag{1}$$

The normal coordinate Q_1, corresponding to the symmetric stretching frequency ν_1, is proportional to the change in the F—F bond length; the normal coordinate Q_3, corresponding to the antisymmetric stretching frequency ν_3, is proportional to the deviation of the D atom from the center of the bond in the direction of the bond. It follows readily that

$$\langle u_{\|}^2\rangle_{H} - \langle u_{\|}^2\rangle_{F} = (h/16\pi^2 m_F)[\{(2m_F - m_H)/(m_H \nu_3)\} - 1/\nu_1], \qquad (2)$$

where for the normal isotope one uses the mass of the hydrogen and the corresponding frequency while for the heavy isotope one uses the mass of deuterium and its frequency. Figure 2 shows the results of the spectroscopic calculation of eq. (2) versus the neutron results as a function of the distance of the H and D atoms from the center. The best agreement occurs for the symmetric single-minimum potential function. The complementary nature of spectroscopy and diffraction is embodied in the results of figure 2; there is probably no better evidence that the bifluoride ion is a symmetric ion.

There is additional information from the diffraction study that bears on the potential function and hence on the spectroscopy of the FHF and FDF ions. It is found in KHF_2—KDF_2 [2] and in $NaHF_2$—$NaDF_2$ [1] that

$$\langle F-D-F\rangle \quad > \quad \langle F-H-F\rangle$$

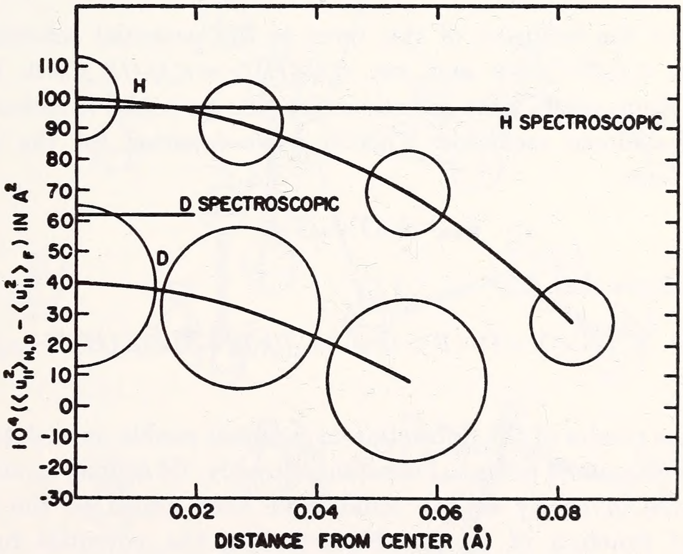

FIGURE 2. The difference in mean-square amplitude of vibration along the bond of H or D and F versus the distance of H or D from the center of the bond [1]. The circles represent the estimated standard deviations of the ordinate.

where $<>$ is used to denote mean value. These results are deduced from the changes in cell constants that result upon substitution of D for H in these two substances. As we point out below, it is generally invalid to deduce changes in mean bond lengths from changes in cell constants. Yet especially in the structure of $NaHF_2$ there is only one FHF in the primitive unit cell and it is along the *c* direction of the crystal: the assumption that the change in the length of the *c* axis reflects a mean bond-length change seems valid. Normally we might write a potential function for this FHF system as

$$2V=(k_1/\mu_1)Q_1^2+(k_3/\mu_3)Q_3^2 \tag{3}$$

with the possible addition of quartic terms in Q_1^4 and Q_3^4. We noted above that Q_1 is proportional to the change in the F—F bond length; hence the expectation value of Q_1, $<Q_1>$, must be isotopically dependent in view of the bond length changes we have described. But since the evidence is that the bond is linear and symmetric, we also require that there can be no terms in the potential function containing odd powers of Q_3. Clearly our simple potential function, eq (3), is not adequate, and we require additional terms to account for the observed diffraction results. Let us couple the symmetric and antisymmetric modes and add a term to eq (3) of the form

$$(k_{13}/(\mu_1^{\frac{1}{2}}\mu_3))Q_1Q_3^2. \tag{4}$$

Note that the inclusion of this term in the potential function still leads to $<Q_3^{2n+1}>=0$ and yet $<Q_1(H)>\neq<Q_1(D)>\neq 0$. Let us take as appropriate basis functions for this potential function those of the harmonic oscillator. Then a wave function for the system has the form

$$\psi_{nm}=\psi_n(1)\psi_m(3) \tag{5}$$

and it follows that [3]

$$<\mathrm{F-H-F}>-<\mathrm{F-D-F}>=(-hk_{13}/(k_1k_3^{\frac{1}{2}}4\sqrt{2}\pi)(\mu_3(H)^{-\frac{1}{2}}-\mu_3(D)^{-\frac{1}{2}}). \tag{6}$$

Hence the results of the diffraction experiment enable us to determine one of the assumed potential constants directly. Of course, terms other than those given by eq (4) could have been added to the simple potential function of eq (3). Nevertheless, the potential function given by these terms has provided a reasonable fit to the observed fundamentals and overtones of the FHF and FDF ions [3].

4. The ClHCl and BrHBr Ions

The impetus to study simple hydrogen-bonded systems led us to examine structures that might contain the bichloride, ClHCl, and bibromide, BrHBr, ions. These ions are less stable than FHF, and compounds such as $NaHCl_2$, or even $CsHCl_2$, are very unstable.

We [4, 5] did, however, discover the unusual systems $CsX\cdot\frac{1}{3}H_3OHX_2$, where X=Cl and Br. The basic structure is shown in figure 3. It consists of strings of bihalide ions and strings of hydronium ions stabilized apparently by coordination of the halide ions to cesium. The pertinent XHX distances, together with $X \ldots X$ distances, are given in table 2. The relatively constant difference may be fortuitous.

These particular compounds containing ClHCl and BrHBr are unstable in the absence of the halide acid, but it still should be possible to obtain infrared spectra. Our own efforts in this direction were unsuccessful. Yet these spectra should be investigated. It is unfortu-

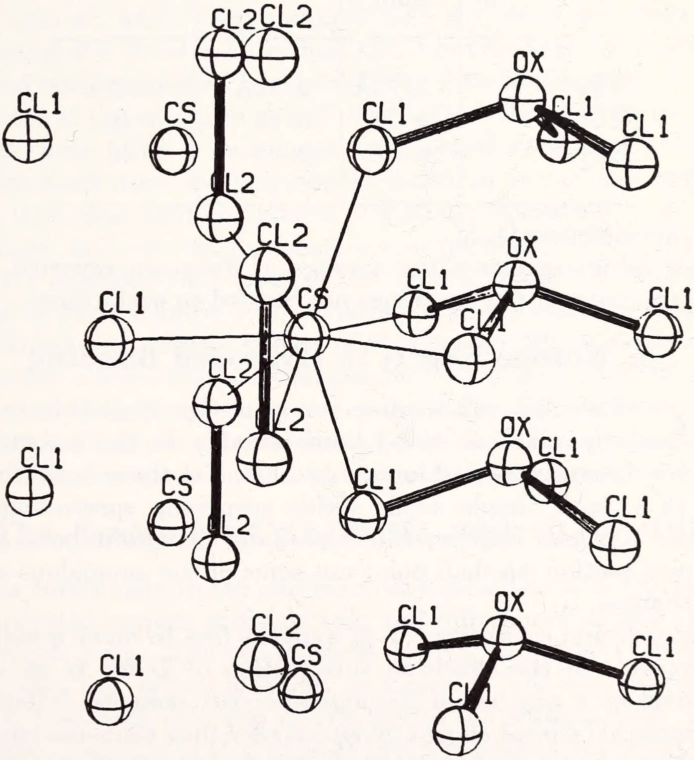

FIGURE. 3. Part of the structure of $CsCl\cdot\frac{1}{3}H_3OHCl_2$ [4]. The c axis is vertical in the figure. The disorder of the oxygen positions is not shown, nor are the hydrogen positions. The shaded lines represent probable hydrogen bonds.

nate that no spectra have been obtained on these compounds, which are the only compounds containing the bichloride and bibromide ions in a known environment.[2] Yet a number of spectra have been obtained on compounds of uncertain structure that contain the bichloride and mixed bihalide ions. The results of Evans and Lo(6,7) are indeed curious. They find two distinct types of vibrational spectra for $MHCl_2$, which they suggest might be due to symmetric and asymmetric ClHCl ions. Yet the correlation with M is surprising:

Type I: asymmetric: Cs^+, $(CH_3)_4N^+$, $(C_4H_9)_4N^+$, . . .

Type II: symmetric: $(C_2H_5)_4N^+$, $(C_3H_7)_4N^+$, $(C_5H_{12})_4N^+$, . . .

Clearly this area needs further work. In particular, it needs cooperative efforts by spectroscopists and diffractionists.

TABLE 2. Comparison of H bonded and van der Waals distances [a]

X—H—X	Radius Sum	$X—X_{obs}$	Difference
HF_2^-	2.73Å	2.26Å	0.47Å
HCl_2^-	3.62	3.14	0.48
HBr_2^-	[b] 3.81	3.35	0.46

[a] From references [4, 5].

[b] This value represents the average of distances reported for the closest approach of two bromines not bonded to each other.

5. Isotope Effects in Hydrogen Bonding

The use of isotopic substitution is a generally applicable technique in spectroscopy that has aided immeasurably in the assignment of bands and determination of force constants. Yet the substitution of D for H in various simple solids yields surprising spectroscopic and diffraction changes. Here we will discuss the changes in bond lengths; in the next section we shall point out some of the anomalous spectroscopic changes.

Ubbelohde and co-workers [2, 8] were the first to make quantitative measurements of the effects of substitution of D for H on the cell parameters of a number of hydrogen-bonded systems. Where there was a single AHA bond along a given cell edge they made the reasonable assumption that any change in that cell edge on substitution of D for H directly reflected a change in the mean A—A bond length on going from AHA to ADA. More often, however, there were several independent AHA bonds that could contribute to the change in the cell edge, and so the interpretation of the results became more arbitrary. Maximum cell changes are about 0.06 Å on substitution of D for H, and since A—A distances could not be determined with an estimated error of less than perhaps 0.03 Å in those days, it was clearly necessary to use the changes in cell constants to deduce indirectly the changes in bond lengths. Direct determinations of these AHA and ADA bond lengths would not have yielded precise enough answers to enable one to detect significant changes in bond lengths on deuteration.

---

[2] Note added in proof. Such spectra, both infrared and Raman, have now been obtained by L. W. Schroeder and will be reported separately.

The situation has now changed, and in reasonably simple systems containing first row elements, such as C or O, along with H, it is possible to determine O—O bond lengths to an apparent precision of around 0.002 Å, and so to attach significance to differences in ODO and OHO distances of the order of 0.01 Å. We have carried out a complete single-crystal study of both normal and deuterated oxalic acid dihydrate [9]. We chose oxalic acid dihydrate because Robertson and Ubbelohde [10] had found the isotope effect to be very large for this substance; when they assumed that the effect was only in the strongest of the three independent OHO bonds, they concluded that this bond was lengthened by about 0.041 Å on deuteration.

A sketch of the structure and of our results is shown in figure 4. Note that all three OHO bonds lengthen on deuteration, and that the strongest bond does not lengthen as much as one of the very weak bonds. It is clear that the effects of isotopic substitution are indeed long range, and are not localized in the particular strong hydrogen bond. We conclude that most of the results in the literature on the changes in bond lengths with deuteration are unreliable, since these are obtained from measurements of changes in cell constants in cases where there is more than one independent bond along the cell edge. It would seem that there is a severe paucity of reliable information on the effects of isotopic substitution on bond lengths in the solid state and that much experimental and theoretical work needs to be done.

6. The Systems $HCrO_2/DCrO_2$ and $HCoO_2/DCoO_2$

Let us turn finally to the chromous and cobaltous acid systems that have provided various spectroscopic and diffraction puzzles over the past several years. The structure of $HCrO_2$, which is typical of all members of this series, is shown in figure 5. The structure is very simple indeed, with only one HMO_2 unit in the primitive cell. The site symmetry around M is D_{3d}, at least to a first approximation. The only positional variables in a crystallographic sense are the position of the O atom along the threefold axis and the position of the H atom. In a desire to understand the nature of the potential well in this OHO

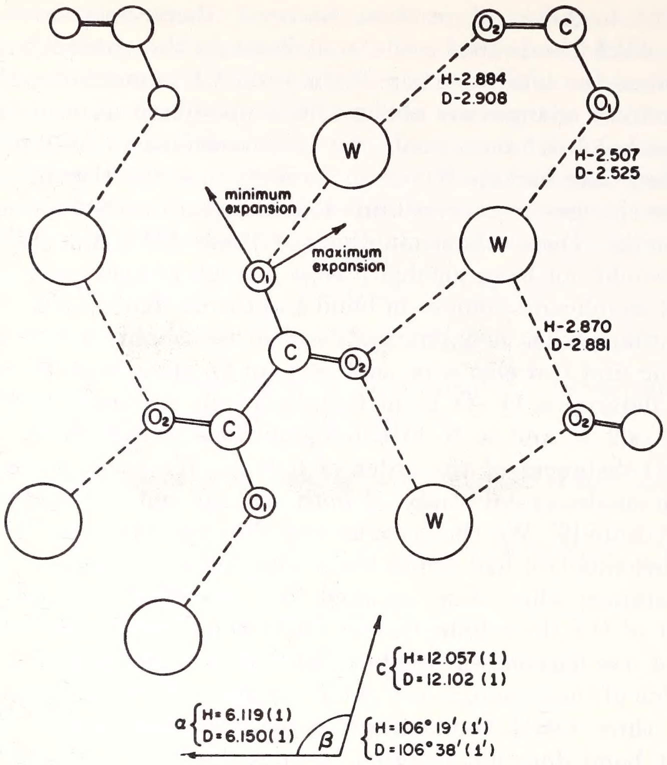
O2
C
H-2.884
D-2.908
O1
W
H-2.507
D-2.525
minimum expansion
maximum expansion
O1
W
C
O2
H-2.870
D-2.881
O2
C
O2
O1
W
c {H=12.057(1) D=12.102(1)
a {H=6.119(1) D=6.150(1)
β
{H=106°19′(1′) D=106°38′(1′)

FIGURE 4. Part of the structure of oxalic acid dihydrate projected onto the *a–c* plane [9]. There is a symmetry center midway along C–C. The independent O–H–O and O–D–O bond lengths are shown. Each has an estimated standard deviation of 0.002 Å. Standard deviations of the lattice parameters are shown in parentheses. The directions of minimum and maximum expansion are from Ref. 10.

system a number of physical studies were undertaken. These include an NMR study [11], a neutron diffraction study [12], and spectroscopic studies [13, 14] on the Cr system (stimulated by an initial x-ray study [15]) and various spectroscopic, neutron diffraction, and inelastic neutron scattering experiments on the Co system [16, 17]. The diffraction and NMR studies have been hampered by the lack of single crystals; all attempts to obtain suitable single crystals of these materials have failed.

The structure illustrated in figure 5 is completely analogous to that for $NaHF_2$ and again there is only one AHA bond in the *c* direction. Deductions made from the change in cell constants on deuteration of these systems are:

Cr system: $<ODO> = <OHO> + 0.06$ Å; $<O–D–O> = 2.55$ Å

Co system: $<ODO> = <OHO> + 0.06$ Å; $<O–H–O> = 2.49$ Å.

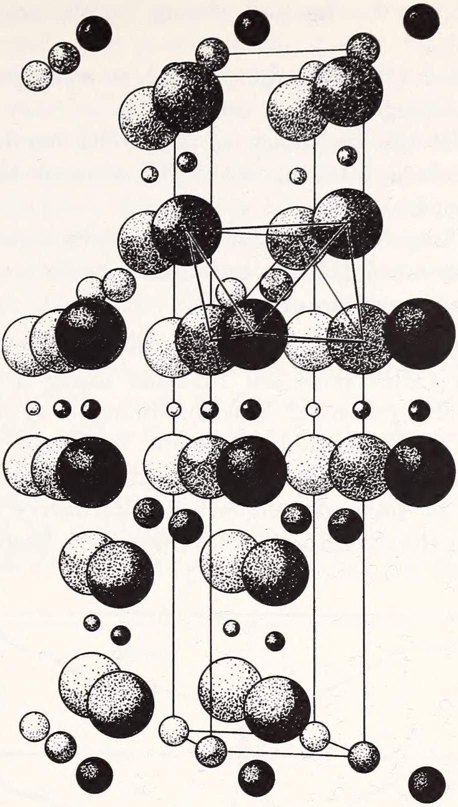

FIGURE 5. The atomic arrangement in $HCrO_2$: Perspective view along the line ($x=\frac{1}{4}y$, $z=\frac{1}{2}$) from 40 Å of four hexagonal unit cells [12]. The largest spheres are oxygen atoms; those of intermediate size are chromium; and the smallest are hydrogen, shown in the central position of the O–H–O bond. One of the CrO_6 octahedra is outlined.

The neutron diffraction studies of the Cr compounds are most readily interpreted in terms of a double-minimum potential well for the ODO system. The results for the OHO system are ambiguous.

Typical spectroscopic results on these systems are shown in figure 6, where the infrared spectra for $HCrO_2$ and $DCrO_2$ are shown in the region 3000 to 400 cm^{-1}. The results for the Co compounds are essentially analogous, although some general shifts of the bands occur. Moreover, in both the Cr and Co systems there are no additional bands in the region 400 to 30 cm^{-1}. The various difficulties with the spectroscopic results, as deduced from the spectra presented in figure 6, are:

(1) The O–H stretching band in $HCrO_2$ is centered around 1640 cm^{-1}. No O–D stretching band occurs in $DCrO_2$ at the expected

place (1300–1200 cm^{-1}). Instead strong bands are observed near 1750 cm^{-1}.

(2) The assigned OH stretching band is a singlet, whereas the assigned OD stretching band is a doublet.

(3) The ratio of the frequency of the OHO bending mode to the ODO bending mode is 1.487 at −196 °C, whereas the value for the harmonic oscillator is 1.386.

(4) There are two bands in the lattice-mode region (700 cm^{-1} to 30^{-1}) of the spectrum of $HCrO_2$, but there are six such bands in this same region of the spectrum of $DCrO_2$.

We have suggested previously [13] that these observations are compatible with the OHO potential function being a single-minimum type and the ODO potential function being a symmetric, double-minimum type, as illustrated in figure 7. These one-dimensional potential functions are supported by model calculations. Moreover, no one appears to have developed an alternative explanation for these results, and the experimental findings have been verified several times [14, 16, 17].

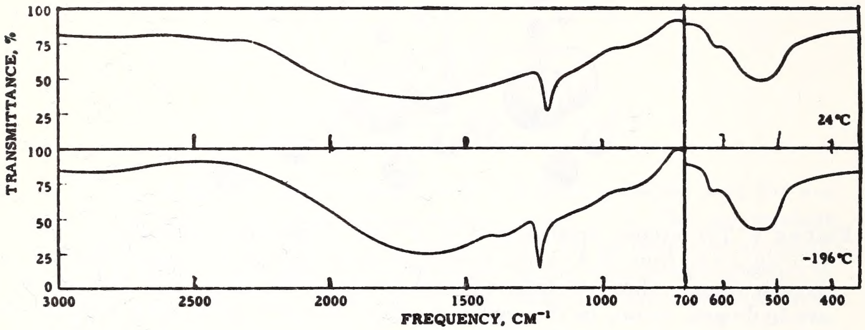

FIGURE 6a. Infrared spectrum of $HCrO_2$ at 24° and at −196°C. (3000–700 cm^{-1} 2.47 mg and 700–400 cm^{-1} 0.62 mg of $HCrO^2$ in 1-in. KBr disks) [13].

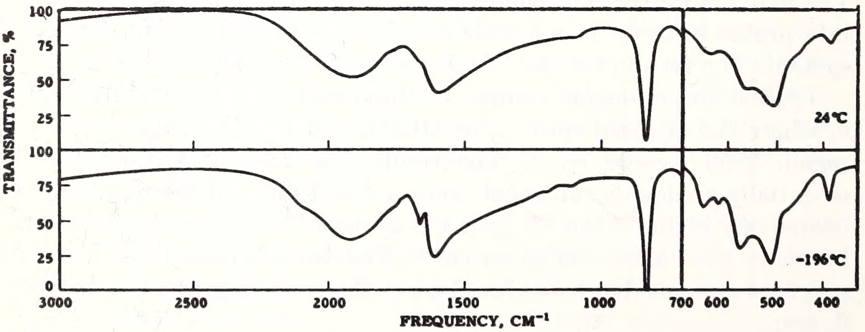

FIGURE 6b. Infrared spectrum of $DCrO_2$ at 24° and at −196°C (3000–700 cm^{-1} 2.49 mg and 700–400 cm^{-1} 0.63 mg of $DCrO_2$ in 1-in KBr disks).

If one assumes that some coupling between the antisymmetric stretching mode and other modes in the system might be responsible for the apparent change in symmetry in going from H to D, then one may be able to rationalize the results. Such coupling, of course, is similar to that suggested earlier [3] for the FHF–FDF system, but the coupling must be much greater to account for the far larger isotope effects. Suppose that in the Cr and Co systems there is a symmetric, double-minimum potential function. Then H will lie nearer to the top of the barrier than will D. Owing to its more rapid tunneling through the barrier and its coupling with the other modes the H atom may effectively "see" a symmetric environment. The D atom, however, because of its lower position in the well may not be able to track with the other modes and hence will "see" an asymmetric environment. We attempted to make model calculations in which we coupled the symmetric and antisymmetric modes in these systems, as described in Section 3. Yet the magnitude of the coupling term k_{13} required by the large isotope effect is such that our variational calculations did not converge even when we used Hamiltonians

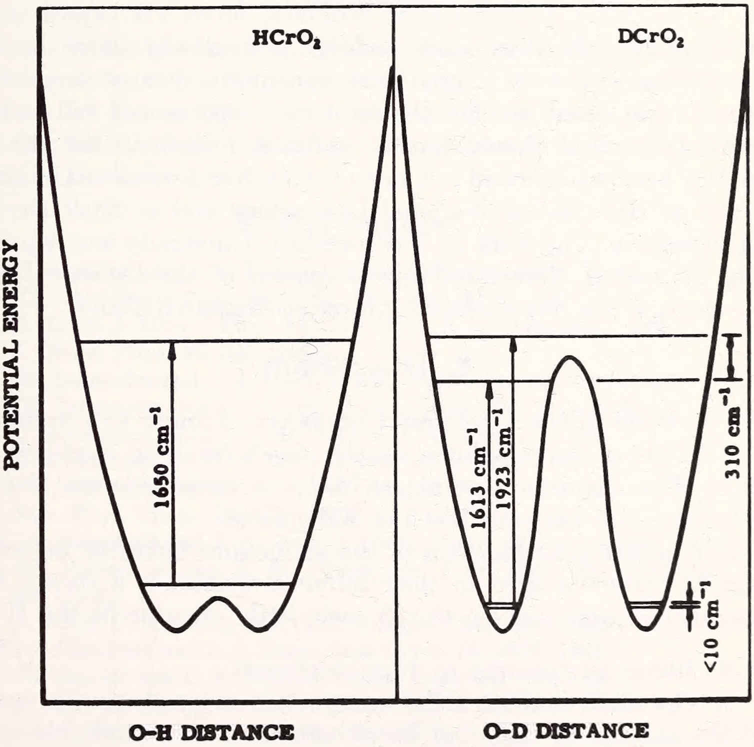

FIGURE 7. Potential energy curves for the hydrogen bond of $HCrO_2$ and $DCrO_2$ [13].

of as high an order as is compatible with our computer. We have therefore studied what happens to the various levels as we gradually increase the k_{13} term. It would appear that the idea of coupling of the antisymmetric stretching mode with other modes of the system may have some merit in explaining the puzzle of the very large spectroscopic changes on deuteration in the $HCrO_2$ and $HCoO_2$ systems. Yet clearly there is great need for new and inventive theoretical work on these systems.

7. Summary

In this lecture I have tried to touch on a few topics that I hope will be of interest to both the diffractionist and the spectroscopist. Let me again emphasize that the study of simple hydrogen bonds in solids is one route to an understanding of hydrogen bonding in general, and that such systems offer the advantage that the spectroscopic and diffraction results are complementary and lead, when combined, to a more thorough understanding than would have been obtained from the individual results of either method.

It is not feasible here to acknowledge individually all of the many collaborators who have shared with me in the fun of some of the studies I have described. For the most part their names will be found in the references. I should like to indicate, however, that the work described here was carried out not only at Northwestern University, but also at Brookhaven National Laboratory and at Shell Development Company. The work at Northwestern University was supported by the Advanced Research Projects Agency of the Defense Department through the Northwestern Materials Research Center.

8. Discussion

W. J. Potts (Dow Chemical Company): I have two comments:

1. Mulls in fluorocarbons usually don't result in chemical reactions. The chemical reaction is likely to occur between the ionic substance and the ionic NaCl or KBr plates.

2. A possible explanation of the anomalous behavior between H and D chromous acid in their infrared spectra is a strong Fermi resonance interaction in the D case, little or none in the H case.

J. A. Ibers: In response to your comments:

1. The $CsX \cdot \frac{1}{3}$ (H_3O HX_2) compounds are apparently unstable in the absence of HX. Our initial efforts to obtain reliable spectra were not successful. We encourage others more experienced in obtaining spectra of reactive materials to look at these substances.

2. Although I can't eliminate the possibility of Fermi resonance, I don't believe it affords an explanation of the dramatic differences in spectra in the lattice-mode regions of these two substances.

K. Harmon (Harvey Mudd College): We have repeated the spectroscopic work of Evans and Lo on $H\,Cl_2^-$ with $H\,Br_2^-$ cations and find a steady progression in the spectra from tetramethylammonium to tetrabutylammonium compounds. Has any spectroscopic work shown evidence for type I and type II vibration spectra with the HF_2^- ions? All of the reports I have seen are with small cations, where a type I spectrum would be expected.

J. A. Ibers: I'm aware of no spectral or diffraction work on salts containing both the HF_2^- ion and large cations.

J. Schiffer (Temple University): I noted in your bifluoride-ion calculation, you considered only a stretch-stretch term in your expression for potential energy. I know this is partly a matter of curve fitting, but still might be real. Did you consider stretch-bend interactions as influencing the isotope effect?

J. A. Ibers: We could probably have achieved a similar fit using coupling with the bending, rather than with the antisymmetric stretching frequency. Since we were also interested in fitting the overtones of the antisymmetric stretching frequency, we restricted our potential to terms related to the symmetric and antisymmetric stretching modes.

9. References

[1] B. L. McGaw and J. A. Ibers, J. Chem. Phys. **39,** 2677 (1963).
[2] A. R. Ubbelohde, Proc. Roy. Soc. (London) **A173,** 417 (1939).
[3] J. A. Ibers, J. Chem. Phys. **41,** 25 (1964); R. G. Delaplane and J. A. Ibers, J. Chem. Phys. **48,** 539 (1968).
[4] L. W. Schroeder and J. A. Ibers, J. Am. Chem. Soc. **88,** 2601 (1966).
[5] L. W. Schroeder and J. A. Ibers, Inorg. Chem. **7,** 5944 (1968).
[6] J. C. Evans and G. Y. -S. Lo, J. Phys. Chem. **70,** 11 (1966).
[7] J. C. Evans and G. Y. -S. Lo, J. Phys. Chem. **70,** 20 (1966).
[8] For a bibliography on measured isotope effects see J. A. Ibers, Ann. Rev. Phys. Chem. **16**, 375 (1965).
[9] R. G. Delaplane and J. A. Ibers, J. Chem. Phys. **45,** 3451 (1966).
[10] J. M. Robertson and A. R. Ubbelohde, Proc. Roy. Soc. (London) **A170,** 222 (1939).
[11] J. A. Ibers, C. H. Holm, and C. R. Adams, Phys. Rev. **121,** 1620 (1961).
[12] W. C. Hamilton and J. A. Ibers, Acta Cryst. **16,** 1209 (1963).
[13] R. G. Snyder and J. A. Ibers, J. Chem. Phys. **36,** 1356 (1962).
[14] J. J. Rush and J. R. Ferraro, J. Chem. Phys. **44,** 2496 (1966).
[15] R. M. Douglass, Acta Cryst. **10,** 423 (1957).
[16] A. Benoit, Spectrochim. Acta **19,** 2011 (1963).
[17] R. G. Delaplane, J. A. Ibers, J. R. Ferraro, and J. J. Rush, J. Chem. Phys., in press.

[illegible]

R. [illegible]

J. A. [illegible]

[illegible]

J. A. Pierce: [illegible]

6. References

[illegible]

STRUCTURE AND DYNAMICS IN MOLECULAR CRYSTALS; SOME COMPARISONS [1]

WALTER C. HAMILTON

Chemistry Department
Brookhaven National Laboratory, Upton, New York 11973

1. Chemists and Molecules

In a recent conversation with a colleague, I learned that he was associated with the School of Molecular Science in a new university. The explanation that he was really a member of the chemistry department should have been expected, for the best definition of the chemist is that he is a *molecular scientist.*[2] He is concerned with the *structure of molecules, the dynamics of molecules,* and the *synthesis of molecules.* These three areas have as a matter of fact been suggested by the Westheimer Committee [1][3] as the proper divisions of chemistry, as opposed to the traditional physical, organic, and inorganic chemistries.

We are concerned in these colloquia with two of these broad areas of chemistry—the structure and dynamics of molecules. We must be careful not to define the latter area too narrowly, for the chemist is interested not only in the dynamics of individual molecules, the thermal motions in pure crystals or liquids for example, but in the dynamics involved in chemical change—for in a narrower sense it is chemical change that is what chemistry is really all about. The chemical industry is based on an extension of the alchemist's attempts to generate valuable materials from worthless ones. Thus some of my colleagues consider that the study of chemical kinetics—how molecules react—is the heart of all chemistry.

It thus behooves us, as molecular scientists actively engaged in the study of the detailed structure and dynamics of pure substances, to consider how our techniques can be of value to the chemist who is actually doing chemistry.

The configurational and metrical aspects of molecular structure determination—so well exemplified by x-ray crystallography—have been and will continue to be of great importance to the chemist in obvious ways. Reaction mechanisms and chemical syntheses can only be understood if one has some feeling for the relative positions of the atoms in the molecules. This area of structural chemistry has been of growing importance in recent years, perhaps reaching its pinnacle in the attempt to relate geometrical configuration to activity in protein enzymes. It is also clear that inorganic chemistry has received a tremendous shot in the arm from the fact that small molecular structures can be determined in a quite routine fashion nowadays.

---

[1] Research performed under the auspices of the U.S. Atomic Energy Commission.

[2] The current breed of physicist in this country always seems a bit uncomfortable when faced with molecules, but perhaps this is because he—in contrast to his chemical friends—knows that molecules are rather easily understood and does not care to bother with them.

[3] Figures in brackets indicate literature references at the end of this paper.

In this paper, however, I would like to address myself more to the question of molecular dynamics and leave the questions of geometrical structure somewhat to one side. The practical chemist is interested in the energy of his reacting system as a function of the geometrical parameters of the system. If he has in his hands an accurate description of this reaction surface, he is in a better position to predict the mechanism and rate of a reaction: Which configuration of reacting species is involved in the transition state? From our present point of view, we would like to ask whether such information can be obtained from structural studies of the type we are discussing here. Can studies of molecular motion in pure compounds give some insight into the way in which these molecules will react with other molecules? Can we determine the details of the force field surrounding a molecule? I will try in the following pages to give some perspective to the problems of determining interesting things about potential functions from neutron and x-ray diffraction and neutron inelastic scattering studies. I will emphasize the desirability of the use of complementary techniques; I will discuss the importance of models; I will give some report of the present status of these techniques; and I will finally indulge in some speculation regarding the future of neutron inelastic scattering as applied to chemical problems. Most of these problems will be discussed in some detail by other contributors to this symposium, so I will feel free to leave out a great deal of detail while apologizing in advance for any substantial overlap.

2. Molecules and Models

The two classical methods of studying molecular structure are diffraction and spectroscopy. The first gives information on position (and information on the change in position averaged over time); the second gives information on energy levels. From both, we would like to determine potential functions. In many practical cases when we are examining a particular mode of molecular motion we are measuring a system which is initially in its lowest energy level with respect to this motion. At best, we are dealing with a Boltzmann population of the lowest few energy levels. It is clear that it is impossible to construct a complete potential surface from such measurements.[4] Normally a model for the potential is chosen—a simple harmonic potential for example—and parameters of the model are fit to the data. These parameters only have meaning if the assumed model is correct. By comparing various measurement techniques, which are affected by the model in different ways, we hope that we can define the model and test its correctness far better than we could by using one technique alone. Furthermore, it is often important that numerical calculations be used to establish the qualitative features of a model, while the experiment is used to determine precisely the quantitative parameters to be associated with this model if it is indeed correct.

The importance of models can best be understood by examination of some simple one-dimensional problems. In diffraction methods, we measure an amplitude of motion. In spectroscopy we measure an energy level difference. The model of the harmonic oscillator is usually chosen as the best approximation for molecular motions. An extreme model for a vibrational mode is that of a particle in a one-dimensional box (square-well with infinitely high potential walls). By formulas which are developed in every elementary quantum mechanics book, we can show that the following relationships exist between the mean square amplitude of vibration in the ground state $<r^2>$ and the vibrational frequency ω between the ground and first excited states: For the harmonic oscillator in its ground state [5,6]

$$<r^2> = \frac{h}{8\pi^2 m\omega c} = \frac{16.8}{m\omega} \tag{1}$$

For the particle in the box in its ground state

$$<r^2> = \frac{h}{m\omega c}\,\frac{3}{8}\left[\frac{1}{12} - \frac{1}{2\pi^2}\right] = \frac{16.3}{m\omega} \tag{2}$$

The constants 16.8 and 16.3 are valid for $<r^2>$ expressed in Å^2, m in a.m.u. and ω in cm^{-1}.

For a particle with a mass of 1.5 atomic mass units and a frequency of 275 cm^{-1}, we find root mean square (rms) amplitudes $<r^2>^{\frac{1}{2}} =$ 0.202 and 0.199 Å for the two cases (see fig. 1). Thus the relationship between the vibrational amplitude and the first vibrational level

---

[4] One of the great bugaboos of spectroscopy has been that although in principle we know that a complete knowledge of the energy levels of a system will allow us to calculate all thermodynamic functions—and hence all chemistry—we first of all do not have all the energy levels, and secondly do not have adequate models from which to infer all the energy levels from the few that we have measured. This situation is especially valid for molecules of any interesting complexity. Given that we have measured the energy levels of a system, what have we learned about chemistry?

[5] The notation $<r^2>$ means the average value of r^2 over the probability density function for the motion.

[6] An actual measurement of the amplitude by diffraction would measure the average over all populated levels. We ignore this difference for the purposes of this illustration.

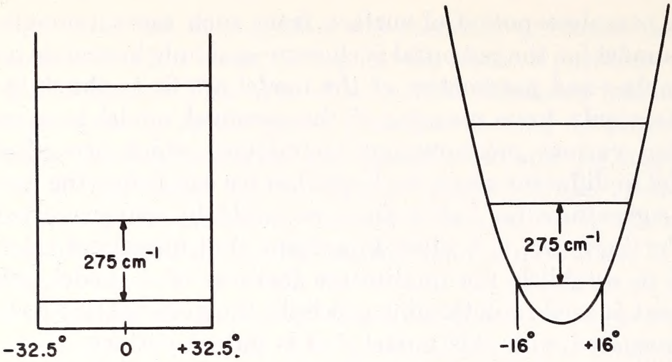

FIGURE 1. Square-well potential and harmonic potential, each having the 0–1 transition at 275 cm^{-1}. For a particle with mass 1.5 atomic mass units, the root-mean-square amplitude of vibration is 0.20 Å in each case. If the model is applied to the internal rotation mode in ethane, the root-mean-square amplitude is 11.0°.

transition is relatively insensitive to the shape of the potential function. This is an important result and suggests to us that the assumption of harmonic motion in the prediction of spectroscopic transition frequencies from diffraction-determined amplitudes is not a limiting assumption. Indeed, excellent agreement is often found when the diffraction studies (which rarely determine vibrational amplitudes to better than 10 percent) are carefully carried out.

The use of the particle-in-a-box as a model for interatomic forces is not so unrealistic as it might at first sight seem. In the context of this paper, we are interested in learning something about "non-bonded" intermolecular potentials. These potentials are often characterized by a sum of a rather weak attractive term and a very strong repulsive term, which is often adequately approximated by a hard barrier. (Witness the success of hard sphere models in the study of simple structures and statistical thermodynamics.) Thus particle-in-a-box models may be closer representations of intermolecular potentials than are harmonic functions.

The particular parameters in the example above are pertinent to the internal rotation in ethane. If we take equations (1) and (2) and divide by R^2, the square of distance from the axis of rotation, we may write the mean square angular displacement in radians as

$$\langle\phi^2\rangle = \frac{16.8 \text{ or } 16.3}{I\omega} \qquad (3)$$

where I is the moment of inertia of the rotating group. The internal rotation in ethane is equivalent to the rotation of a single group with half the moment of inertia or mass against an infinite mass; hence the mass 1.5 taken above. Taking the C–H bond length as 1.09 Å and a tetrahedral bond angle, we find

$$<\phi^2>^{1/2}=11.0.$$

For the square-well model, this corresponds to a well width of 61°.

Let us consider now a pair of more realistic potentials for the internal rotation in ethane: potentials with a period of 120°. Two extreme models may be taken for the motion, one a periodic square-well potential and the other a potential of the form $V=\frac{1}{2}V_o(1\text{-}\cos 3\theta)$, where θ is the angle of rotation. These are illustrated in figure 2. The dimensions of the potentials are such as to reproduce the first three energy levels as derived from thermodynamic and spectroscopic data [2, 3].

The height of the barrier is the only degree of freedom for the cosine potential, and a barrier height of 2750 cals/mole or 960 cm^{-1} was found to give a good fit to the data. There are two parameters for the square-well potential—the height and width of the barrier; again a good fit may be obtained with a barrier height of 1700 cal/mole (595 cm^{-1}) and a barrier width of 76°. It is interesting to note that the width of the potential well of 44° is somewhat less than the 61° for the infinitely deep square well which has the same first transition energy of 275 cm^{-1}. As the barrier comes down, the well width also decreases; there is a simultaneous decrease in the energy of the higher levels.

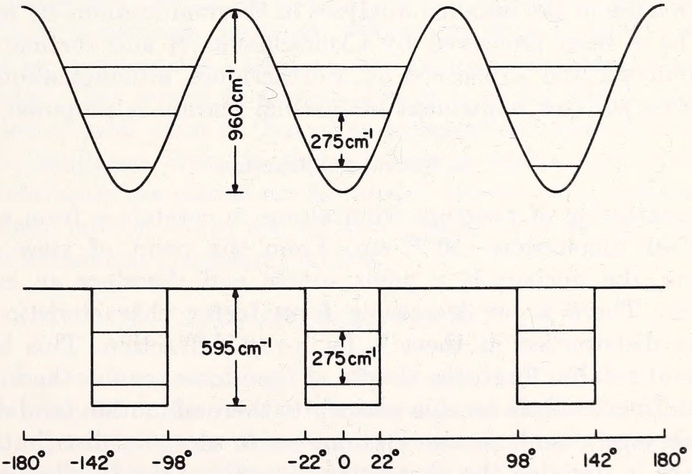

FIGURE 2. Square and sinusoidal periodic potentials for the internal rotation in ethane. The first three energy levels are virtually the same for both potential functions.

The really important point of this example is that the derived barrier *height* is sensitively related to the shape of the barrier and may have little relationship to the actual height if the functional form chosen is incorrect. As noted above, potential functions for rotations of groups in crystals may more nearly approximate square well type potentials than the cosine potentials commonly assumed in interpretation of spectroscopic and diffraction data. This point will be further illustrated in some of the examples discussed later in the paper.

In this case again, we expect the amplitude of vibration to be very nearly equal for the two cases and to be simply related to the vibrational frequency, so that the comparison between spectroscopic and diffraction data will again be valid, independent of the shape of the barrier.

3. Models and Techniques

3.1. Diffraction and Vibration Amplitudes

In some of the examples below, we will discuss the results of neutron diffraction studies in which vibration amplitudes have been derived from the diffraction data. Other participants in this conference have discussed in considerable detail how this is done and what types of information can be obtained. I would like to make three points in this section: one, that neutron diffraction may provide better measurements for these vibration amplitudes in many cases of interest than does x-ray diffraction; second, that the particular model assumed for the refinement of the diffraction data is of some significance although it may often be ignored; and finally that there is a wealth of information available in the detailed analyses of thermal motions by methods which have been pioneered by Cruickshank [4] and further refined by Schomaker and Trueblood [5]. Furthermore, a modification of the usual least squares refinement of thermal motion is proposed.

a. Neutron Diffraction

The scattering of neutrons from atoms in crystals is from a region of nuclear dimensions—10^{-13} cm. From the point of view of 1 Å neutrons, the nucleus is a point source and therefore an isotropic scatterer. There is no decreasing form factor characteristic of the electron distribution as there is for x-ray diffraction. This has two important results. First, the shapes of the atoms seen in the inversion of the diffraction data are due entirely to thermal motion (and disorder in the crystal), and no assumptions as to electron distribution are necessary in deriving the parameters describing the thermal motion.[7]

---

[7] The combination of neutron and x-ray diffraction on the same crystals has been used in an elegant way by Coppens [6] to obtain accurate electron density distributions in crystals. This work has been discussed in another paper at this conference.

The second important result of the lack of form-factor dependence is that the scattering extends with appreciable intensity to much higher scattering angles, and thus more accurate data may be obtained.

For many of the problems in which I have been interested, neutron diffraction has been essential for another reason. Namely, hydrogen atoms do not scatter x-rays with enough intensity for it to be possible to obtain accurate parameters for their thermal motion. Neutron diffraction offers a considerable improvement, for the ratio of the scattering cross section of hydrogen to that for carbon is about 0.4, while it is 0.03 for x rays. The practical effect is that we can determine bond lengths involving hydrogen atoms to better than 0.01 Å and the thermal motion parameters of these hydrogen atoms to a few percent. Most of the work I will discuss later on is devoted to studies of the hydrogen bond, but I will also assert that most interesting molecules have hydrogen around their periphery, so that if we are to study the forces between interacting, interesting molecules we are forced to study the dynamics of hydrogen atoms with great accuracy.

b. Validity of the Usual Models

The second point I would like to make in this section concerns the validity of models used in the refinement of diffraction data, the amount of information we can obtain from diffraction data and whether we can still obtain interesting information even if our models are wrong. The most direct method of understanding a diffraction experiment is to look at the representation of the scattered density as revealed in a Fourier inversion of the diffraction data. This may give a qualitative feeling for the nature of the thermal motion. For a quantitative measure, however, diffraction data is almost always analyzed by carrying out a least squares refinement of the parameters of a model. This model is almost always a model which describes the motion of each atom as that of an independent three-dimensional harmonic oscillator. Even in the refinements where rigid body and other constraints are placed on the model, the model is still confined to harmonic motion. Thus the motion of each atom is described by a three-dimensional Gaussian function

$$\rho(\mathbf{r})=\rho_o(\mathbf{r})\exp\{-\tfrac{1}{2}\mathbf{r}'\mathbf{A}\mathbf{r}\} \tag{4}$$

where $\mathbf{r}$ is a vector describing the atomic position and $\mathbf{A}$ is a matrix whose inverse $\mathbf{A}^{-1}$ is the matrix of mean-square displacements.

Now any distribution function $\rho(\mathbf{r})$ is completely specified by specifying all of its moments:

$$m^{abc}=\int\rho(\mathbf{r})\,x^a y^b z^c\,dx\,dy\,dz \tag{5}$$

The matrix $\mathbf{A}^{-1}$ defined in eq (4) contains the second moments m^{002}, m^{020}, m^{200}, m^{011}, m^{110}, m^{101}. The assumption of the particular form (eq (4)) implies certain relations between these moments and higher moments of the distribution. In particular, all the odd moments are zero and the higher moments are given by expressions of the type

$$m^{(0,2n,0)}=(2n-1)m^{(0,2n-2,0)}m^{(0,2,0)} \tag{6}$$

Thus the average value of x^4 is

$$m^{0,4,0}=<x^4>=3<x^2>^2 \tag{7}$$

If we assume that the scattering density function is approximately Gaussian, we may wish to add as further parameters in the refinement the departures of the higher moments from their ideal values. Such a procedure does of course add extra parameters to the refinement, and it is only natural that the agreement between the observed and calculated data improve. The most desirable approach is one that first uses a theoretical model to ascertain which of the many possible additional parameters are likely to be of any importance, then refines these parameters by a least squares procedure, and finally assesses the improvement in the agreement by a valid statistical test [7].

Experience and theory tell us that the harmonic approximation is probably valid to a high degree of accuracy for most of the internal modes of motion of a molecule. It is not so likely to be valid for the very low frequency modes involved in intermolecular interactions and in internal rotations in molecules and crystals. Convincing evidence for departures from the harmonic approximation has been given by Willis [8] and Dawson [9] for the ionic crystals CaF_2 and UO_2.

Pawley [10] has suggested directly refining the rigid group vibration parameters of molecules rather than the vibrational parameters of individual atoms, from which the group vibrational parameters may be derived with the Schomaker-Trueblood [5] formalism. This has the desirable effect of greatly reducing the number of parameters to be determined in a crystal structure refinement.

I would like to propose the following scheme to put a few parameters back in. Since one of the main interests in determining vibrational parameters is in the study of intermolecular forces, a sensible approach might be as follows:

(1) Use vibrational parameters for the internal modes obtained from spectroscopic measurement on the same or related molecules.

(2) Refine parameters describing the rigid body motions as well as parameters describing internal rotations.

(3) Include in the parameters refined in (2) more sophisticated models of thermal motion than the harmonic. Thus include refine-

ment of higher moments of the rigid groups—not of individual atoms. It is just in the low-frequency motions of whole molecules and groups within molecules that the anharmonic terms are likely to be of most importance. Introducing them in this way will still lead to fewer parameters than the usual complete harmonic refinement for individual atoms and may well lead to much better descriptions of thermal motion in molecular crystals than we have had up to now. Some efforts in this direction are being made in our laboratory.

Complete, general descriptions of the rigid body motions should teach us much about the forces between molecules. We have a unique situation in the crystal in that we can easily measure the directional properties of intermolecular forces.

3.2. Neutron Inelastic Scattering

Neutron inelastic scattering promises to be the most important of the techniques for the study of the dynamics of motion in molecular crystals. Here again, a useful first approximation for a crystal model is that of harmonic motion. But again, for the more interesting motions involving weak intermolecular forces, it is the departures from harmonic motion that may be of the most interest.

In the ideal inelastic scattering experiment, we can control the following parameters:

(1) The energy E_o of the incident neutrons.

(2) The energy E_s of the detected scattered neutrons.

(3) The scattering angle. This may be expressed in the change in vector momentum $\Delta\mathbf{P}=\mathbf{P}_o-\mathbf{P}_s$ of the neutron, or usually as the change in the wave vector $\boldsymbol{\kappa}=\mathbf{k}_o-\mathbf{k}_s$ with $\mathbf{k}=\mathbf{P}/\hbar$.

(4) The orientation of the crystal lattice with respect to the scattering vector $\boldsymbol{\kappa}$.

(5) The temperature of the crystal and, hence, the population in various energy levels.

In any real experiment, we may average over one or more of these quantities. In some cases, this may lead to simpler theoretical expressions for the scattered intensity. In others, it may lead to nasty problems in resolution.

The change in energy $\Delta E=E_o-E_s$ of the neutron must of course be equal to the change in energy in the scattering system; thus it must represent a transition between stationary states of the scattering system. By studying the scattered intensity as a function of energy change, we obtain a spectrum which is characteristic of the energy level scheme of the crystal. By varying the crystal orientation we are able to obtain information concerning the polarization characteristics of the normal modes, i.e., the directions of atomic motions. Finally, by variation of the direction and magnitude of the scattering vector κ, we are able to obtain bounteous information on the intermolecular force constants—if we choose a force constant description. The advantages over infrared spectroscopy are enormous; infrared spectroscopy is limited to the measurement of frequencies where the motions of all unit cells are in phase; on the other hand, in neutron scattering we have the facility to examine the scattering as a function of the phase relationships between the various unit cells; since these relationships are governed by the intermolecular forces, a powerful tool is in our hands (see fig. 3). Rather than just the $3N-3$ frequencies available from infrared, we have available for measurement $3N$ continuous functions—the dispersion surfaces. The data thus obtained can be analyzed in terms of refinement of parameters of a model or in a more direct way, these two ways corresponding to the least-squares and Fourier techniques in elastic diffraction studies.

Let us denote the initial and final states of the scattering system by U_o and U_s. The important quantities entering the expressions for the scattered intensity are the matrix elements.

$$M_i^{os} = \int U_s^* e^{i\mathbf{k}\cdot\mathbf{r}_i} U_o dt \tag{8}$$

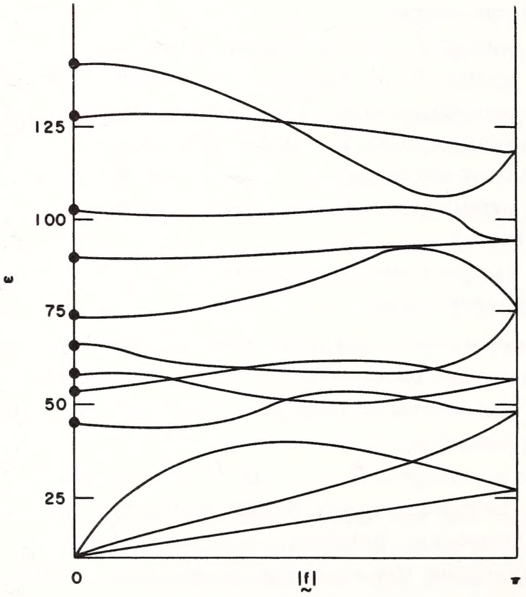

FIGURE 3. Calculated dispersion curves for the intermolecular vibrations in anthracene. All unit cells are in phase for $\mathbf{f}=0$. For $\mathbf{f}=\pi$ the motions in adjacent cells are 180° out of phase. Adapted from G. S. Pawley [11].

defined for each atom i in the crystal. The scattered intensity for given values of $\boldsymbol{\kappa}$ and ΔE may be expressed as

$$I(\boldsymbol{\kappa},\Delta E) \propto \frac{k_s}{k_o} \sum_{i=1}^{N} \sum_{j=1}^{N} a_i^* a_j M_i^* M_j \tag{9}$$

where a_i and a_j are the scattering lengths for the nuclei and the summations are over all atoms in the crystal. If there is random occupancy of a given unit cell site in the crystal, it becomes theoretically advantageous to separate the expression for the total scattering into a coherent part and an incoherent part. Defining [8]

$$a_i^{\text{inc}} = [\langle a_i^2 \rangle - \langle a_i \rangle^2]^{1/2} \tag{10}$$

and

$$a_i^{\text{coh}} = \langle a_i \rangle, \tag{11}$$

we may obtain expressions for the incoherent and coherent scattering as

$$I_{\text{inc}} \propto (k_s/k_o) \sum_i |a_i^{\text{inc}} M_i|^2 \tag{12}$$

and

$$I_{\text{coh}} \propto (k_s/k_o) \sum_{i=1}^{N} \sum_{j=1}^{N} a_i^{\text{coh}*} a_j^{\text{coh}} M_i^* M_j. \tag{13}$$

The latter expression may of course be written as

$$I^{\text{coh}} = \frac{k_s}{k_o} \left| \sum_i^N a_i^{\text{coh}} M_i \right|^2 \tag{14}$$

The sum is still over the whole crystal but eq (14) suggests that the coherent scattering may be written as the square of a structure factor. If this is true, it seems clear that the Fourier transformation of this measured structure factor may then be used to directly obtain a map which is related to the momentum distribution in the crystal.

If a model of harmonic motion is assumed, we can obtain the following results:

Let the displacement $\Delta\mathbf{r}_i$ of an atom i in one unit cell be expressed in terms of the normal coordinate q, the polarization vector $\mathbf{C}_i$, the atomic mass m_i and the number of unit cells N in the crystal by

$$\Delta\mathbf{r}_i = \mathbf{C}_i q (N m_i)^{-1/2} \tag{15}$$

The intensity of the incoherent scattering may now be written

$$I \propto \frac{k_s}{k_o} \sum_{\text{cell}} a_i^{\text{inc}^2} T_i^2 \frac{(\boldsymbol{\kappa}\cdot\mathbf{C}_i)^2}{m_i} \frac{n\hbar}{2\omega} \tag{16}$$

---

[8] <> denotes average value over all atoms in the same crystallographic site.

where T_i is a Debye-Walter factor and ω is the transition frequency. The coherent scattering may be expressed in terms of a structure factor

$$H(\boldsymbol{\kappa})=\sum_{\text{cell}} e^{i\mathbf{k}.\mathbf{r}_i^0} a_i^{\text{coh}} T_i m_i^{-1/2}(\boldsymbol{\kappa}\cdot\mathbf{C}_i); \tag{17}$$

The scattered intensity is then

$$I \propto \frac{k_s}{k_o}\frac{n\hbar}{2\omega}\,|H|^2\delta(\boldsymbol{\kappa}-\mathbf{f}-\boldsymbol{\tau}). \tag{18}$$

The δ-function involving the scattering vector $\boldsymbol{\kappa}$, the reciprocal lattice vector $\boldsymbol{\tau}$ and the phonon wave vector $\mathbf{f}$ shows us that the scattering process is such that we can indeed measure the intensity along the dispersion curve.

In both of these formulas, we see that the following general conclusions may be drawn concerning the intensity of scattering:

(1) k_s/k_o should be large. This implies that the scattered energy should be greater than the incident energy. It is best, from this point of view, for a low-energy neutron to pick up energy from the lattice. Many experiments are actually done this way. Alternatively the incident energy must be high enough so that the residual k_s is still large after the neutron loses energy to the lattice.

(2) The appearance of the frequency of transition in the denominator implies that the intensity will be greatest for small energy transfers.

(3) The intensity will be greatest for an atom of small mass.

(4) The scattering will be great if the momentum transfer is in the same direction as the largest vibrational component of the atom for the particular normal mode being examined: $(\boldsymbol{\kappa}\cdot C_i)$ must be large.

(5) There must be an appreciable number of molecules in the initial state. If deexcitation is important or in a case where population out of the ground state is appreciable, any real experiment must take into account the fact that it is averaging over transitions from all occupied levels.

There are several levels of approach in the interpretation of neutron scattering experiments. One of the most fruitful has been that of measuring the largely incoherent scattering from hydrogen-containing materials. Because the incoherent scattering formula contains little information on the structure of the crystal, the measurement of the scattering as a function of energy transfer directly gives a spectrum of the energy levels in the crystal. Since the experiment is incapable of measuring the dependence on the phonon wave vector $\mathbf{f}$, what is obtained is a projection of the dispersion curve onto the $\mathbf{f}=0$ axis

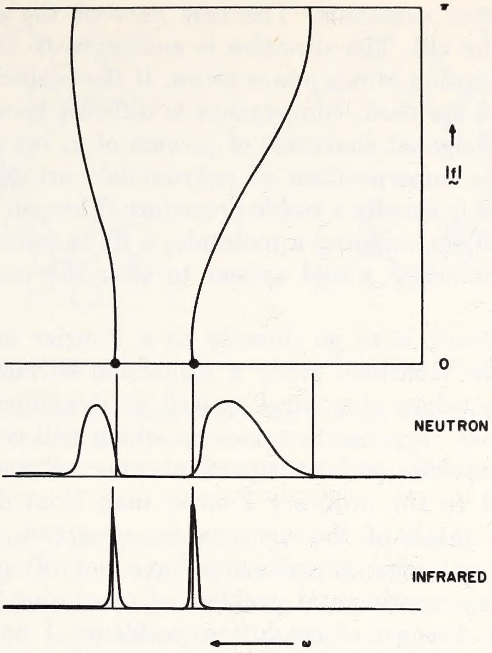

FIGURE 4. Infrared spectroscopy measures a frequency for $\mathbf{f}=0$; the line is moderately sharp. In an incoherent scattering experiment from a polycrystalline material, there is no resolution of the momentum transfer; hence a broadened spectrum which is the projection of the dispersion curve on the $\mathbf{f}=0$ axis is observed. Averaging over all populated levels also occurs.

(see fig. 4). The peaks are broader than would be observed in the infrared and the peak intensities will not necessarily occur in the same places as the $\mathbf{f}=0$ bands observed in the infrared. The results to date—some of which will be discussed below in connection with our own diffraction experiments—have been largely on polycrystalline materials, so that no information has been obtained regarding the polarization vectors. Examination of the scattering from a single crystal would often be useful in sorting out and identifying the normal modes; to date, this approach has not been vigorously pursued.

The examination of the coherent scattering from a single crystal clearly will give the most information regarding the complete force field in a crystal. The method traditionally employed has been to measure the dispersion curves and to fit the parameters of a particular force constant model (or in the first experiments just to see if a particular model fit the data). The models chosen have often been ones which gradually add force constants out to a higher order of neighbors. Such an approach suffers from the fact that the addition of new force constants often changes the picture entirely with respect to the values of the lower force constants. The new part of the solution is not orthogonal to the old. The situation is analogous to that of fitting a function by expansion into a power series. If the coefficients of powers of the argument are used, convergence is difficult because of the extremely non-orthogonal character of powers of x; on the other hand expansion into a superposition of polynomials orthogonal over the interval of the fit is usually a stable procedure. Thus, in the description of the force field surrounding a molecule, a fit to parameters of a set of orthogonal functions would appear to offer the most satisfactory approach.[9]

Another approach is to go directly to a Fourier inversion of the intensity data as measured along a dispersion surface. Such an inversion would produce structural as well as dynamical information. Peaks will appear near atomic positions which will contain information on the atomic motion for the particular normal mode in question. This is opposed to the ordinary Fourier map from diffraction data where the sum totals of the motions are observed. Intensity data from coherent scattering experiments have not often been used in this way, for the experimental problem of measuring intensity is extremely difficult because of resolution problems. I nevertheless look forward to the day when this will prove to be the most sophisticated use of scattering data.

We should ultimately be in a position to analyze this wealth of information in terms of anharmonic models, particularly in terms of directional effects in forces between molecules—getting away from the spherical potentials usually associated with van der Waals or Lennard-Jones potential functions where the intermolecular potentials are expressed simply as the sum of individual atomic potentials.

Both rigid-group refinement of diffraction data and detailed examination of the frequencies and intensities of inelastic scattering may be expected to provide us in the coming years with information concerning forces which is of real use to the chemist. We now turn to some systems which have been studied by the simpler techniques.

4. Techniques and Results: Some Examples From Hydrogen-Bonded Systems

4.1. Phosphonium Iodide

Phosphonium iodide (fig. 5) has been studied by Rush [12] by the method of neutron inelastic scattering. He has found a peak frequency of 327 ± 11 cm^{-1}, which he has assigned to the frequency of torsional

---

[9] We should expect that we can obtain better convergence properties in the study of intermolecular forces than has often been achieved with forces in ionic or metallic crystals because of the shorter range forces usually involved; thus for molecular crystals the force constant expansion may prove to be good enough.

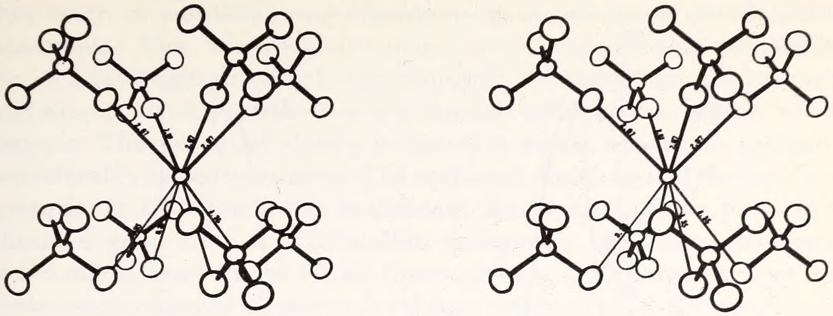

PHOSPHONIUM IODIDE PHOSPHONIUM IODIDE

FIGURE 5. Surroundings of a single iodide ion in phosphonium iodide PH_4I. Each PH_4^+ ion is also surrounded by eight iodides at the corners of a tetragonal prism. The postulated rotation is around the vertical $\bar{4}$ axis. (This is a stereo pair.)

oscillation of the phosphonium ion in the crystal lattice. Basing his analysis on that of Gutowsky, Pake and Bersohn [13] for Phase III of ammonium bromide (which has an analogous structure), where a three-dimensional trigonometric potential with one parameter was assumed, he derived a barrier to rotation of 6.7 kcal/mole. We [14] have carried out a neutron diffraction study of this crystal and find that the r.m.s. amplitude of vibration in a direction corresponding to rotation around the four-fold inversion axis of the crystal is 8.5 degrees. The corresponding frequency of 250 cm^{-1} is in good agreement with the neutron-scattering spectroscopic value. In an attempt to understand the height of the potential barrier, we carried out calculations of the crystal energy using a point charge electrostatic model and the computer program MANIOC written by Baur [15].

The purely electrostatic model gives a minimum in the potential energy which is 90° in rotation away from the experimental minimum. The electrostatic contribution to the energy (assuming a charge of $+\frac{1}{4}$ on each hydrogen atom and -1 on each iodide ion) is shown by the dashed curve in figure 6. The potential minima are separated by a broad hump about 9 kcal/mole high. It was immediately obvious that the equilibrium structure must be largely determined by repulsive forces between the hydrogen atoms and iodide atoms rather than by the electrostatic forces. We repeated the calculation, adding to the electrostatic energy an interaction energy of the Lennard-Jones type:

$$E_{ij}=4\epsilon[(\sigma_{ij}/r_{ij})^{12}-(\sigma_{ij}/r_{ij})^{6}] \qquad (19)$$

where r_{ij} is the interatomic distance, σ_{ij} is a parameter which is equal to 0.8909 times the equilibrium van der Waals contact distance, and ϵ is an energy parameter which gives the depth of the van der Waals

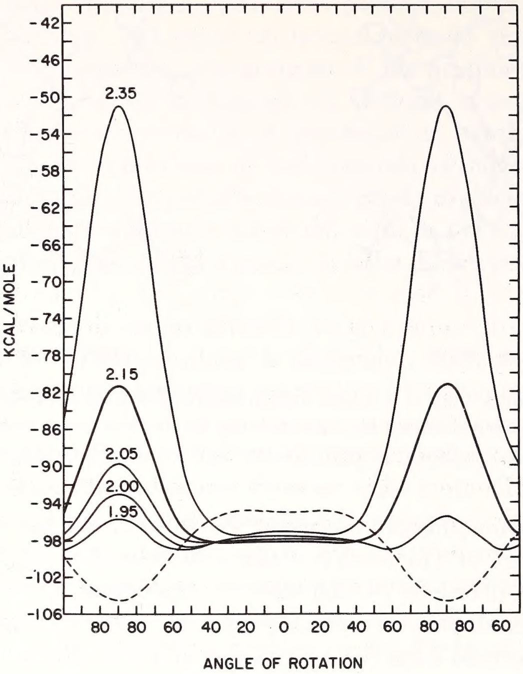

FIGURE 6. Calculated potential energy curves for rotation of the phosphonium ion around the $\bar{4}$ axis. The dashed curve is the electrostatic energy alone and gives a minimum in the wrong place. The heavy solid curve includes both the electrostatic energy and repulsive and attractive forces as described by a Lennard-Jones 12–6 potential. The other curves are for different choices of the minimum van der Waals contact distance; the van der Waals radius of iodine is indicated; that for hydrogen was taken as 1.2 Å.

well. The value chosen for σ_{ij} was based on a van der Waals radius of 2.15 for iodide and 1.20 for H. The value of ϵ was taken as the geometric mean of the values for the nearest rare gas atoms (Xe and He); the shape of the potential is independent of ϵ, and small changes in ϵ will change the barrier height only slightly.

For the parameters chosen in our earlier study, we obtained the heavy curve shown in figure 6. The equilibrium position is correctly given (the small hump at the bottom of the well is well below the first energy level), and a barrier height of 16 kcal/mole is obtained. This barrier height is however extremely sensitive to the van der Waals diameter (fig. 6) assumed. A measurement of the barrier height thus can in fact establish quite good values for the coefficient $4\epsilon\sigma^{12}$ of the repulsive term in the I^-—H potential—given that the $1/r^{12}$ model is suitable. The potential shown is far from a cosine of harmonic potential, however, and the derivation of a barrier height from the observed frequency or amplitude of vibration is, as we have noted above, hazardous. The vibration frequency from the inelastic scattering model and the amplitude of vibration from the diffraction study would correspond to a particle-in-a-box model with a box width of 50 degrees. The potential shown in figure 6 would appear to predict a considerably lower frequency. The apparent dominance of the repulsive potential in this case seems to indicate that it may not be possible to obtain a great deal of information concerning the shape parameter of the attractive van der Waals (here taken as $1/r^6$) potential from the gross measurements of energy level separation or vibration amplitude. It is possible of course that a much stronger long range attractive potential or perhaps a longer range repulsion than $1/r^{12}$ would give a deeper minimum and hence a larger frequency of vibration. We are now studying this question in detail.

In any case, it becomes quite clear here that the assistance provided by a calculated potential for a model may be extremely important in the interpretation of neutron scattering and diffraction results; perhaps the quantitative results of the calculation are unimportant, but the qualitative choice of a model might be greatly facilitated.

4.2. Ammonium Fluorosilicate

The rotation of the ammonium ion in another salt has been studied by both neutron inelastic scattering and neutron diffraction by Schlemper, Hamilton, and Rush [16]. The structure is shown in figure 7. The neutron spectroscopic frequency of 168 cm^{-1} was assigned to the hindered rotation; this corresponds to a barrier height of 2.1 kcal for a three-fold cosine type barrier. The crystal is disordered—either statically or dynamically—and a map of the scattering density in the plane in which the hydrogen atom is expected to lie is shown in figure 8. The model proposed in our original paper was that the energy transition actually observed was due to the excitation of a level which kept the hydrogen atom in approximately the same place—free to move over the large region indicated by the Fourier synthesis. One could in fact in this case postulate much larger barriers between the positions related by three- and two-fold rotations. The r.m.s. rotation amplitude corresponding to the measured frequency, however, is about 10°, and this is not inconsistent with the amplitudes of 10–20° obtained for a conventional harmonic motion refinement of three statically disordered hydrogen atoms in the diffraction study.

It seemed reasonable to carry out some electrostatic energy calculations to attempt to shed some light on what seemed at best a rather speculative model. A number of calculations were made assigning a charge of $+\frac{1}{4}$ to each hydrogen atom and $-\frac{1}{3}$ to each fluorine atom.[10]

---

[10] One could argue with these particular choices; as a matter of fact they are not terribly crucial.

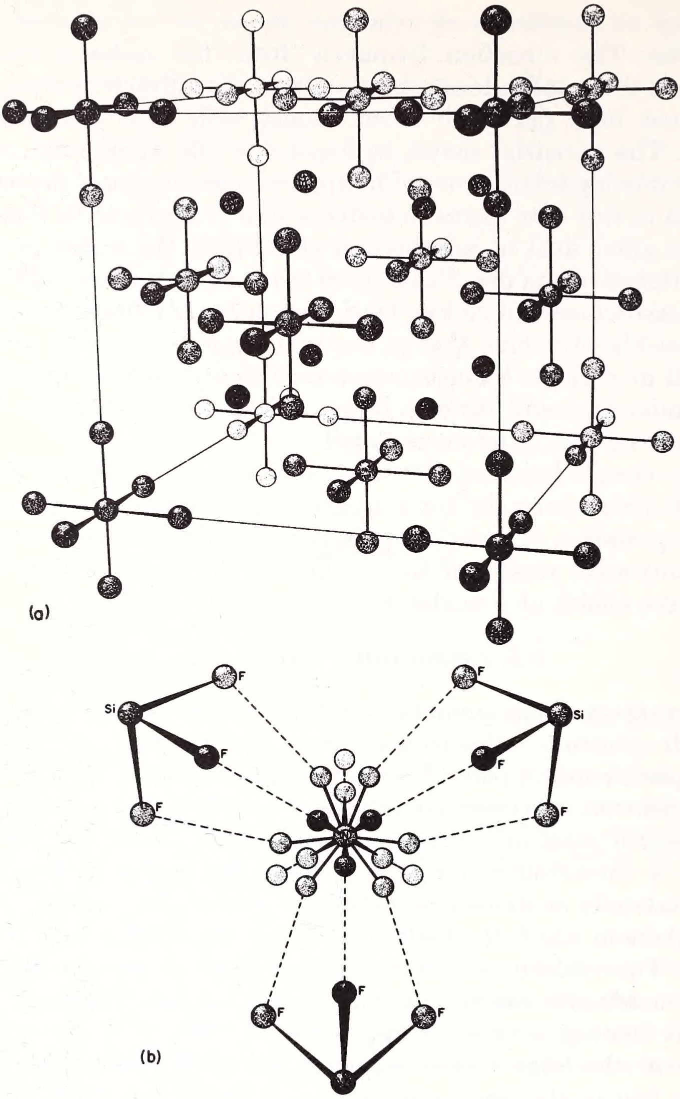

FIGURE 7. The structure of ammonium fluorosilicate. a) One unit cell; only the nitrogen on the ammonium group is shown with a tweedy appearance. b) Postulated 12-fold static disorder in the hydrogen atom positions; the nearly linear hydrogen bonds are clearly seen.

A complete calculation of the energy surface as a function of the three parameters specifying the orientation of the ammonium ion has not as yet been carried out. The following two calculations have been completed.

(1) Motion of a single hydrogen atom on the surface of a sphere; interactions with the other hydrogen atoms and bending force con-

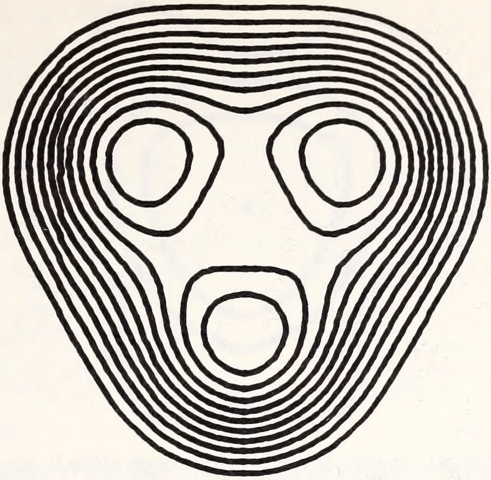

FIGURE 8. Scattering density in a plane perpendicular to the three-fold axis of ammonium fluorosilicate. The hydrogen atoms should lie approximately in this plane. This experimental result may be understood either in terms of the static disorder suggested by figure 7 or by a more dynamic situation.

stants were ignored. This calculation provides a map of the potential generated by the fluorine atoms and seen by the hydrogen atoms.

(2) Cross sections through the complete energy function were taken by calculating the energy as a function of rotation around the three-fold axis of the ion. The results of these calculations are seen in figures 9 and 10.[11] The result of calculation 1 shows that there is indeed a broad, slightly featured minimum in the neighborhood of the crystallographic three-fold axis. The equilibrium position is not at the exact center of the axis but off-set—much as the three peaks in the scattering density map indicate.

The rotation around the three-fold axis however does approximate a cosine potential with a barrier height of 2.5 kcal/mole in excellent agreement with the neutron spectroscopic results. We conclude that in this case the simple interpretation of the spectrum has given a realistic result. We will however calculate the three-dimensional potential surface to provide a more definitive picture of the dynamic structure.

These results are not inconsistent with deuteron resonance experiments of Blinc [17], although the interpretation is perhaps not so straightforward. Blinc observes two relaxation mechanisms, one of which may involve the more limited motion in the broad well and, the other, motion which interchanges hydrogen atoms related by a three-fold axis.

---

[11] The Lennard-Jones energy was included in the calculations but is so small in this case as not to obscure the main points, despite any uncertainties in the parameters.

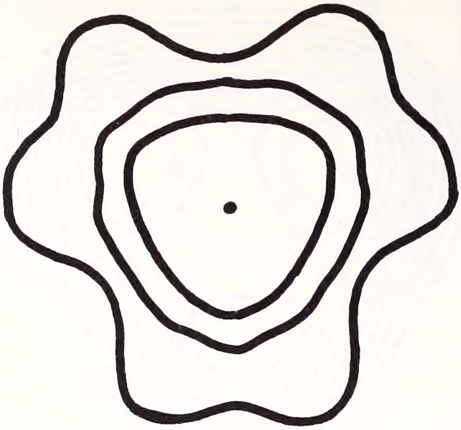

Figure 9. Electrostatic energy of a single hydrogen atom in ammonium fluorosilicate as a function of polar coordinates measuring its displacement from the three-fold axis. The minimum is at the center and the contours are drawn at intervals of 0.05 kcal mole^{-1}. The outer contour lies approximately at the $\theta = 30°$ line.

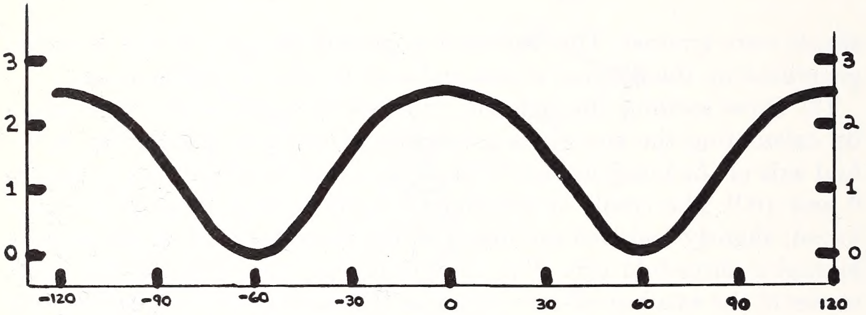

Figure 10. Electrostatic and Lennard-Jones energy of ammonium fluorosilicate as the ammonium ion is rotated around its three-fold axis. The energy units are kcal-mole^{-1}. The abscissa reads in degrees.

4.3. Potassium Hydrogen *Bis*acetylsalicylate

As a final example (one that has been studied only by neutron diffraction and not by neutron scattering), I will discuss the hydrogen bond in a typical type A acid salt—the potassium acid salt of aspirin (fig. 11). This structure has been the subject of a definitive x-ray structure investigation by Manojlovič and Speakman [18]. The two aspirin anions are connected by a hydrogen bond with an O—H—O distance of 2.456 ± 0.004 Å. The bond in this type of compound is thought to be symmetric. It was in order to shed further light on this problem that we decided to undertake the neutron diffraction study

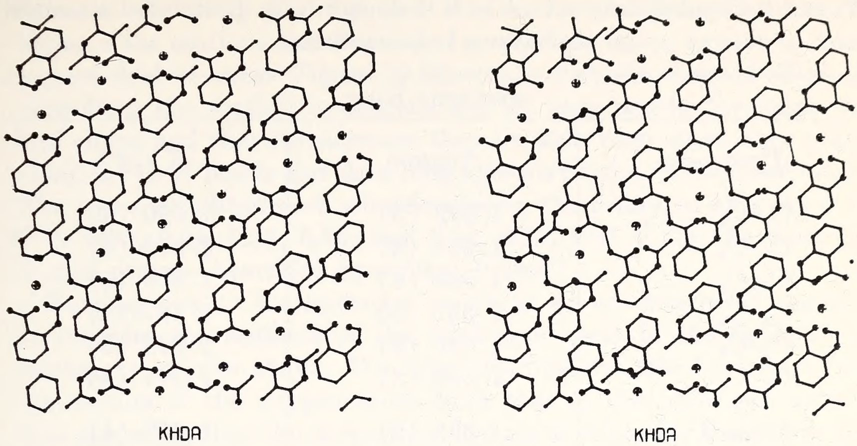

FIGURE 11. One layer of the crystal structure of potassium hydrogen diaspirinate (KHDA). The K$^+$ ions are represented by the isolated balls. The lines connecting pairs of anions are the short hydrogen bonds.

[19]. The results of the study are gratifying in that they agree extremely well with the x-ray work. In fact we consider these two pieces of work to provide the best comparision that exists today between any moderately complex structures as determined by the two methods. The quality of the agreement may be judged by examination of some of the bond lengths which are given in table 1. The agreement between the heavy-atom bond lengths is seen to be quite remarkable. The consistency and small standard deviations of the C—H distances on the benzene ring in the neutron study are also worthy of note in comparison with the x-ray values; this illustrates my previous point regarding the advantages of neutron diffraction for hydrogen atom location.

The agreement between the anisotropic thermal parameters is also satisfactory for the heavy atoms; these were not refined in the x-ray case for the hydrogen atoms. Typical mean-square amplitudes of vibration were 0.0300–0.0600 Å^2 in both studies. The corresponding standard deviations were 0.0030 Å^2. The agreement between the two studies was within two standard deviations in every case except for the mean-square amplitude in the c direction of the crystal, where the neutron values were consistently about 0.0150 Å^2—several standard deviations—less than the values from the x-ray study. The reason for this is not known, but there are probably sources of systematic error unaccounted for in one or the other of the studies or both.

We were interested in having a careful look at the hydrogen atom motions as we had determined them by neutron diffraction. We had hopes that we could believe in these because of the good agreement

TABLE 1. Bond distances in Å in KH diaspirinate. Estimated standard deviations in parentheses

Benzene Ring		
Parameter	*Neutron*	*X ray* [a]
C_1–C_2	1.392 (3)	1.390 (4)
C_2–C_3	1.394 (4)	1.372 (6)
C_3–C_4	1.399 (4)	1.390 (5)
C_4–C_5	1.382 (3)	1.387 (4)
C_5–C_6	1.395 (3)	1.393 (5)
C_6–C_1	1.393 (3)	1.394 (4)
Mean C–C	1.393 (3)	1.388 (4)
C_2–H_2	1.081 (6)	0.93 (5)
C_3–H_3	1.083 (6)	1.03 (6)
C_4–H_4	1.080 (7)	0.85 (4)
C_5–H_5	1.088 (5)	1.01 (4)
Mean C–H	1.084 (2)	0.95 (4)
Carboxyl Group		
C_6–C_7	1.501 (3)	1.504 (4)
C_7–O_2	1.217 (4)	1.221 (4)
C_7–O_1	1.284 (3)	1.284 (4)
O_1–H_1	[b] 1.224 (2)	[b] 1.228 (2)
Acetyl Group		
C_1–O_3	1.390 (4)	1.392 (4)
O_3–C_8	1.356 (4)	1.360 (4)
C_8–C_9	1.491 (4)	1.477 (6)
C_8–O_4	1.204 (4)	1.199 (4)
C_9–H_7	[c] 0.98, 1.13 (2)	0.93 (7)
C_9–H_8	1.01, 1.15 (2)	0.83 (10)
C_9–H_9	0.99, 1.17 (2)	1.13 (12)
Mean C–H	1.15 (1)	0.96 (9)

[a] Reference 18.

[b] Assumes that hydrogen atom is fixed at origin by symmetry.

[c] The first figure is a raw value. The second includes a probably incorrect correction for thermal motion. Because of the very large thermal motion, these distances are rather inaccurate.

between the x-ray and neutron studies for the heavy atoms and because the motions for the methyl group hydrogens appear to make a good deal of sense. Figure 12 illustrates that the thermal ellipsoids describing the methyl hydrogens are all very nearly the same size and shape and that furthermore they lie with their short axes nearly along the C–H bonds and their long axes perpendicular to these bonds. The r.m.s. amplitudes of vibration along the principal axes are 0.24, 0.31, 0.60; 0.24, 0.33, 0.59; and 0.24, 0.37, 0.61 Å for the three hydrogen atoms—beautiful agreement indeed!

Turning now to the hydrogen in which we are interested, we wish to consider the motions of this hydrogen atom in the field of two stationary oxygen atoms. We may approximate this by subtracting the motion of the oxygen atom from that of the hydrogen atom—thus assuming that the three-atom system is riding on the lattice and that the hydrogen atom has a further motion relative to the oxygen's that is superimposed on the more general motion. Thus

$$U_{ij}^{\mathrm{corr}}=U_{ij}^{H}-U_{ij}^{0}$$

The resulting difference tensor was then diagonalized to obtain the motions for the hydrogen atom given in table 2 and illustrated in figure 13. The long axis is found to lie along the bond, and the two

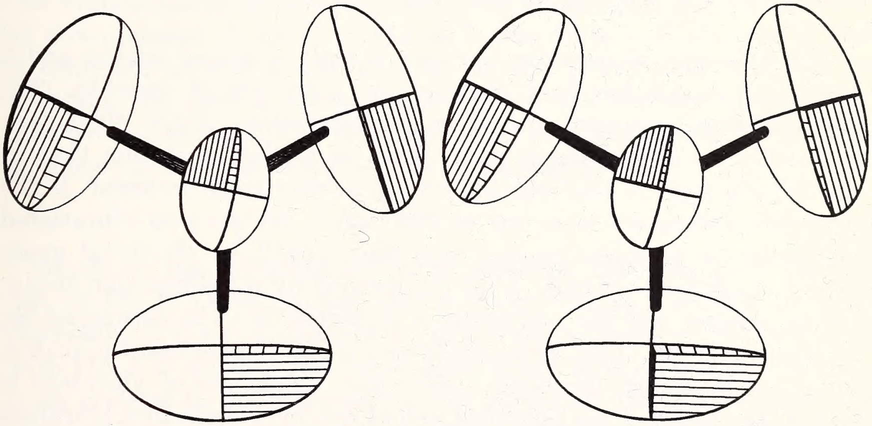

FIGURE 12. Thermal ellipsoids for the methyl group in KHDA. The view is down the C–C bond and clearly shows the effects of a wide-amplitude hindered rotation.

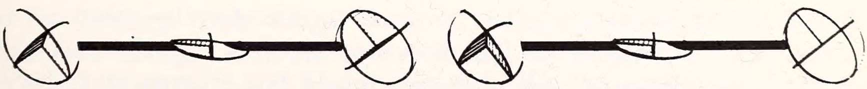

FIGURE 13. The O–H–O bridge in KHDA. The difference ellipsoid for H indicates a large amplitude of vibration along the hydrogen bond.

short axes perpendicular to the bond. The length of the long axis corresponds to a stretching frequency of 470 cm^{-1} if a harmonic potential is assumed. The amplitude determined from the diffraction data is likely to be on the high side if anything; allowing 3σ as a limit of error, one could obtain a frequency as high as 1000 cm^{-1}. There has been some speculation among spectroscopists as to the exact value for this frequency in crystals of this type—but values of 500 to 1500 cm^{-1} have been suggested. Our experimental value is compatible with this range.

TABLE 2. Principal axes of thermal ellipsoids for the H_1 atom and angles which these make with the O-H-O bond

	Total hydrogen motion		*Hydrogen motion-oxygen motion*	
	Amplitude	*Direction*	*Amplitude*	*Direction*
H_1	0. 19 (1)	139 (4)	0. 03 (7)	101 (7)
	0. 26 (1)	52 (4)	0. 08 (2)	87 (10)
	0. 26 (1)	78 (2)	0. 19 (2)	11 (7)

The difficulty of deciding between a truly centered proton and a disordered proton has been discussed on a number of occasions [20]. The following argument, based on a combination of the diffraction data with the spectroscopic data, leads us to the conclusion that in this typical type A acid salt the proton is effectively centered. If the stretching frequency is as low as 1500 cm^{-1}, the squared vibrational amplitude for harmonic motion is at least 0.0112 Å^2. The total mean square amplitude is 0.0361 Å^2 as determined by the diffraction study. Let us assume that the remainder of 0.0249 Å^2 is to be accounted for by static disorder. This corresponds to a static displacement of 0.16 Å from the center of the bond. The r.m.s. amplitude of vibration is 0.11 Å; the width of the potential well at the level of the first vibration is then $\sqrt{2}\times 0.11 = 0.16$ Å. The situation is as shown in figure 14. The first vibrational level lies just at the point of intersection of the two hypothetical wells. Inasmuch as we expect the motion to be at least somewhat anharmonic, the point of intersection is probably lower, and it seems somewhat artificial to consider the potential in terms of two isolated wells. The best description is thus in terms of a single broad potential well of undetermined but unimportant shape at the bottom. In terms of the particle-in-a-box model, the same total vibrational amplitude would be given by a box 1 Å in extent.

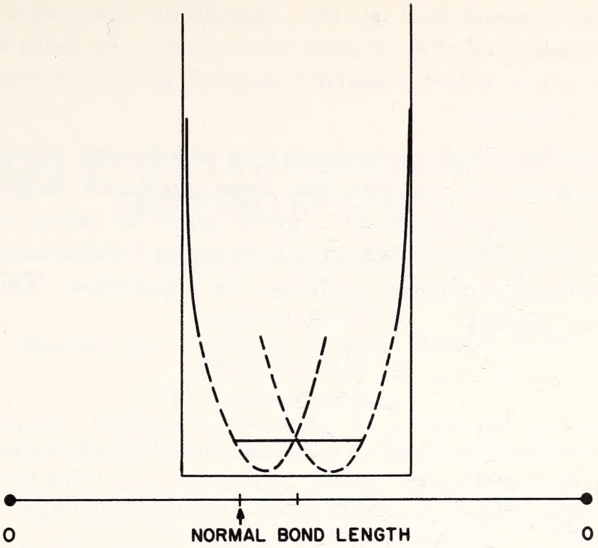

Figure 14. Hypothetical single-minimum energy curves for the short hydrogen bond in KHDA intersect at a level at or below the energy of the first vibrational state. Hence a single symmetric minimum potential is suggested.

This seems very reasonable in view of the 2.45 Å 0 . . . 0 distance. We unfortunately do not have available an inelastic scattering study of this material. A study of the scattering from a single crystal and a complete normal mode analysis should prove very fruitful. In addition, we plan a diffraction study on the deuterated material. The isotope effect on the hydrogen bond may be expected to further enhance our understanding of this interesting system.

Much of the experimental work reported here has been carried out by Dr. E. O. Schlemper, Mr. Anisbert Sequeira and Dr. C. Alan Berkebile. It is also a pleasure to acknowledge the many conversations with Dr. J. J. Rush which have led to much of my work in this area. I am grateful to the organizers of the Materials Research Conference for inviting me to take part in what has been a most stimulating few days.

5. Discussion

G. Dolling (Oak Ridge National Laboratory): I would like to disagree strongly with one of Dr. Hamilton's remarks concerning the separation of the total neutron scattering into coherent and incoherent parts. This is a mathematical separation, of course, but its importance is based on the fact that these two parts can be distinguished experimentally, in contradiction to Dr. Hamilton's statement. The distinguishing feature of the coherent scattering is the delta function in momentum space which does not appear in the cross-section for incoherent scattering.

W. C. Hamilton: But we have no way of knowing whether a given neutron reaching the counter has been scattered incoherently or coherently. A measurement at a given point in energy-momentum space leads to no information on coherence or incoherence. We must use a theoretical model to perform the separation. This was the context of my remark.

6. References

[1] Committee for the Survey of Chemistry, Chemistry: Opportunities and Needs, National Academy of Sciences-National Research Council, Washington, D.C., 1965.
[2] G. B. Kistiakowsky, J. R. Lacher, and F. Stitt, J. Chem. Phys. **7,** 289 (1939).
[3] A. Charlesby, Proc. Phys. Soc. **54,** 471 (1942).
[4] D. W. J. Cruickshank, Acta Cryst. **9,** 754 (1956).
[5] V. Schomaker and K. N. Trueblood, Acta Cryst. **B23,** 63 (1968).
[6] P. Coppens, Science, **158,** 1577 (1967).
[7] W. C. Hamilton, Acta Cryst. **18,** 502 (1965).
[8] B. T. M. Willis, Acta Cryst. **18,** 75 (1965).
[9] B. Dawson, Acta Cryst. **21,** A5 (1965).
[10] G. S. Pawley, Acta Cryst. **17,** 457 (1964).
[11] G. S. Pawley, Phys. Stat. Sol. **20,** 347 (1967).
[12] J. J. Rush, J. Chem. Phys. **44,** 1722 (1966); also T. C. Farrar and J. J. Rush, these proceedings.
[13] H. S. Gutowsky, G. E. Pake, and R. Bersohn, J. Chem. Phys. **22,** 643 (1954)·
[14] A. Sequeira and W. C. Hamilton, J. Chem. Phys. **47,** 1818 (1967).
[15] W. Baur, Acta Cryst. **19,** 209 (1965).
[16] E. O. Schlemper, W. C. Hamilton, and J. J. Rush, J. Chem. Phys. **44,** 2499 (1966).
[17] R. Blinc, private communication.
[18] L. Manojlovic and J. C. Speakman, J. Chem. Soc., 971 (1967).
[19] A. Sequeira, C. A. Berkebile, and W. C. Hamilton, J. Mol. Str. **1,** 283 (1967).
[20] W. C. Hamilton and J. A. Ibers, Hydrogen Bonding in Solids, W. A. Benjamin, New York, 1967, pp. 108–113.

DYNAMICAL EFFECTS OF DEUTERON INTRABOND JUMPING IN KD_2PO_4 [1]

V. HUGO SCHMIDT

Department of Physics,
Montana State University, Bozeman, Montana 59715

1. Introduction

Four dynamical effects of motion of deuterons within hydrogen bonds in KD_2PO_4 are discussed. These effects are an additional splitting of the deuteron magnetic resonance spectrum below the ferroelectric Curie temperature T_c, a contribution to the deuteron spin-lattice relaxation, dielectric behavior at microwave frequencies, and ferroelectric domain wall motion.

2. Domain Wall Mobility

Figure 1 shows a projection of the structure along the ferroelectric *c* axis. The top and bottom rows contain Slater D_2PO_4 groups of the two zero energy types respectively, and constitute portions of two oppositely oriented domains. The middle row contains Slater D_2PO_4 groups of energy ϵ_0, and forms the domain wall. A typical deuteron jump sequence causing wall motion is as follows: Jump 1 produces a Takagi group pair at cost of energy $2\epsilon_1$. Jumps 2 and 3 in effect move the D_3PO_4 Takagi group to the upper right corner, turning the center group into part of the lower domain and the group above it into part of the wall.

The mobility calculation, which appears in detail elsewhere, [1] [2] assumes that jump probabilities are governed by the Boltzmann factors for the energy changes $\pm\mu_1 E$ per deuteron jump in the applied field E, and by the fractional density N_T/N of Takagi groups which has been previously calculated [2]. The calculated mobility is

$$\mu_w = \frac{N_T}{N}\,\frac{\mu_1 a_0}{kTT_0}\,;\ a_0 = 1.86\text{Å};\ \mu_w = 6.8\times10^{-5}\,\frac{cm^2}{\text{volt-sec}}\ \text{at } 200\ {}^\circ\text{K}$$

in fair agreement with measured values of Bjorkstam and Oettel [3]. The mean Takagi group jump time T_0 is found from the dielectric behavior in the following calculation.

---

[1] Work supported in part by the National Institutes of Health. A more detailed account of this work appears in Phys. Rev. 164, 749 (1967).

[2] Figures in brackets indicate the literature references at the end of this paper.

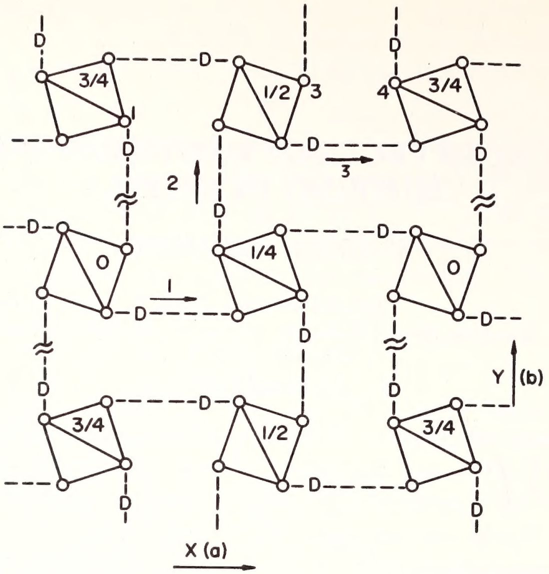

FIGURE 1. Projection of structure along ferroelectric *c* axis.

3. Dielectric Constant

The calculation of dielectric constant above T_c is based on the same expressions for jump probabilities as the domain wall mobility calculation. These probabilities yield an expression for the rate of change of polarization in an alternating electric field, from which the following expression for the susceptibility is obtained; the notation follows ref. 2:

$$\chi-\chi_0=\frac{\alpha\mu_0\mu_1 N/VkT}{1+j\alpha\omega T_w};\ \frac{N_T}{N}=\frac{T_0}{T_w};\ \epsilon'-j\epsilon''=1+4\pi\chi;$$

$$\alpha=\frac{1}{2}\left[\frac{e^{-\epsilon_0/kT}+e^{-\epsilon_1/kT}-\frac{1}{2}}{1+e^{-\epsilon_1/kT}}-\frac{\beta}{kT}\right]^{-1}$$

Figure 2 shows a Cole-Cole plot of these expressions compared with Ludupov's [4] data at room temperature. The best fit results if the only adjustable parameter T_0 is set at 6 x 10^{-14} sec. This value is near h/kT or a typical lattice vibration period, implying little correlation between successive jumps of Takagi groups.

4. Deuteron Magnetic Resonance

The autocorrelation function for the electric field gradient (efg) fluctuations seen by a deuteron jumping between its two positions in a hydrogen bond is calculated from the jump probabilities for a deuteron at each bond position. The autocorrelation time $T_{we}=$

$(1-p^2)T_{oe}N/NT$, where T_{oe} is effective jump time and p is fractional spontaneous polarization. Below T_c the rapid drop in $1-p^2$ causes T_{we} to decrease, explaining the lack of line broadening at the transition as observed by Bjorkstam [5].

Figure 3 compares experimental deuteron spin-lattice relaxation results [6] with theory. For intrabond motion the spectral density of

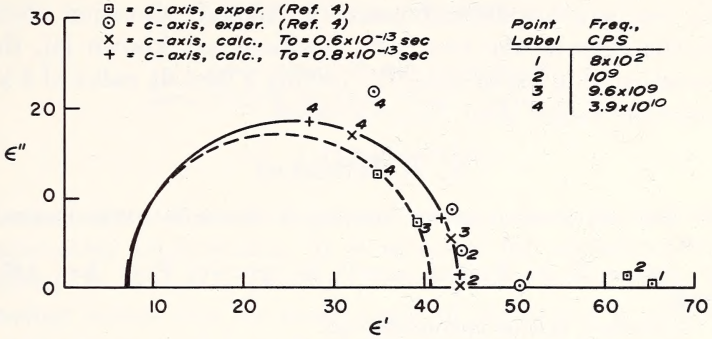

FIGURE 2. Cole-Cole plot of expressions compared with Ludupov's [4] data at room temperature.

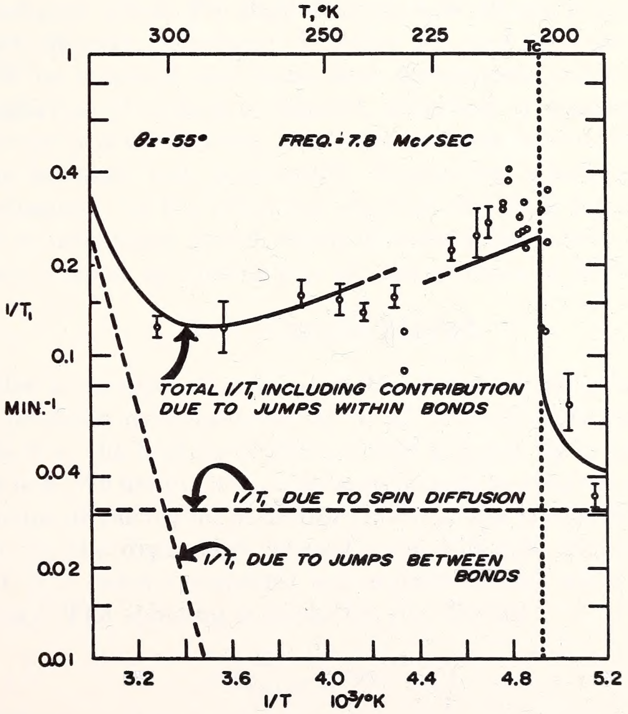

FIGURE 3. Experimental comparisons of deuteron spin-lattice relaxation results [6] with theory.

the efg fluctuations is given by

$$J(\omega)=\frac{1}{2}(1-p^2)T_c/(1+\omega^2T_c^2)\simeq\frac{1}{2}(1-p^2)T_{we}.$$

The rapid drop in $1/T_1$ below T_c results from the decrease of both $1-p^2$ and T_{we}. The gap in the curve is due to the onset of interbond jumping. The Takagi group activation energy ϵ_1 of 0.078 eV is found from the temperature dependence of intrabond relaxation above T_c. Because the efg's at the two bond positions are known [5], there is only one adjustable parameter, T_{oe}, having a best fit value of 8×10^{-14} sec., somewhat larger than T_o as expected.

5. References

[1] V. H. Schmidt, Proc. Internat. Meeting on Ferroelectricity, Prague, **2,** 97 (1966).

[2] H. B. Silsbee, E. A. Uehling, and V. H. Schmidt, Phys. Rev. **133,** A165 (1966).

[3] J. L. Bjorkstam, private communication.

[4] Ts.-Zh. Ludupov, Soviet Phys., Crystallography **11,** 416 (1966).

[5] J. L. Bjorkstam, Phys. Rev. **153,** 599 (1967).

[6] V. H. Schmidt and E. A. Uehling, Phys. Rev. **126,** 447 (1962).

THE DETECTION OF ATOM TUNNELING IN SOLIDS

I. PELAH [1] **and Y. IMRY** [2]

Israel Atomic Energy Commission
Soreq Nuclear Research Centre, Yavne, Israel

1. Introduction

The tunneling of atoms between two or more potential minima is an interesting phenomenon. It is essential for understanding ferroelectricity in KH_2PO_4 (KDP)[1][3] and probably in other crystals. Tunneling occurs also for many cases of impurities in solids.

In this paper we discuss *direct* measurements of tunneling, employing the interaction of the tunneling atom with external radiation. This includes experiments like IR absorption, neutron scattering and Mossbauer effect. We shall describe how effects peculiar of tunneling are directly detectable. Existing IR and neutron studies of KDP will be reviewed and some new experiments suggested.

The behavior of radiation emitted, absorbed or scattered by two distinct sources is well known. Our basic problem is that of one source tunneling between two positions[2]. Interesting interference effects can be obtained. In the following we shall discuss a mathematically simple two mimimum model which illustrates the above points and is, in fact, a good approximation for the protons in KDP.

2. A Simple Model

Consider a particle of mass m in the following potential[3]. Two jointed parabolic wells centered at $\pm x_o$, the oscillator frequency in each well is ω, the bottom of the left well is lower by B than that of the right one. We assume that ω is large enough so that we can neglect the influence of the higher oscillator levels on the ground level.

For $B=0$, the degenerate ground state will split into two levels, $|1>$ and $|2>$, with symmetric and antisymmetric wave functions, respectively. The splitting is given by $E_2-E=2\Omega$

$$\Omega=\frac{2}{(\pi)^{1/2}}\,q\exp\left(-q^2\right)$$

---

[1] Present address: Argonne National Laboratories, Solid State Physics Div., Argonne, Illinois

[2] Present address: Dept. of Engineering Physics, Cornell University, Ithaca, New York

[3] Figures in brackets indicate the literature references at the end of this paper.

with $q=X_o(\hbar/m\omega)^{-1/2}=\frac{x_0}{\sigma}$. Ω is the "tunneling matrix element."

For the asymmetric case, $0<B\ll\hbar\omega$, the splitting increases: $E_2-E_1=2(\Omega^2+B^2/4)^{\frac{1}{2}}$. $|1>$ is more concentrated in the deeper well and $|2>$ in the higher well. The concentration is complete for $B\gg\Omega$. If we denote the relative weights of the wave function $|1>$ in the two wells by α and β, with $\alpha^2+\beta^2=1$, we can characterize the degree of localization by the parameter $\alpha\beta$ ranging from ½ for $B=0$ to 0 for $B\gg\Omega$.

We shall need the following matrix elements:

$$<1|\exp(ikx)|1>=\exp(-k^2\sigma^2)[\alpha^2\exp(-ikx_o)+\beta^2\exp(ikx_o)]$$

$$<2|\exp(ikx)|2>=\exp(-k^2\sigma^2)[\alpha^2\exp(ikx_o)+\beta^2\exp(-ikx_o)]$$

$$<1|\exp(ikx)|2>=2i\alpha\beta\exp(-k^2\sigma^2)\ \sin kx_o.$$

Using these matrix elements, we can find the cross sections for the processes of interest.

a. *Infrared Absorption*—The transition dipole is

$$M=2\ Qx_o\alpha\beta$$

where Q is the effective charge of the tunneling particle. We note that Qx_o is much larger than σ—typical transition moment for a single well. The absorption will, however, decrease sharply with asymmetry (due to the factor $2\alpha\beta$) because of decreasing overlap between the wavefunctions.

The isotope effect is interesting. A substitution of higher mass will greatly reduce Ω. In a symmetric well the transition energy will thus decrease, but the intensity will be unaffected. In a strongly asymmetric well ($B\gg\Omega$), the transition energy, roughly equal to B, will change only slightly, while the intensity will drop sharply. These effects will be complicated by the fact that in KDP, for example, the asymmetry, which is determined by interactions between the protons, will also change with deuteration [1].

b. *Neutron Scattering*—We are interested in incoherent scattering from a system of protons each moving in its own potential. This is meaningful for KDP when it is understood that the asymmetry for each proton is determined [1] by interactions with its neighbours. Because of the high incoherent cross section of H, it will contribute most of the cross section for KDP.

We denote the component of the momentum transfer **K** parallel to the tunneling direction by k and obtain for the elastic part

$$\left.\frac{d\sigma}{d\Omega}\right)_{\text{el}}=\exp(-2k^2\sigma^2)(\alpha^4+\beta^4+2\alpha^2\beta^2\cos 2kx_0).$$

Note the periodic dependence on $\mathbf{K},\mathbf{x}_o$ due to the interference between the two wells. In the inelastic part this interference is even more important. For "one phonon (E_2-E_1) energy loss processes we get

$$\left(\frac{d^2\sigma}{d\Omega d\omega}\right)_{\omega=E2-E1} \propto 4\alpha^2\beta^2 \exp(-2k^2\sigma^2) \sin^2 kx_o$$

The inelastic cross section, and the $\mathbf{K},\mathbf{x}_o$ dependent part of the elastic cross section, decrease sharply with the asymmetry.

c. *Recoilless Emission by Tunneling Impurities*[2]. Here one has to take into account the following result, due to Lipkin.[4] We assume the impurity to move in some effective potential, with energy levels E_n and recoilless emission matrix elements f_n. The usual expression

$$f_1(T)=\sum_n w_n|f_n|^2$$

for the Mossbauer fraction, where w_n is the thermal weight of the nth level, is correct only when the relaxation time, T_R, of the "oscillator" levels is much longer than the lifetime, T_N, of the nuclear level. If $T_R \ll T_N$ (as is almost always the case, since $T_N \sim 10^{-8}$ sec, $T_R \sim 10^{-11}$ sec) we have for the Mossbauer fraction:

$$f_2(T)=|\sum_n w_n f_n|^2$$

i.e., a coherent averaging.

For the case where the impurity potential is harmonic, the ratio between f_1 and f_2 is a Bessel function factor. For our tunneling model we obtain:

$$f_1(T)= \exp(-2k^2\sigma^2)(\alpha^4+\beta^4+2\alpha^2\beta^2 \cos kx_o)$$

$$f_2(T)= \exp(-2k^2\sigma^2)\left[\cos^2 kx_o+ \tan \mathrm{h}^2\left(\frac{E_2-E_1}{2kT}\right)(\alpha^2-\beta^2) \sin^2 kx_o\right].$$

The difference between f_1 and f_2 can be extremely large, and the "interference pattern" is temperature dependent. This type of effect will occur also for three dimensional models. In the case $B \gg \Omega$, $kx_o \sim \pi/4$, the temperature dependence of f_2 is very sharp. This might be the explanation for the experimental results for Kr in hydroquinone clathrates [5]. Another case where a Mossbauer source probably performs tunneling is Fe in AgCl.

3. Review of the Experiments in KDP

A hydrogen mode around 400 cm^{-1} was found by Pelah, Lefkovitz, Kley and Tunkello [6] for KDP, using inelastic, energy gain, neutron scattering. This was assumed to be the splitting $E.-F.$, in a double minimum well. Further IR neutron measurements [1] have substantiated this result.

It is believed that in the ordered, ferroelectric state the protons are effectively localized in their single wells by the interactions, which provide large static asymmetry for each double minimum well.

In the nonordered state, the asymmetries are changing slowly with time; the average situation is symmetric, but $<|B|> \neq 0$. The disappearance of tunneling below the Curie point is demonstrated by the changes in the IR spectrum. The absorption around 400 cm^{-1}, which is connected with tunneling, drops sharply upon the transition (at 123 °K) [1]. The same experiment is planned using neutrons and an energy loss method.

It turned out that a simple experiment which would again support this picture was possible [7]. The hydrogen bonds in KDP, along which the protons tunnel, are directed along the lattice x and y axes. Therefore, the total scattering cross sections for neutron beams parallel, σ_z, and perpendicular, σ_x, to the z axis should differ. In fact it is easy to see that σ_x should be higher than σ_z. Both σ_x and σ_z were measured [7] as a function of neutron energy and of temperature (with special attention to the vicinity of the Curie point).

The results are in a good agreement with calculations based on a model in which the protons tunnel along the H-bonds and make harmonic vibrations (with the experimental frequencies) perpendicular to the H-bonds. Interesting changes were found in the vicinity of the Curie point.

Further experiments for the measurements of the dependence of the cross section on $\mathbf{K},\mathbf{x}_0$ are planned. Preliminary results confirm that the inelastic cross section rises with $\mathbf{K},\mathbf{x}_0$. Quantitative results will give an independent determination of $\alpha\beta$ and x_0. It would be interesting if high energy neutrons could be used to see the periodic variation with $\mathbf{K},\mathbf{x}_0$. Finally, the collective proton modes, with which we have not dealt here, seem to be a most interesting problem.

4. References

[1] Y. Imry, I. Pelah and E. Wiener, J. Chem. Phys. **43**, 4332 (1965).
[2] Y. Imry, Lecture delivered at the Nato Advanced Study Inst. on Tunneling, Riso, 1967, (to be published).
[3] R. Blinc and D. Hadzi, Molec. Phys. **1**, 398 (1958).
[4] H. J. Lipkin, Ann. Phys. (N.Y.) **26**, 115 (1964).
[5] Y. Hazony, P. Hillman, M. Pasternak and S. Ruby, Phys. Letters **2**, 337 (1962).
[6] I. Pelah, I. Lefkovitz, W. Kley and E. Tunkello, Phys. Rev. Letters **2**, 94 (1959).
[7] Y. Imry, I. Pelah, E. Wiener and C. Zafrir, Solid State Comm. **5**, 41 (1967).

PROTON DELOCALIZATION IN INORGANIC SOLIDS

J. J. FRIPIAT, P. G. ROUXHET, H. JACOBS, and A. JELLI

Laboratoire de Physico-Chimie Minérale
Institut des Sciences de la Terre
42, de Croylaan, Heverlee-Louvain (Belgium)

This paper aims to show that in the special case of solids containing hydroxyl groups, infrared spectroscopy may contribute to the study of lattice defects arising from proton delocalization. In these solids, heated progressively to elevated temperatures, a decrease of the integrated intensities of the stretching as well as of the deformation and torsion OH bands is observed, the initial intensity being fully restored on cooling the sample.

These effects seem to occur in several kinds of inorganic solids including micas [1],[1] boehmite, [2] and decationed zeolites [3].

1. Perturbation Due To Sample Emission

Recording infrared spectra at high temperature requires careful protection for sample emission, even if discrete emission bands are not detectable [4].

In the used double beam IR spectrograph, this is achieved by stopping the second chopper between the sample and the optics in a position where 50 percent of the intensities of the two beams are collected and by using larger slits. In an earlier work [1] the effect of the continuous emission was unfortunately neglected. Subsequent data were always obtained with only the first chopper between the source and the sample in operation.

2. Decrease in Intensity of the OH Vibration Bands

Several hypotheses may be proposed to explain the decrease in intensity of the OH vibration absorption band of inorganic solids heated at high temperatures.

(1) In an monocristalline solid a change in the orientation of the OH transition moment could be invoked. Careful measurements made on mica monocrystals ruled out very clearly this possibility [1, 5].

---

[1] Figures in brackets indicate the literature references at the end of this paper.

(2) The temperature increase could effect the electron distribution in the OH bond, producing a change in the magnitude of the transition dipole. This explanation cannot be accepted because the decrease in intensity of the stretching, deformation and torsion OH bands are almost identical in boehmite [2].

(3) A more probable explanation could be supported by considering the well known intensity decrease of OH stretching bands caused by the release of hydrogen bonding. This explanation, however, is again ruled out by the observation that for the various materials already studied, no correlation was found between the frequency shift of the OH stretching band and the decrease in intensity. Moreover, calculations founded on the perturbation of the vibrational energy levels by the weakening of the H bonds fails to reproduce the right order of magnitude of the intensity loss [2].

(4) In view of the impossibility of explaining the intensity loss of OH vibrations by any of the effects listed above, it has been proposed that it may be accounted for by assuming that the protons are, to some extent, delocalized at increasing temperatures.

3. Interpretation of the OH Band Intensity Loss in Boehmite [2]

Among aluminum hydrates, boehmite presents the unique feature of a distribution of hydrogen bonded hydroxyls along a zig-zag chain.

Table 1 gives the loss of relative intensity obtained for the stretching modes of untreated and deuterated bohemite. A similar evolution is observed for the other vibrational modes. The activation energies obtained by plotting the integrated intensities against T^{-1} (°K^{-1}) averages 2 kcal.

It is assumed that any vibrational transition starting from a level approximately located 2 kcal above the fundamental level does not contribute to the discrete absorption of radiant energy. Therefore, increasing the sample temperature shifts the populations of the vibrational levels in such a way that an increasing number of OH oscillators does not contribute furthermore to the band intensity.

The condition of inefficiency of these optical transitions would originate from the broadening of the upper vibrational levels where the tunneling probability becomes noticeable with respect to the vibration period. At this level, the probability for a proton to escape from its initial potential well during the vibration period is such that it may be considered as delocalized. This phenomenon might involve two adjacent potential wells of the zig-zag chain or, several potential wells by flipping, for instance, a complete row of OH bonds. Approxi-

TABLE 1. Change of relative absorbance with respect to temperature for the stretching modes of boehmite

AlOOH		AlOOD	
Temp. (°K)	Relat. absorbance	Temp. (°K)	Relat. absorbance
300	1. 00	300	1. 00
391	0. 91	373	0. 85
439	0. 865	436	0. 76
541	0. 79	487	0. 72
576	0. 755	569	0. 59
652	0. 65	629	0. 56

mate calculations of the tunneling probability per period of stretching vibrations P_w^s lead to the result that P_w^s has a noticeable value above the energy levels corresponding to 11 kcal or $h\nu_v+2$ kcal. As shown in table 1, experimental data and theoretical results deduced from this hypothesis agree quite well. Taking into consideration their respective periods of vibration, a similar agreement is found for the deformation and torsion bands. Proton tunneling is probably favored by the decrease of the height of the energy barrier resulting from oxygen atoms vibrations.

Recent dielectric and deuterium diffusion data support the above mechanism [6]. A rather strong Debye dipolar absorption (fig. 1A) has been observed in the frequency region of 800–16,000 Hz in the temperature range between 100 and 200 °C. The activation energy of Debye dipolar absorption approximates 0.68 eV. The activation energy obtained from deuteron diffusion measurement carried out in the presence of D_2O in the same temperature range is almost identical (fig. 1B). The activation energy of the conductivity process by free charge carriers, superimposed to the dipolar absorption, was about 0.22 eV.

Assuming that, in agreement with the previous results, the formation energy of an ions pair defect approximates 0.45 eV (or 11 kcal) and that the rotation energy of such a defect is of the order of magnitude of a few hundredths eV, the activation energies obtained for both the dipolar absorption process and for the free charge carrier conductivity may be accounted for.

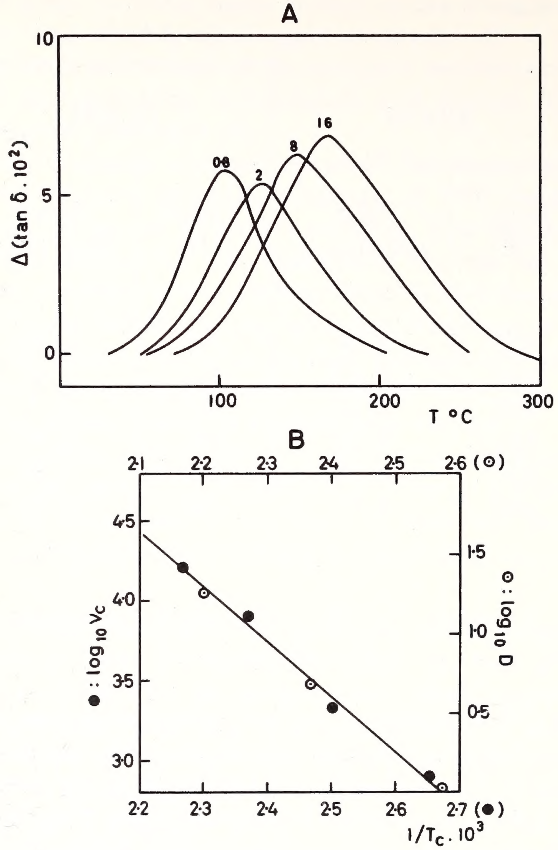

Figure 1. A. Contribution of Debye Dipolar Absorption (D.D.A.) to tan δ, the corresponding frequencies being in kHz. B. $\log_{10} \nu_c$ and $\log_{10} D$ against T^{-1} (°K^{-1}). The diffusion coefficient D is expressed in arbitrary units.

4. Intensity Loss in Micas (Muscovite and Phlogopite)

It might be objected that the special hydrogenic structure of boehmite would favor the delocalization process which should then be restricted to structures characterized by strong hydrogen bonds. In micas, OH groups are isolated within an octahedral cell characterized by cationic vacancies. Muscovite and phlogopite differ in that the OH dipoles are slightly tilted above the ab plane in muscovite [1, 7], whilst they are oriented almost perpendicularly to this plane in phlogopite [1]. As shown previously [1, 5] heating has no noticeable effect on these orientations. The loss of absorbance observed for the OH stretching bands for both samples are shown in figure 2. If the hypothesis made for boehmite is accepted, it must be assumed that heating muscovite

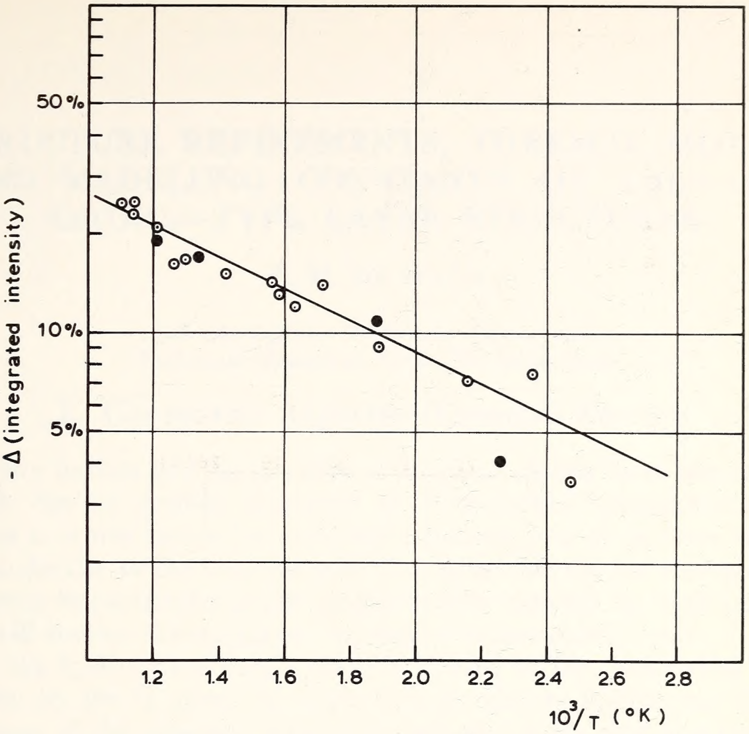

FIGURE 2. Decrease of the absorption intensity as a function of the inverse of temperature for the stretching band of a muscovite (○) and a phlogopite (●) sample.

or phlogopite up to 600 °C shifts approximately 20 percent of the oscillator population to energy levels from which the photon absorption will not contribute further to the discrete OH stretching bands. The proton at the upper energy levels might jump from its lattice position to an adjacent oxygen orbital or to an octahedral vacancy.

5. References

[1] J. J. Fripiat, P. G. Rouxhet and H. Jacobs, Am. Miner. **50,** 1937–1958 (1965).

[2] J. J. Fripiat, H. Bosmans and P. G. Rouxhet, J. Phys. Chem **71,** 1097–1111 (1967).

[3] J. B. Uytterhoeven, R. Schoonheydt and J. J. Fripiat, Int. Symp. on React. Mechanisms of Inorg. Solids, Univ.of Aberdeen **5,** 2 (1966).

[4] J. J. Fripiat, P. Rouxhet, H. Jacobs and A. Jelli, Bull. du Groupe Français des Argiles **19** 43–52 (1937).

[5] J. J. Fripiat, H. Jacobs and P. Rouxhet, Silicates Industriels, **31,** 311–313 (1966).

[6] A. Matta and J. J. Fripiat, Trans. of the Faraday Society, **63**, 2936–2944 (1967).

[7] W. Vedder and R. S. McDonald, J. Chem. Phys. **38,** 1583–1590 (1963).

STRUCTURE REFINEMENTS, THERMAL MOTION AND MADELUNG CONSTANTS OF CdI_2—AND $Cd(OH)_2$—TYPE LAYER STRUCTURES

Y. M. DE HAAN

Laboratorium voor Technische Natuurkunde
Technische Hogeschool, Delft, The Netherlands

1. Geometric Aspects—Thermal Motion

Many halides and hydroxydes of bivalent metals have structures which can be crudely described as close-packed arrangements of anions in which the cation-occupied octahedra join up to form layers perpendicular to the trigonal axis. The layers have a net charge zero and may be regarded as giant molecules held together by weak forces. We will assume the intralayer bonding to be essentially ionic.

In the hydroxydes, each proton is located in the tetrahedral hole formed by the O atom, to which it is covalently linked, and three O atoms of the adjacent layer. The indications are that there is no hydrogen bonding [1].[1]

The close-packing may be

hexagonal	(C6–or $Cd(OH)_2$ structure),
cubic	(C19–or $CdCl_2$ structure), or
mixed	(C27–or Cd(OH)Cl structure and many structures with longer stacking periods, or with stacking faults).

In all these structures the layers (sandwiches) are of essentially the same type.

A different classification can be made on the basis of the ratio of the ionic radii: $\rho = R_{M++}/R_{X-}$. Although the critical value for octahedral coordination is 0.414, many CdI_2-type halides (particularly iodides) have much lower ρ-values. MgI_2 ($\rho = 0.33$) is a particularly good example of such a "*rattling structure*".

On the other hand, many hydroxydes and chlorides have high ρ-values; in this case we will speak of *expanded structures*. A typical example is $Ca(OH)_2$: $\rho = 0.71$.

Whereas the octahedra in rattling and "nicely fitting" structures are expected to be fairly regular (see table 1), the expanded structures (with relatively large cations) may have their octahedra considerably distorted, from cubic to trigonal symmetry. The radius ratio deter-

---

[1] Figures in brackets indicate the literature references at the end of this paper.

TABLE 1. Crystallographic data[a] and Madelung factors for five selected compounds

	NiI_2	$NiCl_2$	CdI_2	$Cd(OH)_2$	$Ca(OH)_2$[b]
Type	C19	C19	C6	C6	C6
R_M/R_X[c]	0.36	0.42	0.48	0.70	0.72
$\sin \epsilon$	+0.027	+0.029	+0.009	+0.141	+0.148
c'/a[d]	1.683	1.665	1.616	1.344	1.366
z'_X[e]	0.233	0.235	0.2492	0.241	0.2330 (0.2341)[b]
a	3.927	3.483	4.244	3.499	3.593
c'	6.610	5.800	6.859	4.701	4.909
L	2.742	2.428	2.988	2.316	2.371
$B_x(M)$	0.6	2.0	1.8	0.6	0.68 (0.70)
$B_z(M)$	1.1	2.0	3.2	1.3	1.50 (1.25)
$B_x(X)$	0.7	2.0	1.8	1.0	0.9 (0.73)
$B_z(X)$	0.9	2.0	1.8	1.0	0.8 (0.93)
A	4.431	4.435	4.388	4.636	4.644
$A+\Delta A(\dot{\alpha})$[f]	5.3	5.1	5.2	5.25	5.22

[a] Obtained by the author and co-workers, except for $Ca(OH)_2$[1, 2] and $NiCl_2$ [3].

[b] Neutron diffraction data [1] shown in parentheses

[c] With effective anion radii 2.02 Å for I^- and 1.75 Å for Cl^-, as indicated by the interionic distances.

[d] $c'=c$ (C6), $c'=c/3$ (C19).

[e] Anion coordinate relative to c'.

[f] Polarizabilities according to ref. [4]; $\mu_p(OH^-)=1.5D$.

mines the extent to which the octahedra might be either *flattened* or *elongated*. Let us consider the bond angle X_1MX_2 (X_1 and X_2 in the same anion layer) and define a distorsion angle, ϵ, according to:

$$\angle X_1MX_2=90+\epsilon. \tag{1}$$

Flattened and elongated octahedra have $\epsilon>0$ and $\epsilon<0$ respectively. By treating the ions as rigid spheres we can show that

$$|\sin\epsilon|\leqq 1-\frac{2}{(\rho+1)^2}. \tag{2}$$

In actual expanded structures the octahedra are always flattened. This observation, deduced from structure refinements (see table 1), tempted the author to calculate the Madelung constant, A, as a function of ϵ (section 2). Temperature factors, also obtained from these refinements (see table 1), indicate that in both rattling and expanded structures the cations vibrate anisotropically with the larger amplitude perpendicular to the layers. The anions have a fairly isotropic thermal motion.

2. Structural Dependency of the Crystal Energy

The Madelung constant A is related to the coulomb energy U per molecule according to:

$$U=-A\frac{e^2}{4\pi\epsilon_0 L} \tag{3}$$

(L is the shortest interionic distance).

Our calculations show that a layer of coupled octahedra tends to have its octahedra flattened. When $\sin\epsilon$ goes from -0.2 to $+0.2$, A increases by about 30 percent (corresponding with a gain in lattice energy of 100–150 kcal/mole) to a maximum, 4.75, for $\sin\epsilon=0.33$ ($\angle X_1MX_2=109°$).

We have extended the ionic description of these structures by including the interaction energy ΔU associated with the induced and permanent dipoles carried by the anions. The following equation

$$\Delta U=-2\frac{\frac{1}{2}\alpha E_q^2+E_q\cdot\mu_p+\frac{1}{2}g\mu_p^2}{1-g\alpha} \tag{4}$$

holds for our layer structures, in which α and μ_p are the polarizability and the dipole moment of the anions. E_q is the monopole field at the anion sites and g is defined as E_μ/μ, E_μ being the field at the anion sites due to dipole moments μ of the anions.

It is of interest that g is negative, indicating that the dipole-dipole interaction (eq (4), third term) is antibonding. The denominator reflects the depolarizing influence of the induced dipoles themselves. This effect is often neglected in calculations of this type.

ΔU can be represented by a dimensionless quantity, ΔA (eq (3)), to be added to the Madelung constant. ΔA can be obtained directly from eq (4) by replacing α by $\dot{\alpha}=\alpha/4\pi\epsilon_0 L^3$, E_q by $\dot{E}_q=E_q\, 4\pi\epsilon_0 L^2 e^{-1}$, etc.

ΔA is of the order of 1 (20 percent of A), for both hydroxydes and halides, and decreases rapidly as the octahedra are flattened. The maximum of $A+\Delta A$ shifts towards lower values of ϵ as $\dot{\alpha}$ increases.

Actual structures follow the behaviour of $A(\epsilon)+\Delta A(\epsilon,\ \dot{\alpha})$ qualitatively. The above-mentioned shift of the maximum explains, for instance, why the octahedra are strongly flattened in $Cd(OH)_2$, less flattened in $CdCl_2$, and fairly regular in CdI_2.

We finally remark that our results for A and ΔA hold for one individual layer (A_l, ΔA_l) as well as for complete structures (A_s, ΔA_s): $(A+\Delta A)_s-(A+\Delta A)_l$ could be shown to amount to less than 0.2 percent of $A+\Delta A$, regardless of the structure type.

3. References

[1] W. R. Busing, H. A. Levy, J. Chem. Phys. **26**, 563 (1957).
[2] H. E. Petch, Acta Cryst. **14**, 950 (1961).
[3] A. Ferrari, A. Braibanti, G. Bigliardi, Acta Cryst. **16**, 846 (1963).
[4] J. R. Tessman, A. H. Kahn, W. Shockley, Phys. Rev. **92**, 890 (1953).

THE AQUATED HYDROGEN ION: SINGLE CRYSTAL DIFFRACTION INVESTIGATIONS OF COMPOUNDS CONTAINING THE $(H_2O \cdot H \cdot OH_2)^+$ ION[1]

JACK M. WILLIAMS

Metallurgy Division
Argonne National Laboratory, Argonne, Illinois 60439

While hydrates of the type $H^+(H_2O)_n$, with $n = 1\text{–}8$, have been observed in the gas phase [1][2], only compounds containing the oxonium[3] ion $(H_3O)^+$ have been extensively studied in the crystalline state [2–4]. The *diaquohydrogen ion* [5],[4] $(H_2O \cdot H \cdot OH_2)^+$, first postulated by Huggins [6] as a component of acid solutions, has been observed in a 3-dimensional neutron diffraction study of *trans*-$[Co(en)_2Cl_2]^+Cl^-(H_5O_2)^+Cl^-$ [5]. The most probable geometry of the $(H_2O \cdot H \cdot OH_2)^+$ ion involves *cis*-, *trans*-, or *gauche*- conformations.[5] The *cis*- and *trans*- configurations correspond to conventional "boat" and "chair" forms, respectively. Another possibility for $(H_5O_2)^+$ is $(H_3O)^+ \cdot H_2O$. For the *diaquo*- species the *trans*- configuration minimizes both H-H repulsion and lone-pair electron repulsion of the oxygen atoms, but other configurations are observed most likely because of formation of relatively strong O-H. . . X bonds in addition to crystal packing effects.

Table 1 includes compounds where the presence of the $(H_2O \cdot H \cdot OH_2)^+$ ion has been fully, or in some cases partially, substantiated. Numerous compounds not included in table 1 may also contain the ion [7].

From table 1 it seems likely that the *cis*-, *trans*-, and *gauche*- configurations of $(H_2O \cdot H \cdot OH_2)^+$ all exist in crystalline compounds. It also appears that the terminal hydrogen atoms of $(H_5O_2)^+$ may be involved in hydrogen bond formation with Cl^- [5, 9, 14], Br^- [12, 13], O of H_2O and Cl^- [9], O from H_2O only [11], and possibly O from $(ClO_4)^-$ [10].

---

[1] Research supported by the United States Atomic Energy Commission.

[2] Figures in brackets indicate the literature references at the end of this paper.

[3] The $(H_3O)^+$ ion is a complex of oxygen and not simply a *hydrated* proton.

[4] This is the preferred 1960 I.U.P.A.C. nomenclature. See ref. 16, p. 5529.

[5] In this paper *cis*- and *gauche*- (linear or nonlinear O-H-O) imply point symmetry $mm(C_{2v})$ and $1(C_1)$, respectively. *Trans*- (linear O-H-O) implies point symmetry $2/m(C_{2h})$.

TABLE 1. Summary of single crystal diffraction studies of compounds containing the $(H_2O{\cdot}H{\cdot}OH_2)^+$ ion

Investigative method [a]	Compound [b]	(O—H—O) (Å) [c]	Configuration $(H_2O{\cdot}H{\cdot}OH_2)^+$	Symmetry at bridging H site
N(1967)[5]	$[Co(en)_2Cl_2]^+Cl^-[H_5O_2]^+Cl^-$	2.50±0.03	*trans-*	$\bar{1}$
X(1952)[8]	$[Co(en)_2Cl_2]^+Cl^-[H_5O_2]^+Cl^-$	2.66	*trans-*	$\bar{1}$
X(1967)[9]	$[H_5O_2]^+Cl^-$	2.41±0.01	*gauche-*	none
X(1967)[9]	$[H_5O_2]^+Cl^-{\cdot}H_2O$	2.43±0.01	*gauche-*	none
X(——)[10]	$[H_5O_2]^+ClO_4^-$	2.42±0.01	*trans-*	$\bar{1}$
X(1967)[d][11]	$C_6H_2O_8N_2{\cdot}6H_2O$[e]	2.44±0.01	*gauche-*	none
X(1960)[12]	$[Cr(en)_2Br_2]^+Br^-[H_5O_2]^+Br^-$	2.56	*trans-*	$\bar{1}$
X(1959)[13]	$[Co(en)_2Br_2]^+Br^-[H_5O_2]^+Br^-$	2.60	*trans-*	$\bar{1}$
X(1962)[14]	$[Co\ l\text{-}pn_2Cl_2]^+Cl^-[H_5O_2]^+Cl^-$	[f] 2.57	*cis-*	2

[a] *N*, neutron diffraction; *X*, x-ray diffraction; and (publication date).

[b] (en), ethylenediamine and (pn), propylenediamine.

[c] Until 0–0 distances listed above greater than 2.55Å are confirmed by 3-dimensional analyses, it is felt such distances in $(H_2O{\cdot}H{\cdot}OH_2)^+$ ions likely vary between 2.40–2.50Å. Such a generalization may fail if $(H_5O_2)^+$ is present as $(H_3O)^+{\cdot}H_2O$ or if the bridging proton in the *diaquohydrogen* ion is in crystallographic disorder.

[d] As interpreted by E. A. [11] the compound contains an infinite chain of hydronium ions and water molecules of composition $(H_7O_3)_n^{n+}$. An alternate interpretation, consistent with the bond distances and angles, is that the compound contains $(H_5O_2)^+$ ions and normal water molecules suggesting the alternate formulation $[(H_5O_2)^+{\cdot}H_2O]_2(C_6O_8N_2)^=$.

[e] Nitranilic acid hexahydrate.

[f] Although either the *cis-* or *trans-* configuration is possible based on the presence of the 2-fold axis, the O . . . Cl distances and crystal packing suggest *cis-* as most probable.

In the one neutron diffraction study, in which all proton positions were determined, the $(H_5O_2)^+$ ion was observed to have the *trans*-configuration [5]. The distances, angles, and associated O-H. . . Cl hydrogen bonding scheme are shown in figure 1.

Full 3-dimensional neutron diffraction data for $[Co(en)_2Cl_2]^+Cl^-(H_5O_2)^+Cl^-$ has been recollected because of partial sample decomposition in the original study [5]. For this reason the distances and angles given in figure 1 are to be considered correct only within the significance limits of the errors given. The water molecule configuration is *trans*-with the central hydrogen atom of $(H_2O{\cdot}H{\cdot}OH_2)^+$ having *apparent* site symmetry $\bar{1}$ and involved in a short hydrogen bond (0–0=2.50 ±0.03 Å). It is of course impossible to determine from the diffraction data alone if the bridging proton is actually centered (ordered) or removed slightly with closely spaced lattice sites (disordered). The H-O-H angle in the aquo portion of the complex agrees well with that found in crystalline hydrates [15].

In a recent infrared spectroscopic study [7] it was also concluded that the $(H_2O{\cdot}H{\cdot}OH_2)^+$ ion is present in *trans*-$[Co(en)_2Cl_2]^+Cl^-(H_5O_2)^+Cl^-$, in agreement with the neutron diffraction results [5]. In the same infrared study it was demonstrated that the compound did not contain H_2O of crystallization or the $(H_3O)^+$ ion.

In conclusion, the results of several single crystal neutron and X-ray diffraction studies, and infrared spectroscopic studies, have verified the existence of the $(H_2O{\cdot}H{\cdot}OH_2)^+$ ion in the crystalline state. However, the *aquo-oxonium ion* $[(H_3O)^+{\cdot}H_2O]$, which may also be formulated as $(H_5O_2)^+$, has not yet been observed in crystalline materials.

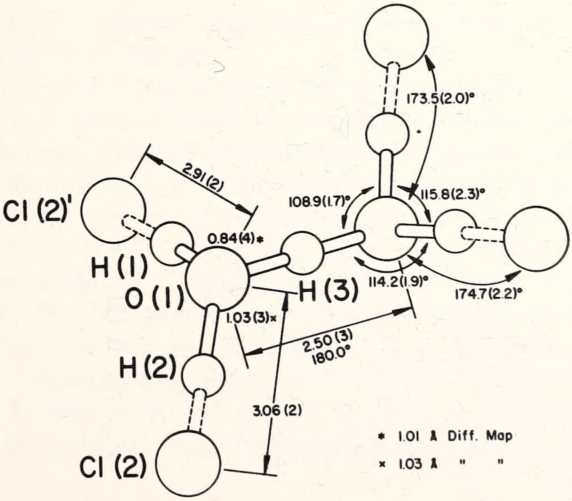

FIGURE 1. Hydrogen Bonding Scheme of the Trans-Diaquohydrogen Ion.

The author wishes to thank Dr. I. Olovsson for preprints of his work prior to publication.

References

[1] P. Kebarle and A. M. Hogg, J. Chem. Phys. **42**, 798 (1965).
[2] R. E. Richards and J. A. S. Smith, Trans. Faraday Soc. **47**, 1261 (1951).
[3] Y. K. Yoon and G. B. Carpenter, Acta Cryst. **12**, 17 (1959).
[4] C. C. Ferriso and D. F. Hornig, J. Chem. Phys. **23**, 1464 (1955).
[5] J. M. Williams, Inorg. Nucl. Chem. Lett. **3**, 297 (1967).
[6] M. L. Huggins, J. Phys. Chem. **40**, 723 (1936).
[7] R. D. Gillard and G. Wilkinson, J. Chem. Soc. 1640 (1964).
[8] A. Nakahara, Y. Saito and H. Kuroya, Bull. Chem. Soc. Japan **25**, 331 **23**, 966 (1967); **23**, 971(1967). (1952).
[9] J-O. Lundgren and I. Olovsson, Acta Cryst. **23**, 966 (1967); **23**, 971 (1967).
[10] I. Olovsson, private communication.
[11] E. Andersen, Acta Cryst. **22**, 204 (1967).
[12] S. Ooi, Y. Komiyama and H. Kuroya, Bull. Chem. Soc. Japan **33**, 354 (1960).
[13] S. Ooi ,Y. Komiyama, Y. Saito and H. Kuroya, Bull. Chem. Soc. Japan **32**, 263 (1959).
[14] Y. Saito and H. Iwasaki, Bull. Chem. Soc. Japan **35**, 1131 (1962).
[15] W. H. Baur, Acta Cryst. **19**, 909 (1965).
[16] A. Silverman, J. Am. Chem. Soc. **82**, 5529 (1960).

INFRARED INVESTIGATION OF ORDERING AND STRUCTURAL CHANGES IN AMMONIUM HALIDES

C. W. GARLAND and N. E. SCHUMAKER
Department of Chemistry

Massachusetts Institute of Technology, Cambridge, Massachusetts 02139

1. Introduction

Ammonium chloride and ammonium bromide undergo transitions involving the relative orientations of the ammonium ions. At low temperatures, both salts have a CsCl-type cubic structure with all the ammonium ions oriented "parallel" to each other. NH_4Cl exhibits an order-disorder transition of the lambda type at 242 °K (249 °K in ND_4Cl). Above the lambda point, the crystal is randomly disordered with respect to the two equivalent orientations of the tetrahedral NH_4^+ ion in the cubic unit cell. The situation is more complex in the bromide because of the existence of an ordered tetragonal phase in which chains of "parallel" NH_4^+ ions are surrounded by nearest-neighbor chains with the opposite orientation. NH_4Br exhibits a complicated order-order transition between the cubic and tetragonal structures at ~108 °K (~ 167 °K in ND_4Br) *and* a lambda-type transition between ordered tetragonal and disordered cubic structures at 235 °K (214 °K in ND_4Br).

Previous infrared investigations [1][1] have contributed greatly to establishing the order-disorder nature of the lambda transitions in ammonium halides. The present investigation of normal and deuterated ammonium chloride and bormide extends the earlier work in two important ways: (a) spectra have been recorded for crystalline samples (~100μ thick) as well as sublimed films (~3μ thick); (c) spectra have been recorded as a detailed function of temperature between 21 °K and 300 °K. This report cannot present the complete results but will summarize two features of special interest. In section 2 we shall deal with the librational motion of NH_4^+ ions and the potential barrier to rotation. In section 3, the degree of order in the crystal will be discussed in terms of an anomalous component of the allowed ν_4 band.

---

[1] Figures in brackets indicate the literature references at the end of this paper.

2. Librational Motion

The potential barrier in the ammonium halides is high enough to prevent the ammonium ions from rotating even at 300 °K. Thus, the ammonium ions librate (undergo torsional oscillations) about their equilibrium positions in both the ordered and disordered phases. The fundamental band for libration is not infrared active, but the value of ν_6 can be determined from the combination band $\nu_4 + \nu_6$. The binary overtone $2\nu_6$ and the tertiary overtone $3\nu_6$ are infrared active, and both have been observed at low temperatures. The values obtained at 21 °K for ν_6, $2\nu_6$ and $3\nu_6$ in the cubic ordered phases of NH_4Cl, NH_4Br, ND_4Cl and ND_4Br are given in table 1. These experimental frequencies clearly indicate the anharmonic character of the torsional oscillation.

TABLE 1. Observed and calculated libration frequencies for ordered cubic ammonium halides

Transition	NH_4Cl	NH_4Br	ND_4Cl	ND_4Br
ν_6(obs)	389	349	280	252
ν_{100}	389	349	282	253
$2\nu_6$(obs)	749	672	545	490
ν_{110}	772	692	560	504
$3\nu_6$(obs)	1110	987	815	728
ν_{210}	1132	1012	827	742

Nagamiya has proposed a potential function for the tetrahedral ammonium ion moving in the cubic field of a CsCl lattice, and Gutowsky, Pake and Bersohn [2] have given an approximate solution for the energy levels of such a three-dimensional torsional oscillator. The position of these levels is determined by I, the momeut of inertia of the ammonium ion, and V_0, the height of the potential barrier for rotation about a two-fold axis of the ion. The values of I are known for both NH_4^+ and ND_4^+, and we have chosen $V_0 = 1860$ cm^{-1} (5.32 kcal mole^{-1}) for the chloride and $V_0 = 1520$ cm^{-1} (4.35 kcal mole^{-1}) for the bromide. With these empirical V_0 values, one can calculate values of $\nu_{ijk} = (E_{ijk} - E_{000})/hc$. As shown in table 1, the calculated frequencies are in reasonable agreement with the observed frequencies. Moreover, Nagamiya's potential predicts that $V_0 \sim a^{-5}$, where a is the cubic lattice parameter. Using $a(NH_4Br) = 4.00$ Å and $a(NH_4Cl) = 3.82$ Å at 20 °K one finds that $[a(\mathrm{Br})/a(\mathrm{Cl})]^5 = 1.25$, in good agreement with $V_0(\mathrm{Cl})/V_0(\mathrm{Br}) = 1860/1520 = 1.22$. Thus, it seems possible to establish appropriate values for V_0 in spite of the fact that the calculated anharmonicity is less than that observed.

3. Effects of Disorder

Although the spectra contain several indications of changes due to ordering, we shall limit this discussion to the behavior near the infrared active, triply-degenerate bending vibration (ν_4) of the NH_4^+ ion. The behavior of the deuterated salts is qualitatively in agreement with that described below.

NH_4Cl films. At 21 °K, the ν_4 bending vibration gives rise to a single strong band at 1403 cm^{-1}. However, at temperatures above $\sim$120 °K an anomalous component (denoted by ν_4') is observed at 1444 cm^{-1}. $I\nu_4'$, the intensity of this component, has been measured as a function of temperature and can be shown to be quite simply related to the orientational disorder [3].

NH_4Br films. The situation here is more complex because ν_4 is split by a tetragonal crystal field, and one observes a second component near the strong 1400 cm^{-1} ν_4 band in the ordered tetragonal phase at 110 °K. The behavior of $I\nu_4'$ near the lambda point at 235 °K thus reflects changes in both the tetragonal distortion of the lattice and the disorder of the NH_4^+ orientations. The most surprising feature is the large variation of $I\nu_4'$ observed in the cubic phase between 20 and 110 °K. Thermal measurements [4] show a sluggish first-order transition at 108 °K and strongly indicate that the cubic NH_4Br at 100 °K is as completely ordered as is NH_4Cl at that temperature. In fact, the spectra demonstrate that a considerable amount of equilibrium "disorder" exists in the cubic phase and the transition is by no means a simple first-order change.

4. References

[1] E. L. Wagner and D. F. Hornig, J. Chem. Phys. **18,** 296, 305 (1950).
[2] H. S. Gutowsky, G. E. Pake and R. Bersohn, J. Chem. Phys. **22,** 643 (1954).
[3] C. W. Garland and N. E. Schumaker, J. Phys. Chem. Solids **28,** 799 (1967).
[4] M. Sorai, H. Suga and S. Seki, Bull. Chem. Soc. Japan **38,** 1125 (1965).

NUCLEAR MAGNETIC RESONANCE AND NEUTRON-SCATTERING STUDIES OF HINDERED ROTATION IN PHOSPHONIUM IODIDE

T. C. FARRAR and J. J. RUSH [1]

Institute for Materials Research
National Bureau of Standards, Washington, D.C. 20234

The phosphonium halides are chemically analogous to the ammonium halides, although considerably less stable [1].[2] The tetragonal crystal structure of PH_4I [2, 3] is similar to that of NH_4Br and NH_4I in their low-temperature phases [4, 5]. However, heat capacity measurements on PH_4I between −180 and 10 °C show no evidence of crystal phase transitions such as those which are observed between −25 and −50 °C for NH_4Cl, NH_4Br and NH_4I and attributed to the ordering of the NH_4^+ ions. Moreover, a recent neutron scattering measurement on PH_4I [6] by one of us indicated a barrier to rotation for the PH_4^+ ions higher than for any of the ammonium halides in their equivalent phases [7]. In addition, a neutron diffraction study of PH_4I [3] shows that although the unit cell is similar to Phase III of NH_4Br and NH_4I, the PH_4^+ ions are ordered in positions displaced from the NH_4^+ orientations by 90° rotation around the $\bar{4}$ axis. This suggests that repulsive interactions may be important in determining the structure and dynamics of PH_4I, whereas the spectroscopic and structural results for the ammonium halides seem to be fitted rather well on the basis of an electrostatic model [7]. Indeed calculations of crystal energy vs. orientation for the PH_4^+ ions in PH_4I [3] using both electrostatic and repulsive terms predict the correct equilibrium positions for the ions. They further indicate that the repulsive terms are dominant and that the potential is quite anharmonic, with a high barrier to rotation.

The above comparison of the results on the phosphonium and ammonium salts suggested that a study of the motion of the PH_4^+ ions in the phosphonium halides by NMR techniques could provide valuable information on the potential energy surfaces in these crystals. In this paper we discuss the results of preliminary line-width and T_1 measurements on phosphonium iodide, and compare them with neutron-scattering results for PH_4I and the ammonium halides.

---

[1] Now with the Center for Radiation Research, National Bureau of Standards, Washington, D.C.

[2] Figures in brackets indicate the literature references at the end of this paper.

The neutron spectrum for PH_4I at room temperature [6] exhibits peaks at 327±11 and 614±40 cm^{-1} which are assigned primarily to the 1→0 and 2→0 transitions of the PH_4^+ torsional oscillations. If one assumes a 4-fold cosine potential[3] and a slightly anharmonic oscillator [6, 7], a barrier of 6.7±0.5 kcal/mole is calculated from the observed torsional frequency of 327 cm^{-1}. This barrier is considerably higher than those calculated under the same assumptions for the low-temperature phases of the ammonium halides [7, 8], as shown in table 1.

TABLE 1. Barriers to rotation derived from NMR and neutron-scattering measurements on the ammonium halides and phosphonium iodide

Compound	Neutron scattering		NMR (T_1)
	ν_{tors} (cm^{-1})[a]	V_0 (4-fold)	Activation energy
NH_4Cl	389	5.2 kcal	4.7 kcal[b]
NH_4Br	335	3.9	4.0[b]
NH_4I	290	3.0	2.0—2.9[c] 3.2[d]
PH_4I	327±11[d]	6.7±0.5	7.2[d]

[a] The frequencies for NH_4Cl, NH_4Br and NH_4I are from reference 8.
[b] Reference 9.
[c] Reference 7 and R. E. Richards and T. Schaefer, Trans. Faraday Soc. **57**, 210 (1961).
[d] Present work and reference 6.

The results of the proton T_1 measurements at 9 MH_Z as a function of temperature for PH_4I are shown in figure 1. Correlation times (τ_c) were derived from these data, and an activation energy (E_a) of 7.2 kcal/mole was calculated for the reorientation of the PH_4^+ ions from the temperature dependence of τ_c, as well as directly from the T_1 curve. This result is shown in table 1, along with values previously obtained by neutron and NMR techniques for the ammonium halides. Also included in the table (in brackets) is an activation energy for NH_4I derived from preliminary T_1 measurements we made recently on this compound in view of the uncertainty of previous results. The

---

[3] This assumption neglects the difference between a 4-fold and a $\bar{4}$ axis.

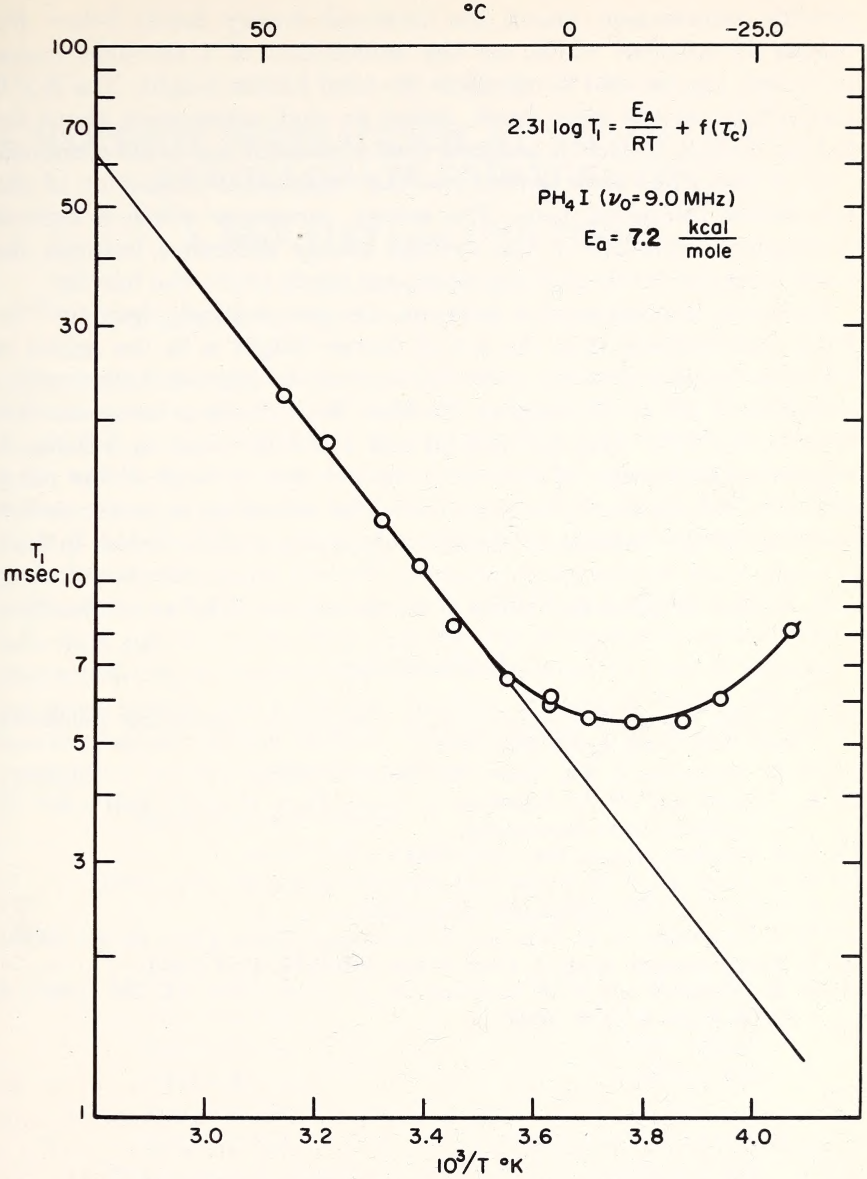

FIGURE 1. Spin-lattice relaxation times versus temperature for polycrystalline PH_4I at a resonance frequency of 9MHz.

agreement between the neutron and NMR results for PH_4I (and the ammonium salts [7–9]) is reasonably good. This is in part fortuitous, however, since the two experiments measure somewhat different things. As discussed above, the neutron (or infrared) measurements provide information about the torsional energy levels below the barrier to rotation which, on the assumption of a four-fold cosine potential, can be used to calculate the total barrier height. The NMR method [7], on the other hand, makes no such assumption about the barrier height. Rather it assumes that a classical activated reorientation of the PH_4^+ ions determines the temperature behavior of the spin-lattice relaxation time. The energy parameter which is derived is roughly a measure of the average energy difference between the lower torsional levels and the rotational levels above the barrier.

However, the agreement between the two derived "barriers" for PH_4I does indicate that the actual barrier height is in the region of 7 kcal/mole, and that the potential is closer to harmonic than recent calculations [3] would suggest. Further the difference in orientation between the PH_4^+ ions in PH_4I [3] and the NH_4^+ ions in NH_4Br [5] suggests that a study of the structure and dynamics of all the phosphonium halides could be quite useful for obtaining a better understanding of the balance of electrostatic and repulsive forces in such crystals. Such studies are in progress. We will report the results along with a more detailed discussion of our results on PH_4I at a later date.

References

[1] J. R. Van Wazer, Phosphorus and Its Compounds, Interscience Publishers, Inc., New York, **1,** 207–211 (1961).

[2] R. G. Dickinson, J. Am. Chem. Soc. **44,** 1489 (1922).

[3] A. Sequeira and W. C. Hamilton, J. Chem. Phys. **47,** 1818 (1967); also W. C. Hamilton, these proceedings.

[4] J. A. Ketelaar, Nature **134,** 250 (1934).

[5] H. A. Levy and S. W. Peterson, J. Am. Chem. Soc. **75,** 1536 (1953).

[6] J. J. Rush, J. Chem. Phys. **44,** 1722 (1966).

[7] H. S. Gutowsky, G. E. Pake and R. Bersohn, J. Chem. Phys. **22,** 643 (1954).

[8] G. Venkataraman, et al., J. Phys. Chem. Solids **27,** 1103 (1966).

[9] D. E. Woessner and B. S. Snowden, Jr., J. Phys. Chem. **71,** 952 (1967); J. Chem. Phys. **47,** 378 (1967).

A NEUTRON DIFFRACTION STUDY OF LITHIUM PERCHLORATE TRIHYDRATE [1]

A. SEQUEIRA [2] and IVAN BERNAL

Chemistry Department
Brookhaven National Laboratory, Upton, New York 11973

Studies of the physical properties (i.e., viscosity, nmr, I.R., and Raman spectra, etc. . . .) of ionic aqueous solutions have resulted in a set of empirical rules which characterize the behavior of the electrolytes with respect to the solvent. In particular, the ability of an ion to form stronger hydrogen bonds with water than water can form with itself if measured by a parameter called "the structure-breaking character" of the ion.

The isomorphous compounds $LiClO_4{\cdot}3H_2O$ and $LiMnO_4{\cdot}3H_2O$ contain two anions which differ considerably in their structure-breaking characteristics, as measured by these techniques. In view of this result we have studies the hydrogen bonding scheme in $LiClO_4{\cdot}3H_2O$ by means of single crystal neutron diffractometry. The resultsof our investigation are summarized as follows:

Space Group = $P6_3mc$
$a = 7.629 \pm 0.007$ Å
$c = 5.527 \pm 0.005$ Å
$Z = 2$ for $d(\text{meas}) = 1.89 \pm 0.05$
$R(F) = 6.6\%$

Li–0(1) = 2.112 Å
0(2) = 2.112
0(3) = 2.112
0(4) = 2.150
0(5) = 2.150
0(6) = 2.150
These are all water
oxygens; see figure 1
$0(2)-H-0(H_2O) = 161.4$ °
$0(2)-H = 113.0$°
$0(1)-H = 154.7$
$0(2)-H = 118.0$

$0(H_2O)-H = 0.936$ Å
$-0(1) = 3.015$
$-0(2) = 2.954$
$-H = 3.075$

$0(1) - Cl = 1.449$ Å
$-0(2) = 2.362$
$-H = 2.587$
$0(2)-Cl = 1.428$ Å
$-H = 2.052$
$-0(2) = 2.319$
$-H = 2.939$

$0(1)-Cl-0(2) = 110.4$°
$0(2)-Cl-0(2) = 108.6$°

---

[1] Research supported by the U.S. Atomic Energy Commission.

[2] Atomic Energy Establishment, Trombay, Bombay, India

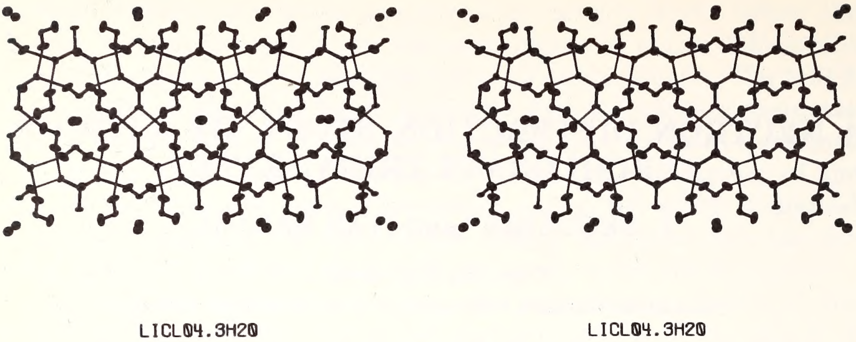

FIGURE 1.—Packing in lithium perchlorate trihydrate, as seen down the *c*-axis. This is a stereo pair which may be studied with a hand-held stereo viewer.

The difference in cell constants between lithium permaganate trihydrate and those of the perchlorate is easily understood since the average Mn–O distance [1][3] is 1.629 ± 0.008 Å, as opposed to the value of 1.438 ± 0.005 Å for the Cl–O bond in the perchlorate. Consequently, if the "iceberg" model of ionic solutions is qualitatively valid one can see that the two anions differ in their structure-breaking properties either by their unequal ability to order sheets of $(MO_4)_x\ (H_2O)_{3x}$, or by the difference in the lifetime of the cluster.

The Raman spectrum of single crystals of $LiClO_4 \cdot 3H_2O$ has been studied by Couture-Mathieu and Mathieu [2] who found that all three normal modes of water are observed and that their frequency has been shifted as expected from the hydrogen bonding to the perchlorate. No data is available on the $LiMnO_4 \cdot 3H_2O$, due no doubt, to its being a highly colored substance. Hopefully, this will be remedied by the current availability of Raman laser spectrometers. However, $LiSO_4 \cdot H_2O$ has been studied by x-ray [3] and neutron diffraction [4], by Raman techniques [5] and by various solution techniques [6].

The Raman study [6] indicates that in this case, the waters behave nearly as unbound molecules; likewise the hydrogen bonds found by Smith [4] are unusually long. Finally, the solution studies [6] classify this ion as a "structure former".

In conclusion we would like to point out that there seems to be an area of general agreement between results of various techniques of studying solutions and those obtained by spectroscopy and diffraction. We believe that the study of isomorphous substances in which only one ion changes (i.e., ClO_4^- versus MnO_4^-) may yield some further insight into the theory of ionic solutions.

---

[3] Figures in brackets indicate the literature references at the end of this paper.

References

[1] G. Palenik, *Inorg. Chem.* **6,** 503 (1967).

[2] L. Couture-Mathieu and J. P. Mathieu, *Acta Cryst.* **5,** 571 (1952).

[3] A. C. Larson, *Acta Cryst.* **18,** 717 (1965).

[4] A. Smith, *Acta Cryst.* **18,** 717 (1965), private communication to A. C. Larson.

[5] C. Bassas-Dubuisson, *J. Chim. Phys.* **50,** C98 (1953).

[6] See E. R. Hightingale, Jr., in *Chemical Physics of Ionic Solution,* B. E. Conway and R. G. Barradas, Eds., John Wiley and Sons, New York, pp. 87–100 (1966).

THE STRUCTURE OF SEVERAL URANYL NITRATE COMPOUNDS AS DETERMINED BY NEUTRON DIFFRACTION[1]

M. H. MUELLER and N. KENT DALLEY [2]

Argonne National Laboratory, Argonne, Illinois 60439

The use of neutron diffraction in the crystal structure determinations of $[UO_2(H_2O)_2(NO_3)_2]$ [1][3], $[UO_2(H_2O)_2(NO_3)_2]\cdot 4H_2O$ [2] and $[UO_2(H_2O)\{CO(NH_2)_2\}_4](NO_3)_2$ [3], hereafter referred to as I, II and III respectively, made it possible to obtain more accurate positions for light atoms and to make a more complete study of the hydrogen bonding present in each compound than would have been possible using x-rays. This is a result of the more favorable atomic scattering factor ratios and a smaller absorption problem in neutron diffraction.

It was found that the uranium coordination in all three compounds supports the conclusions of Evans [4] which he set forth in a review of uranyl compounds, and the U–O distances are in accord with those predicted by Zachariasen and Plettinger [5]. The uranyl ion is linear within experimental error in all three compounds though only in I is this required by the space group symmetry. All three compounds have a nearly planar (within 0.2 Å) arrangement of oxygen atoms perpendicular to the uranyl ion; in I and II the coordination consists of six oxygens, two from two water ligands and four from two bidentate nitrato groups; and in III it consists of five oxygens, one water oxygen and four carbonyl oxygens from the four urea groups. The pentagon of III is more regular than the hexagons of I and II; the unpuckered hexagon of I and II being possible only because of the presence of the highly polarizing NO_3^- group which allows the O–O approach of the oxygens to be less than is normally encountered.

Previous investigators had attempted to determine the structure of these compounds by other methods. In an infrared study of I [6] the nitrate group showed C_{2v} rather than the higher D_{3h} symmetry, hence it was concluded that the nitrate groups were covalently bound to the uranium as bidentate ligands. It was also shown [7] that there were no loosely bound water molecules outside the coordination sphere. These results were substantiated by the present neutron study. An earlier x-ray study of I [8] had reported the same type of configuration but because of erroneous bond lengths and lattice parameters it must be considered of doubtful value.

---

[1] This work was sponsored by the U.S. Atomic Energy Commission.

[2] Student Research Associate from University of Texas, Austin, Texas.

[3] Figures in brackets indicate the literature references at the end of this paper.

In a previous attempt to determine the structure of II, Gatehouse and Comyns [9] suggested the structure to be $[UO_2(H_2O)_6]\cdot 2NO_3$ from infrared studies but shortly thereafter Allpress and Hambly [10] showed that the infrared spectra of II was only slightly different from that of I and they indicated that there were covalent nitrates in both compounds. This was also shown in an infrared study by Ferraro and Walker [6]. Two previous diffraction experiments [11, 12] had not settled the question, however the findings of this neutron study confirmed the presence of bidentate nitrato ligands in II and also agreed with both the infrared study of Ferraro and Walker and an inelastic neutron scattering study [13] on II which indicated several different water environments.

The infrared work on III left many questions unanswered. A Russian study [14] showed that in such a compound the urea ligands would replace the nitrato groups in the primary coordination sphere, which suggested a fivefold coordination of the uranyl ion. However other investigators [15, 16] suggested a coordination of six about the ion with the possibility of a monodentate nitrato ligand or a tetramer. The neutron results showed it was indeed a case of fivefold coordination.

The hydrogen bonding in I is a rather simple chain type linkage. Only the water hydrogens of one of the two nonequivalent kinds of molecules are involved in hydrogen bonding; one hydrogen bond linking to the uncoordinated nitrato oxygen of the other kind of molecule and the second hydrogen bond terminating at the uranyl oxygen of the same kind of molecule. In II the hydrogen bonding is much more complicated with the basic structural units joined together by a network of water sheets. These sheets consist of the four water molecules outside the primary coordination sphere of the uranium atom. There are fairly strong hydrogen bonds from the coordinated water molecules to the water sheets and then weaker bonds from the waters of the sheet to the uncoordinated nitrato oxygens. The water molecules of the sheets are also joined together by hydrogen bonds (see fig. 1). In III most of hydrogen bonds involve the oxygens of the nitrato groups. Thus the nitrate groups perform an important cohesive function in the crystal.

The thermal motion in these compounds has, as would be expected, the larger components of motion perpendicular to the bond direction. In III there is large thermal motion in which the isotropic temperature factors for some of the oxygens of the nitrate groups are nearly eight. However there is no indication of any disorder.

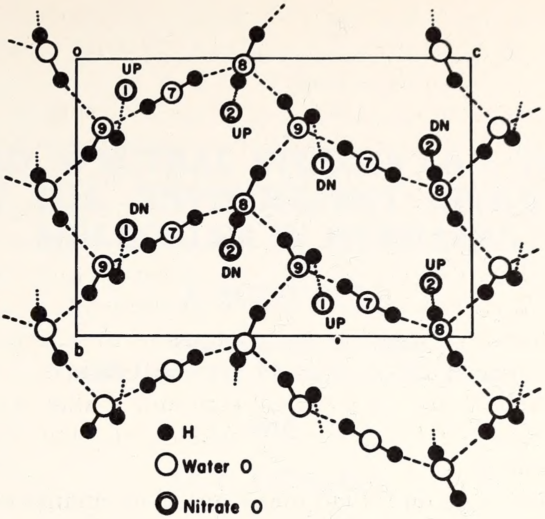

FIGURE 1. Water sheets of uranyl nitrate hexahydrate (after ref. 2). O(7)'s are water oxygens in the primary coordination sphere.

References

[1] N. Kent Dalley, M. H. Mueller, and S. H. Simonsen, American Crystallographic Association Program and Abstracts, Paper J–9, p. 71 (Jan. 1967).
[2] J. C. Taylor, and M. H. Mueller, Acta Cryst. **19,** 536 (1965).
[3] N. Kent Dalley, and M. H. Mueller, American Crystallographic Association Program and Abstracts, Paper T–6, p. 98 (Aug. 1967).
[4] H. T. Evans, Jr., Science **141,** 154 (1963).
[5] W. H. Zachariasen, and H. A. Plettinger, Acta Cryst. **12,** 526 (1959).
[6] J. R. Ferraro and A. Walker, J. Chem. Phys., **45,** No. 2, 550 (1966).
[7] B. Jeżowska-Trzebiatowska and B. Kedzia, Bull. Acad. Polon. Sci. Ser. Sci. Chim. **12,** No. 4, 251 (1964).
[8] V. M. Vdovenko, E. V. Stroganov, A. P. Sokolov, and G. Lungu, Radiokhimiya **4,** No. 1, 59 (1962).
[9] B. M. Gatehouse and A. E. Comyns, J. Chem. Soc. **802,** 3965 (1958).
[10] J. G. Allpress, and N. A. Hambly, Austral. J. Chem. **12,** 569 (1959).
[11] V. M. Vdovenko, E. V. Stroganov, A. P. Sokolov, and V. N. Zandin, Radiokhemiya **2,** 24 (1960).
[12] J. E. Fleming and H. Lynton, Chem. and Ind. **79,** 1416 (1960).
[13] J. J. Rush, J. R. Ferraro, and A. Walker, Inorg. Chem. **6,** 346 (1967).
[14] A.V. Babaeva, V. P. Markov, O. N. Evstaf'eva, and I. V. Tsapkina Fiz. Probl. Spektroskopii, Akad. Nauk. SSSR, Materialy 13-go [Trenadtsatago] Soveshch. Leningrad 1960, **1,** 417-20 (Pub. 1962).
[15] L. S. Campisi, Thesis, Fordham University (1965).
[16] P. S. Gentile, Private Communication.

INFRARED SPECTRAL STUDIES AS A TOOL FOR SENSING THE ENVIRONMENT ABOUT WATER MOLECULES IN HYDRATES

J. SCHIFFER

Department of Chemistry
Temple University, Philadelphia, Pa. 19122

and

D. F. HORNIG

Office of Science and Technology
The White House, Washington, D.C. 20500

The isotope dilution technique has proven very useful for sensing the environment about water molecules in hydrates [1]. In principle, it involves recording vibrational spectra of hydrates, containing varying admixtures of H_2O, HOD and D_2O.

The utility of this technique is based on the following considerations: A hydrate prepared from a salt solution, containing a small percentage of D_2O relative to H_2O, has as its next major component to H_2O, the isotopic species HOD. The OD motions of these HOD's will be both intra and intermolecularly uncoupled from their environments, since they are far removed in frequency from vibrations of molecules surrounding them. The same applies to OH motions of HOD in highly deuterated hydrates. Absorptions due to these uncoupled modes will henceforth be designated ν_{OH} and ν_{OD} bands. The number of these bands directly reflects the number of physically different OH and OD bonds in a hydrate, their frequencies reflect the extent to which each bond is hydrogen-bound in the solid, and their frequency shifts from vapor values, in conjunction with frequency shift—OH—X correlations [2, 3] give reasonable estimates of the geometric environment about each bond of a water molecule in a hydrate. We may also obtain estimates of OH bond distances from a frequency shift—r_{OH} correlation [4].

As the percentage of D_2O is increased in a hydrate, the probability increases for having HOD molecules adjacent to one another and for having two deuteriums on the same water molecule. These lead to the appearance of additional bands in the OD stretching region due to (1) ν_1 and ν_3 motions of uncoupled D_2O molecules and (2) intermolecular coupling components of adjacent OD oscillators. A parallel pattern is expected in the OH stretching region as the concentration of H_2O is increased stepwise in a deuterated sample. These additional features are useful for associating pairs of uncoupled ν_{OH} (and ν_{OD}) bands with particular water molecules [1]. Criteria needed for these assignments are (1) intra and intermolecular coupling components split about their corresponding uncoupled bands, and (2) splitting is greater for OD than OH motion if coupling is intramolecular, with the reverse applying for intermolecular coupling [1]. Using these criteria, we can associate particular ν_{OH}'s with particular water molecules and so obtain the complete environment about each type of water molecule in a hydrate. In addition, the magnitudes of observed splittings can and have been used for obtaining valuable information about intra and intermolecular forces in hydrates [1].

Let us now illustrate the above points with specific examples drawn from infrared spectra of $NaCl{\cdot}2H_2O$, $NaBr{\cdot}2H_2O$, $CaSO_4{\cdot}2H_2O$ [5], $BaCl_2{\cdot}2H_2O$ [5], and their deutero-analogues.

The infrared spectrum of $NaCl{\cdot}2D_2O$ (containing ½% H_2O) contains four bands in its OH stretching region at −195 °C [1]. These appear at 3530, 3434, 3426 and 3416 cm^{-1}. Three of these merge into one at −78 °C. This reflects temperature broadening rather than a phase transition, as shown by additional spectral studies. The appearance of four bands indicates there are four different OH environments in this hydrate. Although no x-ray work has been performed on it, by analogy with the isomorphous $NaBr{\cdot}2H_2O$, we expect two types of water molecules to exist in $NaCl{\cdot}2H_2O$ with four physically different OH groups. The four uncoupled ν_{OH} bands confirm this and further indicate that of the two types of water molecules present, one is considerably distorted by its potential environment while the other is nearly undistorted. This is reasoned from one ν_{OH} band being considerably removed from the remaining three.

A study of coupling between ν_{OH}'s has revealed that the 3530 and 3416 cm^{-1} bands correspond to one molecule, (I), while the remaining two belong to the nearly undistorted one, (II) [1]. If we now assume only OH—Cl bonds, we predict O—Cl distances at −195° C to be [3]: Molecule (I), 3.26 and 3.35 Å (or less if bifurcated bonding): Molecule (II), 3.267 and 3.271 Å. Confirmation of these predictions must await a diffraction study of this hydrate.

The second example is that of $NaBr\,2H_2O$. An x-ray determination of this reveals there are three different O—Br distances, two of length 3.36 Å and one of 3.38 Å [6]. The infrared spectrum of 1¼ percent deuterated $NaBr\,2H_2O$ indicates there are four ν_{OD} bands appearing at 2608, 2544, 2532, and 2522 cm^{-1} at −195 °C. Again, as in the chloride hydrate, we predict two types of water molecules, one distorted and one nearly undistorted. The predicted O—Br distances are: Molecule (I), 3.40 and 3.49 Å (or less if bifurcated); Molecule (II), 3.41 and 3.42 Å. These agree reasonably well with Carpenter's values and suggest further analysis of the x-ray data to identify the environment about the weakly hydrogen-bonded OH group.

In our next example, gypsum, we see a clear illustration of the extreme sensitivity of this method relative to that of diffraction methods. A neutron diffraction analysis by Atoji and Rundle [7] indicates the single type of water molecule in gypsum forms linear OH—O bonds of length 2.816 ± 0.014 Å and 2.824 ± 0.015 Å. The small difference in bond lengths suggests the uncoupled ν_{OH} (and ν_{OD}) bands should fall very near one another in frequency. This is not realized experimentally. The ν_{OH} bands are found at 3411 and 3494 cm^{-1} at -195 °C (3405 and 3501 cm^{-1} at 33 °C) while ν_{OD} bands are observed at 2517 and 2574 cm^{-1} (-195 °C), and at 2516 and 2583 cm^{-1} (33 °C). The frequency separations are quite large, indicating the extreme sensitivity of the vibrations to small changes in environment. The small collapse in frequency on deuteration reveals the ν_{OH} bands do not originate in splittings due to the presence of a double minimum potential for proton motion.

As our final example, we consider the hydrate, $BaCl_2 \cdot 2H_2O$. The spectrum of a 5 percent deuterated sample of this, at -195 °C, shows four ν_{OD} bands appearing at 2440, 2447, 2465, and 2521 cm^{-1}; we obtain the same pattern as in $NaBr \cdot 2H_2O$, only with stronger hydrogen bonding evident: three OH's should be in similar environments with a fourth less strongly bound. This is in excellent agreement with neutron diffraction predictions on $BaCl_2 \cdot 2H_2O$ [8], made after the private communication of our infrared results. The three similar OH environments correspond to OH—Cl distances 3.130, 3.179, and 3.182 Å, all slightly nonlinear. The weaker bond is bifurcated, being highly nonlinear, with O—Cl distances, 3.302 and 3.238 Å.

References

[1] J. Schiffer, Ph. D. Thesis, Princeton University, 1963.
[2] K. Nakamoto, M. Margoshes and R. E. Rundle, J. Am. Chem. Soc. **77**, 6480 (1955).
[3] O. Glemser and E. Hartert, Naturwiss. **42**, 534 (1955).
[4] G. C. Pimentel and A. L. McClellan, The Hydrogen Bond, W. H. Freeman and Co., San Francisco, Calif., p. 90 (1960).
[5] Work performed by R. Kling, Temple University, 1967.
[6] W. R. Haaf and G. B. Carpenter, Acta Cryst. **17**, 730 (1964).
[7] M. Atoji and R. E. Rundle, J. Chem. Phys. **29**, 1306 (1958).
[8] W. R. Busing, private communication, 1962.

NUCLEAR MAGNETIC RESONANCE STUDIES OF MOLECULAR MOTION IN CLATHRATE HYDRATES

C. A. MCDOWELL and P. RAGHUNATHAN

Department of Chemistry,
University of British Columbia, Vancouver, British Columbia, Canada

Although the overall crystal structures of the clathrate hydrates are now well-known [1],[1] studies of the nature and extent of molecular motion undergone by the "guest" molecules inside their clathrate structures have been comparatively few [2–6]. A study of the nuclear magnetic resonance absorption of the guest species should be of particular advantage, since the hydrate frameworks provide selective isolation of the guest molecule. The use of magnetic resonance techniques for the study of motional processes in analogous structures has been demonstrated by Gilson and McDowell [7] and by Meyer et al. [8, 9]. A problem which often arises in the application of the NMR technique to most clathrate hydrates is that the guest molecule and the lattice alike contain proton spins, and computations of dipole-dipole interactions in such structures become complex. Isotopic substitution of the lattice protons using D_2O reduces these interactions considerably. Alternately, choosing a fluorocarbon molecule as "guest" in the hydrate host-structure simplifies the problem greatly since for such a case the F^{19} resonance may be studied.

In this report we shall summarize our results pertaining to the temperance-dependence of NMR line shapes and spin-lattice relaxation times for a variety of molecules enclathrated in hydrate structures. The results were obtained with a crossed-coil, wide line NMR spectrometer operated at 30MHz. The resonance line shapes were rationalized on the basis of precise calculations of theoretical second moments for various dynamical models of the guest molecules. These calculations consisted of "intra-guest" second moment contributions from a single host-lattice cavity as well as "interguest" contributions for all occupied cavities in the neighbourhood.

For convenience we shall divide the clathrates studied into four categories. In the first category may be placed the hydrates of CF_4 and SF_6. From F^{19} magnetic resonance line shapes we conclude that the guest molecules in these clathrates experience but little restriction from the walls of the host cavities, and freely reorient about a chosen axis of symmetry at low temperatures. Random motion sets in only at higher temperatures. Below 250 °K, spherically symmetric force fields are indicated inside the cavities of these crystal lattices. The guest molecules spend all their time reorienting in these cavities and translational motion appears to be quite hindered. For example, we have demonstrated by means of a rigorous second moment analysis that, at temperatures above 150 °K, SF_6 undergoes a very limited isotropic translational motion up to a distance of 0.5 Å from the centre of the clathration volume. In the limit of fully quantized reorientation, the dominant mechanism of relaxation of the fluorine spins would be expected to be a spin-rotation interaction [10, 11].

---

[1] Figures in brackets indicate the literature references at the end of this paper.

The hydrate of propane appears to belong to a category of clathrates in which the temperature-induced translational motion of guests is a maximum. Proton resonance of propane has been studied in two specimens of the deuterated hydrate, one of which was richer in guest content than the other. From the temperature-dependence of the line shapes of these specimens it has been suggested that, below 160 °K, propane assumes a staggered C_2-configuration inside the clathrate cavity. Reorientations about the molecular C_2-symmetry axis superimposed on methyl reorientations are thought to occur, and an activation energy barrier of 1.70 ± 0.08 kcal.mole^{-1} has been computed for the above composite motion from the proton spin-lattice relaxation times in the temperature range of 77–110 °K. Both adiabatic fast passage and progressive signal saturation methods were used for measuring the relaxation times, and the results obtained by the two techniques were in excellent agreement. Closer to the melting point of the clathrate, diffusion of propane through the host lattice is indicated. Diffusional activation energies of 1.40 ± 0.02 kcal.mole^{-1} and 0.75 ± 0.05 kcal/mole have been obtained for the guest-rich and guest-deficient clathrates, respectively.

Somewhat different results were observed for the three monohalomethane hydrates, CH_3X ($X = Cl, Br, I$). For these clathrates, which make up the third category, our low-temperature proton resonance studies indicate that there are definite constraints to the reorientational and translational motion of the guest molecules. Experimental second moment data obtained at 77 °K for the monochloro- and monoiodomethane clathrates show evidence for only low-amplitude oscillatory motions of the CH_3 groups. For the monobromomethane clathrate, a triplet line shape has been observed at 77 °K which indicates some alignment of the guest molecules. At higher temperature it is presumed that the hydrate lattice expands to permit free reorientations about the C_3 axis of the CH_3 groups of the three guest molecules. From the associated linewidth transitions, values of 2.48 ± 0.32, 9.30 ± 0.25, and 6.80 ± 0.50 kcal/mole^{-1} have been calculated for the activation energy barrier hindering methyl reorientation in the CH_3Cl–, CH_3Br–, and CH_3I hydrates, respectively. The motional model proposed for the higher temperature range is adequately supported by measurements of the proton spin-lattice relaxation times.

The clathrate hydrates of the two dihalomethanes, CH_2Cl_2 and CH_2F_2, may be placed in the fourth and last category, where all motional effects which could affect the absorption line shape were virtually absent below 90 °K. For the dichloromethane clathrate hydrate, a clearly resolved doublet characteristic of rigidly aligned proton pairs has been obtained at 77 °K. This doublet has been analyzed by means of an IBM 7040 computer program to yield an H–H distance of 1.73 ± 0.04 Å for the "guest" dichloromethane molecule. The F^{19} resonance line of the CH_2F_2-clathrate was very broad but possessed no structure, presumably owing to a strong broadening by H^1–F^{19} intramolecular dipolar interaction. Analysis of this line shape gave a value of 2.14 ± 0.04 Å for the F–F distance in a CH_2F_2 "guest" molecule

The general trend of our results indicates that, at least in specific cases, refinements to the currently existent approximations of "spherically-symmetric" host cages are necessary. Indeed, in extreme cases of tight-fitting guest molecules, it is even possible to envision the heretofore neglected "exchange interactions" arising from the overlap of the electronic wave functions of the guest molecules with peripheral orbitals of host-lattice oxygens. Alternately, a low-temperature contraction of host lattices of such clathrates in the direction of non-cubic symmetry is another distinct possibility, and low-temperature x-ray crystal structure studies of such hydrates should be of interest. One might recall in this context that earlier work on quinol clathrates of large molecules (e.g., SO_2, CH_3CN) has led to the proposal of distorted host-lattice cavities.[12]

We thank the National Research Council of Canada for their generous support of this work.

References

[1] G. A. Jeffrey, Dechema-Monographien **47,** 849 (1962).
[2] G. J. Wilson and D. W. Davidson, Can. J. Chem. **41,** 264 (1963).
[3] V. McKoy and O. Sinanoglu, J. Chem. Phys. **38,** 2846 (1963).
[4] D. W. Davidson, M. M. Davies and K. Williams, J. Chem. Phys. **40,** 3449 (1964).
[5] K. B. Harvey, F. R. McCourt and H. F. Shurvell, Can. J. Chem. **42,** 960 (1964).
[6] S. Brownstein, D. W. Davidson and D. Fiat, J. Chem. Phys. **46,** 1454 (1967).
[7] D. F. R. Gilson and C. A. McDowell, Mol. Phys. **4,** 125 (1961).
[8] H. Meyer and T. A. Scott, J. Phys. Chem. Solids **11,** 215 (1959).
[9] S. Foner, H. Meyer and W. H. Kleiner, J. Phys. Chem. Solids **18,** 273 (1961).
[10] W. R. Hacklemann and P. S. Hubbard, J. Chem. Phys. **39,** 2688 (1963).
[11] P. S. Hubbard, Phys. Rev., **131,** 1155 (1963).
[12] L. A. K. Staveley in Non-stoichiometric Compounds, Ch. 50, Ed. L. Mandelcorn (Academic Press, Inc., 1964).

CALCULATION AND ANALYSIS OF PULSED-NMR LINE SHAPES OF CRYSTALS[1]

MARCEL KOPP[2]

One may calculate the absorption spectrum of a spin system by diagonalizing its Hamiltonian; but for a crystal of spins ½ (strictly dipolar broadening) the large number of spins to be considered makes the matrices untractable. One can, however, calculate the Fourier-transform of the spectrum, the decay of the free precession signal, which is the response of the system to a powerful pulse of resonant frequency. The method [1, 2][3] was successful for reproducing the shapes of fluorite (CaF_2), a simple-cubic lattice of spins where drastic simplifications are permitted [1]. We have applied the formulae of Lowe and Norberg [1] (LN) and of Evans and Powles [2] (EP) to lattices containing up to 81 spins where no symmetry is required, but the computation time is accordingly increased. The early decays coincide for both formulations; however, the later behavior diverges for LN (without additional farther-neighbor attenuation) but converges for EP. In the latter case, a Fourier transformation to the absorption shape is successful.

Deductions about the molecular shape are often drawn from the second moment of the absorption line and from its doublet splitting if it occurs. Information may also be derived from their Fourier transforms, the second derivative of the precession decay at its time origin, and the first zero of the oscillating decay, respectively. However, it is difficult to extract detailed structural information from spectral moments. Even peak-to-peak splittings are not relevant, but rather the center-of-gravity splitting, or first moment of the shape [3]. Similarly, the first zero t'_{0F} of the decay shape $F(t)$ is not relevant and one must deduce the zero t'_{0U} of the first term $U(t)$ of the LN-series or EP-Dyson expansion. The difference $t'_{0F}-t'_{0U}\equiv\Delta t'_0$ can be computed from lattice parameters using either expansion (since only the early decay is involved), and variations of the parameters has but little effect on $\Delta t'_0$. The relevant splitting is then

$$S_{jk}=\frac{\pi}{2}/t'_{0U}\propto(1-3\cos^2\theta_{jk})/r^3{}_{jk}.$$

---

[1] Work performed while the author was a visitor with the Department of Physics, University of Pittsburgh (1965–1966), where hospitality is gratefully acknowledged. The computation costs, at the Centers of the University and of Mellon Institute, were covered by the National Science Foundation.

[2] Present Address: Mellon Institute, Pittsburgh, Pennsylvania 15213.

[3] Figures in brackets indicate the literature references at the end of this paper.

Knowing the angle θ_{jk}, between the spin-spin vector and the field $\mathbf{B}_o$, one can extract the spin-spin distance r_{jk}, or vice-versa.

The precision of broad-line absorption spectroscopy is impaired by the necessarily large field modulation, and often by a slow spin-lattice relaxation. Pulse spectroscopy is free from these handicaps, but the observed trace decay $V(t)$ must be corrected to the decay shape $F(t)$ because of delays characteristic of the receiver circuit and coherent detector [4]. The correction is simple, but still the early decay shape (where all spectral moments are contained) is obscured by an instrumental blocking time. The available corrected decay shape must therefore be extrapolated to time origin. A convolution analysis (decomposing the decay as a product of simple functions) was suggested by Abragam [5], and applied to some well-behaved shapes in order to deduce second moments [6]. But, in general, the fit of an even polymonial of high degree (e.g., 20th) to the available decay up to about the second zero is more appropriate and successful. Once the decay shape is completed to time origin, it can be Fourier-transformed into the absorption shape. We have thus analyzed numerically the experimental decay shapes of Barnaal [7] for fluorite and ice.

The particular line shape for $B_o \parallel c$-axis in ice is of special interest because all six intramolecular doublets then merge into one. The first zero is found at $T'_{oF}=11.4\pm0.3$ μsec. The difference $\Delta t'_o=1.5$ μsec. is measured on the computed shapes. (Averages taken over the 6 non-equivalent molecular orientations and the 18 configurations of the molecule and its six nearest protons, surrounded by 45 other protons in randomly-chosen but hydrogen-bonding arrangements.) The effects of molecular vibrations and librations on the first-neighbor splittings are discussed to nearly cancel each other to -1.5 percent on S_{jk}, but to appreciably *reduce* the second-neighbor splittings. The zero of $u(t)$ can thus be located at $t'_{oU}=12.3\pm0.3$ μsec *or less*. This yields for the intramolecular HH distance the value (1.635 ∓ 0.015) Å *or less*, which is somewhat smaller than the distance 1.65 Å expected from a tetrahedral HOH angle (with OH=1.01 Å as determined by neutron diffraction at D_2O[8]).

The aim of the present study was to determine what structural information can be derived about the intra- and inter-molecular configurations in ice from its n.m.r. line shapes. The methods were tested on fluorite, a simple-cubic spin lattice, and on gypsum and hydrogen sulphide, simple hydrates, and may be applied to other suitable hydrates or molecular crystals.

References

[1] I. J. Lowe and R. E. Norberg, Phys. Rev., **107,** 46 (1957).
S. Clough and I. R. McDonald, Proc. Phys. Soc., **86,** 833 (1965).
S. Gade and I. J. Lowe, Phys. Rev., **148,** 382 (1966).

[2] W. A. B. Evans and J. G. Powles, Phys. Letters **24A,** 218 (1967).

[3] B. Pedersen and D. F. Holcomb, J. Chem. Phys., **38,** 61 (1963).

[4] D. E. Barnaal and I. J. Lowe, Rev. Sci. Instr., **37,** 428 (1966).
See also, J. G. Powles and J. H. Strange, Proc. Phys. Soc. **82,** 6 (1963); J. Jeener and P. Broekaest, Phys. Rev. **157,** 232 (1967).

[5] A. Abragam, The Principles of Nuclear Magnetism (Clarendon, 1961), p. 120.

[6] D. C. Look, I. J. Lowe, and J. A. Northby, J. Chem. Phys., **44,** 3441 (1966)
D. E. Barnaal and I. J. Lowe, Phys. Rev., **148,** 328 (1966), J. Chem. Phys., **46,** 4800 (1967).

[7] D. E. Barnaal, Thesis, Univ. of Minnesota (1965), Univ. Microfilm #65–7867, and Ref. 6.

[8] S. W. Peterson and H. A. Levy, Acta Cryst., **10,** 70, 344 (1957). R. Chidambaram, Acta Cryst., **14,** 467 (1961)

THE VAPOR PRESSURE OF CO/N_2 SOLID SOLUTIONS

J. A. MORRISON, D. M. T. NEWSHAM,[1] AND R. D. WEIR[1]

Division of Pure Chemistry
National Research Council of Canada, Ottawa, Canada

1. Introductory Remarks

This investigation continues previous work [1][2] in which some thermodynamic properties of condensed CO (accidentally containing about 2.6 percent N_2) were measured. Deviations from the properties of pure CO were used to make some deductions about the behavior of the solution of N_2 in CO in the region of the λ-type transition that occurs in the pure substances and in the solutions [2]. Because of the close similarity of N_2 to CO with respect to mass, molecular properties [3] and crystal structure, substitution of N_2 into the CO lattice does not perturb the solid too severely. By contrast, for some other molecular crystals, it has been found that drastic changes in the shape of the λ-transitions are produced by diluting the crystal lattice with molecules of similar volume but different mass. For example, the well-known λ-transition that occurs in solid CH_4 at about 20.4 °K disappears when Kr in excess of 16 mole percent is added [4].

In this brief report, we are concerned only with vapor pressures of the solutions; no other thermodynamic properties have been measured. Two different measuring techniques have been used with the same apparatus. The second technique was developed to circumvent difficulties encountered in the attainment of equilibrium in the solutions in the region $T<0.9T$ (melting point).

2. Experimental Method

The vapor pressure cell and cryostat were constructed in the form of a simplified adiabatic calorimeter assembly of the type widely used to measure the thermodynamic properties of condensible substances at low temperatures. The cell was a thick-walled copper cylinder (2.5 cm dia. x 7.5 cm long) with an internal volume of 2.5 cm^3. It carried a heater wound on the outer surface and a capsule-type platinum resistance thermometer set into a re-entrant well with Wood's metal. A German silver tube (1 mm. outer dia., 0.1 mm wall-thickness) that carried a close-wound heater over its entire length in the cryostat connected the cell with a gas-handling system on the outside. The cell and surrounding adiabatic shield were hung in a vacuum space and connected by difference thermocouples in the usual way.

---

[1] National Research Council of Canada postdoctoral fellow.

[2] Figures in brackets indicate the literature references at the end of this paper.

Pressures were determined to a precision of ±0.005 mm with a fused quartz Bourdon gage (Model 140, Texas Instruments Inc.). The manufacturer's calibration was checked by comparing the gage with a mercury manometer; some significant deviations were found. The zero point of the gage showed no detectable shift with continuous use over the pressure range 0 to 250 mm.

The CO and N_2 used in the experiments were of so-called spectroscopic purity. The main impurities were found in the CO: up to 680 p.p.m. CO_2 and 268 p.p.m. He. An attempt was made to reduce the latter by a crude distillation before the CO specimen was put in the vapor pressure cell.

3. Experimental Results

The vapor pressure measurements on pure CO condensed in the cell were straightforward and reproducible at all temperatures to within the precision of the pressure gage. Moreover, the triple point and transition point temperatures and pressures agreed with those in the literature [5, 6] within their assigned accuracies. From a plot of log P against $\frac{1}{T}$ for the α and β solid phases, the enthalpy change of the transition was estimated to be 162 ± 11 cal/mole, in reasonable agreement with calorimetric results [1, 5].

The behavior of the solutions was different. Long equilibrium times were observed and, as a consequence, the vapor pressures were not reproducible at the lower temperatures, within the precision of the measuring gage. It was found possible to achieve equilibrium in the β-phase just below the melting point in about five hours. If it is assumed that equilibrium is achieved by diffusion and that the activation energy is of the magnitude of the heat of sublimation, then the estimated equilibrium time at 50 °K would be about a month—a clearly impracticable time interval.

As a result of these findings with a bulk solid phase ($\sim$2 cm^3 of solid solution), a second technique for measuring the vapor pressures was tried and found to be successful. It was a variation of a dew-point method in which vapor in the cell was compressed by decreasing the external volume until a very small amount ($\sim 10^{-4}$ cm^3) of solid formed. The pressure corresponding to an infinitesimal amount of solid, in equilibrium with its vapor, was obtained from the point at which the rate of change of pressure with volume altered abruptly. Vapor pressures of the solutions were determined in this way with a reproducibility better than ±0.05 mm for pressures exceeding 10 mm.

Preliminary analyses of the latter data indicate that solutions of N_2 in CO at concentrations of 20 percent or less behave nearly ideally. For example, if the data are plotted on a reduced scale ($\log(P/P_\lambda)$ versus T_λ/T), the curves for the solutions and pure CO are nearly coincident. Earlier conclusions that gross departures from a regular solution model occurred in the α-phase [7] appear now to have been due to the fact that equilibrium was not achieved with a bulk specimen. A more detailed account of the work has since been published [8].

4. Conclusions

The main conclusion to be drawn is that the thermodynamic properties of solid solutions can only be measured practically in the region $T<0.9T$ (melting point) if an infinitesimal amount of solid is present. This essentially rules out calorimetric measurements that require gross specimens.

The vapor pressure data obtained in this work should provide a rigorous test for discussing the various theories of solutions that are available. This is not the case for liquids because the detailed microscopic structure of the solution is not known. It is perhaps surprising that so much experimental emphasis has been placed on liquid solutions.

One conclusion that can be drawn from the present work is that the transitions in CO and N_2 occur for the same physical reason since the solutions show almost the same thermodynamic behavior as the pure components when they are considered on a reduced basis.

5. References

[1] E. K. Gill and J. A. Morrison, J. Chem. Phys. **45,** 1585 (1966).
[2] M. J. Angwin and J. Wasserman, J. Chem. Phys. **44,** 417 (1966).
[3] L. A. K. Staveley, J. Phys. Chem. Solids **18,** 46 (1961).
[4] A. Eucken and H. Veith, Z. Physik Chem. **38B,** 393 (1938).
[5] J. O. Clayton and W. F. Giauque, J. Amer. Chem. Soc. **54,** 2610 (1932).
[6] A. G. Duncan and L. A. K. Staveley, Trans. Farad. Soc. **62,** 548 (1966).
[7] See figure 5 of reference [1].
[8] J. A. Morrison, D. M. J. Newsham, and R. D. Weir, Trans. Farad. Soc. **64,** 1461 (1968).

STRUCTURAL STUDY OF Ti_5O_9

L. K. KEYS [1]

Materials Research Laboratory Pennsylvania State University, University Park, Pennsylvania 16802

The crystal structure of Ti_5O_9 has been characterized by x-ray diffraction studies by Anderson [1].[2] It was found that the structure can be described as being built up of rutile-type elements, with a complicated arrangement of the metal atoms in the interstitial positions of the lattice formed by the packing of the anions. More explicitly the crystal structure of Ti_5O_9 is triclinic, with a space group P1 and unit cell constants given as: $a=5.569$ Å, $b=7.120$ Å, $c=8.865$ Å, $\alpha=97.55°$, $\beta=112.34°$, and $\gamma=108.50°$. There are 2 Ti_5O_9 per unit cell [1]. The structure is believed to to be formed from TiO_6-octahedra which are arranged in slabs of rutile structure (sharing edges and corners) of finite height of five such octahedra. The height of the rutile slabs is limited (or bounded) by the formation of shear chains or stacking faults. Across the faults these slabs share octahedral faces, and this results in a close metal-metal distance (2.81 Å) between cations occupying these face-sharing octahedra. This close distance has led to the postulation of a metal-metal bond forming between the cations occupying these octahedra [2, 3]. Such effects have also been described in other metal oxides [4].

The five-octahedral width slab can be considered to have a cation arrangement of the form $Ti^{3+}-Ti^{4+}-Ti^{4+}-Ti^{4+}-Ti^{3+}$ [3]. The bond would then form between the Ti^{3+} cations in the face-sharing octahedra at the boundaries of the slab. Magnetic susceptibility studies should be able to confirm this structure as some evidence should appear for the cation-cation interactions [5].

The magnetic susceptibility study of Ti_5O_9 has actually shown it to resemble antiferromagnetic behavior [6] as indicated by figure 1. The magnetic susceptibility shows a complex dependence on the inverse of the temperature above the indicated Néel temperature. The apparent Néel temperature observed for this phase occurs at about 130 °K. This can be interpreted as confirming a moderate exchange interaction occurring between the face-sharing TiO_6–octahedra.

---

[1] Present Address: Nuclear Systems Programs, General Electric Company, Cincinnati, Ohio 45215.

[2] Figures in brackets indicate the literature references at the end of this paper.

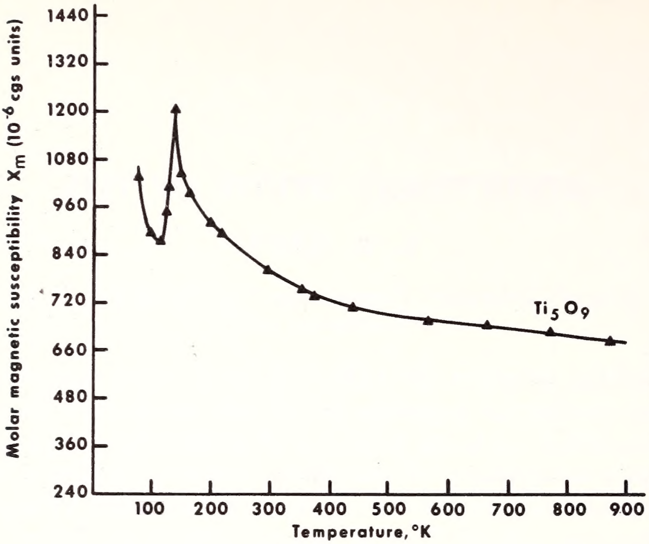

FIGURE 1. Molar magnetic susceptibility of Ti_5O_9 as a function of temperature.

With this antiferromagnetic-like behavior it would be expected that some evidence should also be found for such a transition via electron-spin-resonance measurement. The result of electron-spin-resonance study from 77 °K to ~160 °K indicates a narrow peak with a *g*-value of 1.98 ± 0.02. As the temperature was varied from ~120 °K to 160 °K, the signal intensity decreased rapidly and the line width broadened sharply as shown in figure 2.

These effects may result from electrons which are localized becoming delocalized as well as from the effects of the apparent antiferromagnetism. The delocalized electrons have shorter relaxation times and thus may contribute to the broadening. The low temperature asymmetric spectra becomes symmetric at high temperatures as shown in figure 3. The asymmetry parameter is defined as A/B where A is the peak height of the first derivative of the absorption peak above the base line, and B is the depth of the peak below the base line. This change in symmetry may reflect the effects of the antiferromagnetic interaction and/or electron delocalization; however, this is not certain.

The magnetic susceptibility thus appears to confirm the existence of the cation-cation interactions expected for such a shear structure. The electron-spin-resonance study indicates an anomalous behavior which is probably related to the effects of the stacking fault; however, its interpretation is not as clearly evident.

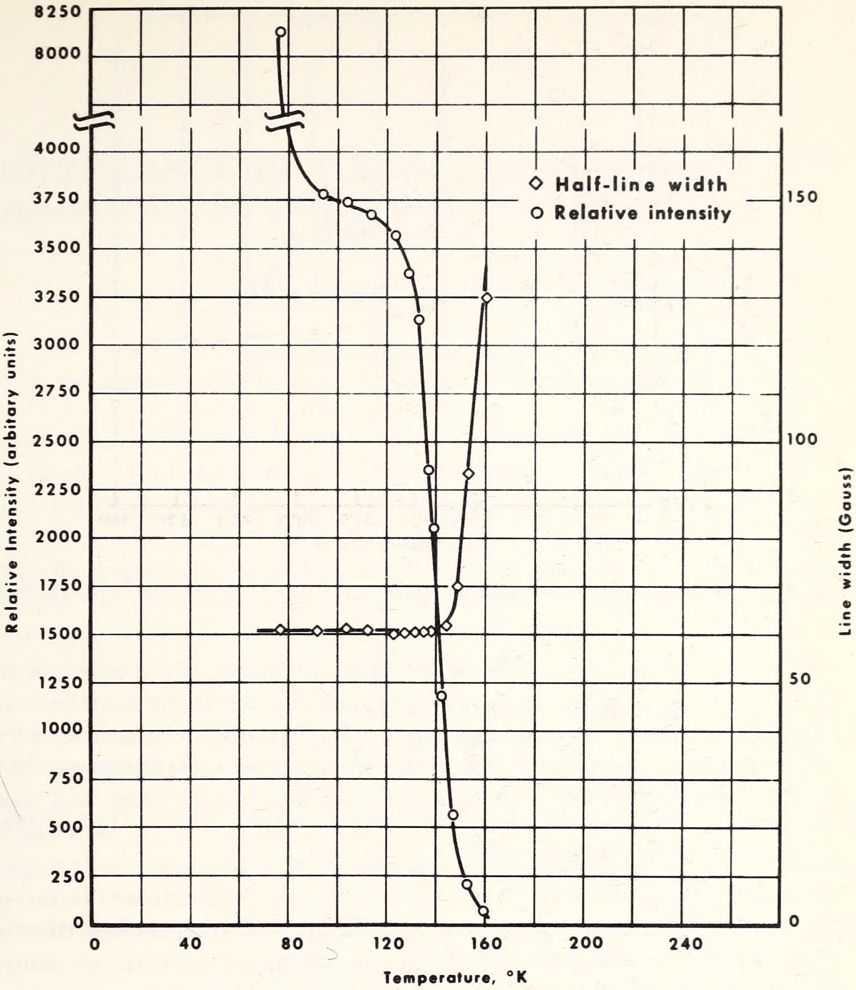

FIGURE 2. Dependence of the relative intensity of the electron-spin-resonance spectra and half-line width on temperature.

These studies were supported by the United States Atomic Energy Commission by a grant, USAEC [Contract AT(30–1)–2851], to the Materials Research Laboratory of the Pennsylvania State University and were initiated by Dr. L. N. Mulay. The author is grateful to the above for their support, and especially to Dr. L. N. Mulay for his guidance and encouragement throughout these studies. The cooperation of the Nuclear Systems Programs of the General Electric Company and Dr. J. Moteff is also acknowledged.

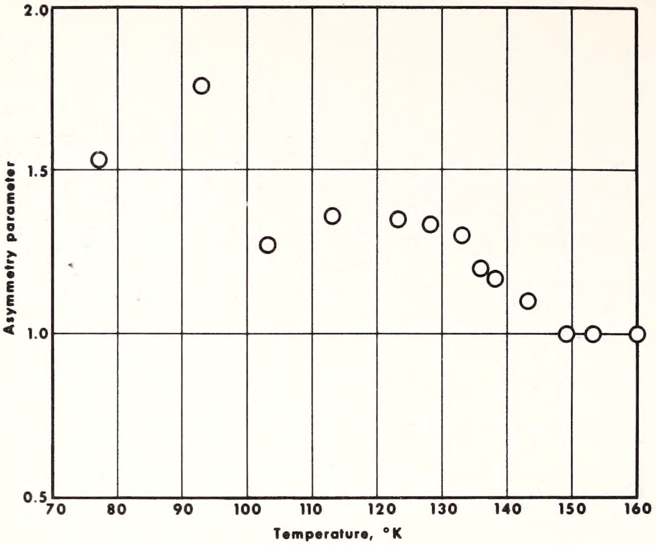

FIGURE 3. Variation of the asymmetry parameter (*A*/*B*) with the temperature.

References

[1] S. Anderson, Acta Chem. Scand. **14,** 1161 (1960).

[2] B. Marinder and A. Magneli, Acta Chem. Scand. **11,** 1635 (1957).

[3] J. B. Goodenough, Magnetism and the Chemical Bond, Interscience Publishers Inc., New York, New York, p. 272 (1963).

[4] L. Pauling, The Nature of the Chemical Bond, 3rd Ed., Cornell Univ. Press, Ithaca, New York, p. 437 (1960).

[5] P. W. Selwood, Magnetochemistry, 2nd Ed., Interscience Pub., New York, New York (1956).

[6] L. K. Keys, International Congress on Magnetism, Boston, Massachusetts, September 11, 1967, Paper BF–6.

SIGNIFICANCE OF WEIGHTING SCHEMES IN AN ANISOTROPIC LEAST SQUARES REFINEMENT OF RUBY

J. W. McCAULEY[1] **and G. V. GIBBS**[2]

Materials Research Laboratory
Pennsylvania State University, University Park, Pennsylvania 16802

The structural and vibrational parameters of a ruby synthesized by Barks, [1][3] containing 5.2 mole percent Cr_2O_3 (a=4.770(1), c=13.020(5) Å) were refined by least-squares and Fourier methods employing 3D counter diffractometer intensity data. A study of the crystal's diffraction symmetry and intensity data reveal that $R\bar{3}c$ and $R\bar{3}$ are the most probable alternate space groups. Two anisotropic least-squares refinements, one using 197 non-equivalent intensities in $R\bar{3}$ and the other using 66 symmetry combined intensities in $R\bar{3}c$, resulted in a weighted R-factor (Cruickshank's weighting scheme [4]) of 6.7 percent for $R\bar{3}c$ and 11.2 percent for $R\bar{3}$. These results suggest that the crystal possesses space group symmetry $R\bar{3}c$ which necessitates that the Cr and the Al atoms be randomly distributed in the cation sites.

The effect of various absolute and relative weighting schemes on the final parameters was subsequently examined in several least-squares refinements using the 66 intensities consistent with $R\bar{3}c$ symmetry. Absolute weights corresponding to systematic and anisotropic errors inherent in the intensity measurement [2] were estimated in two ways: (1) from the standard deviation of averaged symmetry equivalent reflections and (2) from the range estimate [3]. Relative weights were estimated from empirical expressions suggested by Cruickshank [4] and by Hanson [5] and from the least-squares derivation of standard deviations from the assumed linear relationship between the calculated standard deviations and the observed absolute amplitudes. Unitary weights were also utilized in a refinement.

The final positional and vibrational parameters calculated in the refinements using the above weighting schemes are listed in table 1. All the positional parameters are statistically identical and do not significantly differ from those obtained for corundum by Newnham

---

[1] Now at the Army Materials and Mechanics Research Center, Watertown, Mass.

[2] Now at the Department of Geological Sciences, Virginia Polytechnic Institute, Blacksburg, Virginia.

[3] Figures in brackets indicated the literature references at the end of this paper.

TABLE 1.—RESULTS OF REFINEMENTS EMPLOYING VARIOUS WEIGHTING SCHEMES IN $R\bar{3}c$

Parameter	Standard deviation		Range estimate		Least squares wts.		Cruick-shank wts.		Hanson wts.		Unitary wts.	
	Value	σ	Value	σ	Value	σ	Value	σ	Value	σ	Value	σ
Scale Factor	0. 1427	0. 0026	0. 1431	0. 0024	0. 1518	0. 0040	0. 1486	0. 0031	0. 1518	0. 0031	0. 1416	0. 0022
Oxygen: x	0. 3068	0. 0005	0. 3071	0. 0004	0. 3069	0. 0006	0. 3069	0. 0006	0. 3073	0. 0007	0. 3062	0. 0011
β_{11}	0. 0096	0. 0012	0. 0097	0. 0010	0. 0054	0. 0007	0. 0046	0. 0010	0. 0048	0. 0015	0. 0043	0. 0020
β_{22}	0. 0121	0. 0012	0. 0110	0. 0012	0. 0064	0. 0014	0. 0061	0. 0016	0. 0062	0. 0019	0. 0064	0. 0027
β_{33}	0. 0006	0. 0002	0. 0006	0. 0002	0. 0019	0. 0003	0. 0016	0. 0003	0. 0019	0. 0003	0. 0011	0. 0004
β_{12}	0. 0060	0. 0006	0. 0055	0. 0006	0. 0032	0. 0007	0. 0031	0. 0008	0. 0031	0. 0009	0. 0032	0. 0013
β_{13}	0. 0003	0. 0001	0. 0002	0. 0001	0. 0017	0. 0001	0. 0001	0. 0002	0. 00006	0. 0003	0. 00005	0. 0003
β_{23}	0. 0005	0. 0003	0. 0004	0. 0002	0. 0003	0. 0002	0. 0002	0. 0003	0. 0001	0. 0005	0. 0001	0. 0007
Equiv. B	0. 613	0. 067	0. 597	0. 068	0. 690	0. 086	0. 604	0. 093	0. 669	0. 104	0. 477	0. 147
Al-Cr: z	0. 3519	0. 0001	0. 3519	0. 0001	0. 3520	0. 0001	0. 3519	0. 0001	0. 3516	0. 0002	0. 3519	0. 0002
β_{11}	0. 0073	0. 0013	0. 0072	0. 0012	0. 0071	0. 0018	0. 0049	0. 0016	0. 0050	0. 0016	0. 0024	0. 0016
β_{22}	0. 0073	0. 0013	0. 0072	0. 0012	0. 0071	0. 0018	0. 0049	0. 0016	0. 0050	0. 0016	0. 0024	0. 0016
β_{33}	0. 0009	0. 0003	0. 0010	0. 0002	0. 0018	0. 0003	0. 0017	0. 0003	0. 0019	0. 0002	0. 0012	0. 0002
β_{12}	0. 0036	0. 0006	0. 0036	0. 0006	0. 0035	0. 0009	0. 0025	0. 0008	0. 0025	0. 0008	0. 0012	0. 0008
β_{13}	0. 0	------	0. 0	------	0. 0	------	0. 0	------	0. 0	------	0. 0	------
β_{23}	0. 0	------	0. 0	------	0. 0	------	0. 0	------	0. 0	------	0. 0	------
Equiv. B	0. 544	0. 083	0. 554	0. 071	0. 732	0. 106	0. 601	0. 095	0. 657	0. 086	0. 386	0. 089
$\left[\frac{\Sigma w(F_o-F_c)^2}{m-n}\right]^{1/2}$	1. 319	------	1. 001	------	0. 655	------	0. 121	------	0. 231	------	0. 413	------
Weighted R	2. 6%	------	4. 1%	------	7. 5%	------	6. 7%	------	6. 0%	------	5. 8%	------

and De Haan [6]. There are, however, significant differences between the refined anisotropic temperature factors.

The magnitude and orientation of the principal axes of the atomic vibration ellipsoids calculated from the data of the various refinements utilizing the OR–FFE program of Busing, Martin and Levy [7] are listed in table 2. There are significant variations among the data; however, it appears that the vibrational data derived from the absolute weight refinements are the most plausible physically, based on the assumption that an atom will vibrate less in a smaller void than in a larger one.

Figure 1 is a stereographic projection showing the angular relationships between the principal axes of vibration (V_j) of the oxygen ion and the tetrahedrally coordinating cations (R_i) for the absolute weight data. Note that the smallest vibration direction ($V_1 = 0.07(1)$ Å)

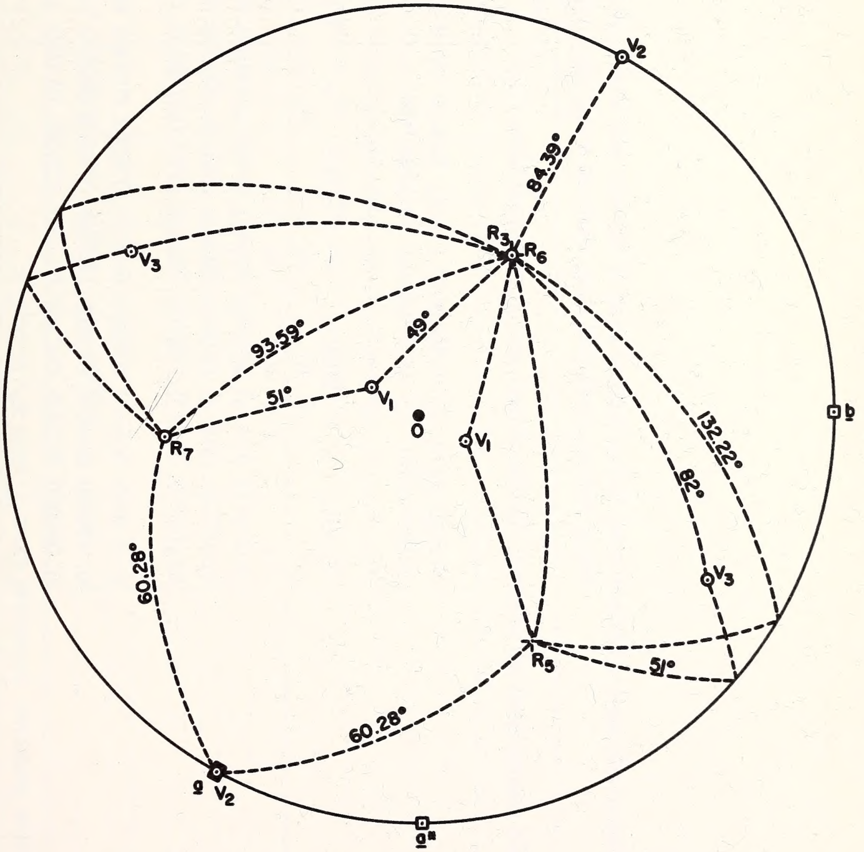

FIGURE 1. Stereographic projection of principal axes of vibration (V_j) and tetrahedrally coordinating cations (R_i) of oxygen (0).

Table 2. Magnitude and orientation of the principal axes of the oxygen and cation (Al,Cr) vibration ellipsoids calculated from refinements utilizing various weighting schemes

(a) RMS component of thermal displacement along principal axes (V_j).

	Standard deviation		Range estimate		Least sq. wts.		Cruickshank wts.		Hanson wts.		Unitary wts.	
	RMS	σ	RMS	σ	RMS	σ	RMS	σ	RMS	σ	RMS	σ
Oxygen V_1	0. 0701	0. 011	0. 0693	0. 0098	0. 0662	0. 0039	0. 0591	0. 0093	0. 0609	0. 016	0. 0562	0. 023
V_2	0. 0873	0. 008	0. 0895	0. 0068	0. 0639	0. 0083	0. 0726	0. 0096	0. 0731	0. 011	0. 0745	0. 016
V_3	0. 1038	0. 0057	0. 0986	0. 0055	0. 1276	0. 0101	0. 1191	0. 0110	0. 1277	0. 011	0. 0970	0. 019
Al–Cr V_1	0. 0793	0. 0069	0. 0786	0. 0063	0. 0782	0. 0104	0. 0653	0. 0098	0. 0656	0. 010	0. 0457	0. 015
V_2	0. 0793	0. 0069	0. 0786	0. 0081	0. 0782	0. 0099	0. 0653	0. 0120	0. 0656	0. 010	0. 0457	0. 015
V_3	0. 0898	0. 0126	0. 0919	0. 0110	0. 1235	0. 0110	0. 1197	0. 0096	0. 1264	0. 008	0. 1024	0. 0097

(b) Angles between principal axes V_j and **a***, **b**, and **c**.

	Axis	Angle	σ	Angle	σ	Angle	σ	Angle	σ	Angle	σ	Angle	σ
Oxygen V_1	**a***	97. 09	3. 22	96. 31	3. 45	30. 00	----	30. 00	----	30. 00	----	30. 00	----
V_1	**b**	102. 34	5. 66	100. 97	6. 06	120. 00	----	120. 00	----	120. 00	----	120. 00	----
V_1	**c**	14. 29	6. 59	12. 70	7. 04	90. 00	----	90. 00	----	90. 00	----	90. 00	----
V_2	**a***	150. 00	----	150. 00	----	119. 88	0. 22	119. 92	0. 27	119. 99	0. 11	119. 92	1. 14
V_2	**b**	60. 00	----	60. 00	----	149. 63	0. 55	149. 76	0. 79	149. 96	0. 37	149. 77	3. 39
V_2	**c**	90. 00	----	90. 00	----	85. 01	3. 81	86. 00	6. 5	88. 41	7. 25	86. 10	27. 97
V_3	**a***	61. 02	0. 93	60. 81	0. 88	87. 51	1. 90	88. 00	3. 24	89. 20	3. 62	88. 05	13. 96
V_3	**b**	32. 94	2. 60	32. 34	2. 52	85. 68	3. 30	86. 53	5. 63	88. 62	6. 27	86. 62	24. 21
V_3	**c**	75. 72	6. 60	77. 30	7. 04	4. 99	3. 82	4. 01	6. 50	1. 59	7. 25	3. 91	27. 96
Al-Cr		V_3 parallel to **c** V_1, V_2 perpendicular to **c**											

almost bisects the angles R_7–O–R_3 and R_6–O–R_5, both at 93.59(3)°; the intermediate vibration direction ($V_2=0.087(8)$Å) bisects the angles R_7–O–R_5 at 120.5(1)° and R_3–O–R_6 at 84.4(1)°, the mean being 102.47°; and the maximum vibration direction ($V_3=0.104(6)$Å) bisects approximately the angles R_5–O–R_3 and R_7–O–R_6, both at 132.22(5)°.

In sum, then, the absolute weight data suggest that the vibrational anisotropy of the oxygen ion is controlled by the coordinating cations and, furthermore, that the cation (Al–Cr) is vibrationally isotropic and not anisotropic as indicated by the data from the relative weight refinements. This latter conclusion indicates that if cation-cation orbital overlap is exhibited by apparent cation anisotropic vibration then there seems to be no overlap present in this structure.

It is apparent from the preceding analysis that weighting schemes must not be used indiscriminately in least-squares refinements if physicially meaningful information regarding anisotropic vibrational states of atoms is desired. Any relative scheme which weights the data according to an empirical function of the magnitude of the Fo values, regardless of which Fo is the most precise, must in fact erroneously bias the temperature factor calculation.

We would like to thank Dr. R. E. Newnham and Dr. E. P. Meagher for many helpful suggestions. This work was supported by ARPA grants SD–132 and DA–49–083 OSA–3140.

References

[1] R. E. Barks, Flux growth of single crystal R_2O_3 oxides with the corundum structure: Ph. D. thesis in Geochemistry, The Pennsylvania State University (1966).
[2] S. C. Abrahams, Acta Cryst., **17**, 1327–1328 (1964).
[3] J. A. Ibers, Acta Cryst., **9**, 652–654 (1956).
[4] D. W. J. Cruickshank, "Computing Methods in Crystallography," edited by J. S. Rollet, pages 112–116 Pergamon Press, New York, (1965).
[5] A. W. Hanson, Acta Cryst., **19**, 19–26 (1965).
[6] R. E. Newnham and Y. De Haan, Zeit. Krist., **117**, 235–237 (1962).
[7] W. R. Busing, K. O. Martin, and H. A. Levy, OR–FLS, A fortran crystallographic least-squares program: ORNL–TN–305, Oak Ridge, Tennessee (1962). W. R. Busing, K. O. Martin, and H. A. Levy, OR–FFE, A fortran crystallographic function and error program: ORNL, Oak Ridge, Tennessee (1964).

THE CRYSTAL STRUCTURE OF $C_8Al_{2.1}B_{51}(AlB_{10})$

A. J. PERROTTA, W. D. TOWNES, and J. A. POTENZA

Institute for Exploratory Research
U.S. Army Electronics Command, Fort Monmouth, New Jersey 07703

Of the higher aluminum borides, only the structure of AlB_{10} has been reported. Three stoichiometries, AlB_{10} ($Z=5.2$) [1, 2],[1] C_4AlB_{24} ($Z=2$) [3] and C_4AlB_{26} ($Z=2$) [4] have been proposed, the major uncertainties being the presence of carbon and the role it plays in the structure. In addition, questions regarding the orientation of B_{12} icosahedra [2, 3] and the nature of intericosahedral atoms [2, 4] have emerged. The present study gives the first detailed structure report of this interesting boride.

Cell parameters [1] are C2/m2/c21/m; $a=5.690\pm0.001$, $b=8.810\pm0.001$, $c=9.100\pm0.002$ Å; $\rho=2.537\pm0.003$ g/cm³. A total of 762 observed reflections were collected for *hkl*, $0\leq h\leq 11$, to $\sin\theta/\lambda \leq 1.21$ using $Mo_{k\alpha}$ radiation and a G.E. XRD-6 semi-automatic diffractometer. Preliminary structure factor calculations showed that one proposed structure [2] was unsatisfactory, the correct icosahedral orientation being that determined by Matkovich [3]. Final site assignments (table 1) as Al, B or C were made by comparing discrepancy indices for a number of models and by requiring that all nearest neighbor contacts be as close to the sum of the covalent atomic radii as possible to minimize charge transfer [4]. The presence of C was verified by electron microprobe analysis. The stoichiometry was determined by analysing peak heights from the final ($R_F=0.050$) Fourier based on an average B peak height of $5e^-/A^3$. This procedure, necessitated by partial site occupancy, led to a calculated density of 2.53 g/cm³, and the formula $C_8Al_{2.5}B_{51}$, which is close to $C_8Al_2B_{52}$, an ideal ternary compound proposed by Hoard [4].

Two interesting comparisons emerge from the arrangement of B and C atoms. First, the hexagonal close packing of icosahedra (fig. 1) is similar to that for a proposed polymorph of boron [5]. Each three-center bond in the proposed structure is replaced by a C atom in the present structure. Carbon then completes six-fold coordination about ½ of the icosahedral B atoms; remaining icosahedral contacts in both structures are B—B. Second, all C atoms are in tetrahedral environ-

---

[1] Figures in brackets indicate the literature references at the end of this paper.

TABLE 1. Atomic parameters[a] and bond distances[b]

Atom	Type	X	Y	Z	B	Multiplier
1	B	0.1615	0.0170	¾	0.4444	8
2	B	0.3403	0.1805	¾	0.5076	8
3	B	0	0.0467	0.4138	0.4412	8
4	B	½	0.2492	0.5902	0.4341	8
5	B	0.2543	0.1518	0.3480	0.4856	16
6	C	½	0.1529	0.4390	0.4135	8
7	Al	0.3175	0.0414	0.5524	0.4878	0.937
8	Al	0	0.2105	¾	0.3784	0.651
9	B	½	0	½	0.6446	3.67
10	Al	0	0.16	0.62	0.45	0.12

Atoms	Distance (Å)	Atoms	Distance	Atoms	Distance
B–B Intraicosahedral		5–6	1.625	5–10	2.194
1–1′	1.838	6–9	1.467	6–7	1.768
1–3	1.840			6–7′	2.015
1–5	1.823	*B(C)–Al*[c]		6–8	2.104
2–2′	1.817	1–7	2.017	6–10	1.755
2–5	1.817	1–8	1.949	7–9	1.200
3–4	1.813	1–10	1.946		
2–5	1.817	2–7	2.186	*Al–Al*[c]	
3–5	1.823	2–8	1.955	7–7′	1.204
4–5	1.784	2–10	2.261	7–7″	2.076
5–5′	1.784	3–7	2.204	7–7′′′	2.400
		3–7′	1.993	7–10	2.189
B–B Intericosahedral		3–10	1.867	8–10	1.236
1–2′	1.773	4–7	2.145	10–10′	2.304
3–3′	1.775	4–10	2.104		
		5–7	1.974		
B–C		5–7′	2.133		
4–6	1.620	5–8	2.060		

[a] Coordinates are in fractions of cell edges. All parameters were taken from the $R_F=0.050$ least-squares data, including multipliers.

[b] B–B and C–B random errors average to 0.003Å, while those for Al–B and Al–C range up to 0.02Å.

[c] Some of these distances may not be real due to partial site occupancy.

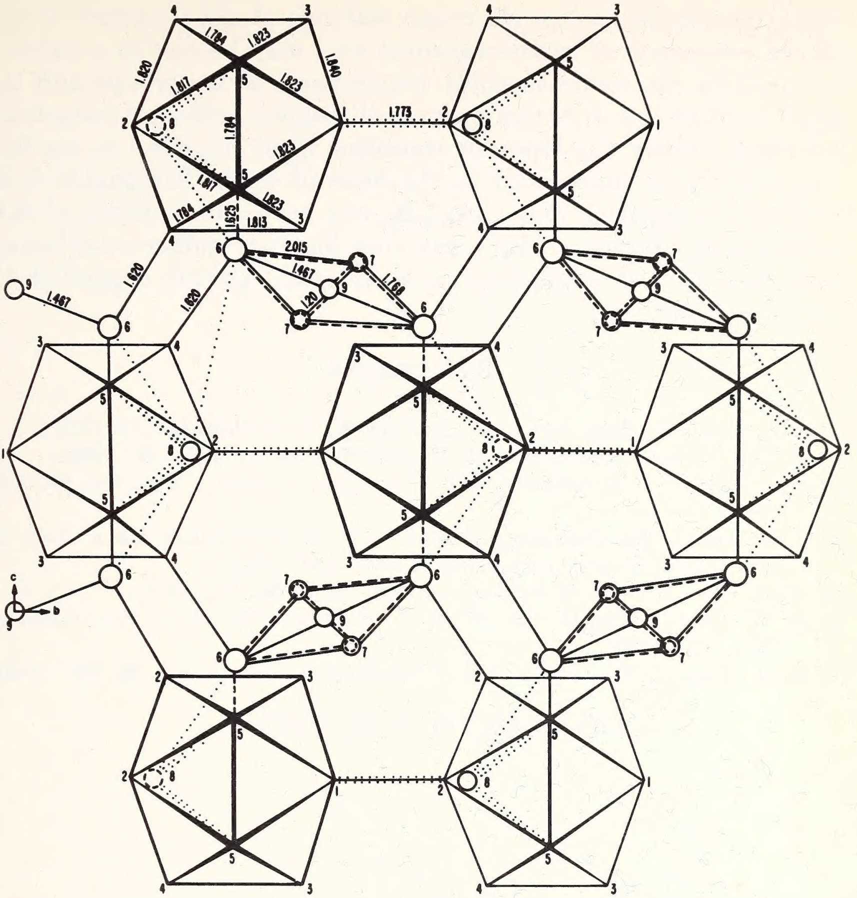
1.784
1.823
1.820
1.817
1.840
1.823
1.773
1.784
1.823
1.817
1.823
1.784
1.625
1.813
2.015
1.467
1.769
1.20
1.820
1.467
1.820
1
2
3
4
5
6
7
8
9
c
b

FIGURE 1. Hexagonal close packing of icosahedra

ments and complete linear C–B–C chains similar to those found in B_4C which contains cubic close packed icosahedra. In addition, all comparable B—B and B—C distances agree to within 0.05 Å. Thus, C and B roles in $C_8Al_{2.15}B_{51}$ are similar to those for B_4C leading directly to electronic comparisons. For B_4C, a structure consisting of B_{12}^{-2} icosahedra linked to $(C—C—C)^{+2}$ chains has been postulated [6]. Hence, icosahedra should be electron acceptors, chains electron donors.

Aluminum atoms, all on partially occupied sites, are irregularly coordinated to B and C atoms at short distances ranging from 1.76 to 2.26 Å. The extremely short Al(7)–B(9) distance of 1.20 Å precludes simultaneous occupancy of both sites such that when Al(7) is present, B(9), which completes the C—B—C chain, is absent. These observations suggest electron donor behavior for intericosahedral atoms which contributes to the electronic stability of the structure. Thus, partial occupancy of intericosahedral sites may be due to a balance between the electronic acceptor requirement of B_{12} groups and the space available for donor atoms once the rigid icosahedral framework is formed. Finally, the topotatic transition [7] of "C_4AlB_{24}" to the B_4C structure can be understood on the basis of similar bonding in both structures, suggesting that $C_8Al_{2.15}B_{51}$ is a crystalline solution of B_4C stabilized by aluminum. B_4C may then have an undiscovered hexagonal close packed polymorph, a modification already suggested for elemental boron [5].

References

[1] J. A. Kohn, G. Katz and A. A. Giardini, Z. Kristallogr. **111,** 53 (1958).

[2] G. Will, J. Amer. Chem. Soc. **85,** 2335 (1963); Nature **212,** 175 (1966).

[3] V. I. Matkovich, J. Economy and R. F. Giese, J. Amer. Chem. Soc. **86,** 2337 (1964).

[4] J. L. Hoard, The Chemistry of Boron and its Compounds, Chap. Two. E. Muetterties, Editor (John Wiley & Sons, Ltd.; 1966),

[5] W. N. Lipscomb and D. Britton, J. Chem. Phys. **33,** 275 (1960).

[6] H. C. Longuet-Higgins and M. de V. Roberts, Proc. Roy. Soc. (London) **230A,** 110 (1955).

[7] R. F. Giese, J. Economy and V. I. Matkovich, Acta. Cryst. **20,** 697 (1966).

LATTICE DYNAMICS

LATTICE DYNAMICS OF MOLECULAR SOLIDS [1]

GERALD DOLLING [2]

Solid State Division, Oak Ridge National Laboratory
Oak Ridge, Tennessee 37830

1. Introduction

The development of new experimental techniques for the study of the solid state, of which neutron inelastic scattering is perhaps the most valuable, has been accompanied by a renewed interest in the dynamical theory of crystal lattices. The problems which this theory has to deal with fall into two main classes: (i) what is the nature and magnitude of the forces between the atoms and molecules in a crystal and (ii) how may the various measurable properties of a crystal be calculated if the forces are known? The classic paper by Born and von Kármán [1] [3] provided a framework within which the latter problems might be solved, and there is now a considerable literature on the subject of calculations of the frequencies of normal modes of vibration of crystals and related properties. The standard text-book is that of Born and Huang [2], and there are several more recent reviews both of the theory and its application to particular solids [3–5]. The potential energy V of the crystal is expanded in powers of the displacements of the atoms from their equilibrium positions. The coefficients of the displacements in the quadratic term V_2 of this expansion are the harmonic force constants which couple the atom (lk) to that at $(l'k')$, where the labels l and k denote the particular unit cell and atom type, respectively. If the cubic and all higher order terms in the expansion are neglected, then the equations of motion for the atoms lead to a temperature-independent dispersion relation, $\nu=\nu_j(\boldsymbol{q})$, between the frequencies, ν, and wave vectors, $\boldsymbol{q}$, of the normal modes of vibration (j is a polarization index). Anharmonic effects may be calculated by taking into account appropriate higher order terms [6, 7, 8]. Relatively little progress has been made, however, toward quantitative *a priori* calculations of the basic interatomic and intermolecular forces in solids; these are customarily represented by arbitrary parameters, i.e., the coefficients of the various terms in the potential energy expansion, whose values are adjusted to give agreement with selected physical

---

[1] Research sponsored by the U.S. Atomic Energy Commission under contract with the Union Carbide Corporation.

[2] On leave from Chalk River Nuclear Laboratories, Chalk River, Ontario; now returned.

[3] Figures in brackets indicate literature references at end of this paper.

properties. The numerical values thus obtained can then be used to compute other properties of the solid.

The purpose of this paper is firstly to show how the dynamical theory for a relatively simple solid has been treated, along the lines suggested above, secondly to indicate the difficulties which arise in the study of crystals of more complicated structure, and thirdly, to discuss various methods which have been developed to avoid or overcome those difficulties. The interactions (aside perhaps from the coulomb forces between charged ions which can be calculated exactly) will be represented by disposable parameters or force constants, whose values will be obtained by comparison with appropriate physical properties. In section 2, we briefly outline the Born-von Kármán theory and certain extensions which have been made in order to describe the lattice dynamics of a simple alkali halide. Experimental results and theoretical calculations for lithium fluoride (LiF) [9] are presented as a typical example. In section 3, the somewhat more complicated cases of sodium nitrite ($NaNO_2$) [10] and hexamethylenetetramine (HMT) [11, 12, 13] are considered, in which the practical limitations of the straightforward Born-von Kármán model become apparent, but where it is still feasible to represent the interionic and/or intermolecular force constants by arbitrary disposable parameters. For more complicated crystals still, such as naphthalene and anthracene, the number of such parameters becomes so large that alternative approaches must be found. In section 4 are described the ideas of Kitaigorodskii and co-workers [14, 15], and the lattice dynamical calculations of Pawley [16], in which one such alternative approach is explored.

2. Dynamical Theory for a Simple Solid

We shall assume without discussion that the well-known adiabatic approximation and cyclic boundary conditions [2] may be applied. We write the quadratic term in the expansion of the crystal potential energy in the usual way [2, 3]

$$V_2=\frac{1}{2}\sum_{lkx}\sum_{l'k'y}\phi_{xy}(lk,\ l'k')u_x(lk)u_y(l'k') \tag{1}$$

where $\phi_{xy}(lk,l'k')=[\partial^2V/\partial x(lk)\partial y(l'k')]$, $u_x(lk)$ is the displacement in the x-direction of the kth atom in the lth unit cell, and the derivatives are to be taken at the equilibrium positions of the atoms. (Strictly speaking, this statement applies at 0 °K and in the absence of anharmonic effects, but in practice it is often convenient [7] to make use of a "pseudo-harmonic" approximation in which the second derivatives are evaluated at the equilibrium positions of the atoms at the temperature of interest. The force constants then implicitly involve certain anharmonic terms and are temperature-dependent.) The equation of motion for the (lk) atom can then be treated by means of a traveling wave solution

$$u_x(lk)=U_x(k\mathbf{q})\ \exp\ i[\mathbf{q}\cdot\mathbf{r}(lk)-2\pi\nu(\mathbf{q})t] \tag{2}$$

where $\mathbf{r}(lk=\mathbf{r}(l)+\mathbf{r}(k)$ specifies the equilibrium coordinates of the kth atom within the lth unit cell. The resulting equations of motion, only $3n$ in number (there are n atoms in the unit cell), may be concisely expressed in matrix notation

$$4\pi\nu^2\underline{\underline{m}}\mathbf{U}=\underline{\underline{M}}\mathbf{U} \tag{3}$$

where $\underline{\underline{m}}$ is a diagonal matrix whose elements are the ionic masses m_k, and $\underline{\underline{M}}$ is a square matrix of order $3n$ x $3n$:

$$M_{xy}(kk',\mathbf{q})=\sum_{l'}\phi_{xy}(lk,\ l'k')\ exp\ i\mathbf{q}\cdot[\mathbf{r}(l'k')-\mathbf{r}(lk)]. \tag{4}$$

The sum over all atoms l' includes the atom (lk) itself, and the so-called "self term" $\phi_{xy}(lk,\ lk)$ is defined as the negative of the sum of the forces acting on the (lk) atom due to all its neighbors. This ensures that the condition of translational invariance is satisfied. For each value of the wave vector $\mathbf{q}$, eq (3) has $3n$ solutions $\nu_j(\mathbf{q})(j=1\ .\ .\ .\ .\ 3n)$, each with its associated eigenvector $\mathbf{U}j(\mathbf{q})$, describing the $3n$ normal modes of vibration of the crystal for that wave vector. The wave vector is arbitrary to the extent of the addition of any reciprocal lattice vector τ of the crystal,

$$\nu_j(\mathbf{q})=\nu_j(\mathbf{q}+2\pi\tau) \tag{5}$$

and it is customary to reduce all normal-mode wave vectors into the first Brillouin zone by subtracting suitable reciprocal lattice vectors.

The application of this (pseudo-harmonic) theory to the dynamics of a given crystal is now straightforward. The interaction between any pair of atoms (lk) and $(l'k')$ is represented by a (3x3) matrix of force constants $\phi_{xy}(lk,l'k')$; in general, there will be very many of these parameters, but it is customary to limit the number, (a) by restricting the range of interaction so as to include only a few near-neighbor pairs, (b) by applying the symmetry of the crystal (see below for examples of this procedure) and (c) by specifying the interaction to be of some special type (e.g. central forces). For sufficiently simple crystals, having highly symmetric structures, only a few distinct atom types, and relatively short range forces, it is easily possible to set up the matrix elements of eq (4) without an excessive number of disposable parameters $\phi_{xy}(lk,l'k')$. The diagonalization of the matrix is not a difficult machine computation, at least for small values of n, and so calculation of the normal mode frequencies can be performed, together with many other physical properties which depend on those frequencies. It should be borne in mind, however, that this discussion has not touched upon one of the basic problems of lattice dynamics, namely the evaluation of the force constants themselves from some more fundamental theory. Attempts to treat this problem have been made for alkali halides [17,18] and for so-called "simple" metals [19–22], but a discussion of these topics is outside the scope of the present paper.

We now describe the application of the above theory to a relatively simple solid, in order to facilitate the discussion of more complicated solids in the subsequent sections. Since one of the latter is at least partly ionic ($NaNO_2$), it is convenient to introduce the subject of coulomb forces by choosing an alkali halide, LiF, as our example. The lattice dynamics of alkali halides has a long history, and several important contributions to the subject have been made in recent years (see reference 5 for a review). Indeed, efforts are still being made [23] to improve upon the successful "shell model" of Dick and Overhauser [24], as developed by Cochran and co-workers. For the present purpose, however, it is appropriate to consider only the coulomb forces between the monopole charges on the ions; the added refinements of a shell model for molecular crystals in which the ionic and molecular polarizabilities are taken into account, will no doubt become necessary as the study of such crystals intensifies. If the charge on the kth ion (assumed to be rigid) is Z_k, then the contribution to the crystal potential arising from coulomb forces is

$$V^c=\frac{1}{2}\sum_{lk,l'k'} Z_k Z_{k'}/|\mathbf{r}(l'k')-\mathbf{r}(lk)| \qquad (6)$$

This term may be expanded in powers of the ionic displacements, in the same way as the potential arising from all other sources. The dynamical matrix $\underline{\underline{M}}$ can be written as a sum of two parts.

$$M_{xy}(kk',\mathbf{q})=R_{xy}(kk',\mathbf{q})+Z_k Z_{k'} C_{xy}(kk',\mathbf{q}) \qquad (7)$$

where $\underline{\underline{R}}$ involves arbitrary force constants representing (purely phenomenologically) all the non-coulomb interactions, and $\underline{\underline{C}}$ is a matrix whose elements may be computed explicitly for any given crystal structure.

The classic paper in this field is that of Kellerman [26], to which the reader is referred for full details of this calculation in the case of NaCl.

Thus, in the case of LiF, if we know the charge Z, the coulomb contribution to the dynamical matrix involves no disposable parameters. We have only to consider the form of $\underline{\underline{R}}$, that is to say, to decide the number of independent parameters $\phi_{xy}(lk,l'k')$ required by symmetry to specify the non-coulomb interactions. In the most general case, the force constants defined by eq (1) can be expressed as a (3×3) array

$$\Phi(lk,l'k')=\begin{pmatrix}\phi_{11} & \phi_{12} & \phi_{13}\\ \phi_{21} & \phi_{22} & \phi_{23}\\ \phi_{31} & \phi_{32} & \phi_{33}\end{pmatrix}. \tag{8}$$

The number of independent ϕ_{ij} is, however, severely restricted by the high degree of crystal symmetry in LiF. If we represent an allowed symmetry operation by a transformation matrix $\underline{\underline{S}}$, then clearly

$$\underline{\underline{S}}\Phi(lk,l'k')\underline{\underline{\tilde{S}}}=\Phi(l''k'',l'''k''') \tag{9}$$

since the lattice remains unchanged by this operation. Certain types of symmetry operation, which we call class A (following the notation of Cochran and Pawley [11]), leave both the origin atom (lk) and the neighbor $(l'k')$ in their original positions $(l=l'', l'=l''')$. In this case clearly the transformed matrix $\Phi(l''k'',l'''k''')$ and the original $\Phi(lk, l'k')$ must be identical. Other types of symmetry operation, class B, involve a translation of the $(l'k')$ atom from $r(l'k')$ to $-r(l'k')$, i.e. $l'=-l'''$. In this case it is easily seen from the definition (1) that

$$\Phi(lk, l'k')=\tilde{\Phi}(lk, l'k') \tag{10}$$

As an example of a class A symmetry operation in LiF, consider the mirror plane perpendicular to the z axis, with the (lk) and $(l'k')$ atoms taken to be at (0,0,0) and (a/2,0,0) respectively. This operation is represented by the transformation matrix

$$S=\begin{pmatrix}1 & 0 & 0\\ 0 & 1 & 0\\ 0 & 0 & -1\end{pmatrix}. \tag{11}$$

Substitution of this into eq (9) leads at once to the result $\phi_{13}=\phi_{31}=\phi_{23}=\phi_{32}=0$; application of the remaining allowed symmetry operations in the same way finally reduces the matrix to the simple form

$$\Phi=\begin{pmatrix}\phi_{11} & 0 & 0\\ 0 & \phi_{22} & 0\\ 0 & 0 & \phi_{22}\end{pmatrix} \tag{12}$$

specifying the interactions between nearest neighbor ions in LiF. The analogous result for the second nearest neighbor interactions is readily obtained in the same way. We can now construct a simple model for the lattice dynamics of LiF, in which the following forces are taken into account:

(i) Long range coulomb forces between the monopole charges ($\pm Ze$) on the ions.
(ii) Short range "overlap" type forces between nearest neighbor ions, represented by the phenomenological force constants ϕ_{11}, ϕ_{22} of eq (12).
(iii) Short range forces between second nearest neighbor F^- ions, represented by force constants $\phi'_{11}(=\phi'_{22})$, ϕ'_{33}, and $\phi'_{12}(=\phi'_{21})$.

The analogous $Li^+ - Li^+$ forces are neglected in view of the small size of that ion. A further simplification, that the forces are axially symmetric, [27] is often made to eliminate one of these 3 second neighbor force constants, which in this case reduces to the assumption that $\phi'_{12} = \phi'_{11} - \phi'_{33}$.

The contribution of the short range forces to the elements of the dynamical matrix are obtained from eq (4), and the electrostatic contributions calculated as in reference 26. If the 5 parameters ϕ_{11}, ϕ_{22}, ϕ'_{11}, ϕ'_{33} and Z are given, the normal mode frequencies $\nu_j(\mathbf{q})$ can be calculated for all $\mathbf{q}$ from the eigenvalues of the dynamical matrix, eq (3). Alternatively, if a reasonable number of frequencies have been experimentally measured, then a set of 5 parameter values can be obtained, by the method of least-squares, which gives the best fit to the measurements. In view of the difficulty of calculating the parameter values from first principles, mentioned in the introduction, it is the latter procedure which is most commonly employed. The frequencies of normal modes of a large number of different wave vectors in Li^7F have recently been measured [9] at 298 °K by standard techniques of inelastic scattering of slow neutrons. The results for modes propagating along two directions of high crystal symmetry, Δ and Λ (the cube edge and body diagonal respectively), are shown in figure 1. We shall not discuss here the group theoretical methods [28–30] used to label the various branches of the spectrum according to the characters of their irreducible representations. Since there are two ions in the primitive unit cell ($k=1,2$), there are, in general, 6 distinct normal modes for any arbitrary $\mathbf{q}$ value. In these two directions, however, the symmetry is such that the transversely polarized modes (Δ_5, Λ_3) occur in doubly degenerate pairs. Another useful consequence of the high symmetry is that the polarization of the modes can be determined rather easily in inelastic neutron scattering experiments, simply by inspection of the intensities of the coherent one-phonon peaks. In more complex crystals, this problem of identification of the modes becomes very much more serious, as we shall see.

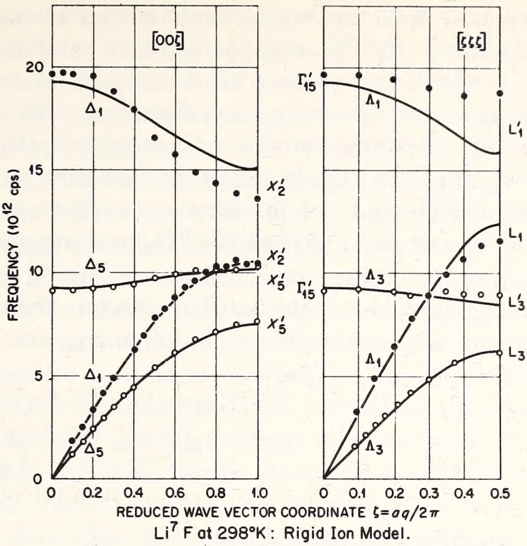

FIGURE 1. Frequencies of normal modes propagating along two directions of high symmetry in ^{7}LiF at 298 °K. The different kinds of polarization of the modes are labelled according to the characters [30] of their irreducible representations. (Note: if we use the notation of reference 28 then L_1' and X_2' should be replaced by L_2' and X_4' respectively.) The solid curves represent the best least-squares fit to the results on the basis of the rigid ion model described in the text.

The result of fitting these data with above-mentioned 5 parameter "rigid ion" model is shown as the solid curves in figure 1. The quality of fit is surprisingly good in view of the fact that the polarizability of the ions has been neglected. (The dielectric constant of LiF is not correctly given by this model.) The best-fit value of the ionic charge is 0.73. A more reasonable value ($\simeq$0.95), together with an excellent fit to the phonon frequencies, may be obtained [9] by making allowance for the polarizability of the F^- ion.

3. More Complicated Solids

3.1. Inorganic Crystals

In this section we discuss possible approaches to the problem of studying inorganic crystals which, though still relatively simple in structure, have more atoms per unit cell and/or a lower symmetry than an alkali halide. Our prime example is sodium nitrite, $NaNO_2$, although many other crystals (e.g. iron disulphide, iodine) can be treated in the same way.

The structure of $NaNO_2$ in its low temperature (below 163 °C) ferroelectric phase is shown in figure 2. It is an extremely interesting material on account of its unusual dielectric behavior as a function of temperature; between 163 °C and 164.5 °C, it exhibits an antiferroelectric phase in which the average electric dipole moment along the *b* axis oscillates as one moves along the *a* direction, with a temperature-dependent period, incommensurate with the *a* lattice parameter. Above 164.5 °C, the NO_2^- dipole moments are directed equally and randomly along the + and $-b$ directions, and the material is paraelectric. A very recent study [31] of $NaNO_2$ has suggested the possibility of an additional ferroelectric phase existing in a very narrow temperature range just below the antiferroelectric region. Such matters are, however, outside the scope of this paper.

The primitive unit cell of $NaNO_2$ contains 4 atoms, and hence a straight-forward application of the Born-von Kármán theory would lead to a (12×12) dynamical matrix, giving, in general, 12 normal modes of vibration for each wave vector. Even if the range of the interatomic forces is assumed to be quite restricted, there are still a large number of different pairs of neighbors (lk) and $(l'k')$, such as N—O, O—O, N—Na, O—Na, Na—Na, N—N, etc., each of which would be assigned a force constant matrix $\Phi(lk,l'k')$. Since the crystal symmetry (Im2m) is not high, only a modest reduction in the number of independent constants would result from application of eq (9). Group theoretical techniques are most useful for deducing the degree of factorization of the (12×12) dynamical matrix. For modes propagating along the *b* axis (a diad axis along the intersection of 2 mirror planes), we obtain the irreducible representations $4\Sigma_1 + 3\Sigma_3 + \Sigma_2 + 4\Sigma_4$, using the character table of Koster [30] for the group C_{2v}. Thus calculation of the eigenfrequencies involves diagonalization of (4×4) and (3×3) matrices. Along the *a* and *c* directions, which have lower symmetry still, only factorization into (7×7) and (5×5)

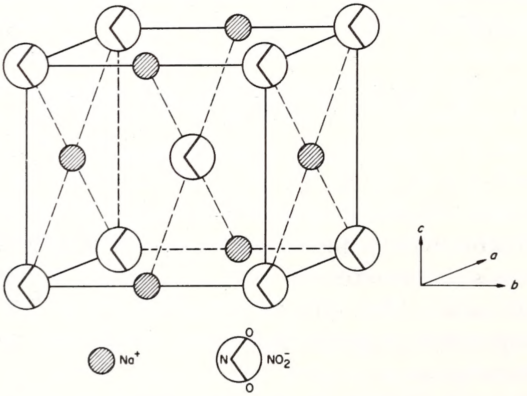

FIGURE 2. Structure of $NaNO_2$ in its ferroelectric phase.

matrices is possible. It is clear, therefore, that this approach to the lattice dynamics of $NaNO_2$ is quite difficult, perhaps prohibitively so. In any event, it is known from Raman scattering experiments that 3 of the 12 normal modes have very much higher frequencies than the other 9, in the range 25 to 40×10^{12} Hz. These are the internal modes of vibration of the tightly bound NO_2^- ion, which are more or less decoupled from the low frequency "lattice" modes. It would seem more profitable, therefore, to think of $NaNO_2$ as a diatomic crystal, like LiF, except that one of the "atoms" has an electric dipole moment in addition to a charge, and librational as well as translational degrees of freedom. This approach has been successful in the study of the dynamics of organic molecular solids, [11, 12, 13, 16] which will be discussed later. To avoid confusion in the subsequent discussion of particular atoms within molecules or groups of atoms like NO_2^-, we shall often refer to such multi-atomic groupings as "molecules".

We begin as before by postulating force constants $\phi_{xy}(lk,l'k')$ representing the force in the x direction on the (lk) molecule when the $(l'k')$ molecule is displaced a unit amount in the y direction. In addition, we postulate sets of $\phi_{x\beta}(lk,l'k')$ and $\phi_{\alpha\beta}(lk,l'k')$ which relate the forces and couples exerted on the (lk) molecule when $(l'k')$ is rotated about the β axis by a unit amount. The (x,y,z) and (α,β,γ) axis systems need not be coincident; it is often convenient to choose crystallographic axes for expressing the displacements $u_x(lk)$ and principal axes of the molecule for expressing the rotations $\theta_\alpha(lk)$. In $NaNO_2$, however, these two sets of axes coincide with the orthorhombic axes a, b and c. The quadratic term in the crystal potential energy, eq (1), is extended to include products of rotational and translational displacements, and the new force constants are just the second derivatives of the potential with respect to these displacements. Equations of motion of the form (mass × acceleration = force constant × displacement) are supplemented by equations of the form (moment of inertia × angular acceleration = torque × angular displacement):

$$m_k\ddot{u}_x(lk)=-\sum_{l'k'y}\phi_{xy}(lk,\,l'k')u_y(l'k')-\sum_{l'k'\beta}\phi_{x\beta}(lk,\,l'k')\theta_\beta(l'k') \tag{13}$$

$$I_{k\alpha}\ddot{\theta}_\alpha(lk)=-\sum_{l'k'y}\phi_{\alpha y}(lk,\,l'k')u_y(l'k')-\sum_{l'k'\beta}\phi_{\alpha\beta}(lk,\,l'k')\theta_\beta(l'k') \tag{14}$$

m_k is the mass of the kth molecule and $I_{k\alpha}$ is the moment of inertia about the α axis. If a particular atom within a molecule is denoted by the index p, then the displacement of that atom is given by

$$\mathbf{u}(lkp)=\mathbf{u}(lk)+\boldsymbol{\theta}(lk)\times\mathbf{r}(p) \tag{15}$$

where $\mathbf{r}(p)$ is the position of an atom relative to the center of mass of the molecule (lk).

Eqs (13) and (14) can be reduced by substitution of traveling wave solutions in the usual manner, and the normal mode frequencies are obtained as before from a matrix eq (3). The diagonal matrix $\underline{\underline{m}}$ now has two types of elements, m_k and $I_{k\alpha}$, and the eigenvectors **U** have both translational and rotational (or librational) components. If there are n molecular units and n' individual atoms (which are not in molecular units) in the primitive unit cell, then the matrix $\underline{\underline{m}}$ is of order $(3n'+6n)$. For $NaNO_2$, $n=n'=1$, and so $\underline{\underline{m}}$ is a (9x9) matrix. Each eigenvector **U** has 9 components, 3 translational coordinates for the Na^+ ion, 3 for the NO_2^- ion, and 3 librational coordinates for the NO_2^- ion.

We must now consider what simplifications can be achieved by appropriate symmetry arguments both in the number of independent force constants and in the order of the dynamical matrix. The high-temperature paraelectric phase of $NaNO_2$ has, in effect, a rather higher symmetry. Furthermore, no large differences have been observed [10] between the two phases in most of the normal mode frequencies. The following remarks, while strictly applicable only to the paraelectric phase, may be regarded as a useful first approximation to the less symmetric ferroelectric phase.

First we discuss the application of group theory to the dynamics of $NaNO_2$ when we regard a unit cell as containing a NO_2^- ion at the origin and a Na^+ ion at (b/2, 0, 0), the former having librational degrees of freedom. If we assume Immm symmetry, each of the 3 crystallographic axes, a, b, c, is on the same footing, and the (9x9) dynamical matrix factorizes in the same way for all 3 propagation directions. The group of the wave vector for any of these directions is C_{2v}, which contains elements E (the identity operation), C_2 (parallel to $[0\zeta 0]$, say) and two mirror planes σ_v, σ_v' intersecting along $[0\zeta 0]$. We use the translational displacements of the Na^+ and NO_2^- ions along the a, b, and c directions, and the librational displacements of the NO_2^- ion about those 3 axes, as a basis set for reducing the representation of the group. Remembering that a librational displacement is an axial vector, which transforms differently from a polar vector under the operation of mirror planes, we find the characters 9, −3, 1 and 1 corresponding to the 4 symmetry operations listed above. With the help of the character table [30] for C_{2v}, we then obtain the irreducible representations for waves propagating along $[0\zeta 0]$:

$$2\Sigma_1+\Sigma_2+3\Sigma_3+3\Sigma_4 \qquad (16)$$

Σ_1 refers to two longitudinally polarized modes (LO+LA), Σ_2 to a pure librational mode about the b axis, while Σ_3 and Σ_4 are each mixtures of 2 transversely polarized translational modes and a librational mode. For example, Σ_3 represents a mixture of *c*-axis libration and *a*-axis translation (transverse polarization).

For modes of nearly zero wave vector, and also at the zone boundaries in the three main symmetry directions, the appropriate group is D_{2h}, and a greater degree of factorization is obtained:

$$N_2+N_3+N_4+2N_2'+2N_3'+2N_4' \tag{17}$$

where the unprimed symbols refer to pure librational modes about the *b*, *a*, and *c* axes respectively, and the others to pairs of translational modes (optic and acoustic) polarized along *b*, *a*, and *c* respectively. The compatibility relations which enable us to "join up" the various branches in different directions, are given in table 1. Factorization of the (9x9) matrix into (5x5) and (4x4) matrices is obtained for wave vectors lying in the mirror planes of symmetry. In all other directions, however, no reduction of the matrix is possible, since the only allowed symmetry operation is the identity operation, E.

TABLE 1.—Compatibility relations for modes propagating along the *a*, *b*, and *c* directions in (paraelectric) $NaNO_2$, and for modes of zero wave vector, and at the zone boundaries (Z.B.) in each of the 3 directions

$\mathbf{q}=0$ or Z.B.	$\mathbf{q}\|\|a$	$\mathbf{q}\|\|b$	$\mathbf{q}\|\|c$
N_2	Σ_3	Σ_2	Σ_4
N_3	Σ_2	Σ_4	Σ_3
N_4	Σ_4	Σ_3	Σ_2
N_2'	Σ_4	Σ_1	Σ_3
N_3'	Σ_1	Σ_3	Σ_4
N_4'	Σ_3	Σ_4	Σ_1

Next we explore the possibilities for describing the interionic forces in $NaNO_2$ by means of a phenomenological model similar in spirit to that for LiF (section 2). We will need to take into account the long range electrostatic forces not only between the monopole charges Na^+ and NO_2^-, but also those involving the permanent dipole moment of the NO_2^- ion. (A more refined model should also allow for the induced dipole moments arising from the ionic polarizabilities, but for simplicity we shall neglect such effects.) In the paraelectric phase, of course, the average dipole moment on an NO_2^- site is zero, and so only the monopole electrostatic forces need to be considered. As in the case of LiF, a dynamical matrix element is composed of two parts, a short-range part R_{xy} $(kk', \mathbf{q})$ and a coulomb part $Z_k Z_{k'}$, C_{xy} $(kk', \mathbf{q})$, where Z_k is the ionic charge for $k=1$, 2, and Z_3 is the NO_2^- dipole moment (i.e., the effective charge on the nitrogen atom multiplied by the distance of that atom from the mid-point between the pair of oxygen atoms). In principle, then, if we know Z_1 and Z_3, these contributions to the matrix elements may be exactly calculated. Full details of this calculation will be published elsewhere [10]. The only remaining problem is that of representing the short-range interactions. It is convenient to consider an enlarged (9×9) force constant matrix $\Phi(lk,l'k')$ instead of the usual (3×3) matrix. For example, the interactions between the NO_2^- ion at (0,0,0) and the Na^+ ion at (0,b/2,0) are expressed by

$$\begin{array}{ccc|ccc|ccc}
 & & & \phi_{14} & \phi_{15} & \phi_{16} & \phi_{17} & \phi_{18} & \phi_{19} \\
 & 0 & & \phi_{24} & \phi_{25} & \phi_{26} & \phi_{27} & \phi_{28} & \phi_{29} \\
 & & & \phi_{34} & \phi_{35} & \phi_{36} & \phi_{37} & \phi_{38} & \phi_{39} \\
\hline
\phi_{41} & \phi_{42} & \phi_{43} & & & & & & \\
\phi_{51} & \phi_{52} & \phi_{53} & & 0 & & & 0 & \\
\phi_{61} & \phi_{62} & \phi_{63} & & & & & & \\
\hline
\phi_{71} & \phi_{72} & \phi_{73} & & & & & & \\
\phi_{81} & \phi_{82} & \phi_{83} & & 0 & & & 0 & \\
\phi_{91} & \phi_{92} & \phi_{93} & & & & & &
\end{array} \qquad (18)$$

Thus ϕ_{41} is the force exerted on the NO_2^- ion in the x direction when the Na^+ ion is translated unit distance in the x direction; ϕ_{92} is the torque exerted on the NO_2^- ion about the z axis when the Na^+ ion is translated unit distance in the y direction, and so on. This very large number of parameters may be substantially reduced by appropriate symmetry arguments. As before, we represent each allowed symmetry operation by a transformation matrix $\underline{\underline{S}}$. While $\underline{\underline{S}}$ is always appropriate for transforming polar vectors, it is only suitable for transforming axial vectors if it represents a proper rotation. The operation of an improper rotation on an axial vector is correctly expressed by $-\underline{\underline{S}}$. The elements ϕ_{ij} of the matrix (18), for i and $j \leq 6$, relate components of polar vectors (displacements of ions), whereas the other elements involve polar vectors (librations of NO_2^-). Thus the total matrix is correctly transformed by a (9x9) matrix of the form

$$T = \begin{matrix} S & 0 & 0 \\ 0 & S & 0 \\ 0 & 0 & S \det S \end{matrix} \qquad (19)$$

since $\det S = +1$ (-1) for proper (improper) rotations.

In table 2 are shown the transformation matrices for 3 symmetry operations suitable for reducing the number of independent elements of eq (18). One easily finds that only 5 parameters are independent, namely ϕ_{14}, ϕ_{25}, ϕ_{36}, ϕ_{37} and ϕ_{19}. In the same way, it can be shown that the interactions between NO_2^- at (0,0,0) and Na^+ at (a/2,0,c/2), NO_2^- (0,0,0) and NO_2^- (a,0,0), NO_2^- (0,0,0) and NO_2^- (a/2,b/2,c/2), and between NO_2^- (0,0,0) and NO_2^- (0,0,c), can be represented by 9, 8, 21 and 5 independent parameters respectively. Restriction of the short-range forces to these pairs of ions is reasonable in view of the large size of the NO_2^- ion. Even so, we still have a large number of parameters, and it is important to find ways of expressing them in simpler terms. One such way is to assume that all the interactions may be regarded as axially-symmetric forces between appropriate near-neighbor atoms (not ions). Consider the interactions between NO_2^- (0,0,0) and Na^+(0,b/2,0); it seems reasonable to suppose that these are dominated by the interactions between Na^+ and the two oxygen atoms of the (rigid) NO_2^- ion. Let the vector distance between these atoms, Na and O, be $\mathbf{r}$; the assumption of axially-symmetric forces implies

$$\phi_{xy}(\mathrm{Na},\mathrm{O}) = \frac{r_x \cdot r_y}{|\mathbf{r}|^2}(A-B) + B\delta_{xy} \tag{20}$$

where δ_{xy} is the Kronecker delta and

$$A = \partial^2 V/\partial r^2 \quad , \quad B = (1/r)\partial V/\partial r \tag{21}$$

Since the structure of $NaNO_2$ is known, we can readily substitute for r in eq (20) for each ϕ_{xy} (Na, O); summing over the two equivalent Na–O pairs, and comparing the result with the 5 independent parameters of eq (18), enables us to express those 5 parameters in terms of the A and B of eq (21). In fact we find $\phi_{14}=2B$, $\phi_{25}=2(t_1A+t_2B)$, $\phi_{36}=2(t_2A+t_1B)$, $\phi_{37}=2t_3(A-B)$, $\phi_{19}=0$. Here t_1, t_2 and t_3 are simple functions of the geometrical positions of O and Na, and are 0.8766, 0.1234 and 0.3289, respectively. Each of the interionic interactions can be treated in this way, and a considerable reduction in the number of parameters is achieved in a physically reasonable manner.

The detailed derivation of the force constant matrices and dynamical matrix elements is straightforward but rather lengthy [10]. We now proceed to discuss the next problem which arises once we have both a theoretical framework for the calculation of normal mode frequencies and also a set of measurements of those frequencies, obtained by means of infrared, Raman and/or slow neutron spectroscopy. This is the problem of identification of the observed peak (in the absorption or scattering process) with the normal mode involved. In prin-

TABLE 2. Symmetry operations useful for reducing the number of independent parameters specifying the interactions between NO_2^- at (0,0,0) and Na^+ at (0,b/2,0)

Operation	S Matrix	Det S
Inversion (Class B)	$\begin{pmatrix} -1 & 0 & 0 \\ 0 & -1 & 0 \\ 0 & 0 & -1 \end{pmatrix}$	-1
Diad ‖ b (Class A)	$\begin{pmatrix} -1 & 0 & 0 \\ 0 & 1 & 0 \\ 0 & 0 & -1 \end{pmatrix}$	$+1$
Mirror plane ⊥ c (Class A)	$\begin{pmatrix} 1 & 0 & 0 \\ 0 & 1 & 0 \\ 0 & 0 & -1 \end{pmatrix}$	-1

ciple, what we have to do is to calculate the intensity of the scattering process, assuming that it involves each of the possible modes in turn, and to check which of these theoretical calculations matches the observation most nearly. If the modes have sufficiently high symmetry this identification can often be performed simply by inspection; for normal modes in $NaNO_2$, however, except perhaps those of very small wave vector, this is not the case, and detailed calculations are necessary. The intensity of coherent one-phonon scattering of neutrons depends on the eigenvector of the normal mode involved, and this can only be obtained from a lattice dynamical model. To obtain the latter, we must first assign a tentative label to each observed scattered neutron peak and perform a least-squares fit analysis of the results on the basis of an empirical force model as described above. Using the best-fit values of the force constants, we compute the eigenvector of each normal mode and hence the neutron scattering cross-section (or infrared absorption or Raman scattering cross-section, as the case may be) appropriate to the experimental conditions under which each mode was observed.

The coherent scattering cross-section [5, 11] for one-phonon processes, aside from certain trivial factors, is determined by the so-called "inelastic structure factor" f_j^2:

$$f_j^2 = \left|\sum_k \sum_p \mathbf{Q} \cdot (\boldsymbol{\xi}_{kj}(\mathbf{q}) + \boldsymbol{\theta}_{kj}(\mathbf{q}) \times \mathbf{r}_p)\Gamma_p {\nu_j}^{-1/2} \exp\,(2\pi i \boldsymbol{\tau} \cdot \mathbf{r}_k)\right|^2 \tag{22}$$

where $\Gamma_p = b_p \exp(-W_p)\exp(i\mathbf{Q}\cdot\mathbf{r}_p)$, and $\hbar\mathbf{Q}$ is the momentum transfer suffered by the scattered neutrons. The normalized eigenvectors $\boldsymbol{\xi}_{kj}(\mathbf{q})$ and $\boldsymbol{\theta}_{kj}(\mathbf{q})$ are given by

$$\sum_k (m_k|\xi_{kj}(\mathbf{q})|^2+I_k|\theta_{kj}(\mathbf{q})|^2)=m,$$

where, as before, m_k and I_k are the mass and moment of inertia of the kth molecule, $m=\sum_k m_k$, and I_k is defined by

$$I_k|\boldsymbol{\theta}|^2=I_{k\alpha}|\theta\alpha|^2+I_{k\beta}|\theta_\beta|^2+I_{k\gamma}|\theta_\gamma|^2.$$

Thus, for any particular wave vector we can calculate the intensity of the scattered neutron beam for each of the normal modes, and compare with the experimental observations. Unless we have been unusually fortunate in our initial assignments of labels, we will now find various inconsistencies between theory and experiment; changes in the assignments must be made, the least-squares fit analysis repeated, and the new calculated intensities compared with experiment, until finally a completely consistent set of normal mode labels is achieved.

One of the most important factors in eq (22) is the scalar product of **Q** with the total displacement of the molecule k. It is often possible to arrange the experimental conditions so that this has a maximum value for some modes while being negligible for other modes. This provides a useful guide to the initial choice of mode assignments, and considerably reduces the number of detailed structure factor calculations needed. Following this general procedure the phonon dispersion curves for $NaNO_2$ at 296 °K (measured by inelastic neutron scattering techniques) have been analyzed on the basis of various force models; the results are shown in figure 3. Initially, we attempted to fit the results using models with only a few parameters, representing what we estimated to be the most important interionic forces, for example, ϕ_{25} [see eq (18)] which couples the b-axis translational motions of the NO_2^- group at the origin with those of the Na^+ ion at (0,b/2,0). The quality of fit obtained with, say, less than 10 parameters, was unsatisfactory, although the shapes of the dispersion curves were qualitatively correct. As more parameters were added (still restricting the forces to be between the 5 closest interionic pairs, however) the quality of fit gradually improved. Finally, the solid curves in figure 3 represent the best fit obtained with a rather general force model involving a grand total of 20 parameters! Of these, 11 have numerical values greater than 10 percent of the largest force constant, and so could scarcely be considered as negligible. The physical meanings of most, if not all, of these constants have clearly been completely lost, and some method is urgently needed to reduce their numbers while still retaining enough of the physics of the problem to be able to fit the experimental results.

If we restrict the force constants by assuming only axially-symmetric forces between near-neighbor *atoms*, the fit to the results is

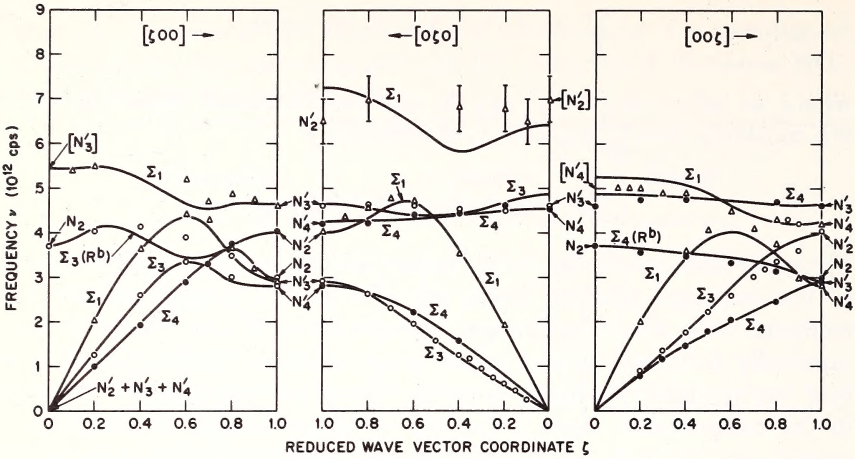

FIGURE 3. Phonon dispersion curves for $NaNO_2$ at 296 °K. The assignment of labels to the various branches is discussed in the text. The solid curves are computed from a rigid ion model involving short-range forces between an NO_2^- ion and its 2 nearest neighbor Na^+ ions and 3 nearest neighbor NO_2^- ions. The symbol R^b denotes a mainly librational mode about the b axis.

fairly good, though definitely less satisfactory. An examination of the calculated eigenvectors for the various modes shows that these fall into fairly well-defined types, e.g. mainly librational, or mainly translational (transverse or longitudinal), even when they are not required to do so by symmetry. This is perhaps not surprising since each branch is required to be purely librational or translational both at zero wave vector and the zone boundary in the three principal symmetry directions. It should be repeated at this point that the results have been analyzed and labelled according to the symmetry of the paraelectric phase, which seems to be a reasonable approximation as far as the existing experimental measurements are concerned. While it is evidently possible to obtain a fairly good description of the normal mode frequencies in $NaNO_2$ with this kind of phenomenological model, it is of course unsatisfactory to have to resort to such a large number of disposable parameters. Furthermore, the dielectric properties of $Na\text{-}NO_2$ cannot be properly discussed in terms of a rigid ion type of model, and the introduction of ionic polarizabilities would inevitably increase the number of parameters needed. Sodium nitrite would seem, therefore, to represent a kind of upper limit to the complexity of materials which might be treated adequately in this way.

3.2. Organic Crystals

A most interesting example of a "molecular" crystal, which, in spite of its name, is simpler in some respects than $NaNO_2$, is hexamethylenetetramine (HMT). This is a highly symmetrical molecule and the crystal structure is body-centered cubic, with only one molecule in the primitive unit cell. Each molecule contains 22 atoms [$(CH_2)_6N_4$], and so a straightforward treatment of the crystal dynamics (i.e., a Born-von Kármán interatomic force model) would lead to a (66x66) dynamical matrix whose elments would contain an enormous number of force constant parameters. However, almost all of the normal modes are internal modes of vibration of the molecular unit; most of these are of rather high frequency and so are virtually unchanged from the analogous modes in the free molecule. We would not expect them to display very much dispersion, and so an adequate knowledge of these modes is obtained by optical studies of their limiting behavior at very small wave vector. The low frequency modes of the system, those in which the molecules behave as more or less rigid units, are of greater interest from the crystal dynamics point of view; these would be expected to show significant dispersion effects, which could be studied in detail by appropriate inelastic neutron scattering experiments. HMT is indeed the first molecular crystal for which comprehensive lattice dynamical calculations [11,13] have been carried out on the basis of a physically reasonable intermolecular force model, which we shall now briefly describe. For full details of these calculations, the reader is referred to the excellent paper by Cochran and Pawley [11]. A much simplified model for HMT has been discussed by Becka and Cruickshank [32].

As in the case of $NaNO_2$ described above, we wish to establish a dynamical model for HMT which will take into account the translational and librational motions of the molecular units, while neglecting their internal modes of vibration. Force constants, representing the forces and couples exerted on a molecule by its near neighbors, are postulated, and the appropriate equations of motion, eq (14), are written down. Maximum use is made of the high symmetry of this crystal to reduce the number of disposable parameters. It turns out that only 6 independent parameters are required to specify the interactions for the first nearest neighbors, and 6 also for the second nearest neighbor interactions. Cochran and Pawley make the further assumptions that the molecule is centro-symmetric (in order to eliminate 2 of these 12 parameters), and that the molecules are rigid (i.e., unpolarizable). Thus coulomb interactions do not enter into the calculations. Since there is only one molecule (and no separate "atoms") per cell, the dynamical matrix is of order (6x6). Roughly speaking, for any wave vector, we find 3 translational acoustic type modes and 3 librational (optic) type modes. The usual kinds of simplifications arise for modes propagating along high symmetry directions. For $\mathbf{q}$ along Δ, or (100), for example, the matrix factorizes into 2 linear equations (longitudinal acoustic and pure librational) and 2 (2x2) matrices giving modes of mixed character. At $q=0$, all three librational modes become degenerate; the frequency of this mode has been measured by Raman spectroscopy. Force constant values were chosen [11] to fit both this frequency and the measured elastic constants. These data are insufficient to specify all the parameters individually, and so various plausible sets of values were tried to see how much the calculated dispersion curves depended on each force constant. The result of one of these calculations is reproduced in figure 4.

As yet, there are no published measurements of the phonon frequencies in HMT, although neutron scattering experiments on a single crystal of fully deuterated HMT are in progress at Chalk River [33]. It is necessary to use deuterated specimens in these *coherent* scattering experiments, since the scattering cross-section of hydrogen is almost completely incoherent. Indeed, incoherent inelastic neutron scattering experiments on many hydrogenous materials can readily be performed [34]. Such experiments can often give valuable, though qualitative, information about the frequency distribution function of the normal modes in a crystal; coherent scattering experiments are needed to obtain the normal mode frequencies themselves. It will certainly be of great interest to see whether the theory of Cochran and Pawley gives an adequate fit to the experimental results when these become available, or whether some more complicated model is needed. Another excellent candidate for such a comparison between theory and experiment is adamantane [13]. Incoherent neutron scattering experiments on this highly symmetric molecular crystal have been performed by Stockmeyer and Stiller [35]. Presumably it would be possible to produce single crystals of the deuterated material, so that some extremely interesting coherent scattering experiments could be made.

4. Even More Complicated Solids

In the previous sections we discussed some examples of crystals which were either highly symmetric (but comprising many different atom types) or composed of only a few different atoms (but having rather low symmetry). A very large number of crystals, however, fall into neither of these categories, and yet are perhaps not so complex as to prohibit all useful discussion of their dynamical properties at this time. Examples of such crystals are organic hydrocarbons, such as benzene, naphthalene and anthracene. The essential characteristic of such crystals from our viewpoint is that it should be a good approximation to divide their normal modes into two more or less distinct groups (i) the lattice modes, translations and librations of (almost) rigid molecules and (ii) the intramolecular modes. Since the

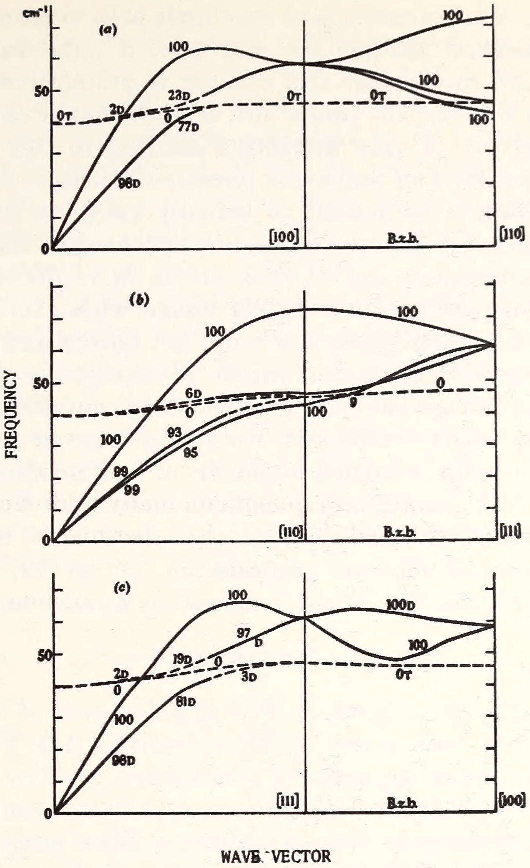

Figure 4. Calculated phonon dispersion curves for hexamethylenetetramine (from reference 11): (a) [000] to [100] to [110], (b) [000] to [110] to [111], (c) [000] to [111] to [100]. The numbers give the percentage translational character of the mode. Predominantly librational modes have broken lines. *D* and *T* denote doubly and triply degenerate branches. B.z.b. ≡ Brillouin zone boundary. To obtain the frequency in 10^{12} Hz units from cm^{-1}, divide by 33.

latter involve distortions of strong covalent bonds, such as those between adjacent carbon atoms, one may hope that their frequencies are appreciably higher than all of the lattice modes. Many organic molecules, such as long chain hydrocarbons, fail to satisfy this requirement and the development of lattice dynamical theories for these cases will no doubt be most difficult.

Naphthalene and anthracene differ from HMT and adamantane in that they crystallize in the rather low symmetry monoclinic space group $P2_1/a$. Thus if we attempt to set up a dynamical model with arbitrary parameters representing the intermolecular forces and couples, then the symmetry is of very little help in reducing the number of independent parameters, and even if only nearest neighbor interactions are considered, this number is prohibitively large. Consequently, as Pawley [16] points out, a model based on fewer parameters is called for. A very attractive solution to this problem is to postulate some kind of empirical potential function (it seems to be out of the question at present to actually calculate such a function from first principles) describing the interactions between an individual atom within a molecule and all other atoms on neighboring molecules. We assume that each atom is rigidly bound within its own molecule, so that intramolecular potentials need not be considered. In certain cases, however, this restriction might advantageously be lifted, but for the moment we ignore this possibility. Naphthalene and anthracene are essentially planar molecules, consisting respectively of two and three benzene rings attached together in the manner indicated in figure 5. The only interatomic potentials needed are for C—C, C—H and H—H bonds. A very popular type of potential which has been invoked for several different purposes [36, 37, 38, 39, 14] consists of an attractive Van der Waals term balanced by an exponential repulsion:

$$V(r) = -A/r^6 + B \exp(-\alpha r). \tag{23}$$

Values for the parameters A, B and α for each of the 3 types of atom pairs have been given by Kitaigorodskii [14]. These were obtained by comparing the heats of sublimation of a few simple hydrocarbons with their lattice energies computed by summing eq. (23) over all pairs of atoms in distinct molecules. Other analytic expressions such as the well-known 6–12 potential, could also be used. One possible objection to all such simple potentials is that they are functions only of interatomic distance r, independent of direction. At present, however, there would seem to be little point in introducing more complicated functions, at least until it has been found that the use of eq (23) fails to provide a satisfactory fit to experimental data.

In order to make use of these potential functions to calculate the "lattice mode" frequencies in naphthalene, for example, we first set up a phenomenological force model similar to those discussed in section 3. As usual, maximum use is made of the limited symmetry to reduce the number of $\phi_{xy}(lk,l'k')$ which must be calculated. In addition to the two classes of operators, A and B, mentioned previously in connection with symmorphic space groups, there is a third class appropriate to non-symmorphic groups such as $P2_1/a$, which relates the appropriate force-constant matrix and the inverse of its transpose. The operation of the screw diad, an example of this class, is described in detail by Pawley [16]. After all possible symmetry arguments have been made, a large number of interaction coefficients remain to be evaluated. For a given pair of molecules (lk), $(l'k')$, we write down the potential for all possible pairs of atoms, always taking one from each molecule. Analytic differentiation with respect to r gives the interatomic forces, which, on summing over all atom pairs, lead to the forces and torques exerted on each molecular unit. When the crystal is in equilibrium, the sum of these forces and torques must be zero, and it may be necessary to adjust the orientations of the molecules within the unit cell in order to insure that this is indeed so.

Let us now consider that intermolecular force constant which represents the force on an origin molecule in the x direction, when a molecule at $r(l'k')$ is rotated slightly about an axis β. This may be conveniently computed in terms of the (A, B, α) values for the 3 interatomic potential functions, simply by numerical differentiation of the forces involved. We rotate the $(l'k')$ molecule by a suitable small angle $\Delta\beta$ from the equilibrium orientation and recalculate the force exerted on the origin molecule. The x component of this force, divided by $\Delta\beta$, gives us the desired force constant. Care must be taken over the

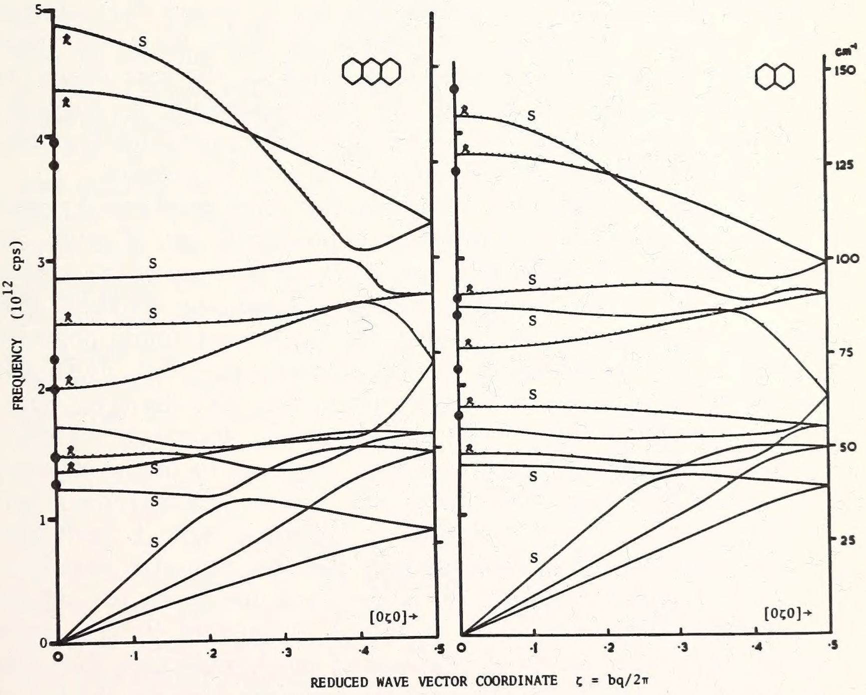

FIGURE 5. Calculated phonon dispersion curves for anthracene and naphthalene (from reference 16), for modes propagating along the b direction. R denotes a mode with librational character, while S indicates a symmetric mode. The filled circles at $\zeta=0$ are the Raman measurements.

choice of increments in displacement and angle used in this numerical differentiation. Pawley [16] found that 10^{-4} Å and 3×10^{-4} radians were most suitable. Once all the force constants have been computed in this way, it is relatively straightforward to set up the dynamical matrix [(12×12) since there are two molecules per unit cell] and diagonalize it to obtain the 12 normal mode frequencies for any desired wave vector. The only "high symmetry direction" in this monoclinic structure is along the *b* axis; here the 12 lattice modes reduce to a set of 6 symmetric modes which preserve the space group symmetry and 6 antisymmetric modes which do not. The lattice-mode dispersion curves calculated by Pawley [16] for naphthalene and anthracene are shown in figure 5. Also shown here are the results of Raman scattering measurements of certain zero wave vector modes. The agreement with the calculations is fairly good, particularly for the lower frequencies. The higher frequency modes would be expected to fit less satisfactorily, since the lowest frequency internal modes of molecular vibration are probably not too far removed from these, and some interaction between them is to be expected.

As in the case of hexamethylenetetramine, single crystals of fully deuterated naphthalene and anthracene are necessary for coherent inelastic neutron scattering experiments on these materials. Such experiments are either in progress or planned for the near future for both anthracene (at Oak Ridge) and naphthalene[40] (at Harwell), and so much more detailed tests of Kitaigorodskii's potential functions and Pawley's normal-mode calculations will soon be possible.

The technique of obtaining intermolecular force constants by summing over the derivatives of interatomic potentials can, of course, be applied to simpler materials, provided there are only one or two atomic species present. Thus the hydrocarbon adamantane [$(CH_2)_6(CH)_4$] could be treated in this way, using the same interatomic potential functions as for naphthalene. Hexamethylenetetramine [$(CH_2)_6N_4$] would be rather more clumsily dealt with in this way, however, since 6 distinct potentials would need to be specified. Inorganic materials of a molecular character, such as iodine, may also be discussed along these lines. A first stage would be to postulate an iodine-iodine potential $V_1(r)$ between atoms belonging to different, rigid I_2 molecules. The intermolecular force constants may then be computed exactly as in the case of naphthalene, and the lattice dynamics of this orthorhombic material expressed in terms of only 3 parameters. Such a model neglects the internal modes of vibration of the I_2 molecules. This may or may not turn out to be a reasonable approximation for the lattice modes; if not, then this restriction might be removed by postulating a second, stronger, iodine-iodine potential, $V_2(r)$, to act only between atoms within a given molecule. The parameters describing $V_1(r)$ and

$V_2(r)$ are chosen to maintain the "dumbbell" nature of the structure, with the known dumbbell orientation as the equilibrium configuration. This would then permit a phenomenological description of all the normal modes of iodine with very much fewer parameters than would be required in the conventional force-constant analysis. Whether or not this approach will provide a satisfactory description of the lattice dynamics could be decided by appropriate neutron inelastic scattering experiments on a single crystal of iodine.

5. Concluding Remarks

The phenomenological framework developed by Born and Huang[2] has been extensively and successfully utilized in the analysis of dispersion curves for simple crystalline solids. Further research in this field falls mainly into two categories, (a) the *a priori* calculation of the basic interatomic forces from more fundamental postulates, and (b) the extension of the conventional framework to be able to deal with more complicated solids, which is the subject of this paper. We have seen how unwieldy the Born-von Kármán type of approach becomes even for what may be regarded as a fairly simple inorganic solid such as $NaNO_2$. The ideas developed in sections 3 and 4 are twofold: (a) that of treating any more or less rigid molecular groupings in the crystal as single entities having both translational and librational degrees of freedom, while neglecting their internal modes of vibration; and (b) that of calculating intermolecular coupling constants by summing over suitable derivatives of empirical interatomic potential functions defined for various pairs of atoms, taken from distinct molecules. Even with the introduction of these ideas, the lattice dynamical calculations are not simple, and little progress could be envisaged without the aid of high-speed computers.

In this paper we have tended to concentrate on the calculation of the phonon dispersion relation $\nu=\nu_j(\mathbf{q})$, which may be directly measured by coherent inelastic neutron scattering. Experimentally this subject is still at a very early stage, although the number of new experiments now in hand suggests an extremely rapid expansion during the next few years. A rather basic restriction of these experiments is that the use of hydrogenous crystal specimens would seem to be virtually prohibited by the enormous incoherent scattering cross section of hydrogen. In the absence of a deuterated specimen, one must perforce make observations of this incoherent scattering, which can only give information about the density of phonon states, $g(\nu)$, in the material concerned. Given a model for the interatomic or intermolecular forces, the function $g(\nu)$ can, of course, be calculated and compared with experiment. The location of sharp peaks or other singular features can often be of value in such comparisons. A recent review of this subject has been given by Boutin[34]. As the crystals being studied become more complex, it is clear that every possible technique, coherent and incoherent neutron scattering, Raman scattering, infrared spectroscopy, elastic constant measurements, and so on, will be needed to achieve a complete picture of their lattice dynamics.

The author is indebted to his many colleagues both at Chalk River and Oak Ridge for stimulating discussions on molecular dynamics in general, to Dr. G. S. Pawley for valuable correspondence concerning naphthalene and anthracene, and to Dr. C. B. Clark for discussions of possible force models for iodine.

6. Discussion

H. Resing (Naval Research Laboratory): Has any use been made of the fact that Smith has shown the barrier to rotation in HMT is 18 kcal/mol by means of NMR measurements?

G. Dolling: No use has been made of this information in setting up the HMT force model. The derivatives of the crystal potential (e.g. the force constants) are not directly related to the barrier height for molecular rotation.

H. Resing: The heat capacity can be calculated from the derived vibration frequencies. Is agreement between such a theoretical heat capacity and the experimental heat capacity a good argument for the validity of the theory?

G. Dolling: As far as I know, the heat capacity of HMT has not been computed from the calculated phonon frequencies, although this could readily be done in the harmonic approximation. One might expect to obtain agreement with the experimental heat capacity to within several percent. To this extent, such a comparison between theory and experiment is quite useful, although anharmonic effects will make it very difficult to deduce from it any more quantitative information about the harmonic model. At this stage, therefore, since we do not have accurate calculations of the anharmonic contribution, the heat capacity is not a particularly sensitive test of a (pseudo-harmonic) force model.

M. Blumenfeld (University of Toronto): I would like to suggest that an ethylene crystal would be interesting to study by the neutron scattering technique. It's a simple molecule in a relatively simple crystal, and one might obtain a more easily interpreted dispersion curve than with some of the more complicated molecules you've been discussing.

G. Dolling: So long as the ethylene molecule satisfies the requirement that the internal vibrations are well separated from the lattice modes, it would be an appropriate case.

M. Blumenfeld: The lattice modes, on the basis of Raman spectra, are in the region of 100 $cm.^{-1}$ The internal modes are in the range from 1000 to 3000 $cm.^{-1}$

J. J. Rush (National Bureau of Standards): Preparation of a large enough crystal at low temperatures might be difficult.

7. References

[1] M. Born and T. von Kármán, Phys. Zeit. **13,** 297 (1912).
[2] M. Born and K. Huang, Dynamical Theory of Crystal Lattices, Clarendon Press, Oxford (1955).
[3] W. Cochran, Reports in Progress in Physics **26,** 1 (1963).
[4] A. A. Maradudin, E. W. Montroll and G. H. Weiss, Lattice Dynamics in the Harmonic Approximation, Solid State Physics, Suppl. 3, editors F. Seitz and D. Turnbull, Academic Press, New York (1963).
[5] G. Dolling and A. D. B. Woods, in Thermal Neutron Scattering, editor P. A. Egelstaff, Academic Press, New York (1965).
[6] G. Leibfried and W. Ludwig, in Solid State Physics, editors F. Seitz and D. Turnbull, Vol. 12, Academic Press, New York (1963).
[7] R. A. Cowley, Advances in Phys. **12,** 421 (1963).
[8] V. N. Kashcheev and M. A. Krivoglaz, Sov. Phys. Solid State **3,** 1107 (1961); translation from Fiz. Tverdogo Tela **3,** 1528 (1961).
[9] G. Dolling, H. G. Smith, R. M. Nicklow, P. R. Vijayaraghavan and M. K. Wilkinson, Phys. Rev. **168,** 970 (1968)
[10] J. Sakurai, R. A. Cowley and G. Dolling, Bull. Am. Phys. Soc. **12,** 282 (1967), and to be published.
[11] W. Cochran and G. S. Pawley, Proc. Roy. Roy. Soc. (London) **A280,** 1 (1964).
[12] H. Hahn and W. Biem, Phys. Stat. Sol. **3,** 1911 (1963).
[13] W. Biem, Phys. Stat. Sol. **3,** 1927 (1963).
[14] A. I. Kitaigorodskii, J. Chim. Phys. **63,** 6 (1966).
[15] A. I. Kitaigorodskii, B. D. Koreshkov and A. G. Kulkin, Sov. Phys. Solid State **7,** 511 (1965); translation from Fiz. Tverdogo Tela **7,** 643 (1965).
[16] G. S. Pawley, Phys. Stat. Sol. **20,** 347 (1967).
[17] P. O. Löwdin, A Theoretical Investigation into Some Properties of Ionic Crystals, Almquist and Wiksells, Uppsala (1948).
[18] S. O. Lundquist, Ark. Fys. **9,** 435 1955); **12,** 263 1957).
[19] T. Toya, J. Res. Inst. Catalysis, Hokkaido Univ. **6,** 183 (1958).
[20] L. J. Sham, Proc. Roy. Soc. (London) **A283,** 33 (1965).
[21] W. A. Harrison, Pseudo Potentials in the Theory of Metals, W. A. Benjamin, New York (1966).
[22] A. E. O. Animalu, Technical Report No. 3, Solid State Theory Group, Cavendish Laboratory, Cambridge (1965).
[23] U. Schröder, Solid State Commun. **4,** 347 (1966). Also V. Nüsslein and U. Schröder, Phys. Stat. Sol. **21,** 309 (1967).
[24] B. G. Dick and A. W. Overhauser, Phys. Rev. **112,** 90 (1958).
[25] W. Cochran, Phys. Rev. Letters **2,** 495 (1959).
[26] E. W. Kellermann, Phil. Trans. **A238,** 513 (1940).
[27] T. Wolfram, G. W. Lehman and R. E. DeWames, Phys. Rev. **129,** 2483 (1963)

[28] L. P. Bouckaert, R. Smoluchowski and E. Wigner, Phys. Rev. **50,** 58 (1936).

[29] These methods are thoroughly described in papers by S. H. Vosko and A. A. Maradudin, and by J. L. Warren, Rev. Mod. Phys. **40,** 1 (1968) and **40,** 38, (1968).

[30] G. F. Koster, in Solid State Physics, editors F. Seitz and D. Turnbull, Vol. V, Academic Press, New York (1957).

[31] S. Hoshino and H. Motegi, Jap. Appl. Phys. **6,** 708 (1967); see also Y. Takagi and K. Gesi, J. Phys. Soc. Japan **22,** 979 (1967), for additional references.

[32] L. N. Becka and D. W. J. Cruickshank, Proc. Roy. Soc. (London), **A273,** 435 and 455 (1963).

[33] B. M. Powell, private communication.

[34] H. Boutin, in Proceedings of the Symposium on Thermal Neutron Scattering Applied to Chemical and Solid State Physics, American Crystallographic Association, **3,** 30 (1967).

[35] R. Stockmeyer and H. H. Stiller, Phys. Stat. Sol. **19,** 781 (1967).

[36] C. A. Coulson and C. W. Haigh, Tetrahedron **19,** 527 (1963).

[37] B. De Santis, E. Giglio, A. M. Liquori and A. Ripamonti, Nature **206,** 456 (1965).

[38] A. I. Kitaigorodskii, Tetrahedron **14,** 230 (1961).

[39] D. P. Craig, R. Mason, P. Pauling and D. P. Santry, Proc. Roy. Soc. (London) **A286,** 98 (1965).

[40] G. S. Pawley, private communication.

EPITHERMAL NEUTRON INELASTIC SCATTERING FROM METAL HYDRIDES[1]

S. S. PAN and M. L. YEATER

Rensselaer Polytechnic Institute, Troy, New York 12180

and

W. E. MOORE

Knolls Atomic Power Laboratory, Schenectady, New York 12301

1. Introduction

This paper summarizes part of the recent neutron scattering research at RPI. The RPI-KAPL scattering facility[2] is designed to study the interactions of neutrons with molecular systems by measuring the energy and angle dependence of the inelastic scattering cross section. Because neutrons having 0.1 to 1 eV incident energy can be used, a wide range of energy and momentum exchange is accessible; single and multiple excitation of the optical modes can be studied in some detail. Comparisons are made between theory and experiment to provide a critical test of a given molecular or atomic vibration model, and indirectly verify certain aspects of the molecular structure. In favorable cases a frequency distribution and scattering law can be derived.

Our analytical procedure for the hydrides is simple because the optical mode is well separated from the acoustic mode. A Debye distribution is assumed for the acoustic mode, and a one-phonon formula is used to deduce a trial frequency distribution from the resolution-corrected cross section data for the optical vibration; an iteration of this distribution is performed in the Debye-Waller factor. Additional improvements are then sought by using the distributed frequency distribution as input to the GASKET-FLANGE [1][3] codes, and comparing the calculated double-differential cross section profiles with the experimental data. Slight modifications of the frequency distribution can generally be made to yield satisfactory comparisons for the range of variables covered by the data.

---

[1] Work supported by the U.S. Atomic Energy Commission.

[2] Some details of the experimental equipment and technique are given in a separate paper in these Proceedings.

[3] Figures in brackets indicate the literature references listed at the end of this paper.

2. Zirconium Hydride

Differential cross sections have been measured at room temperature for incident neutron energies 0.16, 0.24, 0.40, 0.57 and 0.66 eV, and scattering angles ranging from 25° to 150°. Measurements were made at liquid nitrogen temperature with 0.24-eV incident neutrons. Samples having 90 to 95 percent transmission were used, and multiple scattering corrections were applied to some of the data. The measured oscillator energy obtained from the lowest energy runs is 137±3 meV; the higher energy data exhibit equally spaced peaks which are integral multiples (within 5 percent) of this energy, through the third excitation. Careful corrections were applied to the elastic scattering cross sections for the unresolved inelastic scattering of the acoustic mode, and a Debye-Waller factor of 10 eV^{-1} was obtained. The optical-peak width for 0.24-eV incident energy was 26±3 meV, after an 8 percent correction for experimental resolution. The excitation energies and peak widths are in good agreement with other data [2].

Good agreement with the room-temperature data was obtained for a theoretical calculation using a Gaussian frequency distribution for the optical mode, centered at 137 meV and having 22 meV FWHM; the acoustic mode was represented by a Debye distribution up to 24 meV, weighted by the mass ratio 1/91. However, the low-temperature measurement yielded a slightly asymmetric optical mode, as illustrated in figure 1. The frequency distribution deduced in the one-phonon approximation is shown as a dashed line with an arbitrary scale factor. The measured width, 21±3 meV, indicates that Doppler broadening makes only a small contribution to the level widths measured at room temperature. A single-frequency Einstein oscillator model, plus a Debye spectrum, could not be made to fit the observed

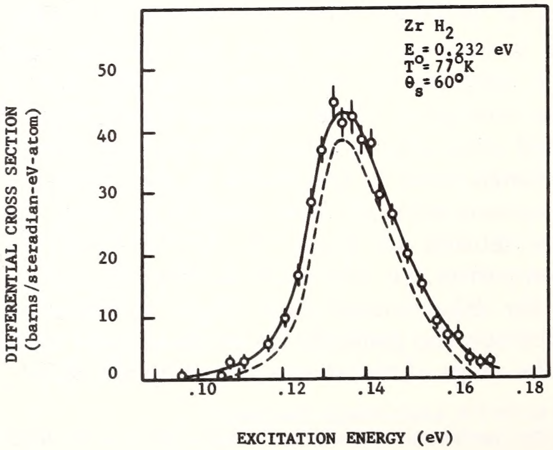

FIGURE 1. Differential cross section for the optical mode in ZrH_2 at liquid nitrogen temperature. The dashed line indicates the derived frequency distribution.

line shape. Angular distributions calculated with the distributed frequency spectrum generally were in better agreement with experiment than calculations based on an Einstein oscillator model.

3. Titanium Hydride

The vibrational energy and level width have been measured for TiH_2 using several incident energies. Again the energies for first, second and third excitations of the optical mode are approximately equally spaced. The one-phonon energy (142±6 meV) is in good agreement with previous neutron scattering experiments [3, 4]. The observed width (39±3 meV) is larger than for zirconium hydride, possibly because the hydrogen-hydrogen interaction through the coupling with the lighter titanium atom is stronger.

4. Niobium Hydride

Scattering cross sections have been measured for a thin $NbH_{0.85}$ sample at room temperature using 0.238—eV incident neutrons. Two well-separated peaks are observed corresponding to energy transfers of 120 meV and 165 meV. The resolution-corrected widths are 18±3 meV. There is no significant evidence for optical levels of lower energy.

Theoretical differential cross sections have been calculated, starting with a one-phonon frequency distribution as outlined above. A Debye acoustic spectrum with a cutoff at 22 meV was used. Two calculations were made, with the Debye mode weighted 1/93, corresponding to a linear chain model, and 1/(6x93), based on an idealized three-dimensional model. The results are shown in figure 2. A small resolution correction (8 percent FWHM Gaussian) has been applied to the data, but multiple-scattering corrections have not been made.

For this range of hydrogen concentration, a niobium hydride β phase is formed with a slightly-distorted bcc lattice [5]. It has been suggested, by considering the vacancies which exist in the lattice, that the hydrogen occupies tetrahedral sites [6]. A recent neutron scattering study of vanadium hydride in its α (bcc) and β (bct) phases [7] also indicates split optical vibrations of 120 meV and approximately 170 meV excitation; these were identified as due to the hydrogens vibrating in the tetrahedral sites. The same work also suggests some population of octahedral sites in the β phase, but the vibration frequencies are considerably lower. We therefore believe that our observations confirm that the hydrogen occupies the proposed tetrahedral sites of the distorted niobium lattice. The splitting of the optical mode is probably due to the anisotropy of these distorted sites. Our results on thorium hydride also show splitting of the optical mode, corresponding to 75 and 125 meV excitation; in this case the widths were approximately 14 and 35 meV, respectively.

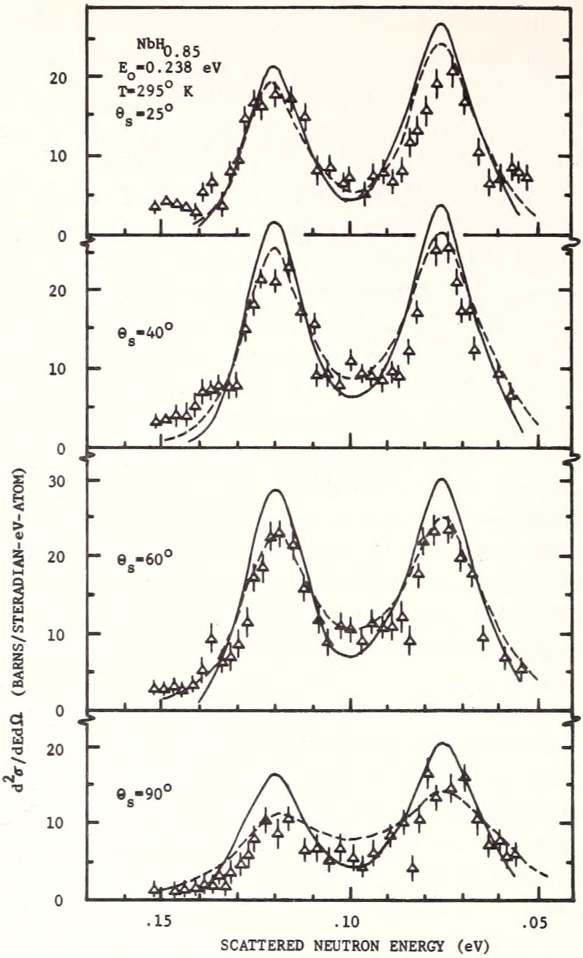

FIGURE 2 Differential cross section for the optical modes in $NbH_{0.85}$ at room temperature. The solid and dashed lines represent calculations with the Debye spectrum weighted 1/(6x93) and 1/93, respectively.

5. References

[1] J. V. Koppel, J. R. Triplett, and Y. D. Naliboff, USAEC Report GA–7417 (1966).
[2] O. K. Harling and B. R. Leonard, Jr., BNL–940 (C–45) p. 96 (1965).
[3] D. H. Saunderson and S. J. Cocking, Inelastic Scattering of Neutrons in Solids and Liquids, Vol. II, p. 265, IAEA, Vienna (1963).
[4] W. L. Whittemore and A. W. McReynolds, Inelastic Scattering of Neutrons in Solids and Liquids, p. 511, IAEA, Vienna (1961).
[5] D. R. Knowles, UKAEA Report IGR–R/C–190 (1957).
[6] G. Hägg, Z. Phys. Chem. **B11**, 433 (1931).
[7] J. J. Rush and H. E. Flotow, private communication (1968), J. Chem. Phys. **48**, 3795 (1968).

VIBRATION SPECTRA OF HYDRIDES POSSESSING THE CUBIC PEROVSKITE STRUCTURE BY THE INELASTIC SCATTERING OF COLD NEUTRONS

ARNULF J. MAELAND

AMMRC, Watertown, Mass. 02172

1. Introduction

Messer and coworkers have, on the basis of x-ray powder patterns and by analogy with $BaLiF_3$, reported $BaLiH_3$, $SrLiH_3$ [1] [1] and $EuLiH_3$ [2] to have inverse perovskite structures. A recent neutron diffraction study of $BaLiH_3$ and $BaLiD_3$ has confirmed the perovskite structure [3]. In the present experiments, we have obtained the vibration spectra of $BaLiH_3$ and $SrLiH_3$ by the energy-gain scattering of cold neutrons. Infrared transmission spectra have also been obtained to supplement the neutron data and assist in the identification of the vibration frequencies.

2. Experimental Procedure

The neutron measurements were made at the AMMRC reactor using a cold beryllium filter spectrometer. The incident neutrons have a mean energy of about 3.5 meV. In the incoherent inelastic scattering process lattice vibrational quanta (phonons) are transferred to the incident neutrons. Energy analysis of the scattered neutrons are obtained by the conventional time-of-flight method. The energy resolution is about 4 percent at low energy transfer and becomes progressively worse at large energy transfers. The infrared transmission spectra were recorded on a Perkin-Elmer 621 spectrometer. The samples were dispersed in nujol and placed between KBr disks.

3. Results

The time-of-flight spectrum of neutrons scattered by $SrLiH_3$ is shown in figure 1. The spectrum for $BaLiH_3$ is quite similar. Each spectrum shows 4 distinct inelastic scattering bands corresponding to four optic modes. The elastic neutron peak begins around channel 156 in both spectra. The neutron scattering cross section is in general not expressable in terms of the frequency distribution function. However,

---

[1] Figures in brackets indicate the literature references at the end of this paper.

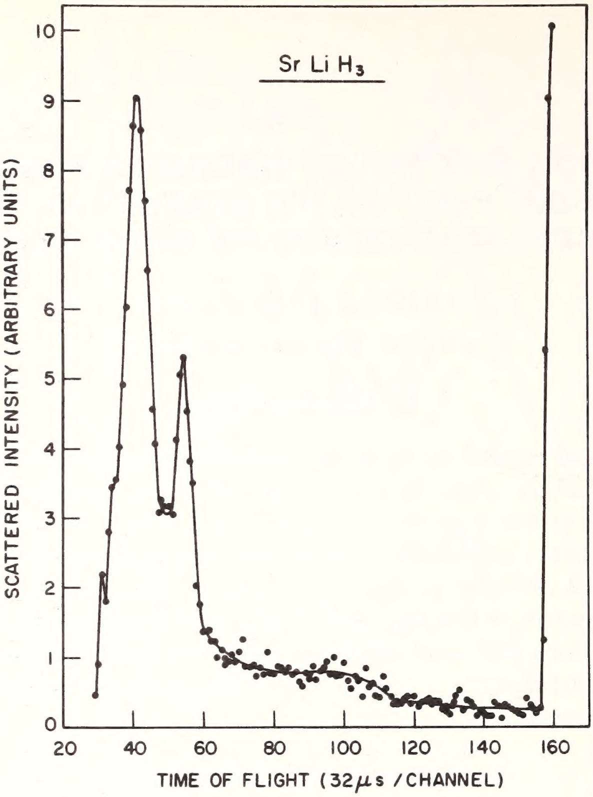

Figure 1. Time-of-flight spectrum of neutrons scattered from $SrLiH_3$.

for a cubic polycrystalline sample, an approximate frequency distribution can be derived from the neutron scattering measurements [4]. The approximate frequency distribution for $SrLiH_3$ is shown in figure 2.

4. Discussion

The cubic perovskite structure belongs to the space group O_h^1 and contains five atoms per unit cell. Hunt, Perry, and Ferguson showed by group theoretical arguments that the twelve nontranslatory modes in the perovskite structure consisted of 3 triply-degenerate normal modes belonging to the symmetry species F_{1u} and 1 triply-degenerate mode of F_{2u} symmetry [5]. The F_{2u} mode is infrared inactive. Quite recently [6] a normal coordinate analysis of perovskite fluorides was published and provided a full description of the vibrational modes in perovskites. Using this description we explain the neutron and infrared results obtained on $BaLiH_3$, $SrLiH_3$ and $EuLiH_3$ and compiled in table 1, as follows. The high frequency band is assigned to the Li-H

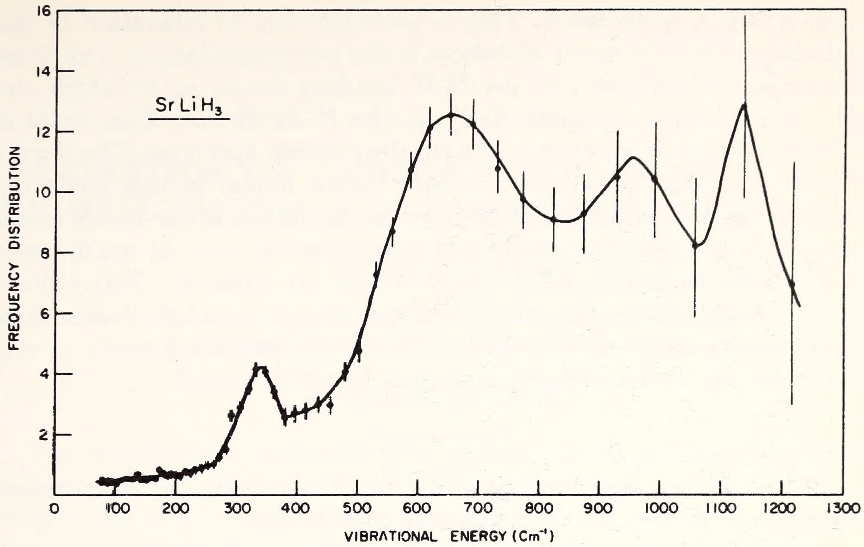

FIGURE 2. Approximate frequency distribution for $SrLiH_3$.

stretching mode ν_1. This frequency will be sensitive to the Li-H distance, a fact which is supported by the experimental data in table 1. In going from $BaLiH_3$ to $SrLiH_3$ the Li-H distance is greatly reduced. Consequently, the Li-H force constant becomes larger and the corresponding frequency ν_1 increases. In $EuLiH_3$ there is a very small decrease in the Li-H distance compared to $SrLiH_3$ and a corresponding small increase in ν_1.

The next band is assigned to ν_4 (F_{2u}) which is infrared inactive, but clearly present in the neutron spectra. However, there appears to be a small shoulder in the I.R. spectra of $EuLiH_3$ and $SrLiH_3$ in the posi-

TABLE 1. Comparison of vibrational frequencies (cm^{-1}) observed in neutron and infrared measurements

$SrLiH_3$		$BaLiH_3$		$EuLiH_3$		Assignment
Neutrons	I.R.	Neutrons	I.R.	Neutrons	I.R.	
1130	1080	920	910	---------	1090	ν_1
950	(930)ia	780	ia	---------	(920)ia	ν_4
660	670	650	650	---------	660	ν_2
340	--------	310	--------	---------	--------	ν_3

tion where ν_4 is expected. This is probably due to relaxation of the selection rules as a result of defects in the perovskite lattice. The third frequency is assigned to the Li-H bending mode, ν_2, in which the H^- ions displace perpendicularly to the H–Li–H line. This mode is observed in the infrared as well as in the neutron spectrum. The lowest band, ν_3, is associated with the M^{+2} lattice mode; in this mode the LiH_3 group oscillates as an entity against the lattice of the heavy metal atoms. It is an external mode and is expected to occur at much lower frequencies than the other modes which are internal. This follows from the assumption that forces between groups are much weaker than those among atoms within a group. The lowest frequency mode, ν_3, was not observed in the infrared because of the KBr cut-off.

This work was supported by Picatinny Arsenal, Dover, New Jersey, through a NAS–NRC Postdoctoral Fellowship.

5. References

[1] C. E. Messer, J. C. Eastman, R. G. Mers, and A. J. Maeland, Inorg. Chem. **3,** 776 (1964).
[2] C. E. Messer and K. Hardcastle, Inorg. Chem. **3,** 1327 (1964).
[3] A. J. Maeland and A. F. Andresen, Paper presented at the 7th International Congress of the International Union of Crystallography in Moscow, U.S.S.R., 12–19 July, 1966.
[4] L. S. Kothari and K. S. Singwi, Solid State Phys. **8,** 109 (1959).
[5] G. R. Hunt, C. H. Perry, and J. Ferguson, Phys. Rev. **134,** A688 (1964).
[6] I. Nakagawa, A. Tsuchida, and T. Shimanouchi, J. Chem. Phys. **47,** 982 (1967).

ABSORPTION OF LIGHT BY THE SOUND WAVES OF ORIENTATIONALLY DISORDERED CRYSTALS

E. WHALLEY

Division of Applied Chemistry,
National Research Council, Ottawa, Canada

1. Introduction

The translational symmetry of a perfect crystal requires that light is absorbed by the nuclear vibrations in a fundamental transition only if the wave vector of the lattice vibration **k** and of the light in the crystal **K** are equal. Any departure from exact translational symmetry relaxes this selection rule and may make all normal vibrations of the crystal active.

The purpose of this paper is to discuss the absorption of light by orientationally disordered crystals in the acoustic branches where the Debye density of states holds. We are interested then in the absorption of light by sound waves.

2. Summary of General Theory

It has been shown recently [1] [1] that all the translational lattice vibrations of an orientationally disordered crystal are active in the infrared and Raman spectra. A detailed study of the far-infrared spectrum of ice [2], particularly of cubic ice (ice Ic), which is orientationally disordered, revealed features that could be identified with features in the density of vibrational states such as the *TO*, *LO*, *LA*, and *TA* maxima, the minimum between the *LO* and *LA* branches, and so on. It is assumed that the potential energy V can be written as the sum of square terms of the internal coordinates

$$2V=\sum_{l,\kappa}\phi(\kappa)s^2(l,\kappa) \tag{1}$$

where $s(l,\kappa)$ is the κth internal coordinate associated with unit cell l and $\phi(\kappa)$ is the corresponding force constant. The change $\Delta\boldsymbol{\mu}$ of the dipole moment of the crystal for the change of the internal coordinates is

$$\Delta\boldsymbol{\mu}=\sum_{l,\kappa}\mathbf{M}(l,\kappa)s(l,\kappa) \tag{2}$$

---

[1] Figures in brackets indicate the literature references listed at the end of this paper.

where $\mathbf{M}(l, \kappa)$ is the dipole moment derivative with respect to coordinate $s(l, \kappa)$. In an ordered crystal $\mathbf{M}(l, \kappa)$ is independent of l, but in a disordered crystal, it is different for different l because of the disorder.

$\mathbf{M}(l, \kappa)$ can be divided into a regular part $\mathbf{M}'(\kappa)$ that has the diffraction symmetry of the crystal. It is independent of l, and is equal to the average value of $\mathbf{M}(l, \kappa)$ over all unit cells,

$$\mathbf{M}'(\kappa) = \frac{1}{N} \sum_l \mathbf{M}(l, \kappa), \tag{3}$$

where N is the number of unit cells. The difference $\mathbf{M}''(l, \kappa)$ between $\mathbf{M}(l, \kappa)$ and $\mathbf{M}'(\kappa)$,

$$\mathbf{M}''(l, \kappa) = \mathbf{M}(l, \kappa) - \mathbf{M}'(\kappa), \tag{4}$$

describes the electrical irregularity of the crystal. A non-zero value of $\mathbf{M}'(\kappa)$ causes the usual activity of low-wave-vector vibrations, whereas a non-zero value of $\mathbf{M}''(l, \kappa)$ causes all vibrations to be active.

If only one coordinate $s(\kappa)$ contributes to the potential energy and if $\mathbf{M}''^2(l, \kappa)$ has only one value $\mathbf{M}''^2(\kappa)$, then the integrated reduced absorptivity $A(\mathbf{k}, j)$ of a normal vibration of wave vector $\mathbf{k}$ in branch j

$$A(\mathbf{k}, j) = V \int_{\substack{\text{band}\\ \mathbf{k}, j}} K(\nu) d\nu, \tag{5}$$

where V is the molar volume, $K(\nu)$ the absorptivity due to the vibration $\mathbf{k}, j$, and ν the vacuum wave number of the light, is

$$A(\mathbf{k}, j) = \frac{\pi}{3c^2} \frac{(n^2+2)^2}{9n} R(\kappa) \omega^2(\mathbf{k}, j). \tag{6}$$

In this equation

$$R(\kappa) = M''^2(\kappa)/\phi(\kappa), \tag{7}$$

$\omega^2(\mathbf{k}, j)$ is the circular frequency of vibration $\mathbf{k}, j$, and the refractive index n allows for the effects of the material on the field. Eq. (6) is also obtained if several coordinates contribute appreciably to the potential energy and the dipole moment, providing that $R(\kappa)$ is the same for each one.

By summing over all vibrations, assuming that each normal vibration has a band width small compared to the frequency interval over which the absorptivity changes appreciably, it can be shown that the absorptivity $K(\omega)$ at frequency ω is given by

$$K(\omega) = \frac{2\pi^2}{3Vc} \frac{(n^2+2)^2}{9n} R\omega^2 g(\omega), \tag{8}$$

where c is the velocity of light and $g(\omega)$ is the density of vibrational states at frequency ω.

3. Debye Distribution

If the frequency is low enough that the Debye distribution holds, then

$$g(\omega)=9N\frac{\omega^2}{\omega_D{}^3}, \tag{9}$$

where ω_D is the Debye frequency and N is Avogadro's number.

The quantity R can be obtained in various ways. One is from the contribution of the translational band to the static dielectric constant. According to a theory as yet unpublished [3], the difference between the limiting low-frequency (ϵ_0) and high-frequency (ϵ_∞) dielectric constants is

$$\epsilon_0-\epsilon_\infty=\frac{4\pi N}{V}\frac{\epsilon_0+2}{3}\frac{\epsilon_\infty+2}{3}R. \tag{10}$$

Hence, from eqs (8–10), in terms of the vacuum wave number ν of the light absorbed

$$K(\nu)=3\pi^2 f(\epsilon_0-\epsilon_\infty)\,\nu_D\left(\frac{\nu}{\nu_D}\right)^4 \tag{11}$$

where

$$f=\frac{\epsilon_0+2}{\epsilon_\infty+2}\frac{1}{\epsilon_0{}^{1/2}}$$

arises from the effects of the internal field. The absorptivity is proportional to the fourth power of the wave number.

4. Application to Ice

For ice, $\epsilon_0=3.1$[4], $\epsilon_0-\epsilon_\infty=1.1$[3], and $\nu_D=157$ cm^{-1} [5]. Consequently, from eq (11)

$$K(\nu)=4.6\times 10^3\ (\nu/\nu_D)^4\ \mathrm{cm}^{-1}.$$

The theoretical absorptivity is compared with experiment in the range 50 to 16 cm^{-1} in figure 1, which is a plot of log $K(\nu)$ against log ν at 100 °K. At the higher frequencies the absorptivity is proportional to the fourth power of the frequency and is nearly independent of temperature, and the value is within a factor of 3 of that predicted by eq (11). In view of the approximations in the theory, particularly the neglect of long-range interactions [6] and of the short-range correlation of orientations, the agreement is satisfactory. There is no doubt that the sound waves are absorbing light as fundamentals.

At frequencies below those shown in figure 1, the absorptivity departs from a fourth power dependence on the wave number. This no doubt is caused by difference bands, whose intensity is expected to be approximately proportional to the square of the frequency [7].

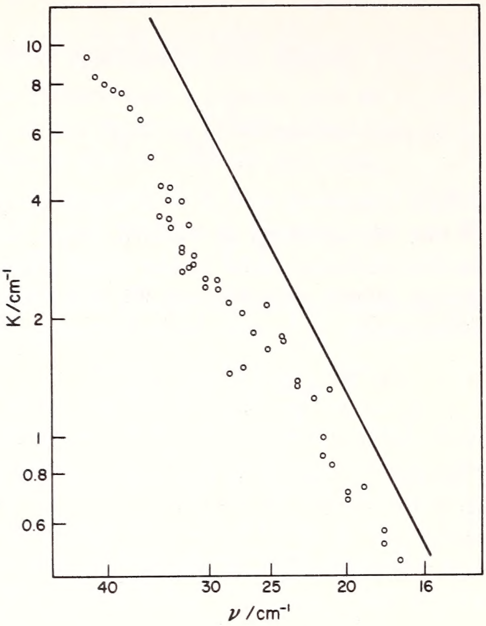

FIGURE 1. Log-log plot of absorptivity of ice against wave number at 100 °K.

5. Future Developments

The treatment outlined in this paper can be applied, with some modifications, to vitreous phases, and the fundamental absorption at low frequencies should also be proportional to the fourth power of the frequency. Departures from this relation may provide information about the departure of the actual frequency distribution from the Debye form. The general considerations should also be relevant to low-frequency absorption in liquids.

Similar considerations should apply to the Raman spectrum but no relevant experimental results have yet been reported.

I am indebted to H. J. Labbé for measuring the absorptivities.

6. References

[1] E. Whalley and J. E. Bertie, J. Chem. Phys. **46,** 1264 (1967).
[2] J. E. Bertie and E. Whalley, J. Chem. Phys. **46,** 1271 (1967).
[3] J. E. Bertie, H. J. Labbé, and E. Whalley, to be published.
[4] J. Lamb and A. Turney, Proc. Phys. Soc. B. **52,** 272 (1949).
[5] P. Flubacher, A. J. Leadbetter, and J. A. Morrison, J. Chem. Phys. **33,** 1751 (1960).
[6] E. Whalley and J. E. Bertie, J. Coll. Interface Sci. **25,** 161 (1967).
[7] B. Szigetti, Proc. Roy. Soc. A **258,** 377 (1960).

LATTICE VIBRATIONS IN SOME SIMPLE MOLECULAR CRYSTALS

J. C. LAUFER, J. E. CAHILL, and G. E. LEROI [1]

Frick Chemical Laboratory
Princeton University, Princeton, New Jersey 08540

Raman spectra of polycrystalline samples of CO_2, N_2O, α–N_2 and α–CO have been obtained on a laser instrument built in this laboratory [1].[2] Several librational lattice modes have been observed and experimental frequencies are compared to theoretical calculations using a pairwise intermolecular potential consisting of a Lennard-Jones (6,12) term and multipole-multipole interactions [2].

The crystal structures of CO_2 [3–5], N_2O[6], N_2[7] and CO[8] are very similar, all forming face-centered cubic lattices with four molecules per unit cell oriented along the body diagonals. Carbon dioxide has a T_h^6 space group with the molecules on S_6 sites. In the other crystals, there is no inversion center; thus the site group is reduced to C_3 and the space group to T^4. In N_2 the molecules are displaced slightly (0.17 Å) along the body diagonals, thus destroying the inversion center. For CO and N_2O, the molecules themselves lack an inversion center. There is some disorder in the CO[9] and N_2O[10] crystals in that the sense of the molecules is random.

For CO_2 there are three librational frequencies (E_g+2T_g) and four translational ($A_u+E_u+2T_u$). The three librations are Raman active and the two T_u translations infrared active. Mixing between librations and translations is strictly forbidden. For N_2, CO and N_2O there are also three librations ($E+2T$) and four translations ($A+E+2T$). All modes are Raman active and the T modes are infrared active. Mixing between librations and translations is no longer forbidden.

The observed frequencies are given in the table. The spectrum of CO_2 is as predicted, showing three bands which do not correspond with the observed far-infrared results [11]. The N_2O results are similar, giving three bands which are assigned as librations because of their strong intensity. The fact that there is no coincidence with the far-infrared spectrum [11] strengthens this assignment and shows that appreciable mixing between librations and translations does not occur. Two strong bands were observed in N_2. Because of their intensity, and the fact that they differ in frequency from the translational motions observed in the far infrared [12, 13] they are assigned as predominantly librational. Only one broad, asymmetric band is observed in CO which has been assigned as a librational motion.

---

[1] Present address: Department of Chemistry, Michigan State University, East Lansing, Michigan 48823.

[2] Figures in brackets indicate the literature references listed at the end of this paper.

TABLE 1. Comparison of observed and calculated frequencies

Molecule	Motion	Observed frequencies	W. and P. calculation[a]	Extended calculation[b]
CO_2	L[c]	74, 92, 131	35, 48, 88	61, 55, 62
	T[d]($2T_u$)	[e]68, 114	74, 113	73, 112
N_2O	L	68, 80, 122	28, 40, 68	43, 40, 44
	T($2T_u$)	[e] 113	64, 92	94, 62
N_2	L	33, 37	28, 40, 68	43, 40, 44
	T($2T$)	[f] 48, 69	48, 71	48, 71
CO	L	48	50, 71, 121	75, 70, 77
	T($2T$)	[f] 49, 85	51, 76	51, 76

[a] Calculations by method of Walmsley and Pople, ref. 1.

[b] Calculations by modification of Walmsley and Pople method described below.

[c] Librational frequencies.

[d] Translational frequencies.

[e] Values taken from ref. 11.

[f] Values taken from ref. 12.

The calculated frequencies presented in the last column of the table were obtained by a modification of the method of Walmsley and Pople. The centrosymmetric structure was assumed in all calculations. The table shows frequencies computed by both methods. Calculations of the translational motions show that the radial Lennard-Jones term is vastly predominant in importance over the multipole-multipole interaction terms. For the torsional modes, however, changes in potential due to angular displacements need to be calculated, and the radial Lennard-Jones term drops out of the calculation. The torsional potential used was derived by expanding a quadrupole-quadrupole potential function in a Fourier series and then weighting the terms so that the new potential function showed an energy minimum about the equilibrium configuration of the molecules in the lattice. The depth of the potential well was taken as the lattice sum of quadrupole-quadrupole interactions.

The calculations of translational lattice modes give good agreement with experimental values. The model used for librational modes predicts these frequencies to be clustered about one small spectral region. The data on N_2 showed this to be the case, with relatively good agreement as to observed and predicted frequencies. The fact that CO shows only one broad asymmetric band in the Raman suggests that several lattice modes lie close to one another and cannot be resolved. The model fails for CO_2 and N_2O, probably because these are rodlike molecules and cannot be forced to fit a point quadrupole model. It should be noted though that between N_2O and CO_2 and between N_2 and CO, the member of the pair with the higher quadrupole moment has the higher librational lattice frequencies. This relationship is evidence that even for molecules that cannot be approximated by a point, the concept of a point quadrupole may be useful in understanding lattice modes.

References

[1] R. E. Miller, D. L. Rousseau, and G. E. Leroi, Technical Report No. 22, ONR Contract 1858 (27), May 1967.
[2] S. H. Walmsley and J. A. Pople, Mol. Phys. **8,** 345 (1964).
[3] J. de Smedt and W. H. Keesom, Proc. Acad. Sci. Amst. **27,** 839 (1924); Z. Krist. **62,** 312 (1926).
[4] H. Mark and C. Pohland, Z. Krist. **61,** 293 (1925); **64,** 113 (1926).
[5] J. C. McLennan and J. O. Wilhelm, Trans. Roy. Soc. Can. **19,** Sec. III (3), 51 (1925).
[6] J. de Smedt and W. H. Keesom, Proc. Acad. Sci. Amst. **27,** 839 (1924); Verslag. Akad. Wetenshap. Amst. **33,** 888 (1924).
[7] T. H. Jordan, H. W. Smith, W. E. Streib and W. N. Lipscomb, J. Chem. Phys. **41,** 756 (1964).
[8] L. Vegard, Z. Physik **61,** 185 (1930); **88,** 235 (1934).
[9] J. O. Clayton and W. F. Giauque, J. Am. Chem. Soc. **54,** 2610 (1932).
[10] R. W. Blue and W. F. Giauque, J. Am. Chem. Soc. **57,** 991 (1935).
[11] A. Anderson and S. H. Walmsley, Mol. Phys. **7,** 583 (1964).
[12] A. Anderson and G. E. Leroi, J. Chem. Phys. **45,** 4359 (1966).
[13] A. Ron and O. Schnepp, J. Chem. Phys. **46,** 3991 (1967).

THE OPTICAL AND ANHARMONIC THERMAL PROPERTIES OF A DIATOMIC MOLECULAR SOLID [1]

GEORGE E. JELINEK

Lawrence Radiation Laboratory
University of California, Livermore, California 94550

1. Introduction

Between 23.9 and 43.6 °K neutron [1] [2] and electron diffraction [2] data indicate that β oxygen has a primitive monomolecular rhombohedral structure with the axis of the molecule oriented parallel to the three-fold axis. The structure of the low-temperature α form of oxygen is monoclinic [3]. The low-temperature α form of fluorine is not known but the diffraction patterns are similar to those of β oxygen [4]. Nitrogen below 35.6 °K has a cubic structure with three non-bonded neighbors at 3.42 Å and six at 3.55 Å [5]. Thus it seems possible that a primitive rhombohedral equilibrium structure with large vibrational excursions from the equilibrium configuration might constitute a reasonable model for the description of the lattice vibrations of oxygen, nitrogen, and fluorine at low temperatures.

2. Potential Model

The assumed structure involves cubic close-packing of cylinders and the effects of the harmonic, cubic, and quartic potential are considered. The force constants have been obtained from the two-body potential between nonbonded atoms. The potentials considered are the modified Buckingham (6-exp) and the Lennard-Jones (6, 12) potential. The parameters of the potential have been evaluated from the observed cohesive energies and the nearest-neighbors distances of oxygen, nitrogen, carbon monoxide, fluorine, chlorine, bromine, and iodine.

3. Anharmonic Thermal Properties

The Born and Huang approach to the problem of the anharmonic contribution to the thermodynamic properties consists in treating the

---

[1] This work was performed under the auspices of the U.S. Atomic Energy Commission.

[2] Figures in brackets indicate the literature references listed at the end of this paper.

anharmonic terms in potential energy expansion as small perturbations [6]. The normal-mode solutions for the harmonic potential, being good zeroth order approximations to the Hamiltonian, serve as the basis set for the calculation of the anharmonic properties. The potential energy is expanded first in terms of the parameters of a homogeneous deformation, then in terms of the nuclear displacements from their equilibrium position in the homogeneously deformed structure.

For both the α and β phases of oxygen the calculated C_p is in very good agreement with the experimental results. For α nitrogen and α fluorine, stable below 35.6 and 45.5 °K, respectively, the calculated C_p is also in good agreement with the experimental results. The calculated thermodynamic properties are less satisfactory for carbon monoxide and poor for chlorine, bromine, and iodine.

4. Discussion of the Infrared Spectra

The β-oxygen structure contains one molecule in the unit cell oriented parallel to the trigonal axis, occupying a site of D_{3d} symmetry. For a one-phonon absorption in the infrared the conservation of energy, $\omega_{\text{light}}=\omega_{\text{phonon}}$ and conservation of momentum, $\mathbf{k}_{\text{light}}=\mathbf{k}_{\text{phonon}}$ require that essentially $\mathbf{k}=0$. There are six polarization vectors for each wave vector. For $\mathbf{k}=0$ the normal modes may be classified according to their symmetry.

In the zero wave vector approximation a combination will be allowed in the infrared spectrum if the character of the combination has the same symmetry as translation (component of x, y, or z in the character table). The character of a combination is determined by taking the direct product of the characters of the two modes. The direct product of A_{1g} with A_{2u} yields A_{2u} and is infrared active. The direct product of A_{1g} with E_u is E_u which is also active. For the dispersion curves of oxygen the transverse acoustic mode, in the zero wave vector limit, has symmetry E_u. The longitudinal acoustic mode has symmetry A_{2u}. Though allowed by factor group analysis, both modes have zero frequency at $\mathbf{k}=0$ and thus neither will appear in the spectrum in combination with A_{1g} (the fundamental vibration) in the infinite wave length limit. The torsional optic mode has symmetry E_g for $\mathbf{k}=0$ and is not infrared active in combination with A_{1g}.

When considering combinations in the infrared spectrum, one is no longer concerned merely with $\mathbf{k}=0$. A combination is a two phonon process and we can get combinations with all wave vectors of the dispersion curves for which energy and momentum are conserved.

$$\omega_{\text{light}}=\omega_1+\omega_2$$
$$\mathbf{k}_{\text{light}}=\mathbf{k}_1+\mathbf{k}_2.$$

Furthermore, the lattice internal rotational mode (E_g and forbidden for $\mathbf{k}=0$) will be active in combination with the longitudinal optical mode. Since the volume in k-space will be greatest at the zone boundary, we will expect combinations with the allowed lattice modes to be more intense for values of the frequencies near those at the zone boundary.

Zone-boundary values of the dispersion curves for the [111] and [011] directions are shown in table 1. Since the band width of the intra-

TABLE 1. Frequencies (cm^{-1}) at the zone boundary for wave vector propagating parallel (3-f) and perpendicular (2-f) to the trigonal axis of the rhombohedral model

Substance	Transverse acoustic		Longitudinal acoustic		Torsional optic		Observed
	3-f	2-f	3-f	2-f	3-f	2-f	
oxygen	37.1	61.8	74.2	85.2	46.5	64.7	47., 69. (45)[a]
		105.4				95.7	
nitrogen	29.5	44.4	59.1	71.6	45.3	65.2	48. (4), 69. (7)[b]
		81.3				74.2	49. (3), 69. (6)[c]
carbon	32.1	48.8	64.1	77.2	47.5	70.4	70.[d] 110.[e]
monoxide	----	87.5			----	80.3	49. (7), 85. (12)[b]
							50.5 (5), 86. (13)[c]
fluorine	31.3	53.2	72.2	80.6	36.1	74.4	
		90.4			----	88.4	
chlorine	25.6	52.5	71.3	78.4	35.6	72.6	62., 90.[f]
LJ(6,8)		87.9			----	86.9	
bromine	13.2	40.9	57.1	61.6	28.5	57.3	49., 74.[f]
LJ(6,9)	----	69.0			----	69.3	
iodine	5.8	36.5	52.1	55.5	26.0	51.7	41., 65.[f]
LJ(6,9)	----	62.2			----	63.1	

[a] Translational, half-width of band given in parenthesis, B. C. Cairns and G. C. Pimentel, J. Chem. Phys. **43,** 3432 (1965).

[b] Translational, A. Anderson and G. E. Leroi, J. Chem. Phys. **45,** 4359 (1966).

[c] A. Ron and O. Schnepp, J. Chem. Phys. **46,** 3991 (1967).

[d] Librational, G. E. Ewing and G. C. Pimentel, J. Chem. Phys. **35,** 925 (1961).

[e] R. M. Hexter, J. Chem. Phys. **46,** 2300 (1967).

[f] Translational, S. H. Walmsley and A. Anderson, Mol. Phys. **7,** 411 (1964).

molecular mode of the model is only about 2 cm^{-1}, the predicted combination spectrum of the model may be obtained from the critical points of the frequency distribution spectrum, $g(\omega)$, with the character of the modes contributing to the critical points determined from the eigenvectors of the various dispersion-curve branches.

Cairns and Pimentel observe that the lattice combination band of oxygen has two broad features, one centered 47 cm^{-1} and the other centered 69 cm^{-1} above the center of the O_2 fundamental at 1549 cm^{-1}. On the basis of the selection rules for the D_{3d} structure they conclude that the lattice bands involve combinations with the translational lattice modes. The frequency distribution function for oxygen for the Lennard-Jones (6,12) potential contains distinct peaks at 56, 71, and 87 cm^{-1}. In view of the large half-width of the combination absorption band (45 cm^{-1}) it is difficult to classify the two peaks observed since the band encompasses nearly the entire range of zone-boundary frequencies for both the translational and rotational lattice modes. It seems apparent, though, that the lattice combination centered at 69 cm^{-1} is a vibration-translation combination of the type longitudinal optic+longitudinal acoustic, as concluded by Cairns and Pimentel. A possible assignment to the broad band centered at 47 cm^{-1} is a vibration-libration of the type longitudinal optic+transverse rotation.

For the other substances as shown in table 1, while there is reasonable agreement between calculated and observed spectra, the model indicates that the combination spectra contain a manifold of translational and librational modes, with the observed spectra containing modes of both translational and librational character.

5. References

[1] Alikanov, Soviet Physics-JETP **45,** 812 (1963).

[2] E. M. Horl, Act Cryst. **15,** 845 (1962).

[3] C. S. Barrett, L. Meyer, and J. Wasserman, J. Chem. Phys. **47,** 592 (1967).

[4] T. H. Jordan, W. E. Streib, and W. N. Lipscomb, J. Chem. Phys. **41,** 760 (1964).

[5] W. E. Streib, T. H. Jordan, and W. N. Lipscomb, J. Chem. Phys. **37,** 2962 (1962).

[6] M. Born and K. Huang, The Dynamical Theory of Crystal Lattices (Oxford University Press, New York, 1954).

NEUTRON SCATTERING STUDIES OF MOLECULAR VIBRATIONS IN ICE

H. PRASK [1] **and H. BOUTIN** [1, 2]
Picatinny Arsenal, Dover, New Jersey 07801

and

S. YIP
Massachusetts Institute of Technology, Cambridge, Massachusetts 02138

It is well known that the phonon frequency distribution function of a monatomic, cubic crystal can be determined from a measurement of the one-phonon incoherent neutron scattering cross-section [1].[3] The exact determination of the frequency distribution of molecular solids, on the other hand, generally involves a formidable computational problem. In this work an extension of the one-phonon incoherent neutron scattering theory for monatomic crystals has been investigated for incoherent scattering molecular solids with particular application to ice.

If one assumes that molecular translations and rotations are separable, a frequency distribution can be associated with each such that $g(\omega)=g_T(\omega)+g_R(\omega)$, where subscripts T and R denote translation and rotation respectively and $g(\omega)$ is the distribution function for the system. If translational motions are treated as small-displacement oscillations and rotations as small angle torsions, a Gaussian expression is obtained for the intermediate scattering function [2]:

$$\chi(\boldsymbol{K}, t)=e^{-2W}e^{K^2/2M}\Gamma(t) \tag{1}$$

$$\Gamma(t)=\int_0^\infty\frac{d\omega}{\omega}\left[\coth\frac{\hbar\omega}{2k_BT}\cos\omega t-i\sin\omega t\right]\left[g_T(\omega)+\frac{M}{M_R}g_R(\omega)\right], \tag{2}$$

where e^{-2W} is the Debye-Waller factor associated with translations, M is the molecular mass and M_R is an effective rotational mass. When eq (1) is applied in the one-phonon approximation, the cross section becomes proportional to an effective frequency distribution, $g_{\text{eff}}(\omega)=g_T(\omega)+(M/M_R)g_R(\omega)$, which allows determination of $g(\omega)$ if

---

[1] Guests at the Army Materials and Mechanics Research Center, Watertown, Mass.

[2] Present Address: Research Laboratories Division, Bendix Corporation, Southfield, Michigan.

[3] Figures in brackets indicate the literature references at the end of this paper.

$g_T(\omega)$ or $g_R(\omega)$ is known *a priori*, or if they do not overlap appreciably. These results are comparable to those of Hahn [3] whose formal analysis, which is closely akin to a normal-mode treatment, differs from the more intuitive approach used here [2].

The theory was applied to "cold" neutron scattering data from a 0.3mm thick sample of hexagonal ice ($\theta = 65°$) at 150 °K. A frequency distribution was extracted and the specific heat calculated. Ice was chosen because the translational and rotational intermolecular modes are quite well separated [4, 5] and the scattering is almost entirely ($\geq 95\%$) from hydrogen and therefore incoherent, so that the model is applicable.

In figure 1 the "effective" frequency distribution of ice is shown after incident beam width and instrumental resolution [6] have been taken into account. The curves labeled I and II correspond to possible choices of the shape of the rotational frequency distribution. Also shown is the two-phonon contribution calculated using $\chi(\boldsymbol{K}, t)$ of eq (1) following Sjolander's development for monatomic crystals [7].

The observed maxima in the translational portion of the density of states are in excellent agreement with optical density/$(\nu)^2$ versus ν

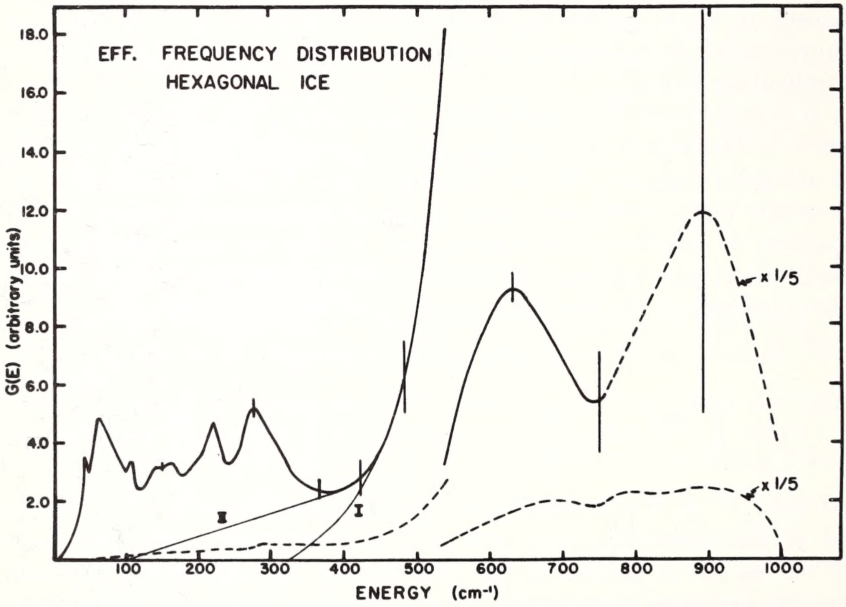

FIGURE 1. The effective frequency distribution of ice obtained from neutron inelastic scattering data on ice at 150 °K (heavy solid line). The dashed line along the bottom corresponds to the calculated two-phonon contribution subtracted out. Lines I and II correspond to two choices of the lowest energy portion of the rotational distribution.

obtained from recent infrared measurements [8, 9], which for a disordered crystal should show features of the density of states [10].

Calculation of $C_v(T)$ in the harmonic approximation was made using both separations I and II indicated in figure 1. The "true" or thermodynamic $g(\omega)$ is determinable if M_R is known. Alternatively, normalization of the observed rotational and translational distributions to equal total degrees of freedom fixes M_R, which in the case of the ice distribution of figure 1 yields $M_R \sim 1.0$. The large statistical errors at high energy transfers make this value somewhat uncertain.

Specific heat calculated from separation II is in excellent absolute agreement with measured values [11, 12] from 0 to 100 °K and deviates by less than 10 percent from C_v, corrected for anharmonicity [5], over the entire range 0—273 °K. The moments of translational distribution II are also in excellent agreement with moments inferred by Leadbetter [5] from a detailed analysis of the measured specific heat. Separation I, which *a priori* seems more reasonable, gives poorer agreement with measured $C_v(T)$ values and the inferred moments. It should be pointed out that multiple scattering has not been corrected for, and could alter these results. The shape of the lowest energy portion of the frequency distribution (0–40 cm^{-1}) is in agreement with that obtained by Leadbetter from analysis of the specific heat.

In conclusion, the theory outlined in this paper provides a model by which an approximate frequency distribution can be obtained for some molecular crystals. The application of the theory to ice, although not conclusive, does give a frequency distribution that gives specific heats in agreement with measurement, frequencies close to optical results, and distribution moments in agreement with inferred values.

References

[1] G. Placzek and L. van Hove, Phys. Rev. **93,** 1207 (1954).
[2] H. Prask, H. Boutin, and S. Yip, J. Chem. Phys. **48,** 3367 (1968).
[3] H. Hahn in Inelastic Scattering of Neutrons. International Atomic Energy Agency, Vienna, *II*, 279 (1965).
[4] Reviewed by N. Ockman, Adv. Phys. **7,** 199 (1958).
[5] A. J. Leadbetter, Proc. Roy. Soc. **287A,** 403 (1965).
[6] K. E. Larsson, U. Dahlborg, S. Holmryd, K. Otnes, and R. Stedman, Ark. f. Fys. **16,** 199 (1959).
[7] A. Sjolander, Ark. Fys. **14,** 315 (1958).
[8] J. E. Bertie and E. Whalley, J. Chem. Phys. **46,** 1271 (1967).
[9] W. Bagdade, Far Infrared Absorption in Ice Ih and Liquid Water, Mid-American Symp. on Spect., Chicago, May, 1967.
[10] E. Whalley and J. E. Bertie, J. Chem. Phys. **46,** 1264 (1967).
[11] W. F. Giaque and J. W. Stout, J. Am. Chem. Soc. **58,** 1144 (1936).
[12] P. Flubacher, A. J. Leadbetter, and J. A. Morrison, J. Chem. Phys. **33,** 1751 (1960).

INFRARED ABSORPTION STUDIES OF INTERMOLECULAR VIBRATIONS IN THE LOW FREQUENCY REGION

NEIL T. McDEVITT

AFML (MAYA)
Wright-Patterson Air Force Base, Ohio 45433

and

R. E. WITKOWSKI and W. G. FATELEY

Mellon Institute
Pittsburgh, Pennsylvania 15213

The solid state is characterized by high cohesion and rigidity, yet the type of force existing between the particles and the relationship between the structure and physical-chemical properties of the crystal still presents a considerable challenge to the researcher.

Infrared spectroscopy is playing its role in the development of the science of materials through the study of crystalline solids. The energy levels of a solid are, of course, essentially a property of the whole system. In our infrared study of solids we are interested in the type of bonding that contributes greatly to the lattice energy of the system. We, therefore, are interested in studying the vibrational modes of a system that are associated with intermolecular forces. As a matter of convenience we have classified intermolecular forces as to the following types: ionic, van der Waals and hydrogen bonding. As examples of materials that we have studied in which these forces are predominant we cite some metal oxides, polynuclear aromatics, and phenols.

Since atoms in the solid state may be held together by forces that can be classified as ionic, covalent or a combination of types, it is necessary to have infrared methods that may help to distinguish between these forces. Three methods have been used in our infrared studies of lattice vibrations: (1) lattice parameter, (2) high pressure diamond cell and (3) low and high temperature studies.

The first method takes into consideration the predominant ionic characteristics of a large number of inorganic materials. Infrared spectra were measured in the region 1000 to 50 cm^{-1}. In general the size and coordination number of the ions determine the tetrahedral and octahedral grouping in most oxides. These groups, in turn, build the unit cell and determine to a large extent the lattice parameters of the crystal. This particular method worked very well in the study of rare earth oxides and garnets. From this study we are able to show how the lattice parameter, and not the reduced mass of the metals, played its role in determining the frequency position of the M—O stretching mode.

Recent high pressure diamond cell studies by Brasch and Jakobsen in the mid-infrared and Ferraro and Mitra in the far-infrared have indicated that useful data can be obtained from this technique. This method was utilized in our study to determine if pressure on a material would affect lattice vibrations in a specific way. The diamond cell studies were performed on a Michelson far-infrared interferometer.

The first material studied under pressure was sodium chloride. Pressure had a dramatic effect on this compound and its lattice frequency shifted from 165 to 218 cm^{-1}. Points were obtained in between these frequencies by cycling the pressure through the maximum range (50 kb) several times and then leaving the sample under a particular pressure for approximately fifteen minutes. The first recording was at one atmosphere and the next at maximum pressure of the particular study. Several more recordings would then be made as the pressure was lowered and the last obtained at one atmosphere again.

The following series of compounds have been studied by both pressure and low-temperature methods. Cuprous oxide has only two optically active modes in the infrared. One in the mid-infrared at 625 cm^{-1} and one in the low frequency region at 147 cm^{-1}. The application of 100 kilobars of pressure to this compound shifts the 625 cm^{-1} band to 690 cm^{-1} while the low frequency band remains the same. At 150 °K under normal pressure the 625 band shifts to 635 and the 147 band to 150 cm^{-1}. This seems to indicate that the metal-to-oxygen stretching mode in this body centered cubic lattice is greatly affected by pressure while the bending mode is not even slightly perturbed.

ZrO_2 and HfO_2 have a series of three bands occurring between 280 and 230 cm^{-1}. For ZrO_2 we found bands at 272, 262 and 233 cm^{-1} while HfO_2 has bands at 270, 260 and 237 cm^{-1}. Although the mass of hafnia is almost twice that of zirconia, we can see that the first two frequencies in ZrO_2 are only slightly higher than for HfO_2. However, the low frequency band at 237 cm^{-1} for HfO_2 is slightly higher than the corresponding frequency in ZrO_2. Pressure increases this band frequency slightly in ZrO_2, while it has more of an effect on HfO_2. Low temperature studies show both bands shifting approximately the same degree; however, this shift is larger than the pressure shift.

We chose anthracene as an example of an organic compound exhibiting van der Waals' forces in the crystalline state. Anthracene has bands at 232, 164, 114, and 60 cm^{-1}. The two high frequency bands have been assigned to molecular vibrations while the band at 114 cm^{-1} is assigned to a lattice mode. At 10 kb the molecular vibrations shift slightly while the lattice mode shifts to 140 cm^{-1}. It appears from this study that van der Waals' bonding is quite sensitive to pressure. There is approximately a ten cm^{-1} shift in this frequency when the temperature is lowered to 100 °K.

Phenol is an interesting compound exhibiting hydrogen bonding characteristics. This material has an O—H———O stretching absorption band in the low-frequency region. When pressure is applied to this compound two different phases may be obtained. Phase II was an O—H———O absorption at 133 cm^{-1} while Phase I has a band at 175 cm^{-1}. Both bands shift approximately 25 cm^{-1} with applied pressure.

Conclusion

The three methods studied in this paper are helpful in studying intermolecular vibrations in the low frequency infrared region. However, not all lattice modes shift with pressure, and there is some indication that the type of motion the atoms undergo in a specific mode may determine its sensitivity to pressure. There also seems to be a definite distinction between sensitivity to pressure and a sensitivity to temperature.

OPTICAL PHONONS IN MIXED SODIUM POTASSIUM TANTALATES

T. G. DAVIS, N. E. TORNBERG, and C. H. PERRY

Spectroscopy Laboratory [1]
Materials Center for Science and Engineering [2]
and Research Laboratory of Electronics [3]
Massachusetts Institute of Technology, Cambridge, Massachusetts 02139

and

N. KNABLE

N.A.S.A., Electronics Research Center

Cambridge, Massachusetts 02138

1. Introduction

The dielectric properties of $KTaO_3$ have been investigated by Wemple [1] and indicate Curie-Weiss law behavior with an extrapolated Curie temperature (T_c) of 1–3 °K. Davis [2] has obtained dielectric data of the mixed crystal system $NaTaO_3$–$KTaO_3$ as a function of temperature. T_c rises to a maximum of 65 °K for a sample containing 48 percent $NaTaO_3$, falls with higher $NaTaO_3$ concentrations, and becomes negative at approximately 72 percent $NaTaO_3$. For materials in the range 35–50 percent $NaTaO_3$, an anomalous "plateau" in the dielectric behavior is observed [2]. This could arise (e.g., in $(Na_{0.4}:K_{0.6})TaO_3$) from a second-order ferroelectric transition at ~55 °K and a transition from cubic to a structurally different phase (e.g. tetragonal) at 37 °K. X-ray data by Davis [2] shows that samples with concentrations to ~70 percent $NaTaO_3$ are cubic at room temperature.

Above 70 percent the structure initially becomes tetragonal, finally shearing to pseudo-monoclinic as the concentration approaches pure $NaTaO_3$. The $(Na_x:K_{1-x})TaO_3$ crystals investigated here by infrared and Raman spectroscopy as a function of temperature had $x=0.0$, 0.12, 0.40 and 0.85.

---

[1] The work of this laboratory is supported in part by the National Science Foundation Grant No. GP-4923.

[2] The work of this laboratory is supported in part by A.R.P.A., S.D.-90.

[3] The work of this laboratory is supported in part by the Joint Services Electronics Program (Contract DA28-043-AMC02536 (E)).

The reflectivity measurements were of considerable importance in obtaining the $\mathbf{k} \approx 0$ infrared allowed modes and helping to positively identify the presence of any first-order Raman bands.

2. Experimental Procedure

The temperature dependence of the infrared spectrum of $KTaO_3$ has been reported by Perry and McNelly [3], and the same instrumentation [4] was used for the present measurements. For the mixed crystal with $x=0.12$ the results are very similar, but as the sodium content increases, splitting of various bands is observed (fig. 1).

For the paraelectric mixed crystals a strongly temperature-dependent peak in the low-frequency conductivity shifts to longer wavelengths as the temperature is lowered toward the "Curie" temperature, in general accordance with Cochran's theory [5] for displacive ferroelectrics.

Raman spectra were obtained using He-Ne laser excitation and X(ZZ)Y scattering symmetry. Most of the second-order bands show a uniform increase in frequency as x is increased. The spectrum of $(Na_{0.4}:K_{0.6})TaO_3$ as a function of temperature (fig. 2) is typical.

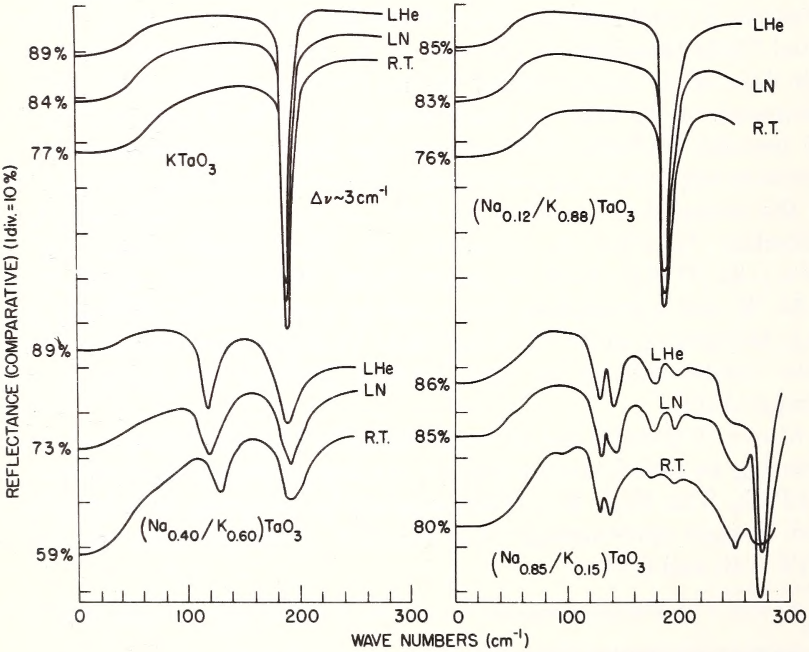

FIGURE 1. Long-wave infrared reflectance spectra for various samples and temperatures.

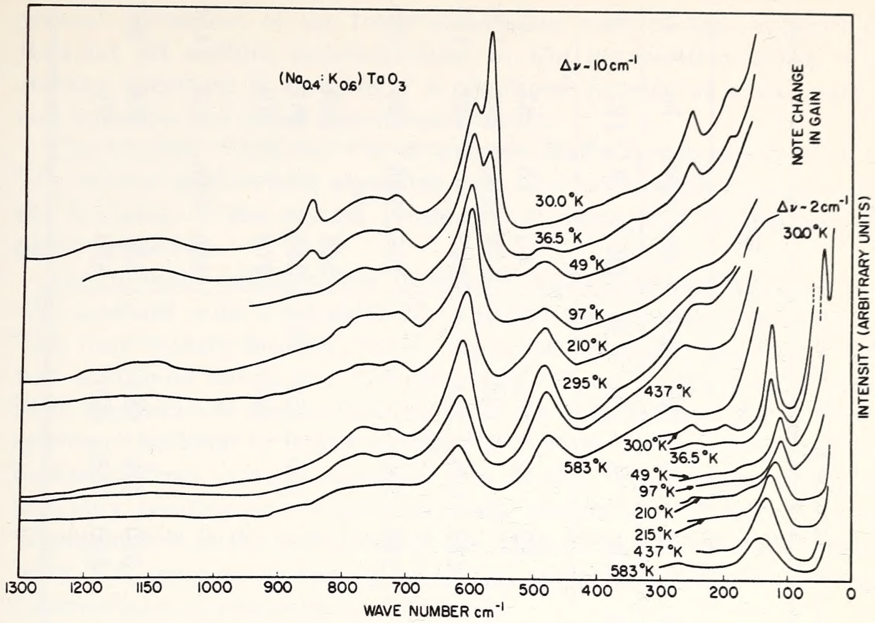

FIGURE 2. Raman spectra for $(Na_{0.4}:K_{0.6})TaO_3$ at various temperatures.

3. Discussion

The interpretation of the second-order Raman spectrum of $KTaO_3$ has been discussed by Perry, Fertel and McNelly [6], and a similar analysis has been applied here. The temperature dependence of the intensities of the bands has been used to differentiate between possible combination and difference processes. Although a classical Brillouin zone is not well defined for these mixed crystals, the multiphonon spectrum still behaves as if it were due only to phonon combinations at the critical points at the edge of the pseudo Brillouin zone.

For $(Na_{0.4}:K_{0.6})TaO_3$ at 49 °K (fig. 2) there is only a slight indication of a superimposed first-order Raman spectrum. In the 36.5 °K and 30.0 °K spectra additional bands appear at approximately 42, 128, 200, 255, 572 and 850 cm^{-1}. These are attributed to the normally Raman forbidden bands for $\mathbf{k} \approx 0$ becoming allowed due to a structural change to lower symmetry.

Similar bands are present in $(Na_{0.85}:K_{0.15})TaO_3$ even at room temperature and increase in strength as the temperature is lowered. These can be similarly explained.

The optic modes at $\mathbf{k} \approx 0$ derived from the infrared reflectance measurements using a Kramers-Kronig analysis are compared with the frequencies obtained from the first-order Raman data in table 1. The

TABLE 1. Comparison of infrared and Raman frequencies for the $NaTaO_3$–$KTaO_3$ system

% Na	12%						40%						85%					
(°K)	295	295	80	110	10	30	295	295	80	97	10	30	295	295	80	109	10	24
Type	IR	R	IR	R	IR	R	IR	R	IR	R	IR	R	IR	R	IR	R	IR	R
TO_1	75		50		48		102		81		39	42	75		60	70	57	65
													132		132	130	132	130
							138		132		129	128	144		147		147	150
LO_1 TO_2	198		198		198		204		201		198	200			196	200	196	205
															246		246	
LO_2 TO_3												255	255	255	258		261	
													270		270		270	
LO_3															430	450	430	450
TO_4	540		540		540		576		573		570	572	584		584		584	580
LO_4	816		816		816		860		855		850	850	870		870		870	

general agreement of the frequencies helps confirm the supposition that for all sodium concentrations in the paraelectric phase, the Raman spectrum is essentially a combined density of states curve and indicates the phase transitions present.

The band at ~130 cm^{-1} in 40 percent $NaTaO_3$ is interpreted as a TO_1 normal mode which separates from the ferroelectric mode due to the lowering of the crystal symmetry to tetragonal at the second phase transition.

The normally orthohombic 85 percent $NaTaO_3$ crystal has a dielectric constant with a considerably reduced temperature dependence. This may explain the behavior of the lowest frequency mode and the two additional bands at ~130 cm^{-1} and 147 cm^{-1}, which show very little temperature dependence in both the infrared and the Raman spectra. The band or bands around 255 cm^{-1} in the two crystals with highest sodium content could be due to the "F_{2u}" mode, which is normally inactive in the cubic crystals, becoming both infrared and Raman active in the tetragonal phase. It should be noted that further work is in progress in the region of the phase transitions on various intermediate concentrations of $NaTaO_3$.

Electric-field induced Raman spectra in the paraelectric phase is presently being investigated by T. G. Davis at M.I.T. and N.A.S.A. (E.R.C.). The temperature dependence of the "soft" mode and the other first-order forbidden modes in these crystals with $x<0.70$ has been observed. However, discussion of these results is beyond the scope of this summary and will be published elsewhere.

4. References

[1] S. H. Wemple, Phys. Rev. **137A,** 1575 (1965).
[2] T. G. Davis, S. M. Thesis, Department of Electrical Engineering, M.I.T. (1965) (unpublished).
[3] C. H. Perry and T. F. McNelly, Phys. Rev. **154,** 456 (1967).
[4] C. H. Perry, R. Geick and E. F. Young, Appl. Opt. **5,** 1171 (1966).
[5] W. Cochran, Advances in Physics **9,** 387 (1960).
[6] C. H. Perry, J. H. Fertel and T. F. McNelly, J. Chem. Phys. **47,** 1619 (1967).

ON THE SECOND ORDER ELASTIC CONSTANTS OF MOLECULAR SOLIDS

M. L. KLEIN*

School of Chemistry
University of Bristol, Bristol, England

In this paper we are concerned with the possible importance of anharmonic effect in the interpretation of the thermoelastic properties of molecular solids. In particular, we shall be concerned with the relationship between elastic constants determined by

(a) Isothermal thermodynamic measurement

(b) Velocity of ultrasound (adiabatic)

(c) Slopes of phonon dispersion curves as measured by the inelastic scattering of neutrons.

For a strictly harmonic solid these three measurements are equivalent and simply related to the harmonic force constants. However, in an anharmonic crystal (i.e., real crystal) these three quantities, in principle at least, show a different temperature dependence. Later we shall use solid Kr to illustrate the posible magnitude of these differences. Solid Kr is chosen because it is a crystal in which anharmonic effects are important, but not dominant, and this situation is likely to be common to many other molecular solids.

1. Isothermal Elastic Constants

Here it is convenient to define isothermal elastic constants as the coefficients in the Taylor series expansion of $(\mathrm{F}/\mathring{\mathrm{V}})$, the Helmoltz free energy density, in powers of the homogeneous strain parameters $\{u_{\alpha\beta}\}$.

$$(\mathrm{F}-\mathring{\mathrm{F}})/\mathring{\mathrm{V}}=S_{\alpha\beta}u_{\alpha\beta}+\frac{1}{2}S^{\mathrm{iso}}_{\alpha\beta\sigma\tau}u_{\alpha\beta}u_{\sigma\tau}$$

Thus
$$\mathring{\mathrm{V}}S^{\mathrm{iso}}_{\alpha\beta\sigma\tau}=(\partial^2F/\partial u_{\alpha\beta}\partial u_{\sigma\tau})_T$$

Since the Helmholtz energy is temperature dependent, so too are the isothermal elastic constants. In particular the lowest order explicit temperature dependence is given by

$$(1/\mathring{\mathrm{V}})\sum_{qj}[\beta_{\alpha\beta\sigma\tau}e-\gamma_{\alpha\beta}\gamma_{\sigma\tau}Tc_v]$$

---

*ICI Fellow.

where

$$\beta_{\alpha\beta\sigma\tau}=\frac{1}{\omega}\left(\frac{\partial^2\omega}{\partial u_{\alpha\beta}\partial u_{\sigma\tau}}\right),\ \gamma_{\alpha\beta}=-\frac{1}{\omega}\left(\frac{\partial\omega}{\partial u_{\alpha\beta}}\right)$$

and e and c_v are the contribution to the internal energy and specific heat of the mode ω. The parameters $\beta_{\alpha\beta\sigma\tau}$ and $\gamma_{\alpha\beta}$, which describe the strain dependence of the normal modes, can be related to the usual anharmonic force constants by perturbation theory.

For a cubic crystal under an isotropic stress $S_{\alpha\beta}=-p\delta_{\alpha\beta}$ the bulk modulus B_T is given by

$$3B_T=S_{xxxx}+2S_{xxyy}+2p.$$

2. Adiabatic Elastic Constants

The adiabatic constants $(\partial^2E/\partial u_{\alpha\beta}\partial u_{\sigma\tau})_S/\mathring{V}$ which determine the velocity of ultrasonic waves can be related to the isothermal constants by thermodynamics. For a cubic crystal one finds.

$$\mathring{V}(S^{\mathrm{ad}}_{\alpha\beta\sigma\tau}-S^{\mathrm{iso}}_{\alpha\beta\sigma\tau})=\gamma^2TC_v\delta_{\alpha\beta}\delta_{\sigma\tau}$$

where $\gamma=(V/C_v)(\partial S/\partial V)_T$ is the usual thermodynamic Grüneisen parameter.

3. Inelastic Neutron Scattering

The inelastic scattering of neutrons can be used to measure the frequency Ω and wave vector $\mathbf{Q}$ of phonons. The limiting slope of phonon dispersion curves can be used to derive wave velocities and hence effective elastic constants.

The explicit temperature-dependent contribution to these constants has the following form [1][1]

$$(1/\mathring{V})\sum_{qj}[\beta_{\alpha\beta\sigma\tau}e-\gamma_{\alpha\beta}\gamma_{\sigma\tau}Tc_vf(\mathbf{Q})].$$

Here $$f(\mathbf{Q})=[C(\mathbf{Q})^2/(C(\mathbf{Q})^2-v(\mathbf{Q})^2)]$$

where $v(\mathbf{Q})$ is the velocity of the probe in the direction $\mathbf{Q}$ and $C(\mathbf{Q})$ is the derivative with respect to wave vector of the mode ω along the direction $\mathbf{Q}$ of the probe. At finite temperatures these constants may not have the same symmetry properties as the macroscopic elastic constants. We note that if $f(\mathbf{Q})=1$ we recover the isothermal result whereas if $f(\mathbf{Q})=0$ the neutron measurement yields the quantity $(\partial^2E/\partial u_{\alpha\beta}\,\partial u_{\sigma\tau})_{\bar{n}}/\mathring{V}$, where $\bar{n}$ is the mean number of phonons in the mode ω. Thus, in general, the slopes of phonon dispersion curves give neither the adiabatic nor isothermal constants at finite temperatures. Quantitative prediction without recourse to a specific model is difficult, but it is clear that for cubic crystals, for example,

---

[1] Figures in brackets indicate the literature references listed at the end of this paper.

$$v_l^{\mathrm{N}}(100) \geq v_l^{\mathrm{ad}}(100).$$

4. Model Calculations and Experimental Results for Solid Kr

Adiabatic and isothermal elastic constants have been calculated for solid Kr using a Mie Lennard-Jones (13–6) central two-body potential with parameters fitted to the latent heat and molar volume at 0 °K [2].

At 77.3 °K the isothermal bulk modulus for this model is calculated to be 20.0 kbars. This value is to be compared with the experimental value 20.8 ± 0.7 kbars [3].

At 77.3 °K the adiabatic longditudinal wave velocity for the (110) direction is calculated to be 1280 m/sec which is to be compared with the recently measured experimental value [4].

$$v_l^{\mathrm{ad}}(2\bar{2}0) = 1370 \pm 80 \text{ m/sec}.$$

Phonon dispersion curves for the (100), (110), and (111) directions in fcc Kr were recently reported [5]. The measurements were carried out at 79 °K on a crystal with lattice parameter 5.725 Å (approximately 0.3 kbars pressure). Typical values of the slopes of the dispersion curves derived from these measurements are

$$v_l^N(100) = 910 \pm 90 \text{ m/sec } (760)$$
$$v_{\mathrm{l}}^N(100) = 1150 \pm 120 \text{ m/sec } (1200)$$
$$v_{\mathrm{l}}^N(110) = 1310 \pm 120 \text{ m/sec } (1280).$$

The values in parentheses are adiabatic velocities calculated for the (13–6) potential. If these values are taken at all seriously then they confirm the prediction that for finite temperatures

$$v_l^{\mathrm{N}}(100) > v_l^{\mathrm{ad}}(100); \text{ and } dv_l^{\mathrm{N}}\ (100)/dT < dv_l^{\mathrm{ad}}\ (100)/dT.$$

With some improvement in the present experimental accuracy this difference will probably be detectable.

5. References

[1] R. A. Cowley, Proc. Phys. Soc. **90,** 1127 (1967).
[2] C. Feldman and M. L. Klein, to be published.
[3] V. O. Urvas, D. L. Losee and R. O. Simmons, unpublished work.
[4] E. Lücher, et al., unpublished work.
[5] W. B. Daniels, G. Shirane, D. C. Frazer, H. Umebayashi and A. Leake, Phys. Rev. Letters **18,** 538 (1967).

STRUCTURE OF ORGANIC CRYSTALS

DIFFRACTION STUDIES OF MOLECULAR DYNAMICS IN ORGANIC CRYSTALS*

K. N. TRUEBLOOD

Department of Chemistry
University of California
Los Angeles, California 90024

1. Introduction

The chief focus in this brief account is on some recent work on two topics relevant to the theme of the symposium: the description of the motion of individual molecules and parts of molecules in crystals and the mechanisms of some reactions in the solid state. Little is said here about a number of important and relevant topics, including the recent contributions of Cochran and Pawley [1–4][1] on the lattice dynamics of organic molecular crystals, the sorts of information available from studies of diffuse x-ray scattering [5] and from neutron inelastic scattering, and the application of data from precise structure analyses to the testing and improvement of the parameters of inter- and intramolecular potential functions [6–9]. All of these are germane to a discussion of molecular dynamics in crystals, but some of them are being considered by others and limitations of time preclude any adequate discussion of them here.

The introduction of high-speed computing techniques in the early 1950's had a profound influence on the course of structure analyses by diffraction methods in several different ways. It made possible for the first time detailed structural studies of large molecules—first with hundreds, now with thousands of atoms—and made practicable the use of direct analytical methods for structure determination without any chemical assumptions. These direct methods have in the past few years become almost routine in many laboratories, at first only for centrosymmetric structures but now increasingly for non-centrosymmetric ones as well. Computers also made possible the development of techniques for fully automatic data collection.

However, our concern here is chiefly with another aspect of the impact of the computer—the development and application of rapid and precise multiparameter refinement techniques. Why is refinement needed at all? The answer to this question is closely related to the central problem of structure analysis by diffraction methods, the "phase problem". The pattern of scattered radiation from an object is the Fourier transform of the distribution of scattering matter in the object—if the radiation can easily be focussed, one can recombine it with appropriate lenses and get an image of the scattering matter. With x-rays and neutrons however, no such physical recombination is possible, so one must resort to analytical methods and perform a Fourier inversion. In order to do that, however, one needs to know not only the intensity of scattered radiation at each point (and thus its amplitude) but also its phase. The amplitudes may readily be determined experimentally, but the phases seldom can be. The process of structure *determination* consists in finding an approximate set of phases, which then may be used with the observed amplitudes in the reconstruction of an approximate image of the scattering matter by Fourier synthesis. *Refinement* consists in systematically altering appropriate parameters of the trial structure until it fits the observed data in an optimum way, i.e., until the scattering amplitudes calculated for the derived structure agree with those observed as closely as is meaningful when one considers the experimental precision and accuracy.

---

* University of California Contribution 2175.

[1] Figures in brackets indicate the literature references at the end of this paper.

When a structure involves only a few parameters—as do the simple and often highly symmetrical structures studied during the first two decades of x-ray crystallography—multiparameter refinement techniques are not needed. However, they became essential by the early 1940's as the complexity of structures under investigation increased, and Hughes in 1941 [10] first applied the least-squares method. This is still by far the most widely used refinement technique; because the observational equations are non-linear, least squares must be applied in an iterative way, and many cycles are often needed for convergence. Hughes' first application of least squares was in a two-dimensional study, and very few organic structures were studied three-dimensionally before the late 1940's because the processing of three-dimensional data was just too tedious. Months of labor were needed for a single Fourier synthesis or diagonal least-squares cycle, and to calculate a "full-matrix least squares"—i.e., to take into account the mutual interactions of the different parameters during refinement—was out of the question. Thus there simply was no opportunity for study of the fine details of even the simplest organic structures and consequently there was no need to measure with high precision the intensities of the diffraction maxima—it is these intensities which reflect the fine details of the arrangement of scattering matter in the unit cell. The moderate precision of photographic methods and eye estimation was quite adequate.

This situation changed markedly when high-speed computers became available to crystallographers, and there was a period when numerous structures were refined beyond the point warranted by the precision and accuracy of the experimental data used. However, this sort of injudicious refinement is now uncommon, in part because appropriate statistical tests are often applied. Furthermore, one now has as a standard the demonstrated consistency and physical plausibility of results obtained in independent studies of many related substances. A reemphasis during the last decade on techniques for precise measurement of the diffracted intensities, including corrections for the various sorts of errors that can occur—chiefly absorption and secondary extinction—has helped significantly in improving the precision of the derived parameters.

Even though approximate structures can often be *determined* with no chemical assumptions, other than the plausible one that the structure contains approximately spherical atoms, the process of structure refinement necessarily involves a model of the scattering matter, since *refinement* consists in adjusting appropriate parameters of a model to get the best fit with the experimental intensity data. The choice of parameters to be refined is in some ways obvious and in some ways subtle. Clearly the total number of adjustable parameters must be far smaller than the number of independent intensity estimates.

One set of these parameters is the positions of atoms not fixed by symmetry—three per atom in the general case, although in complex structures containing reasonably rigid groups of moderately predictable geometry (e.g., phenyl groups), the internal geometry of the group is sometimes assumed and only its center of mass and orientation refined [11]. However, whether one assumes individual atoms or definite groups of atoms, there still remain questions about their atomic numbers, their shapes, and their modes of vibration.

We consider atomic and molecular motions in the next section; with regard to atomic shapes and numbers, the most common assumption currently is that each atom is spherical and of known atomic number (known from some clues about the chemical nature of the compound under study). When there is ambiguity about atomic identity, the atomic number can be a parameter to be determined, and with good x-ray intensity data it can be ascertained with reasonable assurance if there are not many atoms present of much higher atomic number. This topic is considered briefly below.

The assumption that atoms are spherical has until recently seemed adequate for essentially all x-ray studies, but attention is now being directed both experimentally and theoretically to the detection of bonded density and the effects of neglect of aspherical components of charge distributions in the usual treatments [12–14]. These effects are very difficult to detect experimentally since they are manifested primarily in the inner region of the diffraction pattern because of the reciprocal relation between this pattern and the distribution of scattering matter that gives rise to it, and the intensities in this inner region are the most difficult to measure precisely because of extinction and other experimental difficulties. However the effects do seem experimentally detectable, even though small. Dawson's formalism for treating such effects [14] includes also provision for handling anharmonic components of atomic vibration amplitudes.

2. Atomic Vibration Parameters or "Temperature Factors"

Within a year after the discovery of x-ray diffraction, Debye introduced what has come to be known as the "Debye-Waller factor" or simply the "temperature factor" to allow for atomic vibrations in crystals. This factor is a coefficient in an exponential term which reduces the intensity of the diffracted radiation with increasing scattering angle:

$$I=I_0 e^{-2B(\sin^2\theta)/\lambda^2}$$

I_0 is the intensity expected for an atom at rest; the coefficient B is an "isotropic temperature factor", the same for all scattering directions. Inasmuch as the intensity is proportional to the square of the structure factor amplitude $|F|$, an equivalent form is

$$|F|=|F_o|e^{-B(\sin^2\theta)/\lambda^2} \qquad (2.1)$$

In deriving this relation, Debye analyzed the effects of displacements of atoms from their equilibrium sites. He assumed for simplicity that these displacements were independent and (on the average) isotropic, and that the potential function governing them was the same for every atom. In essence this amounts to assuming a simple cubic structure with one atom at every lattice point. Hence there is only a single isotropic vibration parameter for the whole structure—the diminution in intensity arising from this cause depends only on the angle between the incident and diffracted beams and not on the direction from which the incident beam impinges on the crystal. This approximation is a considerable oversimplification for most structures, since the potential functions governing atomic motions often vary widely for different atoms except in the simplest structures, and are isotropic only when symmetry demands that they be. However, until the 1950's, it was seldom possible to take either the anisotropy or the variation from atom to atom into account in calculations.

The first improvement was to allow for individual isotropic "temperature factors" (this name persists even though it was clear from the start that there would be vibrations even at 0 °K and that a static disorder would normally be indistinguishable from the dynamic one implied by this name if studies were made only at a single temperature). As it became possible to handle larger numbers of parameters, it became common to assume that each individual atom was vibrating harmonically in an anisotropic field, so that its general motion could be described by a symmetric tensor with six independent components (corresponding physically to the magnitudes of the three principal axes of an ellipsoid of vibration and the three angles specifying the orientation of this ellipsoid relative to the crystal axes). This description of atomic vibrational motion in terms of individual ellipsoidal "temperature factors" is still by far the most common and is used in most precise refinements because it is easy to handle and a fair approximation in many situations. The most common formulation of it is expressed in terms of the familiar Miller indices of the Bragg "reflecting plane", which are also the indices of the corresponding diffraction maximum in reciprocal crystal space. In this formulation the exponential term analogous to that in eq (2.1) is

$$\exp[-(b_{11}h^2+b_{22}k^3+b_{33}l^2+b_{12}hk+b_{23}kl+b_{31}hl)] \tag{2.2}$$

or

$$e^{-2\pi^2}\sum_i \sum_j U_{ij}s_is_j \tag{2.3}$$

where **s** is the reciprocal vector with components s_i and magnitude $2 \sin \theta/\lambda$,

$$\mathbf{s}=h\mathbf{a}^*+k\mathbf{b}^*+l\mathbf{c}^*,$$

with **a***, **b***, and **c*** the reciprocal axes of the crystal. U_{ij} is a component of a symmetric tensor **U** such that the mean square amplitude of vibration in the direction of a unit vector m_i with respect to the reciprocal axes is

$$u^2=\sum_i \sum_j U_{ij}m_im_j. \tag{2.4}$$

Although the use of individual atomic isotropic and anisotropic vibration parameters has been regarded at times as unjustified and merely a device to improve the agreement of calculated with observed structure amplitudes by introducing additional adjustable parameters, the benefits have in fact far outweighed and outnumbered the abuses. These "vibration parameters" may indeed mask other effects and may even be in part artifacts arising from absorption by the crystal, which simulates a negative temperature factor and may introduce false anisotropy because of irregularities of crystal shape. However, by suitable choice of radiation and crystal size and shape, this effect can be minimized, and if it is significant it can be (and usually now is) corrected for in careful work.

Careful scrutiny of even isotropic temperature factors during least-squares refinement of a structure is one of the most effective ways of discovering spurious "atoms" introduced into a trial structure. If an assumed atom is spurious, its vibration parameter will increase very rapidly—physically this corresponds to a spreading of the scattering matter of this supposed atom over a very large volume, an indication that the assumed position is incorrect. When the position is correct, but the identification of the atom is not—i.e., in x-ray determinations, when its atomic number is wrong—this mis-identification can often be discovered by comparison of the vibration parameters of the assumed atom and its immediate neighbors. If it seems to be vibrating far less than one might have expected, it probably has been assigned too low a scattering factor, so that to compensate the electrons appear more concentrated than they really are. Conversely, if its vibration seems too great, it may have been assigned too high an atomic number, or it may be disordered in any of a variety of ways. These sorts of considerations have been used many times, e.g. to distinguish the oxygen and nitrogen atoms in the amide group of aureomycin [15], and to distinguish supposed oxygen atoms from what was in reality a half-chlorine atom (i.e., chlorine in two-fold disorder) in an iron porphine [16].

Similar examination of anisotropic "temperature factors" can be even more helpful. For example, in the aforementioned iron-porphine [16] and also in a closely related molecule [17], the vibration parameters of the metal atoms were unusually high parallel to **c** but were normal in other directions. This anomaly, together with certain other unusual structural features, suggested that in fact the molecules involved were disordered parallel to **c**. A much improved fit to the data, together with more normal vibration parameters, was found with this model. Even in the absence of disorder, scrutiny of the behavior of anisotropic vibration parameters during refinement can aid in differentiating similar atoms or reveal unsuspected errors. For example, it helped in differentiating nitrosyl and carbonyl groups in $MnNO(CO)_2P(C_6H_5)_3$ [18] and brought to light an inadvertent error in the sign of the y-parameter of one oxygen atom of the phosphate group of calcium thymidylate [19]. Because of the latter error, the assumed position of this atom was 0.55 Å from the correct position along **b**; when refinement was started, the "temperature factor" parallel to the y-axis increased very rapidly, but those in other directions remained normal. At the same time, the refinement process gradually shifted the y-parameter, and as it approached its correct value, the corresponding temperature factor decreased again to a reasonable magnitude.

Some attempts have been made in the past to use more exact descriptions of the scattering from atoms or groups of atoms undergoing librational motion, particularly torsional motion in hindered rotation, but they are unwieldy and have in fact been applied only rarely. However, they are attracting renewed interest [20,21] and more treatments of this sort are to be expected with the better data now available, which warrant more exact analyses.

3. Rigid-Body and Related Treatments

3.1. Rigid-Body Motion

Cruickshank first showed in 1956 [22] how to determine the components of the rigid-body motion of a molecule in a crystal by a least-squares analysis of the individual atomic anisotropic vibration parameters. His treatment involves a description of the molecular motion in terms of two symmetric tensors, one for translation (**T**) and one for libration (which he termed $\boldsymbol{\omega}$). It has been widely adopted and used in many studies of molecular crystal structures.

However, in recent years it has been recognized by several people that Cruickshank's treatment is inadequate when there is no preordained center of libration (e.g., a center of symmetry, which was in fact present in the molecules that he first treated) and attempts have been made to determine and refine the position of an assumed center of libration [23,24]. Actually, Schomaker first recognized in 1963 that an additional tensor was needed to account for correlations of libration and translation, and a complete analysis has now been published [25]. In addition to the translation (**T**) and libration (**L**) tensors, which are symmetric as before and thus involve six parameters each, the screw correlation tensor (**S**) must be included. For a molecule at a sufficiently unsymmetrical site, **S** has eight independent components, one of its diagonal elements being arbitrary, and the contributions to the anisotropic displacement tensors by the rigid-body part of the enormously complicated actual motions can be described in terms of six uncorrelated simple motions: three principal mean-square translations plus three *screw* (*helical*) motions about and along three mutually perpendicular *non-intersecting* axes.

The problem of fitting the observed atomic vibrational displacement tensors (the **U** of eq (2.4)) in terms of rigid-body translation and screw motion involves in the general case a least-squares fit of twenty independent parameters. If the molecule is at a symmetrical site, some or all of the components of **S** are subject to special restrictions; for example, if the molecule is at a centrosymmetric site, **S** vanishes completely and the treatment is identical to Cruickshank's. In any event the fit is always independent of the origin assumed in the description of the motion and can be found by a straightforward linear least-squares process.

3.2. Librational Corrections to Distances

Cruikshank [26, 27] was also the first to treat an important consequence of librational motion, namely that intramolecular distances will appear foreshortened. The corrections for this effect depend only on the libration tensor **L** when rigid-body motion is all that is involved. In more complicated situations, it is only possible to make a meaningful correction by making assumptions about the joint distribution of the motions of the atoms involved [28]. An assumption commonly made is that one atom "rides" on another (essentially that it participates in all of the motion of the atom on which it rides plus some additional motion of its own). This assumption often seems justified, particularly when a light atom is attached terminally to a heavier one (e.g., as in a —OH group).

Becka and Cruickshank have shown convincingly [29] how the correction for rigid-body librational motion removes an apparent small temperature dependence of the C–N bond distance in hexamethylenetetramine. The *uncorrected* distance decreases by more than 0.010 Å as the temperature is raised from 34 to 298 °K; the r.m.s. librational amplitude increases at the same time from 2.4° to 6.6° [30]. When this latter increase is taken into account, the difference in the foreshortening correction at the different temperatures is found to account almost exactly for the apparent change in bond length.

3.3. Pawley's Rigid-Body Method

Pawley [23, 24] has used an approach to the determination of the rigid-body parameters different from that of Cruickshank or Schomaker and Trueblood. He makes the rigid-body assumption at an early stage in the refinement of the parameters of the structure, so that instead of determining *individual* atomic anisotropic vibration parameters, he determines only the components of the overall librational and translational tensors **L** and **T** and the coordinates of a presumed origin of libration.[2]

This approach has the advantage that it reduces the number of parameters and gives appreciably more rapid convergence; it also usually gives somewhat smaller standard deviations for the rigid-body tensors than are obtained by the analysis of refined individual atomic vibration parameters. It is of course suitable only for rather rigid molecules, since the individual atomic anisotropic temperature factors are constrained to fit the parameters of the rigid-body motion. Most of the molecules studied by Pawley [24] were indeed quite rigid boron compounds, but one had $-CH_2Br$ groups which might have been expected to be moderately flexible. Surprisingly, when the constraints on the individual temperature factors were removed at the end of the refinement, there was no significant improvement in the agreement of observed and calculated structure amplitudes.

---

[2] In a private communication just received, Pawley reports that he has modified his parameter-refinement program to include **S** instead of the presumed origin of libration and that the least-squares process no longer converges but rather exhibits all the symptoms lf ill-conditioning.

3.4. Internal Vibrations

Any rigid-body treatment involves either assuming that the internal vibrations are negligible with respect to the rigid-body motion, explicitly correcting for the internal vibrations if they are known [31, 32], or modifying the analysis to include them when they do not increase too greatly the number of parameters to be determined. By far the most common assumption in practice has been to ignore the internal vibrations. This approximation is generally justified as far as bond-stretching vibrations are concerned (except when hydrogen vibrational parameters have been determined and are being used to determine rigid-body motion—this is possible with neutron diffraction although not with x-rays). The approximation is less good for bending modes, but is still acceptable for many molecules; it is much more questionable when there are appreciable torsional modes (e.g., about single bonds).

It has become common practice to make an analysis of possible rigid-body motion at the conclusion of the determination of the structure of a molecular crystal. By comparing the results with and without certain suspect atoms or groups of atoms, and in particular the fit of the vibrational parameters of these atoms to the rigid-body model, the validity of the model can be plausibly tested. For example, the appreciable vibrations of the cyano groups in many cyano-olefins are readily apparent when this sort of comparison is made [33], and the large out-of-plane bending characteristic of carbonyl oxygens and other terminal atoms has been noted many times [34]. A recent survey [35] indicates that the rigid-body postulate may be more widely applicable to molecular crystals than might at first be thought; detailed atom-by-atom comparisons were made, and since Cruickshank's method was used although some of the molecules were not centrosymmetric, the fits were not in fact as good as they would be with the more exact treatment, which has always given a better fit, even when the increased number of parameters is taken into account [25].

In several of the most careful organic structural studies to date, including hexamethylenetetramine [30], 3-*endo*-phenyl-2-*endo*-norbornanol [36], and benzene [37,38], the rigid-body motion has been treated separately from at least the most prominent internal vibrations. The results shown in table 1 for the libration of the benzene molecule about its six-fold axis at various temperatures [37,38] are illustrative. They are qualitatively consistent with n.m.r. evidence concerning the motion of the molecule in the crystal, and agree within the errors of the methods of estimation with the Raman spectroscopic results [39]. The latter indicate that the r.m.s. librational amplitude about the molecular six-fold axis in crystalline benzene is about 6.8° at 273 °K, 4.5° at 195 °K, and 2.6° at 77 °K. At each of these temperatures, Ito and Shigeoka [39] interpret their results (on both benzene and perdeuterobenzene) to indicate that there is a slightly larger libration amplitude about one of the two-fold axes in the molecular plane than about the six-fold axis, in disagreement with the x-ray results at 270 °K [38]. (No librational amplitudes about the two-fold axes were calculated in the neutron diffraction study [37].) However, in each analysis there were some rather serious approximations that had to be made to get the libration amplitudes about the different molecular axes and it seems unlikely that this discrepancy is significant. Ito and Shigeoka suggest that as far as hydrogen-hydrogen contacts are determining, there does appear to be greater freedom for motion about the two-fold axis than about the six-fold axis.

Each of the studies just cited was made at a number of temperatures well below room temperature, a practice which has been urged by Lonsdale [40] for many years. The number of careful structure analyses made at different temperatures is still small, but there have been several within the past year and undoubtedly efforts in this direction will be accelerated. As Cruickshank has pointed out [41], little is to be gained by going below liquid hydrogen temperatures because modes which are thermally excited at room temperature are then populated chiefly in the ground state. In fact, the gain between the temperatures of liquid nitrogen and liquid hydrogen is in most cases so small that it is probably not worth the extra effort unless there is some reason for the low temperature other than the study of the precise molecular and crystal structure, including as many details of the electron density as can be discerned.

TABLE 1. RMS libration amplitude of benzene about the molecular 6-fold axis [37, 38]

Temperature	From Carbon-Atom Vibration Parameters	From Hydrogen-Atom Vibration Parameters
270 ° K	7. 9°	------------------
218 ° K	5. 0°	4. 0°
138 ° K	2. 5°	2. 8°

(The values at the two lower temperatures are from neutron-diffraction data and include correction for the internal vibrations of the molecule).

It is clearly important in attempting to deduce information about internal modes that the data used be of the best possible accuracy. A very ambitious attempt has been made [42] to determine the internal bending modes of di-*p*-xylylene ([2.2]paracyclophane); however, the molecule has high symmetry so there is little redundancy in the vibrational parameters that can be used and hence any errors in them will be important. An extensive further study of this molecule using both diffractometer and film data [43] indicates that the vibration parameters found earlier were sufficiently in error that the conclusions from that analysis concerning the details of the various bending modes of the molecule (which depended chiefly on *differences* in the parameters for the three unique atoms) are not well founded.

A striking demonstration of the physical plausibility of vibration parameters derived by careful analysis of accurate data has recently been given by Johnson in his neutron-diffraction study of 3-*endo*-phenyl-2-*endo*-norbornanol [36]. In one approach, he treated the entire skeleton of non-hydrogen atoms as a rigid body, and then used the motional parameters so derived to calculate the rigid-body contributions to the hydrogen vibrational parameters, assuming them to "ride" on the heavy-atom skeleton. The differences between the actual hydrogen vibrations and those so calculated presumably represent the displacements due to internal vibrations of the hydrogen atoms.

The general pattern so found was physically very plausible: the smallest displacements were along the bond directions, the out-of-plane displacements for the phenyl-hydrogens were greater than the in-plane tangential ones, and the largest displacements for the methylene hydrogens were in the H–C–H plane and nearly perpendicular to the C–H bonds. A far better fit of the heavy-atom parameters was obtained by treating the phenyl group and the norbornanol cage as two separate rigid bodies, and the three plausible patterns of hydrogen-atom movement noted above were then even more apparent. Furthermore the differential hydrogen displacements so derived agree reasonably well with the displacements expected from the usual force constants and frequency assignments.

3.5. Segmented or Coupled Rigid-Bodies

Johnson [44] has recently extended the rigid-body approach to what he terms "segmented rigid bodies", that is a group of individually rigid segments riding on each other and joined by axes of torsional oscillation. He has applied this model with notable success to citric acid, which he treated as consisting of six segments joined by five torsional axes.

A general approach to the problem of coupled rigid bodies has been suggested by Schomaker [45]. It involves no assumptions of riding motion and is just a generalization of the analysis of a single rigid body [25]. For example, if there are two rigid bodies joined at a single point, there will be one overall translational tensor and two librational and screw tensors, a total of 34 parameters; with two rigid bodies joined together at two points, the additional constraint reduces the number of parameters to 26. Since in a large molecule of the sort which is likely to be of interest for this type of analysis there are many atoms, with six vibrational parameters per atom, there should normally be more than sufficient data for determining these additional rigid-body parameters. It remains to be seen, of course, whether they will be physically plausible, but presumably they should be as consistent as those for individually rigid molecules. That these are often extremely plausible physically is shown in the next section.

4. Some Experimental Results Concerning Motion of Molecules and Portions of Molecules

A few examples have been selected from some recent precise structure analyses to illustrate the sorts of patterns of molecular motion that can be discerned from diffraction data. Almost all of the results quoted have been determined by application of the rigid body model, including **S** when needed, to the individual atomic temperature factors after the latter have been determined by least-squares refinement. The only exceptions are for the nitro groups, for which calculations were made as described below, and for naphthalene and anthracene, to which Pawley applied his refinement method [24].

Despite the fact that the individual atomic mean-square displacements are usually precise only to about 5 percent in the best analyses. there are normally sufficient atoms in the rigid body so that its parameters can be determined with fair precision. The r.m.s. discrepancies of the observed and calculated components of the displacement tensors (taking into account the number of independent parameters being determined) were evaluated in every example quoted and the fit was usually well within the estimated precision of the experimentally determined displacements.

Cruickshank's results for anthracene [46, 47] and naphthalene [48] were the first ones obtained with the rigid-body model and demonstrated at once its general plausibility. The principal axes of the translational and librational tensors for each molecule coincided with the molecular axes within experimental error, and the findings were consistent with both thermodynamic and spectroscopic data [49]. Pawley's elegant recent development of a model for the lattice dynamics of each of these crystals [4] gives good agreement of the tensors derived from the diffraction data with those calculated from the known structures using an assumed "6-exp" interatomic potential function.

This model also gives good agreement with the pattern of thermal diffuse x-ray scattering (especially noteworthy at high resolution), and fair agreement with the Raman frequencies and the elastic constants. Refinements of the model require more precise hydrogen positions since these are of prime importance in determining the structures [7, 8, 8a]. Inclusion of low-frequency modes of molecular distortion is needed also to improve the fit of calculated with observed Raman frequencies. Pawley is currently pursuing some of these lines, including the effects of anharmonicity [50].

The physical reality of the patterns of librational and translational motion derived from interpretation of diffraction data on organic molecular crystals to date is supported chiefly by their self-consistency in comparative studies of the same or similar molecules, or rigid portions of a molecule, in closely related structures, as well as by the physical plausibility of the results. We shall focus here entirely on the librational patterns not only because they are more striking but also because they are always independent of the origin assumed in the calculations, while for non-centrosymmetric molecules the translational tensor is not.

Table 2 gives some data on the libration of the molecule of tetracyanoquinodimethane (TCNQ),

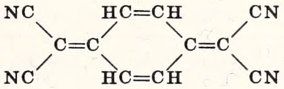

in four different structures [33, 51–53]. In each instance the libration is markedly anisotropic, and the principal motion is a libration with r.m.s. amplitude of 5–6° about an axis nearly coincident with the long axis of the molecule (which is the axis of minimum inertia). The pattern is very much the same whether all of the atoms are included, or just those of the quinodimethane skeleton, omitting the cyano groups (which are evidently "wagging" appreciably in TCNQ [33], as they are in tetracyanoethylene [54]). The librational tensors for three other TCNQ molecules, in $Cs_2(TCNQ)_3$ [54a] and *N*-methylphenazinium TCNQ [54b] have been calculated and are very similar to those in table 2.

In all of these structures, TCNQ molecules are packed with their planes parallel to those of other TCNQ molecules or to a planar group (such as 8-hydroxyquinoline); the minimum interplanar spacings are about 3.45 Å in TCNQ itself, and about 3.2 Å in the other structures, in which the TCNQ molecule is complexed in different ways. The variations in environment are relatively minor in a gross sense, but of course they differ in fine details and when one considers the sensitivity of intermolecular potentials to distances and thus to the details

TABLE 2. Principal axes of libration tensors for TCNQ in four different structures [a]

	TCNQ	$(C_6H_5)_4P$-$(TCNQ)_2$	TMPD $(TCNQ)_2$	TCNQ $(8\text{-HOQn})_2Cu$
		(*a*) *Entire molecule*		
L1	$30(^\circ)^2$	$38(^\circ)^2$	$32(^\circ)^2$	$27(^\circ)^2$
L2	5	4	5	6
L3	2	3	4	0
Deviation*	3°	1°	2°	3°
		(*b*) *Eight central carbon atoms*		
L1	$20(^\circ)^2$	$30(^\circ)^2$	$20(^\circ)^2$	$33(^\circ)^2$
L2	5	4	5	4
L3	1	3	3	4
Deviation*	4°	3°	1°	6°

*Angular deviation of direction of L1 from the long axis of the molecule.

[a] Abbreviations are: TCNQ, tetracyanoquinodimethane [33]
TMPD, N,N,N′,N′-*p*-phenylenediamine [52]
HOQn, 8-hydroxyquinoline [53]

of the molecular environment, these variations might have been expected to be quite significant. It is surprising that the pattern of TCNQ libration is so similar in every structure; the similarity suggests that the pattern of lattice modes is far less sensitive to the details of the intermolecular potential assumed than might at first have been believed.

Table 3 gives librational patterns for some *trans, trans* derivatives of muconic and sorbic acids studied by Schmidt and his collaborators [55–57]. The remarkable consistency of the patterns for these related molecules in different structures, together with the physical plausibility of the strongly anisotropic librations chiefly about the axes of minimum inertia, are once again strong arguments that they do represent actual patterns of molecular motion. These molecules fit the rigid-body model surprisingly well, and even the bending vibrations which might have been anticipated do not seem as pronounced as in some related molecules. It is possible that the very large amplitudes

TABLE 3. Libration tensors for some *trans,trans*-dienes [55–57]

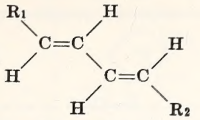

	R_1=-CN R_2=-CN	R_1=-$COOCH_3$ R_2=-$COOCH_3$	R_1=-CH_3 R_2=-$CONH_2$
L1	284(°)^2	84(°)^2	126(°)^2
L2	7	3	8
L3	5	2	3
Deviation*	5°	2°	0°

*Angular deviation of L1 and axis of minimum moment of inertia.

about L1 may include a significant contribution from torsional motion about the central single bond, which does not deviate greatly from the direction of L1.

Table 4 presents some results for the two independent molecules of cyclopropanecarboxamide in the asymmetric unit of the monoclinic crystals of this compound [58]. The librational patterns are remarkably similar, both with respect to the molecular axis of this compact nonplanar molecule (the principal libration is nearly about the axis of minimum inertia, with an amplitude near 10°) and with respect to the hydrogen bonds which tie the structure together. Whether this close relation to the hydrogen-bonding scheme is mere coincidence cannot be decided until more analyses have been made of patterns in similar crystals; however it is certainly suggestive that the molecules are swinging about these connecting links, which nearly coincide with the molecular axes of minimum inertia.

The same *caveat* must be applied to the results of table 4 as to those of table 3; there could be appreciable torsional oscillations about the bond from the amide group to the ring, and since this bond does not deviate greatly from L1 (by 27° and 15° for the two molecules), the overall apparent libration may include some internal torsional component. The fact that each molecule adopts an equilibrium conformation with the amide group nearly normal to the cyclopropane ring, a conformation found in some other similar cyclopropane derivatives as well, suggests that there may be a strong preference for this conformation and that perhaps the barrier to rotation about the bond may be relatively high. Unfortunately, there are too few atoms to permit completely general coupled rigid-body treatment to be made with an precision.

TABLE 4. Principal axes of libration tensors for the two independent molecules of cyclopropanecarboxamide [58]

	Molecule A	Molecule B
L1	$93(°)^2$	$92(°)^2$
L2	25	25
L3	13	11
Angle, L1 to axis of minimum inertia	3°	10°
Angle, L1 to N–H . . . O	8°	15°

Incidentally, the librational patterns for these molecules calculated using Cruickshank's method relative to the center of mass gave markedly different results [25]; inclusion of S was necessary in order to reveal the pattern shown in table 4.

The foregoing examples indicate the sorts of librational patterns characteristic of molecules that are at least moderately rigid. It is often possible to find similar patterns for portions of molecules that are themselves rigid although they may be joined together by links with some flexibility. The example of phenylnorbornanol studied by Johnson [41] has been cited earlier, and the application of his segmented rigid-body approach to citric acid [42] has also been described.

In extreme cases the torsional motion can be discerned readily merely from an examination of displacements in different directions. The marked apparent torsional oscillation characteristic of aromatic nitro groups was noted in 1960 [59]. Table 5 gives some relevant data from the structures of 4-nitroaniline [59] and 3-nitroperchlorylbenzene [60]; the data are typical of many aromatic nitro compounds. Scrutiny of the displacements of different atoms normal to the plane of the nitro group (which in each of these molecules is not far from the plane of the aromatic ring), as well as in different directions in the plane, suggests a marked torsional oscillation about the C–N bond. Although it is clear that there is scatter in the data, which may be real or may merely reflect a lack of precision, the general patterns are remarkably similar in different molecules. If one assumes that all of the difference in the out-of-plane motion of the oxygen and nitrogen atoms is due to torsional oscillation, the data indicate a torsional oscillation with a r.m.s. amplitude near 14° and a frequency of *ca.* 70 cm^{-1} (the frequency for 4-nitroaniline has been revised slightly from the earlier result [59] which was based on the classical approximation). Of course this assumption may be faulted, especially in view of the high out-of-plane amplitudes of vibration of carbonyl oxygen

Table 5. Vibrational parameters of aromatic nitro groups [59, 60]

	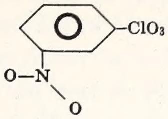	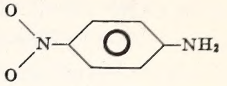
1. Mean square amplitudes:		
⊥ Plane:		
0(1), 0(2)	0. 134, 0. 133 Å^2	0. 166, 0. 123 Å^2
N	0. 063	0. 061
In plane, ‖ bond:		
0(1), 0(2)	0. 070, 0. 057	0. 035, 0. 041
N	0. 070, 0. 063	0. 033, 0. 056
In plane, ⊥ bond:		
0(1), 0(2)	0. 071, 0. 073	0. 074, 0. 046
2. R.m.s. torsional amplitude	14°	13°
3. Estimated torsional frequency	65 cm^{-1}	72 cm^{-1}

atoms [34]; however, if the apparent torsional motion is real, it might be detectable by Raman or neutron spectroscopy.

The foregoing examples are typical of the sorts of effects which can be found; they are not intended in any sense to represent an exhaustive survey, for a great many precise structure analyses have been made and might have been cited. Undoubtedly further surveys of the applicability of the rigid body model, along the lines of the one already mentioned [35], will be forthcoming.

One well-known shortcoming of diffraction methods for studying molecular motion in crystals is that the duration of the experiment is so long that static disorder cannot be distinguished from dynamic effects, at least by experiments at a single temperature. Studies at different temperatures, now being done in increasing numbers, can provide fairly conclusive evidence, since dynamic effects show marked decreases with decreasing temperature, at least for molecular crystals. Most such studies show that the effects reflected in "temperature factors" are indeed temperature dependent, in the expected fashion.

The use of n.m.r. techniques for studying molecular motion in crystals is well known [61], and the results are usually in accord with those found by other techniques, when other techniques are applicable. The final example in this section presents what seems a puzzling contradiction. The crystal structure of the 1:3 complex of silver perchlorate with dioxane has been determined at room temperature (about 22 °C)[62]. Since the silver atom (at the origin) determines essentially all of the signs in this structure, there is little ambiguity about the Fourier synthesis which corresponds to the electron density; it shows quite clearly that at room temperature the dioxane molecules are rotating axially about a line between the oxygen atoms. Detailed structure factor calculations and examination of the anisotropy of the thermal parameters of the oxygen atoms of the dioxane molecule support this model. There is no indication that the dioxane molecules reorient themselves spherically, although the percholate ion does appear to do so.

Recently however· Kawamori and Sakiyama [63] have made measurements of the proton magnetic resonance spectrum of crystals of this complex between −66 and +25 °C. They find two phase transitions (at 14 and 17 °C). By studies of line width, and comparison with calculated second moments, they conclude that axial rotation is present at about 14 °C and that there is spherical reorientation of the dioxane molecules above 17 °C. They imply that the latter result is in accord with the x-ray findings. In fact, it seems to contradict them, but the temperatures involved are not greatly different, and it is not clear whether the apparently contradictory observations were really made on the same phase.

5. Chemical Reactions in Organic Crystals

There has recently been increasing attention to studies of solid state reactions of various sorts, which certainly fall properly within the scope of any consideration of molecular dynamics. Morawetz [64] has reviewed much of the work involving organic crystals; one subsequent study is that of Lonsdale, Nave, and Stephens [65] who made a very detailed investigation of the changes occurring during the photochemical and thermal conversion of a single crystal of anthracene photo-oxide to a single crystal of a mixture of anthraquinone and anthrone. They discuss the observed changes in terms of the details of the molecular structures, thermal vibrations, and packing in the crystals.

The most comprehensive current studies of solid state organic chemistry by a combination of diffraction and other techniques are those of Schmidt and his collaborators at the Weizmann Institute [66, 67]; much of their work has appeared in the Journal of The Chemical Society, chiefly in mid-1964 and early 1967. Their most extensive published studies concern the photochemistry of crystals of *trans* and *cis* cinnamic acid derivatives, various *p*-benzoquinones, and a number of *trans*, *trans*-dienes (principally derivatives of muconic and sorbic acids), and the photochromy, thermochromy, and luminescence of anils of *o*-hydroxy aromatic aldehydes.

The cinnamic acid studies are illustrative, and demonstrate most convincingly the importance of "topochemical" factors (i.e., the details of the mutual arrangement of molecules in the structure). For example, for the *trans* acids, the nature of the photodimer formed on irradiation depends only on the structure of the crystal. Several of these molecules crystallize in a number of polymorphic forms, and one can predict how each form will behave on irradiation simply by knowing the details of the packing of nearby molecules [68]. If they are parallel to each other, related simply by the translational symmetry of the crystal lattice, and the double bonds are separated by about 4.1 Å or less, they will dimerize to a substituted cyclobutane (a β-truxinic acid), which has a mirror plane. If the reactive centers are further apart than about 4.7 Å, no reaction occurs. Finally, if the molecules are head-to-tail, related by a center of symmetry, and are sufficiently close, a centrosymmetric cyclobutane derivative, known as an α-truxillic acid, is formed. The structural relationships are summarized in table 6.

TABLE 6. Relations between molecular packing in *trans*-cinnamic acid derivatives and structures of photodimers formed [68]

Packing	*Symmetry*	*Photodimer formed (if any)*
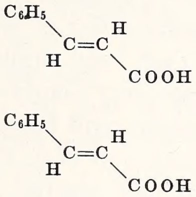	(Translation)	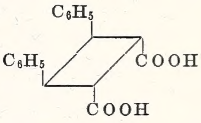 β-Truxinic Acid
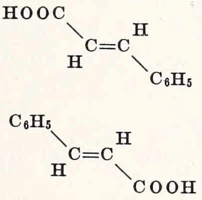	(Centrosymmetric)	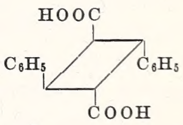 α-Truxillic acid

Irradiation of crystalline *cis*-cinnamic acids may isomerize them to *trans* molecules, which (after local recrystallization) are either trapped in a light-stable structure or photodimerized to the product(s) characteristic of their crystal structure(s) [69]. The isomerization itself appears lattice-controlled, perhaps by a mechanism which requires interaction of an excited C=C in one *cis* molecule with a neighboring-molecule's C=C no more than about 4.4 Å away.

Topochemical control is certainly demonstrated for these reactions, in accord with the postulate [66] that they occur with a minimum amount of atomic or molecular movement. Topochemical factors are expected not to be dominant when reactions involve long-distance migrations of electrons or excitation energy, or in systems of high symmetry (such as many inorganic crystals).

In the studies of *p*-benzoquinones [70] and muconic acid derivatives [71], the results were with very few exceptions also in accord with the postulates of topochemical control. In some of the quinone crystals, the occurrence of close *non-parallel* double-bond contacts appeared to be correlated with the formation of polymeric (rather than dimeric) products. Presumably the interaction of these reactive centers leads to open-chain dimer diradicals which cannot terminate by ring closure and may therefore instead initiate polymerization.

Much of the work on the photochromy, thermochromy, and luminescence of N-salicylideneanilines and related anils has been summarized in the latest paper by Cohen and Flavian [72]. Extensive spectroscopic studies of crystals and solutions, together with studies of crystal structure, have provided evidence that the thermochromic behavior arises as a consequence of a tautomeric proton shift (from oxygen to nitrogen) and that the same ground and excited states are involved in the thermochromic absorption as in the luminescence.

One by-product of these studies of anils was a detailed analysis of the structure of crystalline N-5-chlorosalicylideneaniline at both room temperature and at 90 °K [73]. The structures are very similar at the two temperatures. All atoms of the molecule are very nearly coplanar and in fact the molecule behaves as a moderately rigid body at each temperature; the axis of principal librational motion is in the plane of the molecule and close to the axis of minimum inertia. At room temperature this motion corresponds to a r.m.s. amplitude of about 5°; at 90 °K it is about half as great. Possibly the application of a coupled rigid-body analysis to this molecule would give an improved fit and permit separating a torsional component from this apparent overall librational pattern, but the fit is already quite satisfactory. Once again we see evidence that the rigid-body model has wider applicability than might be supposed.

It is a pleasure to acknowledge my indebtedness to those who sent me published and unpublished information and suggestions, including N. Baenziger, D. W. J. Cruickshank, B. Dawson, A. W. Hanson, C. K. Johnson, E. Maslen, G. S. Pawley, J. Rush, G. M. J. Schmidt, and V. Schomaker. I am also most grateful to Bonnie Warn for her help with many of the calculations reported here.

6. Discussion

J. J. Rush (National Bureau of Standards): Shimanouchi has recently published a very detailed far infrared study on lattice vibrations in solid benzene, and we've also recently published some less well resolved low-energy neutron spectra of benzene. I was wondering if you know of any attempt that has been made to compare the mean-square amplitudes that one would get out of these data with the mean-square amplitudes you showed for benzene.

K. N. Trueblood: I don't. George, do you know if this has been done?

G. E. Bacon (University of Sheffield): Not to my knowledge.

K. N. Trueblood: I'll look into that. Thank you.

E. Prince (Naval Research Laboratory): How good must the data be to yield valid dynamic information? How does one know if the data are good enough?

K. N. Trueblood: These are excellent questions and not easy to answer at all precisely. With regard to the second one, the only way one can know that the dynamic information one has derived is meaningful is to compare it with data obtained in other ways and to try to see if it is physically plausible. As for the first question, the answer is that it certainly ought to be the very best you can get, and the best you can get now is very good. There's no doubt that people have overrefined poor data in the past. It's also clear now, as Coppens will show in just a moment, that if you're trying to get the most precise vibrational parameters, you should take into account anisotropy of form factors, as well as minimizing the usual systematic errors. In the examples that I've cited here, the motion has been quite significant, with fairly large r.m.s. amplitudes, say 5 degrees or more. Under those conditions I would guess that most of the relatively precise x-ray studies now being done would be adequate. But, of course, in many molecules the motions are smaller than that, and if you want to do something of the sort that Carroll Johnson illustrated with the norbornanol derivative, it would be very hard to do it with ordinary x-ray data and get really meaningful results. On the other hand, with the best automatic diffractometer data, I suspect it is possible, but only under the most careful circumstances. Of course with data which is carefully taken but of less than the best obtainable quality one can often find consistent and plausible patterns such as those cited earlier, but one must regard them with some skepticism. I fear this isn't a very satisfactory answer—no doubt the best assurance comes from finding similar information by independent techniques.

Perhaps Dr. Johnson can comment.

C. K. Johnson (Oak Ridge National Laboratory): Systematic errors in the neutron-diffraction Bragg-reflection intensities of 3-*endo*-phenyl-2-*endo*-norbornanol [36] would have much less effect on the accuracy of the mean-square amplitudes of the phenyl hydrogen atoms *relative to* the mean-square amplitudes of the phenyl carbon atoms than these errors would have on the absolute mean-square amplitudes determined for the atoms of the phenyl group. Systematic errors in intensities would, in general, affect the carbon and hydrogen anisotropic temperature factor coefficients in the same manner and this would cancel out in the analysis of mean-square amplitudes of hydrogen atoms relative to carbon atoms because of the similar geometry of hydrogen and carbon atoms on the phenyl group.

G. E. Bacon: Have you considered, or do you think it would be possible to consider, the formulation of some factor which would express—in a rough way at least—the extent to which the thermal data is compatible with rigid-body motion? I am struck by the contrast between some of the molecules which you have described and cases, like potassium hydrogen bisphenylacetate, where we concluded that the molecule moved as a whole, but not rigidly.

K. N. Trueblood: I have not thought about that, but it certainly might be helpful qualitatively to have some such measure, and it ought to be considered further. (*Added later:* Some function of the ratio of the r.m.s. ΔU_{ij}, corrected for the number of parameters being determined, to the average e.s.d. of an individual U_{ij}, could measure how well any particular model fit. One would have to specify what that model was—e.g., a completely rigid molecule, or one composed of several coupled rigid segments. For more than this one needs to examine the fit of the tensors of the individual atoms as Burns et al. have done [35]).

R. D. Gilardi (Naval Research Laboratory): I was wondering about the question of separability of the internal vibrational motion from rigid-body translations and librations with the unit cell. I should think that a symmetrical molecule, such as CO_2, would appear the same whether it was *vibrating* in a symmetric bend or *librating* within the crystal lattice. Do you think this inseparability is confined to special symmetrical cases or whether it might, to some extent, affect all such diffraction analyses of dynamics?

K. N. Trueblood: I'm sure you're right about CO_2. The question of distinguishing the symmetrical bending of CO_2 from a possible libration about an axis normal to the plane of the bending vibration is analogous to the difficulty of distinguishing torsional motion about a bond from libration of the whole molecule about the bond. Diffraction data, involving both time- and lattice-averaging, cannot separate the two, at least if the molecule is symmetrical about the bond. (If it is not, the individual parts may have significantly different torsional amplitudes, and some resolution of the motions would be possible.) However, for general internal modes of larger and less symmetrical molecules, I don't believe this sort of inseparability would normally be a major problem; furthermore, of course, the amplitudes of most stretching and many bending vibrations are appreciably less than those consistent with common patterns of libration of molecules. In the work of Duax and Baenziger [74] on CS_2, the problem did not arise because they used spectroscopic data to get the librational amplitudes rather than attempting to derive them from the diffraction data. (This answer is amplified from that given at the time.)

W. C. Hamilton (Brookhaven National Laboratory): In the light of Professor Trueblood's talk, I would like to restate the method I proposed for the refinement of molecular motions from diffraction data. Let us express the total thermal motion M_T of a molecule in a crystalline solid in the following way:

$$M_T = M_I + M_{RB}^H + M_{RB}^A$$

where

M_I = internal molecular modes

M_{RB}^H = harmonic rigid body motion (the **T**, **L**, and **S** of Professor Trueblood's paper)

M_{RB}^A = anharmonic contributions to the rigid body motions.

Pawley's approach was to refine M_{RB}^H, assuming that the other two terms were zero. I propose using spectroscopic values for M_I and refining both M_{RB}^H and M_{RB}^A. Of course this approach is rigorous only if there is no serious coupling of the internal modes, that is if the dispersion curves for these modes are flat. This will be one very interesting question for the neutron lattice dynamics people to answer, "How flat are the dispersion curves for the internal optical modes in molecular crystals?"

7. References

[1] W. Cochran, Reports on Progress in Physics **26,** 1 (1963).

[2] W. Cochran and G. S. Pawley, Proc. Roy. Soc. **A280,** 1 (1964).

[3] W. G. Cochran, in Phonons and Phonon Interactions (T. Bak, editor), p. 102, W. A. Benjamin, New York (1964).

[4] G. S. Pawley, Phys. stat. sol. **20,** 347 (1967).

[5] W. A. Wooster, Diffuse X-ray Reflections from Crystals, Oxford University Press, Oxford (1962).

[6] A. I. Kitajgorodskij, J. chim. Phys. **63,** 9 (1966).

[7] D. P. Craig, R. Mason, P. Pauling, and D. P. Santry, Proc. Roy. Soc. **A268,** 98 (1965).

[8] D. E. Williams, J. Chem. Phys. **45,** 3770 (1966).

[8a] D. E. Williams, Abstracts of the American Crystallographic Association, p. 54, Atlanta, Georgia (1967).

[9] P. K. Gantzel and K. N. Trueblood, Acta Cryst. **18,** 958 (1965).

[10] E. W. Hughes, J. Amer. Chem. Soc. **63,** 1737 (1941).

[11] S. J. LaPlaca and J. A. Ibers, Acta Cryst. **18,** 511 (1965).

[12] A. M. O'Connell, A. I. M. Rae, and E. N. Maslen, Acta Cryst. **21,** 208 (1966).

[13] G. C. Verschoor, Nature **202,** 1206 (1964) and Thesis, Groningen.

[13a] R. F. Stewart, Abstracts of the American Crystallographic Association, p. 51, Atlanta, Georgia (1967).

[13b] P. Coppens, This Symposium, paper F1 (1967).

[13c] P. Coppens and A. L. Bednowitz, Abstracts of the American Crystallographic Association, p. 52, Atlanta, Georgia (1967).

[14] B. Dawson, Proc. Roy. Soc. **A298,** 255, 264 (1967).

[15] J. Donohue, J. D. Dunitz, K. N. Trueblood, and M. S. Webster, J. Amer. Chem. Soc. **85,** 851 (1963).

[16] J. L. Hoard, G. H. Cohen, and M. D. Glick, J. Amer. Chem. Soc. **89,** 1992 (1967).

[17] M. D. Glick, G. H. Cohen, and J. L. Hoard, J. Amer. Chem. Soc. **89,** 1996 (1967).

[18] J. H. Enemark and J. A. Ibers, Inorg. Chem. **6,** 1575 (1967).

[19] K. N. Trueblood, P. Horn, and V. Luzzati, Acta Cryst. **14,** 965 (1961).

[20] G. M. Brown and R. Chidambaram, Abstracts of the American Crystallographic Association, p. 21, Atlanta, Georgia (1967).

[21] E. N. Maslen, Acta. Cryst. **A24,** 434 (1968).

[22] D. W. J. Cruickshank, Acta Cryst. **9,** 754 (1956).

[23] G. S. Pawley, Acta Cryst. **17,** 457 (1964).

[24] G. S. Pawley, Acta Cryst. **20,** 631 (1966).

[25] V. Schomaker and K. N. Trueblood, Acta Cryst. **B24,** 63 (1968).

[26] D. W. J. Cruickshank, Acta Cryst. **9,** 757 (1956).

[27] D. W. J. Cruickshank, Acta Cryst. **14,** 896 (1961).

[28] W. R. Busing and H. A. Levy, Acta Cryst. **17,** 142 (1964).

[29] L. N. Becka and D. W. J. Cruickshank, Proc. Roy. Soc. **A273,** 435 (1963).

[30] L. N. Becka and D. W. J. Cruickshank, Proc. Roy. Soc. **A273,** 455 (1963).

[31] P. W. Higgs, Acta Cryst. **8,** 99 (1955).

[32] S. J. Cyvin, Spectrochim. Acta **15,** 828 (1959).

[33] R. E. Long, R. A. Sparks, and K. N. Trueblood, Acta Cryst. **18,** 932 (1965).

[34] K. Lonsdale, D. Walley, and K. El Sayed, Acta Cryst. **20,** 13 (1966).

[35] D. M. Burns, W. G. Ferrier, and J. T. McMullan, Acta Cryst. **22,** 623 (1967).

[36] C. K. Johnson, This Symposium, paper C5 (1967).

[37] G. E. Bacon, N. A. Curry, and S. A. Wilson, Proc. Roy. Soc. A **279,** 98 (1964).

[38] E. G. Cox, D. W. J. Cruickshank, and J. A. S. Smith, Proc. Roy. Soc. A **247,** 1 (1958).

[39] M. Ito and T. Shigeoka, Spectrochim. Acta **22,** 1029 (1966).

[40] R. E. Gilbert and K. Lonsdale, Acta Cryst. **9,** 697 (1956).

[41] D. W. J. Cruickshank, Acta Cryst. **9,** 1005 (1956).

[42] K. Lonsdale, H. J. Milledge, and K. V. K. Rao, Proc. Roy. Soc. A **255,** 82 (1960).

[43] D. A. Bekoe, H. S. Maddox, and K. N. Trueblood, unpublished.

[44] C. K. Johnson, Abstracts of the Amer. Cryst. Assoc., p. 82, Minneapolis, Minnesota (1967).

[45] V. Schomaker, private communication (1967).

[46] D. W. J. Cruickshank, Acta Cryst. **9,** 915 (1956).

[47] D. W. J. Cruickshank, Acta Cryst. **10,** 470 (1957).

[48] D. W. J. Cruickshank, Acta Cryst. **10,** 504 (1957).

[49] D. W. J. Cruickshank, Rev. Mod. Phys. **30,** 163 (1958).

[50] G. S. Pawley, private communication (1967).

[51] P. Goldstein, K. Seff, and K. N. Trueblood, Acta Cryst. **B24,** 778 (1968).

[52] A. W. Hanson, Acta Cryst. **B24,** 768 (1968).

[53] R. M. Williams and S. C. Wallwork, Acta Cryst. **23,** 448 (1967).

[54] D. A. Bekoe and K. N. Trueblood, Z. Kristallogr. **113,** 1 (1960).

[54a] C. J. Fritchie and P. J. Arthur, Jr., Acta Crystallographica **21,** 139 (1966).

[54b] C. J. Fritchie, Acta Crystallographica **20,** 892 (1966).

[55] S. E. Filippakis, L. Leiserowitz, and G. M. J. Schmidt, J. Chem. Soc. B, 290 (1967).

[56] S. E. Filippakis, L. Leiserowitz, and G. M. J. Schmidt, J. Chem. Soc. B, 297 (1967).

[57] S. E. Filippakis, L. Leiserowitz, and G. M. J. Schmidt, J. Chem. Soc. B, 305 (1967).

[58] R. E. Long, H. S. Maddox, and K. N. Trueblood, submitted to Acta. Cryst.

[59] K. N. Trueblood, E. Goldish, and J. Donohue, Acta Cryst. **14,** 1009 (1961).

[60] G. J. Palenik, J. Donohue, and K. N. Trueblood, Acta Cryst. **24,** in press (1968).

[61] E. R. Andrew, J. Phys. Chem. Solids **18,** 9 (1960).

[62] R. J. Prosen and K. N. Trueblood, Acta Cryst. **9,** 741 (1956).

[63] A. Kawamori and M. Sakiyama, J. Phys. Soc. Japan **18,** 1218 (1963).

[64] H. Morawetz, Science **152,** 705 (1966).

[65] K. Lonsdale, E. Nave, and J. F. Stephens, Phil Trans. A **261,** 1 (1966).

[66] M. D. Cohen and G. M. J. Schmidt, J. Chem. Soc. 1996 (1964).

[67] F. L. Hirshfeld and G. M. J. Schmidt, J. Polymer Sci. A **2,** 2181 (1964).

[68] G. M. J. Schmidt, J. Chem. Soc., 2014 (1964).

[69] J. Bregman, K. Osaki, G. M. J. Schmidt, and F. I. Sonntag, J. Chem. Soc., 2021 (1964).

[70] D. Rabinovich and G. M. J. Schmidt, J. Chem. Soc. B, 144 (1967).

[71] M. Lahav and G. M. J. Schmidt, J. Chem. Soc. B, 312 (1967).

[72] M. Cohen and S. Flavian, J. Chem. Soc. B, 334 (1967).

[73] J. Bregman, L. Leiserowitz, and G. M. J. Schmidt, J. Chem. Soc., 2068 (1964).

[74] N. C. Baenziger and W. L. Duax, J. Chem. Phys. **48,** 2974 (1968).

INFORMATION ON MOLECULAR MOTION DERIVED FROM ANISOTROPIC TEMPERATURE FACTOR COEFFICIENTS [1]

CARROLL K. JOHNSON

Chemistry Division
Oak Ridge National Laboratory
Oak Ridge, Tennessee 37830

1. Rigid-Body Model

The anisotropic temperature factor (ATF) coefficients derived through a crystal-structure analysis describe the time-averaged mean-square displacement in 3-space for each crystallographically distinct atom in the crystal. Correlations between the displacements of different atoms are not experimentally obtainable from x-ray or neutron Bragg reflection data. Consequently, it is necessary to adopt a model which fixes the interatom correlations of motion in order to formulate a description of overall molecular motion from the ATF coefficients.

The simplest possible model for molecular motion is the rigid-body model in which all intramolecular interatomic distances are held constant. A recent detailed analysis of the mathematics for rigid-body motion of a molecule in a crystal is given by Schomaker and Trueblood [1].[2] If the time-averaged mean-square amplitudes of displacement due to internal molecular vibration in the same molecule or a similar molecule are known, the effect of these displacements can be subtracted from the observed ATF coefficients before fitting the rigid-body model.

2. Internal Molecular Vibrations

A normal coordinate treatment of spectroscopic data from the gas and liquid phases can be used to obtain time-averaged mean-square amplitudes of displacement due to internal molecular vibration. Three-by-three symmetric matrices defining the mean-square amplitude in 3-space for each of the N atoms in the molecule are present along the block diagonal of the complete $3N$-by-$3N$ symmetric "cartesian mean-square amplitude matrix." The cartesian mean-square amplitude

---

[1] Research sponsored by the U.S. Atomic Energy Commission under contract with Union Carbide Corporation.

[2] Figures in brackets indicate the literature references at the end of this paper.

matrix can be calculated with a computer program written by J. H. Schachtschneider [2]. The results of two such calculations using Schachtschneider's program and the published internal coordinates and force constants for benzene [3] and cyclobutane [4] are shown pictorially [5] in figure 1.

3. Mean-Square Displacements of Phenyl Hydrogen Atoms

The crystal structures [6] of 3-*endo*-phenyl-2-*endo*-norbornanol-5-*exo*-7-*anti*-d_2 and the nondeuterated isomorph were determined by neutron diffraction. There are two molecules in the asymmetric unit and two different isomorphous crystals; consequently, we obtain four independently determined sets of ATF coefficients for the molecule.

A description of rigid-body motion for the carbon atoms in the phenyl groups was calculated from the derived ATF coefficients after correcting for the displacements due to internal vibration as obtained from the spectroscopic study of benzene. The ATF coefficients of the hydrogen atoms were entered into the calculation in such a way that the hydrogen atoms were allowed to "ride" on the carbon ring with additional radial, in-plane, and out-of-plane mean-square displacements. The average resulting rms displacements of a hydrogen atom are 0.08 ± 0.02 Å along the bond, 0.13 ± 0.01 Å in the plane and 0.20 ± 0.01 Å out of the plane. These values are to be compared with the corresponding values of 0.077, 0.116 and 0.150 Å obtained from the spectroscopic study of benzene. The out-of-plane displacement value is significantly different from that of benzene, but the other values are essentially in agreement. Further work is underway to investigate the cause of the discrepancy.

4. Segmented-Body Model

Many molecules have large-amplitude modes of internal vibration, such as torsional oscillation about a single covalent bond. In such cases a "segmented-body" model can often be used to allow for this internal motion. The segmented-body model [7] is a network of coupled rigid-bodies. The freedom of motion between any two coupled segments of the model can be constrained to approximate a specific internal molecular motion such as torsional oscillation.

The type of segmented-body model most easily treated mathematically is the "riding model" [8], in which a segment B is assumed to "ride" on another segment A. Segment B has all the mean-square displacement caused by the motion of segment A as well as the additional mean-square displacement arising from the freedom of motion of the coupling joint connecting segment B to segment A. The additional

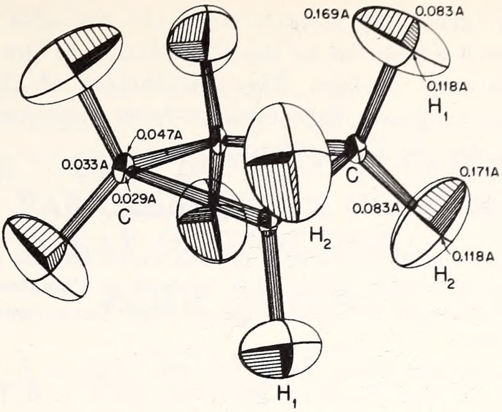

CYCLOBUTANE INTERNAL VIBRATION

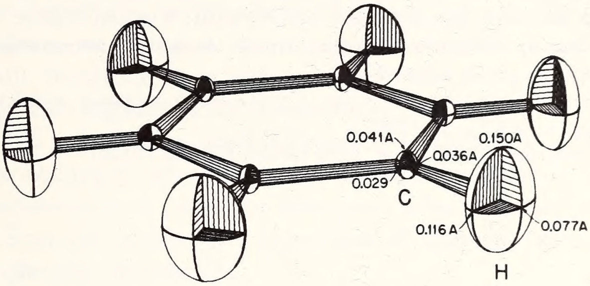

BENZENE INTERNAL VIBRATION

Figure 1. Probability ellipsoids for thermal motion from internal molecular vibrations, as determined by normal coordinate analyses of spectroscopic data for benzene and cyclobutane. The ellipsoid axes are drawn three times the rms displacement along the axes and the ellipsoidal surfaces enclose 97 percent of the normal distribution density. This figure was drawn with an incremental *xy* plotter controlled by the computer program ORTEP.

component of motion arising from the coupling joint is uncorrelated with the motion of segment *A*.

Once the riding segmented-body description of molecular motion has been obtained by a linear least-squares procedure, families of other models with different types of intersegment correlation of motion are obtainable which give the same calculated ATF coefficients. The major problem is to choose the member of the family of models which is the most realistic. However, useful information, such as the correction of interatomic distances within each rigid segment for the apparent shortening caused by libration [1,8], can be calculated directly from the riding model.

The author gratefully acknowledges the valuable discussions with Dr. H. A. Levy which led to the formulation of the segmented-body model for thermal motion. The calculations of the time-averaged values of mean-square displacement from spectroscopic data were performed by Dr. M. D. Danford.

5. References

[1] V. Schomaker and K. N. Trueblood, Acta Cryst. **B24,** 63 (1968).

[2] J. H. Schachtschneider, Vibrational Analysis of Polyatomic Molecules. III, Vibrational Secular Equation Programs, Shell Development Co. Tech. Rept. 263–62 (1962).

[3] a. S. J. Cyvin, Acta Chem. Scand. **11,** 1499 (1957); b. F. A. Miller and B. L. Crawford, J. Chem. Phys. **14,** 282 (1946), and c. E. B. Wilson, J. C. Decius and P. C. Cross, Molecular Vibrations, McGraw-Hill, New York (1955).

[4] R. C. Lord and I. Nakagawa, J. Chem. Phys. **39,** 2951 (1963).

[5] C. K. Johnson, ORTEP: A Fortran Thermal Ellipsoid Plot Program for Crystal Structure Illustrations, ORNL–3794, Revised (1965).

[6] C. K. Johnson, Abstracts of Amer. Cryst. Assoc. winter meeting at Georgia Inst. of Tech., F–3, p. 46 (1967).

[7] C. K. Johnson, Abstracts of Amer. Cryst. Assoc. summer meeting at Univ. of Minnesota, Q–6, p. 82 (1967).

[8] W. R. Busing and H. A. Levy, Acta Cryst. **17,** 142 (1964).

INFLUENCE OF BONDING EFFECTS ON THERMAL PARAMETERS AS DETERMINED BY X-RAY DIFFRACTION [1]

PHILIP COPPENS

Chemistry Department
Brookhaven National Laboratory, Upton, New York 11973

1. Introduction

X-ray temperature parameters obtained in conventional least-squares refinement using a free-atom model will generally contain contributions resulting from asymmetry of the valence electrons due to bonding. An experimental measure of the effect is obtained by comparative x-ray and neutron diffraction analyses. The few analyses of sufficient accuracy which have been undertaken indicate that the effect is appreciable at least for first row atoms. X-ray temperature factors for first row atoms are therefore of limited usefulness in the study of molecular dynamics.

2. Analysis of the Effect

We want to list three perturbations causing atomic asymmetry:

(1) *Bond Density.* A wave function describing a covalent bond AB contains a cross term between the atomic wave functions $\psi(A)$ and $\psi(B)$. This cross term represents the bond density or "overlap density." Its presence indicates that a certain amount of valence electronic charge has migrated from the atom into the bond region.

(2) *Lone-Pair Electrons.* When all atomic orbitals are either half-filled or doubly-filled the charge cloud is spherically symmetric. In the prepared state or valence state part of the orbitals may be doubly filled. The extra electrons in these "lone pair orbitals" cause an appreciable atomic asymmetry.

(3) *Ionicity.* Polarity of a bond will bring additional charge to specific atomic orbitals. An electronegative atom in a conjugated system will, for example, have extra charge in its p_π orbital.

These effects have been discussed from the standpoint of the diffractionist by, among others, McWeeny [1] [2], Dawson [2] and Coppens and Coulson [3]. The asymmetry results in a measurable shift in

---

[1] Research performed under the auspices of the U.S. Atomic Energy Commission.

[2] Figures in brackets indicate the literature references at the end of this paper.

the centroid of the charge density of first row atoms, for which the valence electrons form a considerable fraction of the total electron cloud. Similarly the temperature factors will be affected.

Bonding density may be simulated, for example, by an increase in the temperature parameters. Both Allmann [4] and Stewart [5] have calculated the variation in shape of a Fourier maximum with variation of the isotropic temperature parameter B. From their results it can be derived that for a carbon atom with B in the range 2.5–5.0 Å^2 and for Cu-Kα cut-off of reflections, an increase of 1 Å^2 in B corresponds to a migration of 0.22 electrons of the $1s^2$ shell into the region about 0.7 Å from the nucleus, which is the midpoint of a typical bond. The corresponding number for the $2sp^3$ shell is only 0.05. Thus, the free-atom model in x-ray structure analysis compensates for the diffuseness of the valence electrons by a smearing out of the core electrons of the 1s shell.

Dawson's treatment of the diamond structure gave an experimental value of 0.108 electrons/atom/bond for the overlap density [6]. This indicates that a trigonal first-row atom may have a total overlap density of about 0.33 electrons, and its temperature parameter may therefore increase by as much as 1.5 Å^2, a relative error of 40 percent!

An increase in B shifts the bonding density equally in all directions, while the arrangement of the bonds is obviously not spherically symmetric. However, more sophisticated models for thermal motion can absorb bonding asymmetry with greater ease. Thus, the routinely used anisotropic harmonic approximation will produce results which are especially erroneous when the deviations from spherical symmetry are centrosymmetric, while a model incorporating anharmonic motion can allow for any bonding asymmetry.

3. Experimental Evidence

Separate refinement of high-order x-ray data can provide an estimate of true atomic motion, as the valence electrons contribute relatively little to high-order reflections. Such a refinement by Hall and Maslen [7] on orthanilic acid has produced temperature factors which are generally 5–10 percent lower than those obtained from all data. The drawbacks of this procedure are, first, that the amount of data is considerably reduced by exclusive use of high-order reflections and, second, that even the high-order reflections contain some contribution from the valence electrons [8, 5]. Comparison of x-ray and neutron parameters do, however, yield the requested information without any of these drawbacks. Data of sufficient accuracy are available on a few compounds, they include: α-oxalic acid [9, 10], α-deutero oxalic acid [9, 11], *s*-triazine [12] and hydroxyapatite [13]. In the last compound the diagonal elements β_{ii} of the thermal vibration tensor as

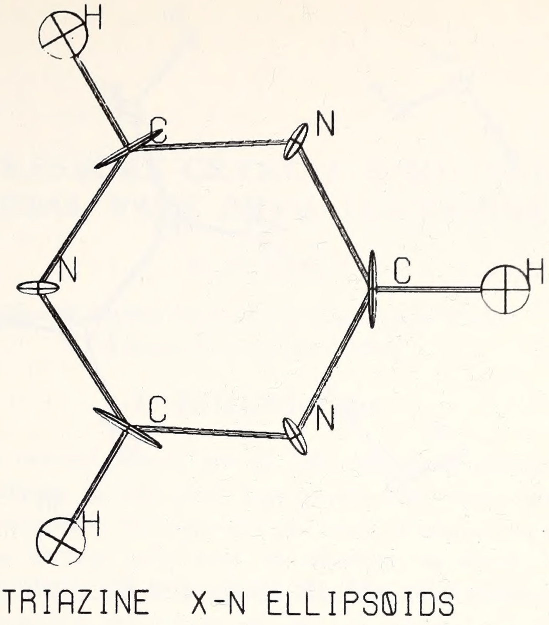

FIGURE 1. Ellipsoids showing the difference between x-ray and neutron thermal-vibration tensors for *s*-triazine.

obtained with x rays are larger than the neutron parameters for three out of four light (oxygen) atoms. In the first three compounds x-ray β_{ii} values are larger for all but one of a total of 30 elements. The differences vary between 4 and 52 percent, 11 and 47 percent and -5 and 50 percent for the three compounds respectively. Most of the discrepancies Δ are highly significant in terms of the least-squares standard deviations σ, especially in α-deutero oxalic acid for which the average of Δ/σ is 6.9. Moreover, the variation of the differences with direction is meaningful in terms of the atomic environment.

This is best illustrated by plotting the ellipsoids representing the difference between the x-ray and neutron tensors. Such a plot for *s*-triazine obtained with the ORTEP program [14] is reproduced in figure 1 (the ellipsoids are 70 percent probability ellipsoids; the slightly negative $\Delta\beta_{22}$ for carbon has been reset to a very small positive value). The apparent thermal motion of the carbon atom is in the direction of the C-N overlap density, while the effect of the overlap density is more than offset by the lone-pair electrons of the nitrogen atom. Similar plots are obtained for α-deutero oxalic acid (fig. 2) in which, very strikingly, the oxygen difference ellipsoids are extended in the direction of the lone pair electrons, while the ellipsoid of the trigonal carbon atom is almost a sphere.

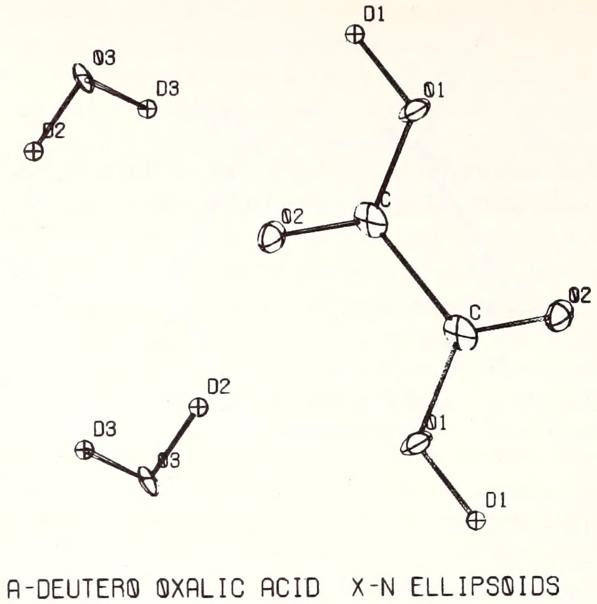

FIGURE 2. Difference ellipsoids for α-deutero oxalic acid.

The discussion given above emphasized systematic errors in x-ray temperature parameters. It should be noted that chemically meaningful information can be obtained by a more sophisticated treatment of x-ray data [6, 15] or by combined analysis of x-ray and neutron data [12]. Such treatments can yield parameters, unobtainable with other techniques, which are directly comparable with results of theoretical calculations.

4. References

[1] R. McWeeny, Acta Cryst, **6,** 631 (1953).
[2] B. Dawson, Acta Cryst. **17,** 997 (1964).
[3] P. Coppens and C. A. Coulson, Acta Cryst., in press (1967).
[4] R. Allmann, Acta Cryst. **22,** 434 (1967).
[5] R. F. Stewart, private communication.
[6] B. Dawson, Proc. Roy. Soc. **A298,** 264 (1967).
[7] S. R. Hall and E. N. Maslen, Acta Cryst. **22,** 216 (1967).
[8] A. M. O'Connell, A. I. M. Rae and E. N. Maslen, Acta Cryst. **21,** 208 (1966).
[9] R. G. Delaplane and J. A. Ibers, Abstracts A.C.A. winter meeting, Atlanta, paper G3 (1967).
[10] T. M. Sabine, B. M. Craven and G. W. Cox, to be published.
[11] P. Coppens and T. M. Sabine, to be published.
[12] P. Coppens, Science, **158,** 1577 (1967).
[13] K. Sudarsanan and R. A. Young, Abstracts A.C.A. summer meeting, Minneapolis, paper Q5 (1967).
[14] C. K. Johnson, A Fortran Thermal-Ellipsoid Plot Program ORNL–3794 (1965).
[15] B. Dawson, Proc. Roy. Soc. **A298,** 255 (1967).

HIGH PRESSURE CRYSTAL STRUCTURE OF METAL FREE PHTHALOCYANINE

R. S. Kirk

General Electric Research and Development Center
Schenectady, New York 12301

1. Introduction

The known crystal structures of the phthalocyanines have been rapidly multiplying in the past few years. For each new chemical variation there seems to be a new crystal form. Although any particular phthalocyanine shows only one or another structure for sizable single crystals, there are indications that in their metastable forms such phthalocyanine can occur in all the known structures. The difficulty of obtaining good single crystals has hindered efforts to prove this fact.

It has been found that under high pressures macroscopic single crystals of the phthalocyanine can be transformed to new crystal structures. The quality of the new crystals has indicated the possibility of accurate structural determination. Unfortunately, it is not possible to quench to one atmosphere pressure, the new crystal form. Furthermore, single-crystal x-ray studies at high pressures require a considerable amount of effort. However, it has been found that by following the changes in the morphology of the single crystals as they transform from the known to the unknown crystal forms, probable new lattices may be constructed for the high pressure forms. Although similar transformations occur in a wide variety of compounds, this report will deal exclusively with the behavior of metal-free phthalocyanine, (H_2P_c).

2. Equipment

High pressure experiments with H_2P_c single crystals were performed in a high pressure cell consisting of diamond anvils compressing a liquid-filled gasket (see fig. 1) [1].[1] A gasket of Inconel, 0.015 cm thick with a 0.025 cm hole, was filled with heptane and a crystal of sample. The diamonds contain the pressure and still allow the sample to be examined optically. The combination of liquid and metal gasket

---

[1] Figures in brackets indicate the literature references at the end of this paper.

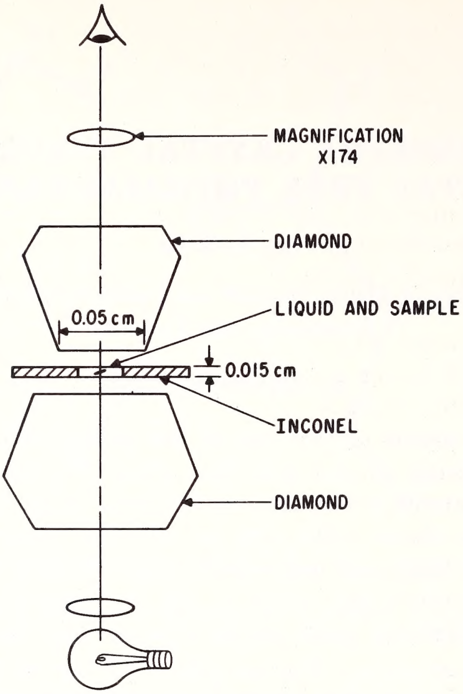

FIGURE 1. Schematic diagram for the generation of pressure and observation of samples within the diamond high-pressure cell

concentrates the pressure gradients within the gasket, leaving the pressure in the liquid close to hydrostatic.

The pressures were determined by using the applied force from a compressed spring as a scale for the pressure, which was calibrated by means of two internal standards: the melting of the heptane and the appearance of the trapped bubble of air. The latter occurred at such low pressures ($\approx$ 10 bars) that it was considered zero pressure. Using the melting point of the heptane served to eliminate any problems of liquid supercooling. With high-purity heptane and slow release of pressure, the estimated uncertainty for the pressure was half a kilobar.

The phthalocyanine crystals used in this experiment showed no electron spin resonance absorption, indicating an absence of the common metallic salts of phthalocyanine. The crystal structure was of the β form [2].

It was possible to place crystals individually into the pressure transmitting liquid. The crystal dimensions were measured from the projections perpendicular to the axis of view.

The angle between the crystal faces was measured by the following: an unusually thick phthalocyanine crystal was illuminated by both transmitted and dark field lights. This made it possible to measure directly the projection of one plane on the other.

3. Results

The most dramatic effect of high pressure on the phthalocyanine crystals is the transformation at 7.1 ± 0.7 kbar. The 001 plane appeared to shorten by twenty percent, and to thicken by twenty percent in a transformation that occurred so quickly that the whole crystal appeared to change at once. The transformation was found to be identical in both water and heptane. The transformation was reversible at approximately the same pressure (± 1 kilobar) for increasing and decreasing pressures. Single crystals could be maintained through several transformations. In one instance the transformation was observed to stop part way through a crystal, and for a short time the relation between the dimensions in the two crystal forms was shown.

In the 7.1 kilobar transformation, although all the linear dimensions of the crystals undergo change, the large differences between the three external axes at one atmosphere enable one to identify their counterparts in the new crystal. For example, the longest crystalline dimension, corresponding to the b axis in the low-pressure β form transforms to the longest dimension at high pressure. It will be called the b axis in the high-pressure form. Two other axes may be similarly identified in the high-pressure form.

With the axes so defined, the effect of the transformation may be calculated:

$$\frac{\Delta a}{a} = +0.195 \pm 0.02$$

$$\frac{\Delta b}{b} = -0.197 \pm 0.005$$

$$\frac{\Delta c'}{c'} = -0.03 \pm 0.03$$

(a, b, c' at 7.1 kbar in the β phase; c' lies in the $20\bar{1}$ plane, perpendicular to the b axis.) The external angles between b and a, and b and c' are both within a degree of 90° in the high pressure form. The external angle, between the two developed surfaces ($20\bar{1}$ and 001 in the low pressure form) decreases from 99.1 to 96.2° ± 1°. These results give for the change in the volume of the crystals at 7.1 kilobar

$$\frac{\Delta V}{V} = -0.064 \pm 0.06.$$

In the high pressure form the so-called *a* and *c′* axes remain perpendicular to the longest axis suggesting that the new crystal form remains in the monoclinic system. In addition the exterior angle between the two most developed faces (001 and $20\bar{1}$ in the low pressure form) transforms to 96.2 ±1°, close to the angle found between the 001 and 201 surfaces in platinum phthalocyanine (95.2°), suggesting that the new form might be related to the monoclinic structure found for platinum phthalocyanine. Considering the two most developed faces in the high pressure form as 001 and $20\bar{1}$, the axes of the unit cell can then be determined. By using the changes in crystal axes, so defined, it is possible to derive a new cell at high pressures from the unit cell at low pressures. This cell in the new crystal form, when extrapolated to room pressures, bears a remarkable resemblance to the room pressure unit cell of platinum phthalocyanine. (Table 1 compares the dimensions and angles of the two structures.)

TABLE 1

Metal free phthalocyanine high pressure crystal form ($P \approx 0$ kilobar)	Platinum phthalocyanine [a] ($P=0$ kilobar)
"a_0"$=23.72\pm0.4$ Å	23.9 Å
"b_0"$=3.91\pm0.08$ Å	3.81 Å
"c_0"$=16.12\pm0.55$ Å	16. 9 Å
"β"$=130.3\pm2°$	129. 6°

[a] J. M. Robertson, J. Chem. Soc., 36 (1940).

In summary, although these results do not prove the crystal structure of the high pressure form is isomorphous with that of the platinum compound, they do show a high degree of consistency with this one structure. Needless to say, efforts are now being made to prove this speculation by direct x-ray evidence.

4. References

[1] A. Van Van Valkenburg, High Pressure Measurement, Butterworths, Washington, pg. 93, (1963).

[2] J. M. Robertson, J. Chem. Soc., 615 (1935).

X-RAY DIFFRACTION AND RADIOFREQUENCY SPECTROSCOPIC INVESTIGATION OF DIMETHYLTIN DICHLORIDE*

JACK D. GRAYBEAL[1] **and DOMNIC A. BERTA**[2]

Department of Chemistry, West Virginia University, Morgantown, West Virginia 26506

1. Introduction

Previous nuclear quadrupole resonance (NQR) investigations [1, 2][3] have shown that there is a much larger change of the observed NQR frequency of ^{35}Cl in going from $SnCl_4$ to organotin chlorides than for comparable substitutions on other group IVA tetrahalides. This phenomenon, along with observed positive temperature coefficients for several dichlorides, indicates that there is either a large change of π-bonding or ionic character with substitution of organic groups. An NQR Zeeman study was instigated in order to determine the magnitude and direction of the principal electric-field gradient (EFG) tensor components and hence provide additional bonding information. A knowledge of the crystal structure is necessary to specify the EFG axis directions. The combined study has provided an excellent sample of how the results of an NQR Zeeman experiment can aid in an x-ray crystal structure determination.

2. Experimental Work

Crystals of dimethyltin dichloride, $(CH_3)_2SnCl_2$, suitable for x-ray studies were prepared by the slow evaporation, in a dry box, of a saturated solution of $(CH_3)_2SnCl_2$ in CCl_4. A large (2 cm^3) crystal for the Zeeman study was obtained by growing from a melt in a Bridgman furnace. The density of $(CH_3)_2SnCl_2$ was found to be 2.30 ± 0.09 g cm^{-3} using a standard pycnometric method with trimethylamine and N,N′-bis(1-ethyl-3-methylpentyl)diethylenetriamine as immersing liquids.

The x-ray crystal structure determination was done using a prismatic crystal 0.5mm × 0.7mm × 0.7mm at 25 °C. Initially the cell parameter *c* was determined from a rotation photograph, and upon

---

*Supported by a grant from the National Science Foundation.

[1] Present address: Department of Chemistry, V.P.I., Blacksburg, Va. 24061.

[2] Present address· Allegheny Ballistics Laboratory, Cumberland, Md. 21502.

[3] Figures in brackets indicate the literature references at the end of this paper.

addition of a Weissenberg camera, a zero-level Weissenberg photograph was used to determine a and b. The unit cell was found to be orthorhombic with $a=7.76 \pm 0.04$ Å, $b=8.83 \pm 0.04$ Å, $c=9.29 \pm 0.03$ Å and to contain 4 molecules. The nature of the systematic absences indicated a body-centered Bravais lattice with the possibility of six space groups, Immm, Imm2, Im2m, I2mm, I222 and $I2_12_12_1$. A positive spoon text eliminated the Immm group. An equi-inclination Weissenberg photograph was taken and the intensities of 353 reflections were visually measured by comparison to a 45 spot grey scale prepared from a zero-level reflection.

The loci of zero splitting for the Zeeman-split NQR transitions were determined at 25 °C using a bidirectionally-modulated marginal oscillator and a two-circle goniometer as described elsewhere [3]. The loci and the resulting principal EFG-axis systems are shown in figure 1.

3. Discussion

Using the available intensity data a Patterson map was constructed. This indicated the most probable space groups to be ones with the Sn atoms and Cl atoms lying in the yz-plane. The Imm2 space group appeared to be the most probable and it was used as a basis for a

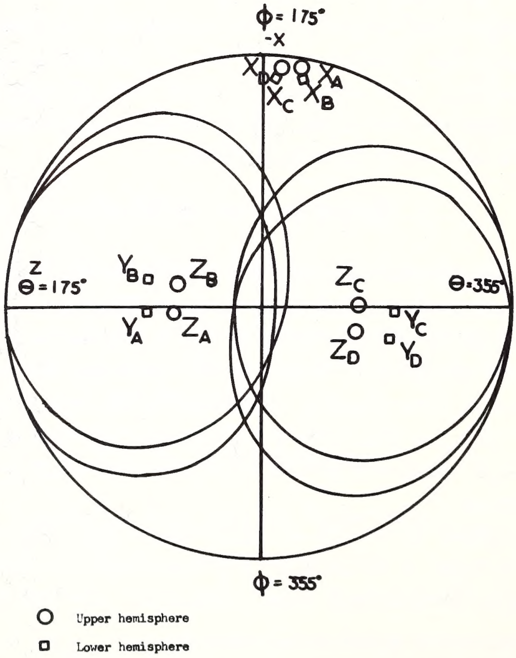

FIGURE 1. Plot of the loci of zero splitting on a stereographic net.

TABLE 1. Atomic Positions, Bond Angles and Bond Lengths

	x(Å)	y(Å)	z(Å)	$\sigma(x)$	$\sigma(y)$	$\sigma(z)$
Sn(1)	0	2.21	1.95	0	0	.01
Sn(2)	3.88	2.21	−1.95	0	0	.01
Sn(3)	3.88	6.62	6.59	0	0	.01
Sn(4)	7.75	6.62	2.69	0	0	.01
Cl(1)	−0.15	4.03	0.38	.03	.02	.02
Cl(2)	4.03	4.80	5.03	.03	.02	.02
Cl(3)	7.91	8.45	4.27	.03	.02	.02
Cl(4)	3.73	0.39	−0.38	.03	.02	.02
Cl(5)	3.73	8.45	5.03	.03	.02	.02
Cl(6)	0.15	0.39	0.38	.03	.02	.02
Cl(7)	4.03	4.03	−0.38	.03	.02	.02
Cl(8)	7.60	4.80	4.27	.03	.02	.02
C(1)	−2.03	2.42	2.65	.08	.13	.09
C(2)	5.91	6.46	7.30	.08	.13	.09
C(3)	9.79	6.81	2.00	.08	.13	.09
C(4)	1.85	2.02	−2.65	.08	.13	.09
C(5)	1.85	6.81	7.30	.08	.13	.09
C(6)	2.03	2.02	2.65	.08	.13	.09
C(7)	5.91	5.91	−2.65	.08	.13	.09
C(8)	5.73	5.73	.200	.08	.13	.09

Angles

Apex	End	End	Angle	σ
Sn(4)	Cl(8)	C(3)	109.8°	2.7°
Sn(4)	Cl(8)	Cl(3)	98.8°	1.8°
Sn(4)	Cl(8)	C(8)	95.0°	2.7°
Sn(4)	C(8)	C(3)	141.9°	4.2°

Lengths

Atom 1	Atom 2	Length	σ
Sn(4)	Cl(8)	2.41Å	.04Å
Sn(4)	Cl(3)	2.41Å	.04Å
Sn(4)	C(8)	2.16Å	.18Å
Sn(4)	C(3)	2.16Å	.18Å

least squares refinement. Using the usual Lorentz polarization corrections, an isotropic temperature factor of 2.5, and no absorption correction, a structure was determined with an R of 27. Even though the large prismatic crystal used limited the use of any absorption correction, it was believed that a lower R factor should be obtained.

At this point in the investigation the zero splitting loci had been obtained, and reference to figure 1 shows that rather than having two loci with their principal EFG Z-axes separated by the ClSnCl bond angle, there are two pairs. The individual members of each pair have principal EFG Z-axes separated by only $10 \pm 2°$. This indicates that the plane of the ClSnCl skeleton is tilted out of the yz-plane by $5 \pm 2°$.

This twisting of the ClSnCl skeleton would change the space group to $I2_12_12_1$. Four possible modes of twisting the molecule within the unit cell were considered and a full matrix least-square refinement in the $I2_12_12_1$ space group was attempted for each. The best agreement, an R of 21, was obtained with the atom positions and bond parameters given in table 1. The ClSnCl skeleton is twisted out of the yz-plane by $3 \pm 2°$.

The zero splitting loci were used to obtain the directions of the EFG principal axes and the EFG asymmetry parameter. The latter was found to be $\eta = 0.34 \pm 0.06$. Using this value of η; the observed NQR frequency, 15.712 ± 0.003 MHz; the known nuclear quadrupole moment for ^{35}Cl, $Q = -0.0789 \times 10^{-24}\,\mathrm{cm}^3$; and allowing for the contribution to the EFG of partial ionic charges on the atoms in neighboring molecules, the π-bond character of the Sn–Cl bond is calculated to be $\pi = \pi_x + \pi_y = 0.207 \pm .002$ with $\pi_y - \pi_x = -.0.095 \pm 0.02$.

4. References

[1] E. D. Swiger and J. D. Graybeal, J. Am. Chem. Soc. **87,** 1464 (1965).
[2] P. J. Green and J. D. Graybeal, J. Am. Chem. Soc. **89,** 4305 (1967).
[3] G. L. McKown and J. D. Graybeal, J. Chem. Phys. **44,** 610 (1966).

THE CRYSTAL AND MOLECULAR STRUCTURE OF TETRAETHYLAMMONIUM BIS-(3)-1,2-DICARBOLLYLCUPRATE (II)

RICHARD M. WING

Department of Chemistry
University of California, Riverside, California 92502

1. The Descriptive Chemistry of Dicarbollylmetalloids

1.1. The Dicarbollyl Group

The dicarbollyl dianion $C_2B_9H_{11}^{-2}$ is the fragment remaining when $(BH)^{2+}$ is "formally" extruded from an icosahedral $C_2B_{10}H_{12}$ group. Of interest to the present discussion is that species in which the five-atom open face produced above has carbons as near neighbors.

The electronic structure of the fragment bears a strong resemblance to the cyclopentadienyl ion $C_5H_5^-$, in that the five-atom face with six electrons in delocalized orbitals directed roughly at the position vacated by $(BH)^{2+}$ is comparable to the delocalized π electrons of $C_5H_5^-$.

1.2. Dicarbollyl Analogs of Sandwich π-Cyclopentadienides

M. F. Hawthorne and coworkers have synthesized a number of transition-metal derivatives of the dicarbollyl dianion, which seem to to be directly analogous to the corresponding metal cyclopentadienides [1].[1]

X-ray crystal structure studies by Zalkin [2, 3] et al., for the iron (III) and rhenium (I) derivatives and electron spin resonance work by Maki [4] on the iron (III) derivatives convincingly illustrate the analogy.

The organometallic chemistry of copper has no representatives in π sandwich chemistry, however, so when Hawthorne and Warren [5] isolated a blue crystalline compound of copper from an aqueous, strongly basic solution of cupric chloride and (3)⁻1,2-dicarbollide dianion we were anxious to study this unusual compound.

1.3. Physical Criteria for a Sensible Descriptive Chemistry

It is this author's opinion that atom positions, while certainly necessary, do not generally supply information sufficient to describe a molecular structure. Indeed in some instances the accuracy of bond lengths scales the difference of two chemistries, e.g., the double versus the triple bond.

---

[1] Figures in brackets indicate the literature references at the end of this paper.

Thus it becomes important to add the information to be found in other measurements such as electronic and vibrational spectroscopy and magnetic resonance, which in turn become better experiments if they can be done on single crystals.

In this study single-crystal visible and electron spin resonance spectroscopy have been used in conjunction with a crystal structure determination in an effort to formulate a molecular description of the bis-dicarbollylcuprate (II) ion.

2. X-Ray Structure [6]

2.1. Crystal Data

The blue crystals are triclinic; $\mathbf{a}_0=12.98$ Å, $\mathbf{b}_0=9.09$ Å, $\mathbf{c}_0=8.73$ Å, $\alpha=93.5°$, $\beta=90.1°$, $\gamma=117.1°$. There is one formula unit per cell.

2.2. Molecular Framework Structure

With only one heavy atom per unit cell, the structure was assumed to be centrosymmetric, and a Fourier was computed assuming all structure factors to be positive. The images of the 21 unique non-hydrogen atoms were clearly visible at this point.

This structure was refined by full matrix least-squares variation of all positional and temperature factors. Following six cycles of such refinement during which all cage atoms were assumed to be borons, the residual *R* was 0.14, and all eleven cage hydrogens were visible in a difference Fourier.

2.3. Choosing the Cage Carbons

Two factors made the choice of the cage carbons clear. First the temperature factors of two of the (cage) atoms were **ca.** 30 percent smaller than the other nine. Second the intra-cage atom-atom distances clearly factored into three classes, containing respectively, 1 short, 6 medium, and 18 long bonds. These facts considered separately lead to identical choices for the two carbon atoms, CB2 and CB3 in figure 1.

The two atoms referred to above were treated as carbons, cage hydrogens were added but not refined, and all thermal motion was treated anisotropically, with the result that after 8 additional cycles of refinement the residual was 0.09.

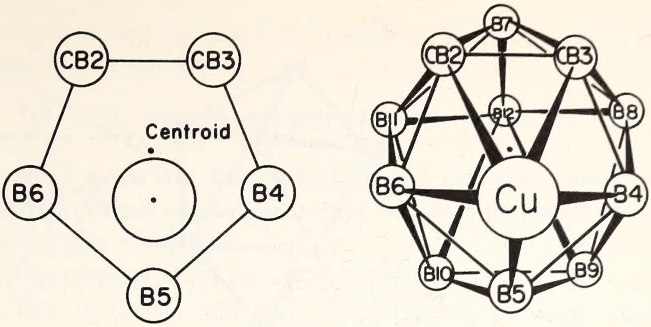

FIGURE 1. Projection of the $Cu(C_2B_9H_{11})_2^{-2}$ anion down the perpendicular to the C_2B_3 face. Only the far cage is shown.

3. Optical and Magnetic Resonance Spectroscopic Experiments

3.1. The Presence of a Molecular 2-Fold Axis

The crystals are very dichroic, and when the single-crystal visible spectrum is taken with the direction of light propagation being **a*** (fig. 2), it is found that the bands at 6200 Å and 5150 Å, which are very strong when the electric vector is oriented along $\mathbf{c}_0$, are nearly absent when the electric vector is oriented along $\mathbf{b}_0$.

The *g* tensor derived from single crystal electron spin resonance measurements diagonalizes to a set of principle values which again supports the presence of a molecular two-fold axis [7].

3.2. The Cu to B_3 Centroid as an Important Molecular Direction

The principle values and directions of the *g* tensor are indicated in figure 2. The largest value which corresponds approximately in magnitude to g_{11} found in copper (II) symmetric top molecules is directed at the B_4, B_5, B_6 centroid.

4. Description of the Structure

4.1. Valence Bond Description

Although a complete description of the bonding in the compound will require additional calculations, a very satisfying topological description (fig. 3) is suggested by the present experimental results.

This is quite consistent with the molecular C_{2h} symmetry, the short C–C bond (1.53 Å as against 1.61 and 1.58 in the previously studied symmetrical compounds [2, 3]), the short Cu–B distances (2.20 Å) as compared to Cu–C (2.51 Å), and the directions of the principle *g* values.

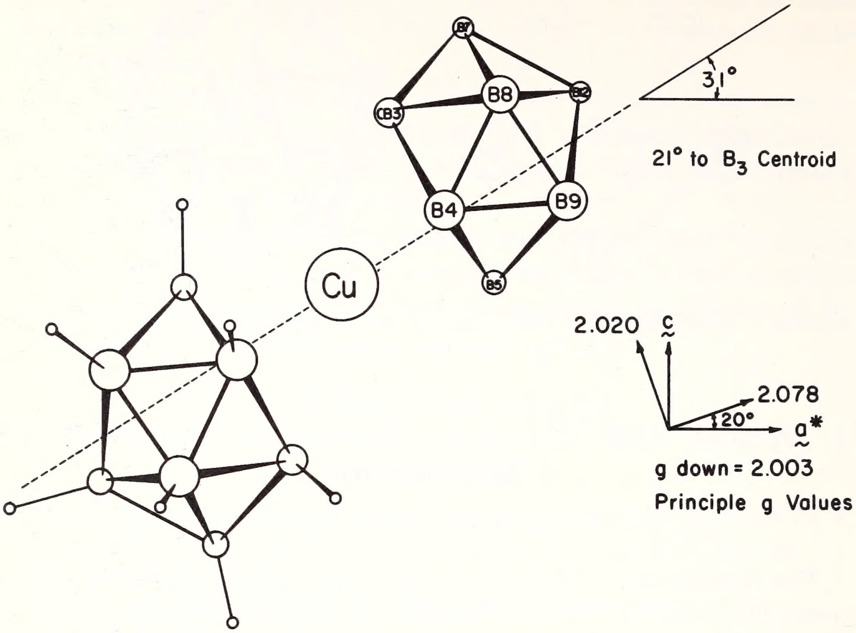
B7
CB3
B8
B12
B4
B9
B5
Cu
31°
21° to B_3 Centroid
2.020 c
2.078
20°
a*
g down = 2.003
Principle g Values

FIGURE 2. The $Cu(C_2B_9H_{11})_2^{-2}$ anion viewed down its molecular 2-fold axis (a 10°38′ counterclockwise rotation about $\mathbf{c}_0$). The dotted line represents the perpendicular from copper to the C_2B_3 carborane face. Hydrogen atoms are pictured on the lower left-hand cage only.

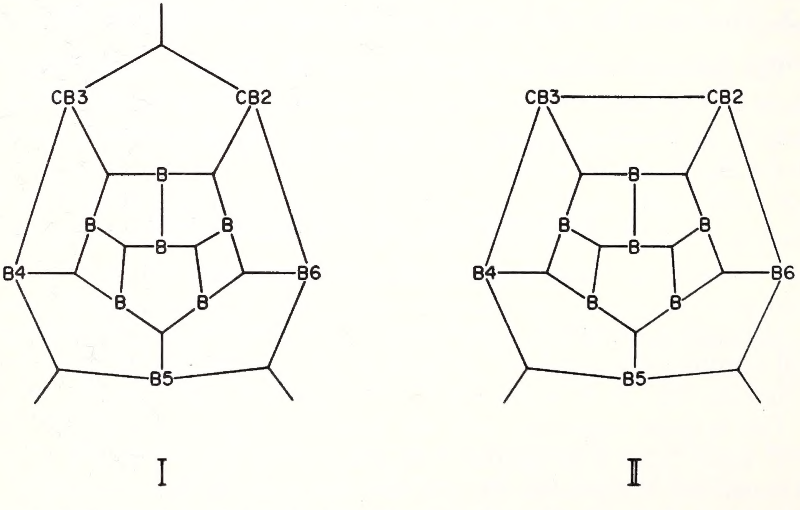
CB3
CB2
B
B
B
B
B
B
B4
B6
B5
I
CB3
CB2
B
B
B
B
B
B
B4
B6
B5
II

FIGURE 3. A topological description of the bonding of a dicarbollyl anion to a metal ion; a symmetrical π sandwich (I), and a distorted π allyl (II).

The proposed description closely relates this compound to the bis-allyl nickel (II) molecule.

4.2. Electron-Rich Metalloaromatics

Theoretical work on this molecule and related "sandwich" compounds indicate that a combination of two factors are needed to cause the observed slip distortion.

(1) The system must be electron rich.

(2) The aromatic ring must be heterocyclic, or unsymmetrical in some other way (e.g. bridged naphthalene).

For heterocyclic rings, the direction of distortion can be predicted from simple electronegativity considerations.

4.3. Organometallic?

One must be especially careful in descriptive areas in the choice of words.

Thus this author hesitates to classify this molecule as an organometallic since the copper and carbon atoms interact minimally if at all in this system.

5. References

[1] L. F. Warren, Jr., and M. F. Hawthorne, J. Am. Chem. Soc. **89,** 470 (1967) and references therein.

[2] A. Zalkin, D. H. Templeton and T. E. Hopkins, J. Am. Chem. Soc. **87,** 3988 (1965).

[3] A. Zalkin, T. E. Hopkins and D. H. Templeton, Inorg. Chem. **5,** 1189 (1966).

[4] A. H. Maki and T. E. Berry, J. Am. Chem. Soc. **87,** 4437 (1965).

[5] M. F. Hawthorne and L. F. Warren, private communication. A full account of the chemistry of these compounds is in press, M. F. Hawthorne, et. al., J. Am. Chem. Soc.

[6] Richard M. Wing, J. Am. Chem. Soc. **89,** 5599 (1967), for a full report on the structure.

[7] August H. Maki and D. D. Scott, private communication.

NUCLEAR MAGNETIC RESONANCE STUDIES OF SINGLE CRYSTALS OF TRICHLOROACETIC ACID [1]

DAVID C. HADDIX [2] **and PAUL C. LAUTERBUR** [3]

Department of Chemistry,
State University of New York at Stony Brook,
Stony Brook, New York 11790

1. Introduction

Although the magnetic shielding of a nucleus is in general a tensor quantity, only the average shielding (equal to one-third the trace) is observable in isotropic fluids. Some information on shielding anisotropies can be obtained from the NMR spectra of small molecules in nematic solvents [1] [4] and studies of solids, either polycrystalline or single crystals [2] can allow determination of the complete tensor in favorable cases. The small differences in average nuclear magnetic shieldings (chemical shifts) found for protons can usually be expected to be obscured by large dipolar couplings among the protons. At a frequency of 100 MHz, for example, a typical proton chemical shift of 10 ppm corresponds to 1 kHz, very much smaller than a typical line width in the solid of 20 G, or about 85 kHz. If proton shielding tensors in solids could be studied, however, they would provide information on the nature of the bonding and on the effects responsible for the shifts. We have therefore searched for opportunities to make such measurements.

In the example reported here, trichloroacetic acid, success is attributable to two circumstances. First, there are relatively few protons per unit volume in the crystal lattice, and these are in chemically identical, but differently oriented molecules. The individual peaks in the spectrum can become as narrow as 1.2 kHz. This would still not permit resolution of the peaks from the differently oriented molecules, except for the happy circumstance that the nuclei are closely coupled in pairs. Since the strengths of the couplings depend upon the orientation of the crystal in the magnetic field, the pair of otherwise overlapping lines can be split into a pair of well-separated doublets. One such spectrum is shown in figure 1. The sharp line is

---

[1] This work was supported in part by the Research Foundation of State University of New York and by the National Science Foundation.

[2] Deceased.

[3] Alfred P. Sloan Fellow.

[4] Figures in brackets indicate the literature references at the end of this paper.

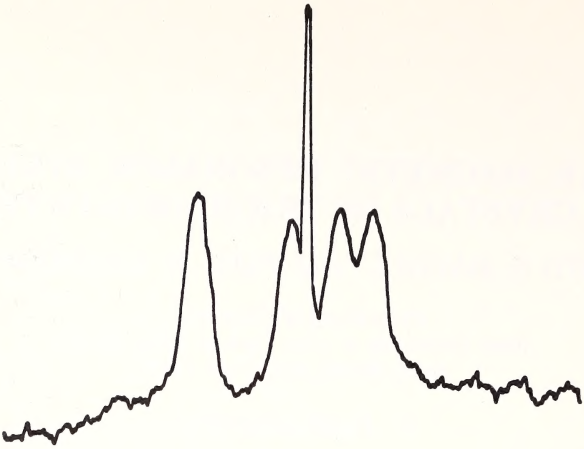

FIGURE 1. Proton nuclear magnetic resonance spectrum of a single crystal of trichloroacetic acid at 100 MHz.

the resonance from occluded aqueous solution. The outer pair constitute one doublet, the inner another. The displacement can be seen readily at this orientation.

2. Experimental Details

All spectra were obtained at 100 MHz, using a slightly modified Varian HR–100 NMR spectrometer operating at room temperature. The crystals were grown from the melt and were about 2.5 mm in diameter and 3 mm long. They were rotated about a vertical axis and spectra were taken every five degrees over 180°, referenced to a capillary of tetramethylsilane. The data were fitted with the equation

$$S=A+B\cos 2\theta+C\sin 2\theta$$

as shown in figure 2. The shielding plots were further analyzed by a computer program STISC to obtain the shielding tensors in their principal-axis systems.

An x-ray diffraction study indicated a space group $P2_1/c$, $a=5.7$ Å, $b=9.7$ Å, $c=12.0$ Å, $\beta=118°$, with two dimers in the unit cell [3]. The orientation of one crystal was also determined by x-ray diffraction [4] after completion of the NMR measurements.

3. Results

The magnitudes of the principal components of the shielding tensors, and their orientations relative to the corresponding proton-proton lines, are given in table 1. The disagreement between the tensors for dimers A and B leaves some doubt as to the reality of the apparent

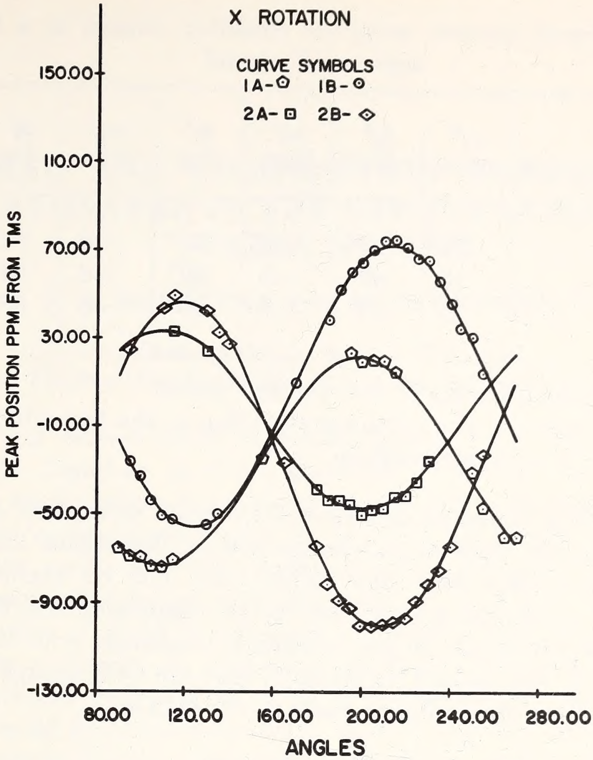

FIGURE 2. Positions of 100 MHz proton nuclear magnetic resonance lines of a single crystal of trichloroacetic acid as a function of rotation angle about an arbitrary axis. The curves have been fitted to the experimental points by a least squares technique.

deviations from axial symmetry, but an as yet incomplete error analysis suggests that they are genuine. Our two H–H lines are at 28° to one another, in fair agreement with the angle of 31° found by Goldman [5] and our H–H distance of 2.58 Å agrees well with his value of 2.56 Å. Our dipolar splitting data also show that the hydrogen bonds cannot be switching rapidly in the dimer, certainly not faster than 10^4 sec $^{-1}$. The angle between the planes defined by the proton-proton line and the largest component of the shielding tensor in each dimer is approximately 85°.

4. Discussion

The average shielding anisotropy of 18 ppm is somewhat larger than might be estimated from published theoretical calculations on hydrogen-bonded protons, but the contribution of the ordinary O—H single bond is uncertain. If the largest component of the shielding tensor lies approximately in the O—H—O direction, the result is not un-

TABLE 1. Proton nuclear magnetic shielding tensors in a trichloroacetic acid crystal

Site	σ_1[a] ppm	θ_1[b] deg	σ_2[a] ppm	θ_2[b] deg	σ_3[a] ppm	θ_3[b] deg	σ_{ave}[c] ppm
A	11	79°	−2	51°	−9	52°	−12
B	13	85°	−5	30°	−8	64°	−12
Ave	12	82°	−4	40°	−8	58°	−12

[a] Principal components of the traceless tensor.

[b] Angle relative to the proton-proton line in the respective dimer.

[c] Relative to tetramethylsilane.

reasonable. The apparent deviation from axial symmetry cannot be discussed usefully until more information on the crystal structure is available, especially since the dimer may not be planar[6]. The assumptions made above which led to the suggestion that the dimers are nearly perpendicular to one another is consistent with the suggestion of Dunell, Reeves and Strømme[7] that the CCl_3 groups pack just above and below the hydrogen pairs in the lattice.

5. References

[1] See A. D. Buckingham and K. A. McLauchlan, Chapt. 2 in Progress in Nuclear Magnetic Resonance Spectroscopy, Vol. 2, edited by J. W. Emsley, J. Feeney and H. Sutcliffe, Pergamon Press, New York, 1967, for a recent review.

[2] See P. C. Lauterbur and J. J. Burke, J. Chem. Phys. **42,** 439 (1965) for an example and references.

[3] The authors thank Dr. W. C. Hamilton for this experiment.

[4] By Mr. John Ricci of this Department.

[5] M. Goldman, J. Phys. Chem. Solids **7,** 165 (1958).

[6] G. A. Jeffrey and M. Sax, Acta Cryst. **16,** 430 (1963).

[7] B. A. Dunnel, L. W. Reeves and K. O. Strømme, Trans. Faraday Soc. **57,** 381 (1961).

THERMAL AND COMPOSITION EXPANSION OF CLATHRATES IN THE ETHYLENE OXIDE-WATER SYSTEM

J. A. McINTYRE and D. R. PETERSEN

Chemical Physics Research Laboratory
The Dow Chemical Company, Midland, Michigan 48640

Water and certain small, relatively non-reactive molecules can be crystallized together to form clathrate structures in which H_2O molecules are hydrogen-bonded into an array of contiguous polyhedral cages which enclose guest molecules. In the Type I clathrate structure (fig. 1), the cubic unit cell consists of two pentagonal dodecahedra and six somewhat larger tetrakaidecahedra. The unit cell formula, assuming that all eight of the cages are filled, is $8M{\cdot}46H_2O$, where M is the guest molecule. An important result of a theoretical treatment of the clathrate hydrates, however, is the prediction that such compounds should be nonstoichiometric and of variable composition[1].[1] The nonstoichiometric nature of the ethylene oxide-water clathrate was verified by McMullan and Jeffrey[2] by means of a single-crystal x-ray structure analysis.

In their study, they found the cubic cell parameter to be 12.03 ± 0.01 Å at −25 °C for the compound crystallizing from a melt containing 8 mole percent ethylene oxide. Using this cell edge, Glew and Rath[3] were able to demonstrate the variable composition of this compound by comparison with their observed density values. However, a more positive demonstration of this property requires that the unit cell parameter as a function of temperature be known for a variety of compositions. This report contains the results of such a study[4].

Through x-ray diffraction experiments, thermal expansion relations were established for several specific compositions over the temperature range from −140 to −20 °C. Figure 2 shows a plot of the clathrate unit-cell parameter versus temperature for the samples containing 2.3, 4.8, 9.3, and 12.8 mole percent ethlyene oxide.

The values derived from the few cell-parameter measurements made on the sample containing 2.3 mole percent ethylene oxide could be fitted by the 4.8 mole percent ethylene oxide curve within the error of measurement. The curves shown were drawn from the quadratic

---

[1] Figures in brackets indicate the literature references listed at the end of this paper.

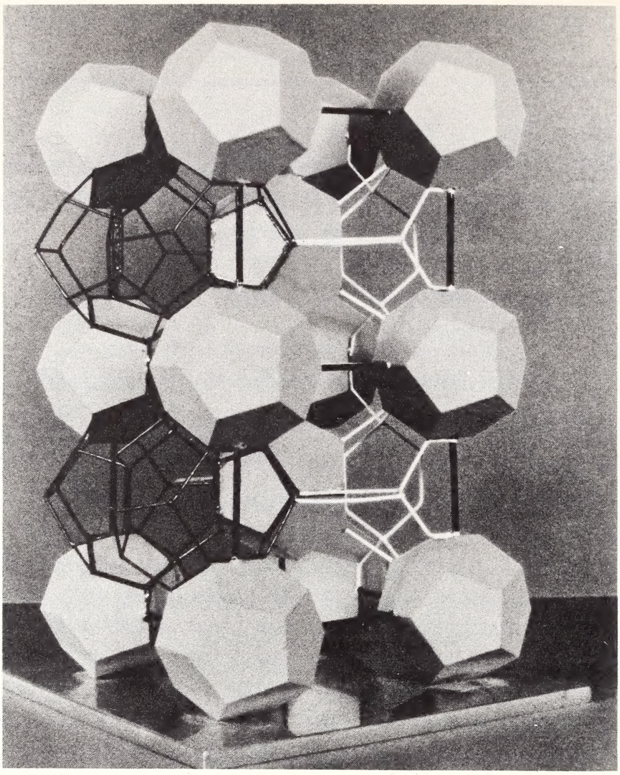

Figure 1. The Type I Clathrate Hydrate Structure.

equations which resulted from a least-squares treatment of the data. The equations are:

(a) for 12.8 mole percent ethylene oxide:

$$a = 4.582 \times 10^{-6} T^2 + 1.624 \times 10^{-3} T + 12.087$$

(b) for 9.3 mole percent ethylene oxide:

$$a = 3.691 \times 10^{-6} T^2 + 1.269 \times 10^{-3} T + 12.053$$

(c) for 4.8 mole percent (and 2.3 mole percent) ethylene oxide:

$$a = 0.991 \times 10^{-6} T^2 + 0.724 \times 10^{-3} T + 12.016$$

with T in °C and a the cubic cell edge in Å.

This measured thermal expansion of H_2O in the Type I ethylene oxide clathrate structure is somewhat greater than that of H_2O in the normal ice structure, over the temperature range from -140 to $-20°$, for the various compositions studied.

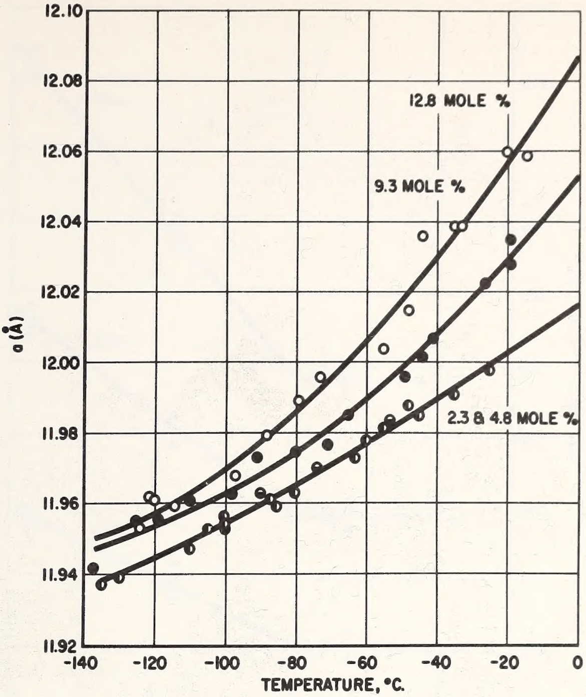

FIGURE 2. The dependence of the unit-cell parameter of ethylene oxide clathrate hydrate on composition and temperature.

One quite interesting observation which can be made from the above results is an apparent break in the composition expansion curve. In figure 3 is shown the relation between the observed unit cell volume and the number of ethylene oxide molecules per unit cell, at several temperatures.

It is suggested from our results that the addition of ethylene oxide to the cage structure does not cause an expansion of the unit cell until some composition near three molecules ethylene oxide per unit cell is reached. Above this critical concentration, the unit cell expands with increasing addition of ethylene oxide. We interpret this observation to mean that up to half of the six larger tetrakaidecahedral cages in the unit cell can be filled with guests, perhaps with some "internal" distortion of the remaining empty cages, before expansion occurs.

A further interesting result of this investigation is the preparation by rapid quenching of clathrate hydrates containing concentrations of guest molecules as low as 2.3 mole percent, or about one guest molecule per unit cell. We believe that clathrate hydrates of such low guest molecule concentration have not been observed positively before. This study has indicated that such compounds are not stable at temperatures above about −20 °C.

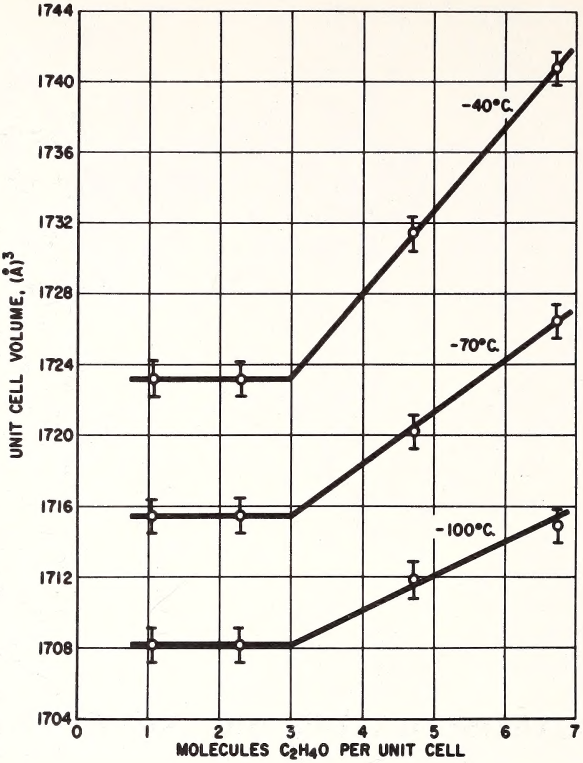

Figure 3. The relation between unit cell volume and number of molecules o ethylene oxide per unit cell at different temperatures.

References

[1] J. C. Platteeuw and J. H. van der Waals, Mol. Phys. **1**, 91 (1958); Advan. Chem. Phys. **2**, 1 (1959).

[2] R. K. McMullan and G. A. Jeffrey, J. Chem. Phys. **42**, 2725 (1965).

[3] D. N. Glew and N. S. Rath, J. Chem. Phys. **44**, 1710 (1966).

[4] J. A. McIntyre and D. R. Petersen, J. Chem. Phys. **47**, 3850 (1967).

SPECTROSCOPY OF ORGANIC CRYSTALS

NUCLEAR MAGNETIC RESONANCE AND MOLECULAR MOTION IN ORGANIC CRYSTALS

E. R. ANDREW

Department of Physics
University of Nottingham
Nottingham, England

1. Introduction

In this article I shall first discuss a representative group of related organic solids in which molecular reorientation about one preferred axis had been examined by the nuclear magnetic resonance (n.m.r.) method. I shall then draw attention to experiments in which narrowing of n.m.r. spectra of solids is achieved by rapidly spinning the specimens, since this gives insight into the narrowing mechanism and lends support to the underlying ideas. I shall then go on to consider a group of organic solids in which not only is the molecule as a whole capable of rotational motion, but in which there is also rotational motion of groups within the molecule. Next I shall discuss solids in which as the temperature is raised progressively more general motions of the molecules are excited. This leads to a discussion of the diffusion of molecules in solids. Finally, I shall mention the way in which quadrupole effects can provide information about molecular motion in solids.

2. Molecular Motion About One Preferred Axis

The proton magnetic resonance spectrum of polycrystalline organic materials usually consists of one broad resonance line which sometimes exhibits partially resolved structural features. The spectral breadth is caused predominantly by the magnetic dipolar interaction between the protons; in simple physical terms the protons in the material experience a variety of local magnetic fields generated by their neighbours. Only in simple examples can the spectral profile be calculated in detail, but in all cases one important parameter of the spectral line, namely the mean square width or second moment, can be calculated in terms of the crystal structure [1].[1] If the molecules are not fixed in the crystal but undergo reorientation, the magnetic dipolar interaction between the protons becomes time-dependent, and if the motion is sufficiently rapid, it is the average value of the interaction which determines the n.m.r. spectral breadth and its second moment. The average value of the interaction is usually smaller than the static interaction and consequently the spectral line is narrowed. For a full quantitative discussion the reader is referred elsewhere [2], and it will suffice here to state that for polycrystalline materials the contribution to the second moment of the resonance spectral line from any two interacting protons in the same molecule is reduced by a factor

---

[1] Figures in brackets indicate the literature references at the end of this paper.

$$F(\gamma)=\tfrac{1}{4}(3\cos^2\gamma-1)^2 \qquad (1)$$

where γ is the angle between the axis about which rotation takes place and the direction of the proton-proton pair. For protons in different molecules the reduction factor is more complicated but is calculable.

At a sufficiently low temperature the molecular motion is usually absent (though we shall discuss an exception presently) and the spectral line is broad. As the temperature is raised the rate of molecular reorientation increases until it is sufficient to cause the spectral line to narrow. Very many examples of this behaviour have been observed and figure 1 illustrates polycrystalline benzene which I investigated as long ago as 1949 [3, 4]. This material is taken as my basic example partly because it still provides one of the clearest examples of the n.m.r. method, and partly because with more recent work a connected theme may be developed.

Although there were on interesting anomalies in the heat capacity of solid benzene, nevertheless the high symmetry of this simple molecule in a weakly-bound molecular solid suggested that molecular reorientation about the hexad axis might occur sufficiently fast to be noticed by the n.m.r. method. A highly symmetrical molecule such as this has no permanent electric dipole moment and therefore the dielectric method cannot be used to investigate molecular motion in this material. The dielectric method has successfully revealed molecular freedom for less symmetrical polar molecules, which are likely to be more strongly bound in the solid state. It is therefore to be expected that more symmetrical non-polar molecules may exhibit considerable molecular freedom capable of investigation by the n.m.r. method.

By making measurements on benzene and 1,3,5-trideuterobenzene the intramolecular and intermolecular contributions to the second moment of the n.m.r. line were disentangled [4] and the intramolecular contribution was found to be reduced by a factor 0.25 ± 0.02 above 120 °K. This provides strong support for the view that the spectral narrowing is caused by reorientation about the hexad axes of the molecules, since in this case the angle γ is $\pi/2$ for all intramolecular proton

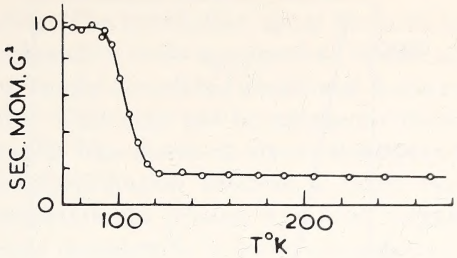

FIGURE 1. Dependence on temperature of the n.m.r. spectrum second moment of solid benzene [4]. The narrower spectrum above 120 °K arises from hindered rotation of the molecules about their hexad axes.

pairs; motion about this axis is therefore expected, from equation (1), to lead to a reduction by a factor ¼ in the intramolecular second moment.

The time-dependent part of the magnetic dipolar interaction between the protons provides a mechanism for proton spin-lattice relaxation. The spin-lattice relaxation time T_1 is shortest when the mechanism is most efficient, namely when the rate of molecular reorientation is close to the proton magnetic resonance frequency. At low temperatures the rate of reorientation is too slow for the process to be efficient, and equally at high temperatures it may be too fast. Consequently the temperature-dependence of T_1 frequently shows a characteristic minimum, and this is found for solid benzene (fig. 2).

Assuming the molecular motion to be a random reorientation between the six equivalent positions of the molecule, and assuming that the random process can be characterised by a single correlation time τ_c, then the measurements of T_1 may be translated into measurements of τ_c as a function of temperature and these are shown in figure 3. The straight line plot of ln τ_c against $1/T$ suggests that a simple activation law is followed, and the activation energy obtained from the slope is 3.7 ± 0.2 kcal/mole, or 1.6×10^4 J/mole or 0.17 eV.

More accurate T_1 data, using a short-pulse method of measurement, have been reported recently by Anderson [5] on solid C_6H_6, solid 1,3,5-$C_6H_3D_3$ and solid solutions of C_6H_6 in C_6D_6, which in all cases give an activation energy 3.95 ± 0.05 kcal/mole in reasonable agreement with the earlier value [4]. By assuming that the intermolecular contribution to the spin-lattice relaxation rate is proportional to the C_6H_6 concentration in the solid solutions Anderson was able to separate the intermolecular and intramolecular contributions to the relaxation time. For pure C_6H_6 the intermolecular relaxation is 69 percent and it is of interest that the intermolecular contribution to the second moment is closely similar, 68 percent [4]. This is not entirely surprising since both parameters involve the interproton separations to the

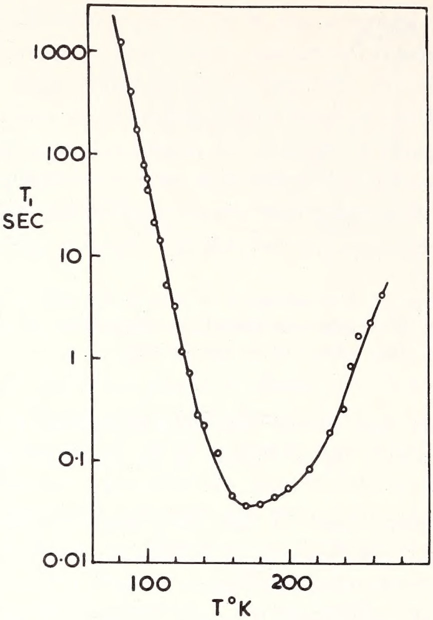

FIGURE 2. Dependence on temperature of the proton spin-lattice relaxation time T_1 in solid benzene [4].

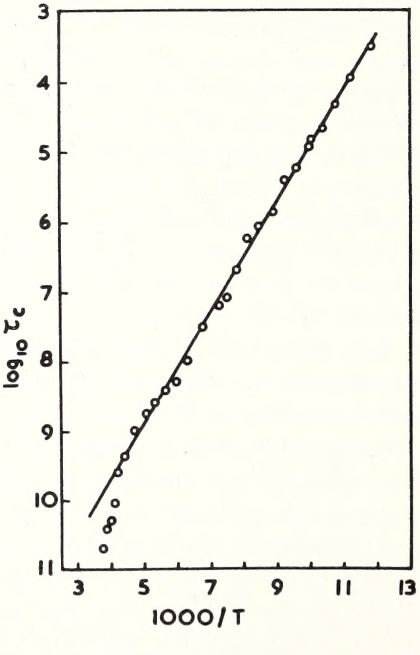

FIGURE 3. Logarithmic plot of the correlation time τ_c of the benzene molecular motion against inverse temperature. The slope of this straight line yields an activation energy for the hindered rotational motion of 3.7 kcal/mole.

inverse sixth power. The correlation times for both intermolecular and intramolecular relaxation rates appeared to be the same and Anderson interprets this to imply correlated rotational motions of neighbouring benzene molecules. This may not be unreasonable since the molecules pack into the crystal like sheets of six-toothed gear wheels [6]. On the other hand the interpretation assumes a single correlation time for the random reorientational process and this may not be quite true even in this simple compound; in more complicated materials a wide spread of correlation times sometimes has to be assumed in order to account for the data. A distribution of correlation times is of course a common feature in the interpretation of dielectric relaxation measurements.

Anderson and Slichter [7] have investigated the dependence of T_1 for solid benzene on both temperature and pressure (up to 680 atmospheres). Increase of pressure at constant temperature increases the correlation time τ_c of the molecular reorientation, no doubt because intermolecular constraints are increased by reduction of specific volume. The correlation time is much less dependent on temperature at constant volume than at constant pressure; the activation energy at constant volume is only 1.4 kcal/mole in comparison with 3.9 kcal/mole at constant pressure. Again this agrees with qualitative expectations since at constant pressure the expansion of the lattice with increasing temperature reduces the intermolecular constraints on molecular reorientation.

The reorientation rates in solid benzene range from about 10^3 Hz at 80 °K to about 10^{11} Hz at 270 °K, just below the melting point, and this is a typical range of values that can be obtained from relaxation measurements. The more recent use of rotating-frame measurements of relaxation times $T_{1\rho}$ enables correlation times as long as several seconds to be measured [8]. The method therefore has great sensitivity.

The benzene molecule spends most of its time, even close to the melting point, in one of its six equivalent orientations, about which it undergoes angular oscillations. The x-ray diffraction investigation of Cox, Cruickshank and Smith [6] at -3 °C therefore gave no direct evidence of molecular reorientation, since it provides a time-averaged electron density map of the unit cell. Nevertheless the n.m.r. data [4] did provide support for the considerable amplitude of angular oscillation of the molecules which the x-ray work revealed at -3 °C. A correction [6, 9] for this anisotropic motion of the carbon atoms brought the C–C bondlength into agreement with the Raman value [10]. A neutron diffraction investigation of solid benzene by Bacon, Curry and Wilson [11] has confirmed the x-ray work, and has extended it down to 138 °K where the amplitude of angular oscillation is found to be much smaller.

The angular oscillations of the molecules in solid benzene may be studied through the low-frequency Raman lines which they generate [12, 13]. The random reorientation of the molecules revealed by n.m.r. limits the lifetime of the molecules in the oscillatory states and endows them with a breadth of order $1/\tau_c$. This breadth should therefore increase with temperature and at 270 °K should be of order 10^{11} Hz or 3 cm^{-1}. This is in fact rather less than the width observed by Fruhling [12] at this temperature; the interpretations of the n.m.r. and Raman data are therefore mutually consistent.

Lawrenson and Lewis [14] have measured the ^{19}F n.m.r. spectrum of a fully substituted benzene, solid chloropentafluorobenzene. Calorimetric studies had revealed thermal anomalies at 191 °K and 245 °K. Below 191 °K the second moment (see fig. 4) is that of an essentially rigid array of molecules, but above this transition temperature the second moment falls to a value which is consistent with reorientational motion about an axis perpendicular to the plane of the molecule. Brot and Darmon [15] have found a similar motion in three other fully substituted benzenes, namely pentachlorotoluene, tetrachloroparaxylene, and pentachlorobenzenethiol from the proton magnetic resonance spectrum.

The behaviour of benzene molecules has also been studied in a variety of other environments. Nakajima [16] has investigated the proton magnetic resonance spectrum of benzene enclathrated in ammonia nickel cyanide. The benzene molecules reorient about their hexad axes in much the same manner as in their own crystal; the activation energy of the motion is almost the same, although the n.m.r. spectral line narrows at a higher temperature. However, for the less-symmetrical aniline molecule in this clathrate it is likely that only

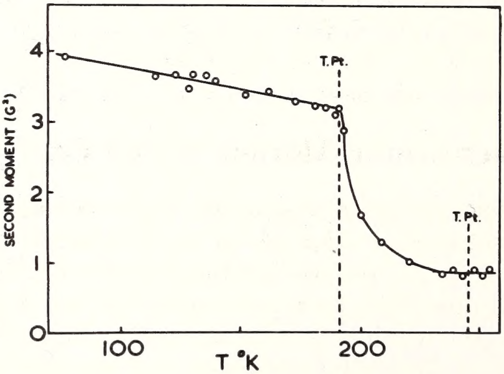

FIGURE 4. Dependence on temperature of the n.m.r. spectrum second moment of solid chloropentafluorobenzene [14]. Above the transition point at 191 °K reorientation of the molecules about an axis normal to the molecular plane caused spectral narrowing.

the amino group has rotational freedom, while the pyridine molecule shows little rotational freedom at all. Hindered rotation about their hexad axes has also been established for benzene molecules in a number of other clathrates [17]. The relative isolation of the benzene molecules in clathrates leads to longer proton spin-lattice relaxation times [17].

Benzene molecules have also been found by n.m.r. to show freedom of reorientation about their hexad axes in certain solid complexes. One example [18] is dibenzene chromium, $Cr(C_6H_6)_2$, in which the chromium atoms are sandwiched between pairs of benzene molecules which have a common hexad axis. Another example is provided by the less-symmetrical benzene-silver-chlorate complex [19]. In ferrocene, ruthenocene and titanocene dichloride the metal atom is sandwiched between two cyclopentadienyl (C_5H_5) rings, forming a molecular arrangement similar to the dibenzene chromium complex, and in similar fashion there is found to be ring-reorientation about the pentad axes [18, 20, 21, 22].

Another environment in which benzene molecules have been studied is when adsorbed on solid surfaces. Both on charcoal surface [23] and on silica gel [24], proton magnetic resonance studies demonstrate that the molecules are reorienting about their hexad axes down to liquid nitrogen temperatures. In fact the rotational freedom is greater than in solid benzene [4], which is in turn greater than in the dicyano-ammine-nickel clathrate [16]. Benzene has also been studied when dissolved in nematic liquid crystals [25]. The high mobility of the molecules ensures the averaging out of intermolecular contributions to the proton magnetic resonance spectrum, but their environment among long host molecules aligned with the magnetic field causes them to be partly oriented, with the result that intramolecular dipolar interactions are not fully eliminated. As a consequence the spectrum examined under high-resolution conditions displays a wealth of fine lines which supply the signs of the J coupling constants [26]. Hexafluorobenzene, C_6F_6, has been similarly studied [27].

3. Macroscopic Motion About One Axis

In the previous section a number of examples have been given in which rapid molecular motion about one preferred axis within the solid is believed to be responsible for the narrowing of the n.m.r. spectra. I shall now describe experiments in which we have demonstrated in a direct manner that rotation does indeed cause spectral narrowing [28–35]. If a solid specimen is rapidly rotated in the applied magnetic field, the coherent rotational motion is impressed upon every internuclear vector in the specimen, and the average magnetic dipolar linewidth should as a consequence be reduced by a factor $\frac{1}{2}(3\cos^2\alpha - 1)$, and the second moment by the square of this, where α is the angle between the axis of rotation and the direction of the applied magnetic field. The time-dependent part of the interaction generates satellite lines on either side of the narrowed central line, and these are set at integer multiples of the rotation frequency on either side of the center.

These effects are illustrated in figure 5 which shows the ^{23}Na n.m.r. spectra [29] of crystalline sodium chloride (a) when static, (b) when rotated at 800 Hz and (c) when rotated at 1600 Hz. These spectra were recorded for the case where α has the special value 54°44′ ($\cos^{-1} 1/\sqrt{3}$) which causes the reduction factor $\frac{1}{2}(3 \cos^2\alpha - 1)$ to be zero. In this situation the central line becomes very narrow. The satellite lines are clearly observed and as the speed of rotation increases they move out from the central line and become weaker, so that at 3 kHz only the narrow central line remains observable. In this situation the dipolar broadening has been effectively removed from the spectrum by motional averaging about one well-chosen axis; in a liquid it is removed by isotropic motion. Rotation about an axis perpendicular to the applied field ($\alpha = 90°$) reduces the second moment to one quarter, and more general angles have also been examined [28, 29, 36]. When molecular motion occurs within solids the rotational frequencies cover a wide band of frequencies of order

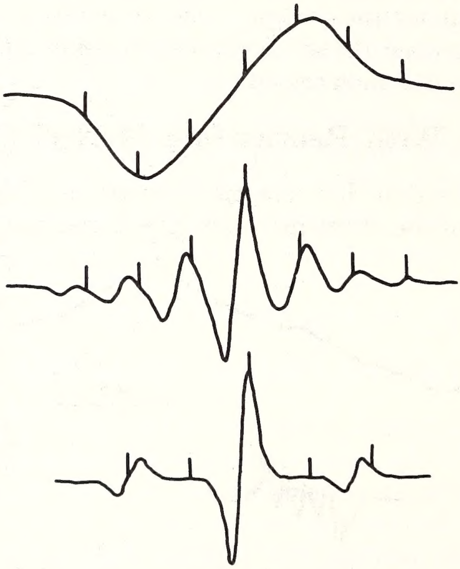

FIGURE 5. The effect of rapid rotation on the n.m.r. spectra of a solid [28]. Top: ^{23}Na n.m.r. derivative spectrum of a sodium chloride crystal at rest. Middle: spectrum for the same crystal rotated at 800 Hz about the magic axis. Bottom: spectrum for the crystal rotated at 1600 Hz about the magic axis. The markers are 800 Hz apart.

$1/\tau_c$, and the satellite lines are therefore spread too thinly to be observable.

These experiments not only demonstrate that rotational motion does reduce or remove dipolar broadening, but also they show, as figure 5 indicates, that the criterion for spectral narrowing is that the rate of motion should be comparable with the static linewidth. While the second moment of the central line is reduced in the manner expected, the second moment of the entire spectra including satellite lines is invariant with respect to the motion. The use of the second moment in interpreting spectral narrowing has therefore been placed on a firmer basis, and the conditions have been examined under which the invariance of second moment may be expected to apply [37].

N.m.r. spectra which have been narrowed by macroscopic rotation may exhibit fine structure which is otherwise obscured by the dipolar broadening and by other anisotropic interactions. Chemically-shifted fine structures have been found in several solid phosphorus compounds [33, 38], while recently we have been able to resolve spin-spin multiplets in the n.m.r. spectra of two rapidly-rotated polycrystalline specimens [35]. The ^{19}F n.m.r. spectra of one of these, namely potassium hexafluoroarsenate $KAsF_6$, are shown in figure 6. The upper recording is for the static material, which has a breadth between turning points of 13.2 kHz. The lower recording is for the specimen rotated at 5.5 kHz about the "magic" axis, revealing a quartet due to the interaction between the six equivalent fluorine nuclei and the ^{75}As nucleus whose spin number is 3/2.

4. Molecules With Reorienting Methyl Groups

The methyl group with its low moment of inertia is a highly mobile rotor. Motional narrowing of the proton magnetic resonance spectrum

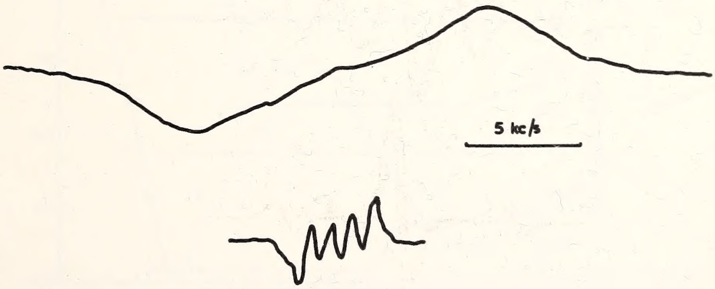

FIGURE 6. A spin-spin multiplet resolved in the n.m.r. spectrum of a solid by the technique of rapid specimen rotation [35]. The upper trace is the ^{19}F n.m.r. derivative spectrum of a static specimen of polycrystalline hexafluoroarsenate, $KAsF_6$. The lower trace is the spectrum for the specimen rotated about the magic axis at 5.5 kHz displaying a quartet structure due to electron-coupled interaction between ^{19}F and ^{75}As nuclei.

for methyl groups in solids is consequently often found to persist to low temperatures. We have been examining the proton magnetic resonance spectrum and relaxation time in a number of solid polymethylbenzenes down to liquid helium temperatures, and these provide good examples of the mobility of the methyl groups and moreover continue the earlier theme of benzene and its derivatives.

Hexamethylbenzene provides an example of a combination of two motions [3]. The temperature dependence of the second moment [39, 40] is shown in figure 7. The "rigid-lattice" value of the second moment would be approximately 33G^2, and the lower values observed below 150 °K indicate reorientation or tunnelling of the six methyl groups. The much lower value above 170 °K is ascribed to rotational motion of the entire molecules about their hexad axes superposed on the internal motion of the methyl groups.

It is to be noticed that there is no significant change in second moment on passing through the phase transitions at 116° and 383 °K. On the other hand the loosening of the structure at these temperatures is accompanied by discontinuities in the correlation times as is evidenced by the discontinuities in T_1 shown in figure 8. The low temperature minimum is associated with methyl group motion, while that at about 265 °K is associated with rotational motion of the whole molecule. Above 50 °K the correlation times extracted from the T_1 data below 116 °K follow a simple activation law with activation energy 1.9 kcal/mole. Rush and Taylor [41] using the neutron-scattering method obtain a barrier height of 1.35 kcal/mole. These two measured energies are clearly closely related but are not

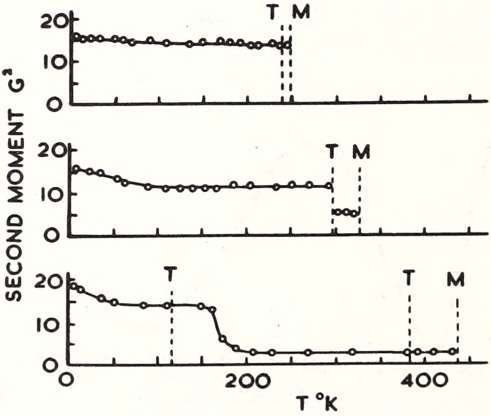

FIGURE 7. Dependence on temperature of the n.m.r. spectrum second moment for three solid polymethylbenzenes [39, 40, 42]. Top: 1,2,3,5-tetramethylbenzene. Middle: Pentamethylbenzene. Bottom: Hexamethylbenzene. *M* is melting point; *T* is transition point.

necessarily expected to be identical. The activation energy obtained from the n.m.r. results represents an average energy of excitation from a torsional state above the minimum of the potential curve to a rotational state above the barrier. This energy can be expected to be only roughly equal to the barrier height. In the neutron scattering experiments torsional frequencies of the methyl groups are determined; a barrier height is determined from these frequencies assuming a particular shape for the barrier, usually sinusoidal in absence of other information. It is therefore satisfactory that the energies obtained by the two methods are found to be roughly equal; no more than this should be expected.

Below 50° K there are systematic deviations of the correlation times from a simple activation law. At the lowest temperatures tunnelling must play a dominant role in the spectral narrowing. In the phase above 116 °K the activation energy for methyl group motion is 1.6 kcal/mole, a decrease of 16 percent; the barrier height determined by neutron scattering [41] showed a decrease of 21 percent, which is comparable. The activation energy obtained from the T_1 results for reorientation of the whole molecule about its hexad axis in this phase was found to be 6.7 kcal/mole. Anderson and Slichter [7], who have examined T_1 between 200° and 370 °K, found very similar values for the activation energy at constant pressure at both one atmosphere and at 680 atmospheres. As in the case of solid benzene, discussed in section 1, the activation energy at constant volume is much lower, namely 3.6 kcal/mole.

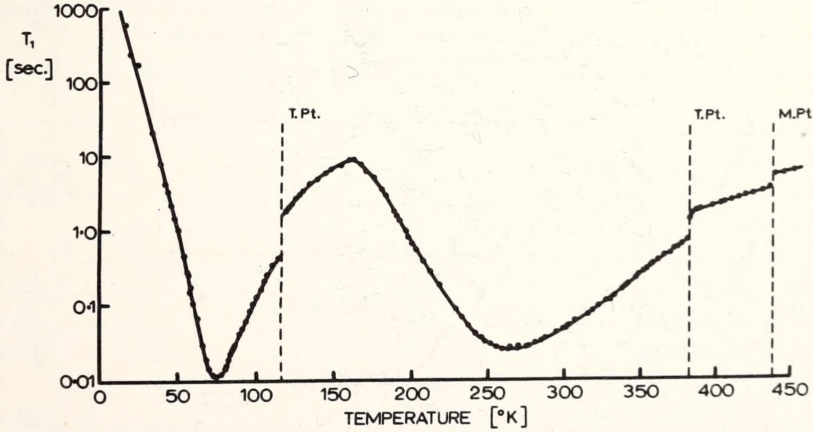

FIGURE 8. Dependence on temperature of the proton spin-lattice relaxation time T_1 in solid hexamethylbenzene [41]. The minimum at 74 °K is associated with methyl group reorientation, while that at 265 °K is associated with reorientation of the molecule about its hexad axis.

All the other eleven polymethylbenzenes also show motional narrowing of the proton magnetic resonance spectrum down to liquid helium temperatures [39, 42, 43], which can be ascribed to methyl group reorientation or tunnelling; some examples are shown in figure 7. The T_1 measurements are not always so readily interpreted as they were for the more symmetrical hexamethylbenzene. For example solid 1,2,3,5 tetramethylbenzene exhibits three minima at 48°, 74° and 118 °K (figure 9), while 1,2,3 trimethylbenzene shows two minima at 50° and 77 °K (fig. 10). It is possible that different values of τ_c and of T_1 characterize methyl groups with different molecular environments, and if this is so the additional minimum for 1,2,3,5 tetramethylbenzene at 118 °K may be associated with the additional methyl group at position 5. In fact, as table 1 indicates, the number of minima is in most cases equal to the number of structurally different methyl groups in the molecule. However this explanation may be too facile, and in order to cast light on this problem work is now in progress in our laboratory using deuterated compounds. Where a simple activation law is followed by the correlation times the activation energies for methyl group motion range from 0.6 to 2.2 kcal/mole. The potential barriers found by neutron scattering [45] for several of these poly-

TABLE 1. Minima in the proton T_1 versus temperature curves for solid polymethylbenzenes at 25 MHz

Compound	Temperature of minima associated with methyl group motion (°K)	Temperature of minima associated with motion of whole molecule (°K)	References
C_6H_6	----------------	170	4
$C_6H_5CH_3$	50	----------------	43
1,2 $C_6H_4(CH_3)_2$	77	----------------	43,44
1,3 $C_6H_4(CH_3)_2$	32	----------------	43
1,4 $C_6H_4(CH_3)_2$	52	----------------	43
1,2,3 $C_6H_3(CH_3)_3$	50,77	----------------	42,43
1,2,4 $C_6H_3(CH_3)_3$	85	----------------	42,43
1,3,5 $C_6H_3(CH_3)_3$	63	----------------	42,43
1,2,3,4 $C_6H_2(CH_3)_4$	20,96	----------------	42
1,2,3,5 $C_6H_2(CH_3)_4$	48,74,118	----------------	39,42
1,2,4,5 $C_6H_2(CH_3)_4$	82	----------------	39,42
$C_6H(CH_3)_5$	39,114	----------------	39,42
$C_6(CH_3)_6$	74	265	40

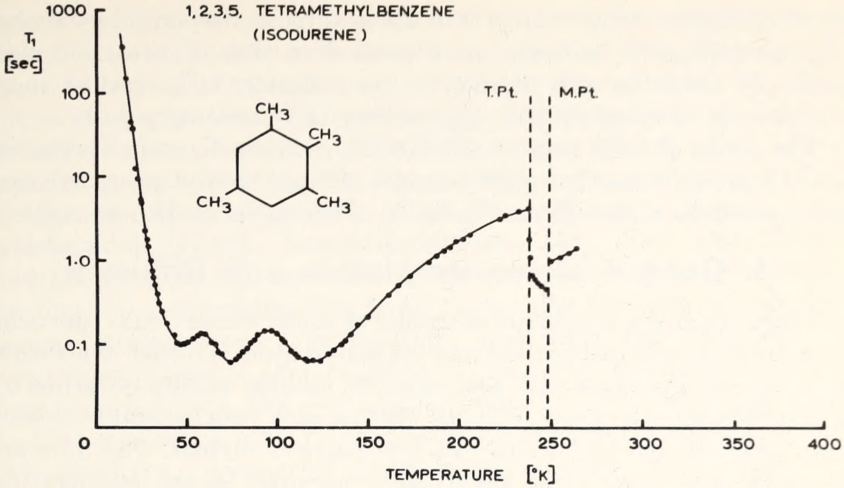

FIGURE 9. Dependence on temperature of the proton spin-lattice relaxation time T_1 in solid 1,2,3,5-tetramethylbenzene [39].

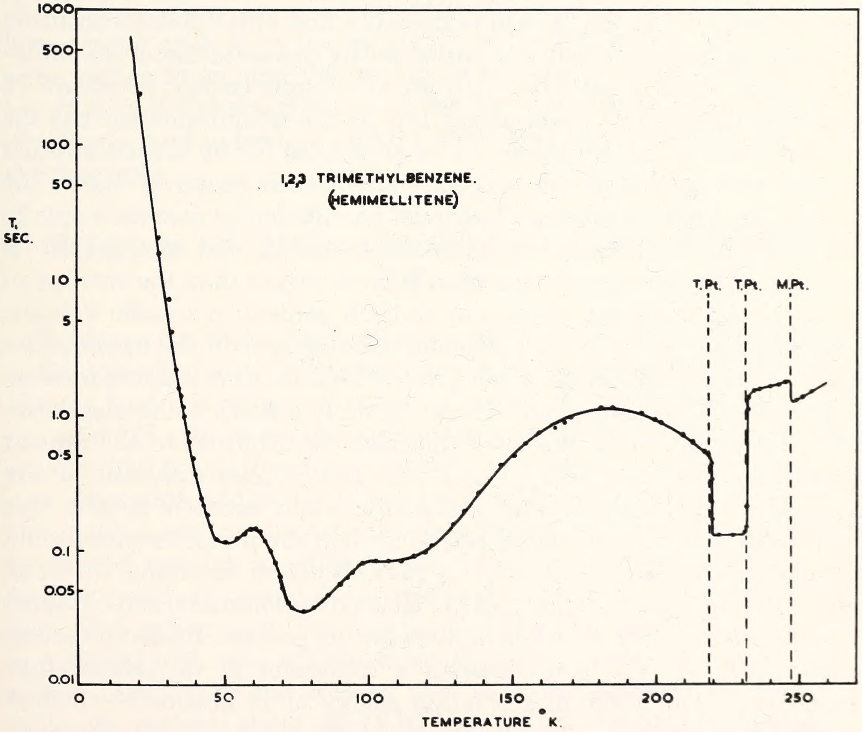

FIGURE 10. Dependence on temperature of the proton spin-lattice relaxation time T_1 in solid 1,2,3-trimethylbenzene [42].

methylbenzenes range from 1.0 to 2.2 kcal/mole. Second moment and $T_{1\rho}$ measurements indicate more general motion of the molecules, probably about an axis normal to the molecule, in several of these compounds at temperatures approaching their melting points.

The series of solid compounds $X(CH_3)_4$, where X is C, Si, Ge, Sn and Pb provides another good example of rapid methyl group rotation superposed on a general reorientation of the molecule [46, 47, 48].

5. General Molecular Motion and Diffusion

There are now a number of examples of solids whose n.m.r. spectrum narrows in several distinct steps as the temperature is raised. The rate of each process increases with temperature, though usually governed by quite different activation energies, and as each rate becomes comparable with the spectral width, the line narrows further. The different processes and their rates are usually mirrored in the temperature dependence of spin-lattice relaxation time behaviour, as we saw with hexamethylbenzene in the previous section.

An early example in this category which we studied some years ago is solid cyclohexane [49]. The second moment falls from 26.0 G^2 at 100 °K to 6.4 G^2 at 186 °K where there is a first order phase transition. This can be quantitatively accounted for by reorientation of the molecules about their triad axes with an activation energy of about 11 kcal/mole. In the new phase above 186 °K the second moment has the smaller value of 1.4 G^2 which can be accounted for by the assumption of a general motion of the molecules about their center of mass. The motion need not be isotropic but must be sufficiently near-isotropic to cause the intramolecular contribution to the second moment to be removed. The entropy of transition is much larger than the entropy of melting, and there is a change of about 8 percent in specific volume. This implies a much looser molecular arrangement in the upper phase which gives the molecules much greater freedom of rotational motion. Above 220 °K the spectrum narrows again to a sharp width characteristic of a liquid. Even the intermolecular contribution to the dipolar broadening has now disappeared and this implies diffusion of the molecules through the crystal lattice at a rate in excess of 10^4 Hz. This diffusional motion, postulated [49] to explain the n.m.r. results of solid cyclohexane has been confirmed by the radiotracer technique by Hood and Sherwood [50,51], who used ^{14}C labelled cyclohexane, and obtained an activation energy of 16.3 kcal/mole for the process. Recent measurements [52] of $T_{1\rho}$ have revealed a minimum in its temperature dependence, and yield an activation energy of 10 kcal/mole which is significantly lower.

The behaviour of solid cyclohexane is typical of many so-called "plastic crystals", which are characterized by at least one phase transformation accompanied by a large heat of transition, usually larger than the heat of fusion. Such transitions are sometimes referred to as "pre-melting". The molecules are globular in shape and in the upper temperature phase exhibit considerable molecular freedom. Besides cyclohexane some examples of the large number of such solids which have been examined by the n.m.r. method are cyclobutane [53], cyclopentane [54], neopentane [47,48,55], perfluorocyclohexane [56], cyclohexanol [57,58], hexamethyldisilane [59], 2,2- and 2,3-dimethylbutane [60,61], succinonitrile [62], camphor [63], triethylenediamine [64], quinuclidine [65]. In all these solids the molecules show a general quasi-isotropic reorientation, and with the exception of quinuclidine there is also evidence of molecular diffusion. Most of these materials have, like cyclohexane, a heat of transition greater than the heat of melting, often much greater. In the case of camphor, whose molecules have a permanent electric dipole moment, there is dielectric evidence of molecular motion consistent with the n.m.r. results.

Solid cyclohexanol [58] is an interesting case in that the molecular tumbling and diffusion narrow the n.m.r. spectral line sufficiently to enable a high-resolution spectrum to be observed consisting of three chemically-shifted proton lines with intensity ratios 1:1:10. These lines clearly arise from the resonance of the OH group, the H on the same carbon atom, and the remaining ten ring protons. The spectrum has in fact the characteristics of the high-resolution n.m.r. spectrum of a liquid, and indeed on melting there was no discernible change in the spectrum.

6. Evidence of Molecular Motion From Quadrupole Effects

Evidence for molecular motion in solids which has been discussed in the preceding sections has been derived from the magnetic-resonance spectra, and relaxation behaviour of nuclei of spin ½, such as the proton and ^{19}F. However the examination of nuclei with spin number greater than ½, and therefore possessing an electric quadrupole moment, can often give additional information. Molecular motion modulates the nuclear electric quadrupolar interaction, enabling the motion to be studied through its effect on the electric quadrupolar coupling tensor, its principal axes and principal values, and on the nuclear spin-lattice relaxation time. The first work of this kind was that of Ketudat and Pound [66], who examined the deuteron resonance in monocrystalline $Li_2SO_4 \cdot D_2O$ and showed that at room temperature the water molecule reorients about the DOD bisector between its two equivalent positions 180° apart, while at 148 °K the spectrum corresponded to that of stationary water molecules. The same type of behaviour has been found in deuterated oxalic acid dihydrate $(COOD)_2 \cdot 2D_2O$ by Chiba [67], and in deuterated Rochelle salt by Bjorkstam [68].

In our laboratory, Derbyshire, Gorvin and Warner [69] have recently studied the deuteron magnetic resonance spectrum in a single crystal of glycine $N^+D_3CH_2COO^-$. The monoclinic unit cell contains four glycine molecules related by a plane of symmetry and a center of symmetry. Thus there are six different N–D directions, and yet at room temperature only two pairs of lines are found in the quadrupole split spectrum, an example of which is shown in figure 11. The angular variation of the two pairs of lines for rotation of the crystal about three mutually perpendicular axes is shown in figure 12. This result is consistent with the view that the N^+D_3 group is reorienting about an axis equally inclined to the three N–D directions. The principal values obtained for the two tensors were +51.3 kHz, −32.6 kHz and −18.7 kHz; the rate of reorientation must therefore have been greater than 10^5 Hz, and as we shall see presently probably much greater than this. The direction of the largest principal value is, as expected, close to the N–C bond direction, but is significantly different from it, the difference being 5° 39′. This implies either that the three electric field gradient tensors experienced by the three deuteron nuclei are not quite equal, or that the N–D bonds do not make equal angles with the N–C bond direction. In view of the probable differences in hydrogen bonding of the three N–D bonds, it is likely that both causes contribute; the observed tensor is in any case not found to be axially symmetrical.

The conclusion that the N^+D_3 group is rapidly reorienting at room temperature is consistent with the proton magnetic resonance spec-

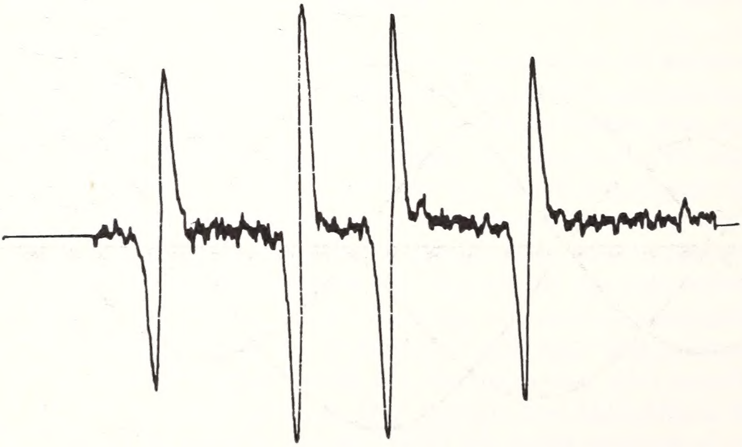

FIGURE 11. Deuteron magnetic resonance spectrum in deuterated glycine at room temperature [69]. The two pairs of lines arise from deuterons in two structurally inequivalent N^+D_3 groups.

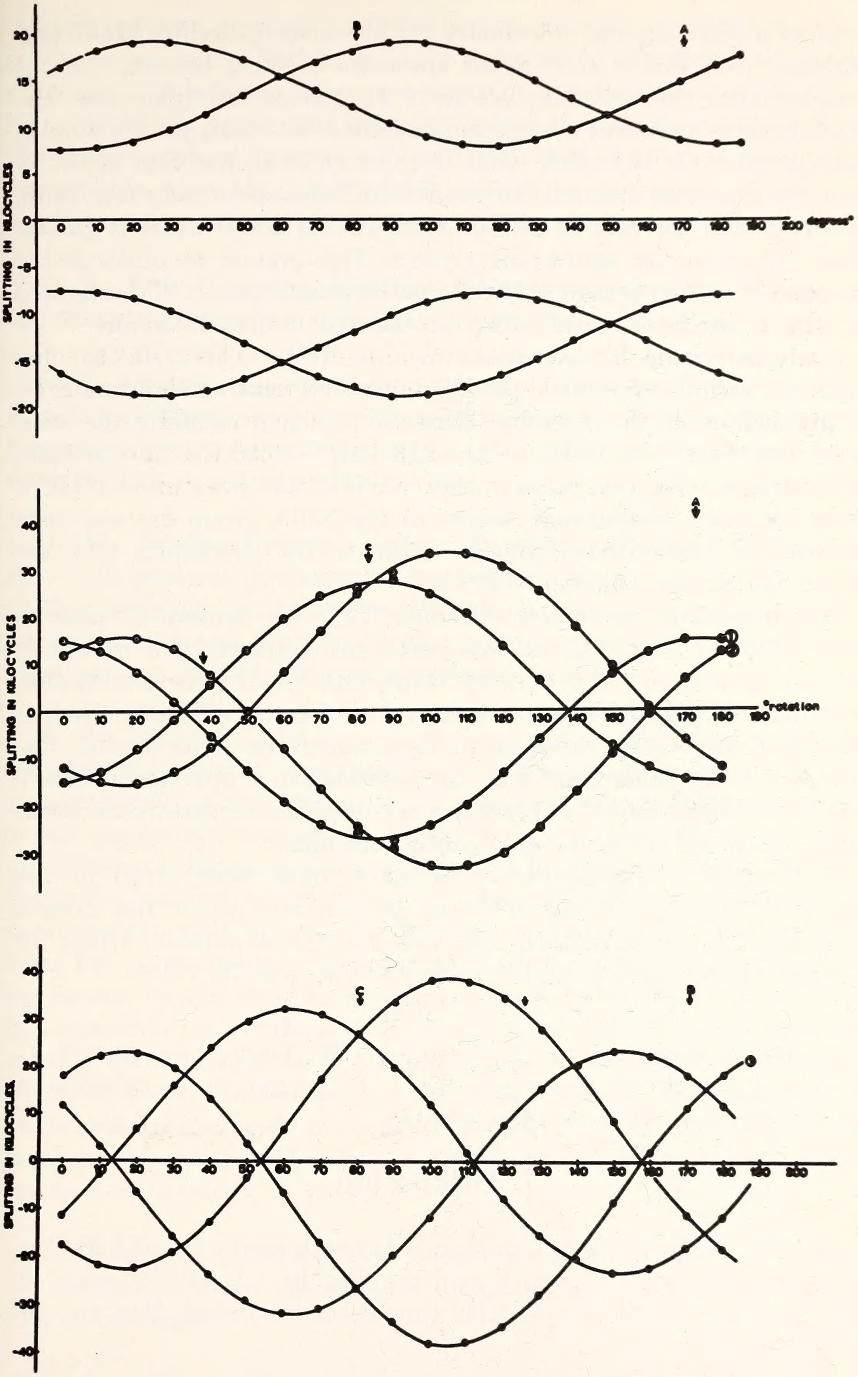

FIGURE 12. Angular dependence of the four lines in the deuteron magnetic resonance spectrum of deuterated glycine at room temperature [69]. The three diagrams refer to rotation of the crystal about three mutually perpendicular axes.

trum of a single crystal of ordinary glycine investigated by Webb and Moulton [70]. Below 150 °K the spectrum is much broader [70, 71] corresponding to essentially static N^+H_3 groups, implying that the rate of reorientation at these temperatures is less than 10^5 Hz in ordinary glycine. On the other hand Derbyshire et al. [72] find at 90 °K that the deuteron magnetic resonance still consists of only four lines, implying that the rate of reorientation at this temperature is greater than 10^5 c/s in the deuterated glycine. This greater mobility in the deuterated species presumably reflects the weaker nature of deuterated hydrogen bonds compared with protonated hydrogen bonds.

A single crystal of deuterated alanine $N^+D_3\ C(CH_3)HCOO^-$ has been studied also [72] and like glycine shows that there is rapid reorientation of the N^+D_3 group. Here the principal values of the averaged tensor are $+49.2$ kHz, -29.0 kHz and -20.2 kHz. The direction of the largest principal value in this case is 3° 40′ away from the N–C bond direction. Rotational motion of the N^+D_3 group has also been studied in deuterated triglycine sulphate by Bjorkstam [73] and Blinc, Pintar and Zupancic [74].

An interesting result was obtained [72] with deuterated malonic acid $CH_2(COOD)_2$. The triclinic unit cell contains two molecules related by a center of symmetry. Thus one would anticipate finding two pairs of lines corresponding to two different O–D directions; in fact four pairs were found at room temperature. This implies that for each O–D bond there are two possible bond directions. This is not of course disclosed by the x-ray investigation of the crystal structure, which did not locate the hydrogen atoms.

A number of representative examples have been given in this paper of different kinds of molecular motion which the nuclear magnetic resonance method has been able to illuminate. Other examples will be found in earlier review articles [75, 76, 77].

I wish to thank Dr. P. S. Allen, Dr. W. Derbyshire, Dr. D. C. Douglass, Dr. R. G. Eades and Dr. I. J. Lawrenson for information on their work in advance of publication.

7. Discussion

D. W. McCall (Bell Telephone Laboratories): In $KAsF_6$ you were able to resolve the As-F spin coupling by a 6 kHz rotation. As the resonance width is $\sim$13 kHz this seems surprising. Can you tell us about this?

E. R. Andrew: Experimentally one finds that you don't have to rotate at quite the rate equal to the linewidth of the static specimen defined between derivative turning points. Usually one finds that the spectrum is already beginning to show the effect of rotation when the specimen is rotated at about a quarter of the derivative width. This is in reasonable agreement with the theory of Clough and Gray that the spectrum should narrow substantially when the rate of rotation is comparable with the r.m.s. width, which in the case of $KAsF_6$ is 4.5 kHz.

R. S. Kirk (General Electric): Does the activation energy of the relaxation time show a change when tunnelling becomes important?

E. R. Andrew: At lower temperatures where tunnelling assumes greater importance, the correlation time deduced from the spin-lattice relaxation time measurements for the solid polymethylbenzenes deviates from a simple activation law.

G. W. Smith (General Motors Research): Various data show that both hexamethylethane and neopentane are 'plastic crystals' and display self-diffusion. However in the analogous compounds hexamethyldisilane and tetramethylsilane, only hexamethyldisilane has a plastic phase. Would you care to comment on this?

E. R. Andrew: I do not think we have a quantitative understanding of the phase transitions in molecular solids. However one can see empirically a progression of behaviour as silicon replaces carbon in the compounds mentioned. Replacing carbon with silicon in hexamethylethane decreases the melting point by 86° from 374 to 288 °K. Replacing carbon with silicon in tetramethylcarbon (neopentane) decreases the melting point by 80° from 254 to 174 °K. The replacement has approximately the same effect on the melting point. Replacing carbon by silicon in hexamethylethane has the effect of *increasing* the transition temperature by 69° from 153 to 222 °K. If the replacement of carbon by silicon in tetramethylcarbon were to have the same result on the transition temperature, the transition temperature for tetramethylsilane would occur at about 209 °K. However the melting point of this compound is low, 174 °K, and consequently the plastic phase does not exist.

C. S. Johnson (University of North Carolina): I wonder if exactly the same activation energies are obtained from linewidths as from second moments.

E. R. Andrew: All the activation energies that I have quoted are based on spin-lattice relaxation data and not at all from spectral narrowing. Consequently they are based on a much wider range of temperature, since the spectrum usually narrows over a small temperature interval. However if T_1 measurements are lacking, estimates of activation energy can be obtained from spectral narrowing. Strictly one should work with the linewidth here and not with the second moment, since the latter is not uniquely obtainable in the region of narrowing.

C. S. Johnson: If you can compare the activation energies from relaxation measurements and from linewidths will they come out the same?

E. R. Andrew: Yes, you can very often give a reasonable account of the line-narrowing process using the activation data from the T_1 measurements.

D. F. R. Gilson (McGill University): The linewidth versus temperature plot obtained by Hoch and Rushworth for cyclobutane indicated two linewidths at the same temperature. Similar results were obtained by G. W. Smith for triethylenediamine and by us for some other compounds. Would you care to comment on this?

E. R. Andrew: I do not recall the details of the work mentioned sufficiently clearly. However both compounds contain pairs of protons which would generate a line structure and in the region where the spectrum is narrowed by hindered rotation the intermolecular broadening may be reduced sufficiently to allow the intramolecular structure to be resolved.

C. Brot (Centre National de la Recherche Scientifique): Do you have any comment on the possible differences between the activation enthalpy (which is most often measured), the activation energy, and the intermolecular potential barrier.

E. R. Andrew: This is an interesting point, since measurements have been made of T_1 by Anderson and Slichter on a number of solids as a function of pressure and temperature. For the more compressible molecular solids they found a significant difference between the activation energy at constant pressure (activation enthalpy) and the activation energy at constant volume. At constant volume one supposes that the potential barriers restraining molecular rotation are held constant and that as the temperature rises more molecules are excited over the potential barriers. On the other hand at constant pressure the lattice expands as the temperature rises and one expects that the potential barriers are progressively reduced while at the same time more molecules are being excited over them. In this case there should therefore be a more rapid variation of molecular reorientation rate with temperature, and hence the activation enthalpy should be greater than the activation energy measured at constant volume, and this is what was found.

J. J. Rush (National Bureau of Standards): I have a comment rather than a question. Professor Andrew and I have already discussed some of this in private, but I think considering the nature of the conference that some comments about correlation between the neutron scattering data and the nmr data might be apropos. By a happy coincidence, as Professor Andrew pointed out, a whole sequence of polymethylbenzenes were studied in the same temperature region and the same phases, by neutron scattering at Argonne, and by Professor Andrew and his collaborators in England. The correlation between these data is quite impressive, particularly in cases such as *o*-xylene and durene where you do have some hope for the potential to approximate a three-fold cosine potential. The activation energies extracted by Professor Andrew and his collaborators are in quite good agreement with the barriers to rotation we calculated from the measured 1–0 transitions. In addition, all of these data are consistent with the activation energies for the gas phase derived from thermodynamic data, also assuming a cosine potential. This, I think, demonstrates that similar types of measurements in parallel directions by these techniques can, in the future, contribute more information about individual motions and potential barriers and changes with state of aggregation than one technique alone.

8. References

[1] J. H. Van Vleck, Phys. Rev. **74**, 1168 (1948).
[2] See for example E. R. Andrew, Nuclear Magnetic Resonance, Cambridge University Press (1955); A. Abragam, The Principles of Nuclear Magnetism, Clarendon Press, Oxford (1961); C. P. Slichter, Principles of Magnetic Resonance, Harper and Row (1963).
[3] E. R. Andrew, J. Chem. Phys. **18**, 607 (1950).
[4] E. R. Andrew and R. G. Eades, Proc. Roy. Soc. **A218**, 537 (1953).
[5] J. E. Anderson, J. Chem. Phys. **43**, 3575 (1965).
[6] E. G. Cox, D. W. J. Cruickshank and J. A. S. Smith, Proc. Roy. Soc. **A247**, 1 (1958).
[7] J. E. Anderson and W. P. Slichter, J. Chem. Phys. **44**, 1797 (1966).
[8] D. C. Ailion and C. P. Slichter, Phys. Rev. **137**, A235 (1965).
[9] E. G. Cox, Rev. Mod. Phys. **30**, 159 (1958).
[10] B. Stoicheff, J. Chem. Phys. **21**, 1410 (1953).
[11] G. E. Bacon, N. A. Curry and S. A. Wilson, Proc. Roy. Soc. **A279**, 98 (1964).
[12] A. Fruhling, Anu. Phys. Paris **6**, 401 (1951).

[13] I. Ichishuma and S. Mizushima, J. Chem. Phys. **18,** 1686 (1950); also M. Ito and T. Shigeoka, Spectrochim. Acta **22,** 1029 (1966).
[14] I. J. Lawrenson and C. Lewis, Proc. Phys. Soc. **89,** 923 (1966).
[15] C. Brot and I. Darmon, J. Chim. Phys. **63,** 100 (1966).
[16] H. Nakajima, J. Phys. Soc. Japan **20,** 555 (1965).
[17] T. Miyamoto, T. Iwamoto, Y. Sasaki and S. Fujiwara, J. Chem. Phys. **45,** 752 (1966).
[18] L. N. Mulay, E. G. Rochow and E. O. Fischer, J. Inorg. Nucl. Chem. **4,** 231 (1957).
[19] D. F. R. Gilson and C. A. McDowell, J. Chem. Phys. **39,** 1825 (1963); the same authors have reported a study of molecular motion in other organic complexes in Can. J. Chem. **44,** 945 (1966).
[20] C. H. Holm and J. A. Ibers, J. Chem. Phys. **30,** 885 (1959).
[21] L. N. Mulay and M. E. Fox, Naturwissenschaften **49,** 446 (1962).
[22] L. N. Mulay and A. Attalla, J. Amer. Chem. Soc. **85,** 702 (1963).
[23] J. K. Thompson, J. J. Krebs and H. A. Resing, J. Chem. Phys. **43,** 3853 (1965).
[24] D. E. Woessner, J. Phys. Chem. **70,** 1217 (1966).
[25] A. Saupe and G. Englert, Phys. Rev. Letters **11,** 462 (1963).
[26] L. C. Snyder and E. W. Anderson, J. Amer. Chem. Soc. **86,** 5023 (1964).
[27] L. C. Snyder and E. W. Anderson, J. Chem. Phys. **42,** 3336 (1965).
[28] E. R. Andrew, A. Bradbury and R. G. Eades, Nature **182,** 1659 (1958).
[29] E. R. Andrew, A. Bradbury and R. G. Eades, Nature **183,** 1802 (1959).
[30] E. R. Andrew, A. Bradbury, R. G. Eades and G. J. Jenks, Nature **188,** 1103 (1960).
[31] E. R. Andrew and R. G. Eades, Disc. Faraday Soc. **34,** 38 (1962).
[32] E. R. Andrew, A. Bradbury, R. G. Eades and V. T. Wynn, Physics Letters **4,** 99 (1963).
[33] E. R. Andrew and V. T. Wynn, Proc. Roy. Soc. A**291,** 257 (1966).
[34] E. R. Andrew, S. Clough, L. F. Farnell, T. D. Gledhill and I. Roberts, Physics Letters **21,** 505 (1966).
[35] E. R. Andrew, L. F. Farnell and T. D. Gledhill, Phys. Rev. Letters **19,** 6 (1967).
]36] I. J. Lowe, Phys. Rev. Letters **2,** 285 (1959).
[37] E. R. Andrew and G. J. Jenks, Proc. Phys. Soc. **80,** 663 (1962).
[38] H. Kessemeier and R. E. Norberg, Phys. Rev. **155,** 321 (1967).
[39] P. S. Allen, E. R. Andrew and A. Cowking, Proc. XIV Colloque Ampere, Ljubljana 1078 (1966).
[40] P. S. Allen and A. Cowking, J. Chem. Phys. **47,** 4286 (1967.)
[41] J. J. Rush and T. I. Taylor, J. Chem. Phys. **44,** 274 (1966).
[42] A. Cowking, Ph.D. thesis, University of Nottingham (1967).
[43] G. P. Jones, R. G. Eades, K. W. Terry and J. P. Llewellyn, (to be published).
[44] J. Haupt and W. Müller-Warmuth, CR XIII Colloque Ampere, Louvain 247 (1964).
[45] J. J. Rush, J. Chem. Phys. **47,** 3936 (1967).
[46] G. W. Smith, J. Chem. Phys. **42,** 4229 (1965).
[47] J. G. Powles and H. S. Gutowsky, J. Chem. Phys. **21,** 1695 (1955).
[48] E. O. Stejskal, D. E. Woessner, T. C. Farrar and H. S. Gutowsky, J. Chem. Phys. **31,** 55 (1959).
[49] E. R. Andrew and R. G. Eades, Proc. Roy. Soc. A**216,** 398 (1953).
[50] G. M. Hood and J. N. Sherwood, Molecular Crystals **1,** 97 (1966).
[51] G. M. Hood and J. N. Sherwood, J. Chim. Phys. **63,** 121 (1966).
[52] D. C. Douglass (private communication).

[53] M. J. R. Hoch and F. A. Rushworth, Proc. Phys. Soc. **83,** 949 (1964).
[54] F. A. Rushworth, Proc. Roy. Soc. A**222,** 526 (1954).
[55] H. S. Gutowsky and G. E. Pake, J. Chem. Phys. **18,** 162 (1950).
[56] A. Fratiello and D. C. Douglass, J. Chem. Phys. **41,** 974 (1964).
[57] P. Averbuch, C.R. Acad. Sci. Paris **244,** 3147 (1963).
[58] H. Suga, M. Sugisaki and S. Seki, Molecular Crystals **1,** 377 (1966).
[59] T. Yukitoshi, H. Suga, S. Seki and J. Itoh, J. Phys. Soc. Japan **12,** 506 (1957).
[60] R. G. Eades, G. P. Jones, J. P. Llewellyn and K. W. Terry, Proc. Phys. Soc. **91,** 124 (1967).
[61] G. P. Jones, Physics Letters **22,** 390 (1966).
[62] L. Petrakis and A. Rao, J. Chem. Phys. **39,** 1633 (1963).
[63] J. E. Anderson and W. P. Slichter, J. Chem. Phys. **41,** 1922 (1964).
[64] G. W. Smith, J. Chem. Phys. **43,** 4325 (1965).
[65] I. Darmon and C. Brot, Molecular Crystals **1,** 417 (1966).
[66] S. Ketudat and R. V. Pound, J. Chem. Phys. **26,** 708 (1957).
[67] T. Chiba, J. Chem. Phys. **41,** 1352 (1964).
[68] J. L. Bjorkstam, Bull. Am. Phys. Soc. **9,** 142 (1964).
[69] W. Derbyshire, T. Gorvin and D. Warner, Molecular Physics **12,** 299 (1967).
[70] W. E. Webb and W. G. Moulton, J. Chem. Phys. **36,** 1911 (1962).
[71] R. A. Kromhout and W. G. Moulton, J. Chem. Phys. **23,** 1673 (1955).
[72] W. Derbyshire, T. Gorvin and D. Warner, (private communication).
[73] J. L. Bjorkstam, Phys. Rev. **153,** 599 (1967).
[74] R. Blinc, M. Pintar and I. Zupancic, J. Phys. Chem. Solids **28,** 405 (1967).
[75] E. R. Andrew, J. Phys. Chem. Solids **18,** 9 (1961).
[76] J. G. Powles, J. Phys. Chem. Solids **18,** 17 (1961).
[77] E. R. Andrew and P. S. Allen, J. Chem. Phys. **63,** 85 (1966).

FAR INFRARED SPECTRA AND SPACE GROUP OF CRYSTALLINE HYDRAZINE AND HYDRAZINE-d_4

F. G. BAGLIN, S. F. BUSH, and J. R. DURIG

Department of Chemistry
University of South Carolina, Columbia, South Carolina 29208

The infrared spectra of crystalline hydrazine and hydrazine-d_4 have been recorded from 33–400 cm^{-1}, and are shown in figures 1 and 2. All spectral bands are assigned to lattice vibrations according to whether they arise primarily from a translational or a librational mode. However, there is strong evidence that these two motions are coupled, and thus may not be described accurately as arising from one type of motion or the other.

Seven bands were observed in the far-infrared spectrum of crystalline hydrazine, and their frequencies are listed in table 1. All three of the translational modes predicted from group theory are assigned and four of the six predicted librations are also assigned. The assignments were accomplished on the basis of similar band contours and isotopic shift data (see table 2) obtained from hydrazine-d_4. The space group of crystalline hydrazine was found to be C_2^2 on the basis of the number of bands observed in the lattice region of the spectrum, and it is believed that far infrared data should be useful in the solution of similar structural problems.

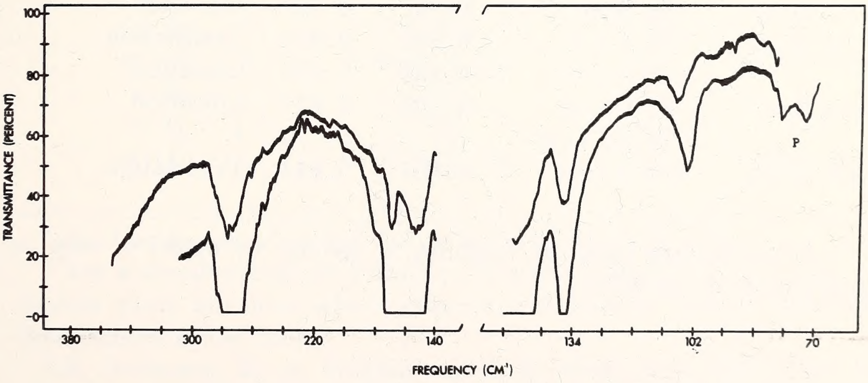

FIGURE 1. Far infrared spectrum of crystalline hydrazine. P indicates polyethylene bands.

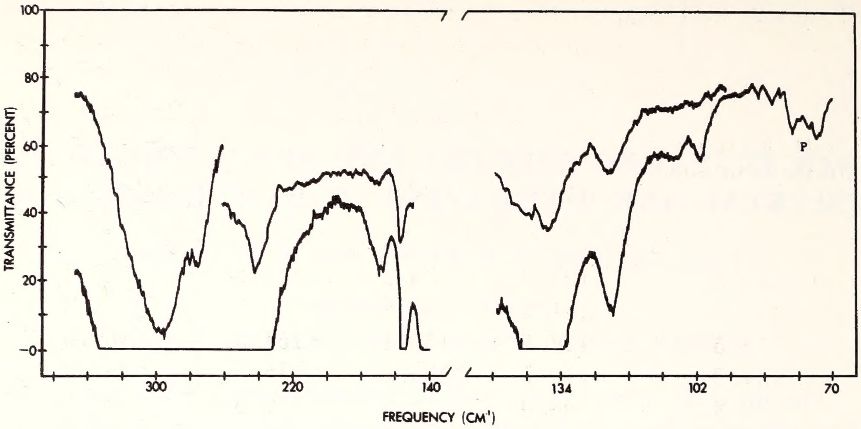

FIGURE 2. Far infrared spectrum of crystalline hydrazine-d_4. P indicates polyethylene bands.

TABLE 1. Optical lattice modes of hydrazine and hydrazine-d_4

Frequencies in cm^{-1}		Observed Ratio	Calculated	Assignment
N_2H_4	N_2D_4	$\frac{\nu_D}{\nu_H}$		
650 (vs)[a]	492 (vs)	--------	--------	
405 (vvs)	298 (vvs)	0. 736	-------	Intramolecular torsion, ν_t
	277 (sh)	--------	-------	
274. 9(s)	243. 0 (s)	0. 884	0. 870	Libration
180. 5(vw)	169. 5 (vw)	0. 939	0. 943	Translation
172. 5(m)	156. 5(m)	0. 907	0. 877	Libration
154. 0(s,c)	142. 3 (s)	0. 924	0. 943	Translation
	136. 9 (s)	0. 889	0. 870	Libration
136. 3(m)	123. 0 (m)	0. 904	0. 877	Libration
	(107. 5)(vvw)	--------	--------	?
106. 7(w)	101. 5 (w)	0. 951	0. 943	Translation

[a] Abbreviations used: m, medium; s, strong; w, weak; v, very; c, composite; sh, shoulder.

TABLE 2. N_2D_4 frequencies generated by moment and mass ratio data from observed N_2H_4 frequencies

N_2H_4 Frequency in wavenumbers	Librational ratios			Translational ratio 0.943
	0.719	0.870	0.877	
274.9	197.7	[b] 239.2	241.1	258.4
180.5	131.2	158.8	160.1	[b] 172.4
172.5	124.1	150.1	[b] 151.3	162.4
154.0	110.7	[b] 134.0	135.1	[b] 145.2
136.3	98.0	118.6	[b] 119.5	128.5
106.7	76.7	92.8	93.6	[b] 100.7

[b] Indicates the N_2D_4 band or bands assigned as arising from the N_2H_4 frequency at the left of the table.

TABLE 3. Intermolecular force constants

Translational force constants in $\frac{\text{m-d}}{\text{Å}}$	Librational force constants in $\frac{\text{m-d}}{\text{Å}}$	Crystalline sample	Reference
0.004–0.008	([a])	Cl_2	([c])
0.006–0.13	([a])	Br_2	([c])
0.006–0.16	([a])	I_2	([c])
[b] 0.21	[b] 0.042	HCl	([d])
[b] 0.20	[b] 0.035	HBr	([d])
0.102	0.0590–0.117	N_2H_4	This work
0.22	0.050	DCl	([d])
0.21	0.043	DBr	([d])
0.110	0.0524–0.104	N_2D_4	This work

[a] No frequencies observed due to infrared selection rules.

[b] For a one-dimensional Born-Von Karman lattice the equations of motion yield solutions which give force constants exactly one-half those stated in the table.

[c] A. Anderson, H. A. Gebbie and S. H. Walmsley, Mol. Phys. **7**, 401 (1964).

[d] S. H. Walmsley and A. Anderson, Mol. Phys. **7**, 411 (1964).

The force constant calculations were carried out using a modified Born-Von Karman model. Two dumbbell-shaped bodies were used to represent the two hydrazine molecules per unit cell. The NH_2 groups were assumed to be connected by a rigid weightless bar, and the dumbbells, in turn, connected by a weightless spring. The masses at the end of the dumbbells were nearly isobaric with the NH_2 group, i.e., an oxygen atom. Thus, a one dimensional "ribbon lattice" was constructed.This model closely matches the configuration of the molecules in the crystal lattice. The results of this calculation are given in table 3.

One of us (FGB) wishes to thank the National Cancer Institute for a postdoctoral fellowship, number 6–F2–CA–35,825–01A1. We also wish to thank the National Aeronautics and Space Administration for their sponsorship of this research through grant NGR–41–002.003.

MOLECULAR ROTATION IN CONDENSED PHASES OF SIMPLE MOLECULES

M. BLUMENFELD

Department of Physics,
University of Toronto, Toronto, Ontario

1. Introduction

The problem of molecular rotation in condensed phases has received considerable attention since the early investigations of Crawford, Welsh and Harrold [1] [1] into the Raman spectra of liquid oxygen, nitrogen, and methane, and solid methane. From the shape and extent of the rotational wings they concluded that these molecules rotated freely in their condensed phases.

1.1. Moment Analysis of Spectral Bands

In a series of articles, Gordon [2] has demonstrated a new method of extracting information regarding molecular rotation from the spectra of molecules in their condensed states. Briefly, the spectrum is analysed in terms of the moments of its intensity distribution, $I(\nu)$, where the nth moment of a Raman band is given by

$$M(n)=\int(\nu-\nu_s)^n\lambda^4 I(\nu)d\nu$$

where ν_s is some suitably chosen band origin.

The lower-order moments yield quantities depending on low order distribution functions. In particular, from the second and fourth moments the magnitude of the intermolecular torque (the angular derivative of the intermolecular potential) hindering the rotational motion can be obtained. This analysis requires that the intensity be accurately known, particularly in the tail ends of the spectral bands. A reinvestigation of the Raman spectra of liquid oxygen and methane, and of solid methane was undertaken to obtain suitable data for such an analysis.

1.2. Rotational Correlation Function Analysis

Gordon [3] has also shown how to recover dynamical information about the molecular rotation from the shapes of the depolarized spectral bands. The normalized intensity distribution, $I(\nu)$, is the Fourier transform of $C(t)$, a normalized correlation function of the anisotropy of the vibrational polarizability, β^v given by

---

[1] Figures in brackets indicate the literature references listed at the end of this paper.

$$\lambda^4 I(\nu)=\frac{1}{2\pi}\int_{-\infty}^{\infty} < \mathrm{Tr}\, \beta^v(0)\cdot \beta^v(t)> e^{\frac{-2\pi i\nu t}{c}}\, dt$$

$$=\frac{1}{2\pi}\int_{-\infty}^{\infty} C(t) e^{\frac{-2\pi i\nu t}{c}}\, dt$$

For a linear diatomic molecule such as O_2 the correlation function can be expressed as

$$C(t)=<P_2(\mathbf{u}(0)\cdot \mathbf{u}(t))>$$

in the classical limit, where **u** is the unit vector along the symmetry axis, and $P_2(x)$ is the second Legendre polynomial.

The same relation holds for a spherical top molecule such as methane, except that the unit vector now points along a twofold axis. The correlation function can be thought of as representing the decay of our knowledge about the rotational motion of the molecule.

2. Experimental Procedure

The cryostat and the method by which the samples were obtained and retained are described elsewhere [4]. The solid samples were clear and flawless throughout, reducing the background due to parasitic light scattered by cracks, bubbles, or crystal boundaries into the spectrograph optics. Excitation was by a Toronto Hg arc; the spectra were recorded on a modified Bausch and Lomb Dual-Grating Spectrograph, using slit widths of about 250 and 500 microns. In the second order at 4625 Å the reciprocal linear dispersion is 8 cm^{-1}/mm.

3. Results and Discussion

3.1. Moment Analysis

a. Liquid Oxygen

The band profile of the anisotropically scattered Raman spectrum of liquid oxygen, shown in figure 1, was obtained by subtracting the properly normalized profile of the Rayleigh line from the total Raman band profile, under the assumption that the isotropic Q branch was the image of the Rayleigh line broadened by the slit. The first four moments about the Q branch peak position, 1551.9 cm^{-1}, were calculated and the mean-squared torque, $<\tau^2>$, obtained from the ratio

$$\frac{M(4)}{M(2)}=32\frac{kT}{hc}B+\frac{hc}{kT}B<\tau^2>\cdot$$

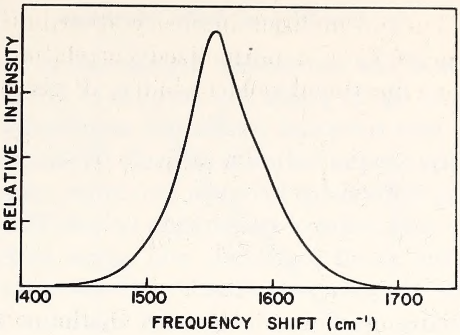

FIGURE 1. The band profile of the anisotropically scattered part of the fundamental vibration in liquid oxygen at 88 °K.

As indicated in table 1, the rms value of the torque obtained was 283 cm^{-1}/rad. An effective rms torsional oscillation amplitude can be defined through the relation

$$<\theta^2>^{1/2}=\frac{180}{\pi}\frac{kT}{hc}\frac{1}{<\tau^2>^{1/2}}$$

In liquid oxygen the amplitude obtained is 12°, indicating the motion is highly hindered, rather than free as was concluded by Crawford et al. [1].

TABLE 1.—Spectral band moment analyses

	Rms torques (cm^{-1}/rad)		kT/hc thermal rotational energy (cm^{-1})	Rms torsional oscillation amplitudes	
	Raman	IR		Raman	IR
Liquid O_2	283		61	12°	
Liquid CH_4	118	[a]148	64	31°	25°
Solid CH_4	201	[a]173	56	16°	19°

[a] Calculated by Gordon [5] from the IR data of Ewing [6].

b. Liquid and Solid Methane

Similar analyses of the completely depolarized ν_3 band in liquid and solid CH_4 (shown in fig. 2) yields rms torques of 118 and 201 cm^{-1}/rad, respectively, and rms torsional oscillation amplitudes of 31° and 16°. The accuracy in the torque values is difficult to ascertain, but, because the torques are the differences between two large, almost equal, terms, they are probably only order of magnitude values. However, the values obtained follow the trend expected, and agree within experimental accuracy with the torques calculated by Gordon [5] from the infrared results of Ewing on liquid and solid methane [6], as shown in table 1. This Raman study therefore confirms the conclusions of Savitsky and Hornig [7], and Ewing [6], from the infrared data, that the molecular rotation in liquid and solid CH_4 at temperatures near its freezing point is hindered.

3.2. Correlation Function Analyses

The correlation function calculated from the experimentally obtained profile of the anisotropic Raman scattering in liquid oxygen is displayed in figure 3. Initially, the behaviour is similar to that expected for a freely rotating molecule. Departure from this behaviour begins at about 2.5×10^{-13} seconds; it is at this point that the inter-

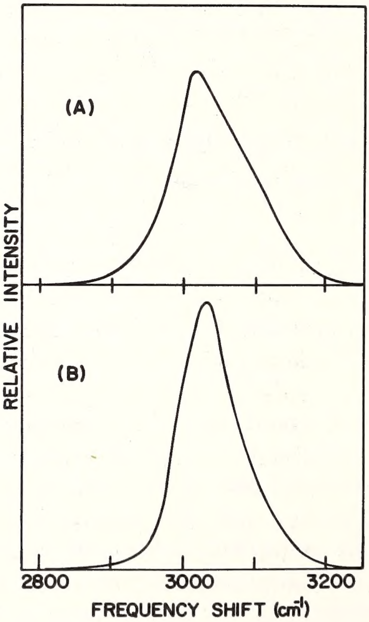

FIGURE 2. The Raman band profiles of the ν_3 vibrational fundamental in (A) liquid CH_4 at 90 °K, and (B) solid CH_4 at 80 °K.

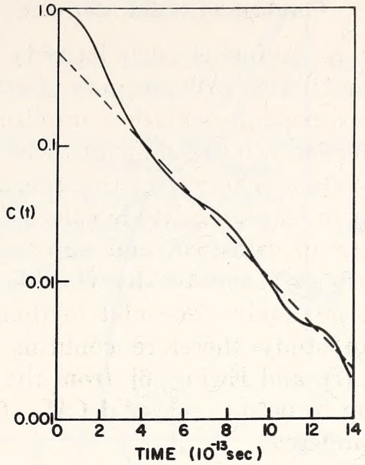

FIGURE 3. The rotational correlation function obtained from the anisotropic Raman vibrational band of liquid oxygen. The correlation function is plotted logarithmically to show the exponential decay at long times.

molecular torques begin to act on the molecule, hindering its rotation. In the period from about 4×10^{-13} seconds till the function becomes effectively zero, at about 15×10^{-13} seconds, the rotational motion has become so complicated by the intermolecular torques that the correlation function is approximated by a random exponential decay, with a time constant of about 2.5×10^{-13} seconds. This time constant has been interpreted by Gordon [3] as the average time between changes in the direction of the angular momentum vector describing the rotational motion of the molecule. Apparently the molecules rotate freely for about 2.5×10^{-13} seconds before a "collision" changes the direction of the rotation.

The behaviour of the liquid methane correlation function, shown in figure 4, is similar to the behaviour of the liquid oxygen function described above. After about 2×10^{-13} seconds the action of the intermolecular torques in hindering the rotation becomes evident. After about 3×10^{-13} seconds the decay is again approximately exponential, with a time constant of about 3.5×10^{-13} seconds. The function becomes essentially zero at about 8×10^{-13} seconds.

As expected, the correlation function for the solid initially lies above that of the liquid, indicating that the mean-squared torque is greater than that of the liquid. After about 3.5×10^{-13} seconds the function drops rapidly to slightly below zero, approaching the zero equilibrium value from the negative side of the axis (as shown in fig. 5).

Thus the correlation function analyses of the anisotropically scattered Raman bands of liquid oxygen, and of liquid and solid

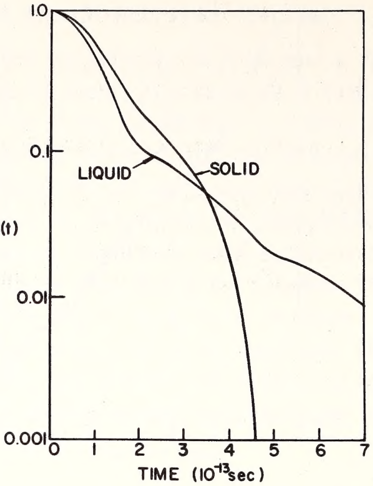

FIGURE 4. The rotational correlation functions computed from the ν_3 Raman band in liquid and solid CH_4. The exponential decay is not as evident in the solid as in the liquid.

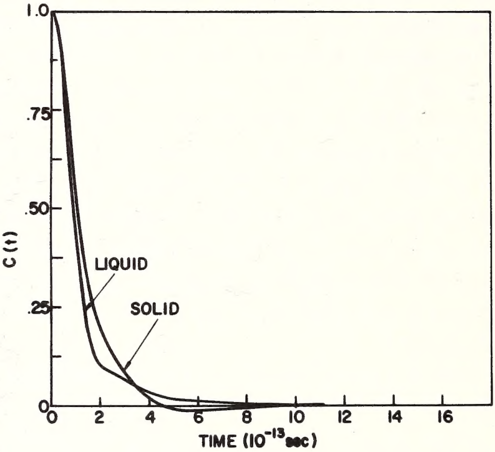

FIGURE 5. The rotational correlation functions computed from the ν_3 Raman band in liquid and solid CH_4. The solid correlation function apparently approaches equilibrium from the negative side of the axis.

methane confirm the conclusion that the rotational motion of these molecules is not free.

I wish to acknowledge gratefully the support and encouragement of Professor H. L. Welsh under whose supervision this work was carried out as part of the research requirements for the degree of Doctor of Philosophy at the University of Toronto.

4. References

[1] M. F. Crawford, H. L. Welsh, and J. H. Harrold, Can. J. Phys. **30,** 81 (1952)

[2] R. G. Gordon, J. Chem. Phys. **39,** 2788 (1963); ibid. **40,** 1973 (1964); ibid. **41,** 1819 (1964).

[3] R. G. Gordon, J. Chem. Phys. **42,** 3658 (1965); ibid. **43,** 1307 (1965); ibid. **44,** 1830 (1966).

[4] M. Blumenfeld and H. L. Welsh, to be published.

[5] R. G. Gordon, private communication (1966).

[6] G. E. Ewing, J. Chem. Phys. **40,** 179 (1964).

[7] G. B. Savitsky and D. F. Hornig, J. Chem. Phys. **36,** 2634 (1962).

CORRELATION OF INFRARED AND INELASTIC NEUTRON SCATTERING SPECTRA OF SOLID METHANE

ASHOK K. AGRAWAL and SIDNEY YIP

Department of Nuclear Engineering, Massachusetts Institute of Technology,
Cambridge, Mass. 02139

It is well known that spectra of infrared absorption, Raman scattering and inelastic neutron scattering all provide information about rotational motions in molecular systems. Recently attempts have been made to correlate these spectra by using time relaxation functions [1],[1] which are obtained from optical band shapes, directly in the analysis of incoherent neutron scattering measurements. The studies thus far have been directed at liquid methane for which optical and neutron data are both available [2, 3]. In this paper we consider similar corelations of infrared and neutron spectra of solid methane near its λ-point. We have obtained an effective frequency spectrum which can be used in cross-section calculations and which is in qualitative agreement with that inferred from the neutron data. We have also deduced an approximate thermodynamic frequency distribution function which leads to a reasonable estimate of the heat capacity.

In the Gaussian approximation the double differential neutron incoherent scattering cross section $\sigma(E_0,E,\theta)$ is completely determined by the mean-square displacement function $W(t)$. For slow neutrons $W(t)$ has contributions from center-of-mass translations and molecular rotations. The rotational contribution can be expressed in terms of the relaxation function $F(t)$, which is the Fourier transform of a normalized infrared absorption band $\hat{I}(\omega)$ [3]. Using measurements at 28 °K[4] we have determined $F(t)$, and the results are shown in figure 1 along with the relaxation function for a free spherical rotor. Curves A and B correspond to slightly different ways of smoothing the experimental $\hat{I}(\omega)$ within the fluctuations in the data. It can be seen that for times less than $t_0 \sim 0.2 \times 10^{-12}$ sec., there is little difference between $F(t)$ (curve A) and the free rotation result. The dimensionless time $t_0^* = (k_B T/I)^{1/2} t_o$ is about 0.55, which is essentially the same as that for liquid methane at 98 °K [1]. Deviation of $F(t)$ from free-rotation behavior beyond t_o indicates the onset of intermolecular torque effects. At long times $F(t)$ appears to approach an exponential

---

[1] Figures in brackets indicate the literature references listed at the end of this paper.

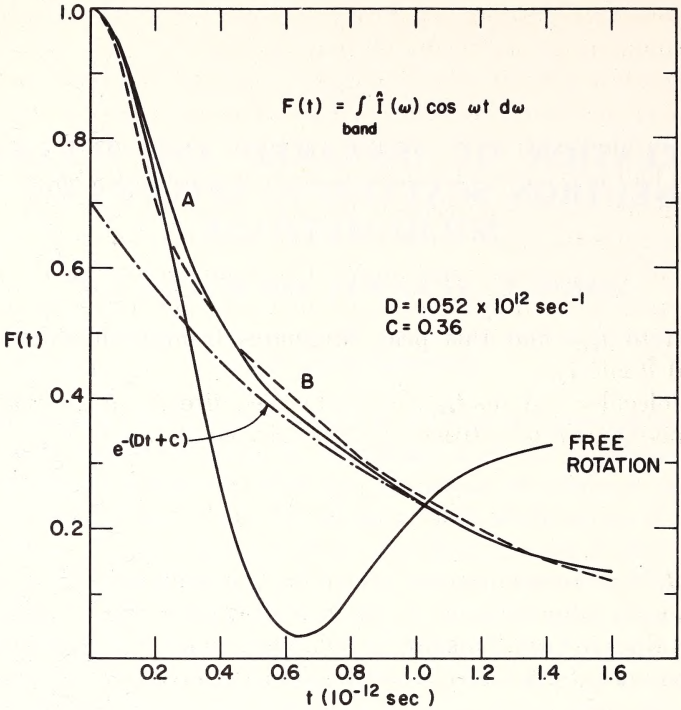

FIGURE 1. Rotational time relaxation function $F(t)$ for solid methane at $T=28$ °K.

decay of the form exp(-Dt-C). The dimensionless rotational diffusion coefficient $D^*=(I/k_BT)^{1/2}D$ turns out to be about 0.4, which is about 40 percent smaller than the corresponding value for the liquid at 98 °K. The value of C seems to be unchanged in the solid and liquid phases.

Measurements of inelastic neutron scattering by solid methane have been recently carried out by Harker and Brugger [5] in the temperature range 5–22.1 °K, and the data used to extract effective frequency distribution functions at various temperatures. In the present approach this distribution function is written as

$$f_{\mathrm{eff}}(\omega)=\frac{\beta/2}{\sinh\beta/2}\, f_T(\omega)+\frac{2Mb^2\omega^2}{3k_BT}\,\hat{I}(\omega) \qquad (1)$$

where $\beta=\hbar\omega/k_BT$, M is the molecular mass, b the scatterer position measured from the center-of-mass, and f_T the normalized spectrum of translational frequencies. The second term in eq (1) clearly represents the rotational contribution. A comparison of eq (1) with the extrapolated result of Harker and Brugger at 22.1 °K is shown in the insert of figure 2 [6]. The infrared data used were those discussed in figure 1 and a Debye spectrum ($\theta_D=150$ °K) was assumed for f_T. By treating translations and rotations separately, we see that in f_{eff} the rotational effects dominate at practically all frequencies.

The absolute magnitudes of $\sigma(E_0,E,\theta)$ at 22.1 °K have been computed using the above frequency spectra. The cross sections computed with an incident spectrum which is taken to be a Gaussian with full width at half maximum of 4 percent, are compared with experimental data in figure 2. The agreement between measurements and results obtained with frequency spectrum A is satisfactory except in the vicinity of energy transfer 7 meV. The shoulder in the theoretical cross section arises from a corresponding peak in the rotational contribution to f_{eff}, and this peak originates from a shoulder in the observed $\hat{I}(\omega)$ [4,7].

For molecular systems f_{eff} can not be used directly in the evaluation of thermodynamic quantities. If we rewrite eq (1) as [8]

$$f_{\mathrm{eff}}(\omega)=\frac{\beta/2}{\sinh\beta/2}\left[f_T(\omega)+\frac{M}{M_r}f_R(\omega)\right] \tag{2}$$

where M_r is a "rotation mass", then an approximate thermodynamic frequency distribution is given by f_T+f_R. Qualitative considerations indicate that for methane M_r should be about $4m_H$, m_H being the hydrogen mass [8]. Following this method we have deduced a thermo-

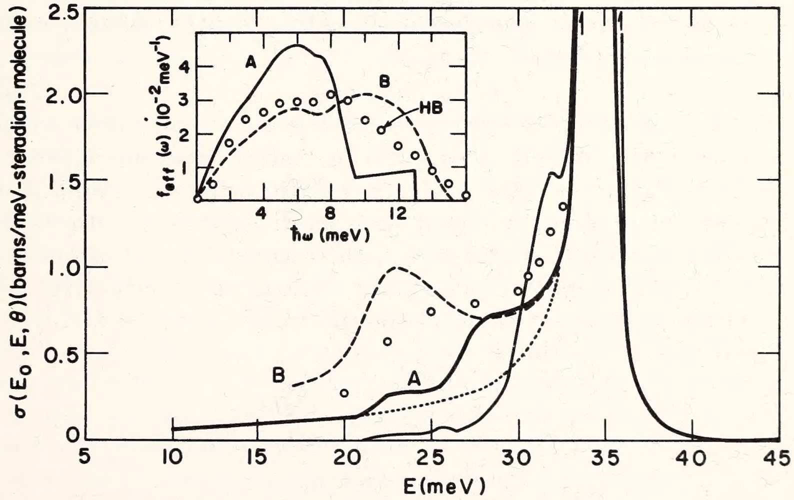

FIGURE 2. Double differential neutron scattering cross section $\sigma(E_0,E,\theta)$ of solid methane at $T=22.1$ °K with $E_0=34.7$ meV and $\theta=15.4°$. Results computed with f_{eff} labeled as A and B are shown as heavy solid and dashed curves respectively. The experimental spectrum (hand smoothed) is shown as a dotted curve. In addition, the cross section computed using the Harker-Brugger f_{eff} is shown by the open circles, and that obtained from a free-rotation theory is shown as light solid curve.

dynamic frequency distribution from spectrum A given in figure 2. The value of M_r deduced from this spectrum is $5m_H$. At 28 °K the value of the specific heat c_v computed with this distribution and assuming a harmonic solid is within the quoted experimental uncertainty [9].

We wish to thank G. E. Ewing and R. M. Brugger for making available large plots of their experimental data. Also we thank H. Prask for the use of a computer program to compute specific heat. This work was supported by Army Research Office—Durham under contract DAHCO4–67–C–0011.

References

[1] R. G. Gordon, J. Chem. Phys. **43,** 1307 (1965).
[2] V. F. Sears, Can. J. Phys. **45,** 237 (1967).
[3] A. K. Agrawal and S. Kip, J. Chem. Phys. **46,** 1999 (1967).
[4] G. E. Ewing, J. Chem. Phys. **40,** 179 (1964).
[5] Y. D. Harker and R. M. Brugger, J. Chem. Phys. **46,** 2201 (1967).
[6] For this comparison we have normalized f_{eff} to have the same area of 0.32 as the Harker-Brugger curve. This normalization is not used in subsequent cross-section calculations.
[7] This shoulder is even more pronounced in the data of G. B. Savitsky and D. F. Hornig, J. Chem. Phys. **36,** 2634 (1962).
[8] S. Yip, H. Prask and H. Boutin, to be published.
[9] J. H. Colwell, E. K. Gill and J. A. Morrison, J. Chem. Phys. **39,** 635 (1963).

THEORY OF PHASE TRANSITIONS IN SOLID METHANES

TSUNENOBU YAMAMOTO, YOSUKE KATAOKA and HIDEO YASUDA

Department of Chemistry, Faculty of Science
Kyoto University, Kyoto, Japan

In the present report we would like to present briefly a quantum mechanical study of the James-Keenan model [1][1] with special emphasis on application to solid light methane.

In 1959 James and Keenan published an elaborate theoretical work on phase transitions in solid heavy methane [1]. It was based on the assumption that the intermolecular interaction which is responsible for the transitions under consideration is essentially the electrostatic octopole-octopole interaction between neighboring molecules. They have succeeded in revealing the main characteristics of three solid phases, I, II, and III, through laborious consideration of the stability of various possible phases, and have reproduced quantitatively the thermodynamical features of the observed double transitions in CD_4 [2].

We have tried to make a *quantum mechanical* continuation of James and Keenan's *classical* theory. At first each of three nuclear spin species A, E, and T were treated separately under the assumption of no interspecies conversion. Then two kinds of mixture of nuclear spin species, normal and equilibrium, were treated with and without the said assumption, respectively. All the calculations were carried out in the framework of the molecular-field approximation method.

Figure 1 shows the upper transition lines of both CH_4 and CD_4.[2] We have made the calculations in the subspace with $J \leqq 9$, J being the rotational quantum number, which is sufficient so long as we are concerned with phenomena below about 30 °K. The value of the coupling parameter at zero pressure can be determined such that the equilibrium mixture of CH_4 has its transition at 20.4 °K, the observed upper transition temperature [3]. Then one sees that solid CH_4 exhibits remarkable *spin-statistics effects*, whereas solid CD_4 does not. From this one infers that the molecules in solid CH_4 are undergoing a sort of *hindered rotation* under the influence from neighboring molecules

---

[1] Figures in brackets indicate the literature references listed at the end of this paper.

[2] The curves for the normal mixtures have already been given by M. J. Freiser, thesis, Purdue University, 1956.

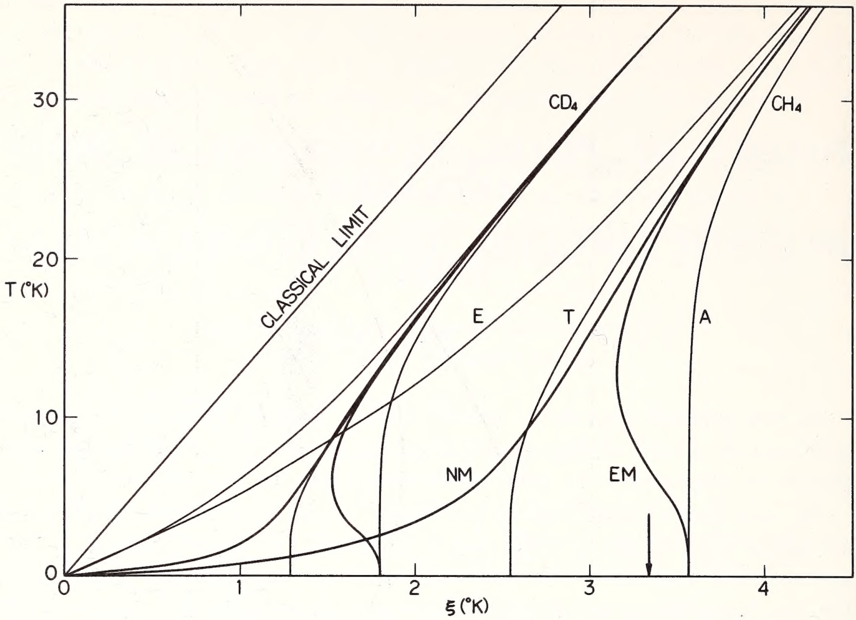

FIGURE 1. Upper transition lines, i.e., transition lines between phases I and II of CH_4 and CD_4. The letters A, E, and T refer to respective pure spin species and NM and EM represent normal and equilibrium mixtures, respectively. The abscissa is the coupling parameter, $\xi = I_3^2/R^7$, I_3 and R being the octopole moment of the methane molecule and the distance between neighboring molecules, respectively. The arrow indicates the predicted value of ξ at zero pressure.

even below the upper transition temperature. On the contrary, in the case of CD_4, one cannot make any definite statement in this respect, because the absence of spin-statistics effects can imply either rotational or librational motion.

We have evaluated the free energies of each of three solid phases, predicted by James and Keenan, for each of the individual species of CH_4 and their mixtures, this time with $J \leqq 4$. Mixtures are assumed to contain A and T species only, species E being omitted for simplicity because of its small concentration. Some results are summarized in figure 2, which shows the phase diagrams of both normal and equilibrium mixtures of nuclear spin species overlapped in one and the same coordinate plane. The shaded region is assigned to the solid state at zero pressure.

Inspection of the figure allows one to make several interesting predictions about the properties of solid CH_4. As regards the normal mixture, the lower transition is expected to occur at about 14 °K. Although such a transition does not seem to have been observed so

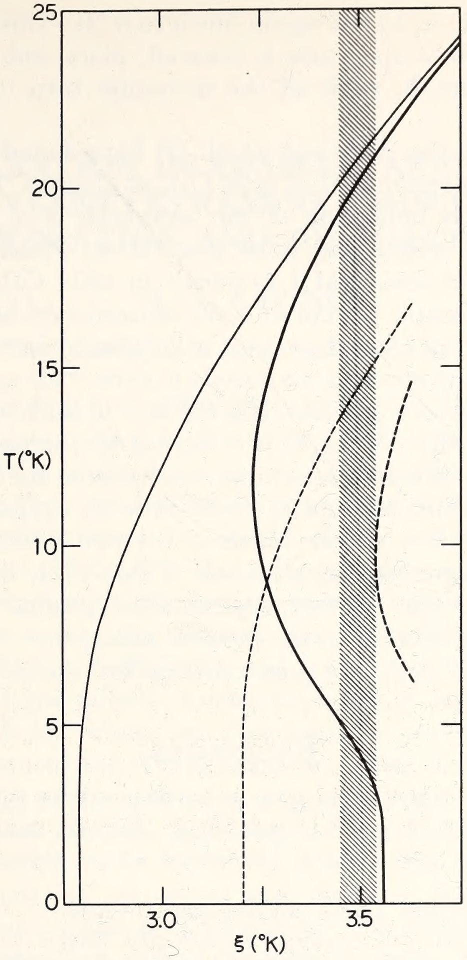

FIGURE 2. Phase diagrams of normal and equilibrium mixtures of species A and T, CH_4. The thin and thick curves correspond to normal and equilibrium mixtures, respectively, and the solid and dotted curves to the upper ($I \rightleftarrows II$) and lower ($II \rightleftarrows III$) transition lines, respectively. The shaded region indicates the solid state at zero pressure.

far, it may be interesting to note that it almost coincides with that which is extrapolated linearly from the observed lower transition line in the CH_4–CD_4 solid solution [4]. The predictions about the behavior of the equilibrium mixture are more complicated and exciting. First of all phase III, which is the lowest-temperature phase in the case of normal mixture, does *not* seem to appear at zero pressure. Even when it does, it can appear only in a narrow temperature region at around 10 °K. Furthermore, if the pressure is increased, the region of phase III increases, which is in accordance with observation [5]. Below about 3 °K we should expect phase I, the highest-temperature disordered phase, to appear again down to 0 °K. This comes from the fact that, as the temperature is lowered, more and more molecules convert to species A, until all the molecules turn to this species at 0 °K.

As is well known, Morrison et al. [7] have found a rather broad anomaly in the specific heat of solid CH_4 at about 8 °K, and proposed to interpret it as indication of the occurence of a lower transition which had been overlooked until then. Now, Pitzer et al. [6] have recently reported that NMR intensity in solid CH_4 increases with time when the sample is kept at some temperature below 10 °K, if it is contaminated by a small amount of oxygen molecules, and that no appreciable change occurs if the sample is pure. This apparently means that the interspecies conversion is prohibited in the lowest temperature region in pure CH_4, but that it is catalyzed by the presence of oxygen molecules. Then one may assign our normal mixture to pure methane and our equilibrium mixture to methane with oxygen. At present it is not easy for us to decide which of the two mixtures corresponds better to the experimental situation of Morrison et al. Thus it is highly desirable that further experimental studies be carried out, particularly calorimetric and infrared-absorption experiments on samples with controlled oxygen content, for the purpose of testing our predictions.

References

[1] H. M. James and T. A. Keenan, J. Chem. Phys. **31,** 12 (1959).

[2] K. Clusius and L. Popp, Z. physik. chem. (Leipzig) **B46,** 63 (1940); J. H. Colwell, E. K. Gill, and J. A. Morrison, J. Chem. Phys. **39,** 635 (1963); **42,** 3144 (1965).

[3] K. Clusius, Z. physik. Chem. (Leipzig) **B3,** 41 (1929).

[4] E. Bartholomé, G. Drikos, and A. Eucken, ibid. **B39,** 371 (1938).

[5] J. S. Rosenshein and W. M. Whitney, Low Temperature Physics, J. G. Daunt et al., Eds., Plenum Press, Inc., New York, p. 1114. (1965).

[6] H. P. Hopkins, Jr., P. L. Donoho, and K. S. Pitzer, J. Chem. Phys. **47,** 864 (1967). See also R. P. Wolf and W. M. Whitney, Low Temperature Physics, J. G. Daunt et al., Eds., Plenum Press, Inc., New York, p. 1118 (1965).

[7] J. H. Colwell, E. K. Gill, and J. A. Morrison, J. Chem. Phys. **36,** 2223 (1962).

NMR RELAXATION IN ADAMANTANE AND HEXAMETHYLENETETRAMINE: MOLECULAR ROTATION AND DIFFUSION

H. A. RESING

U.S. Naval Research Laboratory, Washington, D.C. 20390

The molecular structure of hexamethylenetetramine (HMT) differs from that of adamantane, $C_{10}H_{16}$, only in the replacement of four bridgehead carbon atoms by nitrogen. Both solids melt at about 270 °C. Despite these similarities the crystal structure of HMT is bcc, while that of adamantane is fcc above -65 °C and tetragonal below. A very significant difference is that adamantane is a "plastic crystal" (easily undergoes plastic deformation) while HMT is not. The underlying thesis here is that the difference in plastic behavior is due to a difference in diffusion coefficients, and it is the purpose of this work to measure this latter difference using those NMR methods (relaxation in the local field [1])[1] which are most sensitive to diffusional motion.

We have measured the NMR relaxation times (both in the laboratory and rotating reference frames) and have interpreted the data in terms of molecular rotation and diffusion. The barriers to rotational motion are 19 kcal/mole for HMT, 3.1 kcal/mole for fcc adamantane, and 6.1 kcal/mole for tetragonal adamantane. The barrier to self diffusion for adamantane is 34 kcal/mole; this extremely large value shows that the repulsive part of the intermolecular potential must be quite steep, i.e., adamantane is indeed a hard sphere. While the adamantane diffusional jump time could be followed over nearly seven powers of ten, that for HMT is so long at all temperatures that it has no observable effect on NMR relaxation. At 270 °C therefore, the adamantane diffusion coefficient must be at least five orders of magnitude greater than that for HMT. The adamantane data are shown in figure 1.

Of particular interest in the context of this meeting is the rotation in the high-temperature adamantane phase and in HMT. From figure 1 it can be shown that at the melting point the time between rotational jumps in adamantane is about 2×10^{-12} sec, which is roughly the same as a librational period. Thus the harmonic approximation in lattice dynamics [2] (i.e., small displacements from the equilibrium position) is clearly not valid for adamantane. This conclusion is in accord with

---

[1] Figures in brackets indicate the literature references listed at the end of this paper.

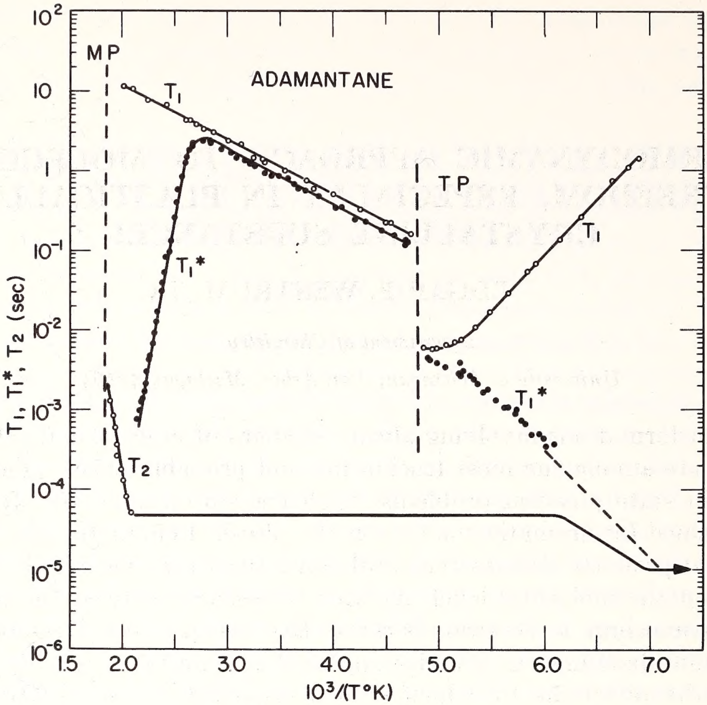

FIGURE 1. Relaxation times for adamantane: T_1, spin-lattice relaxation time; T_1*, spin-lattice relaxation time in the local field; T_2, spin-spin relaxation time; solid line represents broad-line measurements of Douglas and McCall [4].

some recent slow neutron scattering results [3]. Because of the higher rotational barrier in HMT the harmonic approximation is better for this solid.

References

[1] D. C. Ailion and C. P. Slichter, Phys. Rev. **137,** A235 (1965).
[2] G. Dolling, this volume.
[3] R. Stockmeyer and H. H. Stiller, Phys. Stat. Solidi **19,** 781 (1967).
[4] D. C. Douglas and D. W. McCall, J. Chem. Phys. **33,** 777 (1960).

THERMODYNAMIC APPROACH TO MOLECULAR FREEDOM, ESPECIALLY IN PLASTICALLY CRYSTALLINE SUBSTANCES

EDGAR F. WESTRUM, JR.

Department of Chemistry
University of Michigan, Ann Arbor, Michigan 48104

Transformations involving abrupt changes of molecular freedom in solids are among the most fascinating and probably least understood of solid state physical problems. Such transformations are often accompanied by dramatic changes in the physical characteristics seemingly disproportionate to the subtle structural metamorphoses which occur at the molecular level. As we have seen already exemplified in this symposium, a transition is rather like the elephant in the fable of the nine blind men in that its apparent manifestation is dependent upon the technique by which it is approached.

Although many experimental techniques have been shown to provide penetrating insight into the nature and mechanism of molecular freedom in crystalline substances, the solid state researcher is so often occasioned to acknowledge the extraordinary yield of information obtainable from cryogenic thermal capacity determinations that he is tempted to attribute a more fundamental significance to such measurements than to any single method of investigation. Certainly determinations of heat capacity and related thermal phenomena have already contributed much to the interpretation of molecular dynamics as a sensitive parameter of the energetics spectrum of substances and the Gibbs energies and entropies of phases and their transitions. In addition, calorimetric data are particularly relevant for treatment of order-disorder phenomena even at elevated temperatures. An example of such an approach to transitions in which the entropy may be evaluated by $\Delta S = R \ln Q$ is that of succinonitrile [1],[1] $[NC(CH_2)_2CN]$, which, although obviously not very globular in its molecular shape, nonetheless evidences a plastically crystalline phase. X-ray diffraction analysis indicates Crystal II to be completely-ordered monoclinic (consisting only of *gauche* molecular forms), whereas infrared data show Crystal I to be a highly-disordered, body-centered cubic phase (composed of a temperature-dependent, equilibrium mixture of *gauche* and *trans* geometrical isomers).

---

[1] Figures in brackets indicate the literature references at the end of this paper.

In solid-solid transitions in which order-disorder effects predominate, the entropy change may be approximated by $\Delta St = R \ln Q$, in which Q is the ratio of the number of orientational states statistically occupied in the two phases. In the case of succinonitrile, the disordering at the 223.3 °K. transition arises from four terms: (*i*) alignment of the principle axis of the molecule with the cube diagonals ($R \ln 4 = 2.755$ e.u.), (*ii*) rigid rotation of the molecule about this axis ($R \ln 2 = 1.377$), (*iii*) entropy of mixing *gauche* and *trans* isomers ($-R[X_t \ln X_t + X_g \ln X_g - X_g \ln 2] = 2.08$), (*iv*) volume change of the lattice on transition ($R \ln [V_2/V_1]$; "free" volume$=0.18$). The sum of these four calculated contributions, $\Delta St = 6.39 \pm 0.09$ e.u., is in excellent accord with the experimental value, 6.35 ± 0.03 e.u.

The low entropy of melting, 2.68 e.u., at $T_m = 331.3$ °K. indicates that the Crystal I phase of succinonitrile is indeed plastically crystalline. The agreement obtained between the third-law entropy of the gas, 79.04 ± 0.10 e.u. at 298.15 °K., and the corresponding value obtained from the spectroscopic data, 79.09 ± 0.10 e.u., is ample indication of the absence of residual disorder in the structure in Crystal II and justifies the assumptions implicit in calculating the contributions to the entropy.

A similar approach has been used to elucidate the mechanism of transition in the symmetrical-top molecules of table 1 [2]. These bicyclo-hydrocarbon molecules provide interesting symmetry-sensitive regularities.

Guthrie and McCullough [3] treated ΔSt for simple tetrahedral molecules stochastically and concluded that a minimum of about ten distinguishable molecular orientations exists at each lattice site for substances normally considered to be plastic crystals. In this light, rotation can be more adequately described in terms of orientational disorder, with the molecules "flipping" rapidly into discrete, distinguishable positions in the crystal lattice. The treatment of such changes in structure must be applied cautiously, however, until it is more adequately tested by careful crystallographic studies, for there is considerable uncertainty in the magnitude of the vibrational contribution. To minimize this uncertainty, the approach of Guthrie and McCullough may need to be modified by making heat capacity measurements on the high temperature form undercooled to near 0 °K. We are presently endeavoring to do this, and if successful and unhindered by complicating transitions involving metastable phases, we should be able to evaluate $\Delta St_{(0\ \mathrm{oK})}$ and thereby perhaps make an even more convincing interpretation for adamantane [4].

Although the great success of thermodynamics in the determinations of molecular structures has been evident for nearly two decades, this work has been done largely on gaseous molecules. In determining

TABLE 1. Transition data on crystals formed by symmetrical top globular molecules [a]

Compound	T_t	ΔSt	T_m	ΔSm	$\Delta St+\Delta Sm$
Bicyclo[2.2.2]octane	164	6.66	447	4.48	11.14
Bicyclo[2.2.2]octene-2	111	0.78	389	2.43	10.87
	176	7.66			
Bicyclo[2.2.1]heptane	131	7.53	360	3.03	10.62
	306	0.06			
Bicyclo[2.2.1]heptene-2	129	8.98	320	2.43	11.41
Bicyclo[2.2.1]heptadiene-2,5	202	10.57	254	1.58	12.15
Nortricyclene	173	9.0	330	2.5	11.5
1-Azabicyclo[2.2.2]octane	198	6.34	433	3.2	9.54
1,4-Diazabicyclo[2.2.2]-octane	351	7.19	433	4.10	11.29
3-Azabicyclo[3.2.2]nonane	298	11.63	467	3.55	15.18
3-Oxabicyclo[3.2.2]nonane	208	8.22	448	3.61	11.83
The four compounds listed below were studied in the U.S.S.R.:					
Exo-2-cyanobicyclo-[2.2.1]heptane	238	7.79	300	2.34	10.13
Endo-2-cyanobicyclo-[2.2.1]heptane	177	2.82	332	2.13	4.95
Exo-2-methylbicyclo-[2.2.1]heptane	152	7.38	387	1.40	8.78
Endo-2-methylbicyclo-[2.2.1]heptane	160	(?)	164	(?)	12.21

[a] Units: cal., mole, °K.

structures from vapor heat capacities and "third-law" gaseous entropies, the statistical mechanical quantities are usually calculated on the basis of some assumed value and then compared with the measured value. However, utilization of the third-law entropy of the gas requires that the low-temperature, solid-phase heat capacity be augmented by enthalpy of vaporization or sublimation, vapor pressure measurements, and equation of state data for the vapor.

The advantages of determining barrier heights exclusively from crystalline phase heat capacities have recently been demonstrated by Wulff [5]. His method involves the evaluation of the heat capacity contributions of a crystal from (*i*) the intermolecular (lattice) vibrations, (*ii*) the intramolecular vibrations (calculated within the harmonic oscillator approximation by combination of Einstein functions based upon the observed spectra), (*iii*) $C_p - C_v$ (resulting from the expansion of the lattice as occasioned by the anharmonicities of the vibrations), and (*iv*) the internal rotational freedom. Although barriers in the crystalline state potentially involve intermolecular forces which are absent from the gaseous phase, excellent accord between barrier values for gases and crystals has been obtained.

A similar ΔSt approach has been used on ionic crystals, and in the absence of disordering transitions, the resolution of the heat capacity contribution has provided an elucidation of the dynamics of symmetrical ions.

References

[1] C. A. Wulff and E. F. Westrum, Jr., J. Phys. Chem. **67,** 2376 (1963).

[2] Based largely on unpublished studies from the author's research group at Ann Arbor.

[3] G. B. Guthrie, Jr. and J. P. McCullough, J. Phys. Chem. Solids **18,** 53 (1961).

[4] S. S. Chang and E. F. Westrum, Jr., J. Phys. Chem. **64,** 1547 (1960).

[5] C. A. Wulff, J. Chem. Phys. **39,** 1227 (1963).

SPECTRAL ASSIGNMENT IN INELASTIC NEUTRON SCATTERING SPECTROSCOPY BY ATOMIC SUBSTITUTION TECHNIQUES

J. W. WHITE

Physical Chemistry Laboratory, Oxford, England

1. Introduction

When a beam of monoenergetic slow neutrons falls on a sample containing hydrogen (which may be a molecular crystalline solid), the neutrons are scattered incoherently. If the energies of the outgoing neutrons are analysed it is found that some are scattered without any change in energy, whilst others gain or lose energy by their interaction with the molecular modes in the lattice. Measurements of the amount of energy gained by these inelasticly scattered neutrons, when very cold incident neutrons are used, lead directly to the energies of the molecular states responsible for the scattering. The technique resembles closely the Raman scattering of light, which has traditionally been a source of molecular motional constants.

There are two particular virtues of the neutron scattering method which shall concern us in this paper. Firstly, transitions between molecular and crystal states which cannot be seen by optical spectroscopy because they are forbidden by optical selection rules, are observable by neutron scattering. This comes about because the neutron interacts with the molecular vibrations etc., through the neutron-nucleus interaction rather than indirectly through the electron cloud as is the case with light. Secondly the intensities of scattering in largely incoherent systems, such as those containing hydrogen, can be directly related through their angular dependence to the amplitudes of motion associated with particular vibrational frequencies. Under these circumstances it is highly desirable to be able to separate out the neutron inelastic scattering spectrum into contributions from different parts of the molecule, so that the frequencies and the amplitudes for these parts can be determined separately.

In the experiments reported here molecules with two hydrogenous scattering centres, such as CH_3OH, have been studied with cold neutron inelastic scattering. So long as the scattering from each centre in a molecule is largely incoherent, the differential scattering cross section of a molecule with two scattering centres can be written

$$\frac{\partial^2\sigma}{\partial\Omega\partial\omega}=\frac{k}{k_o}\{b_1^2S_1(\mathbf{Q},\omega)+b_2^2S_2(\mathbf{Q},\omega)\} \tag{1}$$

where $\frac{\partial^2\sigma}{\partial\Omega\partial\omega}$ is the differential scattering cross section with respect to fractional angle of scattering $\partial\Omega$ and fractional energy transfer $\partial\omega$ (in frequency units). It is equal to the intensity of the scattering spectrum if the incident neutrons are well defined in collimation and energy. $\mathbf{k}$ and $\mathbf{k}_o$ are the scattered and incident wavevectors of the neutron respectively, $\mathbf{Q} = \mathbf{k}\text{-}\mathbf{k}_o$ is the momentum transferred in the collision, ω is the energy transferred in the collision (in radians $\sec^{-1}$) and $S_j(\mathbf{Q},\omega)$ is the scattering law for the jth different molecular group and is defined by

$$S_j(Q,\omega)=\iint\exp\{i(\mathbf{Q}\cdot\mathbf{r}-\omega t)\}G_j(\mathbf{r},t)d\mathbf{r}dt \tag{2}$$

This is the double fourier transform of the space-time correlation function $G_j(\mathbf{r},t)$ which describes fully the motion of the scattering centre j [1, 2].[1]

It is because of the very explicit connection between the equation of motion of the scattering centre and the neutron scattering spectrum described in the above equation, that there are no selection rules for the spectrum and that there is the possibility of determining the amplitudes of motion from the intensities. In addition the additivity of the spectra contained in eq (1) for incoherent scattering makes the atomic substitution techniques described in this paper possible.

The experiments described were carried out using the cold-neutron time of flight spectrometer on the DIDO reactor at A.E.R.E. Harwell. This has been described by Harris et al. [3]. The incident wavelength was 5.3Å and the energy resolution was approximately 7 percent. Samples of the methanols and acetic acids were especially dried and had purities above 99 percent. There was little change in the spectrum on freezing except in the quasielastic region. All samples were kept as thin as possible to make sure that the scattering at no time exceeded 15 percent and was generally less than 10 percent.

2. Frequency Assignment

Figure 1 shows the elastic and inelastic components of the neutron scattering spectrum from liquid CH_3OH. In the inelastic region the large broad band at a time of flight of about 500 microsec/metre extends from energy transfers of about 20 cm^{-1} to about 300 cm^{-1}.

---

[1] Figures in brackets indicate the literature references at the end of this paper.

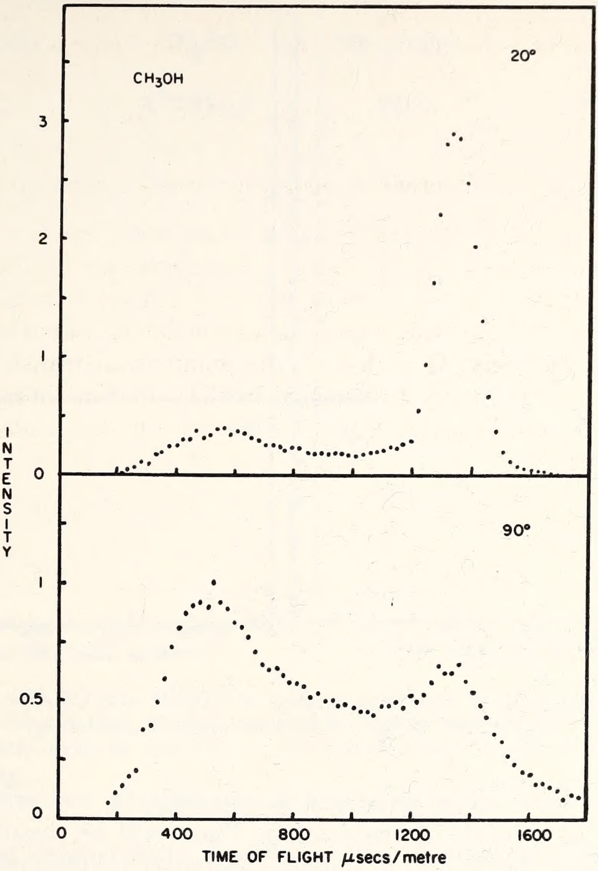

FIGURE 1. Cold neutron scattering spectrum of methanol, CH_3OH, in the liquid state at 300 °K for 20° and 90° angle of scattering.

In this region there must be motions due to the methyl group torsion or hindered rotation, as well as to the OH hydrogen bond bending motions. These two regions cannot be resolved from this spectrum alone. The spectra shown were taken at angles of scattering of 20° and 90° from the incident beam to show the considerable variation of intensity with angle.

In figure 2 the spectra of CD_3OH and CH_3OD taken again at 20° and 90° angles of scattering from the incident beam are shown. The marked change in the inelastic region on substituting D_3 for H_3 is clear from figure 2. The large band at about 400 microsec/metre must be assigned to a CH_3 motion as it has largely disappeared in CD_3OH and returns in CH_3OD. Again, the region near 800 microsec./metre can be assigned to the OH motions as these are much less sensitive to the deuteration. Very large changes in the angular de-

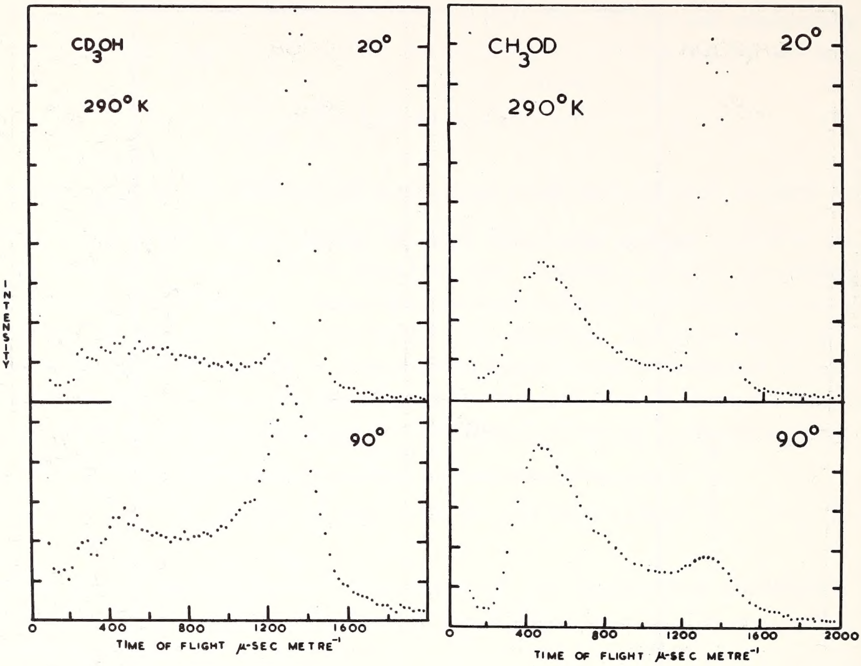

FIGURE 2. Cold neutron scattering spectra of CD_3OH and CH_3OD in the liquid state at 300 °K for 20° and 90° angle of scattering.

pendence of both the inelastic and the quasielastic scattering can also be noticed as a result of deuteration. These will be mentioned later and have been the subject of a more exhaustive investigation [4].

Since isotopic substitution decreases the contribution from a particular scattering law ($S(\mathbf{Q}, \omega)$ in eq 1) to the inelastic spectrum by reducing the value of b_j^2, the same qualitative effect can be achieved by replacing the atoms in a group, not by another isotope of lower scattering power but by another atom of different scattering power, such as fluorine. Figure 3 shows the inelastic scattering spectra of acetic and trifluoroacetic acids taken at 20° and 90° scattering from the incident neutron beam. In the acetic acid spectrum it is clear that again there is the large band which contains both the CH_3 group and the OH group motions for the system. Comparing, say, the 20° spectra the effect of fluorine substitution is very noticeable and the large contribution of the CH_3 group motion to the spectrum is evident. On careful examination of the 90° spectra where inelastic scattering is more probable, it can be seen that at about 700 microsec/metre there is a broad band, or step extending from the inelastic region, which can be assigned to the OH motion in CF_3COOH. Strong angular-dependent effects of substitution are again noticeable.

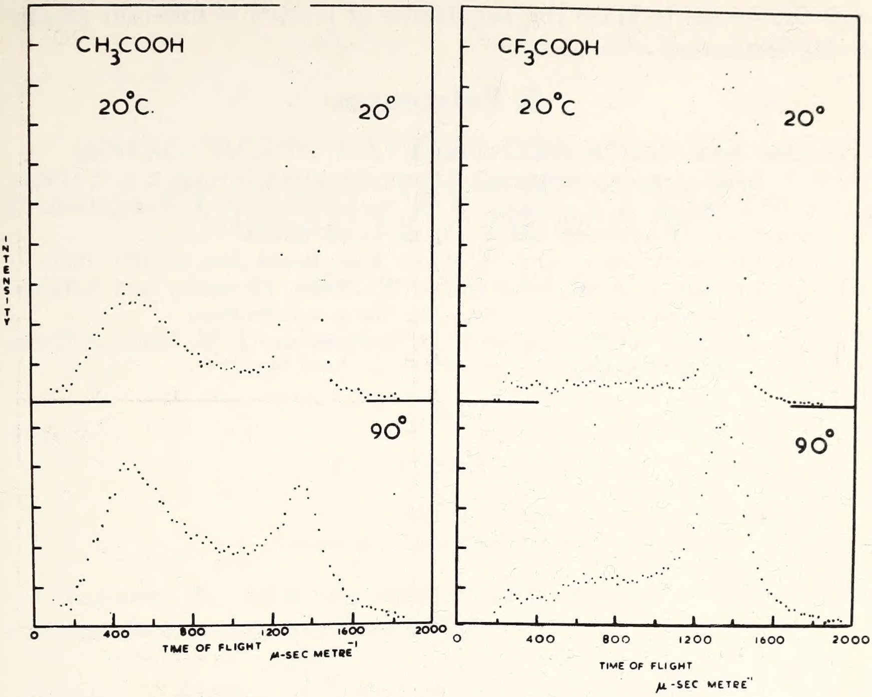

FIGURE 3. Cold neutron scattering spectra of acetic acid (CH_3COOH) and trifluoroacetic acid at 300 °K in the liquid state for 20° and 90° angle of scattering.

3. Motional Amplitudes

It can be noticed from figures 2 and 3 that atomic substitution causes the angular dependence of both the inelastic intensity and the elastic intensity in the neutron scattering spectrum to be modified. In a simple one-phonon harmonic approximation amplitudes of motion may be calculated from the angular dependences [5]. Since the intensity in substituted molecules comes largely from the remaining hydrogen the amplitudes of the motions associated with separate groups may be determined individually. The generality of these ideas is being explored.

4. Conclusion

It is possible by means of isotopic or atomic substitution to assign different parts of the inelastic scattering spectrum from hydrogenous systems to the motion of different parts of the molecules concerned. This seems to be true both for simple molecular systems such as liquids and solids and also for application to polymers containing simple units. Preliminary results on these experiments are presented [6].

Atomic substitution also leads to marked changes in the angular dependence of the inelastic and the quasielastic scattering intensity, and this seems to allow the amplitudes of motion of different groups to be determined separately.

5. References

[1] L. Van Hove, Phys. Rev. **95,** 249 (1954).
[2] K. E. Larson Inelastic Scattering of Neutrons, IAEA, Vienna, **2,** p. 3, (1965).
[3] D. H. C. Harris, S. J. Cocking, P. A. Egelstaff and F. J. Webb, Inelastic Scattering of Neutrons, IAEA, Vienna, **1,** 107 (1963).
[4] B. K. Aldred, R. Eden and J. W. White, Disc. Farad. Soc. **43,** 169 (1967).
[5] J. S. Downes, P. A. Egelstaff and J. W. White, Chemistry and Industry (1967). (Special number on Molecular Sieves and Zeolites).
[6] For application to polymers, see G. F. Lowgster and J. W. White, J. Chem. Phys. **48,** 5271 (1968).

ANISOTROPIC LATTICE DYNAMIC STUDIES OF ORGANO-TIN COMPOUNDS BY MÖSSBAUER SPECTROSCOPY

HANS A. STÖCKLER

Department of Chemical Physics
National Lead Co., Hightstown, New Jersey 08520

and

HIROTOSHI SANO

Department of Chemistry
Ochanomizu University, Tokyo, Japan

The area, A_i, under the ith absorption line of a normalized Mössbauer-effect energy spectrum is [1].[1]

$$A_i = f_s \int_{-\infty}^{\infty} \Big[1 - \exp\left(-f_a(\theta, \varphi) W \sigma_i(E, \theta, \varphi)\right)\Big] dE \tag{1}$$

where $\sigma_i(E, \theta, \varphi)$ is the energy-dependent gamma ray absorption cross-section for the ith nuclear transition, when the principal axis of the perturbing field is oriented at spherical angles θ and φ relative to the incident (or emitted) photon beam. f_s is the source recoilless fraction and $f_a(\theta, \varphi)$ is the angular dependent probability of recoilless γ-ray absorption in the target material. f_a is related to $\mathbf{k}$, the wave vector of the γ-radiation, and to $\mathbf{u}_r$, the ensemble average of the instantaneous displacement of the rth absorbing nucleus from its mean position.

In the harmonic approximation [2],

$$f_a = \exp\left[-\langle(\mathbf{k} \cdot \mathbf{u}_r)^2\rangle\right] \tag{2}$$

Eq 2 is analogous to the Debye-Waller factor for x-ray scattering [3, 4].

It has been shown that the instantaneous mean-square vibrational amplitude, $\langle u_r^2 \rangle$, is significantly smaller in organometallic tin compounds where the Mössbauer ^{119}Sn atom is directly bonded in a three-dimensional polymeric network lattice [5]. Similarly, $\langle u_r^2 \rangle$ for ^{119}Sn in linear-chain polymers, e.g., $[(CH\ )_3SnF]_n$, is considerably smaller compared to a typical monomeric molecular unit such as

---

[1] Figures in brackets indicate the literature references at the end of this paper.

$(CH_3)_4Sn$, especially at higher temperatures. It was also found that these randomly oriented one-dimensional polycrystalline polymers displayed temperature-dependent asymmetric quadrupole doublet line intensities due to the anisotropic recoilless fraction associated with each nuclear spin state ($\pm 3/2$, $3/2+$ and $\pm 1/2$, $3/2+$), i.e., the Karyagin effect [6, 7, 8, 9].

The present investigation includes the analysis of a typical organotin layer structure, viz, $[(CH_3)_2SnO]_n$. The tin in dimethyltinoxide is pentacoordinated with three nearest-neighbor oxygen atoms to form a two-dimensional polymeric CdI_2-type layer lattice [10] with a well-ordered intermolecular arrangement [11]. The present isomer shift and quadrupole splitting data support the earlier [11] conclusion that the tin-oxygen bond is relatively ionic with perhaps a minimum of dative bond character which presumably gives rise to a pseudo-ionic lattice structure. $[(CH_3)_2SnO]_n$ is being compared here with a typical monomeric trigonal bipyramidal covalent compound $(CH_3)_3SnCl\cdot$pyridine [12].

The isomer shifts, with respect to SnO_2, for $[(CH_3)_2SnO]_n$ and $(CH_3)_3SnCl\cdot$pyridine are 0.93 ± 0.09 mm/sec and 1.33 ± 0.09 mm/sec, respectively. This means that the *s*-electron density, $\Sigma\psi_s^2(0)$, at the tin nucleus is less in $[(CH_3)_2SnO]_n$ than in $(CH_3)_3SnCl\cdot$pyridine. The quadrupole splitting for $[(CH_3)_2SnO]_n$ is 2.07 ± 0.09 mm/sec, while it is 3.44 ± 0.09 mm/sec for $(CH_3)_3SnCl\cdot$pyridine.

Figure 1 shows $<u_r^2>$, in (angstroms)^2 versus temperature, in degrees Kelvin, for $(CH_3)_3SnCl\cdot$pyridine (curve 1) and $[(CH_3)_2SnO]_n$ (curve 2.) The lattice-dynamic behavior can be interpreted by considering the anisotropic mean-square displacement tensor [13, 14], $\mathbf{U}^r$. We have

$$<u_r^2> = \sum_{i,j=1}^{3} U^r_{ij}\, l_i l_j + \sum <u_r^2>_d \tag{3}$$

where $<u_r^2>_d$ corresponds to non-rigid-body distortional vibrations [15]. The contribution of internal modes (e.g., high frequency infrared active modes) to $<w_r^2>$ is probably much less significant than that of lattice modes. Using the analysis suggested in reference 14, we have

$$U^r_{ij} = T_{ij} + G_{ijkl} L_{kl} + H_{ijkl} S_{kl} \tag{4}$$

where $\mathbf{T}$ is the translation tensor, $\mathbf{L}$ is the libration tensor, and $\mathbf{S}$ is the tensor that correlates translation and libration. $\mathbf{U}^r$ represents a vibrational ellipsoid in $<u_r^2>$—space with components $<u_r^2>_x$, $<u_r^2>_y$, and $<u_r^2>_z$. It is expected that the components of $\mathbf{U}^r$ will be smaller for a polymeric layer structure at almost all temperatures. Thus, $<u_r^2>$ for $[(CH_3)_2SnO]_n$ and $(CH_3)_3SnCl\cdot$pyridine is 0.0053Å^2 and 0.0107Å^2 at 70 °K, while at 170 °K it is 0.0151Å^2 and 0.0285Å^2, respectively.

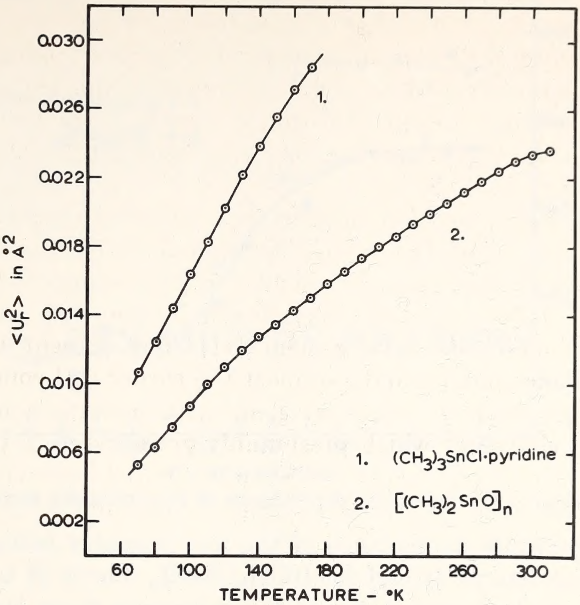

FIGURE 1. Mean-square vibrational amplitudes, $<u_r^2>$, versus temperature for $(CH_3)_3SnCl \cdot$pyridine and $[(CH_3)_2SnO]_n$.

The lattice-dynamic spatial anisotropy associated with a polymeric layer structure can be determined by measuring the relative line intensities of quadrupole doublets in polycrystalline material. The line intensities are determined by the total radiative transition probabilities, $I_\pm$, and the recoilless fraction. Thus, the total relative intensity ratio is

$$\left[\frac{I_2}{I_1}\right]=\frac{\int_0^{2\pi}\int_0^{\pi} I_+[\theta,\ \varphi;h(T))f_a(\theta,\ \varphi;g(T)]\sin\theta d\theta d\varphi}{\int_0^{2\pi}\int_0^{\pi} I_-[\theta,\ \varphi;h(T))f_a(\theta,\ \varphi;g(T)]\sin\theta d\theta d\varphi} \tag{5}$$

I_2 corresponds to the line component with higher energy. For a molecular system with an axially-symmetric electric field gradient (*efg*) tensor and with vibrational symmetry, i.e., $<u_r^2>_x=<u_r^2>_y$,

$$\left[\frac{I_2}{I_1}\right]=\frac{\int_0^{\pi}[(1+\cos^2\theta)f_a(\theta;g(T)]\sin\theta d\theta}{\int_0^{\pi}[(5/3-\cos^2\theta)f_a(\theta;g(T)]\sin\theta d\theta} \tag{6}$$

It is assumed that the principal axes of the efg tensor and $\mathbf{U}^r$ coincide and that $I_\pm$ is temperature independent.

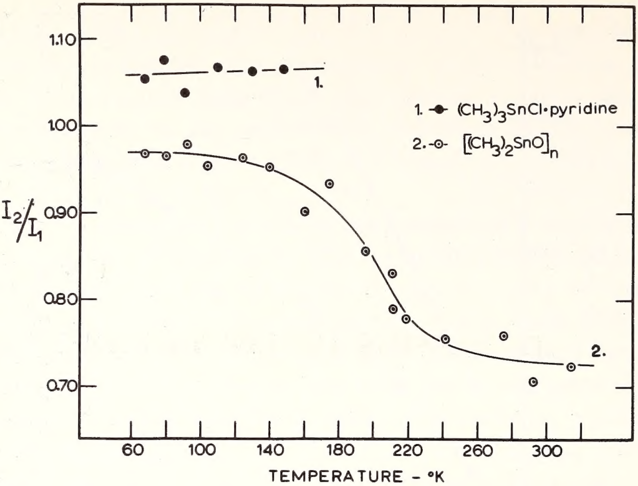

FIGURE 2. Temperature dependence of line-intensity ratios.

The temperature dependence of the line intensity ratio for $(CH_3)_3SnCl\cdot$pyridine (curve 1) and for $[(CH_3)_2SnO]_n$ (curve 2) is illustrated in figure 2. At low temperatures, the polymeric layer lattice (curve 2) can be approximated by a vibrational sphere, i.e., $\langle u_r^2\rangle_x \approx \langle u_r^2\rangle_y \approx \langle u_r^2\rangle_z$. At high temperature a significant anisotropic thermal behavior is observed for the layer type polymer. The eccentricity of the vibrational ellipsoid is maximized with $(\langle u_r^2\rangle_x \approx \langle u_r^2\rangle_y) \neq (\langle u_r^2\rangle_z)$.

The lattice-dynamic anisotropy arises from the strong intermolecular forces operating in the plane of the layer network, whereas weaker short-range forces are effective between the layers. The monomeric crystal $(CH_3)_3SnCl\cdot$pyridine (curve 1) displays an almost isotropic behavior, although small deviations from isotropy, i.e., $(I_2/I_1) \neq 1$, are expected due to the characteristic molecular packing in such organotin compounds.

References

[1] G. Lang, Nucl. Instr. Methods **24,** 425 (1963).
[2] L. van Hove, Phys. Rev. **95,** 249 (1954).
[3] H. J. Lipkin, Ann. Phys. (N.Y.) **26,** 115 (1964).
[4] R. L. Mössbauer and D. H. Sharp, Rev. Mod. Phys. **36,** 410 (1964).
[5] H. A. Stöckler, H. Sano, and R. H. Herber, J. Chem. Phys. **47,** 1567 (1967).
[6] H. A. Stöckler and H. Sano, Phys. Rev. **165,** 406 (1968).
[7] H. A. Stöckler and H. Sano, Physics Letters **25A,** 550 (1967).
[8] S. V. Karyagin, Dokl. Akad. Nauk. (S.S.S.R.) **148,** 1102 (1963); English transl.: Proc. Acad. Sci. U.S.S.R., Phys. Chem. Sect. **148,** 110 (1963).
[9] S. V. Karyagin, Fizika Tverdogo Tela **8,** 1739 (1966); English transl.: Soviet Physics—Solid State **8,** 1387 (1966).
[10] D. L. Alleston, A. G. Davies, and M. Hancock, J. Chem. Soc., 5744 (1964).
[11] W. T. Reichle, J. Polymer Science **49,** 521 (1961).
[12] R. Hulme, J. Chem. Soc. **287,** 1524 (1963).
[13] E. W. J. Cruickshank, Acta Cryst. **9,** 754 (1956).
[14] V. Schomaker and K. N. Trueblood, Acta Cryst. **21,** A247 (1966).
[15] K. Lonsdale, Acta Cryst. **14,** 37 (1961).

DYNAMICS OF POLYMERS

RELAXATION IN SOLID POLYMERS [1] [1]

David W. McCall

Bell Telephone Laboratories
Murray Hill, New Jersey 07971

1. Introduction

In this paper we make an attempt to summarize the present state of knowledge relating to molecular motions in solid polymers [2]. The discussion is concerned only with organic materials of high molecular weight, in the glassy, crystalline and rubbery states. Oriented materials will not be discussed. Even with these restrictions the existing literature on the subject, both experimental and theoretical, is very large. The aim is doubtless presumptuous and the attempt can only be partially fulfilled.

A survey of available experimental data has been conducted and the results are presented in the form of "transition maps." Dielectric, dynamic mechanical, nuclear magnetic resonance and some dynamic birefringence results are included. These transition maps locate the relaxation processes with respect to frequency and temperature. The fact that the various techniques yield points tending to lie on the same loci is taken as empirical evidence that common molecular motions are responsible for the various experimental observations. That is to say, the different experimental methods are sensitive at the same relaxation frequencies, and these frequencies can often be identified with motions of specific molecular groups.

Transition maps say rather little about relaxation strengths or intensities. Very often the intensities for corresponding relaxation mechanisms differ markedly. For example, a very weak dielectric loss may lie on the same transition map locus as a very strong mechanical loss. Further, in a material showing two transition loci, one transition may be stronger in the dynamic mechanical sense while the other is stronger in the dielectric sense. To understand this feature it is necessary to look into the manner in which the experiment couples to the molecular motion. This is a difficult problem even in the most favorable circumstances.

In NMR and dielectric relaxation experiments the experimenter imposes a force field that is nearly uniform throughout the specimen.

---

[1] Figures in brackets indicate the literature references at end of this paper.

The interaction between the field and the specimen can be written down in molecular terms with some considerable confidence. For example, there is no doubt that dielectric relaxation in many systems can be properly described in terms of the time dependence of the orientation of permanent electric dipoles. The energy of interaction with an applied field **F** is simply $E = -\boldsymbol{\mu}\cdot\mathbf{F}$. Similarly, NMR can be analyzed in terms of molecular reorientation and diffusion.

In dynamic mechanical experiments it is less certain that the forces applied to the surfaces of the specimen will be transmitted uniformly throughout the volume of the specimen. Many polymers exhibit a complex crystalline-amorphous morphology and the mechanical properties of the amorphous parts may differ by orders of magnitude from the mechanical properties of the crystalline parts even though the dielectric properties differ only slightly. This matter complicates the dynamic mechanical problem enormously, and much remains to be done on both experimental and theoretical aspects of the problem. Progress in this line could greatly enhance the usefulness of dynamic mechanical measurements.

Inasmuch as we shall refer frequently to relaxation frequencies, correlation times and relaxation times it is in order to discuss these parameters briefly. By relaxation time we mean the characteristic time associated with *macroscopic* experimental effects. Generally it is taken to be the reciprocal of a frequency of maximum loss. A correlation time is a time associated with events on a *molecular* scale. As it turns out the distinction is numerically unimportant for mechanical and dielectric experiments, because the macroscopic and molecular times are nearly equal, and is well understood for NMR experiments. This result is by no means obvious but it is a reliable theoretical conclusion. The relaxation frequency as used in this paper is defined in terms of experimental variables which differ from one method to another.

For the present purposes dielectric loss, ϵ'', was plotted against log (frequency) at constant temperature and the frequency of maximum loss was taken to be ν_c at that temperature. In some cases results were reported as tan δ ($= \epsilon''/\epsilon'$), and in these cases we simply used tan δ plots instead of ϵ'' plots. Mechanical loss G'', E'', J'' or tan δ ($= G''/G'$, E''/E', or J''/J') were handled in the same way. In most mechanical-loss studies the frequency range covered was insufficient to allow this type of treatment. Although it is less desirable, plots of loss *versus* temperature at constant frequency were used in such cases. ν_c was taken as the measurement frequency at the temperature of maximum loss.

NMR relaxation results come n three varieties, spin-lattice relaxation (T_1), spin-spin relaxation (T_2 or line width) and "rotating frame" relaxation ($T_{1\rho}$). NMR results were almost always analyzed with relaxation time-temperature plots. ν_c was taken to be the resonance frequency at the temperature of a T_1 minimum. A change in T_2 (or resonance width, δH) with temperature marks the onset of motion of frequency $\sim 1/2\pi(T_2)_{LT}$ (or $\sim \gamma \delta H_{LT}/2\pi$) where "$LT$" implies the low temperature or rigid lattice condition. ν_c was taken as this frequency at the middle of the transition temperature range. This point is usually difficult to pick out with accuracy. As most resonances are of the order of 10 G wide at low temperatures, ν_c from T_2 is always of the order of 10^4 to 10^5 Hz. NMR experiments in the "rotating frame" have recently come into use and serve to extend the range of ν_c to lower frequencies. $\nu_c \cong \gamma H_1/2\pi$ at the temperature of a $T_{1\rho}$ minimum (H_1 is the strength of the rf magnetic field). As H_1 is typically of the order of one to 10 G, ν_c for a $T_{1\rho}$ minimum corresponds to the same frequency range as that probed by T_2 studies. At lower temperatures, when conditions are favorable, ν_c becomes $\sim 1/2\pi T_{1\rho}$.

In defining the ν_c's in these ways we have neglected various factors of order unity that may properly be applied. The attempt is to keep as close as possible to measured quantities. In any case, for our purposes the corrections are insignificant.

The use of the term correlation frequency often leads to the mistaken notion that the molecules are undergoing a periodic reorientation. In fact, the correlation frequency is $\nu_c = 1/2\pi\tau_c$ where τ_c is some sort of average time between motional events. The event might be the reorientation from one postion to another or it might be a diffusive jump. Of course, the frequencies encountered in resonance spectra, e.g. microwave spectra of gases, do correspond to frequencies of molecular motion in the classical sense. The transition from resonance to relaxation behavior is an important matter of current interest owing to very far infrared and sub-millimeter microwave methods now being employed.

The magnitudes of ν_c of interest here vary over a wide range. In mobile liquids $\nu_c \sim 10^{10}$ to 10^{11} Hz, whereas in glassy or crystalline solids ν_c is very small, perhaps zero. Polymeric materials range widely between these extremes and measured results are available from 10^{-4} to 10^9 Hz. Even these bounds are primarily an indication of experimental limitations and in no way imply limits characteristic of the spectrum of polymer motions. One should keep in mind that many polymer systems have two or more motional mechanisms active under the same conditions. For example, in PMMA [2] at 250 °K there are processes with identifiable ν_c's of 10^7, 10^5 and 10^{-2} Hz. The presence of simultaneous resolvable relaxations in itself provides clues concerning the molecular processes involved.

---

[2] See Appendix 1 for a translation of the abbreviations used in designating the polymers discussed in this paper.

Molecular motions in polymers [3] can be loosely classified under the following headings:

1. Primary main chain motion in crystals.
2. Primary main chain motions in amorphous materials.
3. Secondary main chain motion in crystals.
4. Secondary main chain processes in amorphous materials.
5. Side group motions.
6. Impurity motions.

Primary main chain motion in crystals is a hindered rotation about the main chain axis. All of the chains in the crystalline regions may be involved. The motion could occur *via* a defect mechanism. Activation energies tend to be high, greater than 30 kcal/mole. In PTFE this motion sets in at a first-order polymorphic transition. In polyethylene it is probable that the "α-transition" involves the onset of such motions. In this case it sets in gradually. The presence of mobile imperfections or kinks has been suggested. Translation along the chain axis may also occur.

The primary main-chain motions in amorphous regions begin at the glass transition. The glass transition marks the onset of large-scale main chain motions, both rotational and translational. The rigid glass becomes a viscous liquid as the temperature is raised. Arrhenius plots, i.e. plots of log ν_c *versus* $1/T$, are often curved and the resulting variable activation energies are very large; 100 kcal/mole is not unusual. The temperature dependence is usually analyzed in terms of an alternate expression due to Williams, Landel and Ferry [4]. PIB and PMMA are good examples of amorphous materials, that exhibit glass transitions. The amorphous regions in semicrystalline polymers also undergo similar changes in their state of motion; e.g. the "β-transition" in polyethylene is probably of this nature.

Secondary main-chain processes are thought to be more localized than the primary motions just described. The secondary processes are characteristic of linear polymers which tend to be semicrystalline. Activation energies in the neighborhood of 10 to 15 kcal/mole are normally encountered. It may be that only a fraction of the chains are involved. For example, in crystalline regions it may be that only those chain segments which lie near a row vacancy (possibly associated with a chain end) are free to move. In a glassy structure composed of linear chains there are probably chain lengths of limited size with enough free volume to permit some motion. Loose folds at crystal surfaces may also have some freedom of motion. We emphasize that these mechanisms are particularly speculative. The "γ-transition" in polyethylene is an example of this type of process.

Side-group motions are quite common and tend to occur well below the glass transition temperature. Activation energies may be above 20 kcal/mole for large or highly polar side groups but can be as low as 2 kcal/mole for methyl-group rotations. As only a few atoms are included in the moving unit, it is possible to establish these mechanisms with some certainty. PMMA exhibits three transitions of this type, rotation of the ester side group (the "β-transition"), rotation of the main chain methyl group and rotation of the ester methyl group.

Low molecular weight impurities can dominate relaxation at very low temperatures. In such cases the motions of the polymer are frozen out and the small impurity molecules provide the only relaxation mechanism. The very low temperature process in polystyrene could be an impurity effect.

In all relaxation phenomena the key physical process is the dissipation of energy. This is simply the conversion of work into heat. A sinusoidal stress produces a sinusoidal strain, where the stress may be a mechanical pressure and the strain a volume change, or the stress could be an electrical voltage and the strain an electrical charge. If the stress and strain always remain in phase, that is, if the response of the specimen is much faster than the change in stress, the work done on the specimen during half a cycle is stored and returned to the stress-making device during the other half cycle. This is a reversible system, no net work is done (per cycle) and no heat is generated. The electronic polarization is a good example of such a mechanism. On the other hand, if there is some sluggish factor in the response of the specimen, the stress and strain get out of phase, net work is done (per cycle) and heat must be generated.

In simple mathematical terms, consider the mechanical problem. The work done in an interval dt is

$$dW = f\,dl$$

where f is the force and dl is the displacement in dt. For a sinusoidal stress, ignoring transient terms,

$$f = f_o \sin \omega t$$

and

$$l = l_o \sin(\omega t + \varphi)$$

where φ is the phase difference.

$$dl = l_o\omega \cos(\omega t + \varphi)\,dt.$$

The work done is

$$W = f_o l_o \cos\varphi \int (\sin \omega t)(\cos \omega t)\,\omega dt - f_o l_o \sin\varphi \int (\sin^2 \omega t)\,\omega dt.$$

or

$$W = -\pi l_o f_o \sin\varphi \text{ per cycle.}$$

The first integral is the elastic part which integrates to zero over an integral number of cycles.

On a molecular scale one is confronted with the problem of explaining dissipative phenomena by means of statistical mechanics, based on conservative force laws. It seems probable that this can be done, but it is difficult to obtain an intuitive grasp of the mechanics of dissipation. An explicit model calculation would be helpful but we know of no satisfactory example. Most theoretical work does not address itself to this problem. Recent activity has centered upon the description of macroscopic properties in terms of statistical averages of the time dependence of various molecular quantities, i.e., the correlation functions [65, 66]. A calculation of the correlation functions from first principles would clarify the situation, but this has not been produced.

In order to describe the relaxation process explicity we must state a mechanism, i.e., designate a part of the system which participates by converting the coherent excitation supplied by the experiment into excitation of the phonon bath of the specimen. The phonon bath can be regarded as a collection of oscillators characterized by a distribution function. Mechanical excitation can be regarded as creation of coherent phonons (i.e., in phase with one another) of the experimental frequency. These phonons interact with the designated part of the system and leave it in some excited state. The excitation can subsequently decay by emitting phonons coherent with the excitation, in which case no dissipation occurs, or the excitation can decay by producing one or more phonons of different phase or frequency, i.e., dissipate energy into the heat bath. The transition probabilities which describe these competing processes are very complicated in extremely simple systems, and it is unrealistic to hope for a detailed calculation for polymeric media. For this reason the phonon bath is not introduced explicitly but its presence is felt whenever a temperature appears in the analysis.

2. Some Theories of Relaxation

Theoretical treatments of relaxation processes are numerous and it is not our intent to review all the theories or any one exhaustively. Rather, we will attempt to describe some of the physical ideas underlying these theories and assess their success and rationality as applied to polymers.

2.1. Transition State Theory

The transition state theory [5] of time-dependent processes is one of the oldest and most successful theories available. Eyring has been the principal spokesman for this point of view, but others have contributed significantly, and the ideas have been known for a long time. The theory is limited in some respects, but it is extremely useful. Eyring has been successful in applying the ideas to a wide variety of phenomena. The basic step is to set the characteristic frequency of any process equal to a fundamental vibration frequency, (kT/h), multiplied by an exponential activation energy term, $\exp(-\Delta G^{\ddagger}RT)$,

$$v_c = (kT/h) \exp(-\Delta G^{\ddagger}/RT). \tag{1}$$

This leads to an activation energy (actually an enthalpy),

$$\Delta H^{\ddagger} = -R(\partial \ln v_c/\partial(1/T))_p \tag{2}$$

and an activation volume,

$$\Delta V^{\ddagger} = -RT(\partial \ln v_c/\partial p)_T. \tag{3}$$

It is easily shown that the activation energy at constant volume,

$E_V = -R(\partial \ln v_c/\partial(1/T))_V$ is given by

$$E_V = \Delta H^{\ddagger} - p_i \Delta V^{\ddagger} \tag{4}$$

where

$$p_i = T(\partial p/\partial T)_V. \tag{5}$$

The model can be visualized as follows. A molecule oscillates subject to forces specified by two potential wells separated by a barrier. If kT is very small compared with the barrier height the molecule tends to stay in one well, making transitions to the other well only occasionally. This is the situation for processes of interest here. Crudely speaking, (kT/h) is the frequency with which the molecule approaches the barrier, and the exponential term is the probability that it will have the necessary energy to surmount the barrier. Relaxation experiments couple to the molecules with energies weak compared with kT and $\Delta H^{\ddagger}$. Thus, the experiments cause only small changes in the thermal motions.

When polymers are under consideration the unit whose motion is to be described is usually not the entire molecule but some much smaller portion such as a side group or a limited length of chain. This is not very different from the case of low molecular weight considerations except that the potential may be of intramolecular as well as intermolecular origin. The oscillation considered may be either translational or rotational in nature.

Interpretation of the parameters derived on analysis of the experiments must be undertaken with great care. The great generality and wide applicability are the results of a nonexplicit basis. The graphs in section 4 attest to the constancy of $\Delta H^{\ddagger}$, and this parameter is extremely useful in keeping track of data. (The glass transition does not usually yield a constant $\Delta H^{\ddagger}$, as will be discussed.) Small activation energies can often be associated with specific motions of small groups, but large activation energies can refer to less definite rearrangements.

When a rigid linear molecule, n segments in length, is considered to rotate about its long axis, it is reasonable to write [3]

$$\Delta H^{\ddagger}=\Delta H^{\ddagger}_{\text{end}}+n\cdot\Delta H^{\ddagger}_{\text{seg}} \tag{6}$$

and

$$\Delta S^{\ddagger}=\Delta S^{\ddagger}_{\text{end}}+n\cdot\Delta S^{\ddagger}_{\text{seg}}. \tag{7}$$

As we have noted, many relaxation studies consist of temperature dependencies at constant frequency, so it is desirable to solve the rate expression, eq. (1), for the temperature of maximum loss, T_{max}. With the rigid-rod assumptions this becomes

$$T_{\text{max}}=T_o\left(\frac{a+n}{b+n}\right) \tag{8}$$

where $T_o\equiv\Delta H^{\ddagger}_{\text{seg}}/\Delta S^{\ddagger}_{\text{seg}}$, $a\equiv\Delta H^{\ddagger}_{\text{end}}/\Delta H^{\ddagger}_{\text{seg}}$ and $b\equiv(\Delta S^{\ddagger}_{\text{end}}-R\ln(h\nu/kT))/\Delta S^{\ddagger}_{\text{seg}}$. We recall that ν as used here is the experimental frequency.

When chain twisting is introduced [3, 6, 7]

$$\Delta H^{\ddagger}=\Delta H^{\ddagger}_{\text{end}}+f(n)\cdot\Delta H^{\ddagger}_{\text{seg}} \tag{9}$$

and $\Delta S^{\ddagger}$ is assumed to be a similar function of n. $f(n)$ must be equal to n at small n (rigid behavior) and reach a limiting value for large n. That is, the activation energy should become independent of chain length when twisting occurs to such an extent that only a small fraction of the chain is near the rotational barrier at any given time. For realistic potentials it is found that twisting does not occur at all until the molecule becomes fairly long (e.g., this n may be greater than 100 for paraffin chains). Thus the rigid-rod behavior may be widely applicable.

This result is not obvious but a simple physical model can make the basis clear. The chain-twisting potential and a sinusoidal barrier potential are given as,

$$U(\varphi)=\frac{A^2a^2}{2}\left(\frac{d\varphi}{dz}\right)^2+\frac{B^2}{2}\sin^2\varphi \tag{10}$$

where z is the distance along the chain, φ the angle of rotation, a the segment length and A and B are constants governing the twist energy (A) and the rotation energy (B). It is desired to find the minimum energy that will be sufficient to make the molecule pass over the barrier. A flexible molecule will have only one segment at the top of barrier, $\varphi = \pi/2$, at a time. Consider a molecule with all of its segments at the top of the barrier. We must ask whether twisting the chain will reduce $(B^2/2)\sin^2\varphi$ more than $(A^2a^2/2)(d\varphi/dz)^2$ is increased. For long chains the reduction occurs because the end segments can move appreciably away from the barrier without making $(d\varphi/dz)$ large for any point along the chain. It can be shown [7] that this occurs when $n > A/B$.

The size of the relaxing unit in a polymer can vary over a wide range. It can be as small as a single proton or as large as an entire molecule. For most processes occurring in the solid state it seems reasonable that units small compared with the entire polymer molecule will generally be most important. We shall be concerned with side-group motion, end-group activity, local main-chain motions and rigid and flexible rod rotation for lengths of chain as long as a fold period or a loop length at a fold. Of course, above the glass transition the low-frequency motions correspond to really large scale rearrangements.

2.2. Site Model Theory [8, 9, 10, 11]

Hoffman [8] has developed a model for dipolar relaxation that explains the main empirical features in terms of the potential-well diagrams of transition state theory. This theory is particularly useful in connection with the treatment of long-chain molecules. In the simplest case a dipole is allowed to rotate subject to hindering forces defined by a potential such as that shown in figure 1. Usually $\Delta H^{\ddagger} >> RT$ and the dipole tends to spend most of its time near one of the potential minima, i.e., at a site. If there are N dipoles, each subject to this potential, with N_1 at site 1 and N_2 at site 2, $(N = N_1 + N_2)$,

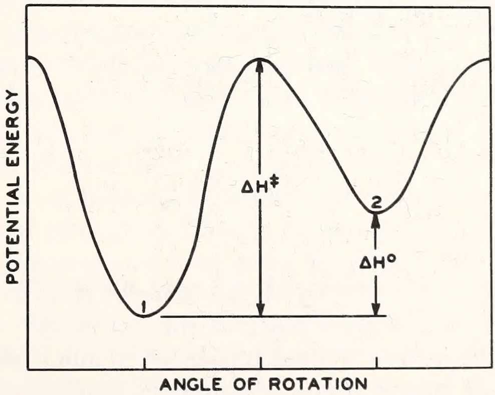

FIGURE 1. Schematic potential energy diagram of the type considered in the analysis of relaxation through molecular reorientation.

then the dipole moment of the system is $N_1\mu_1+N_2\mu_2$. The dielectric constant is proportional to the component of this polarization along the measuring field, **F**. Hoffman solves the coupled equations for N_1 and N_2,

$$\frac{dN_1}{dt}=-2kN_1+2k'N_2$$

$$\frac{dN_2}{dt}=2kN_1-2k'N_2 \tag{11}$$

where $2k$ is the transition probability for a jump from site 1 to site 2 and $2k'$ refers to the reverse jump.

k and k' are simply the characteristic frequencies of the transition-state theory,

$$k=A\exp\left[-(\Delta H^{\ddagger}+\Delta H^{0})/RT\right] \tag{13}$$

and

$$k'=A'\exp\left(-\Delta H^{\ddagger}/RT\right). \tag{14}$$

The differences between A and A' reflect entropy of activation factors The shape of the potential wells is not a critical factor.

After the field F is switched on suddenly, the system approaches its equilibrium polarization exponentially in time. The correlation frequency is given by $2(k+k')$. The transition probabilities place the center of the loss region on a frequency scale, and the magnitude of the polarization is directly related to the intensity of the dielectric loss. The parameter $\Delta H^{\ddagger}$ is the activation energy for the shift of frequency with temperature. The parameter ΔH° can be deduced from the temperature dependence of the loss intensity. The intensity is low at both low and high temperatures and passes through a maximum when ΔH° and RT are of the same magnitude. In addition to the factor involving ΔH° and temperature, the loss intensity is proportional to $N\mu^2$, where μ^2 is the square of the component of the molecular dipole moment perpendicular to the axis of rotation.

A more complex model using three sites reveals the existence of two relaxation rates and thus gives the possibility of explaining distributions of relaxation times. In general, more sites tend to give more relaxation rates and the lower rates tend to correspond to the larger polarizations. Of course, there may be other origins of relaxation-time distributions within the framework of the site model, e.g. a distribution of $\Delta H^{\ddagger}$ arising from a distribution of dipole motion potentials.

The site-model theory gives a satisfying description of dipole relaxation and has been notably successful where it has been applied with care. The parameters of the theory can also be analyzed in terms of molecular properties and intermolecular interactions. This has been done for long-chain dipolar compounds in clathrate complexes and the results are impressive [12].

Hoffman, Williams and Passaglia [3] have recently presented a discussion of relaxation in solid polymers based on the site model. In this ambitious project the authors considered many mechanisms of motion, made proposals concerning the complex transition behavior observed with linear polymers and carried through a calculation of the dynamic mechanical loss based on the site model. We shall take up their specific applications in section 4.

2.3. Free Volume Theories [4, 13]

Free volume has been invoked widely in approximate theoretical studies of liquids. The free volume has been defined in a variety of ways, and it would take us too far afield to try to do justice to this area of activity. However, the mechanism of the glass transition has often been discussed in terms of free volume, and it is relevant to give a brief summary of the kinetic aspects of the arguments here.

The free volume is a measure of the looseness of the structure of the solid or liquid, and it is plausible to associate looseness with molecular mobility. Of course, the average free volume as measured by macroscopic parameters is not necessarily a clear-cut indication of the local free volume, as it may vary from point to point in the substance. Moreover, the manner in which free volume fluctuates in time is important. For these, and other reasons it can be argued that the results of free volume theory will be rather insensitive to the details of the definition of the free volume.

Let the free volume and the total volume be denoted V_f and V. Let the free volume fraction be defined by $f=V_f/V$. It is assumed that a unit of N segments can move when the local free volume fraction exceeds some critical value f_c. ν_c is set equal to the product of the probability that the local free-volume exceeds f_c, and a frequency factor, A, so that

$$\nu_c=A\int_{f_c}^{\infty}\Phi(f)df \tag{15}$$

where $\Phi(f)$ is a distribution function for local free volume. Bueche [14] has used this technique for the description of glass-forming substances. He evaluated $\Phi(f)$ by means of a free-energy expansion and showed, with some approximations, that,

$$\nu_c=\nu_g \exp\{-Nf_c[(1/f)-(1/f_g)]\} \tag{16}$$

where f is the average free-volume fraction and the subscript g refers to values at the glass temperature. Using

$$f=f_g+\alpha(T-T_g), \tag{17}$$

it is easily shown that,

$$\ln(v_c/v_g)=(Nf_c/f_g)(T-T_g)/(T-T_g+f_g/\alpha) \tag{18}$$

which is a form of the WLF (Williams, Landel, Ferry) equation. The WLF equation is usually deduced [4] from the Doolittle viscosity relation,

$$\eta=A' \exp(BV/V_f), \tag{19}$$

where the constant B is of order unity. Equation (16) is seen to be analogous to the Doolittle relation.

The free volume depends only upon intermolecular potential energies, and computations of V_f for relatively simple liquids are well known [13]. The application of these methods to polymers is more complex, however, owing to uncertainty concerning the size and composition of the unit engaged in motion. Usually V_f is taken as the difference between the melt volume and an "occupied" volume. $f_g \cong 0.025$ for most polymers.

2.4. Statistical Mechanical Theory [15, 16]

Gibbs and DiMarzio [15] have argued that the glass transition in polymers is a kinetic manifestation of a thermodynamic transition which lies typically 50° C below T_g. At this transition the system ceases rearrangements ($v \rightarrow 0$) owing to the fact that there are no configurations available into which the system may rearrange. At least, the number of configurations has become sufficiently small that other configurations are not accessible. The configurational entropy becomes zero at the transition temperature, T_2. Beginning from this point of view Adam and Gibbs [16] have discussed polymer relaxation in the glass-transition region. Only the most general statistical mechanical principles are required.

The transition probability is written as a product of a frequency factor and the probability that the system is in a state for which rearrangements are possible.

$$v_c=A \exp(-z^*\Delta\mu/kT) \tag{20}$$

where z^* is the smallest number of segments that can compose a unit capable of rearrangement. $\Delta\mu$ is the free-energy difference that determines the concentration of states permitting rearrangement.

It is then argued that z^* is proportional to $1/S_c$, where S_c is the configurational entropy of the specimen.

also
$$v_c = A \exp(-C/S_cT), \tag{21}$$
where
$$C = \Delta\mu s_c^*/k \tag{22}$$

and $s_c{}^*$ is the configurational entropy of a unit of size z^*. This is a key step because Gibbs and DiMarzio [15] had based their earlier analysis on the assumption that $S_c = 0$ at the thermodynamic transition temperature T_2. Thus S_c at any other temperature is given by,

$$S_c(T) = \Delta C_p ln(T/T_2) \tag{23}$$

where ΔC_p is the difference in heat capacity between the equilibrium melt and the glass at T_g. ΔC_p is assumed to be independent of temperature.

The foregoing considerations lead directly to an equation of the form of the WLF equation,

$$ln(v_c/v_g) = a_1(T-T_g)/(a_2+T-T_g) \tag{24}$$
where
$$a_1 = C/\Delta C_p T_g ln(T_g/T_2) \tag{25}$$
and
$$a_2 = T_g\, ln\,(T_g/T_2)/\{ln(T_g/T_2) + [1+T/(T-T_g)]ln(T/T_g)\} \tag{26}$$

which is slightly temperature dependent. T_g as used here need not be the glass temperature but could be some other reference temperature.

The key step mentioned above, leading to the proportionality between z^* and S_c^{-1}, comes about simply. The configurational entropy of a unit composed of z^* segments is s_c^*. If S_c refers to one mole of segments, then
$$S_c = (N_A/z^*)s_c^* \tag{27}$$

because N_A/z^* is the number of units composed of z^* segments (N_A is Avogadro's number). Thus,

$$z^* = (s_c^* N_A/S_c) \tag{28}$$

and equation (21) follows if $\Delta\mu$ is expressed in molar terms. The physical content of this development is that, as the system becomes more disordered, units consisting of fewer segments become able to rearrange. Whereas this is a plausible result, it is less obvious that all of the temperature dependence is contained in TS_c. We are accustomed to regarding $\Delta\mu$ as temperature independent in transition-state theory. However, s_c^* is the configurational entropy of a section of chain, i.e., a rearrangeable unit, whose length varies with temperature, and we have no definite notion concerning its temperature behavior. We would welcome a theoretical development of this quantity [21].

The success of this theory and the free volume theories is reckoned in terms of the qualitative "reasonableness" of the parameters derived by fitting the theoretical equations to experimental data. In view of the enormously complicated systems described, the results are gratifying.

2.5. Chain Dynamics Theories

Each of the preceding theories expresses the correlation frequency as a product of a frequency factor and a conditional probability for the motional transition. In this section we mention an entirely different theoretical approach that has been developed by Bueche [17], Rouse [18], Zimm [19] and others [20, 4]. A single polymer molecule is considered in a fluid solvent. The molecule is considered to be composed of sub-molecules (of, say, 30 segments) and a differential equation for the position of each sub-molecule is the starting point. This equation is just a balance of the forces on the sub-molecule, and the set of equations is coupled owing to the fact that the sub-molecules are connected to one another. The forces include a Brownian motion term and a frictional force that involves an empirical "friction factor per segment". A normal coordinate transformation serves to uncouple the system of equations, and the solution consists of eigenfunctions that are linear combinations of the positions of the sub-molecules. Each eigenfunction describes a configuration that decays with a time constant given by an associated eigenvalue.

This type of theory is attractive because it deals directly with the long-chain character of polymers. A distribution of relaxation frequencies arises naturally in terms of the normal modes, and it is perhaps worth considering the physical picture to be associated with these modes. Consider a large number of polymer molecules each with its segments numbered from 1 to N. The positions of the segments of a molecule relative to the center of gravity of that molecule specify the molecule's configuration. If the system is unoriented, the average position of segment 1 taken over the entire ensemble is zero. The same statement is true for any given segment. An eigenfunction specifies a displacement for each (ensemble average) segment position. Now if the ensemble has an initial average set of displacements given by an eigenfunction, the theory shows that the displacements will decay to zero with an exponential time dependence. The time constant for the decay will be given by the corresponding eigenvalue. In general eigenfunctions that specify nearly equal displacements for neighboring segments decay slowly. Figure 2

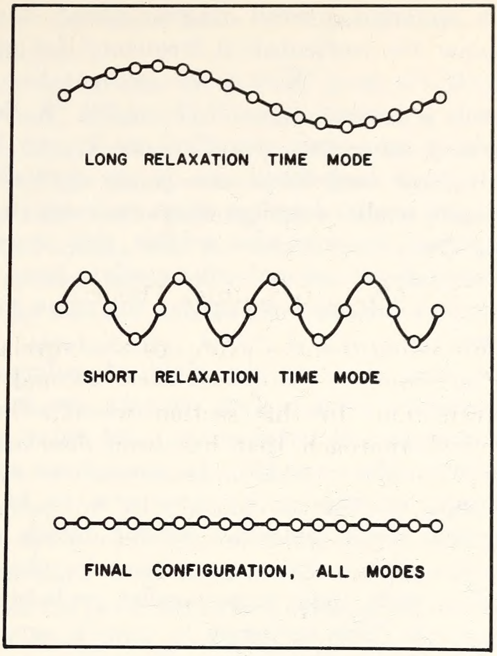
LONG RELAXATION TIME MODE
SHORT RELAXATION TIME MODE
FINAL CONFIGURATION, ALL MODES

Figure 2. Relaxation "modes". The vertical displacements represent ensemble average departures from the center of mass of the molecule.

gives a schematic representation of the situation. The ensemble average displacements are shown vertically and the segments are spread out horizontally for clarity. This type of representation tends to emphasize the analogies between this analysis and the analysis of the vibrations of a string. These analogies are valuable but it must be kept in mind that the displacements of interest here are ensemble averages and that they decay without oscillation.

In these theories interchain interactions are neglected, and it is far from obvious that the discussion holds for undiluted polymer systems. This matter has been carefully considered by Ferry [4] who concludes that this type of theory can be applied to bulk polymers in the glass transition region. Indeed, in some respects bulk polymers are simpler than dilute systems.

3. Mechanisms for Molecular Motion

In this section we review qualitatively several mechanisms for molecular reorientation that would appear to be relevant to polymer systems. Simple group rotations can occur in solids at remarkably low temperatures [22]. Furthermore, even fairly large molecules (say

MW>100) can undergo overall reorientation. For example, in hexamethylbenzene the reorientation frequency for methyl rotation is greater than 10^3 Hz at 1 °K and the reorientation frequency for the entire molecule is greater than 10^3 Hz at 200 °K. Many examples can be cited. Many long-chain paraffins are known to undergo reorientation about their long-chain axes in the crystalline state, and these materials have similar freedom when enclosed in urea clathrate cages [23]. Long-chain ketones also exhibit this type of molecular activity [24]. Thus well-defined molecular motions have been identified in relatively simple solids, and we expect the same sorts of motions in solids polymers.

Although the vast and complex field of polymer morphology cannot be summarized here, a few remarks are in order because morphological concepts and terminology must enter into the assignment of relaxation mechanisms [25]. In amorphous systems, such as atactic polystyrene, we expect the structures to be disordered in the same sense that lower molecular weight liquids are disordered. Long-range order is absent, but the tendency for chain molecules to arrange themselves with their axes parallel probably extends over considerable distances. This tendency to parallel arrangement could help make chain axis rotations easy. Crystalline polymers always exhibit a parallel chain structure. In recent years the chain-folded morphology has been shown to be very common in bulk polymers. As the crystal thickness is of the same order of magnitude as the length of chain required for chain twisting, the chains may or may not behave as rigid rods. The tightness of the fold structures would seem to be a crucial factor. If the folds contain only three or four segments, any chain rotations that occur must be coupled closely to fold or defect motions. If the folds are loose, containing ten or more segments, it is possible that the folds and interior crystal chains may reorient at quite different frequencies. In a loose fold structure a substantial fraction of the total number of segments in the specimen occurs in the folds. Extended-chain crystals have also been identified, but the extent to which they occur is still unknown. The amorphous regions of semi-crystalline polymers are largely uncharacterized. They include partially-fractionated, low-molecular weight material, large disordered regions, and disordered or partially disordered surface layers on crystals. The level of crystallinity is important. When the specimen is less than 30 percent crystalline it seems likely that the structure of the amorphous regions is similar to the structure of a completely glassy or rubbery polymer. However, when the specimen is greater than 80 percent crystalline, crystal surfaces and internal defects probably play an important role. In general we do not know how to evaluate the importance of these factors at intermediate levels of crystallinity.

Relaxation measurements have been used to measure the degree of crystallinity but, at best, the methods can be considered only as secondary. Relaxation results contain information concerning molecular mobility, and the interpretation of these results in terms of the state of disorder amounts to nothing more than a plausible hypothesis. For dielectric and mechanical relaxation the intensity of a loss peak can often be related empirically to the crystalline or amorphous content. Then, by suitable calibration, the loss intensity can be used to evaluate the crystallinity. NMR is somewhat more powerful in that the resonance can often be divided into two parts on the basis of differing T_2's (or resonance widths), and the relative concentration of crystalline and amorphous material is given simply by the relative intensities of the two components [26, 27]. This NMR method is an excellent procedure for estimating the mobile fraction, and this is frequently close to the complement of the degree of crystallinity when the temperature range of measurement is suitably chosen.

Two comments are pertinent. First, criticism of the use of relaxation as a means to determine crystallinity is usually in part a criticism of the crystallinity parameter itself. The degree of crystallinity in polymers is by its very nature an approximate concept. When considering the use of relaxation in this connection, we frequently forget the uncertain features of the x-ray, density and infrared techniques. Second, information relating to the mobile character of a specimen is very often more relevant to our practical needs than the state of order. Of course, both types of information are important.

Reneker [28] has described an interesting defect for polymer chains, which could be important in connection with motional processes. The defect consists of inserting an additional segment into a polymer crystal. Consider a paraffin chain. The chain is rotated by 180° on one side of the defect. Thus, as the defect slides along the chain the chain is rotated by 180°. This type of mechanism is attractive because only a local section of chain needs to be activated in order to bring about main chain reorientation. Figure 3 shows a schematic representation of this type of defect.

The correlation frequency is determined by the number of defects, as well as by the frequency associated with the process of moving the defect by one segment. If there are N segments and n_d defects, then each defect will need to relax about N/n_d segments. If each defect makes a jump every τ_d seconds, the time to relax the specimen will be of the order of $N^2\tau_d/n_d^2$ and

$$\nu_c \cong n_d^2 N^2 \tau_d. \tag{29}$$

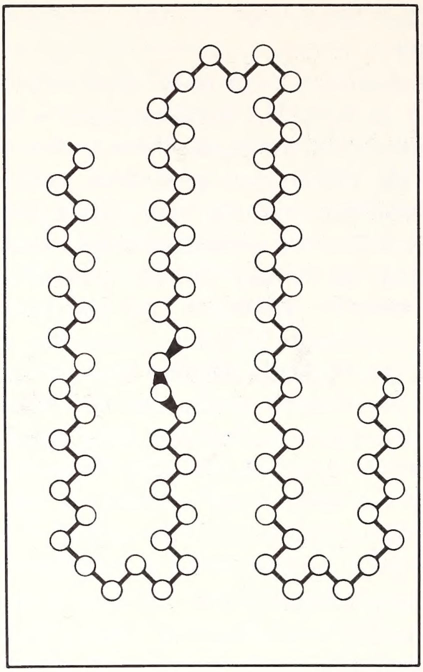

FIGURE 3. Schematic representation of a Reneker defect.

(In this estimate we assume the defects move about by a diffusive mechanism.) τ_d^{-1} may be many orders of magnitude larger than ν_c.

Hoffman, Williams and Passaglia[3] have made a number of explicit proposals to describe the molecular motions of polymer chains with no rotatable side groups. Molecular rotation around the long-chain axis is envisioned. A small translation parallel to the axis of rotation may occur and chain twisting may be involved. The various models can be briefly indicated as follows:

1. chain rotation with a closely-coupled fold reorientation,
2. chain rotation with more or less independent fold reorientation,
3. chain rotation of an extended chain molecule with a vacancy at the end to permit any necessary translation,
4. chain rotation at a row vacancy associated with a chain end, *via* a defect mechanism.

These authors have given a detailed description of the applicability of these models to linear chain relaxations. Figure 4 indicates some of these ideas.

Willbourn has proposed that a chain relaxation occurs at rather low temperatures (< -100 °C) when three or four CH_2-groups occur consecutively. This idea seemed to have a fair empirical basis at the

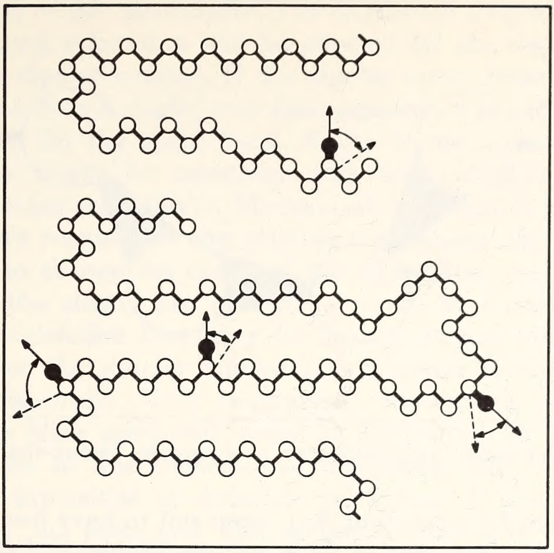

FIGURE 4. Schematic representation of some defects discussed by Hoffman, Williams and Passaglia.

time of Willbourn's proposal, but some subsequent work carried to lower temperatures than available previously has served to weaken the case. This type of mechanism has had considerable popularity in recent years and, in one form, it is referred to as the "crankshaft" mechanism [30, 31]. Figure 5 gives an idealized picture of this motion. The basic notion is that if two C–C bonds are sufficiently separated they can become nearly collinear. The intervening chain can then rotate easily about their common axis. Of course, intermolecular hindrances must be considered and the volume swept out is usually rather large.

Although this mechanism was proposed for low-temperature relaxations, it bears some resemblance to the glass transition mechanism of Adam and Gibbs [16]. As will be recalled, these authors focussed their attention upon the (critical) minimum length of chain capable of rearrangement. Even though the crankshaft picture of figure 5 is an oversimplification, there may be special configurations that are favorable for main chain reorientation.

Molecular motions of groups attached to the main chain can often be identified with some certainty. The identity of the group responsible for side chain relaxation and site model parameters can usually be established. The motions involve the movement of modest numbers of atoms and consist of rotations about one or a few single chemical bonds. The degree of coupling between side-chain and main-chain motions is more difficult to assess.

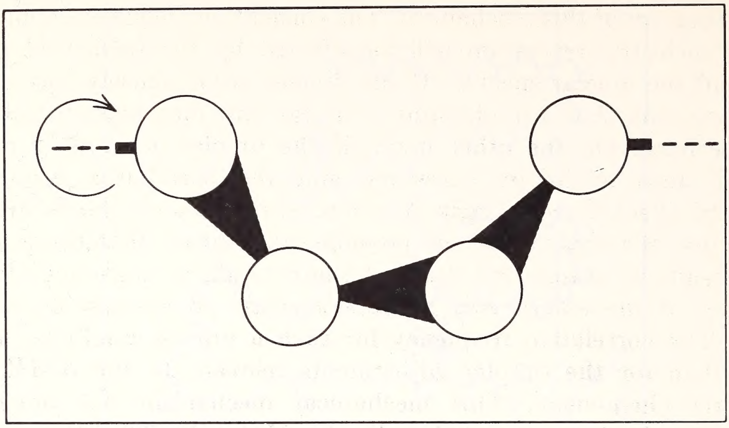

FIGURE 5. Schematic representation of a simple "crank-shaft" motion.

A mechanism for relaxation that seems not to have been considered is that of longitudinal motion. It is well established [32] that polymer crystals thicken at high temperatures and this can be interpreted as evidence for mobility along the chain axis in crystals. At lower temperatures than the refolding region the molecules might have relatively little longitudinal freedom, limited, say, by the reluctance of folds to enter well-formed crystalline regions. However, if the surface of the crystal is rough, or if there is a somewhat disordered surface layer, the molecules might be able to shuttle back and forth appreciably even at relatively low temperatures. The elementary step could, of course, consist of a defect mechanism.

How can this give rise to relaxation? For NMR all that is necessary is a change in internuclear coordinates. The relatively weak intermolecular nuclear dipolar coupling would bring about relaxation of the spin system, and we would expect a T_1 minimum of only modest depth. The correlation frequency of interest would be the segment jump frequency and not the defect jump frequency, as explained above. For dielectric relaxation let us consider a polymer with dipoles perpendicular to the main-chain axis. Rotation about the main-chain axis has already been discussed. Polarization along the crystal axis corresponding to the main chain can only be obtained by orienting the dipoles in the folds or by changing the dipole population of the folds. That is, under the influence of an electric field along the main-chain axis, polymer molecules with longitudinal mobility will arrange themselves such that dipoles will concentrate in folds where they are parallel with the field and abandon folds where they are antiparallel with the field. Figure 6 is a highly schematic representation of this mechanism. The correlation frequency appropriate to dielectric relaxation will be affected by the segmental jump rate and the dipolar spacing. If the dipoles occur densely, say every other segment, then a single jump (per segment) may serve to polarize the specimen. On the other hand, if the dipoles occur only rarely several steps might be necessary and the correlation frequency would be affected accordingly. Mechanical relaxation is more difficult to discuss. We suggest, as one possible mechanism, that the applied stress tends to change the shape of the crystallites, and longitudinal diffusion of the chains can produce a strain to accommodate this stress. The correlation frequency for such a process might be much lower than for the simpler adjustments relevant to the NMR and dielectric phenomena. This mechanical mechanism has much in common with ideas presented earlier by Matsuoka [33, 34].

An objection to this translational mechanism can be phrased on the basis of intensities of dielectric relaxation. If the polarization involves only the folds and fold segments constitute only a small fraction of the specimen, how can an appreciable polarization be achieved? This question can be answered, at least in part, by the following observations. First, when the dipoles occur densely there is a great deal of cancellation and the observed dipolar effects are

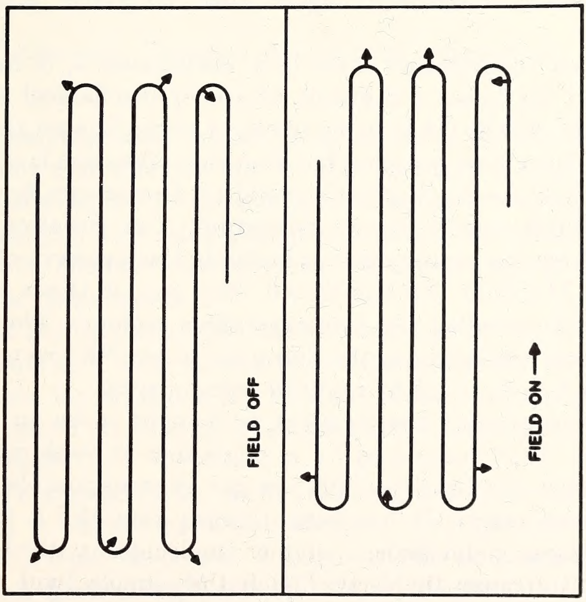

FIGURE 6. Schematic illustration of polarization through longitudinal motions.

measures of the *net* unbalanced dipole moment of the chain. For example, a helical chain will be dipolar only if the length of the chain (or fold period) is not an integral number of helix periods. The fold moment might very well be comparable to this unbalanced moment. Second, when the dipoles occur rarely, say as impurities incorporated in the chain, there is some probability that the dipoles will be concentrated at or near the folds.

4. Relaxation Results and Interpretation

In this section we discuss relaxation results and their interpretations for individual polymer systems. The discussion will be phrased with reference to the transition maps collected here. The transitions will be discussed in order from left to right on these maps, i.e., from high to low temperatures. Although there is some confusion in the literature, we will label these transitions $\alpha, \beta, \gamma, \delta, \ldots$, respectively, when it is desirable.

4.1. Polyethylene (figs. 7 and 8)

Although we have plotted data for linear and branched PE separately, there is very little difference between the transition maps and we discuss them together. In fact these similarities in relaxation behavior are remarkably independent of detailed structure and specimen history.

The highest temperature transition, designated α, is indicated by four lines on the linear PE graph (three for mechanical and one for dielectric and NMR). It is indicated by a single line on the branched PE graph. There is no question but that the relaxation is of crystalline origin and that the mechanical correlation frequencies lie well below those for NMR and dielectric relaxation. The situation is further complicated by the observation of multiple loss peaks in the mechanical results. McCrum [35] has shown that one of these is a surface effect (sometimes called the transcrystalline regions). The three lines for mechanical relaxation in the figure for linear PE are not intended to correspond to the various resolved components.

The next transition, designated β, is thought to be an amorphous phenomenon. It is designated by a single line on each graph. These lines for linear and branched PE are not superimposable and might be of different origin. It has been claimed that the β transition is absent in linear polyethylene and a branch-point mechanism was suggested. More recently Moore [34] and Matsuoka have shown that the β transition can be developed in linear PE, on thermal treatment.

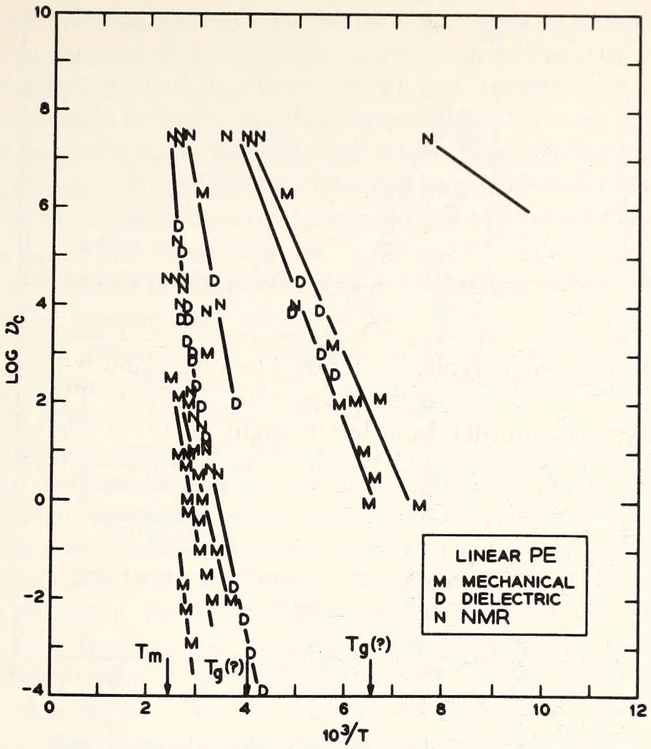

Figure 7. Transition map for linear polyethylene.

The low-temperature γ transition is indicated by two lines on the linear PE plot and a single line on the branched PE plot. This relaxation is believed to be characteristic of both crystalline and amorphous regions, and two relaxation peaks have been resolved in some studies [36, 37]. The two lines for linear PE are not meant to represent these resolved components.

Finally, at low temperatures there is evidence in the NMR results for methyl rotation. This motion is just detectable for linear PE and quite apparent for branched PE in spite of the low concentration of methyl groups. This has been satisfactorily explained in terms of spin diffusion [38].

Thus, there appear to be two crystalline, α and γ, and two amorphous, β and γ, transitions in polyethylene. This situation frequently arises with linear polymers. Morphological complexity bedevils attempts at a general explanation, and a completely satisfying experimental study has not yet come to our attention. We cannot

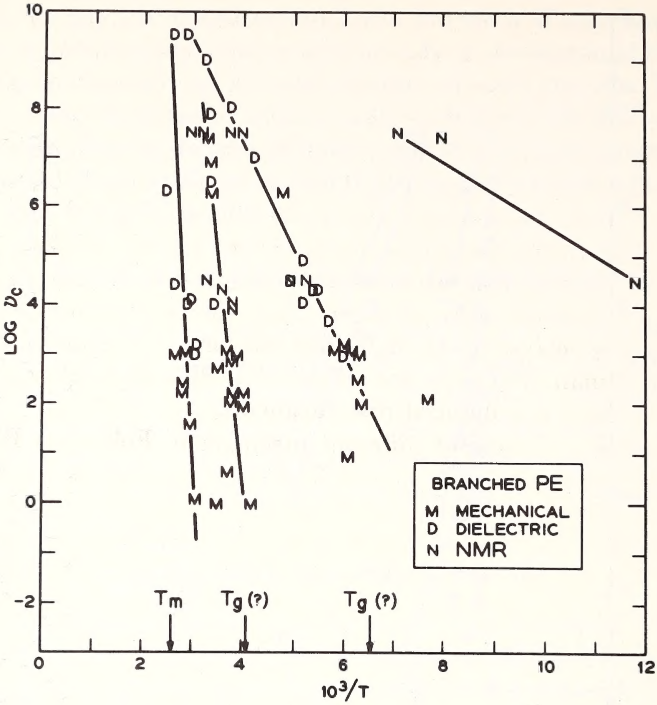

FIGURE 8. Transition map for branched polyethylene.

review all of the published details here, so we will content ourselves with a discussion of the various mechanisms that is strongly influenced by the emphasis on NMR in our laboratory. We recommend the excellent papers of Sinnott [36] and Hoffman, Williams and Passaglia [3] for background.

In linear PE the NMR T_2 for the crystalline component remains at its rigid lattice value to temperatures above 100° C [38]. Thus, in linear PE molecular rotation about the main chain axis cannot occur for any appreciable fraction of the crystalline material below about 100° C. Previous interpretations of the γ transition in terms of molecular reorientations within the crystalline regions must be examined carefully. A strong indication of the γ transition does show up in the NMR T_1 and T_2 results for the mobile fraction. The change in T_2 (mobile) would be consistent with rotations around the main-chain axis, but further narrowing occurs continuously as the temperature is raised through the β relaxation region, showing that more general-liquid-like motions must be involved [39]. T_1 for the crystalline protons follows T_1 for the mobile protons, which indicates a spin diffusion mechanism [38].

For such a mechanism to be effective the mobile and fixed protons must be reasonably close together, say not more than 50 to 100 Å apart. Finally, $T_{1\rho}$ results clearly show the α relaxation. This $T_{1\rho}$ effect corresponds to the crystalline fraction (short T_2) as it should [40].

The dielectric data of Reddish and Barrie [41] indicate only a very weak γ relaxation for linear PE. The mechanical data of Sinnott are ambiguous from the intensity standpoint because of the question of G'' versus tan δ [36]. Sinnott seems to favor G'' while we lean toward tan δ as the desired measure of the loss magnitude. In any case the α transition is considerably stronger than the γ transition. Sinnott assigned the γ relaxation to molecular motions at thermally injected defects. Hoffman, Williams and Passaglia [3] suggested that these defects are chain-end induced row vacancies.

We propose a somewhat different mechanism. Following Blundell, Keller and Connor [42] we picture linear PE crystals as well-formed internal structures with a surface layer that is more or less disordered. For a dilute-solution crystallized specimen that has not been subjected to any damaging treatment, the folds may be well ordered and of quite restricted mobility. These preparations do not exhibit an NMR mobile fraction. On annealing, however, crystals thicken and become less perfect. A partially disordered surface layer is formed. We take this layer to be the amorphous fraction in linear PE. Of course, on less ideal crystallization this layer and other internal defects are probably formed at the outset. The γ relaxation corresponds to chain rotations in these regions, and the β relaxation would correspond to more general motions of the same chains. As we have mentioned the β relaxation is usually not observed in linear PE. NMR results indicate that this is because the region is shifted to higher temperatures (as compared with branched PE) and lies very close to the strong α relaxation.

The crucial experimental fact, as we have pointed out before [39], is the extent of the change in T_2 (i.e., the extent of resonance narrowing). At 75° C T_2 is several times longer than can be accounted for by chain-axis rotations [27]. It is difficult to visualize a molecular motion associated with a row vacancy or any other simple defect that could bring about this increase in T_2.

We note that this proposal has much in common with the views expressed by Sinnott [36] and Hoffman, Williams and Passaglia [3]. The relaxing units are within the lamellae. The active centers have, in a manner of speaking, been collected and placed on the fold surfaces. In bulk linear PE the disordered layers must comprise 10–20 percent of the total lamellar thickness. The thickness of the amorphous layers will vary widely with sample preparation. In general we expect that thick layers of low density will tend to behave as a separate phase.

We propose that the α relaxation corresponds to main-chain rotations in the internal crystalline regions, as suggested previously [39]. Reddish and Barrie [41] analyzed the dielectric intensity approximately and accounted for all of the expected electric moment. Thus, substantially all of the chains are active in the α region. We interpret the mechanical α relaxations, tentatively, as manifestations of longitudinal rearrangements. The chain rotations that dominate the NMR and dielectric relaxations are apparently only weakly active mechanically, if at all. The α relaxation observed dielectrically [43] in oxidized, solution-crystallized linear PE may be an indication of longitudinal mobility, as discussed above. Chain rotation would not be dielectrically active in the crystal mats as they were oriented, so the polarization observed must be of fold origin.

Branched PE has not been subjected to as effective morphological study. The amorphous regions are probably large enough to be considered as a distinct phase. Chain branches (about two or three for every hundred carbon atoms) are known to become incorporated into the crystallites. These branches may be expected to have two more or less compensating effects, first to open up the lattice and second to hinder rotation through steric effects. The α relaxation is more difficult to study in branched PE than in linear PE, owing to lower melting and annealing temperatures.

The mechanisms we visualize here are similar to those proposed for the linear material. The γ relaxation region seems to be primarily amorphous in character. However, the crystalline T_2 is not so easily distinguished as in the linear material and some motion may be present in the crystallites. It is interesting to note that the NMR indication of the γ relaxation occurs at a lower temperature in the linear material while the reverse is true for the β relaxation. Thus, we are led to the following reasonable interpretations. Linear chains are more susceptible to chain-axis rotations but they tend to form structures that are less amenable to more general motions.

Another point deserves comment. Illers [44] has observed a low-temperature mechanical relaxation for several n-paraffins dispersed in polystyrene. The temperature of this relaxation as a function of chain length ties on rather nicely with the results of Sinnott [36] for the γ relaxation temperature as a function of fold length for linear PE. Two comments are relevant. First, NMR studies [45, 46] of n-paraffins give no indication of this transition even though T_1 and $T_{1\rho}$ would be expected to be sensitive to motions of even a small fraction of the chains. Second, Sinnott varied the fold period by annealing, and the state of order and possibly other factors are altered by this treatment.

Inasmuch as these phenomena play a basic role in the development of the mechanisms presented by previous workers it would seem to be worthwhile to further characterize the *n*-paraffin motion and its relevance to the γ transition. The method of specimen preparation is significant in the work of both Illers [44] and Sinnott [36].

Finally, we note that specimens may be available with well-formed crystal interior regions, partially disordered lamellar surfaces and strongly disordered amorphous regions (still possibly attached to the surfaces). This idea was proposed by Matsuoka [33] some time ago and more recently by Bergmann and Nawotki [47]. The observation of two γ relaxations in linear PE may be explained on this basis.

4.2. Polyisobutylene (fig. 9)

The high-temperature transition in PIB is the glass transition, and excellent correlation is observed between the relaxation methods. The curvature observed is the characteristic WLF behavior. The low-temperature transition is clearly a methyl rotation. There are two methyls on every other carbon in the chain and the motion reflects this crowded situation by occurring at higher temperatures than similar methyl motions in other substances, for example polypropylene. The observation of a mechanical loss corresponding to

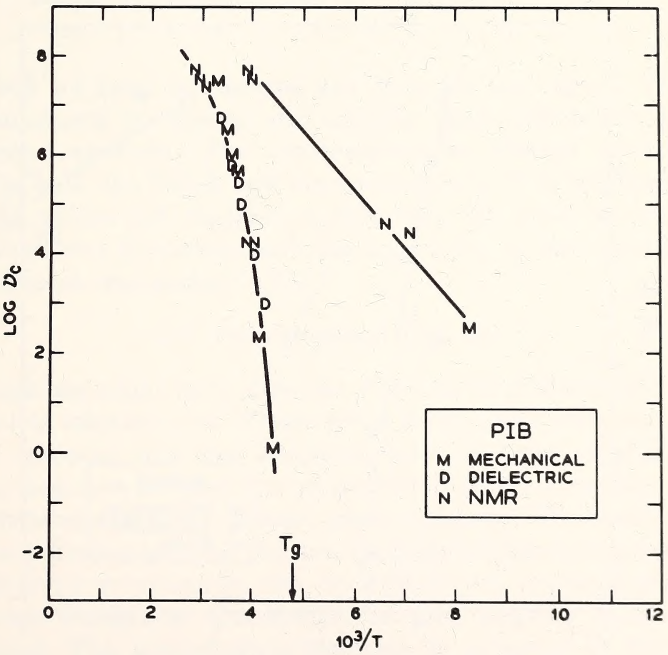

FIGURE 9. Transition map for polyisobutylene.

this locus has led some workers to suggest that the motion must be more complicated than methyl rotation about the C—C bond [48]. We believe that such a methyl motion could be mechanically active, but some cooperative chain motions may be involved as well.

4.3. Rubber (fig. 10)

Relaxation in natural rubber is very similar to that observed in PIB. There is a certain amount of scatter in the data for the glass transition, and this is probably associated with ambiguities in the composition of the polymer. The second set of points (two NMR points and one mechanical point joined by a dashed line) is of unknown origin and may be an impurity effect. We have attempted to reproduce the NMR points in our laboratory with no success. At low temperatures the methyl rotation is again in evidence. This methyl rotation seems to occur at an unusually low temperature.

4.4. Polypropylene (fig. 11)

The data plotted in figure 11 were obtained with isotactic PP and the specimens were partially crystalline. There is probably a high-temperature crystalline relaxation corresponding to the α relaxation

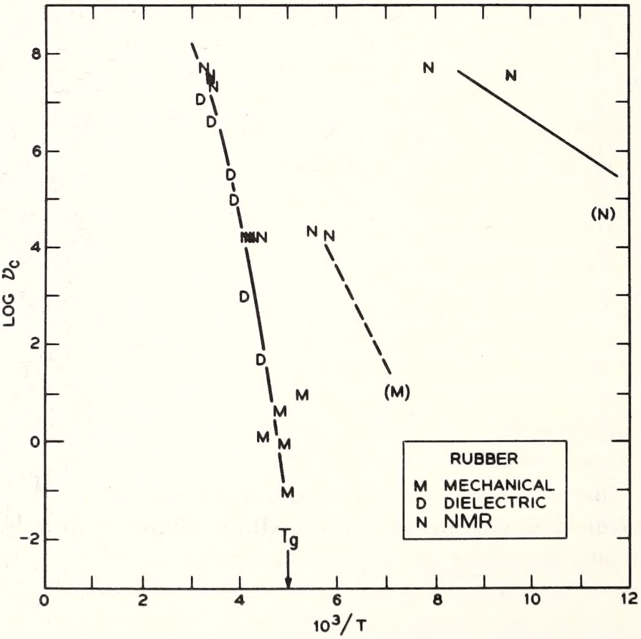

FIGURE 10. Transition map for natural rubber.

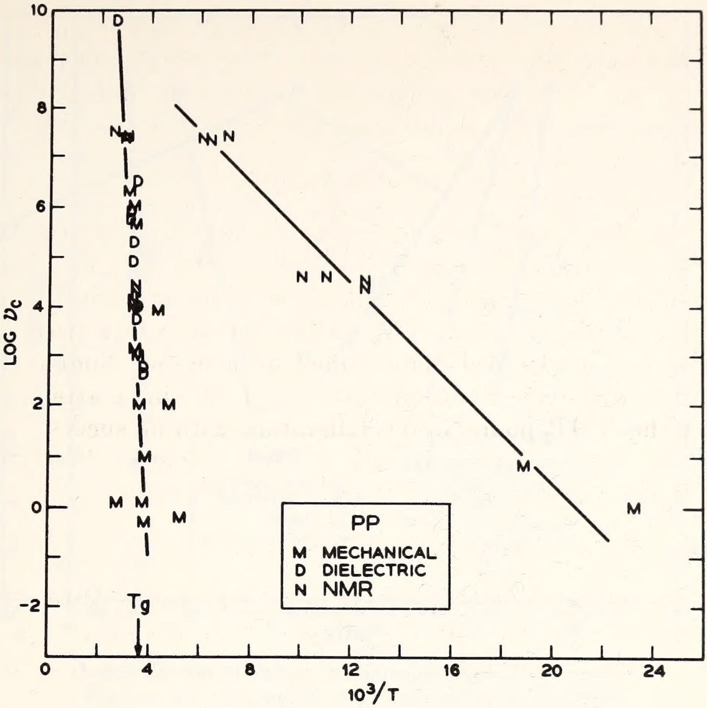

FIGURE 11. Transition map for isotactic polypropylene.

in PE, but we have not located any data for this region. The glass transition shows up clearly and exhibits good correlation between the various methods. The low-temperature methyl relaxation is evident in both the NMR and mechanical data. It is impressive how well these points fall together, considering the great separation in temperature and frequency and the sensitivity of low temperatures on a reciprocal-temperature plot.

4.5. Polybutene-1 (fig. 12)

Although we might have expected PB–1 to be rather similar to PP in respect to relaxation, it is seen to be much more complex. This is isotactic material and the specimens are partially crystalline. In addition, there are at least two crystal forms which interconvert only sluggishly and are often present simultaneously. We have not yet worked out mechanisms for the two medium temperature relaxations, but side-group rotations in the crystalline and amorphous regions are obvious candidates. Correlation between methods is again generally good. The methyl-group rotation is apparent in the NMR results.

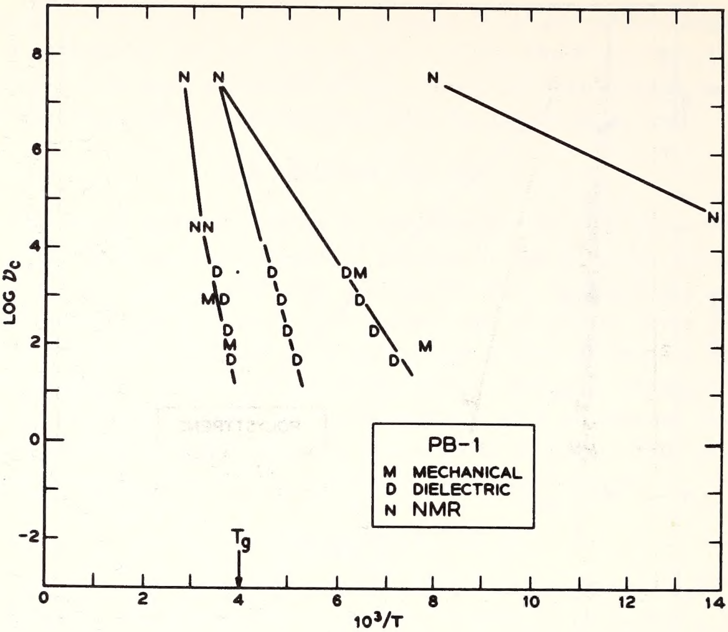

FIGURE 12. Transition map for isotactic polybutene-1.

4.6. Polystyrene (fig. 13)

Relaxation measurements corresponding to the glass transition are in reasonable accord. The temperature scale employed makes the scatter appear somewhat smaller than it would appear on the scale used on the earlier plots. The second transition is active in the NMR and mechanical experiments. This probably corresponds to phenyl-group rotation about the bond connecting the ring to the main chain [49]. The low-temperature NMR point could be an impurity effect, and the dashed line connecting it to the low temperature mechanical point is unsubstantiated.

4.7. Polyvinyl chloride (fig. 14)

Molecular relaxation corresponding to the high-temperature transition in PVC has been discussed in detail by Reddish [50]. His analysis makes it clear that all of the dipoles are active, and indeed the calculated electric moment is so high as to require correlation effects. Whereas this relaxation has usually been interpreted as a glass transition, Reddish discusses the phenomenon as a dielectric "catastrophe" with a Curie point at 74 °C. The number of "correlated dipoles" increases as the temperature approaches T_c, reaching seven at 81°C. This is reminiscent of the Adam and Gibbs treatment of mechanical relaxation above the glass transition [16].

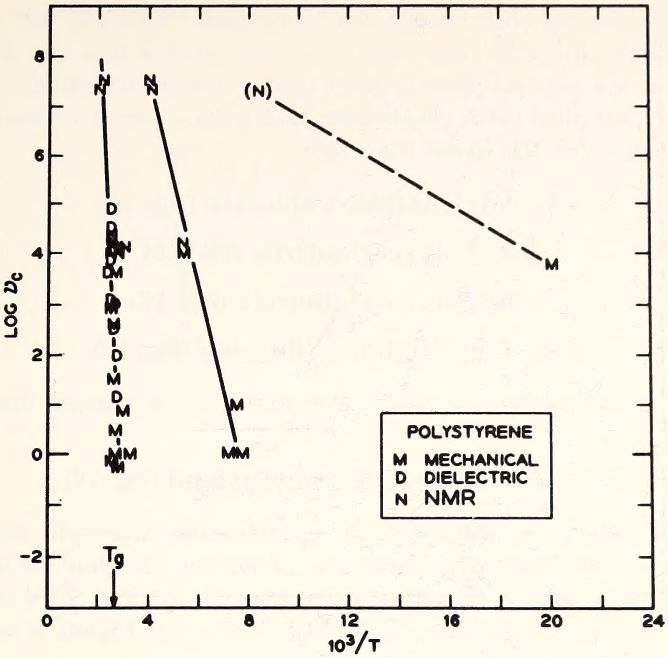

FIGURE 13. Transition map for atactic polystyrene.

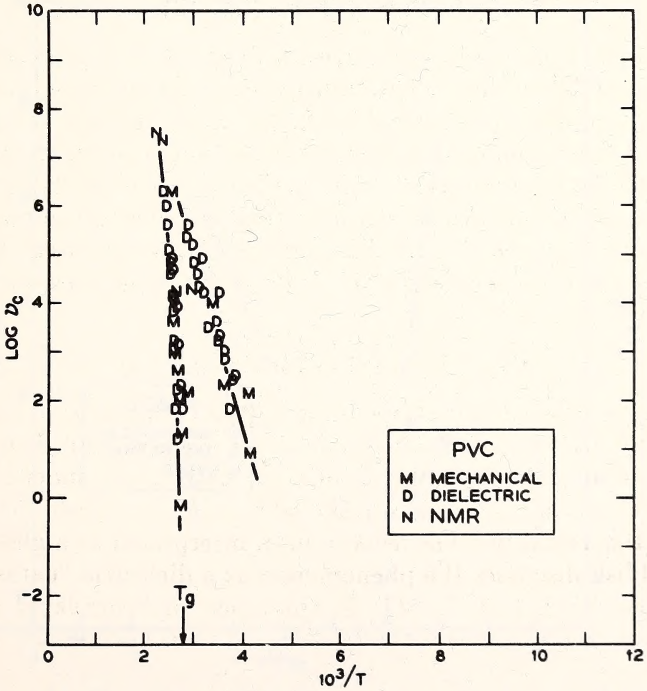

FIGURE 14. Transition map for polyvinylchloride.

The low-temperature relaxation has been reported by several investigators, although it is very weak. Sometimes it is not observed at all and we suggest that it might be an impurity effect. PVC is commonly supplied with plasticizer, and even a small concentration could account for the losses reported.

4.8. Polyvinylidene chloride (fig. 15)

4.9. Polyacrylonitrile (fig. 16)

4.10. Polyvinyl fluoride (fig. 17)

4.11. Polyvinylidene fluoride (fig. 18)

Too little is known about these four materials to warrant discussion here.

4.12. Polychlorotrifluoroethylene (fig. 19)

PCTFE has been subjected to an extensive dielectric study by Scott and co-workers [51]. Particular attention was paid to morphological factors, and measurements were made over a wide range of temperature and frequency. The glass relaxation region is sensitive

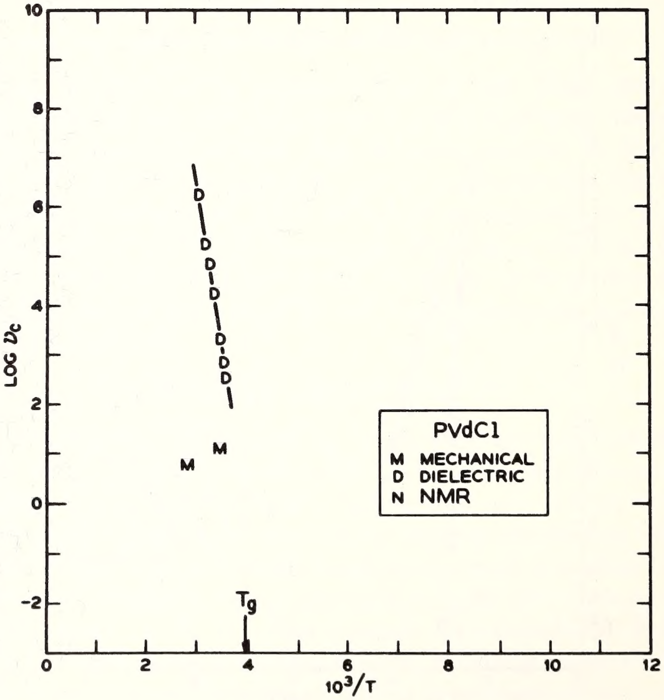

FIGURE 15. Transition map for polyvinylidenechloride.

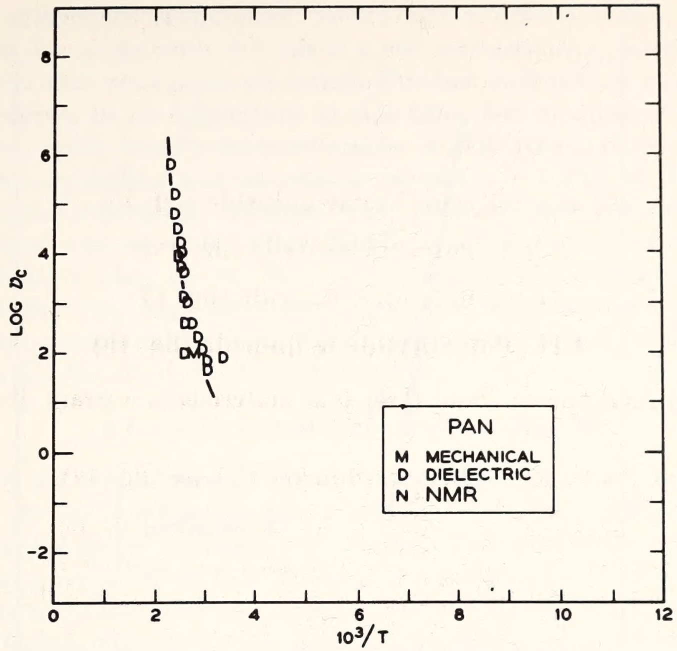

FIGURE 16. Transition map for polyacrylonitrile.

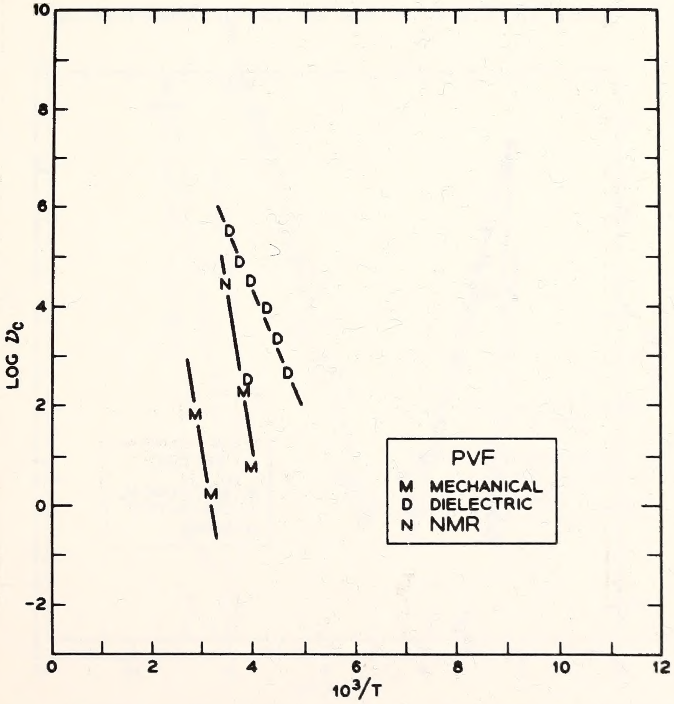

FIGURE 17. Transition map for polyvinylfluoride.

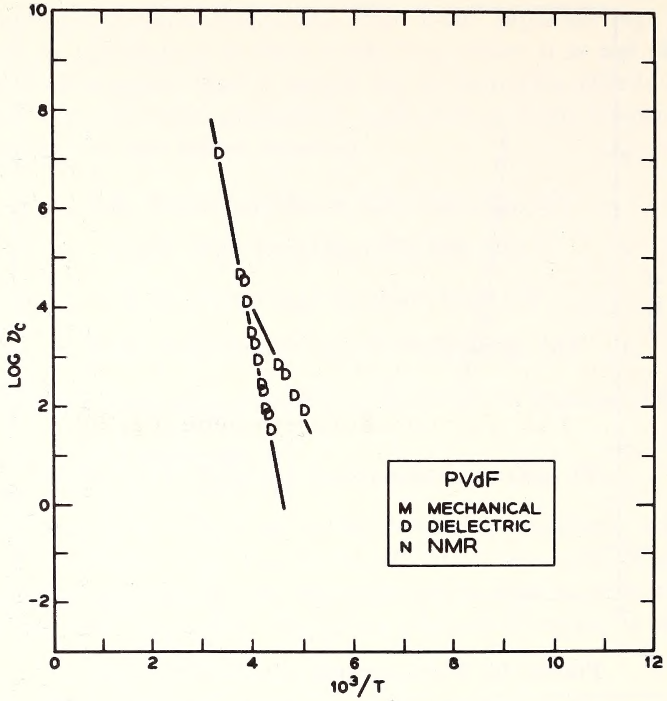

FIGURE 18. Transition map for polyvinylidenefluoride.

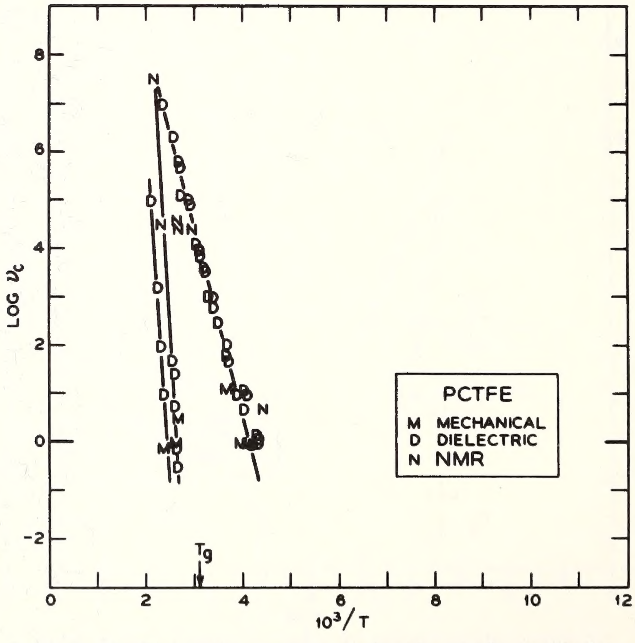

FIGURE 19. Transition map for polychlorotrifluoroethylene.

to the method of preparation, and we have drawn in two lines to indicate the range covered. This is a very complex story and we refer the reader to Scott's paper for details. Further work [52] on this system is in progress in our laboratory at this time, and we are not entirely in accord with Scott's interpretations. NMR results indicate that both the crystalline and amorphous regions are active in the lower temperature relaxation, whereas Scott assigned this motion to the amorphous regions only. (Our NMR specimens were of medium crystallinity.) Also, we can find no evidence in the NMR results to support the very high frequency (very low temperature) crystalline relaxation postulated by Scott. We do not have an entirely satisfactory explanation for all of the data at this time.

4.13. Polytetrafluoroethylene (fig. 20)

PTFE is a crystalline polymer with stiff chains, and it exhibits many unique properties. The relaxation behavior is quite complicated and the morphology is not very well known. Two first-order crystalline transitions are observed in addition to the melting point. We summarize here some assignments made in a recent paper on this system [53].

The high-temperature relaxation is thought by some workers to be the glass transition and is designated α or glass I. We regard this

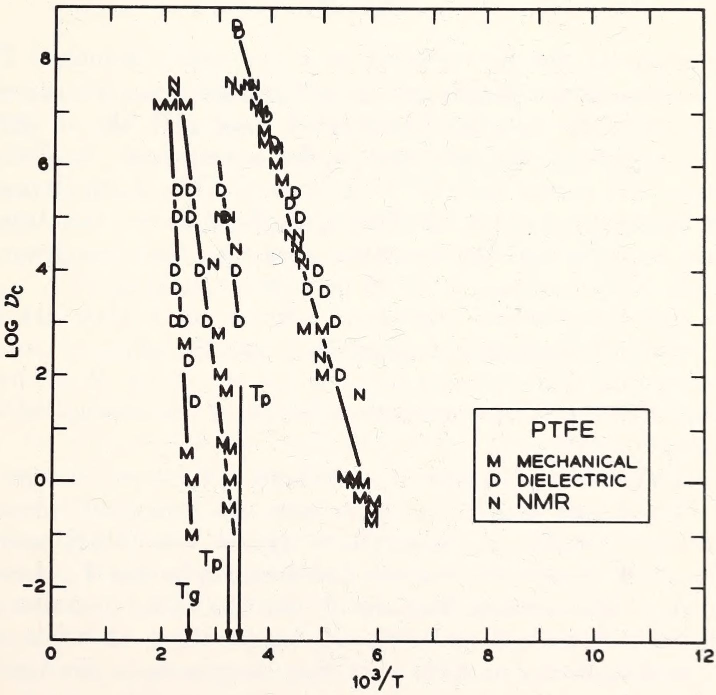

FIGURE 20. Transition map for polytetrafluoroethylene.

assignment as tentative and insecure. The dielectric data could better be interpreted in terms of a crystalline relaxation. No corresponding NMR relaxation is observed (see below).

The second transition, labelled β, is a crystalline phenomenon. We interpret this as a region of extensive longitudinal freedom which extends down to the first-order transition just above room temperature. Clarke [54] has x-ray evidence that may support this suggestion.

The molecules within the crystalline regions obtain rotational freedom abruptly just below room temperature. Here again the x-ray and NMR evidence lead to the same conclusion [55, 56]. The rate of relaxation just above the transition corresponds to $v_c \sim 10^8$ Hz. Corresponding relaxations are observed in the intermediate phase.

The low-temperature transition, designated γ or glass II, is an amorphous phenomenon. The chains gradually attain rotational mobility and longitudinal translational mobility in more or less the same temperature range, as indicated by the continuous increase of the amorphous T_{2a}. It is of interest that T_{2a} becomes independent of temperature above about 180 °C. This is just the region where T_{2a} would be expected to increase sharply if the α transition corresponds to a glass transition in the usual sense.

4.14. Polyhexafluoropropylene-tetrafluoroethylene Copolymer (fig. 21)

This material can be regarded as a somewhat branched PTFE. The branches consist of CF_3 groups and molecular models reveal that they fit compactly into the fluorocarbon chain [57]. One of the most dramatic effects of the branches is the lowering of the first-order transition that occurs near 20 °C in linear PTFE. A copolymer containing about 10 percent hexafluoropropylene shows this transition at about -50 °C and the transition seems to have lost some of its sharpness. This specimen is 30–40 percent crystalline.

The high-temperature relaxation behaves as a glass transition. NMR results indicate two distinct T_2's, and T_{2a} increases rapidly in this region [52]. Quite general motions are visualized. Note that this is entirely different than our interpretation of the corresponding (α) relaxation in PTFE.

Just below this high-temperature relaxation there is a change in the NMR T_2 which we take to signal the onset of longitudinal translations in both the crystalline and amorphous regions. The NMR point with parentheses is taken from a small discontinuity in the $T_{1\rho}$ curve and is probably the remnant feature of the first-order transition that heralds the β relaxation in PTFE. Its temperature, 15 °C, is reasonable in this view. Its position on a frequency scale is not significant [52].

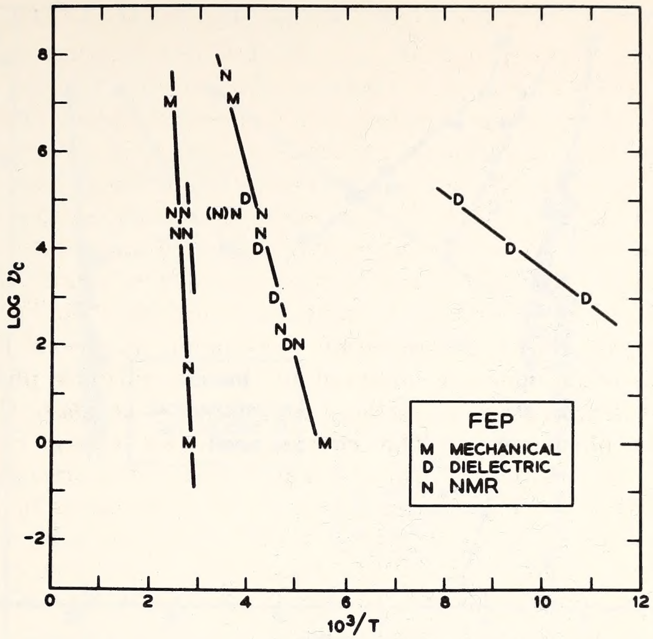

Figure 21. Transition map for a polyhexafluoropropylene-tetrafluoro-ethylene copolymer.

The next lower relaxation locus is probably a composite corresponding to the first-order crystalline transition (20 °C) and the amorphous γ relaxation in linear PTFE. Main-chain rotation is the motional freedom acquired.

Finally, at low temperatures there is dielectric evidence for an impurity relaxation. It has been proposed that this is due to rotations of a few —CF_2H groups [57].

4.15. Polymethylmethacrylate (fig. 22)

The first relaxation is the glass transition, which is very strongly active in the mechanical measurements. The second relaxation, designated β, is apparent in all studies and has been identified with side chain motions of the ester group. We note that by combining the relaxation results, it has been possible to follow this relaxation over eleven orders of magnitude in frequency. The electric polarization is consistent with activity of the entire sample [58].

The dielectric point at 10^4 Hz at -20 °C ($10^3/T=4$) has been ascribed to the presence of water [59]. This is a reasonable interpretation of this weak relaxation.

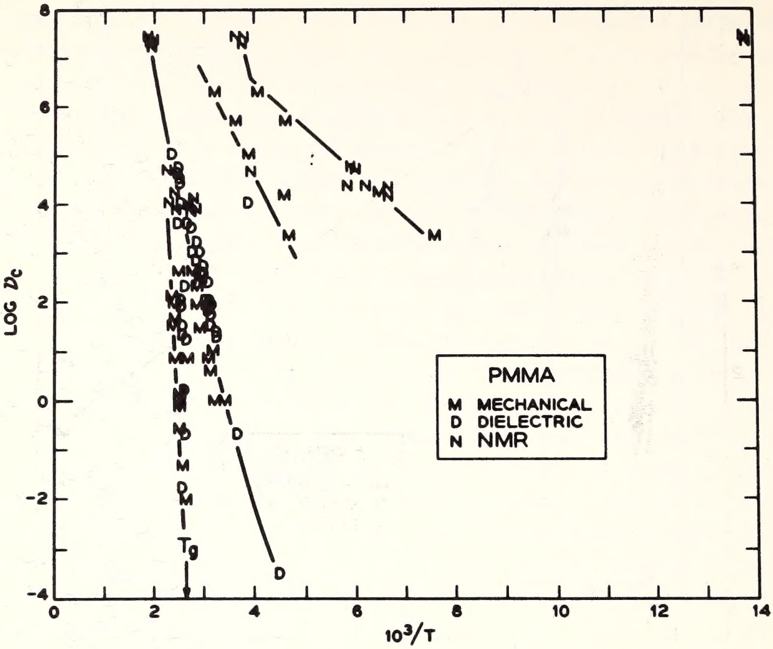

FIGURE 22. Transition map for polymethylmethacrylate.

The low-temperature relaxation detected in NMR and mechanical experiments involves the rotation of methyl groups attached to the main chain. Finally, at very low temperatures there is evidence for rotation of the side-chain methyl groups. Substantially all of the methyls are active in these relaxations. There is some evidence that the side-chain methyl rotation is also mechanically active [60].

4.16. Polyethylmethacrylate (fig. 23)

The relaxation behavior of PEMA is very similar to that of PMMA. The β relaxation lies closer to the glass transition but is still easily resolved. The β motion is the side-chain ester rotation. The low-temperature relaxations are main-chain and ester methyl rotations. The former appears to be mechanically inactive while the latter is active [60]. The interpretation of these low-temperature, mechanically active processes as methyl group reorientations is somewhat controversial and worthy of further study [61].

4.17. Poly *n*-butylmethacrylate (fig. 24)

The glass transition and the β relaxation for PnBMA are indicated by a single line in figure 24 even though separate peaks can be resolved. The presence of the bulky *n*-butyl group tends to make these

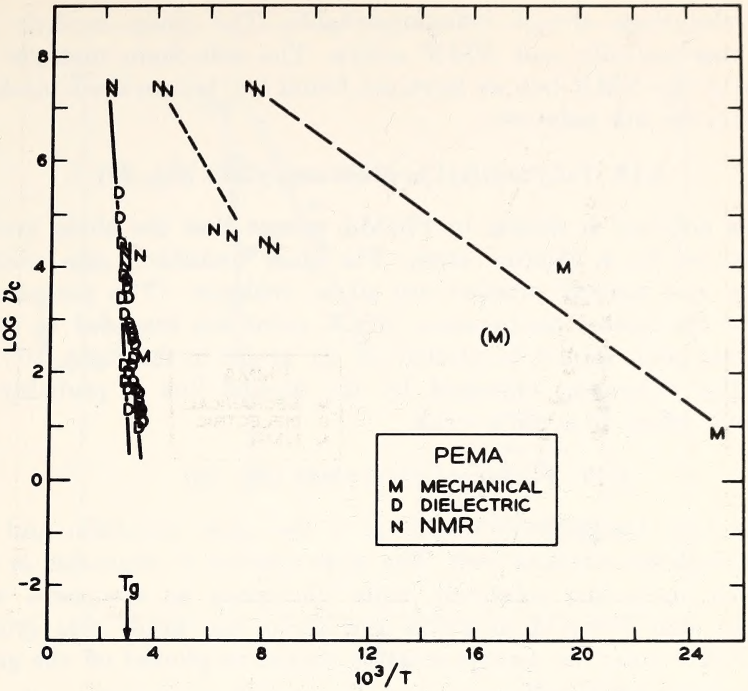

FIGURE 23. Transition map for polyethylmethacrylate.

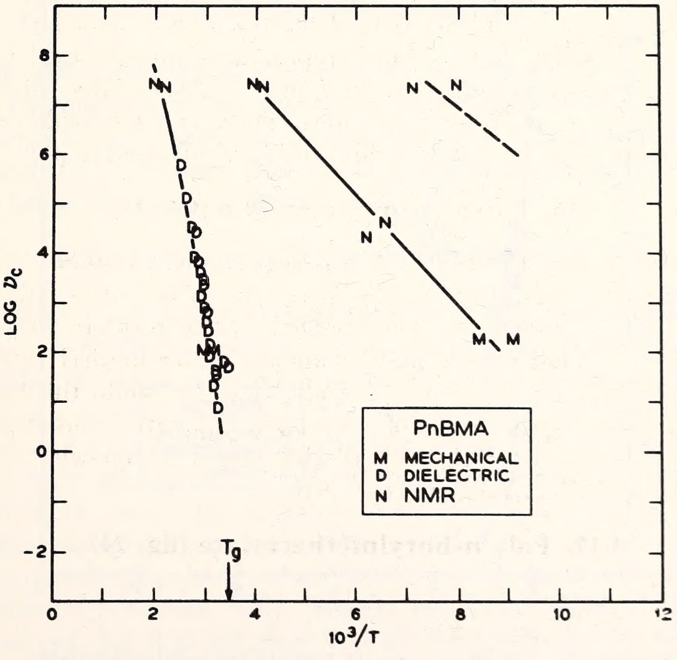

FIGURE 24. Transition map for poly *n*-butylmethacrylate.

two relaxations almost indistinguishable. The chain methyls are both mechanically and NMR active. The side-chain methyls are active in the NMR but we have not found low temperature mechanical data for this polymer.

4.18. Polymethyl α-chloroacrylate (fig. 25)

This polymer is similar to PMMA except that the chain methyl is replaced by a chlorine atom. The glass transition, side chain β motion and methyl rotation are all in evidence. (The parentheses around the lowest temperature NMR point are intended to mean that this point should be plotted off the graph to the right, $10^3/T>12$.) The relaxation indicated by the dashed line is probably an impurity effect. It is quite weak.

4.19. Polymethylacrylate (fig. 26)

The high temperature transition is the glass transition and the three methods correlate well. The ester-rotation β relaxation is well resolved, indicating relatively little hindrance as compared with PMMA and PMαCA in which the chain has other side groups. The NMR point for methyl rotation should be plotted off the graph to the right, $10^3/T>12$.

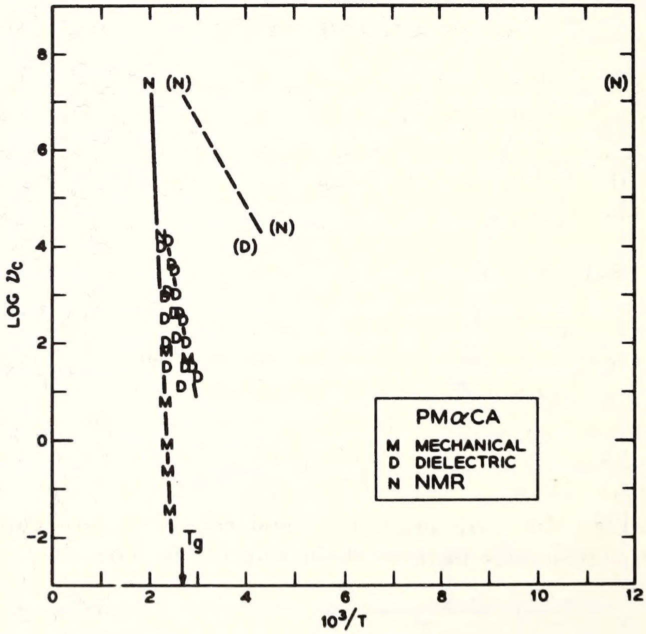

FIGURE 25. Transition map for polymethyl α-chloroacrylate.

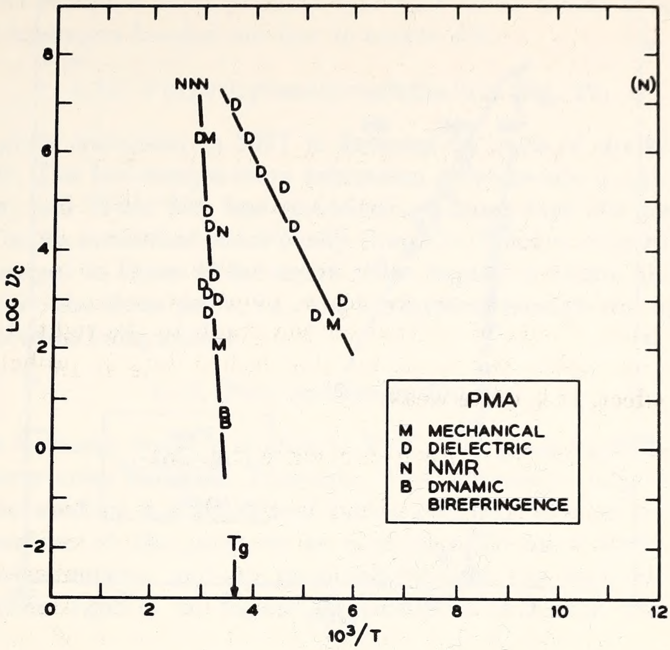

FIGURE 26. Transition map for polymethylacrylate.

4.20. Polyvinylacetate (fig. 27)

From the similarity of structure we expect PVAc to behave as PMA. Comparison of the transition maps confirms this view. It is of interest to note that the β relaxation does not appear in NMR studies of these polymers. The NMR T_1 minimum for methyl rotation occurs below the range of study.

4.21. Polyhexamethyleneadipamide (fig. 28)

The glass transition is evident in each of the relaxation methods for Nylon 6–6. The second transition, evident only in the mechanical and dielectric data, has been ascribed to the presence of water. Drying is a special problem in Nylons, owing to the fact that they are prepared by a reaction that liberates water. As water is removed, it is further generated by further polymerization. The specimens studied were "dry" by ordinary standards. The low-temperature relaxation corresponds to main-chain rotation in both the crystalline and amorphous regions. It is possible that this can be resolved into two separate processes. Both paraffin and polar parts of the chain are involved, but it is not clear that all the amide dipoles are active. A proper dielectric intensity study in the low-temperature region

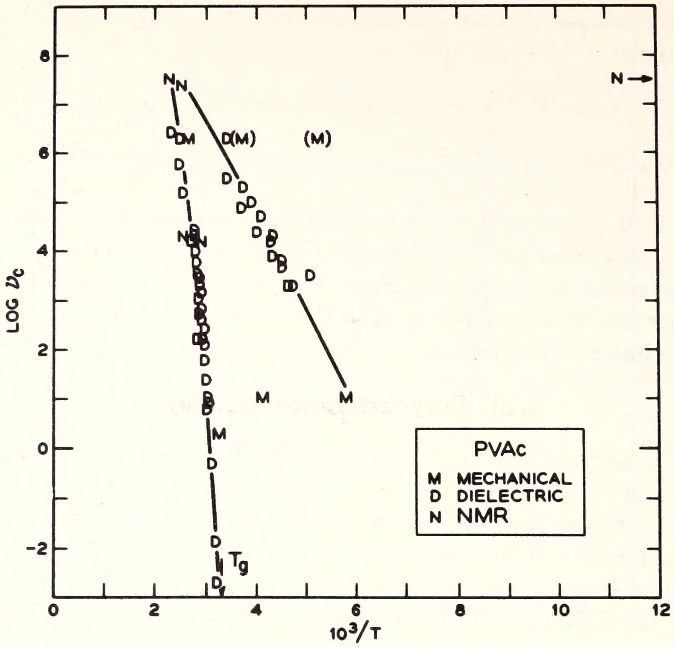

FIGURE 27. Transition map for polyvinylacetate.

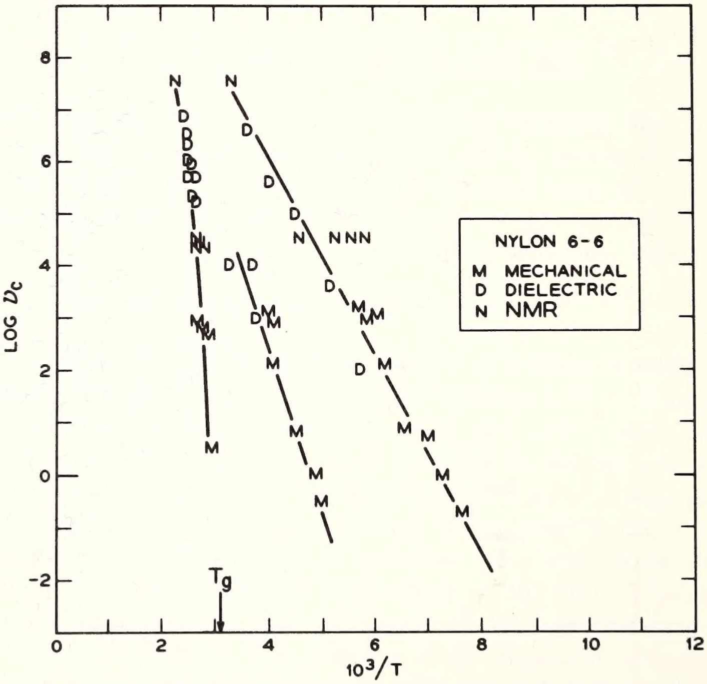

FIGURE 28. Transition map for polyhexamethyleneadipamide.

would be valuable. It is possible that only those amide groups that are not hydrogen bonded are free to rotate [62].

4.22. Polyethyleneterephthalate (fig. 29)

The glass transition in PET is detected by each of the relaxation methods. The low-temperature relaxation corresponds to main chain rotation, and Ward [63] has presented evidence that the methylene groups move somewhat more easily than the benzene rings. It would be of interest to know if the entire chain begins to rotate all at once or whether the three parts, i.e., the methylene, phenyl and carboxyl, are somewhat independent.

4.23. Polycarbonate (fig. 30)

PC is in many respects similar to PET. The glass transition shows good correlation between methods. The secondary relaxation has been discussed by Matsuoka and Ishida [64], who ascribe it to main-chain motion of the polymer as a whole. We have made further NMR observations and we now believe that the carboxyl groups retain their rigidity to higher temperatures than the phenyl and

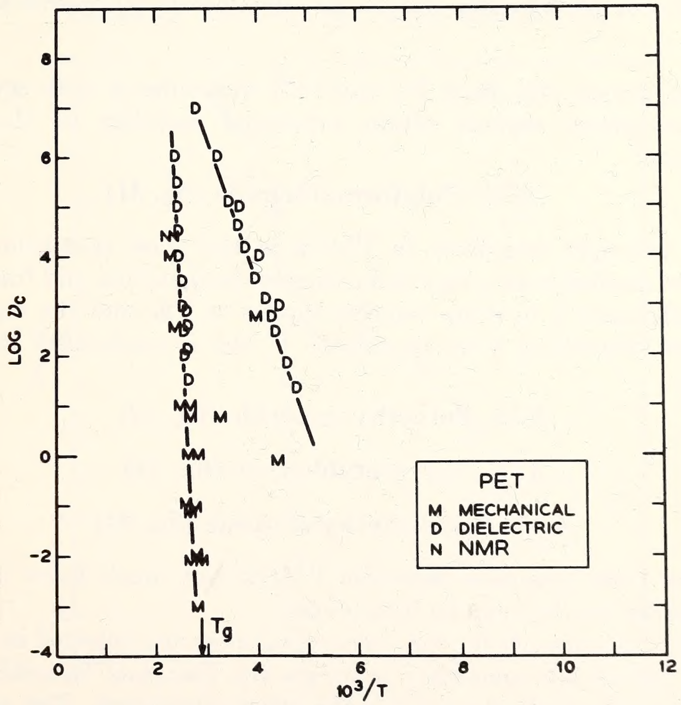

FIGURE 29. Transition map for polyethyleneterephthalate.

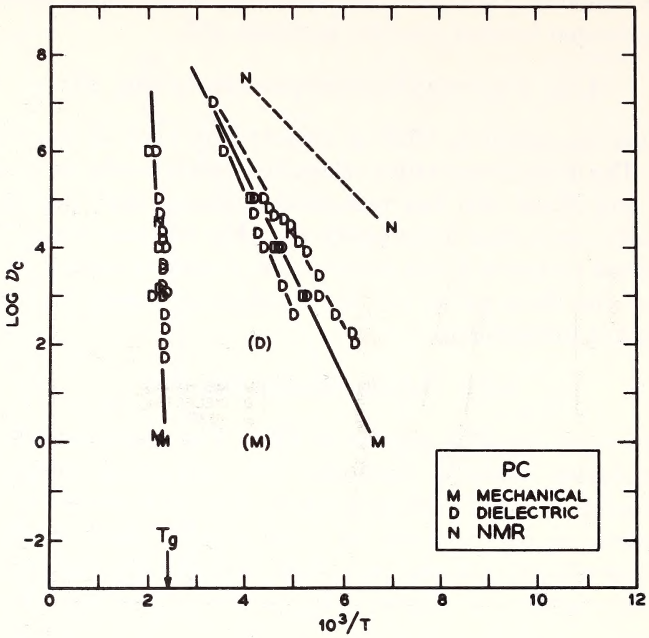

FIGURE 30. Transition map for the polycarbonate of bisphenol-A.

$C(CH_3)_2$ groups [52]. Both PC and PET molecules in both crystalline and amorphous regions attain rotational mobility at the lower relaxation.

4.24. Polyformaldehyde (fig. 31)

The principle transition in PMOx is the glass transition which has been studied over a very wide range of temperature and frequency. This substance is in some respects similar to PE, and the high temperature relaxations may be related to the α mechanism discussed for PE.

4.25. Polyethyleneoxide (fig. 32)

4.26. Polyacetaldehyde (fig. 33)

4.27. Polydimethylsiloxane (fig. 34)

These three polymers resemble PMOx, but much more needs to be done before they can be interpreted.

Activation energies for the various polymers are collected in table 1. These figures are somewhat arbitrary for the glass transitions and not very accurately defined for the other relaxations. The grouping in columns is only intended to match up approximate magnitudes.

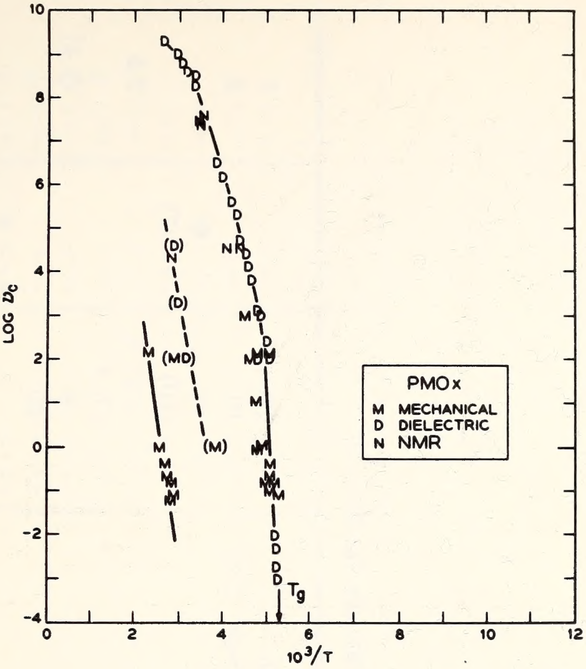

FIGURE 31. Transition map for polyformaldehyde.

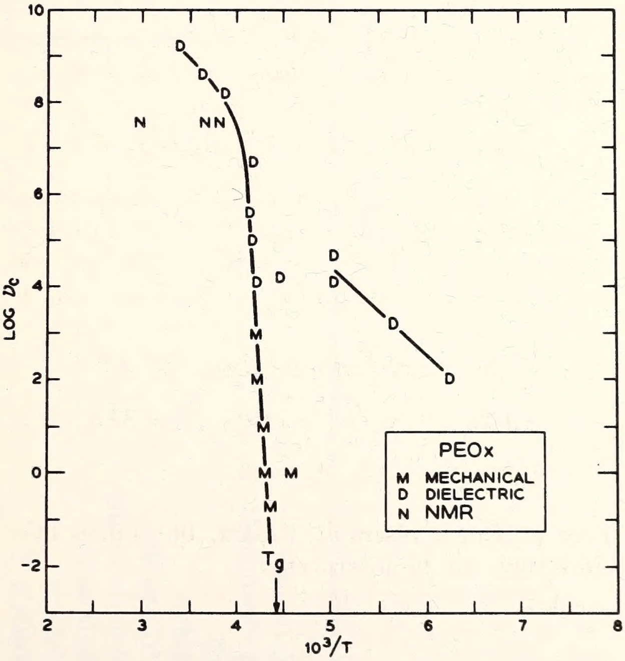

FIGURE 32. Transition map for polyethyleneoxide.

Table 1. Activation energies (kcal/mole)

PE (linear)	>30, 25	 12	...	... ?
PE (branched)	>50, >40	 10	...	... 3
PIB	>50	....	... 6	...
Rubber	>30	.... (10)	... (7)	...
PP(isotactic)	>30	....	...	... 2.3
PB–1 (isotactic)	>20	.... 17, 8	...	...
PSt (atactic)	>50	 9	...	... (1.4)
PVC	>50	 17	...	...
PVdC	>30	....	...	...
PAN	>50	....	...	...
PVF	30, 30	 11	...	...
PVdF	27	 11	...	...
PCTFE	50	 17	...	...

PTFE	>50, 35, 33	 16	...	...
FEP	>50	 18	... 4	...
PMMA	>50	 21	... 4	... ?
PEMA	50	 24	... 4	... 1.7
PnBMA	>30	....	... 4	... ?
PMαCA	>50	 26	...	... ?
PMA	>50	 9	...	... ?
PVAc	>40	 9	...	... ?
NYLON 6–6	>50	.... (15), 9	...	...
PET	>50	 14	...	...
PC	>50	 10	... 5	...
PMOx	>40, >50, >50	....	...	...
PEOx	>50	 8	...	...
PAcAl	>50	....	...	...
PDMS	>50	....	...	...

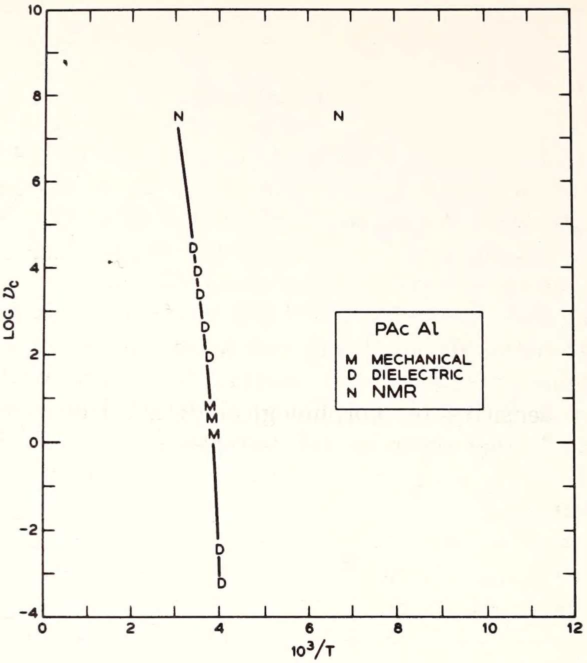

FIGURE 33. Transition map for polyacetaldehyde.

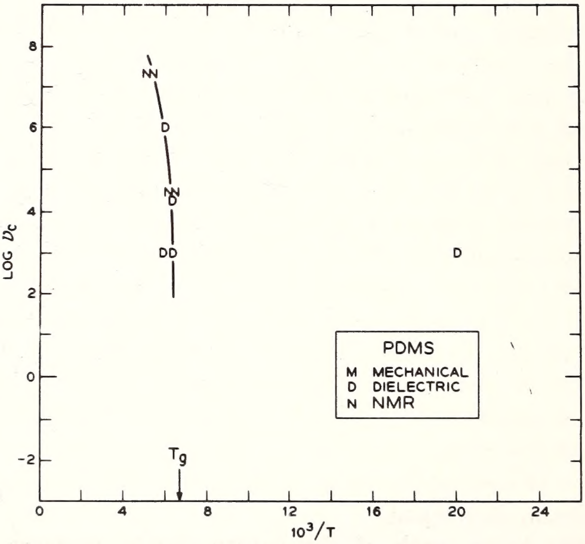

FIGURE 34. Transition map for polydimethylsiloxane.

5. Conclusions

Although the problems associated with understanding relaxation behavior in solid polymers are difficult, progress has been made. Correlations between the various methods are good. It is remarkable just how far our discussion of *relaxation* in solid polymers can be carried with almost no reference to morphological matters. Also, it is remarkable that the correlations work out as well as they do, considering that materials are being compared that have appreciably different origins and histories. It appears that relaxation frequencies are not very sensitive to morphological detail. However, it seems likely that for further experimental characterization of the intensities, it will be necessary to pay close attention to morphology and other structural features.

Assignments of molecular mechanisms for a polymer can usually be made intuitively and checked by comparisons with related polymers and estimates of the magnitudes of relaxation parameters. These assignments are entirely reasonable for many polymers, and we have confidence in most that we have discussed in this paper. This intuitive procedure is less formal, but basically similar to the assignment of resonance spectra, i.e., optical, infrared, etc.

Once a molecular mechanism has been distinguished, the relaxation can usually be described by a very limited number of parameters. Consequently only a limited number of theoretical parameters can be extracted and correspondingly simple models should be chosen. For example, we regard it as unlikely that more than a two-position calculation will be necessary for the description of polymer data. The theories of Bueche and Adam and Gibbs should be useful in understanding glass-transition phenomena. However, it is not obvious that the site model cannot be made to cover this situation as well.

It seems to us that the abundance of relaxation work carried out over the last decade has served its purpose. Future work should follow a different pattern. There is sufficient experimental and theoretical background available that we should begin to emphasize more practical aspects. Oriented and composite materials are obvious candidates. The relevance of basic relaxation studies to engineering matters must be examined and developed.

Finally, the basic work of the future should proceed as a close collaboration between theorists and experimentalists. This is a trend that is already beginning to take shape. The theoreticians are not burdened by an investment in a piece of equipment and thus are more likely to be willing to consider a wide range of experimental sources.

The experimentalists must learn to take a broader view. Practitioners of dielectric relaxation, mechanical relaxation and NMR attend the same meetings, but inter-group communication is usually condescending and lacking in depth. A general theoretical model, not restricted to a single experiment, could provide a medium for broader understanding. With new relaxation tools (e.g. dynamic birefringence) becoming available, the need is urgent.

It is a pleasure to acknowledge a great debt to many friends and colleagues for assistance and encouragement in the preparation of this material. Several sections of this paper were developed in close collaboration with D. C. Douglass, and it would be difficult to overemphasize his contributions. W. P. Slichter and S. Matsuoka contributed frequently and generously in many ways. D. R. Falcone provided much of the original data. W. Reddish, J. D. Hoffman, J. G. Powles, J. Strange, Y. Ishida, T. M. Connor, K. M. Sinnott and E. S. Clark provided material in advance of publication. Professor Powles and the University of Kent kindly provided a haven in which some of this material was prepared. Valuable discussions were provided by G. Willams, B. Read, N. G. McCrum, and I. M. Ward, as well as those individuals mentioned above.

6. Discussion

H. Resing (Naval Research Laboratory): Are the relaxations in the "Ailion-Slichter" experiment always exponential? If they are, how does this fit in with the notion of a distribution of correlation times, e.g. jump times? After all, how can two nuclei with different relaxation environments communicate their spin temperature to one another? Is spin diffusion involved?

D. W. McCall: Dr. Resing has raised an important point. The "Slichter-Ailion" theory predicts that under certain conditions $\tau_c \cong T_{1\rho}$. A distribution in τ_c may or may not be reflected in a distribution in $T_{1\rho}$, e.g. non-exponential rotating frame relaxation curves. If the distribution of τ_c is a sort of macroscopic distribution, e.g. arising from a specimen made up of domains, each with a given τ_c, where τ_c varies from one domain to another, a distribution of $T_{1\rho}$'s can result. We believe this situation occurs in semicrystalline polymers because distinct $T_{1\rho}$ curves appear for the crystalline and amorphous regions. On the other hand, if the various parts of the distribution are coupled strongly to one another, we interpret the Slichter-Ailion model to obtain a single exponential decay in the rotating frame and the resulting $T_{1\rho}$ should be approximately equal to some average τ_c.

7. References

[1] Part of the material included in this paper was presented at the Polymer Research Group Conference, Moretonhampstead, England, April, 1964.

[2] The subject of this paper was considered by a symposium which met at the American Chemical Society meeting at Atlantic City, September, 1965. The papers from this symposium have been published: Transitions and Relaxations in Polymers, edited by Raymond F. Boyer, Interscience Publishers, New York, 1966. This monograph is often listed as: J. Polymer Sci. **C14,** (1966).

[3] Many of the ideas expressed throughout this paper have been drawn from or influenced by: J. D. Hoffman, G. Williams and E. Passaglia, J. Polymer Sci. **C14,** 173 (1966).

[4] J. D. Ferry, Viscoelastic Properties of Polymers, John Wiley & Sons, New York, 1961.

[5] S. Glasstone, K. J. Laidler and H. Eyring, Theory of Rate Processes, McGraw-Hill Book Co., New York, 1941.

[6] H. Frohlich, Proc. Phys. Soc. (London) **54,** 422 (1942).

[7] G. Williams, J. I. Lauritzen and J. D. Hoffman, private communication, to be published.

[8] J. D. Hoffman and H. G. Pfeiffer, J. Chem. Phys. **22,** 132 (1954).

[9] H. Frohlich, Theory of Dielectrics, Oxford Press, 1958, 2nd Ed., Chapter III.

[10] A. H. White, J. Chem. Phys. **7,** 58 (1939).

[11] P. Debye, Chem. Rev. **19,** 171 (1936).

[12] J. I. Lauritzen, J. Chem. Phys. **28,** 118 (1958).

[13] H. Eyring, D. Henderson, B. J. Stover and E. M. Eyring, Statistical Mechanics and Dynamics, John Wiley, New York, 1964, p. 369.

[14] F. Bueche, J. Chem. Phys. **21,** 1850 (1953).

[15] J. H. Gibbs and E. A. DiMarzio, J. Chem. Phys. **28,** 373, 807 (1958).

[16] G. Adam and J. H. Gibbs, J. Chem. Phys. **43,** 139 (1965).

[17] F. Bueche, J. Chem. Phys. **22,** 603 (1954).

[18] P. E. Rouse, J. Chem. Phys. **21,** 1272 (1953).

[19] B. H. Zimm, J. Chem. Phys. **24,** 269 (1956).

[20] R. E. Dewames, W. F. Hall and M. C. Shen, J. Chem. Phys. **46,** 2782 (1967).

[21] M. C. Shen and A. Eisenberg, Prog. Solid State Chem. **3,** 407 (1966).

[22] E. R. Andrew and P. S. Allen, J. chim. phys. 85 (1966).

[23] D. F. R. Gilson and C. A. McDowell, Nature **183,** 1183 (1959).

[24] R. J. Meakins, Trans. Faraday Soc. **51,** 953 (1955).

[25] A discussion of morphology with specific reference to relaxation is given in ref. 3.

[26] W. P. Slichter and D. W. McCall, J. Polymer Sci. **25,** 230 (1957).

[27] D. W. McCall and E. W. Anderson, J. Polymer Sci. **1A,** 1175 (1963).

[28] D. H. Reneker, J. Polymer Sci. **59,** 539 (1962).

[29] A. H. Willbourn, Trans. Faraday Soc. **54,** 717 (1958).

[30] R. F. Boyer, J. Polymer Sci. **C14,** 3 (1966).

[31] T. F. Schatzki, J. Polymer Sci. **C14,** 139 (1966).

[32] W. O. Statton and P. H. Geil, J. Appl. Polymer Sci. **3,** 357 (1960).

[33] S. Matsuoka, discussion at the symposium mentioned in ref. 2.
[34] R. S. Moore and S. Matsuoka, J. Polymer Sci. **C5,** 163 (1964).
[35]_N. G. McCrum and E. L. Morris, Proc. Royal Soc. **A202,** 506 (1966).
[36] K. M. Sinnott, J. Polymer Sci. **C14** (1966).
[37] S. Matsuoka, private communication.
[38] D. W. McCall and D. C. Douglass, Polymer **4,** 433 (1963).
[39] D. W. McCall and W. P. Slichter, J. Polymer Sci. **26,** 171 (1957).
[40] D. W. McCall and D. C. Douglass, Appl. Phys. Letters **7,** 12 (1965).
[41] W. Reddish and I. T. Barrie, I.U.P.A.C. Symp. Wiesbaden, Kurzmitteilen IA3, 1958.
[42] D. J. Blundell, A. Keller and T. Connor, private communication, to be published.
[43] Y. Ishida and K. Yamafuji, Kolloid-Z. **202,** 26 (1965).
[44] K. H. Illers, Rheol. Acta, **3,** 194 (1964).
[45] D. C. Douglass and G. P. Jones, J. Chem. Phys. **45,** 956 (1966).
[46] J. E. Anderson and W. P. Slichter, J. Phys. Chem. **69,** 3099 (1965).
[47] K. Bergmann and K. Nawotki, presented at Mainz, April 1966.
[48] A. E. Woodward, personal conversation.
[49] K. H. Illers, Z. f. Elektrochem. **65,** 679 (1961).
[50] W. Reddish, J. Polymer Sci. **C14,** 123 (1966).
[51] A. H. Scott, D. J. Scheiber, A. J. Curtis, J. I. Lauritzen, and J. D. Hoffman, J. Res. N. B. S. **66 A,** 269 (1962).
[52] D. W. McCall, D. C. Douglass and D. R. Falcone, to be published.
[53] D. W. McCall, D. C. Douglass and D. R. Falcone, J. Phys. Chem. **71,** 998 (1967).
[54] E. S. Clark, unpublished studies, presented at a NASA conference, Case Institute, April, 1967.
[55] E. S. Clark and L. T. Muus, Z. Krist **117,** 119 (1962).
[56] D. Hyndman and G. F. Origlio, J. Appl. Phys. **31,** 1849 (1960).
[57] R. K. Eby and F. C. Wilson, J. Appl. Phys. **33,** 2951 (1962).
[58] D. W. McCall, J. Phys. Chem. **70,** 949 (1966).
[59] D. J. Scheiber and D. J. Mead, J. Chem. Phys. **27,** 326 (1957).
[60] K. M. Sinnott, J. Polymer Sci. **35,** 273 (1959).
[61] A. E. Woodward, J. Polymer Sci. **C14,** 89 (1966).
[62] D. W. McCall and E. W. Anderson, J. Chem. Phys. **32,** 237 (1962).
[63] I. M. Ward, Trans. Faraday Soc. **56,** 648 (1960).
[64] S. Matsuoka and Y. Ishida, J. Polymer Sci. **C14,** 247 (1966).
[65] R. Zwanzig, Annual Reviews of Physical Chemistry, **17** (1966).
[66] Y. H. Pao, private communication.

Appendix 1. Reference List for Transition Maps

Polyethylene (PE)

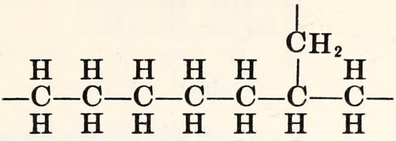

$$-\mathrm{CH_2-CH_2-CH_2-CH_2-CH_2-CH(CH_2{-})-CH_2}-$$

[21, 31, 35, 37, 43, 65, 68, 70, 72, 76, 84, 87, 88, 90, 92, 107, 108, 109, 110, 115, 119, 121, 123, 124, 127, 128, 144, 145, 147, 150, 156, 160, 161, 163, 164, 173, 188, 189, 198, 204].

Polyisobutylene (PIB)

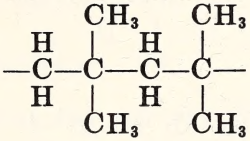

$$-\mathrm{CH_2-C(CH_3)_2-CH_2-C(CH_3)_2}-$$

[16, 38, 71, 118, 136, 137, 150, 156, 170, 171, 183, 186].

Rubber

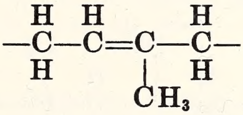

$$-\mathrm{CH_2-CH{=}C(CH_3)-CH_2}-$$

[14, 33, 34, 41, 125, 140, 166, 170, 171].

Polypropylene (PP)
(isotactic)

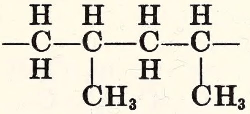

$$-\mathrm{CH_2-CH(CH_3)-CH_2-CH(CH_3)}-$$

[21, 38, 74, 83, 91, 98, 100, 113, 132, 143, 149, 150, 152, 166, 168, 169, 170, 180, 188, 198, 202].

Polybutene-1 (PB–1)

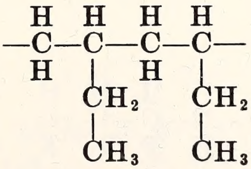

$$-\mathrm{CH_2-CH(CH_2CH_3)-CH_2-CH(CH_2CH_3)}-$$

[61, 91, 150, 166, 169, 170, 202, 205].

Polystyrene (PSt)
(atactic)

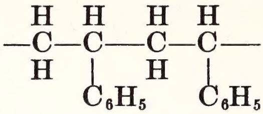

$$\begin{array}{cccc} H & H & H & H \\ -C- & C- & -C- & C- \\ H & | & H & | \\ & C_6H_5 & & C_6H_5 \end{array}$$

[4, 8, 9, 11, 22, 41, 43, 45, 49, 77, 107, 120, 150, 156, 166, 169, 170, 171, 173, 176, 178, 186, 194, 208].

Polyvinylchloride (PVC)

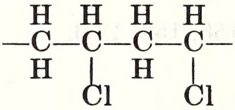

$$\begin{array}{cccc} H & H & H & H \\ -C- & C- & C- & C- \\ H & | & H & | \\ & Cl & & Cl \end{array}$$

[2, 8, 24, 27, 29, 30, 52, 120, 126, 145, 148, 150, 155, 156, 171, 177, 181, 187, 208, 209].

Polyvinylidene chloride (PVdC)

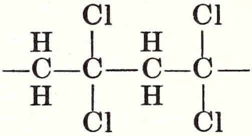

$$\begin{array}{cccc} & Cl & & Cl \\ H & | & H & | \\ -C- & C- & -C- & C- \\ H & | & H & | \\ & Cl & & Cl \end{array}$$

[67, 156].

Polyacrylonitrile (PAN)

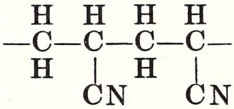

$$\begin{array}{cccc} H & H & H & H \\ -C- & C- & C- & C- \\ H & | & H & | \\ & CN & & CN \end{array}$$

[53, 57, 156, 178, 190].

Polyvinyl fluoride (PVF)

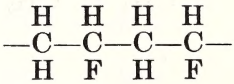

$$\begin{array}{cccc} H & H & H & H \\ -C- & C- & C- & C- \\ H & F & H & F \end{array}$$

[66, 145, 156, 165].

Polyvinylidene fluoride (PVdF)

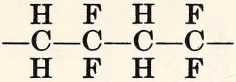

$$\begin{array}{ccccccccc} & H & & F & & H & & F & \\ - & C & - & C & - & C & - & C & - \\ & H & & F & & H & & F & \end{array}$$

[62, 165, 196].

Polychlorotrifluoroethylene (PCTFE)

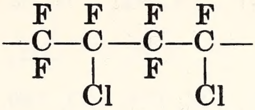

$$\begin{array}{ccccccccc} & F & & F & & F & & F & \\ - & C & - & C & - & C & - & C & - \\ & F & & | & & F & & | & \\ & & & Cl & & & & Cl & \end{array}$$

[29, 78, 94, 114, 117, 156, 158, 181].

Polytetrafluoroethylene (PTFE)

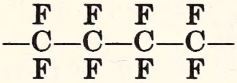

$$\begin{array}{ccccccccc} & F & & F & & F & & F & \\ - & C & - & C & - & C & - & C & - \\ & F & & F & & F & & F & \end{array}$$

[3, 28, 37, 44, 46, 68, 70, 78, 89, 95, 97, 98, 99, 107, 142, 143, 150, 151, 156, 165, 173, 174, 188, 204].

Polyhexafluoropropylene-tetrafluoroethylene copolymer (FEP)

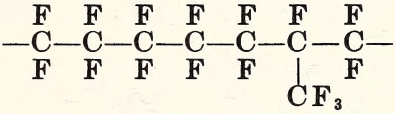

$$\begin{array}{ccccccccccccccc} & F & & F & & F & & F & & F & & F & & F & \\ - & C & - & C & - & C & - & C & - & C & - & C & - & C & - \\ & F & & F & & F & & F & & F & & | & & F & \\ & & & & & & & & & & & CF_3 & & & \end{array}$$

[3, 28, 84, 98].

Polymethylmethacrylate (PMMA)

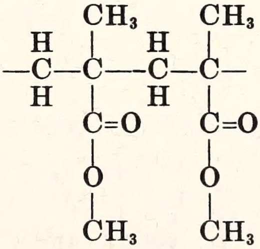

$$\begin{array}{ccccccccc} & & & CH_3 & & & & CH_3 & \\ & H & & | & & H & & | & \\ - & C & - & C & - & C & - & C & - \\ & H & & | & & H & & | & \\ & & & C{=}O & & & & C{=}O & \\ & & & | & & & & | & \\ & & & O & & & & O & \\ & & & | & & & & | & \\ & & & CH_3 & & & & CH_3 & \end{array}$$

[7, 12, 13, 20, 21, 26, 36, 39, 40, 41, 63, 73, 75, 93, 103, 104, 107, 111, 116, 120, 122, 131, 132, 133, 145, 148, 150, 154, 159, 162, 166, 170, 173, 175, 186, 198, 208, 209, 210].

Polyethylmethacrylate (PEMA)

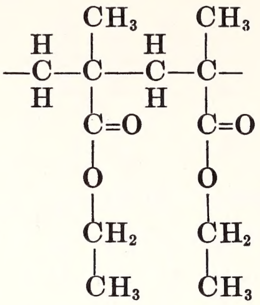

$$-\underset{H}{\overset{H}{C}}-\underset{\underset{\underset{\underset{CH_3}{|}}{\underset{CH_2}{|}}}{\underset{O}{|}}}{\underset{C=O}{|}}{\overset{\overset{CH_3}{|}}{C}}-\underset{H}{\overset{H}{C}}-\underset{\underset{\underset{\underset{CH_3}{|}}{\underset{CH_2}{|}}}{\underset{O}{|}}}{\underset{C=O}{|}}{\overset{\overset{CH_3}{|}}{C}}-$$

[12, 13, 21, 40, 63, 73, 103, 104, 132, 159, 162, 166, 167, 175, 177].

Poly *n*-butylmethacrylate (P*n*BMA)

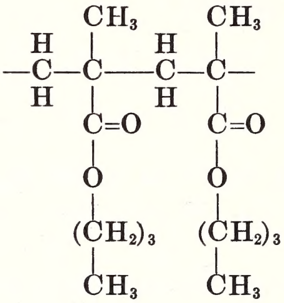

$$-\underset{H}{\overset{H}{C}}-\underset{\underset{\underset{\underset{CH_3}{|}}{\underset{(CH_2)_3}{|}}}{\underset{O}{|}}}{\underset{C=O}{|}}{\overset{\overset{CH_3}{|}}{C}}-\underset{H}{\overset{H}{C}}-\underset{\underset{\underset{\underset{CH_3}{|}}{\underset{(CH_2)_3}{|}}}{\underset{O}{|}}}{\underset{C=O}{|}}{\overset{\overset{CH_3}{|}}{C}}-$$

[12, 13, 40, 63, 73, 102, 103, 132, 166, 167, 198].

Polymethyl α-chloroacrylate (PMαCA)

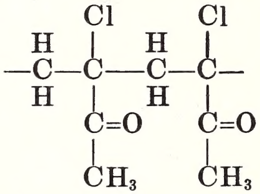

$$-\underset{H}{\overset{H}{C}}-\underset{\underset{\underset{CH_3}{|}}{\underset{C=O}{|}}}{\overset{\overset{Cl}{|}}{C}}-\underset{H}{\overset{H}{C}}-\underset{\underset{\underset{CH_3}{|}}{\underset{C=O}{|}}}{\overset{\overset{Cl}{|}}{C}}-$$

[26, 40, 132, 133, 145, 167].

Polymethylacrylate (PMA)

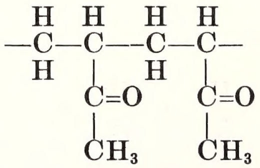

$$-\underset{H}{\overset{H}{C}}-\underset{\underset{\underset{CH_3}{|}}{\underset{C=O}{|}}}{\overset{H}{C}}-\underset{H}{\overset{H}{C}}-\underset{\underset{\underset{CH_3}{|}}{\underset{C=O}{|}}}{\overset{H}{C}}-$$

[12, 13, 50, 73, 75, 105, 132, 140, 141, 156, 162, 173, 175, 201].

Polyvinylacetate (PVAc)

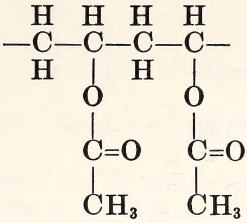

[11, 29, 55, 60, 75, 101, 120, 126, 148, 156, 178, 182, 185, 187, 191, 208].

Polyhexamethyleneadipamide (Nylon 6–6)

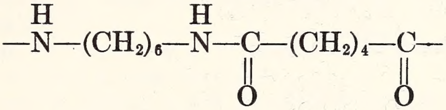

$$-\overset{H}{N}-(CH_2)_6-\overset{H}{N}-\underset{\underset{O}{\|}}{C}-(CH_2)_4-\underset{\underset{O}{\|}}{C}-$$

[6, 10, 21, 23, 25, 32, 47, 48, 69, 85, 86, 150, 156, 169, 172, 198, 203, 204, 206].

Polyethyleneterephthalate (PET)

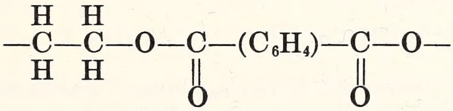

$$-\overset{H}{\underset{H}{C}}-\overset{H}{\underset{H}{C}}-O-\underset{\underset{O}{\|}}{C}-(C_6H_4)-\underset{\underset{O}{\|}}{C}-O-$$

[56, 64, 80, 129, 145, 146, 148, 169, 178, 184, 195].

Polycarbonate (PC)

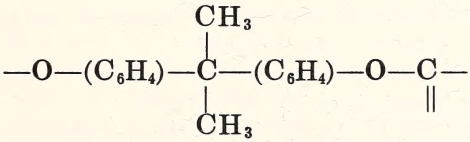

$$-O-(C_6H_4)-\overset{\overset{CH_3}{|}}{\underset{\underset{CH_3}{|}}{C}}-(C_6H_4)-O-\underset{\|}{C}-$$

[15, 29, 72, 78, 82, 84, 106, 112, 116, 126, 157, 193].

Polyformaldehyde (PMOx)

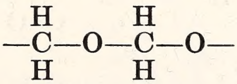

$$-\overset{H}{\underset{H}{C}}-O-\overset{H}{\underset{H}{C}}-O-$$

[19, 51, 54, 96, 128, 139, 170, 188, 197, 206].

Polyethyleneoxide (PEOx)

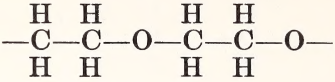

$$-\overset{H}{\underset{H}{C}}-\overset{H}{\underset{H}{C}}-O-\overset{H}{\underset{H}{C}}-\overset{H}{\underset{H}{C}}-O-$$

[1, 2, 18, 58, 59, 170, 197].

Polyacetaldehyde (PAcAl)

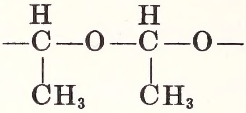

$$-\overset{H}{\underset{CH_3}{C}}-O-\overset{H}{\underset{CH_3}{C}}-O-$$

[17, 138, 200].

Polydimethylsiloxane (PDMS)

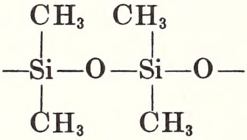

$$-\overset{CH_3}{\underset{CH_3}{Si}}-O-\overset{CH_3}{\underset{CH_3}{Si}}-O-$$

[23, 37, 65, 69, 96, 103].

References for Appendix 1

[1] G. Allen, T. M. Connor and H. Pursey, Trans. Faraday Soc. **59,** 1525 (1963).
[2] E. Amrhein and F. H. Muller, Kolloid-Z. **203,** 159 (1965).
[3] E. W. Anderson, Bell Telephone Laboratories, private communication.
[4] M. Baccaredda, E. Butta and V. Frosini, Polymer Letters **3,** 189 (1965).
[5] E. B. Baker, R. P. Auty and G. J. Ritenour, J. Chem. Phys. **21,** 154 (1953).
[6] W. O. Baker and W. A. Yager, J. Am. Chem. Soc. **64,** 2164 (1942).
[7] N. M. Bazhenov, M. V. Vol'kenshtein, A. I. Kil'tsov and A. S. Khachaturov, Polymer Sci. USSR **3,** 80 (1962). (Vysokomol. soedin. **3,** 290 (1961).
[8] G. W. Becker, Kolloid-Z. **140,** 1 (1955).
[9] F. Borsa and G. Lanzi, J. Polymer Sci. **A2,** 2623 (1964).
[10] R. H. Boyd, J. Chem. Phys. **30,** 1276 (1959).
[11] O. Broens and F. H. Muller, Kolloid-Z. **140,** 121 (1955).
[12] L. de Brouckere and G. Offergeld, J. Polymer Sci. **30,** 105 (1958).
[13] L. de Brouckere and G. Offergeld, Bull. Soc. Chim. Belg. **67,** 96 (1958).
[14] W. C. Carter, M. Magat, W. C. Schneider and C. P. Smyth, Disc. Faraday Soc. 213 (1946).
[15] W. F. Christopher and D. W. Fox, Polycarbonates, Reinhold Publ. Corp., New York, 1962, p. 69.
[16] E. I. Chuikin, Zhurn. Tek. Fiz. **25,** 595 (1955).
[17] T. M. Connor, Polymer **5,** 265 (1964).
[18] T. M. Connor, B. E. Read and G. Williams, J. Appl. Chem. **14,** 74 (1964).
[19] T. M. Connor, Trans. Faraday Soc. **60,** 1574 (1964).
[20] T. M. Connor and A. Hartland, Phys. Letters **23,** 662 (1966).

[21] J. M. Crissman, J. A. Sauer and A. E. Woodward, J. Polymer Sci. **A2,** 5075 (1964).

[22] J. M. Crissman and R. D. McCammon, J. Acoust. Soc. Am. **34,** 1703 (1962).

[23] A. J. Curtis, J. Res. N. B. S. **65 A,** 185 (1961).

[24] J. M. Davies, R. F. Miller and W. F. Busse, J. Am. Chem. Soc. **63,** 361 (1941).

[25] C. W. Deeley, A. E. Woodward and J. A. Sauer, J. Appl. Phys. **28,** 1124 (1957).

[26] K. Deutsch, E. A. W. Hoff and W. Reddish, J. Polymer Sci. **13,** 565 (1954).

[27] A. Dyson, J. Polymer Sci. **7,** 133 (1951).

[28] R. K. Eby and F. C. Wilson, J. Appl. Phys. **33,** 2951 (1962).

[29] D. R. Falcone, Bell Telephone Laboratories, private communication.

[30] R. M. Fuoss, J. Am. Chem. Soc. **63,** 369 (1941).

[31] N. Fuschillo and J. A. Sauer, J. Appl. Phys. **28,** 1073 (1957).

[32] R. E. Glick and R. C. Phillips, J. Polymer Sci. **3A,** 1885 (1965).

[33] H. S. Gutowsky and L. H. Meyer, J. Chem. Phys. **21,** 2122 (1953).

[34] H. S. Gutowsky, A. Saika, M. Takeda and D. E. Woessner, J. Chem. Phys. **27,** 534 (1957).

[35] U. Haeberlen, R. Hausser and F. Noack, Z. Naturforsch **18a,** 689 (1963).

[36] J. Heijboer, Kolloid-Z. **148,** 36 (1956).

[37] K. H. Hellwege, R. Kaiser and K. Kuphal, Kolloid-Z. **157,** 27 (1958).

[38] D. B. Herrmann, Bell Telephone Laboratories, private communication.

[39] P. Heydemann, Kolloid-Z. **195,** 122 (1964).

[40] E. A. W. Hoff, D. W. Robinson and A. H. Willbourn, J. Polymer Sci. **18,** 161 (1955).

[41] L. V. Holroyd, R. S. Codrington, B. A. Mrowca and E. Guth, J. Appl. Phys. **22,** 696 (1951).

[42] C. M. Huggins, L. E. St. Pierre and A. M. Bueche, J. Phys. Chem. **64,** 1304 (1960).

[43] B. I. Hunt, J. G. Powles and A. E. Woodward, Polymer **5,** 323 (1964).

[44] D. Hyndman and G. F. Origlio, J. Appl. Phys. **31,** 1849 (1960).

[45] K. H. Illers, Z. f. Elektrochem. **65,** 679 (1961).

[46] K. H. Illers and E. Jenckel, Kolloid-Z. **160,** 97 (1957).

[47] K. H. Illers, Makromol. Chem. **38,** 168 (1960).

[48] K. H. Illers and E. Jenckel, IUPAC Kurzmitteilungen Sec. 1, Physik Makromol. Stoffe, Verlag Chemie GmbH, Weinheim, 1959. (Cited by A. J. Curtis, J. Res. NBS, **65A,** 185 (1961).)

[49] K. H. Illers and E. Jenckel, J. Polymer Sci. **41,** 528 (1959).

[50] Y. Ishida, Kolloid-Z. **174,** 124 (1961).

[51] Y. Ishida, Kolloid-Z. **171,** 149 (1960).

[52] Y. Ishida, Kolloid-Z. **168,** 29 (1960).

[53] Y. Ishida, O. Amano and M. Takayanagi, Kolloid-Z. **172,** 129 (1960).

[54] Y. Ishida, M. Matsuo, H. Ito, M. Yoshino, F. Irie and M. Takayanagi, Kolloid-Z. **174,** 162 (1961).

[55] Y. Ishida, M. Matsuo and K. Yamafuji, Kolloid-Z. **180,** 108 (1962).

[56] Y. Ishida, M. Matsuo, Y. Ueno and M. Takayanagi, Kolloid-Z. **199,** 69 (1964).

[57] Y. Ishida, M. Matsuo, Y. Ueno and M. Takayanagi, Kolloid-Z. **199,** 67 (1964).

[58] Y. Ishida, M. Matsuo and M. Takayanagi, Polymer Letters **3,** 321 (1965).

[59] Y. Ishida, M. Matsuo, S. Togami, K. Yamafuji and M. Takayanagi, Kolloid-Z. **183,** 74 (1962).

[60] Y. Ishida, M. Matsuo and K. Yamafuji, Kolloid-Z. **180,** 108 (1962).

[61] Y. Ishida, Y. Ueno, S. Togami and M. Matsuo, Kolloid-Z. **199,** 70 (1964).
[62] Y. Ishida, M. Watanabe and K. Yamafuji, Kolloid-Z. **200,** 48 (1965).
[63] Y. Ishida and K. Yamafuji, Kolloid-Z. **177,** 97 (1961).
[64] Y. Ishida, K. Yamafuji, H. Ito and M. Takayanagi, Kolloid-Z. **184,** 97 (1962).
[65] Y. Ishida and K. Yamafuji, Kolloid-Z. **202,** 26 (1965).
[66] Y. Ishida and K. Yamafuji, Kolloid-Z. **200,** 50 (1965).
[67] Y. Ishida, M. Yamamoto and M. Takayanagi, Kolloid-Z. **168,** 124 (1960).
[68] S. Iwayanagi and I. Miura, Institute of Physical and Chemical Research, Bunkyo-ku, Tokyo, private communication. See S. Iwayanagi and I. Sakurai, J. Polymer Sci. **C15,** 29 (1966).
[69] D. W. Jones, Polymer **1,** 203 (1960).
[70] S. P. Kabin, Zhurn. Tek. Fiz. **26,** 2628 (1956).
[71] S. P. Kabin and G. P. Mikhailov, Zhurn, Tek. Fiz. **26,** 511 (1956).
[72] D. D. Kasarda, J. H. Heiss and W. McMahon, Bell Telephone Laboratories, private communication.
[73] T. Kawai, J. Phys. Soc. Japan **16,** 1220 (1961).
[74] T. Kawai, Y. Yoshimi and A Hirai, J. Phys. Soc. Japan **16,** 2356 (1961).
[75] T. Kawai, M. Sasaki, A Hirai, T. Hashi and A. Odajima, J. Phys. Soc. Japan **15,** 1700 (1960).
[76] D. E. Kline, J. A. Sauer and A. E. Woodward, J. Polymer Sci. **28,** 109 (1958).
[77] R. Kosfeld and E. Jenckel, Kolloid-Z. **165,** 136 (1959).
[78] F. Krum and H. Muller, Kolloid-Z. **164,** 81 (1959).
[79] H. Kusumoto, I. J. Lawrenson and H. S. Gutowsky, J. Chem. Phys. **32,** 724 (1960).
[80] R. Land, R. E. Richards and I. M. Ward, Trans. Faraday Soc. **55,** 225 (1959).
[81] W. P. Mason and H. J. McSkimin, Bell System Tech. J. **31,** 122 (1952).
[82] S. Matsuoka and Y. Ishida, J. Polymer Sci. **C14,** 247 (1966).
[83] B. Maxwell and J. E. Heider, SPE Trans. 174 (1962).
[84] D. W. McCall, unpublished studies.
[85] D. W. McCall and E. W. Anderson, Polymer **4,** 93 (1963).
[86] D. W. McCall and E. W. Anderson, J. Chem. Phys. **32,** 237 (1962).
[87] D. W. McCall and D. C. Douglass, Appl. Phys. Letters **7,** 12 (1965).
[88] D. W. McCall and D. C. Douglass, Polymer **4,** 433 (1963).
[89] D. W. McCall, D. C. Douglass and D. R. Falcone, J. Phys. Chem. **71,** 998 (1967).
[90] D. W. McCall and W. P. Slichter, J. Polymer Sci. **26,** 171 (1957).
[91] N. G. McCrum, Polymer Letters **2,** 495 (1964).
[92] N. G. McCrum and E. L. Morris, Proc. Royal Soc. **A292,** 506 (1966).
[93] N. G. McCrum and E. L. Morris, Proc. Royal Soc. **A281,** 258 (1964).
[94] N. G. McCrum, as reported in ref. 158.
[95] N. G. McCrum, J. Polymer Sci. **27,** 555 (1957).
[96] N. G. McCrum, J. Polymer Sci. **54,** 561 (1961).
[97] N. G. McCrum, J. Polymer Sci. **34,** 355 (1959).
[98] N. G. McCrum, Macromol. Chem. **34,** 50 (1959).
[99] N. G. McCrum, J. Polymer Sci. **A2,** 3951 (1964).
[100] M. R. McDonald and I. M. Ward, Proc. Phys. Soc. **80,** 1249 (1962).
[101] D. J. Mead and R. M. Fuoss, J. Am. Chem. Soc. **63,** 2832 (1941).
[102] H. H. Meyer, P. M. F. Mangin and J. D. Ferry, J. Polymer Sci. **A3,** 1785 (1965).
[103] G. P. Mikhailov and T. I. Borisova, Soviet Physics, Technical Physics **3,** 120 (1958). [Zhurn. Tek. Fiz. **28,** 137 (1958)].

[104] G. P. Mikhailov, J. Polymer Sci. **30,** 605 (1958).
[105] G. P. Mikhailov, Zhurn. Tek. Fiz. **21,** 1395 (1951).
[106] G. P. Mikhailov and M. P. Eidelnant, Vysokomolek. soed. **2,** 287 (1960).
[107] G. P. Mikhailov and A. M. Lobanov, Soviet Physics, Technical Physics **3,** 249 (1958). [Zhurn. Tek. Fiz. **28,** 267 (1958)].
[108] G. P. Mikhailov, S. P. Kabin and T. A. Krylova, Soviet Physics, Technical Physics **2,** 1899 (1957). [Zhurn. Tek. Fiz. **27,** 2050 (1957)].
[109] G. P. Mikhailov, S. P. Kabin and B. I. Sazhin, Zhurn. Tek. Fiz. SSSR **25,** 590 (1955).
[110] R. S. Moore and S. Matsuoka, J. Polymer Sci. **C5,** 163 (1964).
[111] E. L. Morris and N. G. McCrum, Polymer Letters **1,** 393 (1963).
[112] F. K. Muller and K. Huff, Kolloid-Z. **164,** 34 (1959).
[113] L. T. Muus, N. G. McCrum and F. C. McGrew, Soc. Plastics Enginrs. J. **15,** 368 (1959).
[114] T. Nakajima and S. Saito, J. Polymer Sci. **31,** 423 (1958).
[115] H. Nakayasu, H. Markowitz and D. J. Plazek, Trans. Soc. Rheology **5,** 261 (1961).
[116] L. E. Nielsen, Mechanical Properties of Polymers, Reinhold, New York, 1962.
[117] A. Nishioka, J. Polymer Sci. **37,** 163 (1959).
[118] A. W. Nolle and J. J. Billings, J. Chem. Phys. **30,** 84 (1959).
[119] W. G. Oakes and D. W. Robinson, J. Polymer Sci. **14,** 505 (1954).
[120] A. Odajima, J. Sohma and K. Koike, J. Phys. Soc. Japan **12,** 272 (1957).
[121] A. Odajima, J. A. Sauer and A. E. Woodward, J. Phys. Chem. **66,** 718 (1962).
[122] A. Odajima, A. E. Woodward and J. A. Sauer, J. Polymer Sci. **55,** 181 (1961).
[123] H. G. Olf and A. Peterlin, Kolloid-Z. **215,** 97 (1967).
[124] N. Oskin and B. Maxwell, cited in private communication from W. Reddish, Imperial Chemical Industries.
[125] A. R. Payne and J. R. Scott, Engineering Design with Rubber, McLaren, London, 1960, p. 30.
[126] W. F. Peck, Bell Telephone Laboratories, private communication.
[127] A. Peterlin and H. G. Olf, Polymer Letters **2,** 409 (1964).
[128] A. Peterlin and H. G. Olf, Polymer Letters **2,** 769 (1964).
[129] P. R. Pinnock and I. M. Ward, Polymer **7,** 255 (1966).
[130] D. J. Plazek, W. Dannhauser and J. D. Ferry, J. Colloid Sci. **16,** 101 (1961).
[131] J. G. Powles and P. Mansfield, Polymer **3,** 336 (1962).
[132] J. G. Powles, B. I. Hunt and D. J. H. Sandiford, University of Kent, Canterbury, private communication.
[133] J. G. Powles, J. Polymer Sci. **22,** 79 (1956).
[134] J. G. Powles and P. Mansfield, Polymer **3,** 340 (1962).
[135] J. G. Powles and A. Hartland, Nat re **186,** 26 (1960).
[136] J. G. Powles and K. Luszczynski, Physica **25,** 455 (1959).
[137] J. G. Powles, Proc. Phys. Soc. (London) **69,** 281 (1956).
[138] B. E. Read, J. Polymer Sci. **C5,** 87 (1964).
[139] B. E. Read and G. Williams, Polymer **2,** 239 (1961).
[140] B. E. Read, in Techniques of Polymer Science, Soc. Chem. Ind. (London) monograph #17, 198 (1963).
[141] B. E. Read, J. Polymer Sci. **C5,** 87 (1964).
[142] W. Reddish, J. G. Powles and B. I. Hunt, Polymer Letters **3,** 671 (1965).
[143] W. Reddish, Imperial Chemical Industries, private communication.
[144] W. Reddish and J. T. Barrie, IUPAC Symposium, Wiesbaden, Kurzmitteilen IA3, 1959.

[145] W. Reddish, Pure and Applied Chem. **5,** 723 (1962).

[146] W. Reddish, Trans. Faraday Soc. **46,** 459 (1950).

[147] R. C. Rempel, H. E. Weaver, R. H. Sands and R. L. Miller, J. Appl. Phys. **28,** 1082 (1957).

[148] S. Saito, Kolloid-Z. **189,** 116 (1963).

[149] J. A. Sauer, R. A. Wall, N. Fuschillo and A. E. Woodward, J. Appl. Phys. **29,** 1385 (1958).

[150] J. A. Sauer and A. E. Woodward, Rev. Modern Phys. **32,** 88 (1960).

[151] J. A. Sauer and D. E. Kline, IX International Congress Appl. Mech., Univ. Brussels **5,** 368 (1957).

[152] J. A. Sauer, A. E. Woodward and N. Fuschillo, J. Appl. Phys. **30,** 1488 (1959).

[153] B. I. Sazhin, V. S. Skurikhina and Y. I. Illin, Vysokomolekul. Soed. **1,** 1383 (1959).

[154] D. J. Scheiber and D. J. Mead, J. Chem. Phys. **27,** 326 (1957).

[155] K. Schmieder and K. Wolfe, Kolloid-Z. **127,** 65 (1952).

[156] K. Schmieder and K. Wolfe, Kolloid-Z. **134,** 149 (1953).

[157] H. Schnell, Ang. Chemie **68,** 633 (1956).

[158] A. H. Scott, D. J. Scheiber, A. J. Curtis, J. I. Lauritzen, and J. D. Hoffman, J. Res. NBS **66A,** 269 (1962).

[159] K. M. Sinnott, J. Polymer Sci. **35,** 273 (1959).

[160] K. M. Sinnott, Grace Chemical, private communication.

[161] K. M. Sinnott, Polymer Letters **3,** 945 (1965).

[162] K. M. Sinnott, J. Polymer Sci. **42,** 3 (1960).

[163] W. P. Slichter, J. Appl. Phys. **31,** 1865 (1960).

[164] W. P. Slichter, J. Appl. Phys. **32,** 2339 (1961).

[165] W. P. Slichter, J. Polymer Sci. **24,** 173 (1957).

[166] W. P. Slichter, Ann. N. Y. Acad. Sci. **83,** 60 (1959).

[167] W. P. Slichter and E. M. Mandell, J. Appl. Phys. **30,** 1473 (1959).

[168] W. P. Slichter and E. M. Mandell, J. Appl. Phys. **29,** 1438 (1958).

[169] W. P. Slichter, Soc. Plastics Enginrs. J. **15,** 303 (1959).

[170] W. P. Slichter, Makromol. Chem. **34,** 67 (1959).

[171] W. P. Slichter, Bell Telephone Laboratories, private communication.

[172] W. P. Slichter, J. Appl. Phys. **26,** 1099 (1955).

[173] G. C. Smith and F. H. Muller, Kolloid-Z. **206,** 137 (1965).

[174] J. A. S. Smith, Disc. Faraday Soc. **19,** 207 (1955).

[175] N. S. Steck, Soc. Plastics Enginrs. Trans. **4,** 34 (1964).

[176] J. M. Stevels, Glass Ind. **35,** 657 (1954).

[177] S. Strella and S. N. Chinai, J. Polymer Sci. **31,** 45 (1958).

[178] H. A. Stuart, Physik der Hoch Polymeren, Bd. IV, Springer Verlag, Berlin, 1956, pp. 549, 563.

[179] M. Takayanagi, H. Harima and Y. Iwata, Mem. Fac. Enginr. Kyushu Univ. **23,** 1 (1963).

[180] M. Takayanagi, Mem. Fac. Enginr. Kyushu Univ. **23,** 41 (1963).

[181] T. Tanaka and Y. Ishida, Prog. Theor. Phys. Sup. **10,** 121 (1959).

[182] K. Tanaka, K. Yamagata and S. Kittaka, Bull. Chem. Soc. Japan **29,** 843 (1956).

[183] D. A. Thomas and D. W. Robinson, British J. Appl. Phys. **6,** 41 (1955).

[184] A. B. Thompson and D. W. Woods, Trans. Faraday Soc. **52,** 1383 (1956).

[185] H. Thurn and K. Wolf, Kolloid-Z. **148,** 16 (1956).

[186] H. Thurn, discussion of paper by R. Kosfeld, Kolloid-Z. **165,** 136 (1959). See also, H. Hendus, G. Schnell, H. Thurn and K. Wolf, Ergebn. exakt. Naturwiss. **31,** 220 (1959).

[187] H. Thurn and F. Wurstlin, Kolloid-Z. **156,** 21 (1958).

[188] N. J. Trappeniers, C. J. Gerritsma and P. H. Oosting, Physica **30,** 997 (1964).

[189] C. A. F. Tuijman, Polymer **4,** 259 (1963).

[190] L. K. H. Van Beek, J. Appl. Polymer Sci. **9,** 553 (1965).

[191] P. F. Veselovski and A. I. Slusker, Zhurn. Tek. Fiz. **25,** 939, 1204 (1955).

[192] J. Volger, Indust. chim. Belge **20,** spec. #128 (1955).

[193] G. Voskotter and R. Kosfeld, Kolloid-Z. **216,** 85 (1967).

[194] R. A. Wall, J. A. Sauer and A. E. Woodward, J. Polymer Sci. **35,** 281 (1959).

[195] I. M. Ward, Trans. Faraday Soc. **56,** 648 (1960).

[196] T. Wentink, J. Appl. Phys. **32,** 1063 (1961).

[197] R. E. Wetton and G. Allen, Polymer **7,** 331 (1966).

[198] A. H. Willbourn, Trans. Faraday Soc. **54,** 717 (1958).

[199] G. Williams, Polymer **4,** 27 (1963).

[200] G. Williams, Trans. Faraday Soc. **59,** 1397 (1963).

[201] G. Williams, Trans. Faraday Soc. **60,** 1556 (1964).

[202] A. E. Woodward, A. Odajima and J. A. Sauer, J. Phys. Chem. **65,** 1384 (1961).

[203] A. E. Woodward, J. M. Crissman and J. A. Sauer, J. Polymer Sci. **44,** 23 (1960).

[204] A. E. Woodward and J. A. Sauer, private communication.

[205] A. E. Woodward, J. A. Sauer and R. A. Wall, J. Chem. Phys. **30,** 854 (1959).

[206] A. E. Woodward, J. A. Sauer, C. E. Deeley and D. E. Kline, J. Colloid Sci. **12,** 363 (1957).

[207] A. E. Woodward and J. A. Sauer, J. Polymer Sci. **35,** 281 (1959).

[208] W. A. Yager, Trans. Electrochem. Soc. **74,** 113 (1938).

[209] A. Zosel, Kolloid-Z. **199,** 113 (1964).

[210] K. Yamamoto and Y. Wada, J. Phys. Soc. Japan **12,** 374 (1957).

LOW FREQUENCY VIBRATIONS IN POLYETHYLENE [1]

W. R. MYERS and P. D. RANDOLPH

Idaho Nuclear Corporation, Idaho Falls, Idaho 83401

1. Introduction

In the last few years there have been several measurements of the neutron scattering spectrum of polyethylene at temperatures ranging from 450 °K down to 77 °K [1].[2] We have extended the measurements by obtaining absolute cross sections for the transverse and longitudinal orientations at 300, 77 and 4.2 °K using the MTR phased-chopper velocity selector. The primary data were taken at low incident energy, which, combined with the low temperature, provides very good resolution in the region of small energy transfers. Our data show the two commonly observed acoustic frequency limits at 25 and 65 meV and provide better definition of some of the weaker singularities. We have also measured the Debye-Waller coefficients used in reducing the cross sections to the directional frequency spectra.

2. Theory

The incoherent neutron-scattering cross section to zero- and one-phonon terms is [1]:

$$\frac{d^2\sigma}{d\Omega d\epsilon}=\frac{\sigma_o}{4\pi}e^{-2W}\left[\delta(\epsilon)+\frac{\hbar^2}{2M}\frac{k_f}{k_i}\frac{1}{\epsilon}\frac{1}{(e^{\beta\epsilon}-1)}\sum_{\alpha\beta}\kappa_\alpha\kappa_\beta G^{\alpha\beta}(\epsilon)\right], \tag{1}$$

where

$$2W=\sum_{\alpha\beta}\frac{\hbar^2\kappa_\alpha\kappa_\beta}{2M}\int_0^\infty\frac{d\epsilon}{\epsilon}\operatorname{ctgh}\left(\frac{\beta\epsilon}{2}\right)G^{\alpha\beta}(\epsilon), \tag{2}$$

and

$$G^{\alpha\beta}(\epsilon)=\sum_{j\mathbf{q}}\gamma_j^{\alpha *}(\mathbf{q})\gamma_j^{\beta}(\mathbf{q})\delta(\epsilon-\hbar\omega_j(\mathbf{q})).$$

σ_o is the bound-atom incoherent scattering cross section and M the mass of the scattering nucleus, $\mathbf{k}_f$ and $\mathbf{k}_i$ are the final and initial neutron wave vectors, $\boldsymbol{\kappa}=\mathbf{k}_f-\mathbf{k}_i$, $\epsilon=\hbar^2(k_f^2-k_i^2)/2m$ is the neutron energy gain, $\beta = (k_BT)^{-1}$, $\gamma_j^\alpha(\mathbf{q})$ is the αth component of the eigenvector for the vibrational mode of branch j having wave vector $\mathbf{q}$. $G^{\alpha\beta}(\epsilon)$ is the amplitude-weighted directional frequency spectrum. For cubic or for polycrystalline monatomic samples, $G(\epsilon)$ is proportional to the true frequency spectrum.

---

[1] Work performed under the auspices of the U.S. Atomic Energy Commission.

[2] Figures in brackets indicate the literature references at the end of this paper.

By appropriate orientation of a uniaxially-oriented target such as fully stretched polyethylene, one may measure two distinct cross sections: the "longitudinal" for $\boldsymbol{\kappa}\cdot\mathrm{S} = \kappa S$ and the "transverse for $\boldsymbol{\kappa}\cdot\mathrm{S} = 0$, where S is the unique direction in the sample. These cross sections are proportional to the directional spectra $G_L = G^{33}(\epsilon)$ and $G_T = (G^{11}+G^{22})/2$, respectively, where the unique direction, S, the chain axis for polyethylene, is represented by $\alpha = 3$.

3. Experiment

The cross sections were measured using six detectors, three on the "left" of the target measuring the transverse cross section, and three on the "right", simultaneously measuring the longitudinal. We used incident energies of 30 meV to provide good resolution for the small energy transfers, 80 meV to extend the measurements to the higher acoustic limit at 65 meV (525 cm^{-1}), and 40 meV to bridge the other two measurements in the energy transfer range 20–35 meV. The detectors were calibrated by measuring the elastic scattering cross section of vanadium corrected for beam attenuation in the target and the vanadium Debye-Waller factor. The polyethylene data are corrected for measured "sample-out" background, beam attentuation in the target using a measured total cross section for polyethylene at room temperature, and an air-scattering contribution which perturbs the data at very low final energies. The orientation conditions were not rigorously satisfied during these measurements, since all energy transfers are sampled simultaneously on a time-of-flight spectrometer, and $\boldsymbol{\kappa}$ has a different direction for each energy. The conditions of the experiment, however, were such that the unwanted component is less than 10 percent of the total over most of the range of interest.

4. Discussion

Figure 1 shows the amplitude-weighted directional spectra for the principal angles. These are calculated from the inelastic cross sections in the one-phonon approximation, eq (1). The cross sections were determined as barns/eV/steradian/CH_2, so that $\sigma_o=160$ barns, and for consistency, $M=14$ amu. The Debye-Waller constants, the coefficients of κ^2 in eq (2), were determined in two ways. By plotting the integrated elastic intensities as a function of κ^2, we find the Debye-Waller con-

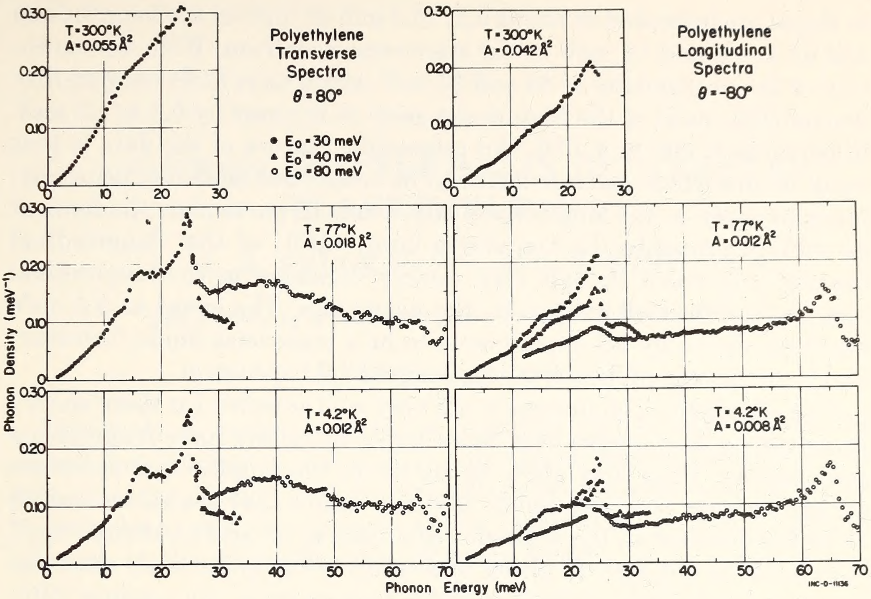

FIGURE 1. Amplitude-weighted directional frequency spectra for uniaxially oriented polyethylene at 4.2, 77 and 300 °K.

stants to be 0.0209 Å² for the transverse and 0.0153 Å² for the longitudinal orientation at 77°, and 0.0127 and 0.0116 Å² for the transverse and longitudinal, respectively, at 4.2 °K. The best least-squares fits were obtained for an intercept of 146 barns which is about 9 percent lower than expected. The other method for obtaining the Debye-Waller constants is to try various values in the conversion of the inelastic cross sections to the frequency spectra, eq (1), and choose the numbers that make the spectra coincide. The values obtained in this manner for the transverse spectra are 0.018 and 0.012 Å² for 77 and 4.2 °K, which are in fair agreement with the numbers determined from the elastic cross sections. It was found that the second method was not definitive for the longitudinal spectra; the values 0.012 and 0.008 Å² make the three spectra for each incident energy coincide, but do not bring the 30, 40 and 80 meV data into agreement. Larger values would accomplish the latter, but would cause divergence in the individual spectra for each incident energy. The set of constants determined from the inelastic data was used in the reduction of the cross sections to the frequency spectra.

In addition to the commonly seen limits at 65 (longitudinal) and 25 meV (primarily transverse), there are strong singularities at 5.5 meV in the longitudinal spectrum and at 12 and 15.5 in the transverse spectrum. Several weak events [3] (characterized primarily by changes in slope) are indicated at about 9.5, 15.5 and 23 meV in the longitudinal and at 4, 6.5 and 18 meV in the transverse spectrum. With the exception of the singularities at 65 and 12 meV which have little temperature dependence, most of the frequencies seem to increase by 0.5 to 1.5 meV in going from 300 to 4.2 °K. An interesting feature of the data is that weak modes which are calculated to be transverse show up, generally, more strongly in the longitudinal spectrum. In particular, the limit at 23 meV is probably the transverse limit, $\nu_5^a(0)$, of the "longitudinal branch", ν_5, which though very weakly indicated in the longitudinal spectra, is not at all evident in the transverse. The event at 9.5 meV has been shown by IR experiments to be a transverse mode, however, and it too shows up better in the longitudinal spectrum.

---

[3] These are seen better in the cross sections; the data will be published in more detail.

The orientation requirements are very well satisfied for these energy transfers, so that modes near these limits definitely have longitudinal components. They may show up better in the longitudinal spectrum simply because it is less dense; the only limits that are calculated [2] to be longitudinal in the acoustic region are at 65 and at about 7 meV (the latter is not seen in either spectrum). It is quite likely that the strong 5.5 meV limit in the longitudinal spectrum is the missing $\nu_9^b(0)$.

Although the amplitude-weighted frequency spectrum is not the appropriate function for the calculation of specific heat, these spectra, normalized to one hydrogen atom, fit the measured specific heat of polyethylene fairly well up to about 50 °K. Above 50° the calculated $C_V(T)$ diverges due to the multiphonon components in the spectra. The two-phonon components have been calculated [3] to become important at about 12 meV, in agreement with this observation.

We see very little credible structure in the range from 25 to 65 meV; while the amplitude in this region is probably due to multiphonon contributions, better calculations and measurements at small κ are needed to demonstrate this. The helium-temperature measurements give much better resolution at the lowest energies, but the two-phonon contribution is not substantially reduced compared to nitrogen temperature measurements at larger energy transfers.

5. References

[1] See for example, W. Myers, G. C. Summerfield, and J. S. King, J. Chem. Phys. **44,** 184 (1966).
[2] See for example, M. Tasumi and S. Krimm, J. Chem. Phys. **46,** 755 (1966).
[3] J. E. Lynch (private communication).

NEUTRON SCATTERING IN DEUTERATED POLYETHYLENE [1]

L. A. FELDKAMP [2] and J. S. KING

The University of Michigan, Ann Arbor, Michigan 48104

1. Introduction

The study of neutron scattering from deuterated polyethylene was undertaken to observe the shift in vibrational frequencies due to the deuterium mass, and thereby clarify features of earlier data on normal polyethylene, and to attempt direct observation of the dispersion relations in the predominantly coherent target.

2. Experimental Method

2.1. Spectrometer

The scattering measurements were made on a triple-axis crystal spectrometer in which the analyzing system was set to observe down-scattering to a final energy of about .030 ev. The sample was maintained at 78 °K to reduce multiphonon events.

2.2. Target Preparation

Several thin disks, formed by pressing $(CD_2)_n$ granules at 160 °C and 1000 psi, comprised the unoriented target, which had a total thickness of .144 in. Strips cut from the disks were later stretched 500 percent under infra-red heat to induce an approximately uniaxial orientation. The distribution of *c*-axis orientations was found from neutron diffraction to have a FWHM of 8°.

3. Discussion of the Data

3.1. Comparison with Normal Polyethylene

The data, for purposes of comparison, have been converted to frequency spectra using the incoherent approximation. The polycrystalline spectrum is compared with earlier data [1] [3] on normal polyethylene in figure 1. The expected shift in vibrational frequencies

---

[1] Work supported by the National Science Foundation.

[2] National Science Foundation Predoctoral Fellow.

[3] Figures in brackets indicate the literature references at the end of this paper.

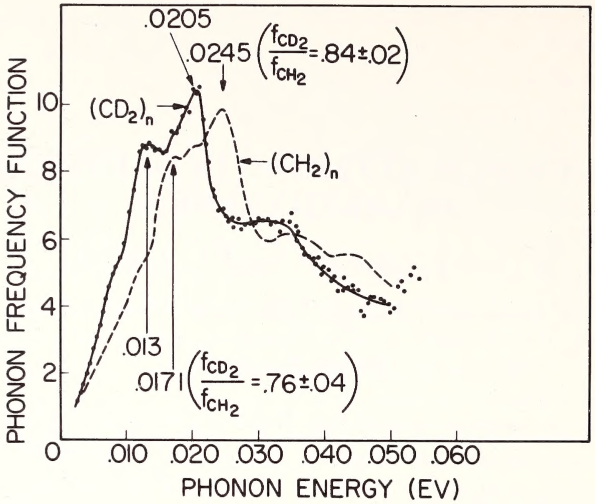

Figure 1. Comparison of unoriented normal and deuterated polyethylene frequency spectra. Scattering angle 90°, temperature 78 °K.

is observed. The ratios of frequencies for the two prominent peaks are in good agreement with the crystalline model calculations of Tasumi and Krimm [2]. The lower frequency event is thus assigned to the $\nu_5^b(0)$ rotatory vibration, and the higher event is confirmed to be the ν_9 torsional-mode cutoff.

3.2. Comparison with Spectrum Calculations

In figure 2 the same deuterated polyethylene data are compared to a frequency spectrum calculation of Lynch [3]. Aside from the difference in resolution, the agreement in the major peaks is reasonably good. The broad maximum in the calculated histogram at .034 ev comes from the two-phonon term in the cross section and is believed to explain the substantial experimental intensity in that region in the present data and in several previous normal polyethylene measurements [1, 4]. Figure 3 is a comparison of the transverse data with Lynch's calculated transverse frequency function. The position of the lower peak is essentially the same as in the unoriented data, but the energy of the higher peak appears to be reduced by about .001 ev.

4. Effect of Coherence

Since the scattering from both deuterium and carbon is primarily coherent, it is to be expected that much of the observed intensity results from coherent processes. The similarity of the normal and deuterated spectra suggests that the orientation average of the

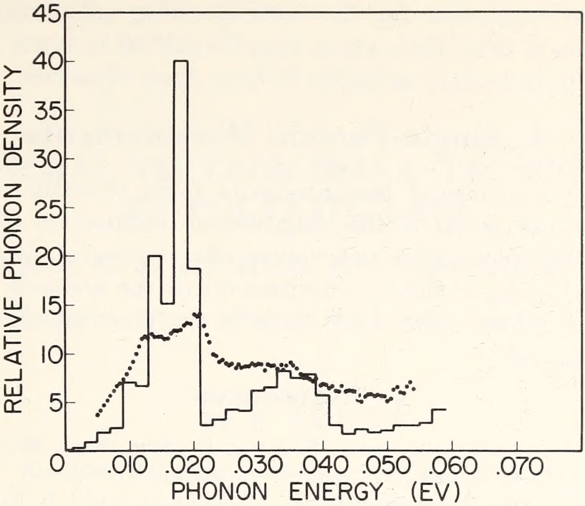

FIGURE 2. Measured and calculated unoriented deuterated polyethylene frequency spectra.

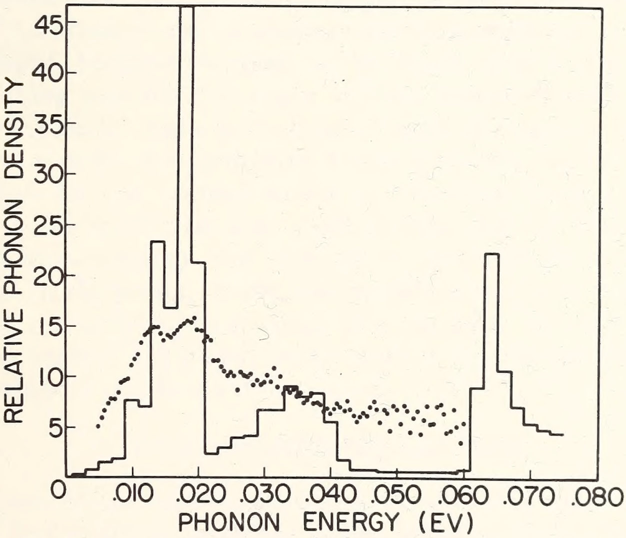

FIGURE 3. Measured and calculated transverse ($\kappa \perp \mathbf{c}$) oriented polyethylene frequency spectra.

$(CD_2)_n$ coherent cross section must yield a shape not too unlike the incoherent cross section. A calculation made for simplified dynamics in which $\omega(\mathbf{q})$ is assumed to depend only on q_z (where $\tilde{z}$ is the chain axis direction) indicates that the coherent cross section is indeed similar to the incoherent and has singularities in the same places.

A qualitative conclusion for the corresponding calculation for the transverse case is that the ν_9 event may be shifted to lower frequency and reduced in intensity, as seems to have been observed.

5. Single-Phonon Measurements

Preliminary constant-Q measurements have recently been made with the oriented target in the longitudinal orientation. Observation of phonons of branch ν_5 for two values of q_z indicates that it should be possible to make a direct measurement of the acoustic dispersion relations for q values along the c^{-1} axis. A complete measurement will soon be attempted.

6. References

[1] W. Myers, J. L. Donovan, and J. S. King, J. Chem. Phys. **42,** 4299 (1965).

[2] M. Tasumi and S. Krimm, J. Chem. Phys. **46,** 755 (1967).

[3] J. E. Lynch, Jr., G. C. Summerfield, L. A. Feldkamp, and J. S. King, J. Chem. Phys. **48,** 912 (1968).

[4] G. J. Safford, A. W. Naumann, and F. T. Simon, J. Chem. Phys. **45,** 3787 (1966); H. R. Danner, G. J. Safford, H. Boutin, and M. Berger, J. Chem. Phys. **40,** 1417 (1964).

EPITHERMAL NEUTRON INELASTIC SCATTERING BY POLYETHYLENE [1]

W. E. MOORE, G. J. KIROUAC, L. J. ESCH, K. W. SEEMANN

Knolls Atomic Power Laboratory, Schenectady, New York 12301

and

M. L. YEATER

Rensselaer Polytechnic Institute, Troy, New York 12180

1. Introduction

The RPI–KAPL neutron scattering system utilizes an electron linear accelerator and phased chopper to produce short neutron bursts of a desired energy; scattered-neutron energies are measured by time-of-flight. Incident energies can be chosen over a range of 0.1 to 1 eV, making possible the study of high energy-transfer modes of molecular systems. Data are compared with calculations based upon theoretical models, thus providing a means of verifying the frequency distribution for the normal modes of vibration. Data can also be reduced to the scattering law, which is extended by these measurements to higher energy and momentum transfers than are usually accessible. In the present work, double-differential cross sections were measured for polyethylene using five incident energies and five scattering angles. The experimental system will be described briefly and examples of the data will be shown.

2. Experimental Method

A diagram of our experimental setup is shown in figure 1. Intense bursts of fast neutrons produced in the tantalum target are partially thermalized in a thin moderator placed nearby. A nearly monochromatic neutron burst is selected by a chopper placed 6m from this source. The Linac is synchronized with the neutron chopper and the phase between the two determines the neutron velocity selected. The chopped beam passes through a thin sample under study and scattered neutrons are detected in banks of ten-atm. ^{3}He-filled counters. Flight times of detected neutrons are recorded by an on-line computer;

---

[1] Work supported by the U.S. Atomic Energy Commission under contract No. W–31–109–Eng.–52 and AT(30–3)–328.

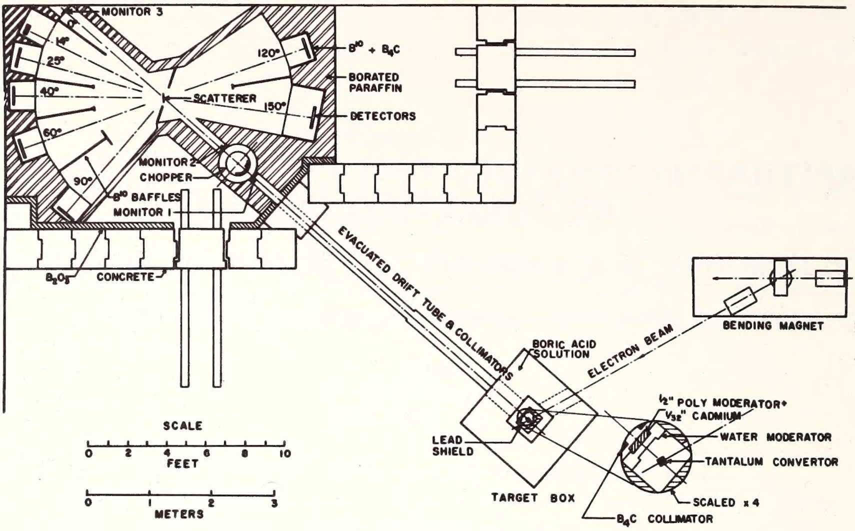
MONITOR 3
0°
14°
25°
40°
60°
90°
120°
150°
SCATTERER
B^{10} + B_4C
BORATED PARAFFIN
DETECTORS
MONITOR 2
CHOPPER
B^{10} BAFFLES
MONITOR 1
B_2O_3
CONCRETE
EVACUATED DRIFT TUBE & COLLIMATORS
BENDING MAGNET
ELECTRON BEAM
BORIC ACID SOLUTION
½" POLY MODERATOR+
1/32" CADMIUM
WATER MODERATOR
TANTALUM CONVERTOR
SCALED x 4
B_4C COLLIMATOR
LEAD SHIELD
TARGET BOX
SCALE
0 2 4 6 8 10
FEET
0 1 2 3
METERS

FIGURE 1. Experimental layout of RPI–KAPL double-differential scattering spectrometer.

detected events are routed to different memory areas according to the scattering angle and type of experimental run. A sequence of runs is repeated every few minutes under computer control, including: (1) a "foreground" run measuring the sample scattering, (2) an empty sample holder background run, and (3) a run measuring the scattering from a standard vanadium sample. The latter serves as a repetitive detector calibration and permits the cross section to be evaluated. Runs are normalized by means of a beam-monitor. Typical operating parameters of the system are shown in table 1.

3. Differential Scattering From Polyethylene

Data were taken at room temperature for a Marlex 6050 sample having 95 percent crystallinity. A 0.012-in. thick sample, having a transmission of 92 percent at 0.16 eV, was used for the present data. Differential cross sections were obtained for incident energies 0.16, 0.23, 0.33, 0.49, and 0.65 eV and 25°, 40°, 60°, 90°, and 120° scattering angles.

It is well known that the double-differential scattering cross section for hydrogeneous materials can be approximated in the incoherent scattering formulation. Symmetry arguments applied to the long-chain molecule made up of units of CH_2 indicate the existence of nine normal modes of vibration. The spectral density, defined as the fraction of modes per unit frequency interval, can be obtained directly from the

Table 1. Parameters for RPI-KAPL double-differential neutron scattering spectrometer

Source: RPI Electron Linear Accelerator
Repetition rate —180–240 bursts/sec.
Pulse width —4.5 μ sec.
Neutron moderator—1 in x 3 in x 8 in H_2O slab

Spectrometer: 20,000 RPM neutron chopper
Motor —0.4 HP hysteresis-synchronous
Rotor —8 in diam., 8 in^2 aperture
Chopping slits —^{10}B epoxy-fiberglass, $\frac{1}{16}$ in-width
Burst width —6.8 μ sec. at 20,000 RPM
Source-chopper distance—5.97 m
Scattered flight path —2.36 m

Incident energy resolution: full width at half maximum measured at chopper exit

E_o (eV)	ΔE_o (eV)	% $\Delta E_o/E_o$
.23	.0051	2.2
.33	.0087	2.6
.50	.014	2.8
.63	.019	3.0

Scattered energy resolution: full width at half maximum at neutron detectors

E_o=.23 eV		E_o=.33 eV		E_o=.63 eV	
E_s(eV)	ΔE_s(eV)	E_s(eV)	ΔE_s(eV)	E_s(eV)	ΔE_s(eV)
.17	.011	.26	.026	.43	.046
.11	.0084	.13	.014	.18	.025

slopes of the dispersion curves. However, the neutron scattering properties must be defined in terms of a weighted frequency distribution. These weights can be determined by a calculation of the polarization vectors for each mode and an appropriate average over molecular orientation. Lacking this detailed information, we have assumed constant weighting within each normal mode and assigned relative weights for different modes.

We have made several cross-section calculations using a spectral density for the CH_2 vibrational modes based on the dispersion curves of Tasumi, Shimanouchi and Miyazawa (TSM)[1] [2] and the density for acoustic and lattice modes predicted by Miyazawa and Kitagawa (KM)[2]. To determine a relative weight for the skeletal modes, Parks[3] makes the simple assumption that the CH_2 molecules move

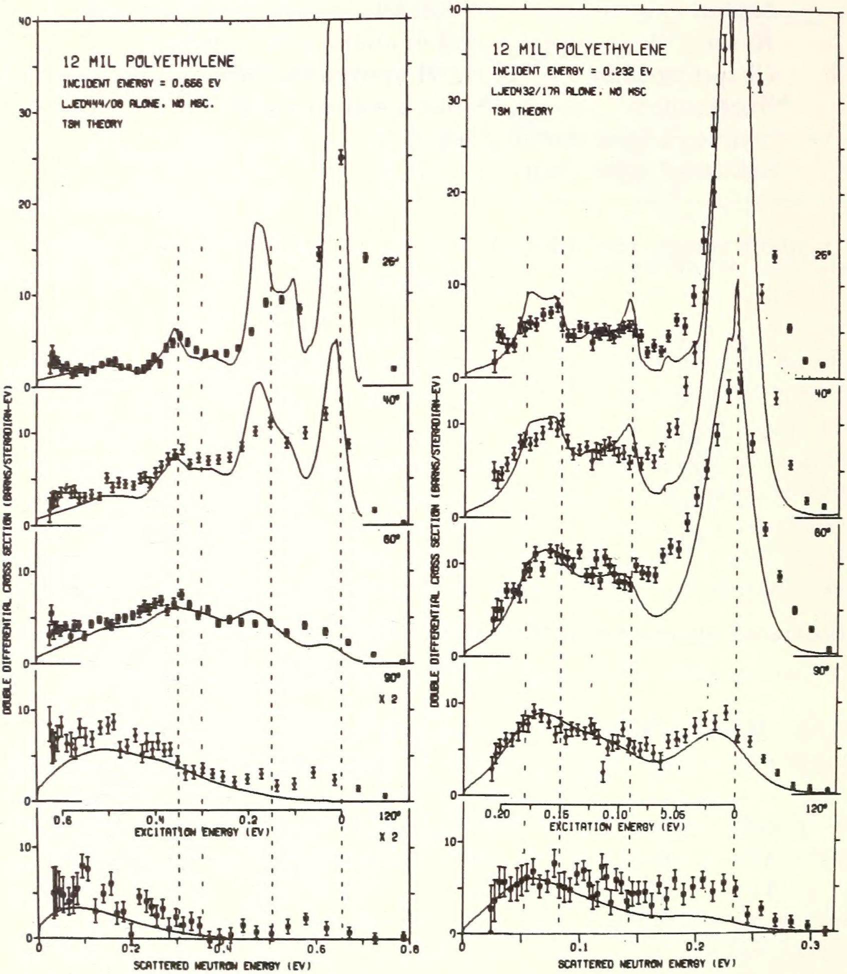

FIGURE 2. Differential cross sections for polyethylene for $E_o = 0.232$ eV and 0.656 eV, compared with theory. Multiple scattering and resolution corrections have not been made.

---

[2] Figures in brackets indicate the literature references at the end of this paper.

like rigid units in the three modes involving skeletal deformation (ν_9, ν_5, and ν_4), and that in the remaining modes the carbon atoms are nearly at rest. We have used his relative weights of 2/15 and 13/15 for these modes in our present calculations. The GASKET [4] code was used, with a continuous frequency distribution below 0.18 eV and a delta function at 0.36 eV. Figure 2 compares the calculated cross section with our data for incident energies of 0.232 eV and 0.656 eV.

Structure in the cross section due to several CH_2 rocking, wagging and twisting modes lying between 0.09 eV and 0.18 eV excitation energy is evident in figure 2. The present model seems to overpredict the scattered neutron intensity from the H–C–H bending mode at 0.18 eV. The high incident energy run clearly shows excitation of the 0.36 eV H–C bond stretching modes. Structure observed at higher excitations is believed to be due to multiphonon contributions, as it also appears in the theory curve. Multiple-scattering and resolution corrections will be applied to permit more definitive conclusions on details of the scattering. Frequency distributions weighted by the polarization vectors are now available [5, 6] and will be compared with our data; a significant reduction is predicted for the ν_2 (0.18 eV) mode.

4. References

[1] M. Tasumi, T. Shimanouchi, and T. Miyazawa, J. Mol. Spec. **9,** 261 (1962).

[2] T. Kitagawa and T. Miyazawa, J. Chem. Phys. **47,** 337 (1967) and J. Polymer Sci. Lett. **2,** 395 (1964).

[3] D. Parks, USAEC Report GA–4659, p. 79 (1964).

[4] J. V. Koppel, J. R. Triplett, and Y. D. Naliboff, USAEC Report GA–7417 (1966).

[5] J. E. Lynch, Jr., G. C. Summerfield, L. A. Feldkamp, and J. S. King, University of Michigan, to be published.

[6] S. F. Trevino, private communication (1967).

THE VIBRATIONAL PROPERTIES OF POLYOXYMETHYLENE

S. F. Trevino

Picatinny Arsenal, Dover, N.J. 07801

and

V. E. LaGarde

Boston College, Newton, Mass. 02740

1. Introduction

Polyoxymethylene POM is a polymer with chemical repeat unit (CH_2O). The chain backbone, consisting of carbon and oxygen atoms, defines a helix of nine chemical units and five turns in the identity period. The unit cell of the crystal is hexagonal and contains one chain [1].[1] The vibrational properties of the polymer have been previously investigated by infrared absorption and Raman scattering studies of Todokoro et al. [2], and reasonably good agreement was obtained between the observed optically-active vibrations and a calculation based on an isolated chain model. These studies were concerned predominantly with high-energy vibrations, and as yet there is very little information on the very low energy modes. The purpose of the present work is an attempt to obtain more extensive information about these low frequency modes which consist of skeletal torsions and deformations.

2. Experimental Procedure

The data obtained consist of measurements of the double differential cross section for inelastic scattering of cold neutrons. The measurements were made using the cold beryllium filter spectrometer located at the AMMRC reactor (2 megawatts, light water moderated).

The polymer scattering sample was oriented by stretching and rolling. The direction of the chains was determined by x-ray measurements to lie along the stretch direction with distribution characterized by an angular width of 13° at half maximum [3]. Two measurements were made on this sample which consisted of alternately placing the chain axis parallel and perpendicular to the direction of momentum transfer. The measured time of flight spectra were corrected for background and instrumental sensitivity. An effective frequency distribution was obtained which reproduced the measured spectrum in the one-phonon approximation. An iterative procedure was used to take into account the instrumental resolution and incident line shape in this fit.

---

[1] Figures in brackets indicate the literature references at the end of this paper.

3. Theoretical

The normal coordinate calculation of the vibrations of the polymer has been performed using the Wilson GF matrix method [4] as modified by Higgs [5]. The model used is that of an isolated helix. The frequencies of the twelve normal modes are calculated as a function of δ which is defined as

$$\delta=2\pi kc \tag{1}$$

k being the phonon momentum and c the distance between adjacent chemical units along the chain axis. The density-of-states function $g(\nu)$ is calculated graphically from the one-dimensional definition

$$g(\nu)=\sum_j\left(\frac{d\nu_j}{d\delta}\right)_{\nu_j(\delta)=\nu} \tag{2}$$

where the sum is over the branches j.

Two functions $g_L(\nu)$ and $g_T(\nu)$ have also been calculated. These are-defined as

$$g_L(\nu)=\sum_j\,(\mathbf{C}_j^c(\delta))^2\left(\frac{d\nu_j}{d\delta}\right)_{\nu_j(\delta)=\nu} \tag{3}$$

$$g_T(\nu)=\sum_j\,[(\mathbf{C}_j^a(\delta))^2+(\mathbf{C}_j^b(\delta))^2]\left(\frac{d\nu_j}{d\delta}\right)_{\nu_j(\delta)=\nu} \tag{4}$$

Here $\mathbf{C}_j^a(\delta)$, $\mathbf{C}_j^b(\delta)$ and $\mathbf{C}_j^c(\delta)$ are respectively the polarization vectors of the hydrogen atoms for branch j along the a, b, and c axes. The c axis is taken as the chain axis and the a and b axes form an orthogonal coordinate system with it. In the one-phonon approximation, these two functions are proportional to the effective frequency distributions described in section 2.

The force field used in the model is of the Urey-Bradley type [6], and consists of describing the potential energy as a series of harmonic forces preventing bond stretching, valence-angle bending and torsions about valence bonds.

4. Discussion

Figure 1 shows the four lowest-energy branches and the corresponding frequency distribution. The large dots on the dispersion curve at values of δ of 0 and $8\pi/9$ correspond to observed infrared frequencies. Inspection of the frequency distribution reveals various frequencies which should be observed in the neutron spectra which are forbidden optically. Figure 2 shows the measured and calculated functions g_L and g_T. The error bars on the measurements reflect statistical uncertainties only. The agreement between the various peaks in the measured spectra and the corresponding caluclations is not very good. There is still considerable adjustment of force constants necessary. There are however various tentative assignments which can be made.

Although not shown in Figure 2, there is a peak observed at 615 ± 15 cm^{-1} which corresponds to the observed infrared frequency of 630 cm^{-1} and is due to a large density of states at $\delta = \pi$ in the highest-energy optical mode of figure 1. The structure at 556 cm^{-1} is assigned to $\delta = 0$ of this same mode which is infrared inactive. The peak at 426 cm^{-1} is due to the lowest optical mode at $\delta = \pi$ and is to be compared with the observed infrared frequency of 455 cm^{-1}. There seems to be a discrepancy in the value of this frequency between the two techniques. The final frequency which can be assigned with some degree of certain is that occurring at 94 cm^{-1}, which corresponds to the high density of states due to the lowest acoustic mode at a value of

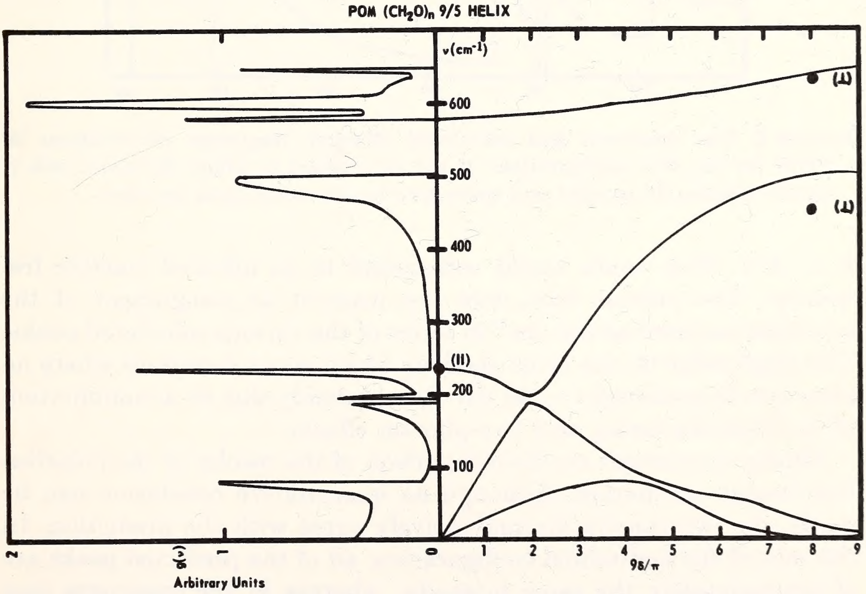

FIGURE 1. The low energy branches and frequency distribution of POM.

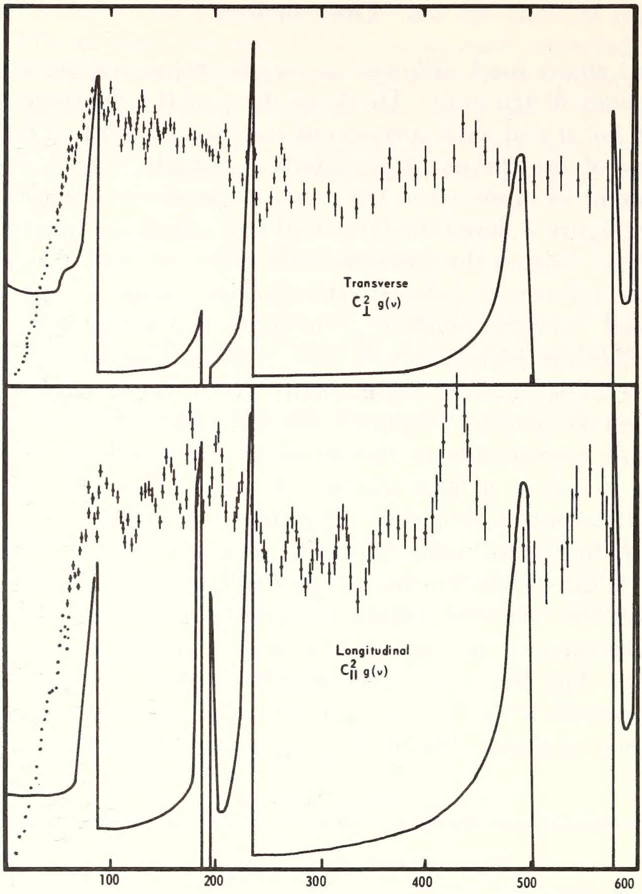

FIGURE 2. The measured and calculated effective frequency distributions of POM for the two configurations of the experiment in which the chain axis is placed alternately parallel and transverse to the momentum transfer.

δ of $.47\pi$. This again would correspond to an infrared inactive frequency. The present data does not warrant an assignment of the structure centered at 200 cm^{-1} in terms of the various calculated peaks. The large value of the cross sections which occur in regions where no structure is predicted ($\sim$350 cm^{-1}) is probably due to a combination of multiple scattering and two-phonon effects.

Finally a comment on the comparison of the results of the polarization vector calculation. Although no quantitative conclusion can be made, the two spectra do qualitatively agree with the prediction. In the case of the logitudinal configuration, all of the predicted peaks are of approximately the same intensity, whereas in the transverse case there is generally some diminishing in the predicted intensity of the higher-energy modes. This general trend is reflected in the measurements.

In conclusion, two frequencies not observable in infrared have been identified in addition to two which have previously been seen. There is a reasonable possibility of identifying more modes in the region of 200 cm^{-1} when the measurements are repeated with an instrument of better resolution. The force constants will be adjusted as soon as this better data is available.

5. References

[1] H. Todokoro, T. Yasumoto, S. Murahashi, and I. Nitta, J. Polymer Sci. **44,** 266 (1960).

[2] H. Todokoro, M. Kobayashi, Y. Kawaguchi, A. Kobayashi, and S. Murahashi, J. Chem. Phy. **38,** 703 (1963).

[3] The sample was provided by Dr. H. Starkweather of E. I. du Pont de Nemours & Co.

[4] E. B. Wilson, J. C. Decius and P. C. Cross, Molecular Vibrations, McGraw-Hill (1955).

[5] P. W. Higgs, Proc. Roy. Soc., London A**220,** 472 (1953).

[6] T. Shimanouchi, J. Chem. Phys. **17,** 245 (1949).

VIBRATION SPECTRA OF POLYGLYCINE

V. D. GUPTA,[1, 2] S. TREVINO,[2] and H. BOUTIN[2, 3]

Explosives Laboratory, Picatiny Arsenal, Dover, N.J. 07801

1. Introduction

Polyglycine $(-CH_2-CO-NH-)_n$ is the simplest of all synthetic polyamino acids, and a study of its normal modes and their dispersion is fundamental to an understanding of more complex polypeptides and proteins. It exists in two forms which differ in chain conformation. Polyglycine I contains fully extended linear zig-zag chains with a two-fold screw axis which are packed in an anti-parallel arrangement. Polyglycine II chains exist in helical form with a three-fold screw axis. They are mostly parallel and are packed in a hexagonal lattice. In both forms the neighboring chains are hydrogen bonded via $N-H...O=C$ bonds. In polyglycine II, Padden and Keith [1] [4] from morphological studies and Krimm [2] from infrared studies have shown the simultaneous presence of both direct and inverted chains. Ramachandran et al. [3] have shown that, as in collagen, hydrogen bonds of the type $C-H...O$ can be formed in polyglycine II. It is found that only one-third the possible number of such bonds can be formed. These observations are in accordance with the infrared studies of Krimm et al. [4].

Fukushima, Ideguchi and Miyazawa [5] have made a normal-mode calculation limited to the in-plane vibrations of polyglycine I and have studied the amide band frequencies. Since the low-frequency vibrations are expected to depend sensitively on the chain conformation, we have recalculated the normal modes for both the in-plane and out-of-plane vibrations and studied their dispersion.

2. Theory

Calculations are carried out according to Wilson's GF matrix method as modified by Higgs [6]. The secular determinant to be solved is:

$$|G(\theta)F(\theta)-I\lambda(\theta)|=0 \tag{1}$$

where I is the identity matrix and θ is the phase difference between successive units. It is related to the phonon momentum K and the distance (a) between adjacent chemical units by $\theta = 2\pi \mathrm{Ka}$. The The frequencies are given by the relation

---

[1] Visiting Scientist on leave from Physics Department, Indian Institute of Technology, Kanpur, India.

[2] Guests of Army Materials and Mechanics Research Center, Watertown, Mass. 02712.

[3] Present Address—Bendix Corporation, Southfield, Michigan.

[4] Figures in brackets indicate the literature references at the end of this paper.

$$\lambda(\theta) = 4\pi^2 \nu^2(\theta) \tag{2}$$

A plot of vibrational frequency ν as a function of $\theta (0 \leq \theta \leq \pi)$ gives the dispersion of the mode. A Urey-Bradley force field was used.

Assuming that a single phonon is involved in the scattering process, the incoherent neutron scattering cross section can be written as:

$$\sigma(\omega) = (E_f/E_i)^{1/2} \frac{(E_i E_f - 2\sqrt{E_f E_i} \cos\phi)}{\omega(e^{h\omega/kT} - 1)} \sum_l a_l^2 e^{-2W_l} g_l''(\omega) \tag{3}$$

where a_l is the incoherent scattering length of the lth nucleus in the unit cell, E_f and E_i are the final and incident neutron energies, M is the neutron mass, ϕ is the scattering angle, e^{-2W_l} is the Debye-Waller factor for the lth particle, $h\omega = E_f - E_i > 0$ is the energy of the phonon from which the neutron is scattered and

$$g_l''(\omega) = (M/M_l) v/(2\pi)^3 \sum_j \int d^3\theta |\mathrm{K} \cdot \mathrm{C}_j^l(\theta)|^2 \delta(\omega - \omega_j(\theta)) \tag{4}$$

where M_l is the mass of the lth particle and v is the volume of the unit cell. For the case of a monoatomic polycrystalline sample the sum over l reduces to

$$\sum_l a_l^2 e^{-2W_l} g_l''(\omega) = a_l^2 e^{-2W} (M/M_l) g(\omega) \tag{5}$$

where $g(\omega)$ is the density of states. Since a knowledge of the polarisation vectors $\mathbf{C}_j^l(\theta)$ is necessary to obtain frequency distributions from the inelastic neutron scattering cross section, our frequency distribution reported here is an approximate one.

3. Results and Discussion

The dispersion curves calculated for polyglycine I are shown in figure 1 and the calculated and observed infrared frequencies with their assignments are given in table 1. The inelastic neutron spectra of polyglycine I and II was obtained using the AMMRC slow chopper. The frequency distributions obtained are shown in figures 2 and 3.

The torsional motion around the amide C–N bond (amide VII) which involves the large displacement of the alpha carbon atom should be sensitive to conformational changes. This band appears as a strong band at 210 cm^{-1} in the neutron spectra and at 215 cm^{-1} in infrared absorption. The corresponding band in P.G.II appears at 365 cm^{-1}.

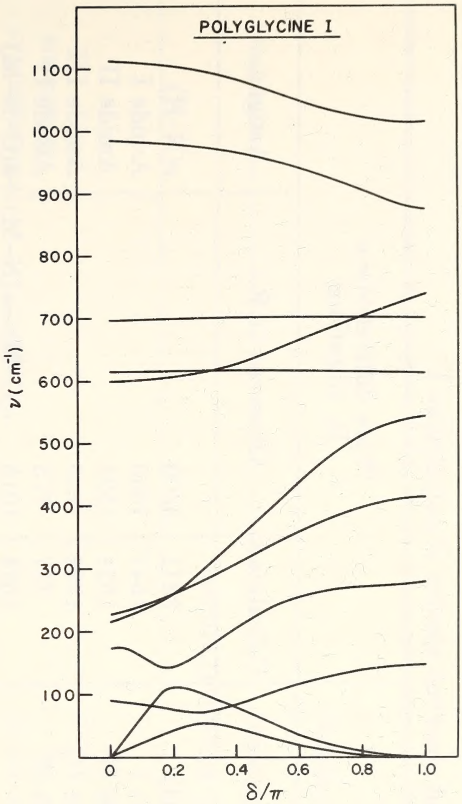

FIGURE 1. Dispersion curves for polyglycine I.

In the neutron spectra this band appears as a weak maximum. Since the peak intensities in neutron spectra are dependent on the amplitude of motion of the hydrogen atoms, it shows that the motion of the hydrogens of the methylene groups in polyglycine II is relatively restricted. This suggests the possibility of the presence of a C–H——O type hydrogen bond in polyglycine II, as suggested by Ramachandran[3].

Knowing the frequency distribution and treating the sample as an assembly of harmonic oscillators one can calculate thermodynamic quantities. Our calculation shows that the difference in the internal energies of the two forms due to the difference in the lattice and conformational energies is of the order of .5 kcal/residue, with polyglycine II having the higher value.

It can be shown that the N—H——O bonds are roughly of the same strength in the two forms and that their conformational energies are also not very different. Assuming that only one-third of the possible

TABLE 1.—Calculated and observed spectra of polyglycine I

Phase difference=0 A$_1$ vibrations			Phase difference=π B$_1$ vibrations		
Calculated	Observed (I.R.)	Assignment	Calculated	Observed (I.R.)	Assignment
3311	3300	ν(N–H)	3311	3300	ν(N–H)
1687	1690	Amide I	1647	1630	Amide I
1516	1514	Amide II	1524	1524	Amide II
1303	1240	Amide III	1294	1220	Amide III
600	628*	Amide IV	737	773	Amide IV
1112	1112	ν(N–M)$-\nu$(M–C)	1014	1015	ν(C–N)$-\nu$(N–M)$+\delta$(C–N–M)
985	987	ν(M–C)$+\delta$(M–C–N)$+\delta$(C–N–M)	874	880	ν(N–M)$+\nu$(M–C)
220	------	δ(M–C–N)$-\delta$(C–N–M)$+$ δ(M–C=0)	541	550*	δ(N–M–C)$+\delta$(M–C–N)
173	------	δ(N–M–C)$-\delta$(C–N–M)	277	282*	δ(C–N–M)$+\delta$(N–M–C)

A_2 Vibrations			B_2 Vibrations		
699	Inactive	Amide V	703	700*	Amide V
618	Inactive	Amide VI	614	600*	Amide VI
231	Inactive 215*	Amide VII	410	413*	Amide VII
91	Inactive	A mixture of τ(C–N), τ(N–M), & τ(M–C)	146	142 (?)	A mixture of 3 torsions
134	N-H—O=C stretch				

All frequencies are in cm^{-1}.
*Frequencies also observed in inelastic neutron scattering.
νBond stretching.
δDeformation mode.
τTorsional mode.

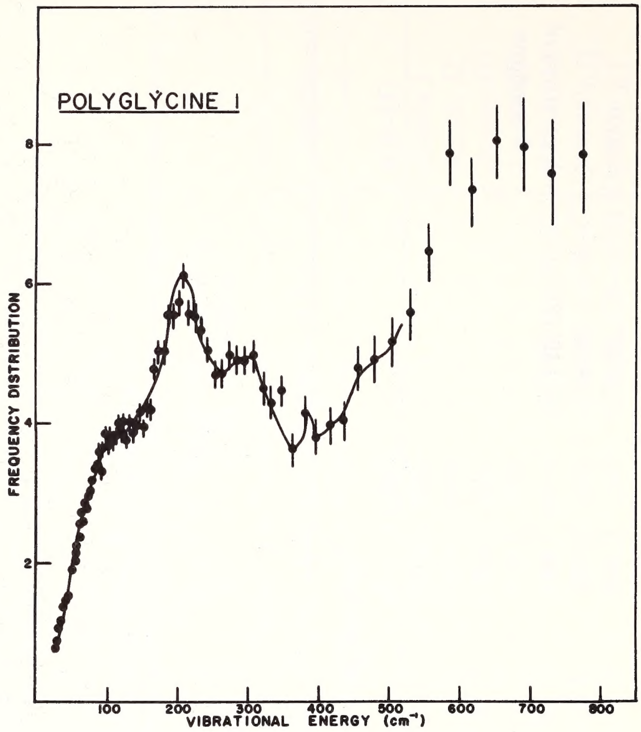

FIGURE 2. Frequency distribution for polyglycine I.

C—H——O bonds are present our approximate calculation shows that the energy of the C—H——O bond should be less than 1.5 kcal/residue. Further free-energy calculation shows that it is higher for polyglycine II which is consistent with the fact that it is metastable.

It is seen that the dispersion curves for the low frequency optical mode ($\theta = 0$ frequency at 173 cm^{-1}) and the acoustic mode (maximum frequency at 110 cm^{-1}) have flat regions in the frequency range 100–140 cm^{-1}. This implies a high density of states and is reflected in the shoulder about these frequencies in the neutron spectra. Of course, in this region there are also lattice-mode frequencies. Similar regions are seen in the frequency range 50–70 cm^{-1}.

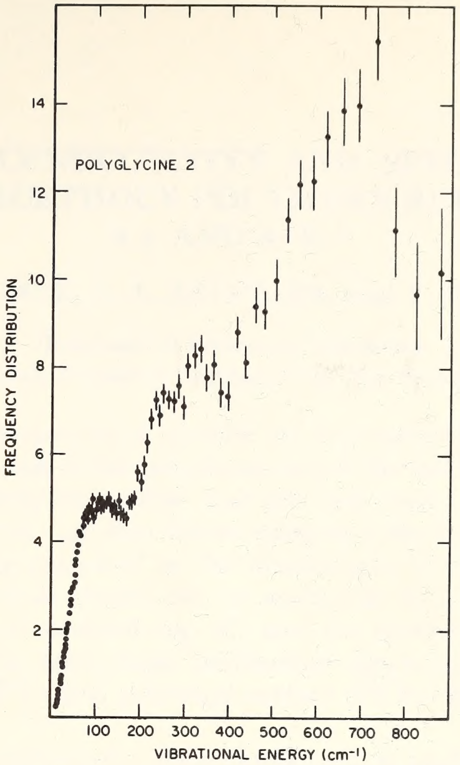

FIGURE 3. Frequency distribution for polyglycine II.

4. References

[1] F. J. Padden and H. D. Keith, J. Appl. Physics **36,** 2987 (1965).

[2] S. Krimm, Nature (London) **212,** 1482 (1966).

[3] G. N. Ramachandran, G. Ramakrishnan and C. M. Venkatachalam, paper presented at the conference on conformation of Biopolymers held at Madras, India (1967).

[4] S. Krimm, K. Kuroiwa and T. Rebane, paper presented at the Conference on Conformation of Biopolymers held at Madras, India (1967).

[5] K. Fukushima, Y. Ideguchi and T. Miyazawa, Bull. Chem. Soc. Japan **36,** 1301 (1963).

[6] P. W. Higgs, Proc. Roy. Soc., London **A220,** 472 (1953).

THERMAL CONDUCTIVITY AND SPECIFIC HEAT OF AMORPHOUS POLYMERS BETWEEN 0.4 AND 4 °K [1]

C. L. CHOY, G. L. SALINGER, and Y. C. CHIANG

Department of Physics and Astronomy
Rensselaer Polytechnic Institute, Troy, New York 12180

The thermal properties of crystals are reasonably well understood theoretically because of the periodic nature of the lattice. The thermal properties of amorphous solids, however, are badly understood. At temperatures low enough that the wavelength of the dominant thermal vibrations is long compared to the microscopic disorder, the theory applicable to crystals should also be applicable to amorphous solids. Thus the thermal conductivity, K, and the specific heat, C, have been measured in amorphous polymethyl methacrylate (PMMA), polystyrene (PSTY) and polyvinyl acetate (PVAc) between 0.4 and 4 °K.

The thermal conductivity, shown in figure 1, is qualitatively similar for all three polymers. It is nearly temperature independent near 4 °K and decreases with an ever increasing power of the temperature as the temperature is lowered. Near 0.4 °K, $K \propto T^{1.5}$. This does not agree with the linear temperature dependence of the thermal conductivity predicted by Klemens[1] [2] for inorganic glasses. Attempts to fit the data by adding internal boundary scattering to the Klemens theory resulted in temperature-independent mean free paths of about 50 μ. This is too long to be physically meaningful.

The Klemens theory may not be applicable since the end-to-end chain length of the polymer chains is the same as the dominant wavelength of the vibrations of the upper part of the temperature range. The thermal conductivity was measured for three different samples of PMMA. The data shown are for a specially prepared pure PMMA (lucite) having a weight average molecular weight of 430,000. For a sample having an average molecular weight of 79,000, the thermal conductivity was 6 percent less over the temperature range. A sample cut from a ¼ inch Rohm and Haas sheet, known to have many short chains, displayed a thermal conductivity about 10 percent less than that shown here. Measurements at lower temperatures may be necessary to make a meaningful comparison with the theory.

---

[1] Figures in brackets indicate the literature refererences at end of this paper.

[2] Work supported by the National Aeronautics and Space Administration.

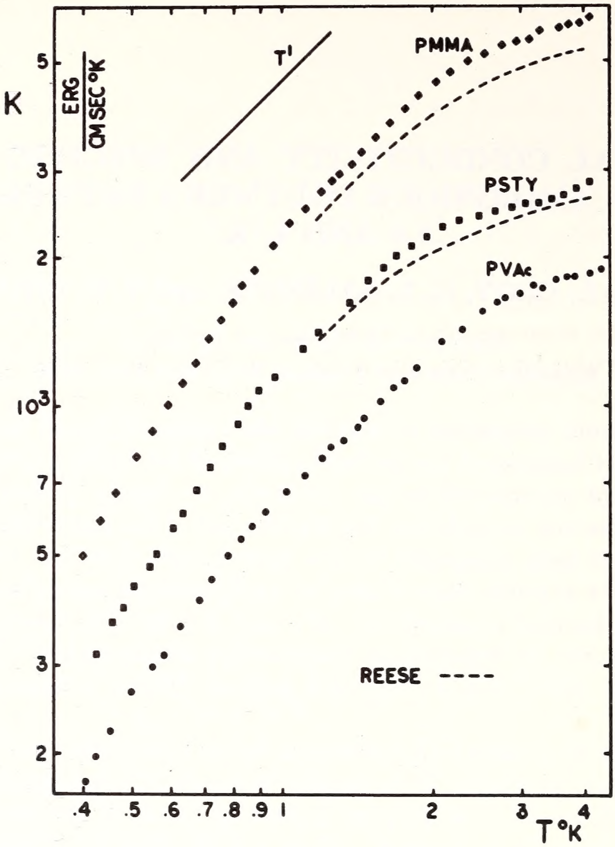

FIGURE 1. The thermal conductivity of polymethyl methacrylate, (PMMA), polystyrene (PSTY) and polyvinyl acetate (PVAc) between 0.4 and 4 °K. The dashed lines refer to the work of reference 2.

The data presented here agree with earlier measurements by Reese [2] within 5 percent for polystyrene and for commercial PMMA samples. This demonstrates that the thermal conductivity is an intrinsic property of the particular polymer and depends only slightly on impurities in this temperature range.

The measurements were made by the steady-state technique in a ^{3}He cryostat. One-eighth watt carbon radio resistors were used to monitor the temperatures, the power dissipation being about 10^{-10} watts. Heat currents of 1 to 200 ergs/sec resulted in a temperature difference between the thermometers of about 2 percent of the temperature of the sample. The shorting effect of the leads is estimated to be about 1 percent.

The thermal diffusivity of the sample could be measured by monitoring one of the thermometers as a function of time. At sufficiently long times, the temperature change becomes an exponential function of time. The time constant τ is related to C and K by $\tau=\frac{4L^2}{\pi^2}\frac{C}{K}$, were L is the effective length of the sample. The specific heats so determined are shown in figure 2 as open squares (PSTY) and open diamonds (PMMA). The values of C/T^3 are fairly constant above 2 °K and agree with those of Reese [2] for PMMA and with earlier work [3] for PSTY. C/T^3 for PVAc is 475 ergs cm^{-3} $°\mathrm{K}^{-4}$.

Below 1.5 °K the time constant became too short and the contact resistance too large for thermal diffusivity measurements. Classical specific-heat measurements were made on samples connected to the ^{3}He refrigerator by a thin pin of the same material. The time constant across the pin was about 100 times the time constant for the sample. The 4 second heat pulse of 1–10 ergs/sec produced a temperature change of about 2 percent in the sample. Heat losses from the sample and systematic errors in the temperature measurement should make the measured values of the specific heat (black circles in fig. 2) larger than the actual values. Below 0.6 °K, the data scattered badly about $C/T^3 = 400$ ergs cm^{-3} $°\mathrm{K}^{-4}$.

Extrapolation to 0 °K of sound-velocity measurements made above 100 °K in our laboratory [4] and above 140 °K by Reese [5]

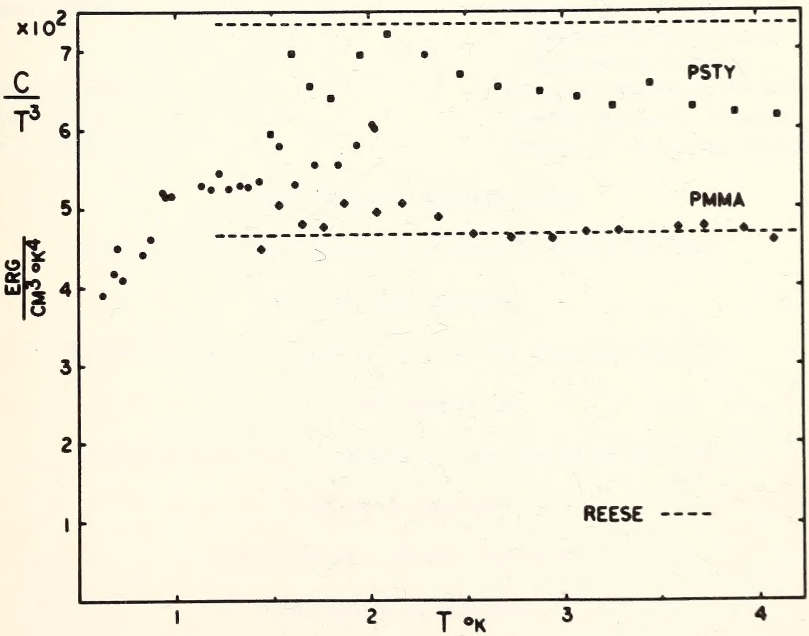

Figure 2. The specific heat per unit volume divided by the cube of the absolute temperature for polystyrene and polymethyl methacrylate. See text for explanation of symbols. The dashed line refers to the work of reference 2.

result in $C/T^3 = 420 \pm 40$ ergs cm^{-3} $°\text{K}^{-4}$ for polystyrene. This value is considerably lower than the measured C/T^3 except at the lowest temperatures. This anomalous specific heat is ascribed to the existence of low frequency non-acoustic modes [5]. The data are consistent with the addition of a 10 °K Einstein mode to the Debye spectrum. We believe that some of the side groups are only loosely coupled to the lattice and contribute to this mode. Recent measurements[6] on irradiation-produced cross-linked polystyrene, which showed no change in the thermal conductivity and a 25 percent reduction in the specific heat between 1.2 and 4 °K, are consistent with this explanation.

References

[1] G. P. Klemens, Proc. Roy. Soc. (London) **A208,** 108 (1951).
[2] W. Reese, J. Appl. Phys. **37,** 864 (1966).
[3] R. J. Noer, C. W. Dempsey and J. E. Low, Bull. Am. Phys. Soc. **4,** 108 (1959).
[4] J. I. Treu (unpublished).
[5] W. Reese, J. Appl. Phys. **37,** 3959 (1966).
[6] W. Reese, private communication.

Appendix I

Molecular Dynamics and Structure of Solids Symposium Committees

Carl O. Muehlhause, General Chairman	Reactor Radiation Division
Vernon W. Myers, Deputy General Chairman	Reactor Radiation Division

Program Committee

Robert S. Carter, Chairman, Reactor Radiation Division

Norman P. Bekkedahl	Polymers Division
Thomas C. Farrar	Inorganic Materials Division
David T. Goldman	Reactor Radiation Division
William G. Hodgson	Research Associate to The Institute for Materials Research, American Cyanamid Company
John D. Hoffman	Polymers Division
David R. Lide	Atomic Physics Division
Edward Prince	Reactor Branch, Nuclear Physics Division, Naval Research Laboratory
Curt W. Reimann	Inorganic Materials Division
John J. Rush	Reactor Radiation Division
Jon J. Spijkerman	Analytical Chemistry Division

Arrangements Committee

Frederick J. Shorten, Chairman, Reactor Radiation Division

Social Committee

Howard T. Yolken, Chairman, Institute for Materials Research

Tours Committee

Frederick J. Shorten, Chairman, Reactor Radiation Division

Ladies Program

Mrs. Edward L. Brady, Chairman

Finance Committee

Ronald B. Johnson, Chairman, Institute for Materials Research

U.S. GOVERNMENT PRINTING OFFICE : 1969 O—311-280

PENN STATE UNIVERSITY LIBRARIES
A000071919645